

2

DOT/FAA/CT-90/11

FAA Technical Center
Atlantic City International Airport
N.J. 08405

Proceedings of the 1990 AIAA/FAA Joint Symposium on General Aviation Systems

AD-A227 355

April 11-12, 1990
Port-O-Call
Ocean City, New Jersey

DTIC
ELECTE
OCT 04 1990
S D

May 1990

This document is available to the U.S. public
through the National Technical Information
Service, Springfield, Virginia 22161

DECLASSIFICATION STATEMENT A
Approved for public release
Distribution Unlimited



U.S. Department of Transportation
Federal Aviation Administration

NOTICE

This document is disseminated under the sponsorship of the U.S. Department of Transportation in the interest of information exchange. The United States Government assumes no liability for the contents or use thereof.

The United States Government does not endorse products or manufacturers. Trade or manufacturers' names appear herein solely because they are considered essential to the objective of this report.

1. Report No. DOT/FAA/CT-90/11	2. Government Accession No.	3. Recipient's Catalog No.	
4. Title and Subtitle PROCEEDINGS OF THE 1990 AIAA/FAA JOINT SYMPOSIUM ON GENERAL AVIATION SYSTEMS April 11-12, 1990		5. Report Date May 1990	
		6. Performing Organization Code	
7. Author(s) Compiled by Augusto Ferrara, Dave Lawrence and Janine Blake		8. Performing Organization Report No. DOT/FAA/CT-90/11	
9. Performing Organization Name and Address American Institute of Aeronautics and Astronautics General Aviation Systems Technical Committee Federal Aviation Administration Technical Center		10. Work Unit No. (TRAIS)	
		11. Contract or Grant No.	
12. Sponsoring Agency Name and Address U.S. Department of Transportation Federal Aviation Administration Technical Center Atlantic Center International Airport, NJ 08405		13. Type of Report and Period Covered Proceedings April 11-12, 1990	
		14. Sponsoring Agency Code ACD-210	
15. Supplementary Notes Held at Port-O-Call Motel, Ocean City, New Jersey			
16. Abstract The 1990 AIAA/FAA Joint Symposium on General Aviation Systems was the result of the combined efforts of the AIAA General Aviation Systems Technical Committee and the Federal Aviation Administration Technical Center. This symposium offered the opportunity to present and review the current state of the art in research that is being conducted in support of general aviation. All told, the papers presented covered the entire spectrum of research and the participants had the opportunity to hear presentations on everything from alternate fuels to developments in air traffic control. <i>Key words</i>			
17. Key Words Proceedings General Aviation Systems AIAA FAA		18. Distribution Statement Document is available to the public through the National Technical Information Service, Springfield, Virginia 22161	
19. Security Classif. (of this report) Unclassified	20. Security Classif. (of this page) Unclassified	21. No. of Pages 395	22. Price

TABLE OF CONTENTS

<u>Title</u> Author/Co-Author	<u>Page</u>
<u>Software Supplier Evaluation and Assessment</u> Robert Kosinski / John M. Gushue Ebasco Services Inc.	2
<u>Mechanical Paint Removal Techniques for Aircraft Structures</u> Joe P. Amro / Jorge E. Talia Wichita State University	16
<u>Surface Condition Effect on the Fatigue Behavior of Aluminum Lithium Alloys</u> Ali Eftekhari / Jorge E. Talia Wichita State University	34
<u>ETBE in General Aviation Aircraft Engines</u> William F. Marshall National Institute for Petroleum and Energy Research	54
<u>Flight Testing with Ethanol in Turboprop Engines</u> Keith Biehl / Paul Demko FAA Technical Center	56
<u>Human Performance in Cockpit-Related Systems</u> Randall Chambers / Mihriban Cihangirili Wichita State University	66
<u>The Enhancement of Air Traffic Control Safety Through Pre-Hire University Based Training Programs</u> Brent Bowen Wichita State University	82
<u>Dynamic Behavior of the Human Body Subjected to Impact Conditions With and Without Restraint</u> Hamid M. Lankarani / Gayle Ermer / Deren Ma Wichita State University	108
<u>Neural Networks: Can They Be Used to Detect Defects in Aircraft Structures?</u> Behnam Bahr / Tarabishy M. Nabeel Wichita State University	132

<u>Title</u> Author/Co-Author	<u>Page</u>
<u>Robotics: Another Choice for Inspection of Aging Aircraft</u> Behnam Bahr / Sami Maari Wichita State University	144
<u>Performance of a Supercharged Direct-Injection, Stratified-Charge Rotary Combustion Engine</u> T. A. Bartrand / E. A. Willis Sverdrup Technology Inc., NASA Lewis Research Center	156
<u>Computational Experience With a 3-D Rotary Engine Combustion Model</u> M. S. Raju / E. A. Willis Sverdrup Technology Inc., NASA Lewis Research Center	180
<u>Advanced Stratified Charge Rotary Engine Technology for General Aviation Systems</u> Robert Mount / Edward S. Wright John Deere Technologies International Inc.	202
<u>Evaluation of Add-on Drag Reduction for Devices Light Aircraft</u> Hubert Smith Pennsylvania State University	222
<u>An Evaluation of Automatic Control System Concepts for General Aviation Airplanes</u> Eric Stewart NASA Langley Research Center	236
<u>Performance Instrumentation for Multiengine Safety</u> Arthur Hoadley Western Michigan University	260
<u>An Airfoil for General Aviation Applications</u> Michael Selig / Mark Maughmer / Dan Somers Pennsylvania State University, NASA Langley Research Center	280
<u>Aerodynamic Transport Efficiency of General Aviation: An Overview</u> Fabio Goldschmied Consulting Engineer	292
<u>Gulfstream IV Flight Management System</u> Steve Runo Honeywell Inc.	312

<u>Title</u>	<u>Page</u>
Author/Co-Author	
<u>Design and Certification of Aircraft for the HERF Environment</u>	330
Jack Glecier / Joseph P. Cross Beech Aircraft Corp.	
<u>The FAA Technical Center's Avionics Data Link Initiative</u>	348
Albert Rehmann FAA Technical Center	
<u>General Aviation and TCAS</u>	358
Carl Jezierski FAA Technical Center	
<u>Summary of the FAA Low Data Rate Voice CODEC Evaluation and Demonstration Program</u>	364
Markus Grable CTA Inc.	
<u>The Pilot's Automated Weather Support System Concept PAWSS</u>	374
Ernie Dash / Norm Crabill Aerospace Consultants	
Appendix A, List of Attendees	385

Delete proprietary information per
telecon Harry Kemp. Federal Aviation
Agency Technical Center/ACM-651. At-
lantic City International Airport, NJ
08405. VHG 12/10/90

Accession For	
NTIS	CLAM
DTIC	TAB
Unannounced	
Justification	
By	
Distribution/	
Availability	
Dist	Availability
A-1	Special

Foreword

The 1990 AIAA/FAA Joint Symposium on General Aviation Systems was the result of the combined efforts of the AIAA General Aviation Systems Technical Committee and the Federal Aviation Administration Technical Center. This symposium offered the opportunity to present and review the current state of the art in research that is being conducted in support of general aviation. All told, the papers presented covered a wide spectrum of research, and the participants had the opportunity to hear presentations on everything from alternate fuels to developments in air traffic control.

The AIAA General Aviation Systems Technical Committee recognizes that the United States general aviation industry has been suffering from a prolonged recession, and this recession is the result of a number of factors. One factor which has contributed to this economic slowdown is the lack of new technology which could make new aircraft more productive than their predecessors. Given this background, the AIAA prepared a position paper titled "The Role of Technology in Revitalizing U.S. General Aviation", a report on an AIAA Workshop December 12-13, 1989 Washington, D.C., published April 19, 1990 by the American Institute of Aeronautics and Astronautics, 370 L'Enfant Promenade S.W., Washington, D.C. 20024-2518, with the intent of promoting government sponsored research in areas which can be used by general aviation manufacturers. The proceedings of this symposium can be viewed as a summary of the research which is being conducted by industry, universities, and the government, and as such they provide the foundation for considering the AIAA position paper.

The Federal Aviation Administration Technical Center and the AIAA General Aviation Systems Technical Committee would like to thank the authors for investing the resources needed to prepare the papers which are contained in this proceedings and Mr. Joseph Del Balzo, Executive Director, AXD-1, for giving the keynote address. We would also like to thank the individuals who acted as technical editor or session chairmen, since their efforts were instrumental in getting the symposium underway. They are as follows:

Jerry Allsup, U.S. Department of Energy, Washington, DC
William Johnson, Galaxy Scientific Co., Atlanta, GA
Dave Lawrence, FAA Technical Center, Atlantic City, NJ
Mark Maughmer, Pennsylvania State University, State College, PA
Trib Singh, Martin Marietta, Atlantic City, NJ
Melvin Snyder, Wichita State University, Wichita, KS
Ed Willis, NASA Lewis Research Center, Cleveland OH

This page intentionally
left blank

SOFTWARE SUPPLIER EVALUATION AND ASSESSMENT

by

R. Kosinski
and
J. M. Gushue
Ebasco Services Inc.
Corporate Quality Programs Division
210 Clay Avenue
Lyndhurst, NJ 07071

For presentation to the AIAA/FAA Joint Symposium on General
Aviation Systems at the Port O-Call Inn, Ocean City, NJ
on April 11, 1990

SOFTWARE SUPPLIER EVALUATION AND ASSESSMENT

R. Kosinski
J. M. Gushue
Ebasco Services, Inc.
Corporate Quality Programs Division
210 Clay Avenue
Lyndhurst, NJ 07071

ABSTRACT

In the design of general aviation aircraft, current technology involves the use of advanced application software. Advanced software systems are called upon to provide reliable and accurate solutions. Software systems enhance our ability to understand complex forces and processes. Thus, the process of software development and maintenance can't be ignored if the aircraft industry is to rely on these advanced systems for the design of state of the art aircraft and the safety of the flying public.

Potential users of advanced application software must establish a level of confidence in the product before it can be applied to engineering and design situations. A software supplier control program can help to provide the necessary level of assurance that advanced application software will perform as required.

Software supplier control programs can help enhance our confidence in the software through: 1) an evaluation of the supplier's Software Quality Assurance Program; 2) an evaluation of its implementation and; 3) an assessment of a supplier's software engineering capability.

Supplier evaluations or audits are a proven technique used to examine suppliers' QA programs, and to determine the acceptability and implementation of the program. The software engineering capability assessment is a technique used to assess the capability of an organization to support and use modern software engineering technology. The emphasis of the software engineering capability assessment is on identifying and promoting modern software development and maintenance processes and practices within the supplier's organization which, in turn, support desirable quality characteristics in the software and software process.

INTRODUCTION

PURPOSE

The engineering and design of complex systems and structures, like general aviation aircraft, increasingly involves the use of software. Software is called on to provide solutions to complex engineering and design problems. The use, and reliance on sophisticated application software

system to solve these engineering and design problems has focused attention on the assurance of software quality and software reliability.

Thus, the assurance of software quality has increasingly become a major consideration to regulators such as the FAA (also FDA, NRC, etc.), users, and developers of software.

BACKGROUND

The awareness that software containing latent defects may adversely affect aircraft safety has caused regulators, software developers, and users to concentrate on software quality and the process functions associated with software development and maintenance. The imposition of new and stringent software quality assurance requirements across many industries has increased dramatically over the last decade. FAA-STD-018a, "Computer Software Quality Program Requirements" (1) are the software QA requirements applicable to contractors under FAA contract or when specifically referenced in a contract or specification governing aviation systems. The FAA standard sets forth the requirements for a computer software quality program and specifically calls for the development, implementation, and maintenance of a Computer Software Quality Program Plan (CSQPP).

Software supplier control is an element of overall software quality assurance planning. The purpose of software supplier control is to ensure that acquired software and services conform to specified requirements. This is accomplished in accordance with an organization's internal policies and procedures, and usually involves personnel from engineering, purchasing, and quality assurance/quality control. Internal procedures are written to ensure that, among other things, software supplier source selection controls are in place and that functional, technical, and quality requirements are properly conveyed to the supplier. These procedures usually make provision for access to the supplier's facilities for the purpose of supplier evaluation/qualification.

The approach to supplier quality uses a supplier qualification practice which involves quality assurance/ quality control personnel. The method most often used to assess the capability of a supplier to meet specified quality requirements is the vendor quality survey or quality assurance program evaluation (2). In general, the purpose of the supplier quality assurance program evaluation is to verify the existence of a documented supplier quality program that meets the purchasers requirements and, based on a review of samples of objective evidence, verification that the quality program is implemented to the satisfaction of the purchaser (3). While nothing has been reported about the correlation between the supplier quality evaluation and the quality of the supplier's product, it is generally felt that the implementation of a quality plan, outlining all the planned and systematic processes and activities necessary to provide confidence that the product conforms to specified requirements, results in improved product quality. The periodic reevaluation and verification of the quality program prevents organizations from drifting away from their stated program thus maintaining quality and confidence in the product. This method has had wide application in such areas as defense, aerospace, nuclear power, medical devices, and industrial applications. The same evaluation approach has been used with respect to the establishment and implementation of a Software Quality Assurance Program/Plan. For example,

IEEE Std 1028 - 1988 "IEEE Standard for Software Reviews and Audits" (4) describes a formal approach for conducting Quality Systems Audits with respect to a software quality assurance program/plan.

The Software Engineering Institute (SEI) of Carnegie Mellon University has developed and described a method for assessing the capability of " ... DOD contractors to develop software in accordance with modern software engineering methods" (5). The purpose of the capability assessment is to objectively and consistently assess the capability of an organization to develop software using modern techniques and to organize and manage the software development process. The methodology has been developed for application to DOD contractors; however, with modification it can be adapted for use in industrial applications.

This approach focuses on the software development process and the organization, management, process control, and resources necessary to ensure a successful software project (i.e. the product exhibits positive attributes such as improved productivity, quality, reliability, and delivered within budget and on schedule). It does not reference specific quality assurance requirements, but does address quality assurance considerations with respect to process control techniques, metrics, and standards and procedures. Objectivity and consistency are achieved through the use of a quantitative method described below.

The supplier evaluation technique can be applied prior to the issuance of a purchase order or contract (pre-award) and during the fulfillment of the purchase order or contract (post-award) at specified time intervals. The assessment technique can be applied during the same intervals.

METHODS AND TECHNIQUES

SOFTWARE SUPPLIER QUALITY ASSURANCE EVALUATION. All government or industry software quality assurance standards include a section addressing the requirements for supplier control. Sections 3.1.12 Supplier Control and 3.1.5 Audits of FAA-STD-018a (1) give the requirements for the control of software suppliers with respect to FAA applications. The software supplier control techniques specified in these sections rely on standard approaches that have been implemented across many industries. Generally, supplier control practices involve engineering, procurement, and quality assurance personnel who contribute to the process with respect to their area of expertise.

Software supplier evaluations are performed to ensure that a software supplier operates in accordance with a Software Quality Assurance (SQA) Program that meets the purchaser's requirements. Quality assurance personnel are called upon to make a "determination of acceptability of the software quality plans and procedures,...." (6). This is usually accomplished through the implementation of a software supplier evaluation program. The program, which should be described in procedures, uses formal methods and techniques to make the necessary "determination" (4). This will involve a visit to the supplier's facilities to evaluate and examine the supplier's software quality assurance program/ plan. The total evaluation process includes: pre-planning and notification to the supplier, performance of the evaluation, reporting, and

follow-up. Pre-planning involves: determining the evaluation criteria such as contract requirements, SQA Plan(s), software standards and procedures; identifying the software, software processes, and software documentation to be examined and; the preparation of evaluation checklists to be used during the evaluation. Checklists are a recognized technique which ensure coverage of the area to be evaluated and acts as a guide to the auditor. The checklists originate from the software quality assurance requirements imposed in the RFP or contract and, thus, drive the evaluation process. For example, a FAA-STD-018a checklist would include sections which address:

- Computer software quality program and plan
- Organization
- Personnel
- Resources
- Development process flow
- Audits
- Standards and procedures
- In-process controls
- Configuration management
- Library controls
- Corrective action; reporting and control
- Tools
- Supplier control
- Test Controls
- Software independent verification and validation (IV&V) interface
- Records
- Reports
- Installation and checkout
- Storage, handling, and shipping

For IEEE Std. 730.1 (7) the checklist would include sections that address:

- Software Quality Assurance Plan
- Purpose
- Reference Documents
- Management
- Documentation
- Standards, practices, conventions, and metrics
- Review and audits
- Test
- Problem reporting and corrective action
- Tools, techniques and methodologies
- Code control
- Media Control
- Supplier control

- Records collection, maintenance, and retention
- Training
- Risk management

Audit checklist questions are concerned with the observation and verification of a particular element or attribute of the software quality assurance requirement imposed by the contract, SQA Plan, or software standards and procedures.

An example of several evaluation questions to assess the area of software standards and procedures would be: 1) does the supplier have standards and procedures to support the software development and maintenance process; 2) do standards address software requirements analysis, software design, coding standards (control logic structures, commentary, statement construction), test, software problem reporting and corrective action, code and media control, and software documentation; 3) are the standards and procedures controlled.

The quality assurance evaluator's job is to verify compliance with the specific software quality requirements. When compliance cannot be verified, a finding or deficiency often results. The deficiency is described in enough detail so that corrective action can be implemented. Findings must identify the organization/ department/group responsible, area or activity, specific QA requirement reference, document or software element (if any) reference, description of deficiency, individual acknowledging deficiency. The cause of the deficiency must be ascertained - this may determine the extent of the corrective action to be implemented. The implementation of the supplier's corrective actions must be verified. The evaluation is often conducted on a periodic basis to ensure supplier maintenance of the software quality assurance program/plan (SQAP/P) as well as implementation.

The supplier quality evaluation rating results from the evaluation process. Numerous rating schemes have been devised including several quantitative measures (2). However, most schemes are qualitative and generally classify the results of an evaluation into three classifications: 1) Adequate, acceptable, or satisfactory - no corrective actions required from the supplier; 2) acceptable with comment, conditional satisfactory, or satisfactory subject to the resolution of findings - identified deficiencies require corrective action; 3) unacceptable or unsatisfactory - significant deficiencies exist, reaudit of supplier's program usually required (3). In summary, the purpose of the software quality assurance evaluation activities are the evaluation and monitoring of the supplier's software quality assurance program/plan thereby helping to ensure that the supplier's overall software development and maintenance activities are defined, controlled, and implemented.

SOFTWARE SUPPLIER SOFTWARE ENGINEERING CAPABILITY ASSESSMENT. The software engineering capability assessment is a technique recently described by the Software Engineering Institute of Carnegie Mellon University (5). The assessment is used to determine whether a software supplier has the capability to develop software using modern software engineering methods and techniques. While the assessment technique and methodology has been developed to assess potential DOD contractors, with modification, it can be used to assess

software suppliers for industrial applications when the application is judged critical.

Generally, the focus of the assessment is to identify those methods and practices which promote quality and quality improvement in the software product and process in the context of the supplier's operations.

In contrast to the quality evaluation, which is a straight forward examination of a software quality program/plan to ensure it meets specified software quality requirements, the assessment approach focuses on the underlying software development and maintenance processes that support desirable characteristics in the software and the software process. Consequently, the assessment approach can be used to supplement the quality evaluation.

The Software Engineering Institute's assessment approach emphasizes concepts which have been accepted and implemented in manufacturing operations. These concepts have to do with process control and technology. SEI "...Assessment questions are based on the following premises:

- The quality of a software product stems, in large part, from the quality of the process used to create it.
- Software engineering is a process that can be managed, measured, and progressively improved.
- The quality of a software process is affected by the technology used to support it.
- The level of technology used in software engineering should be appropriate to the maturity of the process.

..."(5)

The supplier's capability to develop software using modern practices and techniques encompasses three major areas: 1) organization and resource management; 2) software engineering process and its management; 3) tools and technology (5). Within those areas the assessment questions focus on specific qualities and attributes which are identified with modern software engineering practices and techniques - some more advanced than others. Some questions may not be applicable to a supplier; however, this does not necessarily mean that the supplier lacks the capability to develop and maintain software using modern software engineering practice.

Assessment questions in each major area address the major concerns associated with the area. The following concerns within each major area have been addressed:

Organization and resource management
Organizational structure
Resources, Personnel, and Training
Technology management

Software engineering process and its management

- Documented standards and procedures
- Process metrics
- Data management and analysis
- Process control

Tools and technology (5)

The assessment questions are organized according to the major concerns of each area in order to determine the software development and maintenance "process maturity level" of the supplier. Like the supplier quality evaluation the results of the assessment have been classified in a qualitative manner (but arrived at in a quantitative manner). Five software process maturity levels and two stages of technology use have been postulated by the SEI. The five software process maturity levels have been described thus: "...

1. Initial: The initial environment has ill-defined procedures and controls. The organization does not consistently apply software engineering management to the process, nor does it use modern tools and technology...
2. Repeatable: At level 2, the organization has generally learned to manage costs and schedules, and the process is now repeatable. The organization uses standard methods and practices for managing software development activities...
3. Defined: In level 3, the process is well characterized and reasonably well understood. The organization defines its process in terms of software engineering standards and methods, and it has made a series of organizational and methodological improvements. These specifically include design and code reviews, training programs for programmers and review leaders, and increased organizational focus on software engineering...
4. Managed: In level 4, the process is not only understood but it is quantified, measured, and reasonably well controlled. The organization typically bases its operating decisions on quantitative process data, and conducts extensive analyses of the data gathered during software engineering reviews and tests. Tools are used increasingly to control and manage the design process as well as to support data gathering and analysis...
5. Optimized: At level 5, organizations have not only achieved a high degree of control over their process, they have a major focus on improving and optimizing its operation. This includes more sophisticated analyses of the error and cost data gathered during the process as well as the introduction of comprehensive error cause analysis and prevention studies..."(5)

The two stages of software technology described in the SEI Assessment Methodology:..."

- A. Inefficient: Multiple implementations may be available and the practice may be in widespread use, but the technology is no longer effective. An organization that primarily employs inefficient software development technology is likely to be ineffective in developing software...
- B. Basic: Multiple implementations are available, and they have been demonstrated to be effective. An organization that primarily employs basic software development technologies is likely to be moderately effective and, depending upon the maturity of its process, reasonably consistent in its performance."(5)

These classifications must be used with care when applied to suppliers who are not implementing DOD applications. The SEI Assessment Methodology must be modified for the particular application of the software to be acquired. In particular, for software already developed the assessment methodology will focus primarily on the capability of the supplier to maintain the software (i.e. correct defects, implement modifications, and undertake major enhancements) using modern software engineering technology.

With respect to software technology usage, recent development and advances in the implementation of computer aided software engineering (CASE) tools has made the assessment of the technology used very important. Many CASE tools can automate widely accepted software engineering practices and methodologies - including activities like reverse engineering and reengineering of software. Some tools can automate several software life cycle activities using a particular methodology (e.g. structured analysis, design, programming). Often CASE technology is seen as a software engineering panacea by many organizations that have not previously initiated and implemented modern software process practices in their own organizations. The tools may actually have the opposite effect then that expected by the organization. If the tools are not properly evaluated, they may not fit in with the organization's standard software practice. In this case the tools may be misapplied or not used at all.

The SEI Assessment Methodology provides a quantitative procedure to determine a supplier's process maturity level. Simply described, the overall procedure follows from a yes or no response to each question. The questions are grouped with respect to each process maturity level (i.e. Level 2, Level 3, etc.). The percentage of yes responses is determined for the initial level of questions and, based on the percentage of yes responses, the supplier may qualify at Level 2 (if not, the supplier is at Level 1). If the supplier initially qualifies at Level 2, the process is continued until qualification at a higher level has not been achieved - then the supplier qualifies at the lower level (5). The procedure could be modified such that a specific rating is assigned to each question in order to further refine the assessment technique. The rating system might involve these measures: not present; partially present; present. This system can be used to help identify those suppliers who may be ready to move to the next process maturity level.

SOFTWARE SUPPLIER QUALITY EVALUATION/SOFTWARE ENGINEERING CAPABILITY ASSESSMENT. The areas covered in the supplier evaluation and the software engineering capability assessment overlap in many cases such as: organization and management;

standards and procedures; software problem reporting and corrective action; reviews, audits, and inspections. The combination of evaluation/assessment can be used to identify deficiencies and make specific recommendations leading to process improvements. Software supplier quality evaluation deficiencies may be symptomatic of ineffective process controls and inefficient technology. Through the assessment of the suppliers software engineering capability, process improvements can be identified and recommendations made which advance and enhance the suppliers software engineering capability.

For example, during a software supplier evaluation/assessment, purchaser's personnel identify a quality finding with respect to the software supplier's Software Requirements Specifications (SRS).

A software quality requirement states that each software requirement shall be described in sufficient detail such that its implementation and independent verification can be achieved. The evaluation finding determines that the Software Requirements Specification is not sufficiently detailed such that the software requirements can be implemented in design documents and verified. Normally, the supplier would implement corrective actions specific to the documents and software elements indicated in the finding. The SRS may be considered satisfactory once corrective action has been implemented, but if process improvements have not been implemented, this type of finding is likely to recur. The software engineering assessment can be used to assess the supplier's underlying software engineering processes. Negative answers to key assessment questions may indicate where improvements can be implemented. With respect to the software requirements analysis process, recommendations may be made to the supplier which can identify process improvements that enhance the supplier's software requirements analysis process (e.g. investment in software development tools and resources or major changes in standard organizational practices may be suggested). The following assessment questions may help to identify the underlying causes of a deficiency in the area of software requirements analysis.

"... Is a mechanism used for ensuring traceability between the software requirements and top-level design?

Is a mechanism used for ensuring traceability between the software top-level and detailed designs?

Does the software organization use a standardized and documented software development process on each project?

Is a mechanism used for periodically assessing the software engineering process and implementing indicated improvements?

Is a mechanism used for maintaining awareness of the state-of-the-art in software engineering technology?... (5)

Alternatively, the assessment could result in a recommendation to prepare an action plan which

addresses software engineering technology that could improve the organization's software processes. The action plan may identify one or more specific methods, techniques, and practices which can be implemented on a small scale project (e.g. Purchaser initiated enhancement to an existing system). Proper training with respect to the software process method, techniques, etc., as well as, software project management may be needed prior to project initiation. As the supplier gains experience with the software engineering techniques, further process improvements can be recommended, particularly as new software engineering techniques and practices gain general acceptance.

CONCLUSIONS

The industry standards that require suppliers to implement quality programs for the products and services they provide are being imposed, expanded, and improved upon by a growing number of organizations. Not only are quality requirements being tightened in many applications, but many organizations are insisting that their suppliers implement Quality Improvement Programs, Total Quality Management, and other such programs to improve their overall performance if the supplier is to continue to do business with the organization. In the same way the software supplier evaluation/ assessment methodology can be used to ensure compliance with specific software quality requirements as well as exhort suppliers to higher levels of productivity and quality through the implementation of process improvements.

Efforts to apply the evaluation/assessment methodology on suppliers of software have resulted in two major changes: 1) an increased awareness of software quality assurance requirements within an organization as well as in its software suppliers; 2) the recognition that software engineering concepts, practices, and techniques and the establishment of the discipline of software engineering can be important to successful software development and maintenance (cost effective, reliable software).

The increasingly complex problems to which complex software is applied requires a disciplined approach to its development and maintenance if we are to rely on the software to provide accurate results. Much software has been written which was created without the benefit of software engineering practices and techniques and without the benefit of a software quality assurance program/plan.

Through the 1980's a number of software suppliers, providing application software to the nuclear power, aerospace, and petrochemical industries, have been evaluated with respect to their software quality assurance capability. The results of the early evaluations showed, in some cases, significant deficiencies with respect to the implementation of specified software quality assurance requirements. The effect of the evaluations was the gradual improvement in the awareness, development, and implementation of software quality assurance in the suppliers' shop. The increasingly complex software being sought for sophisticated operations and applications has led industry to consider the capability of software suppliers to support a user's technical and quality requirements. The software engineering capability assessment methodology provides a means to

probe the supplier's software development and maintenance processes in order to make a determination as to their software engineering ability. The intent is to focus on those suppliers that demonstrate the use of modern software engineering practices and techniques including process improvements. One impediment, with respect to the application of these techniques, has been the resistance to these changes both within the user organization and in its suppliers. It is apparent that a substantial amount of inertia exists in industry toward technological change with respect to software development and maintenance. Technological change can mean a substantial financial investment in consultants, tools, and resources. And in many quarters software development and maintenance is still viewed as an esoteric art form understood by enigmatic practitioners.

The software supplier evaluation and assessment process should be quantified. A method is needed which indicates the effort needed to "upgrade" a supplier with respect to software quality assurance and software engineering capability. A method should be developed to consistently and objectively evaluate the SQAP/P of the software supplier (the SEI assessment methodology already specifies such a procedure); however, we have seen that such a process is very heavily dependent on the experience, training, and qualifications of personnel performing the evaluations.

With respect to software and software development the overall improvement in software reliability and software quality will not be achieved simply by tightened quality requirements. The state of software engineering technology is advancing such that new techniques and methodologies have been developed which can substantially improve software productivity and quality. However, it appears that software engineering technology is not being implemented with respect to the complex software problems industry is faced with in some critical applications. It is important that software engineering technological changes make their way into the software development and maintenance practices of the software supplier. The supplier's management and software practitioners (i.e. software engineers) should be working to improve their software development and maintenance processes, as their customers continue to monitor and assess their accomplishments.

REFERENCES

- 1) USDOT Federal Aviation Administration Standard, FAA-STD-018a, "Computer Software Quality Program Requirements", September 30, 1987
- 2) J.M. Juran, editor-in-chief, "Quality Control Handbook", 3rd ed. (McGraw-Hill), Chapter 10
- 3) L. M. Johnson, "Quality Assurance Program Evaluation", 1986
- 4) Institute of Electrical and Electronics Engineers - Technical Committee on Software Engineering, IEEE Std 1028 - 1988, "IEEE Standard for Software Reviews and Audits"
- 5) Carnegie Mellon University Software Engineering Institute Technical Report CMU/SEI-87-TR-23, "A Method for Assessing the Software Engineering Capability of Contractors", Sept. 1987
- 6) FAA-STD-018a "Computer Software Quality Program Requirements" section 3.1.12
- 7) IEEE - TCSE, ANSI/IEEE Std. 730.1 - 1989, "IEEE Standard for Software Quality Assurance Plans"

MECHANICAL PAINT REMOVAL TECHNIQUES FOR AIRCRAFT STRUCTURES

by

Joe P. Amro

and

Jorge E. Talia

Department of Mechanical Engineering

The Institute for Aviation Research

The Wichita State University

Wichita, KS 67208

For presentation to the AIAA/FAA Joint Symposium on General
Aviation Systems at the Port O-Call Inn, Ocean City, NJ
on April 11, 1990

MECHANICAL PAINT REMOVAL TECHNIQUES FOR AIRCRAFT STRUCTURES

Joe P. Amro
and
Jorge E. Talia
The Institute for Aviation Research
The Wichita State University

ABSTRACT

The principal objective of this research was to investigate paint removal by mechanical means, i.e., blasting, from aluminum structural aeronautical materials (2024-T3) and to examine the changes on the surface morphology introduced by the paint removal process. Three types of plastic particles were used in this research: Polyextra, Polyplus, and Type III. Scanning electron microscopy has shown that a potentially damaging surface morphology is formed on the surface of the structural material. Multiple microcracks or fissures generated by the stripping could reduce the life and/or change the engineering properties of the material. It was also found that aluminum material stripped using plastic media particles has a very rough surface that may affect the aerodynamic flow of an airplane. The number of microcracks and degree of surface roughness vary with the particle impact angle and velocity. To minimize or eliminate the damage done to the surface during the plastic particle stripping, it was necessary to change the blasting media to softer and smaller particles. Commercial wheat flour was selected for this purpose. With the substitution of these natural particles, the scanning electron microscopy observations of the stripped surface revealed no potential damage (microcracks or fissures) on the structural material, and the surface roughness was also reduced.

1. INTRODUCTION

The predominant industrial method currently used to remove paint from the surface of aircraft and other large vehicles is chemical stripping. The chemical removal of paint is not only costly, but also problematic, leaving large amounts of toxic chemical waste which is very expensive to dispose of without lasting and harmful effects on the environment. Furthermore, to minimize substrate damage caused by the application of chemical strippers [1], chemical removal of paint from aeronautical structures must be followed up by mechanical scraping and sanding in order to remove any remaining paint. This scraping and sanding always entails an important loss of material, thus altering the mechanical properties of the structures. In addition, the Environmental Protection Agency (EPA) is continually applying stricter regulations [2], a situation which makes the chemical removal of paint a less desirable option and increases the need for an alternative method which will not produce detrimental effects on the environment.

To remove paint from their aircraft, the U.S. Navy and Air Force, as well as various commercial companies, have recently adopted a new method: Plastic Media Blasting (PMB) technique. Northwest Airlines and Boeing Co. are also currently considering PMB as an alternative to the use of toxic chemicals in stripping paint from airframes.

The PMB technique, frequently called dry stripping, is a method in which light weight plastic particles are used in blasting in order to remove coatings [2]. The advantages of this method are: a) no hazardous waste is produced, b) the cost is drastically reduced in terms of both the materials and the time required for job completion [1], and c) the loss of material due to scraping and sanding can be eliminated. The use of PMB media thus provides an immediate solution to the ever increasing problems and hazards inherent in the use of chemical strippers [3].

The dry stripping method is, in effect, an erosion process. In this case, the intention is to erode only the paint. However, the process of removing the paint from the surface can also lead to undesired erosion or particle impact damage on the surface of the material. As the first step toward a general application of this new technology, it is necessary to investigate both the process of paint removal by blasting, and the subsequent effects of this process on the substrate morphology. Such a study is necessary because changes in the substrate morphology are capable of altering the mechanical properties of the base material, thus reducing the life expectancy of the aircraft.

Although some guidelines have been proposed for using PMB technology on aircraft skins, very little investigation has been performed to justify the proposed guidelines [2].

This study will provide preliminary information for the selection and development of an optimum paint removal process which is capable of introducing minimal damage to structural materials and which is in full accordance with FAA regulations.

1.1 Previous Work on Dry Stripping

Duhnkrak [1] has investigated the removal of surface coatings without damaging the substrate material on aluminum, titanium, magnesium, steel, and various composites. The plastic particles used were selected from three degrees of hardness: Polyextra, Polyplus, and Type III. The paint removal parameter depended on nozzle size with each media type, pressure, and blasting angle. For instance, aluminum skins with a thickness of 0.022 inches or more, covered with several coats of primer and paint, would require a 3.5 MOH media 20/40 mesh with a 1/2 in. nozzle operated under 25-30 psi at a distance of 24-30 in. using a blasting angle of 15-45 degree, depending on whether the objective is to remove a single layer of paint or to remove all layers at once. However, no details are given in respect to the substrate morphology, the material behavior after blasting, nor are any photomicrographs shown which illustrate the change in the surface morphology caused by the paint removal process.

Shields [4] has investigated the stripping process on T-34C aircrafts; specifically, he has investigated the effect of residual stresses, induced by the impacting media particles, on the fatigue life of the aluminum substrate. Shields reported that the particles remove paint by a combination of chipping and wear. His conclusion is that the fatigue life of stripped aluminum samples is lower than the life of unblasted material. Shields recommended the use of softer particles such as polyextra (MOH 3.0) to minimize the damage to the substrate, but no additional evaluation was given regarding this type of particle.

1.2 Scope of This Research

The scope of this research is the investigation of the effects of dry stripping on the surface morphology of aluminum alloys 2024-T3. Present work is directed toward the detection of surface damage produced by a variety of impact conditions and hardness of the solid particles. Therefore, the experimental procedure and tests were designed to study the substrate morphology after blasting. This was accomplished using a scanning electron microscope and profilometer to measure the roughness of the blasted surface. The principal stripping parameters were: type of particle, incident (impact) angle, abrasive particle size, particle velocity, and the amount of particle needed to remove paint per unit area.

2. EXPERIMENTAL PROCEDURE

Particle media blasting involves a variety of variables including impingement angle, flow rate, pressure, nozzle distance, and particle type. Typical kinds of skin material damage related to PMB are surface roughness, skin warping or distortion, and reduction of fatigue life. The possible blasting parameters which can be varied are related to the type of equipment in use, type of plastic media, and substrate materials.

The abrasive particles used for blast testing were polyextra of media grade 40/60 with grit-size of .016-.009 from U.S. technology and commercial wheat flour. The blast technique is described in detail elsewhere, along with the velocity calibration technique used [5,6]. The blast tests were made using impact angles of 15, 30, 45, 60, 75, and 90 degrees. Particles impacted the surface of the aluminum samples at velocities of 50 m/s through 109 m/s. The surface morphology introduced by each set of conditions was studied using a scanning electron microscope (SEM).

A painted sheet metal of Aluminum clad 2024-T3 with a thickness of .813 mm was obtained from Boeing Military Airplane Company. First, the sheet was cut into small samples of 50 x 100 mm. The sample was mounted on a plate holder capable of changing the particle impingement angle. Second, part of the sample was cut into smaller samples of 7 mm. by 7 mm., allowing the samples to fit on the stub holder of the scanning electron microscope. The blasted area was thus examined at high magnifications for changes on the surface morphology, including investigations such as roughness measurement and optical microscope.

The abrasive plastic particles used for paint removal of aircraft skin were purchased from U.S. Technology. The plastic media were: Polyextra 3.0 MOH hardness, Polyplus 3.5 MOH hardness, and Type III 4.0 MOH hardness with grit-size of .016-plastic media, commercial wheat flour was used as erodent particles. The selection of this natural blasting media was based on environmental concerns and on the similar but lower hardness with respect to the PMB particles.

An air-blast-type system was used for this research, Figure 1 is a schematic of the design. The flight tube of the apparatus is about 2 meters of Tygon plastic tubing, which terminates onto a 25 cm length of high density alumina tube of 3.2 mm internal diameter that acts as a nozzle. Particle feed rate measured in g/s, and the number of particles per unit time are allowed to impact the specimen. In this experiment, the particle feed rate was about .083 g/s. This parameter greatly affects the blasting rate. The selection of this feed rate was based on previous work by Hovis [5].

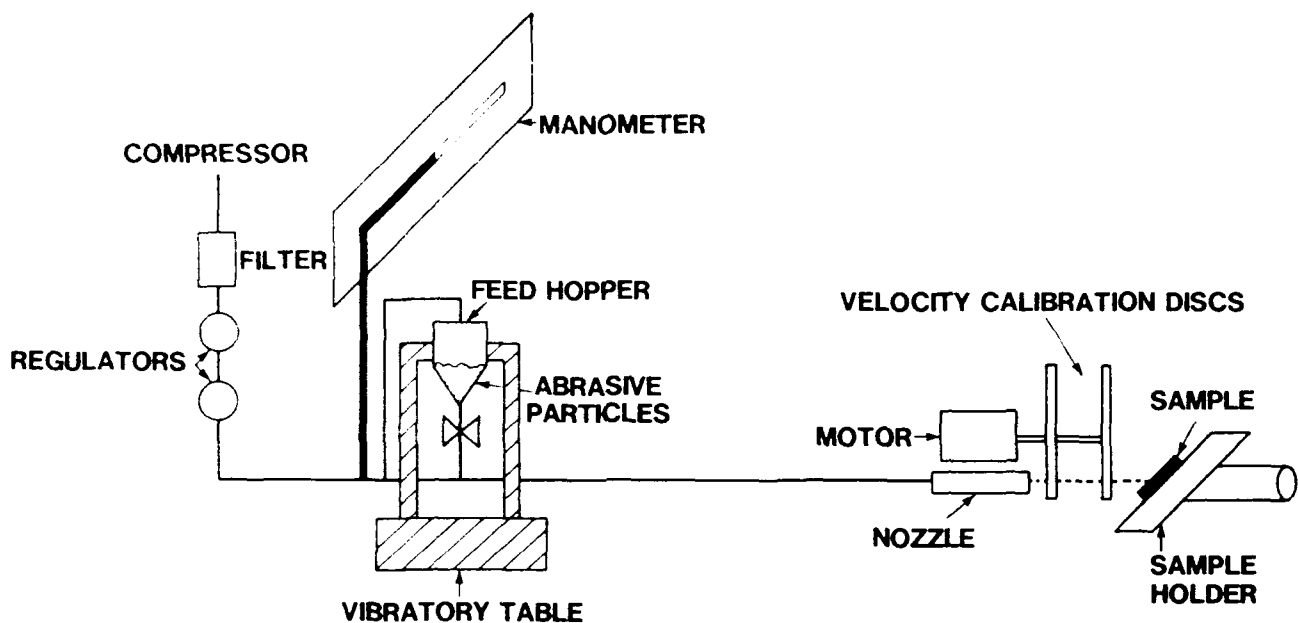


Figure 1 Schematic of the air blast-type system.

The angle of impact between the abrasive particle beam and the sample can be varied from 7-173 degrees. The sample holder allows the incident angle between the abrasive particle beam and sample to be accurately set. It also allows each sample to be centered in the beam so that samples removed for observation can then be reinstalled to the same position for continuation of the test.

The surface roughness of the blasted specimen was measured by a profilometer "Bendix Type MA Tracer." The roughness of the surface was expressed by the arithmetic average values in micrometers.

The Scanning Electron Microscope was used to examine changes on the surface morphology of aluminum samples which had been through the blasting process. SEM was also used to observe the stripped surface in order to determine what damage had formed on the surface as a result of the stripping process. The magnification selector value was 2.02 E3 magnification. All of the micrographs were taken using several samples blasted at different particle angles of incidence, particle velocities, and as further described in the description of the experimental parameters.

3. EXPERIMENTAL RESULTS AND DISCUSSION

The general purpose of this investigation was to examine the surface morphology of Aluminum clad 2024-T3 after the material had been stripped of paint by blasted particles, and to determine what changes, if any, had been introduced. The following particle media were employed in the paint-removal process: 1) U.S. technology 3.0 MOH particles of grade 40/60 with grit sizes of .016-.009, and 2) commercial wheat flour.

3.1 Exploratory Experiments

Before the principal experimental work began, exploratory experiments were performed, they showed that the use of 3.5 and 4.0 MOH particles increases the paint stripping rate. However, the appearance of the surface blasted by 3.0 MOH particles was smoother than the surface blasted by 3.5 MOH and 4.0 MOH media of the same size. The exploratory experiments also showed that the roughness of the surface texture varies, depending upon both the impact angle and a combination of parameters such as pressure inlet, nozzle size, hardness of the particle and media used.

Experiments on this paint removal process were carried out using 3.0 MOH media polyextra 40-60 with grit size 317.5 microns, as well as natural media such as commercial wheat flour. Furthermore, flour blasting yielded a significantly smoother surface morphology than that of a surface blasted by 3.0 MOH media. All of these exploratory tests were performed on aluminum material 2024-T3 with a thickness of .813 mm. This material is used as an exterior aircraft skin by Boeing Commercial Airplane Company.

3.2 Plastic Media Blasting (PMB)

Figure 2 shows surface roughness versus angle of impingement, at particle velocities ranging from 50 m/s to 91 m/s. The figure shows that substrate roughness increases with increasing angle of impact and in the velocity of the particle. The figure also shows that the roughness versus angle of impingement curves of all particle velocities are almost parallel. It is also shown that for a fixed velocity, the roughness at a 90 degree impact is more than twice the roughness at a 15-degree impact. Substrate roughness is seen to increase with increases in particle velocity at all angles of impact. It may also be noted that, for a fixed angle of impact of 15 degrees, the surface roughness at a velocity of 50 m/s is eight times less than that of a 90 degree impact in which the velocity is 50 m/s. Therefore, in order to obtain a smoother surface, both the angle of impact and the particle velocity must be reduced.

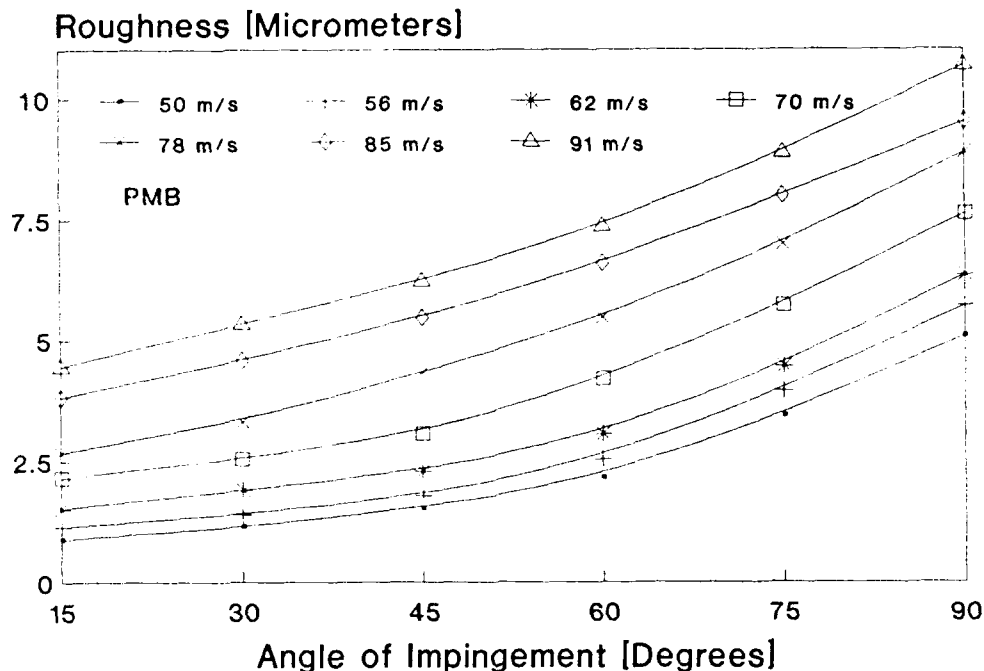


Figure 2 Surface roughness versus angle of impingement at particle velocities ranging from 50 to 91 m/s, using PMB media.

It was observed by the SEM that the use of PMB particles can change the surface morphology of the stripped substrate material. Figure 3 shows photomicrographs of aluminum material which has been stripped by erodent PMB particles at impact angles of 15 and 90 degrees, at a particle velocity of 78 m/s. These micrographs show that the surface damage is severe at all impact angles. Relatively large fissures, or surface microcracks, are shown in Figure 3 (a and b). Folding of material appears to increase at high angles of impact. A comparison of Figures 3 (a) and 3 (b) shows that the size of the cracks generated on the surface decrease as the impact angle decreases. In addition, the effect of velocity on the surface morphology is shown in Figure 4. These samples were stripped using 45 degree impact angles at velocities of 56 m/s and 85 m/s. A comparison of Figures 4 (a) and 4 (b) shows that as the velocity of the particle increases, the size of the cracks on the surface also increase, and great damage is introduced in conjunction with both impact angle and velocity.

Figure 5 presents the amount of erodent material needed to remove paint per unit area as a function of the angle of impingement, at velocities of 50 m/s, 56 m/s, 62 m/s, 78 m/s, 85 m/s, and 91 m/s, using PMB media particles as the erodent material. The figure shows that, at a fixed impact angle, the



(a)



(b)

Figure 3 SEM micrographs of surface morphology introduced by the paint removal process impacted with PMB particles traveling at a velocity of 78 m/s, at angles of impingement of (a) 15 degrees and (b) 90 degrees.



(a)



(b)

Figure 4 Micrographs of eroded surface impacted with PMB particles at an angle of impingement of 45 degrees, traveling at velocities of (a) 56 m/s and (b) 85 m/s.

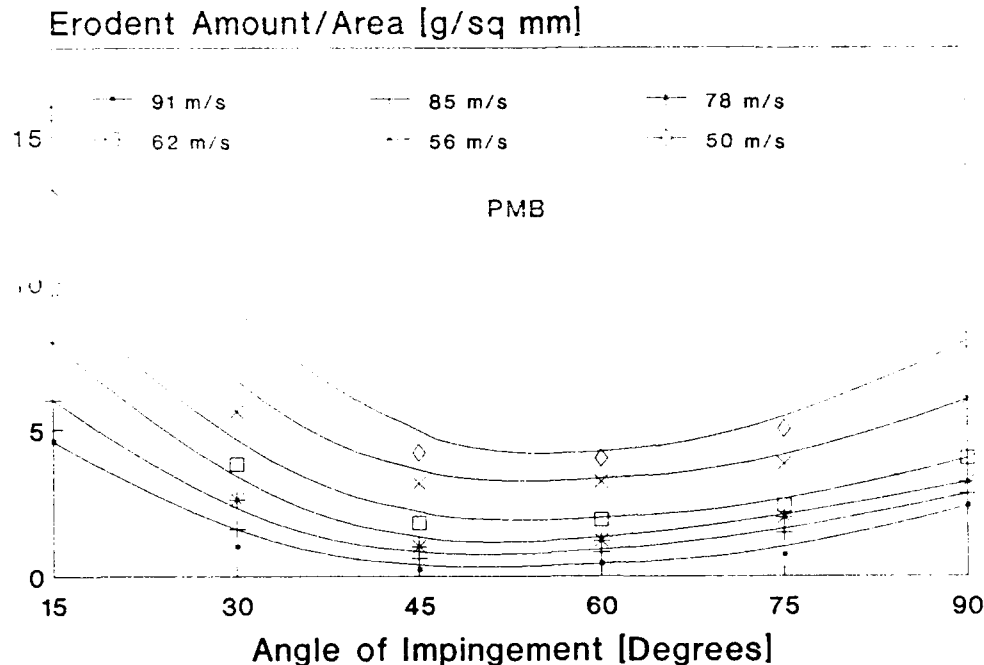


Figure 5 Erodent amount needed to remove paint per unit area versus angle of impact, at velocities ranging from 50 to 91 m/s, using PMB media.

amount of particles needed to remove paint decreases as the particle velocity increases. It is further shown that at a fixed velocity, the amount of particles needed to remove paint depends upon the impact angle. The figures also show that the smallest amount needed is at a 45 degree impact angle and that the maximum amount needed is at a 15 degree impact angle. These results demonstrate that particle velocity is not the only parameter which controls the paint removal capability of an erodent material.

3.3 Commercial Wheat Flour blasting

Figure 6 shows surface roughness versus angle of impingement, at particle velocities of 64 m/s, 75 m/s, 95 m/s, 102 m/s, and 109 m/s. The figure shows that the aluminum substrate roughness increases with an increased impact angle. It was demonstrated that the surface roughness versus angle of impingement curves are almost parallel for all particle velocities. It is also shown that for a fixed velocity the roughness at a 90 degree impact angle is one and one-half times larger than at a 15 degree impact angle. The principle conclusion of these results is that it is possible to obtain a smoother eroded surface by using a low impact angle.

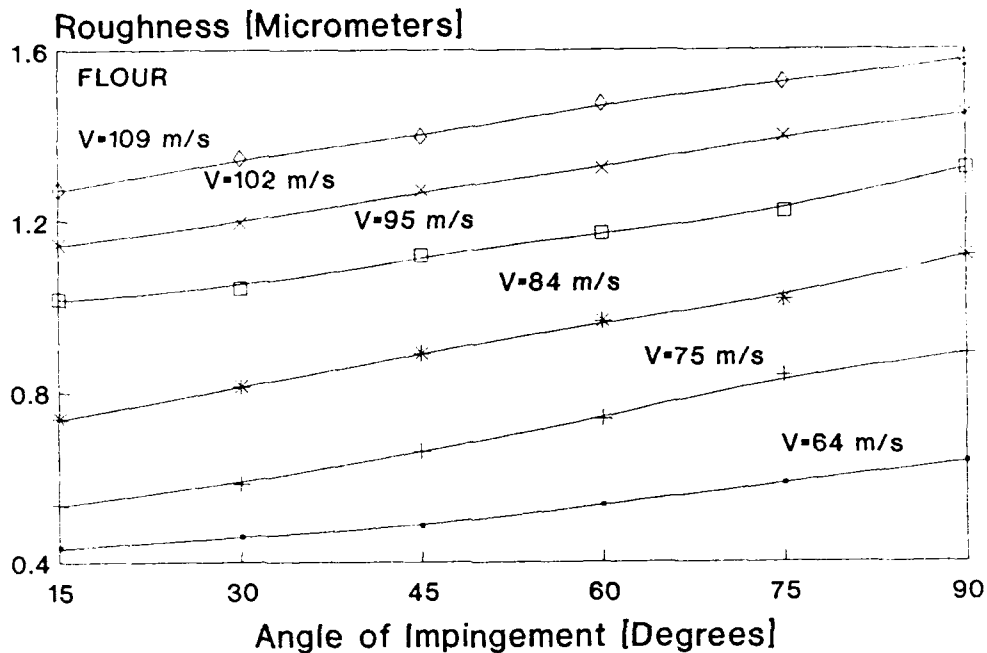
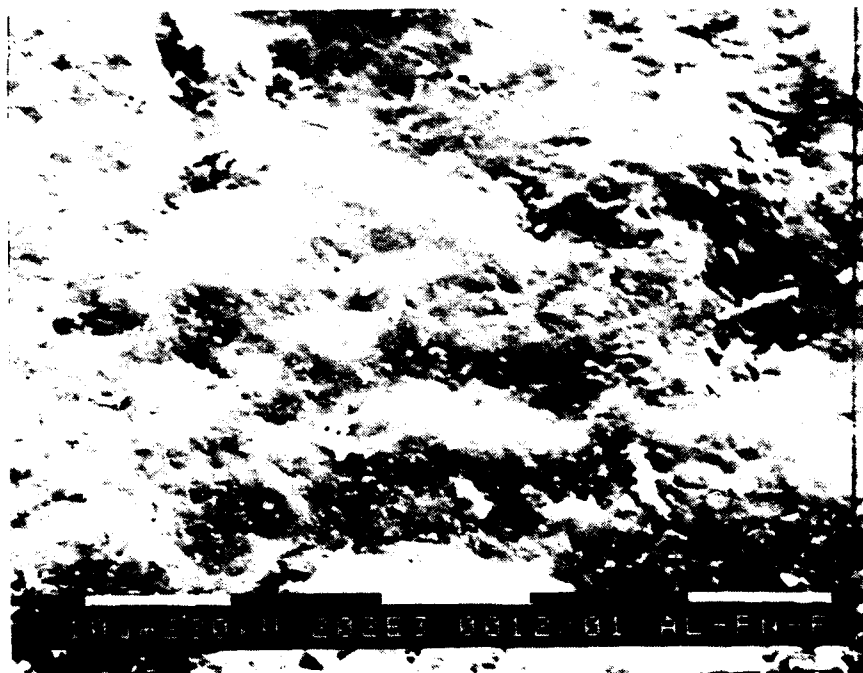


Figure 6 Surface roughness versus angle of impact, with particles traveling at velocities ranging from 64 to 109 m/s, using flour media.

The surface morphology of the stripped sample was studied by SEM with the purpose of investigating changes in the stripped substrate material. Figure 7 shows the photomicrographs of the aluminum material after it has been stripped using commercial wheat flour erodent particles at impact angles of 15 and 90 degrees, at a particle velocity of 84 m/s. It is shown in the micrographs that the surface damage is minor at low impact angles. It may be noted that some flour particles remain on the surfaces blasted at high impact angles; however, no flour particles are seen on the surfaces blasted at low impact angles. This difference may be related to the softness of the underlying material. The effect of flour particle velocity on the surface morphology of the stripped sample is also shown in Figure 8. The samples were stripped at 60 degree impact angles, at velocities of 64 m/s and 109 m/s. Essentially, the damage introduced by the wheat flour particles is small in comparison to the damage introduced by the PMB media particles. However, it is important to note that the least damage to the surface morphology is found at an impact angle of 60 degrees, and at a velocity of 84 m/s; this is well demonstrated in Figure 7. Furthermore, the figure shows that damage to the surface of the substrate increases as the particle velocity increases. This might be related to the increase in particle velocity.

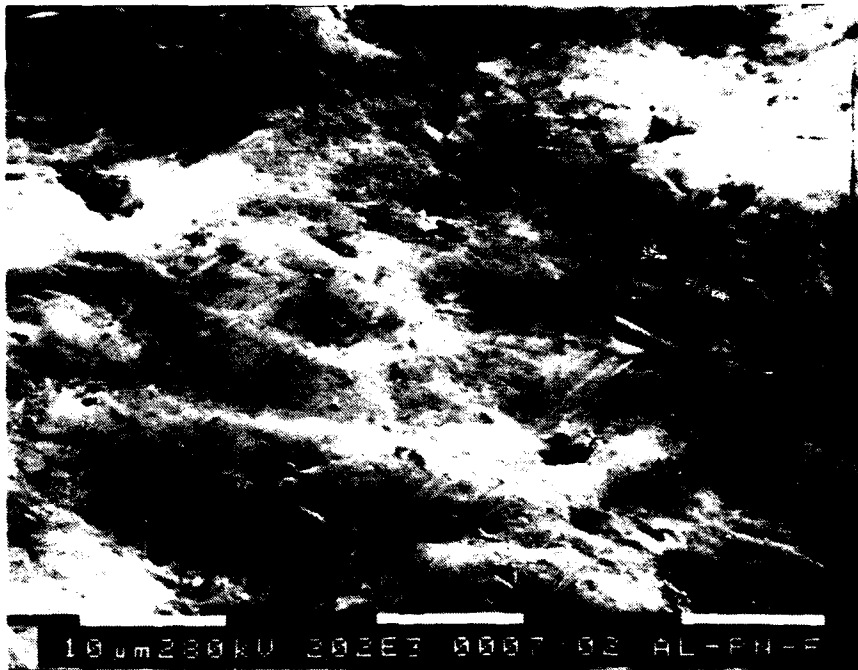


(a)

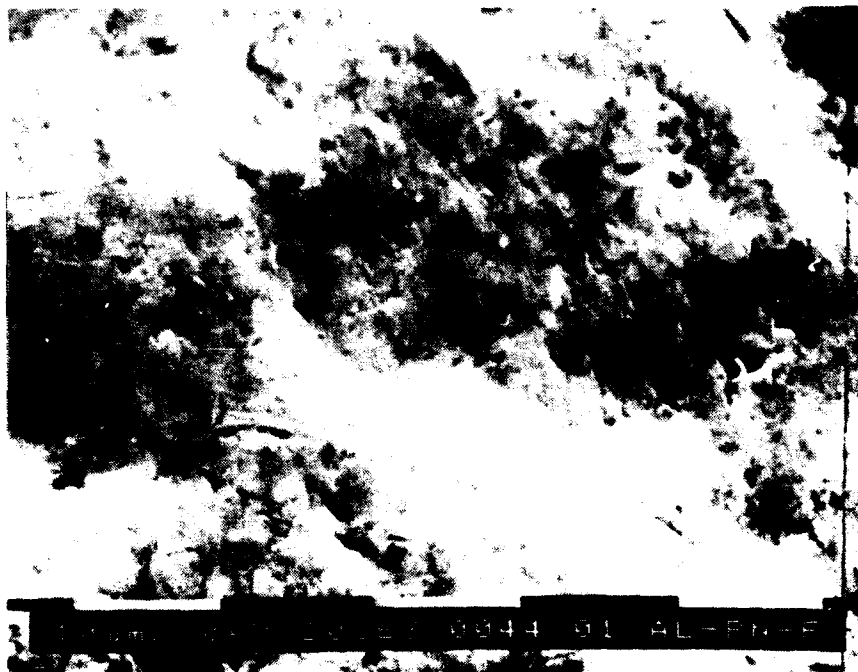


(b)

Figure 7 SEM micrographs of eroded surface impacted with flour media particles, traveling at a velocity of 84 m/s, at angles of impingement of (a) 15 degrees and (b) 90 degrees.



(a)



(b)

Figure 8 Micrographs of surface morphology introduced by the paint removal process, impacted with flour media particles traveling at velocities of (a) 64 m/s and (b) 109 m/s, at an angle of impingement of 60 degrees.

Figure 9 presents the amount of erodent material needed to remove paint per unit area versus the angle of impingement, at impact angles of 15, 30, 45, 60, 75, and 90 degrees, and at velocities ranging from 64 to 109 m/s. It can be seen that, at a fixed velocity, the amount of particles needed to remove paint depends upon the impact angle. As the figure shows, the smallest amount of particles needed to remove paint per unit area at a 60 degree impact angle and the maximum amount needed is at a 15 degree impact angle. These results show, again, that particle velocity is not the only parameter which controls the paint removal capability of an erodent material. It is shown that at a fixed velocity the amount of particles needed to remove paint per unit area decreases as the impact angle increases. Thus, it can be concluded that the smallest amount of erodent material needed to remove paint per unit area is at a 60 degree impact angle, and that the maximum amount required is at a 15 degree impact angle.

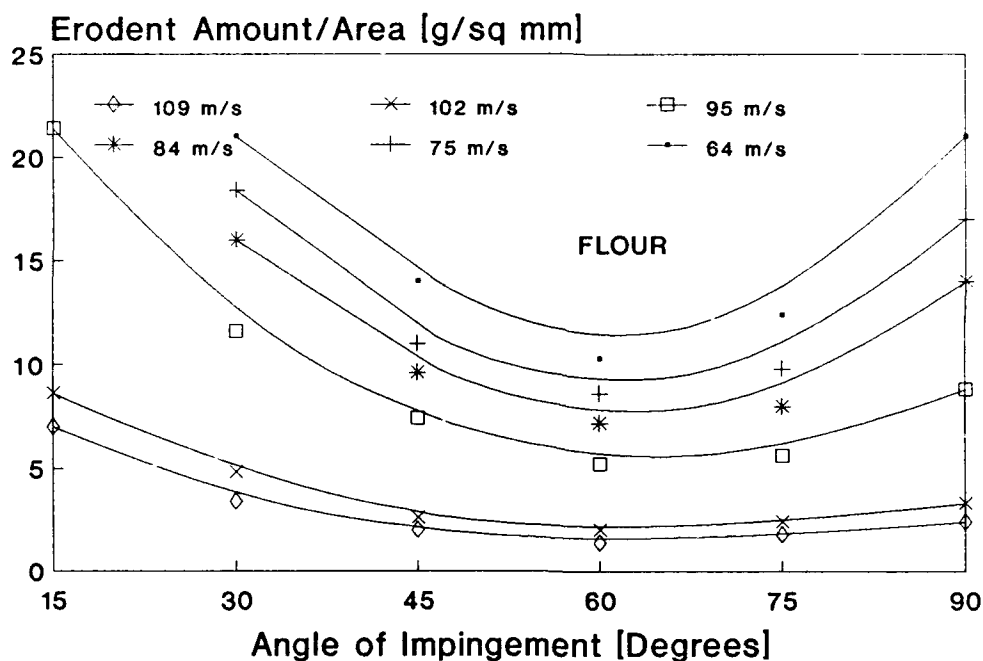


Figure 9 Erodent amount needed to remove paint per unit area versus angle of impact, at velocities ranging from 64 to 109 m/s, using flour media.

4. SUMMARY AND CONCLUSION

The tests showed that blasting the aluminum material with 3.0 MOH plastic media changes the surface morphology, leaving the material distorted and with fissures, or microcracks, all of

which may significantly affect fatigue properties (i.e., number of cycles to fracture). Such changes could reduce the life and/or alter other engineering properties of the material. It was also found that higher blasting particle velocities resulted in higher stripping rates. Observation of surfaces blasted with commercial wheat flour revealed no damage to the structural material. The principal conclusion reached was that while blasting commercial wheat flour at high pressure caused considerably more dust when compared to U.S. media , there was much less damage to the substrate surface of the aluminum material, and the fatigue life of the structural material should be increased in comparison to Al alloy which had been blasted by PMB media.

4.1 Future work

There is ample evidence that the mechanical properties and deformational behavior of metals can be influenced by altering the state of the surface; however, relatively little information is available on how dry stripping affects the fatigue properties of the alloys which are used in the aerospace industry.

With the growing application of the American Damage Tolerance Specifications in design requirements, there is more concern for dangers that arise from manufacturing defects at critical fatigue points. The results obtained from this experimental work, and from work done by others, show that blasting with plastic media causes a very rough surface with fissures or microcracks capable of reducing the fatigue life of the structural material. Therefore, it is important to study the fatigue life of blasted material. The following tests should be applied:

1. Perform the blasting process on test samples of different Al alloys (2024-T3 bare, 7075-T6 clad and bare).
2. Perform fatigue tests under both tension-tension and tension-compression in order to determine fatigue parameters of the above samples.
3. Use X-RAY and Almen strip techniques to provide a means of measuring the amount of compressive stress generated onto the surface.
4. Perform optimization of particle velocities, angle of impact, particle size, and particles hardness.

5. REFERENCES

1. George B. Duhnkrack, Journal of Aviation Week and Space Technology, " Pollution Engineering," DECEMBER, (1987).
2. John E. Heaney, Journal Aviation Week and Space Technology, " Plastic particles peel paint without pollution, " JANUARY, (1987).
3. George B. Duhnkarck. Journal Of Aviation Week and Space Technology, " Application of use dry stripping media," MAY, (1987).
4. S. Shield, Fatigue Tests of PMB Stripped Thin Al Panels, Naval Air Logistics Center, Maryland, JANUARY, (1988).
5. S.K. Hovis, Master Thesis, North Carolina State university, (1985).
6. S.K. Hovis, K. Anand, H. Conrad, R.O. Scattergood, Wear, 101, 69, (1985).

**SURFACE CONDITION EFFECT ON THE FATIGUE BEHAVIOR
OF ALUMINUM LITHIUM ALLOYS**

by

Ali Eftekhari

and

Jorge E. Talia

Department of Mechanical Engineering

The Institute for Aviation Research

The Wichita State University

Wichita, KS 67208

For presentation to the AIAA/FAA Joint Symposium on General
Aviation Systems at the Port O-Call Inn, Ocean City, NJ
on April 11, 1990

**SURFACE CONDITION EFFECT ON THE FATIGUE BEHAVIOR
OF ALUMINUM LITHIUM ALLOYS**

Ali Eftekhari
and
Jorge E. Talia
The Institute for Aviation Research
The Wichita State University

ABSTRACT

Production of Al-Li 2090-T3 alloy by powder metallurgy results in a material with a surface that contains micro and macro defects. In addition, scratches could be introduced to this surface during assembling and/or processing with a drastic decrease in fatigue strength. The effects of scratch are so severe that a smooth sample with a scratch of 200 μm will have a fatigue life as a notched sample with $K_t = 3$, a reduction in fatigue life of about three orders of magnitude. In order to recover this loss, shot peening, polishing, anodizing and some of the combined effects of these techniques have been studied. Depending on the applied stress, the fatigue strength of scratched samples, up to a certain depth, can be partially recovered and some of these treatments have accumulative results on improving the fatigue life. The results are discussed in relation to the potential effects of defects on the nucleation of microcracks and their propagation.

1. INTRODUCTION

Al-Li alloys have recently gathered strong attention in the aircraft industry. Their relatively low density and high stiffness significantly contributes to weight savings which could reduce fuel costs and also increases performance. Compared to conventional high strength aluminum alloys, such as the ones in the 2xxx or 7xxx series, Al-Li alloys offer 10 % increase stiffness along with 10 % decrease in density. However, Al-Li alloys have also shown commercially unacceptable ductility and fracture toughness values [1]. The high elastic modulus and high yield stress, as well as the low fracture toughness, are a consequence of the meta-stable ordered and coherent phase (Al_3Li), which precipitated in aluminum alloys with sufficient lithium [2-4]. This coherent phase causes a strong planarity of slip which introduces high local stress at the grain boundaries and sharp slip lines at the free surface, reducing the life and ductility of the Al-Li alloys.

Knowledge of the influence of scratches on the mechanical properties of metals is becoming more and more important in recent years because of the many engineering applications involving the use of sharp instruments in fabrications. Inchekel and Talia [5] and Toriyama et al. [6] have demonstrated that scratched specimens of aluminum-lithium alloys have lower fatigue strength than unscratched specimens. Scratches on samples of Al-Li alloy, (2090 - T3 and F) reduce considerably their fatigue life if subjected to tensile-tensile cyclic loading. As the depth of the scratches increases, the number of cycles to fracture decreases significantly.

1.1 PURPOSE

The intention of this study is to find a suitable technique capable of reducing the detrimental effects of scratches on fatigue strength and/or life of the Al-Li alloys.

The selected techniques for this purpose were: shot peening, anodizing, and chemical polishing. Several investigators [7,8] report that application of shot peening has improved the fatigue strength. Bannantine et al. [9] and Hertzberg [10], all emphasize that shot peening is most beneficial at the presence of stress concentrations and/or stress gradient. Results of the study by Talia and Mazumdar [11] illustrates that anodizing has influence on fatigue strength. The results obtained clearly indicates that the life decreases initially with film thickness and further increase of the film thickness improves the fatigue strength. To demonstrate the influence of surface on fatigue strength, Raymond and Coffin [12] show that the removal of surface layer at frequent intervals during the fatigue test improves the overall fatigue life. Mann [13] showed, for aluminum alloys, that coarse grinding reduces the fatigue strength by 10-20 %. Oberg et al. [14] displays that electropolished 4.5 % Cu-

Al alloy specimens have a lower fatigue limit than mechanically polished specimens. To understand the effect of polishing, Cina [15] used the X-ray diffraction and stress-relieving experiments to reveal that the low fatigue life of the electropolished specimens is due to the removal of a cold worked surface layer by polishing.

2. EXPERIMENTAL PROCEDURE

Al-Li (2090-T3) alloy in sheet form produced by the Kaiser Aluminum Co. were used in this work. The Al-Li fatigue test specimens were shaped by machining. The specimens were unnotched and notched with a stress concentration factor of 3, ($K_t = 3$). After machining, scratches were generated onto the surfaces of both specimens. The scratch run the full width of the specimen at midway of the gage length. Figure 1 shows the scheme of the specimens used in this study.

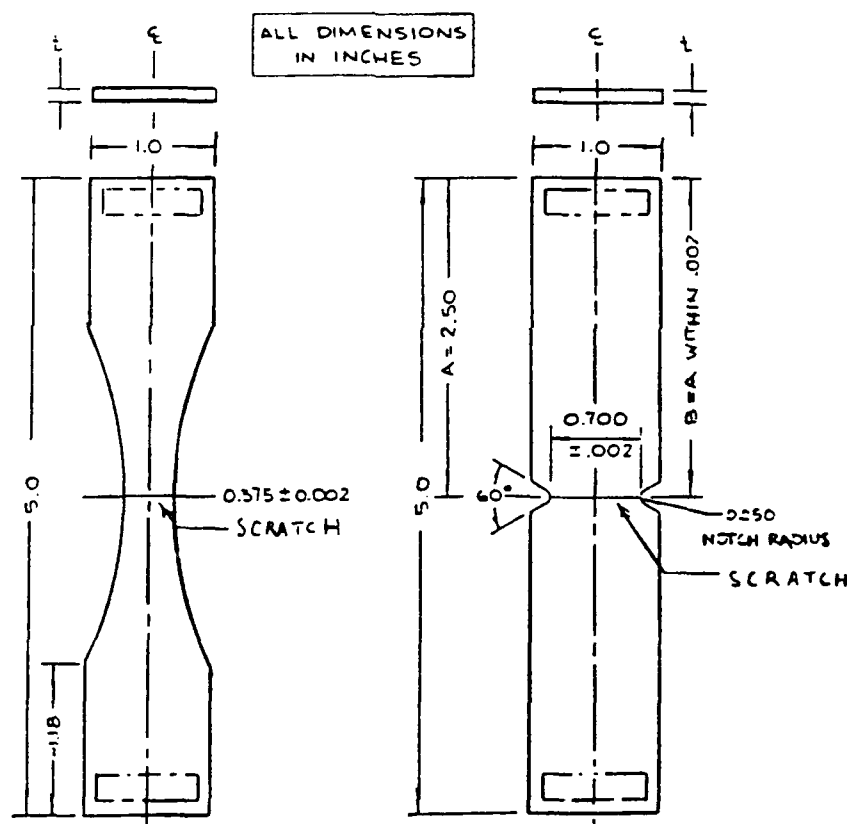


Figure 1. Fatigue-stress endurance (S-N) test specimens.

The scratches were generated by using special made tools having angles of 90 degrees. The tools were mounted in an end mill machine to control the formation of the scratch. For this purpose, a specially designed device holds the specimens at the desired angle to have a symmetric cross section of the scratch.

The scratches were characterized by three parameters, depth (d), their angle (α), and the scratch tip radius. The scratch parameters were determined through the use of an optical microscope. Figure 2 illustrates cross-section of a 90° degree ($\alpha = 90^\circ$) scratch with a depth of about 125 micrometers ($d = 125 \mu\text{m}$). Scanning electron micrograph of the scratch surface of the sample is shown in Figure 3. A careful examination of the surface morphology of the scratch shows that it is rough and chunks of the material have been removed giving evidence that microcracks may have been developed. In addition, the scratch acts as a stress raiser and probably becomes the preferred sites for propagation and/or initiation of microcracks.

50 μm



Figure 2. Cross section of a scratch showing the radius of curvature and an Angle of 90° of the Scratch.

For this study shot peening was performed at Metal Improvement Company. Both faces of the samples were shot peened to the following specifications:

- a) Both sides kept flat
- b) To smooth and flatten any sharp points, micro flaws, and fissures on the surface due to scratches.
- c) To enter into the scratches and possibly blunt the sharpness at the scratch tip.



Figure 3. SEM micrograph of the scratch illustrating irregularities of the scratch surface.

Anodizing was conducted only on notched samples that were freshly scratched $d = 150 \mu\text{m}$. These scratched samples were then anodically oxidized in 1% by volume of concentrated sulfuric acid under a current density of 110 Amp/m^2 for 3 minutes. This resulted in a coating of approximately 1200 nm.

Both unnotched and notched scratched specimens were chemically polished in a solution (80 % phosphoric acid, 5 % nitric acid, 5 % acetic acid, and 10 % water, by volume) and heated to 105°C for five minutes to remove the layer of material that may contain surface defects.

Figures 4 to 7 present scanning electron microscope (SEM) micrograph at 600 magnification of the surface morphology for: as-received, shot peened, anodized, and polished samples.

Finally, the fatigue testing is carried out at room temperature according to ASTM standard using a servohydraulic MTS testing machine. The cyclic loading used was tension-tension, $R = 0.1$ and frequency of 10 Hz. stresses are nominal (Load per minimum cross sectional area). Six tests were carried out for each value plotted. Such a procedure was adopted to reduce the normal scattering associated with the fatigue test. The average of the six tests was taken and the variation given by the standard deviation, in number of cycles, was about ± 10 to 12 % of the mean value.



Figure 4. SEM micrograph of the surface of as-received specimen at 600 magnification.

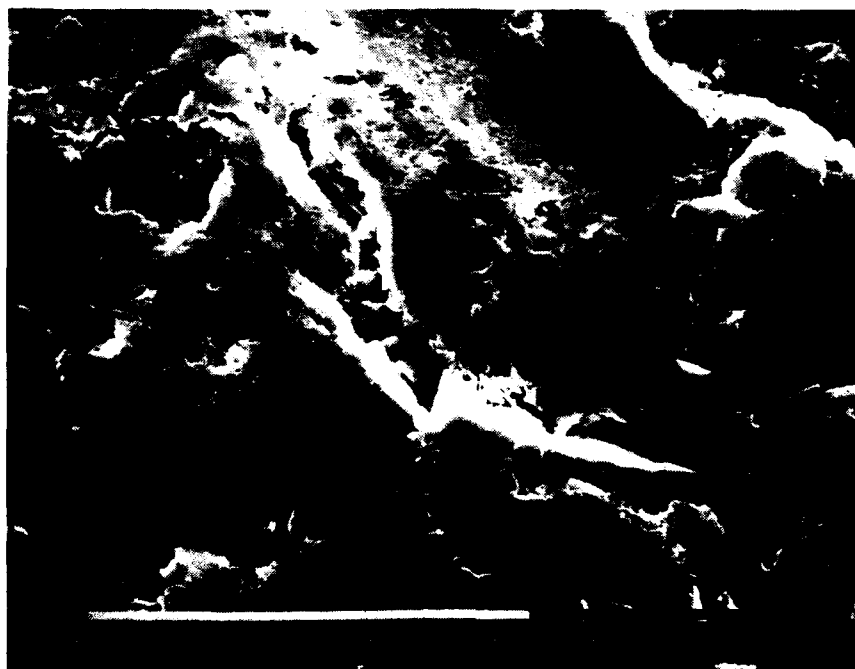


Figure 5. Shot peened surface at 600 magnification.

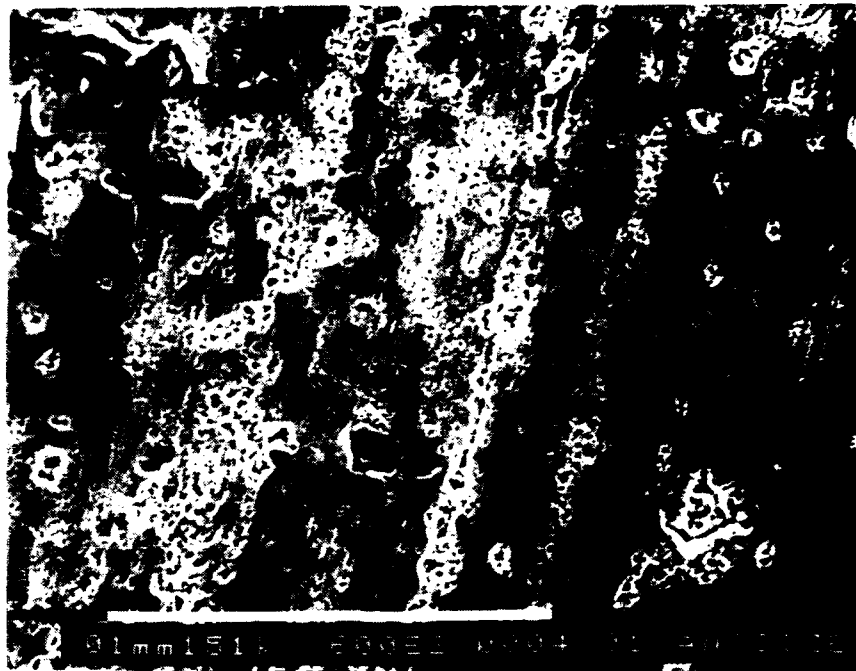


Figure 6. Surface micrograph of an anodized specimen at 600 magnification.

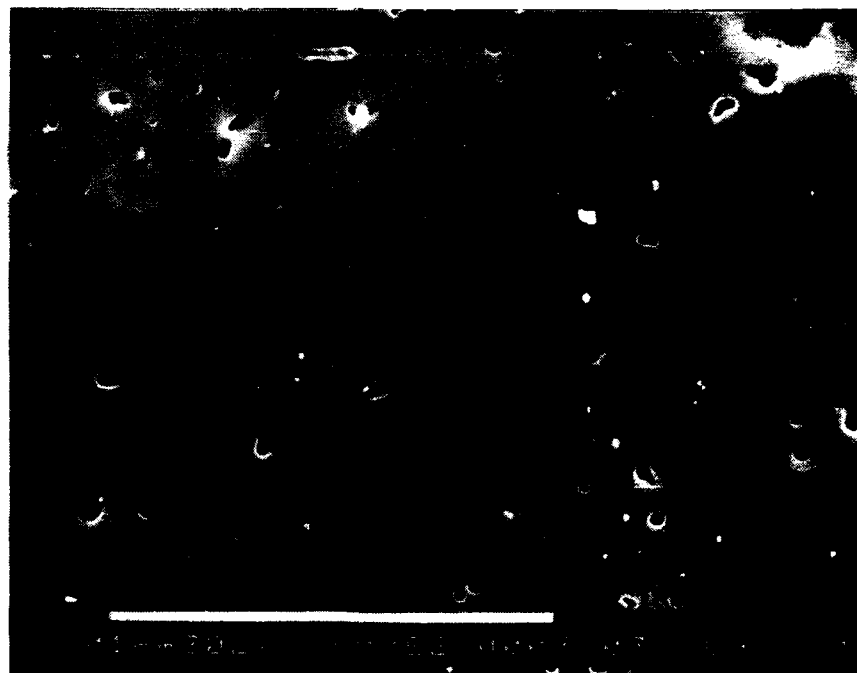


Figure 7. SEM micrograph of the surface of a chemically polished sample at 600 magnification.

3. RESULTS AND DISCUSSION

The effect of the scratch depth on the fatigue life of both unnotched and notched specimens is presented in Figure 8. For both curves fatigue life decreases as scratch depth increases, but the unnotched sample curve decreases more drastically and has a steeper slope for $d < 50 \mu\text{m}$. For the unnotched samples with a scratch depth near $200 \mu\text{m}$, results in fatigue life reduction of 3 orders of magnitude, but for samples with similar scratch depth, the reduction of the fatigue life of a notched sample is only 1 order of magnitude.

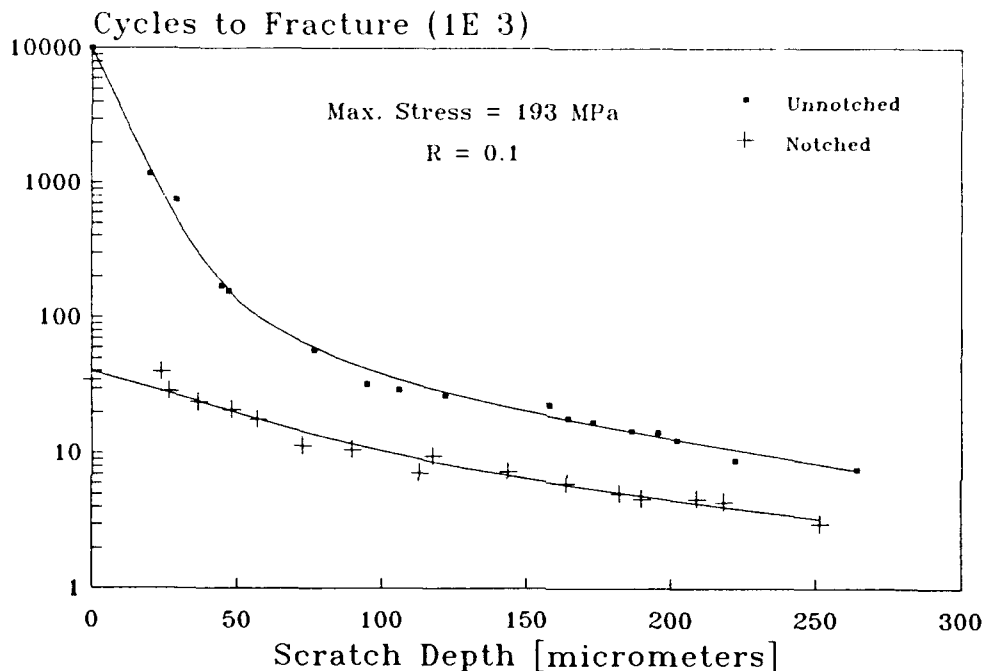


Figure 8. Number of cycles to failure vs. scratch depth for both unnotched and notched specimens.

As displayed earlier in Figures 2 and 3, scratches have a sharp tip and removal of the material is not uniform, resulting in a surface with some areas of sharp cuts. To investigate the effects of the scratch on the fatigue life, the scratch surface morphology was periodically observed during cyclic testing. The same specimen corresponding to Figure 3 ($N = 0$, where N is number of cycles) was fatigue tested for 10,000 cycles. Figure 9 presents a magnified portion of the scratch of Figure 3 after 10,000 cycles. The initial SEM investigation of the scratch did not indicate any important differences within the scratch or anywhere else. Additional cyclic testing of the specimen continued for another 25,000 cycles. Figure 10 shows the same area as in Figure 9 corresponding to $N = 35,000$, some

microcracks have just nucleated and some have already initiated. The observation of the microcracks formation suggested that scratches are sites for microcrack initiation and/or propagation. They may coalesce to form a macrocrack capable of reducing the fatigue life of the sample.



Figure 9. SEM micrograph of scratch surface after 10,000 cycles, 1300 magnification

Surface morphology of a shot peened specimen was studied by SEM with the purpose of investigating changes on the shot peened surface. SEM micrograph in Figure 5, corresponding to shot peened surface, was compared to the micrograph of as-received surface in Figure 4. It is possible to observe in Figure 4 the sample surface prior to shot peening contained several defects (fissures), but after shot peening is performed, the surface roughness has been increased and also most of the surface fissures have been enlarged (compare Figures 4 and 5).

This observation suggested a need to generate stress versus number of cycles to failure (S-N) diagrams, for both unnotched and notched specimens, to determine the effect of shot peening on fatigue strength of the as-received specimens in absence of any scratches. Therefore, in Figures 11 and 12 the S-N diagrams of unnotched and notched samples were examined to determine the effects of shot peening on the as-received surface in the absence of any scratches.

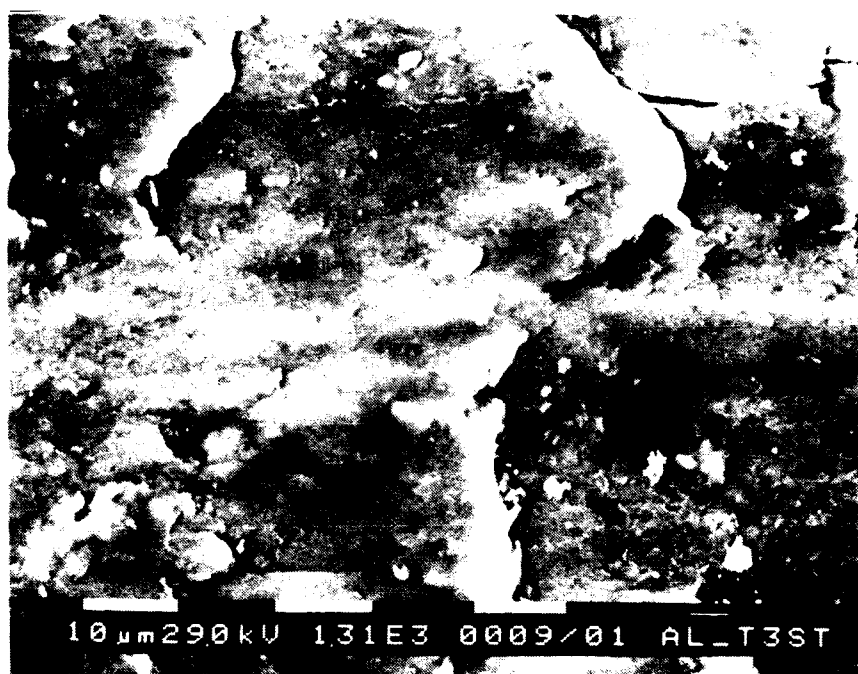


Figure 10. Morphology of the scratch surface after 35,000 cycles, 1300 magnification

Figure 11 presents the S-N diagrams of shot peened and as-received (unnotched) samples. The curve representing the shot peened samples is systematically lower than the one representing the as-received material, but as stress decreases the two curves approach each other. This trend indicates that for stresses below 207 MPa (30 ksi) the shot peened and as-received samples have similar life. Figure 12 shows a S-N diagram of the notched sample. In this figure shot peening is demonstrated to be beneficial only at stresses below 124 MPa (18 ksi). However, for larger stresses shot peening produces a detrimental effect. Both Figures are in good agreement with references 9 and 10.

Figure 13 illustrates the relationship between the scratch depth (d) and the number of cycles to fracture (N_f) for unnotched specimens, tested at $\sigma = 193$ MPa (28 ksi) which is at the lower end of figure 11, when scratches are present. As was expected, shot peening reduces the detrimental effect of the scratches, and it is more beneficial when $d < 50 \mu\text{m}$. It should be noted, however, that full recovery was not possible to achieve, and as scratch depth increases, shot peening becomes less beneficial. Furthermore, for $d > 150 \mu\text{m}$ shot peening enhances the detrimental effect of the scratches.

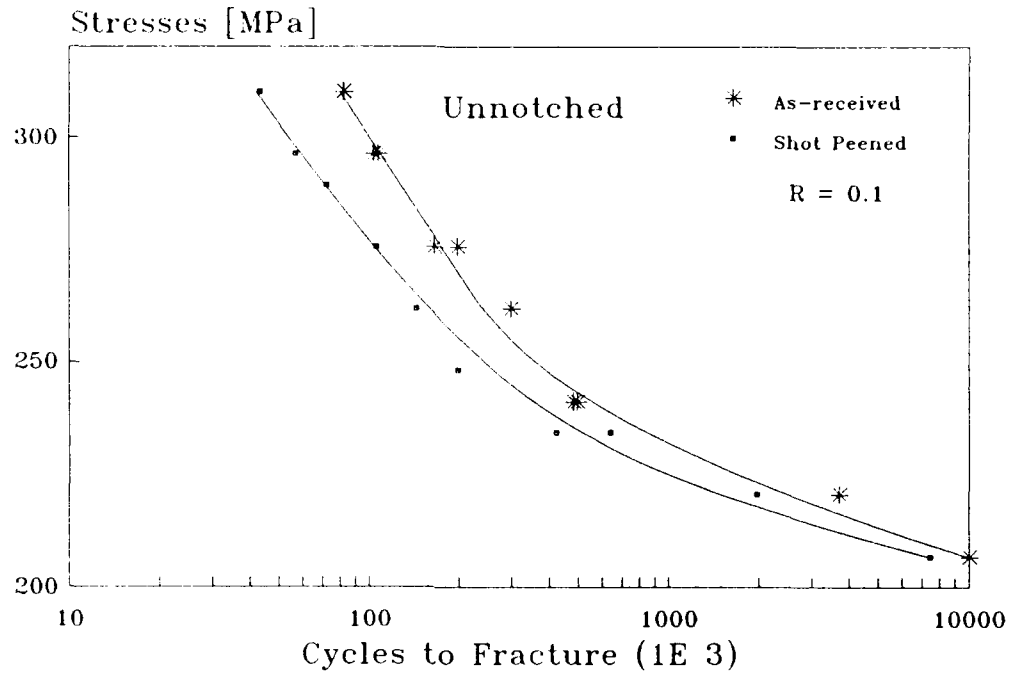


Figure 11. S-N curves for unnotched specimens, shot peened and as-received.

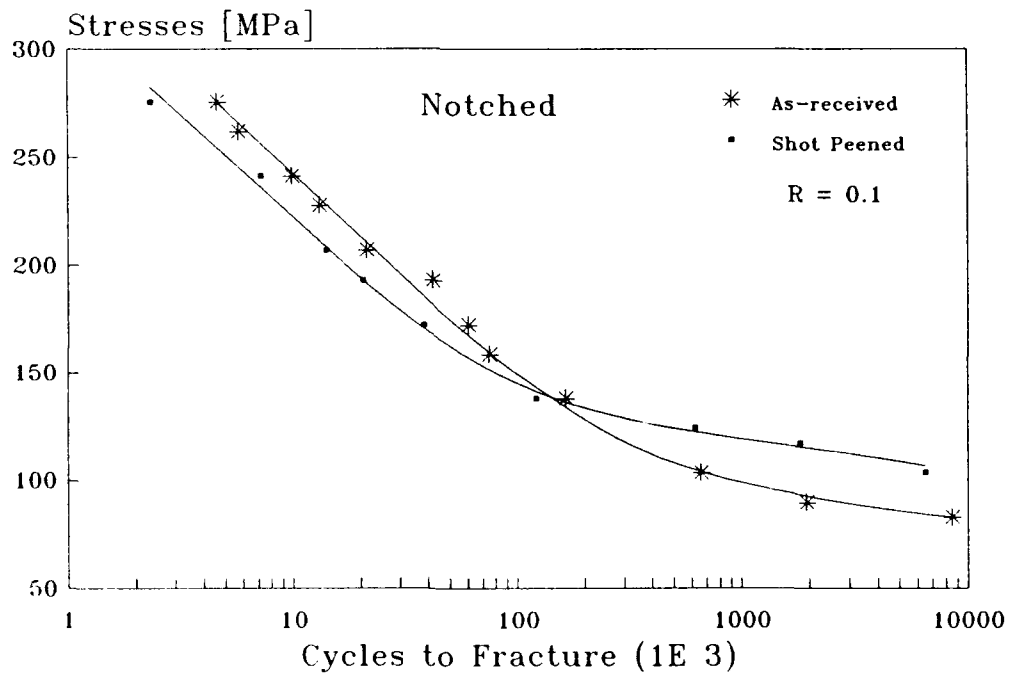


Figure 12. Stress as a function of the fatigue life for notched specimens, shot peened and as-received.

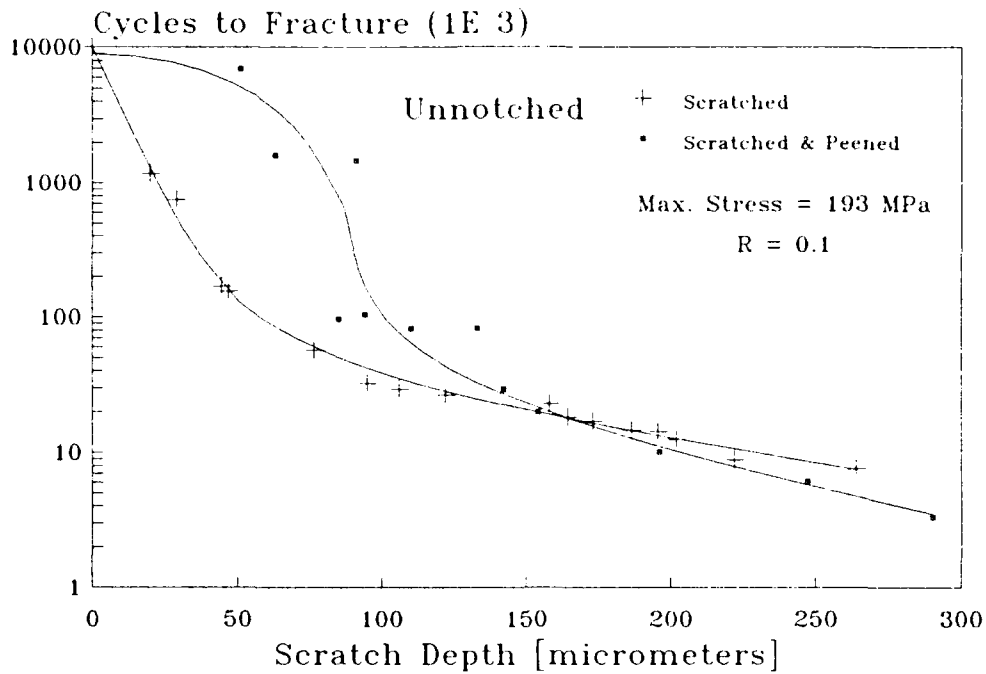


Figure 13. Number of cycles to failure vs. scratch depth for unnotched specimens subjected to $\sigma = 193$ MPa.

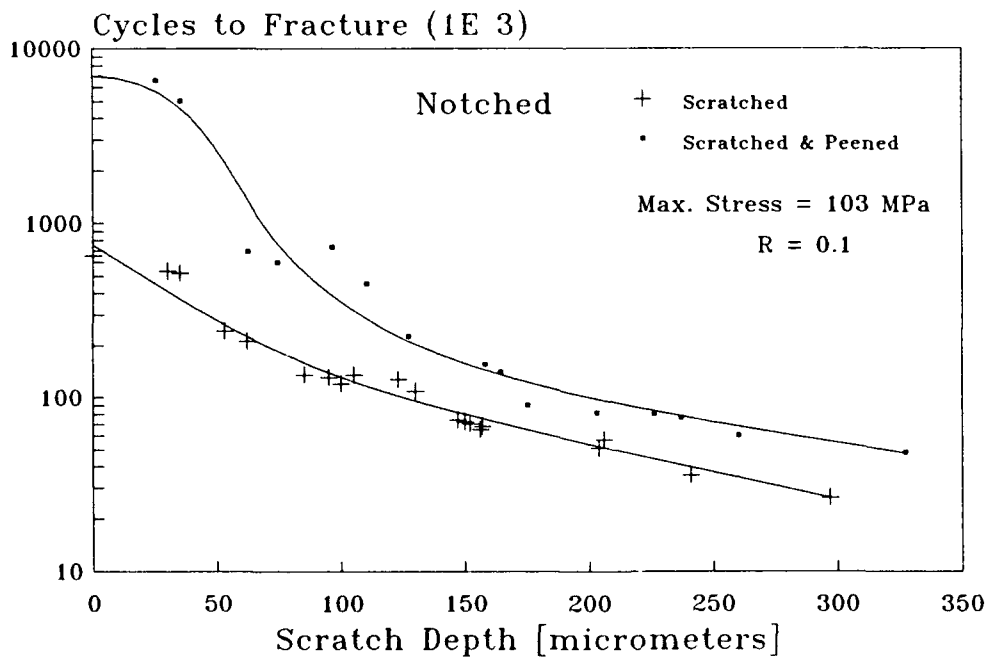


Figure 14. Number of cycles to failure vs. scratch depth for notched specimen subjected to $\sigma = 103$ MPa.

Figure 14 exhibits the N_f versus d curves for scratched notched specimens, the nominal stresses are $\sigma = 103$ MPa (15 ksi), which is at the lower end of Figure 12. Figure 14 displays that shot peening is beneficial in all the ranges studied. Some of scratched samples (up to $d = 75$ μm) fully recover their fatigue life with shot peening.

The S-N curves of samples that have been scratched (depth of 150 μm), scratch and shot peened, and as-received are presented in Figure 15. The curves indicate that when an as-received sample is scratched to $d = 150$ μm , the fatigue life reduces about 85%, ± 5 %. However, the curve corresponding to the scratch and shot peened sample shows that the life of the samples has been increased, specially at lower stresses, and the reduction in life due to scratching can be recovered at stresses lower than 55 MPa (8 ksi). A comparison of Figure 15 to Figure 12 reveals that a scratched, notched specimen will have higher beneficial effect when shot peened. As can be seen in Figure 15 the intersection of the two curves has been shifted to above 207 MPa (30 ksi) from its previous value of about 138 MPa (20 ksi) in Figure 12.

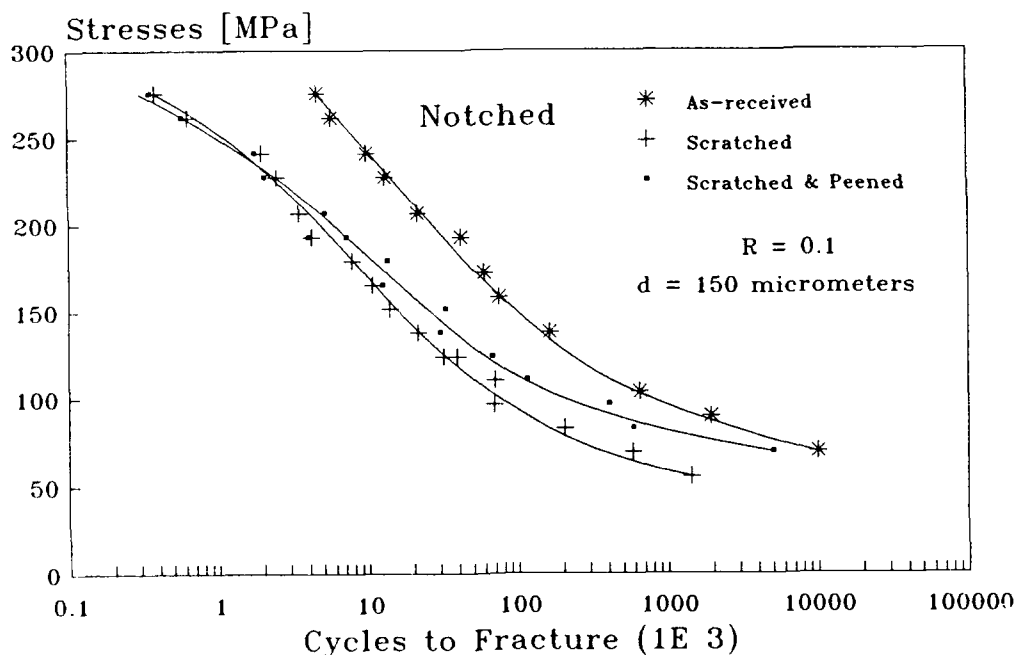


Figure 15. S-N curves for notched specimens.

To analyze the effect of shot peening at higher stresses, reference should be made to Figures 5 and 16. In figure 5 it is noted that shot peening increased surface roughness and enlarged the size of surface microcracks. Furthermore, Figure 16 shows that shot peening not only enlarges surface defects, but also

increases their depth; the defect depth, before shot peening, is almost not detectable with an optical microscope. Consequently, for relatively higher testing stresses, where the compressive residual stresses, generated by shot peening, are overcome by the applied stresses; thus the microcracks can easily propagate, reducing the fatigue life of the samples. However, at lower stresses, the compressed surface layer may arrest the crack propagation, improving the life of the material.



Figure 16. Optical micrograph cross section view of a shot peened specimen 200 magnification.

Shown in Figure 17 are the results of the following three groups of notched samples: the scratched and anodized, scratched only, and as-received. The scratch depth in this experiment is fixed to $d = 150 \mu\text{m}$. This figure shows that, unlike shot peening, anodizing improves the fatigue life consistently at all stresses and does not depend on the applied stress. The effect of shot peening is superior when lower stresses are applied. The improved fatigue life due to anodizing is $50 \% \pm 20 \%$. Figure 6 shows that no major change occurred on the anodized surface.

The fatigue life versus scratch depth (at $\sigma = 193 \text{ MPa}$ for both unnotched and notched samples) curves of chemical polished and unpolished samples are presented in Figure 18. The fatigue curve of the polished notched sample is always lower than the unpolished material. However, polishing is mostly beneficial for unnotched specimens at a scratch depth of $50 \mu\text{m} < d < 70 \mu\text{m}$.

In this region, fracture does not occur at the scratch. At a scratch depth of $50\mu\text{m}$ or less, the fatigue life is sharply reduced. This is attributed to the removal, by a chemical polishing, of the residual stresses due to rolling (compare Figures 4 and 7).

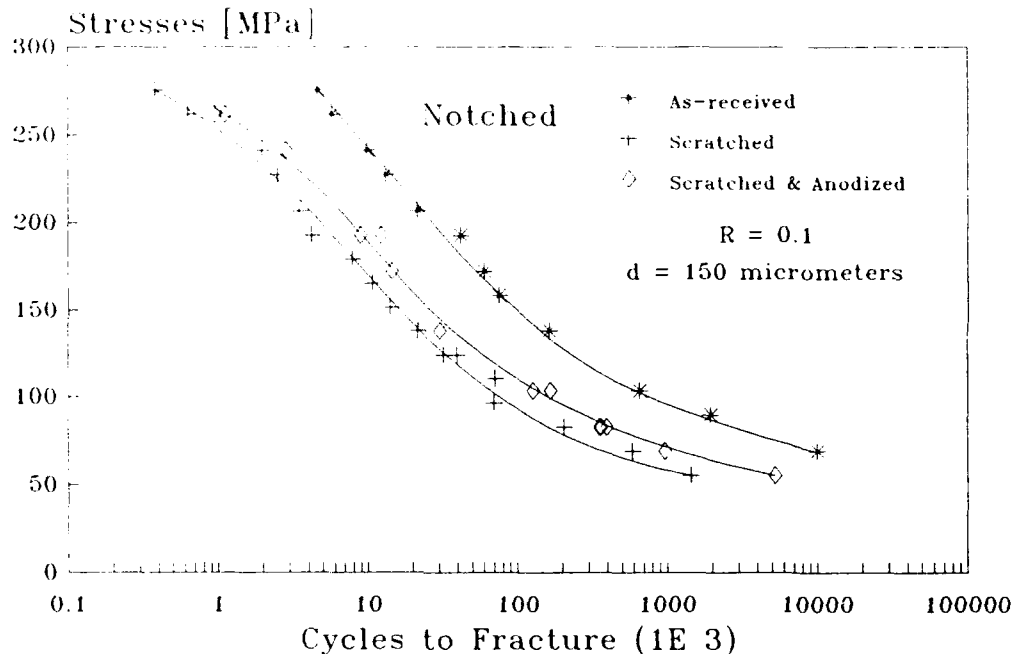


Figure 17. S-N curves for notched specimens.

A few shot peened samples were also anodized, but since the surface was not newly prepared and contained some oxide, the anodizing improved the life by only 10 to 15%. In addition, it was found that scratched ($d = 100 \mu\text{m}$) and then polished samples, when blasted with glass beads, improved their life by about 80% and did not fail from the scratch.

Figures 19 through 21 indicate that the effect of the compressive residual stresses, due to shot peening, can easily be observed from the fracture surface. The shot peening fracture shows that there is a plateau near the surface layer. The end of this plateau should be the transition region from the compressive residual stresses to tensile residual stresses. There is a high probability that failure could initiate from near this transition zone as predicted by Reference 9.

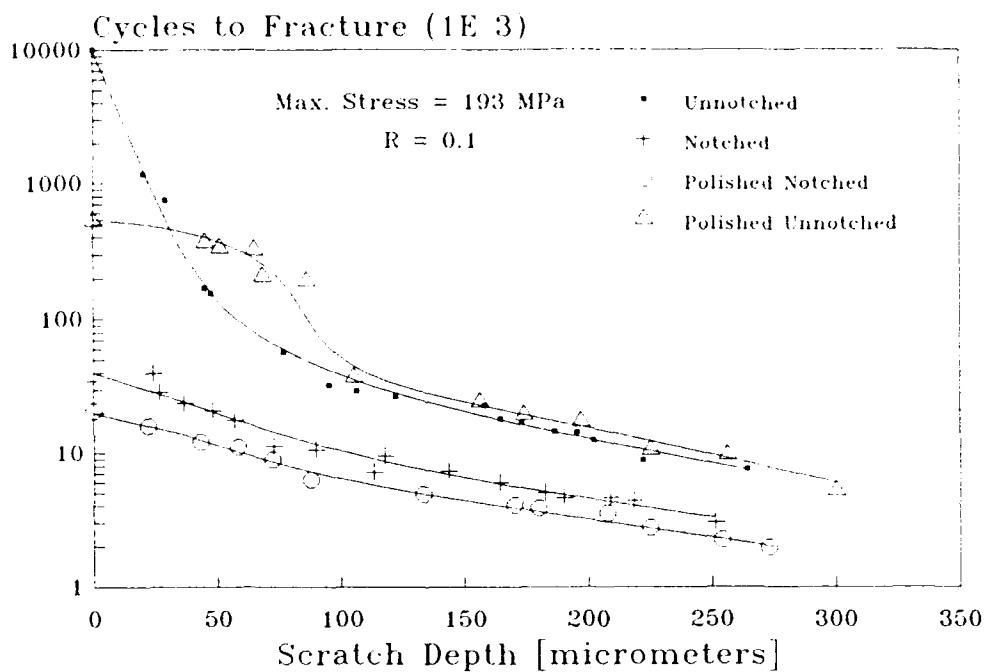


Figure 18. Number of cycles to failure versus scratch depth of as-received and polished samples subjected to $\sigma = 193$ MPa.

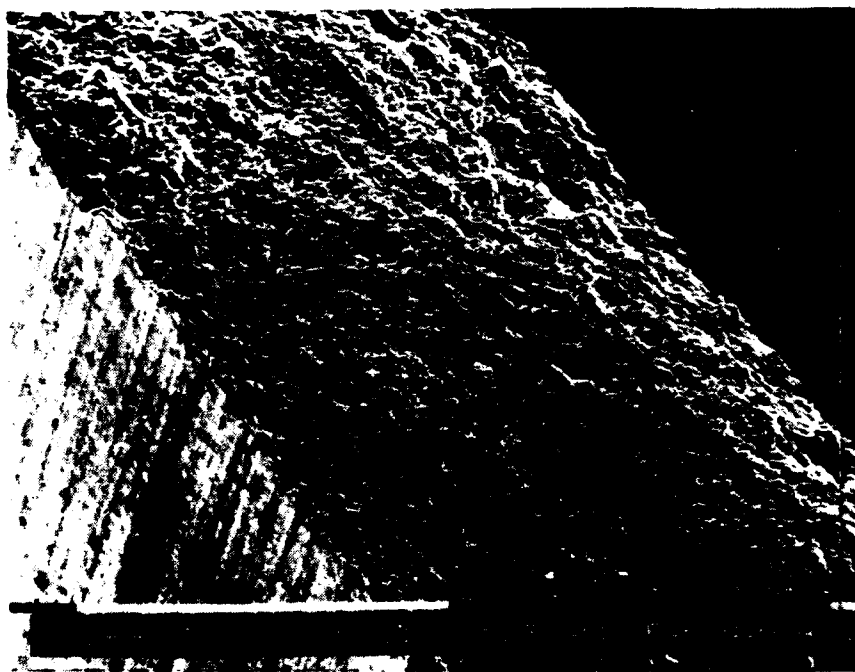


Figure 19. Fractograph of as-received specimen.

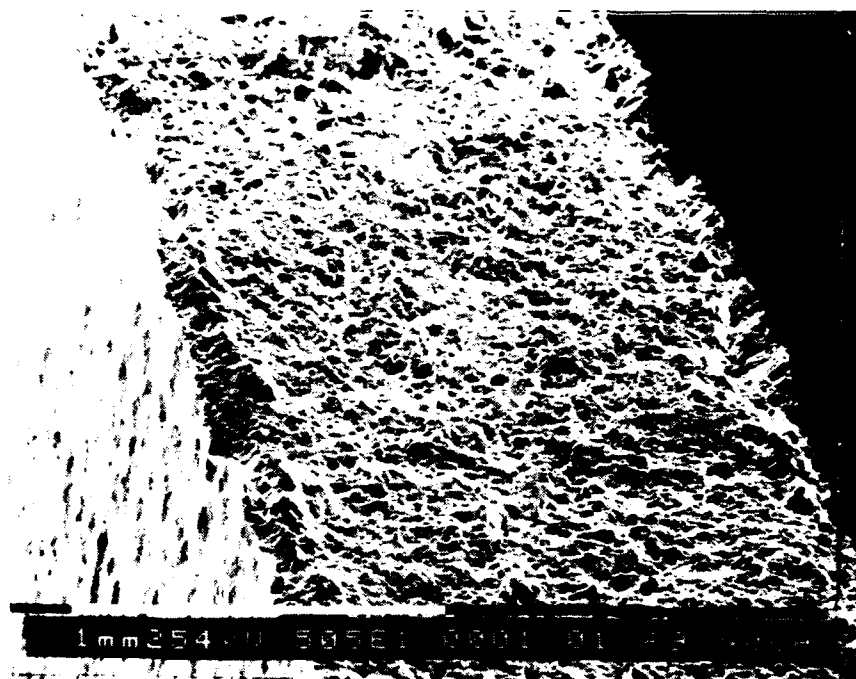


Figure 20. Fracture surface morphology of shot peened material.

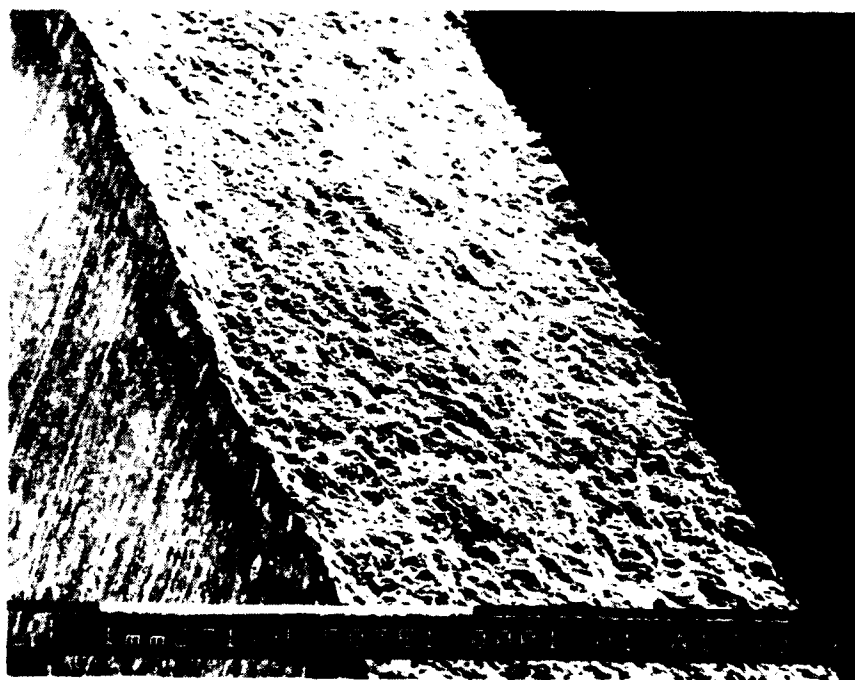


Figure 21. Fractograph of an anodized sample.

4. CONCLUSION

There is ample evidence that the mechanical properties and deformational behavior of metals can be influenced by altering the state of the surface; however, relatively little information is available for Al-Li alloys. Scratches reduced the fatigue strength of Al-Li alloys. This behavior is related to geometry and the uneven removal of material to form the scratch. Scanning electron microscope observation of the scratch, during discrete intervals of fatigue cycling, revealed that microcracks were randomly distributed within the scratch.

SEM observation of surface shows that the surface of the material as-received contains microcracks or fissures and pits. Although, after shot peening the surface was uniform and well covered, it was observed that surface roughness had increased and the surface defects (pits and fissures) have been enlarged and penetrated much deeper into the material. Unnotched and notched specimens without scratches were fatigue tested to distinguish the influence of shot peening on fatigue life. The result indicates that shot peening is not beneficial to the fatigue life of unnotched specimens. However, the notched samples displayed that shot peening is beneficial only at low stresses, and for higher stresses it is detrimental.

Scratched specimens with depth from 0-300 μm were shot peened and fatigue tested at low stresses where beneficial effect of peening had been observed before. For unnotched specimens improvement was observed for $d < 50 \mu\text{m}$, but full recovery was not achieved. As scratch depth increased, the beneficial influence of peening was subsided. Whereas for $d > 150 \mu\text{m}$ the peening acted detrimental to fatigue life. For notched specimens, peening improved the fatigue life for all scratch depths and specimens with $d < 75 \mu\text{m}$ fully recovered. However, much lower stresses should be applied for full recovery of a notched specimen with $d = 150 \mu\text{m}$.

Anodizing did not influence the surface morphology as shot peening. Fatigue life data shows that anodizing improves the life partially. Chemical polishing removes a surface layer that carried the effect of rolling, resulting in reduction of fatigue life for notched specimens. For unnotched specimens, it appears that polished samples with $d < 75 \mu\text{m}$ all have the same fatigue life and do not fail from the scratch. Consequently, life improves in a narrow range, $50 < d < 75$, with no full recovery, and life reduction is observed for $d < 50 \mu\text{m}$.

Fracture morphology of notched specimens at low stresses indicates that, residual stresses due to shot peening contribute to a shear plateau near the surface. This plateau is the transition zone from compressive residual to tensile residual stresses. It is possible that failure could initiate from this transition zone.

A more detailed investigation of these surface-defect-fatigue interaction is needed. Such an investigation will aid the development of models pertinent to the fatigue processes in terms of a balance among defect and/or microcracks generated by surface sources, scratches in particular. This research will aid in selection of better structural materials.

5. REFERENCES

- [1] T. H. Sanders, Final report, Naval Air Development Center, Contract No. N62269-76-C-0271, for Naval Air Systems Command.
- [2] J. M. Silcock, J. Inst. Metals, 88, (1959-1960).
- [3] B. Noble and G. E. Thompson, Metal Sci., J. 5, (1971)
- [4] D. B. Williams, J. W. Edington, Metal Sci., 1975; pp.9
- [5] A. Inchekel and J. E. Talia, Symposium on Light-Weight Alloys for Aerospace Applications Proceedings, 181, Las Vegas, Nevada, February (1989).
- [6] T. Toriyama, P. K. Mazumdar, and J. E. Talia, Fifth International Aluminum-Lithium Conference Proceedings, 1077. Williamsburg, Virginia, March (1989).
- [7] J.F. Watkinson, "International Conference on Fatigue, Institute of Mechanical Engineers", 445 (1956)
- [8] A.G.H. Coombs, F. Sherratt, and J.A. Pope, "International Conference on Fatigue, Inst. of Mech. Eng." 277 (1956).
- [9] J.A. Bannantine, J.J. Comer, and J.L. Handrock, "Fundamentals of Metal Fatigue Analysis", Prentice-Hall, Inc. (1990).
- [10] R.W. Hertzberg, "Deformation and Fracture Mechanics of Engineering Materials", John Wiley and Sons, 3rd edition.
- [11] J.E. Talia and P.K. Mazumdar, Int. J. of Fracture, 40, 67 (1989).
- [12] M.H. Raymond and L.F. Coffin, "Trans. Am. Soc. Mech. Engr." 85, 548 (1963)
- [13] J.Y. Mann, Dept. of Supply, Australia, Aero. Res. Lab. Rep. SM147 (1950).
- [14] T.T. Oberg and E.J. Ward, Wright Air Development Department, Tech. Note, WCRT 53-117, (1953).
- [15] B. Cina, Metallurgia, 55, 11, (1957).

ETBE IN GENERAL AVIATION AIRCRAFT ENGINES

William F. Marshall
National Institute for Petroleum and Energy Research (NIPER)
220 North Virginia
Bartlesville, Oklahoma 74003

ABSTRACT

Tests were conducted to determine the potential of using ethyl tertiary-butyl ether (ETBE) as a fuel for light aircraft engines. An engine was installed on a test stand and operated at two speed-load conditions with five fuels. The fuels were avgas, an unleaded premium autogas, blends of ETBE in the autogas, and neat ETBE. The air-fuel mixture was controlled at five different stoichiometries at each engine mode. Engine performance and exhaust emissions were measured at each condition. The exhaust emissions measurements included hydrocarbon speciation and aldehydes as well as total hydrocarbon, CO, NO_x, O₂, and CO₂.

Results show that the engine performance achieved with ETBE (either blended or neat) was equivalent to that with hydrocarbon fuels. Thermal efficiency was slightly higher for ETBE. The photochemical reactivity of the exhaust was greater for ETBE. However, the lower emission rates of the reactive components with ETBE yields a net effect of lesser effect on air quality.

This paper was unavailable at the time of publishing.

FLIGHT TESTING WITH ETANOL IN TURBOPROP ENGINES

by

Keith J. Biehl
and
Paul S. Demko
FAA Technical Center
Atlantic City Int'l Airport
Atlantic City, NJ 08405

For presentation to the AIAA/FAA Joint Symposium on General
Aviation Systems at the Port O-Call Inn, Ocean City, NJ
on April 11, 1990

FLIGHT TESTING WITH ETHANOL

IN

TURBOPROP ENGINES

Keith J. Biehl
and
Paul S. Demko
FAA Technical Center
Atlantic City Airport, New Jersey

ABSTRACT

Limited flight testing was conducted to evaluate the performance characteristics and functional suitability when operating on a blend of 10% ethanol alcohol with JP-4 jet fuel. Of the 37 hour flight test effort, 20.3 hours were conducted with ethanol blended fuel in the starboard PT6A-41 engine of a Beechcraft King Air 200. Data collection was conducted at 6,000 foot intervals from ground level up to 30,000 feet utilizing step climb to interval altitudes, continuous climbs and endurance cruise profiles.

Ethanol fuel blending was not conducted before flight but rather during flight utilizing a separate onboard ethanol tank with associated fuel lines and mixing valves. This procedure allowed for consistent control of the desired 10% fuel mixture and allowed for a stable mixture with no possibility of phase separation.

While a noticeable power reduction was present when operating with an ethanol mixture, no detrimental conditions were noted. In addition, an engine hot section inspection was performed both before and after flight test operations were completed. No degradation of components were noted by the overhaul facility and the only fuel related part change was a fuel control unit diaphragm. This part change was accomplished during the post flight test inspection as a precaution only.

INTRODUCTION

Over the past decade the aviation community has witnessed a constant push for alternate fuels which would be suitable and approved by the FAA for aviation use. The main emphasis centered around two prominent issues: (1) develop a lower cost fuel; (2) develop fuel with a renewable source of supply which would not be depleted. The general aviation piston engine community has seen numerous test efforts, technical papers/reports and subsequent FAA approval for automotive gasoline use in aircraft as an alternate fuel. However, the turbine engine community has been left watching

with little movement while prices have oscillated to extremes with some spot shortages. While there are avenues available to corporate operators to cover operating expenses, it never the less behoves us to maintain control over operating expenses and ensure a continuous source of supply.

A review of previous alternate jet fuel work has centered on alcohol as both a pure 100% fuel and as an additive or blending agent which would allow more gallons of fuel per barrel of oil. Previous full scale engine test cell analysis has been conducted by both the Naval Air Propulsion Center, reference 1 and the FAA Technical Center reference 2. Both activities utilized T63 engines operating on alcohol/Jet A fuel mixtures with the Technical Center also utilizing a JP-4 fuel blend. Ethanol and methanol were individually used as blending agents with both jet fuels for performance analysis which ultimately indicated ethanol was a better blending agent than methanol. Additionally, concentrations up to 10% ethanol could be accommodated before noticeable performance degradation was experienced.

During September 1989 the FAA Technical Center conducted a 37 hour flight test analysis of 10% ethanol alcohol blended with JP-4 jet fuel. This effort utilized a Beechcraft King Air 200, serial number BB-88, to extract real time "in flight" data which would substantiate turbine engine performance characteristics and demonstrate the functional suitability of using a jet fuel blended with alcohol.

Fuel operations were conducted with JP-4 as the base fuel rather than Jet A simply because of availability. The FAA shares jet fuel purchases with the New Jersey Air National Guard F-16 operations at the Atlantic City International Airport and JP-4 is the preferred fuel. N-4, which was the project test aircraft, had a total airframe time of 4870 hours since new with the #2 engine (starboard) PT6A-41 serial #PCE 80254 having 1967 total hours in use.

As noted above, this flight test effort was an initial look at alcohol usage and not a certification effort. References 3, 4 and 5 provide guidelines and detailed testing procedures required for airframe-engine certification and alternate fuel qualification. A more detailed technical analysis of the overall ethanol flight test effort is provided in reference 6.

TEST APPARATUS

When program discussions began, a review of aircraft requirements versus availability was initiated. As a result, the Beechcraft King Air was selected for several reasons:

- 1) It is a very popular design with a large production base, several models are available and it is a twin engine configuration for safety purposes with nominal single engine performance

- 2) It provided turbine power, PT6A-41, at relatively low fuel consumption, altitude capability up to 35,000 feet and a speed range up to 270 KCAS (Knots Calibrated Air Speed).
- 3) The aircraft afforded sufficient room for modification, instrumentation and a flight test engineer.
- 4) Of the several King Air models currently in the FAA inventory, N-4, King Air 200, serial number BB-88, was assigned to the Technical Center and available for flight test work during the August - October 1989 time period.

Since the King Air does not utilize counter rotating propellers, the initial program installation intentions were to utilize the #2 engine and one of the starboard side wing fuel tanks for the ethanol/JP-4 fuel mixture. However, due to the arrangement of the existing King Air fuel cell interfeed system, figure 1, which includes transfer pumps, bladder tanks and non bladder tanks, it became too difficult to isolate a fuel tank whereby a constant 10% ethanol-fuel blend could be maintained throughout a given two hour flight test period. As a result, a decision was made to remove all cabin seats, tables and lavatory; install an aft facing seat in the forward starboard cabin position for the test engineer; and locate necessary ethanol fuel storage and metering equipment along with required instrumentation inside the cabin. While such an arrangement provided a very convenient installation, it did not allow us the opportunity to utilize an existing "off-the-shelf" aircraft design configuration as an aircraft operator in the field would use under normal flight conditions.

Figure 2 depicts the cabin floor plan as N-4 was finally configured. This installation, as discussed below, afforded us an opportunity to carry a pure 200 proof supply of ethanol fuel in a separate 15 gallon tank which was fed to the engine for mixing with JP-4 just prior to the engine driven low pressure feed pump. As a result, a constant 10% mixture was supplied to the engine with no fear of phase separation or return/bypass flow of JP-4 diluting the test mixture had it been contained in one of the wing tanks.

Figure 3 provides a general three view of the King Air 200. Figures 1, 2 and 3 were extracted from reference 7.

The aircraft cabin carried an instrumentation rack consisting of a project power switch, Zenith laptop computer, data acquisition system, power strip, VHS video camera and an ethanol fuel flow measurement system. A computer based data acquisition system was utilized to read temperatures of both the cabin stored ethanol fuel and the fuel mixture inside the engine nacelle along with cabin tank pressure, aircraft fuel system pressure and pure ethanol fuel flow. For simplicity, a constant nitrogen pressure charge was supplied to the ethanol fuel tank during the entire test period as a means of controlling fuel flow rather than a fuel pump arrangement. This pressure supply arrangement was provided with

a valve connection to the vacant lavatory vent line which would allow for a total system pressure release capability if necessary during flight.

As luck would have it, N-4 contained extended range ferry fuel lines which ran from inside the cabin area out to each engine nacelle area. Since these lines were available and never used for normal aircraft system use, we immediately incorporated their use into our design. After a check valve, pressure transducer and shut-off valve were installed, the cabin ethanol fuel line was connected to the ferry line. At the nacelle end, the ferry line was connected to the engine crossfeed fuel line which then provided continuous ethanol fuel flow into the nacelle for mixing with the JP-4.

Co-pilot's duties required hand recording all test data not recorded by the computer based data acquisition system such as: altitude, interstage turbine temperature (ITT), torque, propeller rpm, gas generator % rpm, engine fuel flow, oil pressure, oil temperature, outside air temperature (OAT) as read from existing aircraft instrumentation. Barometric pressure, ground air temperature, dew point and winds from local airport observations were also manually recorded along with general flight comments.

TEST PROCEDURES

Project personnel consistently followed a set of standardized procedures before and after every test run whether it was a ground test run or a flight test. This included nitrogen pressure check, ethanol fuel tank filling and sealing, test system integrity check, calibration checks and aircraft preflight/systems check. Test runs were grouped into four categories: Ground Test, Step Climb, Continuous Climb and Altitude Endurance Test with all runs starting and stopping on neat JP-4. Once a test condition was set and stabilized on both engines, a full set of data parameters were recorded using neat JP-4. Immediately thereafter an ethanol flow rate at 10% of engine JP-4 flow rate was initiated. After allowing a two minute stabilization period with this fuel mixture, a full set of data parameters were recorded and every five minutes thereafter. It should be mentioned that the initial ground runs were conducted with JP-4 in the ethanol tank so as to note any engine performance shift as a direct result of test system installation/operation. Additionally, the same two test pilots made all test runs alternating seat assignments each time and both agreeing on test point establishment/stabilization prior to data recording or initiating/stopping ethanol fuel flow. When questions developed, the particular test point would be reset.

Ground Run Tests: These were initially conducted with JP-4 only to check system integrity, system impact on normal aircraft systems operations and establish flight team/test systems interaction. Engine power setting test points utilized during data collection on JP-4 in order of use were: low ground idle, high ground idle, descent/approach, 55%, 60%, 65%, 70%, 75%, 80%, 90% of maximum

continuous power and take-off power. Data points utilized during ethanol mixture in order of use were: low ground idle, high ground idle, take-off, descent/approach, 55%, 60%, 65%, 70%, 75%, 80%, 90% of maximum continuous power. During these tests maximum continuous power was equal to take-off power.

Step Climb Tests: This flight profile was conducted twice utilizing an ethanol fuel mixture both times, first with a power setting of maximum continuous (1,900 rpm, 825°C ITT) and then with maximum range power setting (1,700 rpm, 695°C ITT) the second time. The step climb was conducted at 6,000 foot intervals from the surface up to and including 30,000 foot pressure altitude. Each data point was established on neat JP-4 followed by data collection once all parameters stabilized after two minutes. Once everyone was satisfied with the JP4 only data, ethanol flow was commenced at 10% of engine total fuel flow. After five minutes of stabilized parameters, data was again recorded followed by a switch back to JP-4 and climb to the next altitude. At the completion of all data points a normal descent to landing was made.

Continuous Climb Tests: This flight profile was conducted twice utilizing an ethanol fuel mixture both times with a power setting of maximum continuous the first time and maximum range the second time. Once the take-off roll was completed, climb checklist completed and climb clearance received (about 2,000 feet AGL) ethanol fuel flow was commenced at 10% of engine total fuel flow. While power was maintained at a constant rpm/ITT setting, the ethanol fuel flow was continuously adjusted to maintain 10% required until peak altitude was reached at 30,000 foot pressure altitude. Performance data was collected every 3,000 feet during climb and every five minutes while level at 30,000 feet. When a total ethanol run time of 100 minutes had been reached, ethanol fuel flow was terminated and a set of neat JP-4 performance data recorded after test engine stabilization. At the completion of all data points, a normal descent to landing was made.

Altitude Endurance Test: This profile was conducted at 6,000, 12,000, 18,000 and 24,000 foot pressure altitudes with power settings of 1,900, 1,800 and 1,700 rpm, and 695°C ITT. Climb to test altitude and baseline performance data was recorded after five minutes of level stabilized flight with JP-4 only. At that point in time 10% ethanol fuel flow was established and maintained for 100 minutes. Performance data was recorded every five minutes during the test duration with ITT being reset to the initial JP-4 only set point after 30 minutes of operation with ethanol. At the completion of the JP4/ethanol test time another set of baseline data was taken on JP4 only followed by a normal descent and landing.

RESULTS

To measure the overall effects of 10% ethanol on the aircraft engine, a set of hot section inspections were performed: one inspection before the installation of instrumentation and one after

removal of instrumentation from the aircraft. Out of the 37 hours of total testing time, 20.3 hours were accomplished using a 10% ethanol fuel mixture in engine #2 (starboard). This was insufficient time to draw any firm conclusions, however, the inspections revealed no immediate damage caused by operations on 10% ethanol mixtures. One recommendation made by the engine manufacture, up front, at the start of modification discussions was to replace the fuel control unit diaphragm during a post testing hot section inspection as a precaution since material compatibility had not been determined. An item of note which may relate to this, was what appeared to be a change in engine start time. This apparent increase in start time was very subtle over the total test period and not really noticeable until near the end of the flight test program. As such, no specific start times were recorded from program initiation. A cross check was made at program completion between both engines under identical start cycles. Engine #1 required 30 seconds to complete its start cycle while engine #2 required 39 seconds. Remaining start parameters (temperature, rpm, fuel flow) all remained nominal for each engine.

Since the ethanol fuel was not being carried in any of the aircraft wing fuel storage systems, no determination was made relative to materials compatibility or hardware design/fuel flow suitability. However, consideration of these items was not a specific part of this flight test effort. As a precaution to determine that ethanol fuel had not found its way into the aircraft fuel storage system a fuel sample was taken from the nacelle fuel tank after several of the 100 minute endurance test runs. A chemical analysis of this sample indicated no presence of ethanol.

When reviewing the section on Test Procedures it may be noticed that the sequence of data point selection under Ground Run Tests changed with ethanol as to when take-off power was selected. It was noted during JP-4 ground runs that with long test periods at high power settings the oil temperature would reach its red-line limit. Therefore, a decision was made to alter the ethanol sequence to preclude cutting a data point test time short due to unrelated oil temperature problems.

During one altitude endurance run JP-4 baseline data had been completed followed by opening the ethanol fuel valve as per standard test procedure. However, an apparent vapor lock had been induced in the ethanol fuel line during refueling and no ethanol flow was available. Subsequent rapping on the stainless steel ethanol fuel line inside the cabin area relieved this problem with an immediate surge of ethanol fuel. This caught the test crew by surprise leading to a fuel mixture far above 10% since the flow regulating valve was full open. The manifestation of this excess ethanol flow was a drop in torque from 1,700 Ft · lbf to approximately 300 Ft · lbf before proper flow could be reset. All remaining engine parameters were within maximum limits although specific numbers were not noted as the flight crew was preparing to feather the #2 engine if necessary. Once normal ethanol flow was reset at 10% of JP-4 baseline data all engine parameters

returned to normal.

Ground Run Test Analysis: Ambient conditions for all ground runs were close to standard day conditions except for humidity, therefore, data was not corrected to perform the data analysis. Additionally, all ground runs were performed on the same day with constant ambient conditions. This fact also lends itself to the data analysis since we are looking for a delta change under identical conditions rather than a need for specific performance numbers.

The data analysis revealed an average increase in ITT of 0.6% and a 10% drop in torque when changing from neat JP-4 to a fuel test mixture with 10% ethanol. A review of power (torque) versus ITT indicated a 1.7% power decrease (neat JP-4 to 10% ethanol) while the average power change between JP-4 only runs was less than 0.6%. Fuel flow versus ITT indicated an average 3.1% increase in flow with ethanol (for the same power setting without ethanol) while JP-4 fuel flow repeatability was within 0.05%. Another analysis made was to look at brake specific fuel consumption relative to ITT. For 10% ethanol fuel, the consumption was 3.9% higher than with neat JP-4 for the same power setting while JP-4 repeatability was within 0.7%. This 3.9% compares directly with a 3.89% calculated change in energy density with 10% ethanol versus neat JP-4. Also, these trends agree with previous work accomplished during dynamometer testing addressed in reference 2 utilizing a T-63 turboshaft engine.

Climb Test Analysis: Data trends for both the step climb and continuous climb tests paralleled that of the ground testing. Typically, ethanol fuel mixture provided a 4.7% power reduction, fuel flow was relatively unchanged while brake specific fuel consumption was up 5.2%. One item which predominantly stood out during all climb testing was power lever stagger and a lack of maximum torque from the ethanol fueled engine. The power lever for the ethanol engine was always ahead of the neat JP-4 power lever for equal torque and it reached its maximum forward stop before the neat JP-4 power lever of the left engine. This resulted in less total torque during the higher altitudes of the test profile while engine response and other parameters all remained normal.

Altitude Endurance Test Analysis: Performance data trends for all the endurance test profiles also paralleled that of both ground testing and climb testing data trends. In general terms there was always a loss of power with ethanol ranging from 1.36% at 6,000 feet up to 6.99% at 30,000 feet. Fuel flow showed slight fluctuations from a 2.18% increase at 6,000 feet to a 1.16% decrease at 30,000 feet while brake specific fuel consumption increased from 3.57% at 6,000 feet to 6.35% at 30,000 feet. Again the test engine response was smooth and normal with the ethanol mixture except for less available power and the resultant increased brake specific fuel consumption.

As stated throughout the analysis discussion, a couple of general items which were always noticeable from a pilot stand point were: 1) There was never any doubt as to when ethanol fuel entered the engine. There was always a drop in torque, however, this loss was not a hazard nor did it ever impose difficulty in aircraft response. (Except as noted once when ethanol flow rate unintentionally went far in excess of 10%). 2) Power lever stagger was an annoyance but this would resolve itself if both engines were operated on ethanol. 3) If the torque gage were removed from the instrument panel the pilot would not notice when ethanol was being used. 4) Additional flight test time on ethanol fuel was anticipated, however, a malfunctioning oil pressure transducer during the 24,000 foot endurance testing caused a program stoppage. Once replacement parts were available, other project commitments for the aircraft time period forced ethanol equipment removal.

CONCLUSIONS

Based on the short flight test effort conducted with 10% ethanol alcohol added to JP-4, the following conclusions are noted which in themselves may generate additional flight test efforts:

1) At a given interstage turbine temperature, the power developed was lower when operating on ethanol/JP-4 than when operating on neat JP4. In addition, brake specific fuel consumption increased more than was expected based on the change in energy density.

2) At various altitudes the fuel control unit did not have sufficient command authority (i.e., power lever set to maximum travel for full power) to deliver requested power output while utilizing the ethanol mixture. As such a fuel control adjustment must be provided to compensate for change in fuel energy density.

3) Engine relight envelope will require evaluation due to change in fuel control unit response at high altitudes relative to lower power output and perceived start time change.

4) As noted earlier, there was a perceived change in engine start time which may dictate a rescheduling of the fuel control unit start cycle.

5) The engine fuel control unit pressure diaphragm was changed as a precaution. Long term material compatibility testing will be required for both engine and aircraft fuel systems.

6) At one point in the flight test it appeared that vapor lock had been induced into the ethanol fuel system during refueling. As such, the aircraft fuel system on any existing aircraft would need not only material compatibility testing but also a fluid flow analysis for susceptibility to vapor lock and recirculation flow problems.

7) It has been shown from this short flight test effort that a 10% ethanol fuel mixture works quite well in flight operations up to and including 30,000 feet (except for the noted degradation in performance). There still remain several question areas to be addressed: fuel handling from a supply pump, premixture of fuel, phase separation, storage stability, water separation, less energy density per pound of fuel, less cruise performance per pound of fuel, emissions reduction potential, impact on maintenance to name just a few issues. While more flight testing is required, many of these questions may be addressed by ground testing without the need for an aircraft.

8) Will this ethanol fuel work - yes. Is it cost effective to undertake such a research effort, or any alternate turbine fuel research effort - the market place will answer that. What is the long term status of the petroleum based aircraft fuels we now use - How much longer will the great North Slope oil field last - When is it time to look for alternate fuels or fuel extenders - Food for thought.

REFERENCES

1. Naval Air Propulsion Center; NAPC-LR-89-12; 8 June 1989
2. Turbine Fuel Alternatives (Near Term), DOT/FAA/CT-89/23; Furrara, Augusto M., Federal Aviation Administration Technical Center, Atlantic City International Airport, NJ 08405, October 1989
3. Federal Aviation Regulation Part 23 "Airworthiness Standards: Normal Utility, Aerobatic, and Commuter Category Airplanes"
4. Federal Aviation Regulation Part 33 "Airworthiness Standards: Aircraft Engines"
5. FAA Advisory Circular AC20-24B; 20 December 1985
6. In-Flight Evaluation of Turbine Fuel Extenders, DOT/FAA/CT-89/33; Ferrara, A., Rea, C., Federal Aviation Administration Technical Center, Atlantic City International Airport, NJ 08405
7. Super King Air 200 Pilot's Operating Handbook TI4040.10A

HUMAN PERFORMANCE IN COCKPIT-RELATED SYSTEMS

by

Randall M. Chambers
and
Mihriban Cihangirli
Department of Industrial Engineering
Institute for Aviation Research
Wichita State University
Wichita, KS 67208

For presentation to the AIAA/FAA Joint Symposium on General
Aviation Systems at the Port O-Call Inn, Ocean City, NJ
on April 11, 1990

HUMAN PERFORMANCE IN COCKPIT-RELATED SYSTEMS

Randall M. Chambers and Mihriban Cihangirli
Department of Industrial Engineering and
Institute for Aviation Research
Wichita State University
Wichita, Kansas

ABSTRACT

A complex cognitive assessment battery of computerized cognitive performance tests was installed in the cockpit of a flight simulator, and cognitive performance capabilities of thirty volunteer subjects were measured on nine cognitive tests. Research on the effects of cockpit-related conditions on cognitive performance indicated that performance capabilities were affected by the process of attending to and reading selected instruments in the cockpit. Aircraft noise of 90 dBA significantly increased subjective mental workload without altering cognitive performance significantly. Although there were many individual differences among the thirty volunteer test subjects, mean cognitive performance for the fifteen males was not significantly different from the mean cognitive performance of the fifteen females.

INTRODUCTION

In general aviation, the human interface with the cockpit and its environment is an important aspect of airplane safety and flight operations (FAA, 1989; Chambers, 1989). The pilot performs a large number of tasks, many of which involve cognitive performance capabilities. Some of these cognitive performance interface with the cockpit instrumentation during sustained in-flight operations, and these plus a large number of additional ones interface with the cockpit during take-off and landing, and during emergency operations or anticipation of emergency situations. This research examines some of the postulated cognitive performance capabilities of the pilot in the cockpit, assesses a possible series of cognitive performance profiles which may characterize these capabilities in male and female volunteers, and assesses effects of selected specific cockpit-related situations, such as engine noise, attending to selected instrument displays while performing different cognitive tasks within a selected sample of cognitive profiles. Cognitive performance in cockpit-related systems interfaces with flight operations and safety, and is known to have contributory relationships with the incidence of aviation accidents due to human error (Billings and Reynard, 1984; Gerbert and Kemmler, 1986; Dille, 1988; Kayton, 1988). A computerized taxonomy of complex cognitive capabilities (Samet, Geisleman, Marshall-Mies, 1986) appeared to offer a reliable method for assessing components of cognitive skill profiles of volunteer pilots and other subjects within a cockpit during variations in noise and mental workload. The objectives of this research were to measure and

examine a series of cognitive performance capabilities and profiles of men and women in cockpit-related systems, and to assess possible effects of low-level engine noise and effects of attending to selected instruments during simulated in-flight operations.

TEST APPARATUS

The cockpit environment used in this experiment was that of the Learjet 25 Flight Simulator. Two computer monitoring screens were placed in front of the test subject seated in the cockpit: (1), one which displayed airspeed on an airspeed indicator and which also displayed altitude on an altimeter, both of which were controlled by a Silicone Graphics IRIS 3120 computer workstation which was located adjacent to the right-side of the cockpit; and (2), one which displayed CCAB, the Complex Cognitive Assessment Battery, which was controlled by a Zenith computer located behind the flight instrument panel in the fuselage. The cockpit noise was that of a KC-135 airplane simulation recorded by a Bell and Howell model 3181 Tape Recorder during sustained near-level flight at 30,000 feet, played at 90 dBA on a Metal Stereo Cassette Deck RT-160 through Pioneer Two-Way Speaker System Model S-313X. The sound pressure levels in the Learjet simulator for aircraft noise "on" and aircraft noise "off" conditions were checked at the subject's ear level by a Quest model 215 (ANSI Type 2) Sound Level Meter.

Fifteen male and fifteen female test volunteers served as test subjects in the Learjet flight simulator. Their ages ranged between 18 and 48 years of age. The average age for this sample of 30 subjects was 25.1 years; a mean of 25.2 for the males, and a mean of 25.0 for the females. These 30 volunteers were primarily students from the University or employees from local aircraft companies; eight of them were pilots. Their cognitive performance capabilities were measured on the computerized Complex Cognitive Assessment Battery (CCAB), which had been developed by the US Army Research Institute, the US Army Medical Research and Development Command, and the TriService Joint Working Group for Drug Dependent Degradation on Military Performance (Samet, Geiselman, and Marshall-Mies, 1986). CCAB measures cognitive performance capabilities and profiles among fourteen cognitive constructs: attention to detail; perception of form; memory retrieval; time sharing; comprehension; concept formation; verbal reasoning; quantitative reasoning; planning; situation assessment; decision making; communication; problem solving; and creativity.

These fourteen constructs are distributed among nine computerized cognitive tests on the CCAB during presentation to each subject on the display of the computer monitor in the flight simulator:

- (1) Tower puzzle (TP): planning; situation assessment; decision making; problem solving; and concept formation.

- (2) Following Directions (FD): attention to detail; memory retrieval; time sharing; comprehension; and verbal reasoning.
- (3) Word Anagrams (WA): Perception of form; memory retrieval; planning; situation assessment; decision making; and creativity.
- (4) Logical Relations (LR): comprehension; verbal reasoning; and quantitative reasoning.
- (5) Mark Numbers (MN): time sharing; quantitative reasoning; decision making; and memory retrieval.
- (6) Numbers and Words (NW): attention to detail; perception of form; memory retrieval; time sharing; concept formation; and decision making.
- (7) Information Purchase (IP): attention to detail; quantitative reasoning; planning; situation assessment; and decision making.
- (8) Route Planning (RP): perception of form; planning; situation assessment; communication; problem solving.
- (9) Missing Items (MI): attention to detail; perception of form; concept formation; quantitative reasoning; communication; and problem solving.

TEST PROCEDURE

Initial screening in the selection of the 30 volunteer test subjects was conducted as follows: hearing (loudness perception) tests at frequencies of 500, 1000, 2000, 3000, 4000, 6000, and 8000 Hz; vision acuity and color tests; blood pressure; heart rate; exercise; personality; questionnaire; and briefing regarding the objectives and procedures of the research experiment. In the Human Factors Laboratory, each subject received a thorough CCAB familiarization training run on each of the computerized complex cognitive tests in the battery: TP (Tower Puzzle); FD (Following Directions); WA (Word Anagrams); LR (Logical Relations); MN (Mark Numbers); NW (Numbers and words); IP (Information Purchase); and RP (Route Planning); and MI (Missing Items). In the next session in the Human Factors Laboratory, each subject was given two complete baseline runs on CCAB, each lasting approximately 50 minutes, with a 30-35 minute break between trials. After familiarization with the Learjet Flight Simulator, each subject took four complete trials on CCAB (two trials of approximately 50 minutes each, with a 30-35 minute break between trials, within each of two sessions), under varying cockpit conditions. Tests were presented in a randomized order within trials. Two levels of noise were presented: 90 dBA KC-135 cockpit noise, or 50-60 dBA ambient noise; dynamic indicators (changes in readings) of

the altimeter and air speed indicator, or static instrument settings (no change in readings) of altitude and air speed. In all sessions, the mission was straight and level flight, performed by an autopilot. The NASA TLX Operator Workload Index was administered to each subject. The order of presentation of the nine cognitive tests was randomly assigned to each of the 30 subjects. During the four test runs in the cockpit, the subject was required to read the altitude and air speed aloud in response to an auditory signal every 30 seconds. Following the four test trails in the flight simulator, each subject returned to the Human Factors Laboratory and took a final baseline trial on CCAB, and a debriefing session.

Several statistical analyses were applied to the research data. A repeated measure statistical design was used for the comparison of cognitive performance among trials for gender (males versus females). A randomized complete block design was used for the comparison of cognitive performance between gender and among cockpit conditions. The cognitive performance was measured by standardized test scores which were calculated by and recorded by the CCAB software. This data was analyzed by the SSAS statistical package on an IBM 3081 mainframe computer. Analysis of variance (ANOVA) was conducted to assess the effects of cockpit conditions upon cognitive test scores and cognitive performance profiles. Duncan's Multiple Range Test was applied to the CCAB data to investigate the differences among the test means within CCAB during trials in the Human Factors Laboratory and test means in the Learjet Flight Simulator.

RESULTS

The cognitive performance profile for the 30 test subjects who took four trials in the Learjet flight simulator is presented in Figure 1. Each point in the profile represents the mean performance for 30 subjects during four trials on each of the nine cognitive tests in the Learjet Flight Simulator. This profile shows that TP (Tower Puzzle), FD (Following Directions), and MI (Missing Items) had the highest mean scores. Mark MN (Mark Numbers) and WA (Word Anagrams) were the next highest, but significantly lower than the first group of tests. LR (Logical Relations) was next, followed by RP (Route Planning) and IP (Information Purchase). The lowest score was NW (Numbers and words). This profile is based on the mean standardized test scores for each of the nine cognitive tests for the 30 subjects.

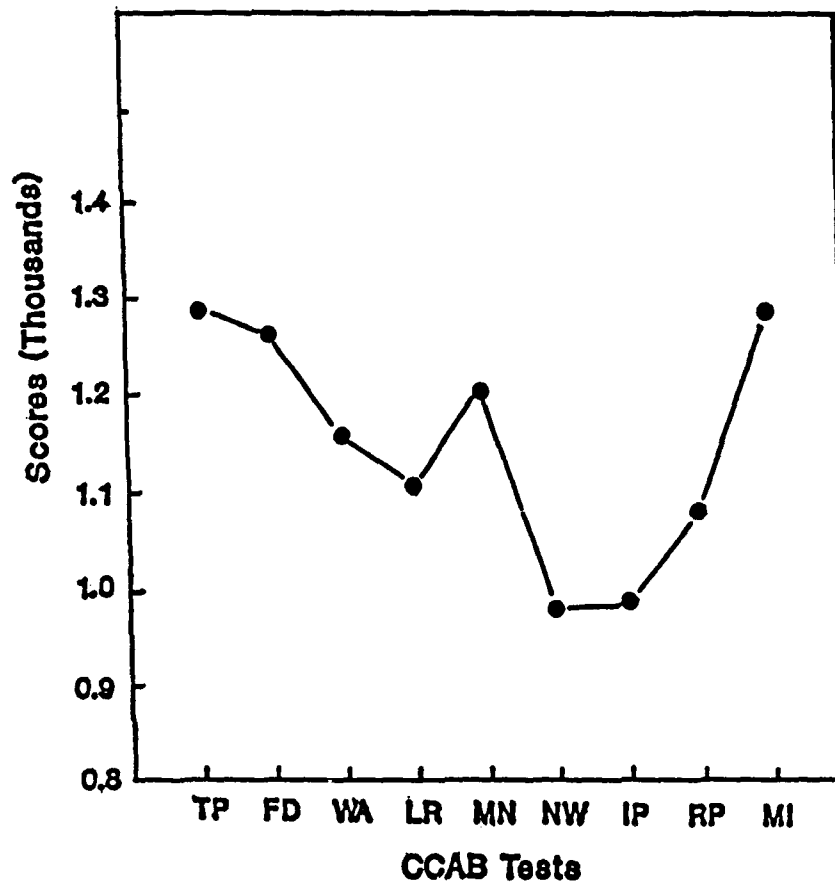


FIGURE 1. COGNITIVE PERFORMANCE PROFILE OF AVERAGE SCORES SHOWING RESULTS FOR 30 SUBJECTS ON EACH OF 9 STANDARDIZED CCAB TESTS.

The results of the analysis of this cognitive performance profile through the application of Duncan's Multiple Range Test are shown in Figure 2. There were five groups of means in terms of their statistical differences among the nine means: (1), MI, TP, and FD; (2) MN and WA; (3) LR; (4), RP and IP; and (5) IP and NW. Group 1 is significantly different from group 2, 3, 4, and 5; group 2 is significantly different from 1, 3, 4, and 5; group 3 is significantly different from groups 1, 2, 4, and 5; group 4 is significantly different from groups 1, 2, and 3; and group 5 is significantly different from groups 1, 2, and 3.

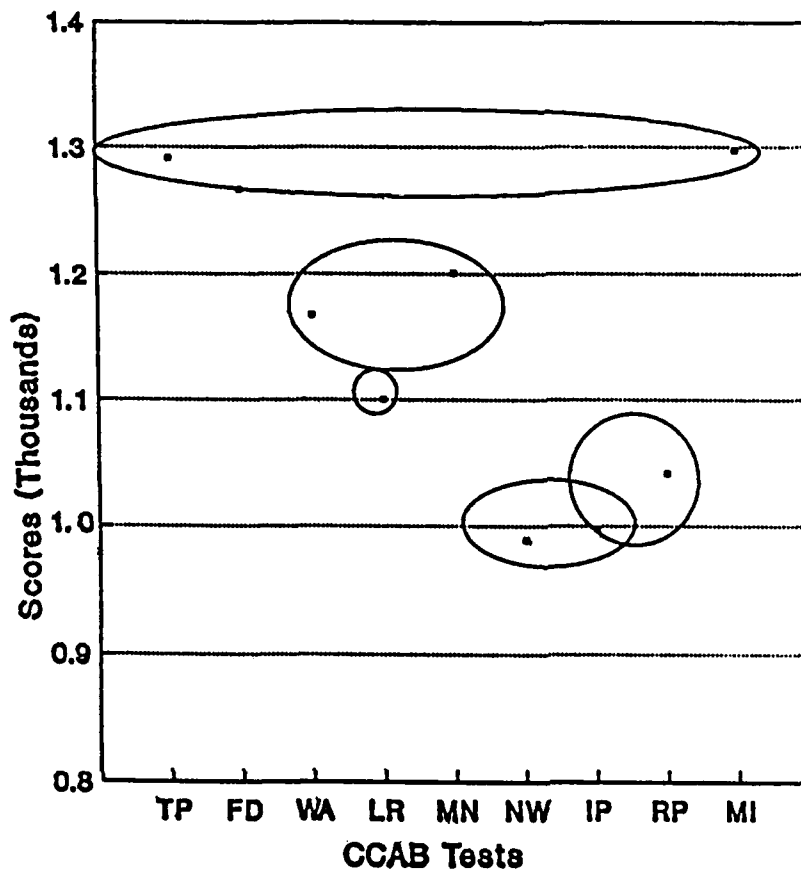


FIGURE 2. APPLICATION OF DUNCAN'S MULTIPLE RANGE TEST ANALYSIS TO CCAB RESULTS.

To assess the effects of cockpit conditions upon cognitive test scores measured in Learjet simulator cockpit, an analysis of variance (ANOVA) was conducted to evaluate differences according to noise effects, instrument effects, individual tests, subjects, and gender. The results of this analysis are shown in Table 1. There were individual differences among subjects. There were no significant gender differences, although males did appear to perform slightly better than females. There were significant differences according to the active versus static instrument variable, and there were significant differences in performance among the nine different cognitive tests. There were no significant significant test scores for performance in the noise (90 dBA aircraft versus the 50-60 dBA) ambient noise. (An analysis of workload data indicated that the subjects worked significantly harder when they were exposed to the aircraft noise than they did under ambient conditions).

TABLE 1. ANALYSIS OF VARIANCE OF CCAB
SCORES IN FLIGHT SIMULATOR

Source	df	SS(Type III)	F
sex	1	51,622.99	0.16
SUB	28	8,998,652.40	11.64 *
instrument	1	410,430.10	14.17*
noise	1	1,831.04	0.07
test	8	13,919,841.97	63.04 *
ERROR	981	27,076,857.80	
total	1020	50,459,236.30	

(* $p < .05$)

To show the means and standard deviations according to gender, instrument, noise, or the nine performance tests, Table 2 is presented to summarize these results. Significant differences are shown among the instrument means and the nine performance test means, but not among the noise means or the gender means.

Figure 3 presents the CCAB test scores graphically, showing the mean static, dynamic, ambient noise, and aircraft cockpit noise scores.

Graphical analysis to illustrate combined effects are shown in Figure 4. This figure presents the individual CCAB test score means according to cockpit test conditions: static (not moving) instruments during ambient (50-60 dBA) conditions; dynamic (moving indicators) during ambient conditions; static instruments during airplane cockpit noise at 90 dBA; dynamic instruments during airplane cockpit noise at 90 dBA.

Analysis of the results of this experiment indicated that neither the altitude nor the air speed readings was sensitive to noise. However, there was a significant gender by instrument interaction, in which the females performed significantly better than the males during dynamic air speed instrument reading conditions. These results are shown in Table 3.

TABLE 2. MEANS AND STANDARD DEVIATIONS FOR
PERFORMANCE TESTS AND COCKPIT
CONDITIONS IN FLIGHT SIMULATOR

Effect	Mean (Standard Deviation)
<hr/>	
Sex	
Male	1152.37 (220.94)
Female	1135.49 (222.54)
Instrument	(*)
Static	1163.81 (222.36)
Dynamic	1124.33 (219.68)
Noise	
Ambient	1144.49 (217.38)
High	1143.47 (226.29)
Test	(*)
TP	1290.74 (271.50)
FD	1266.51 (201.24)
WA	1166.24 (191.46)
LR	1100.47 (210.07)
MN	1200.43 (222.83)
NW	989.24 (183.13)
IP	997.17 (95.34)
RP	1041.34 (177.47)
MI	1297.00 (142.55)
(*) denotes significant difference ($p < 0.05$)	

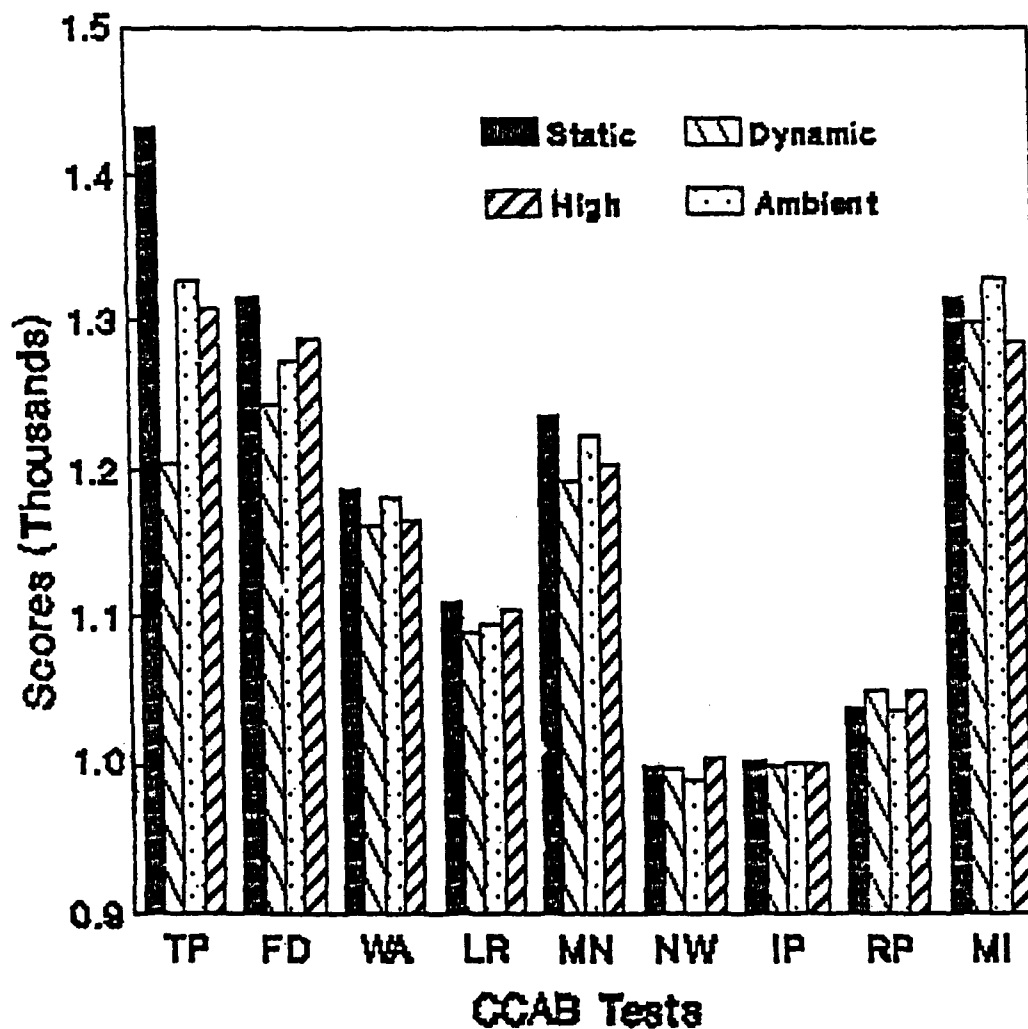


FIGURE 3. EFFECTS OF STATIC INSTRUMENTS, DYNAMIC INSTRUMENTS, COCKPIT NOISE, AND AMBIENT NOISE ON COGNITIVE TEST PERFORMANCE.

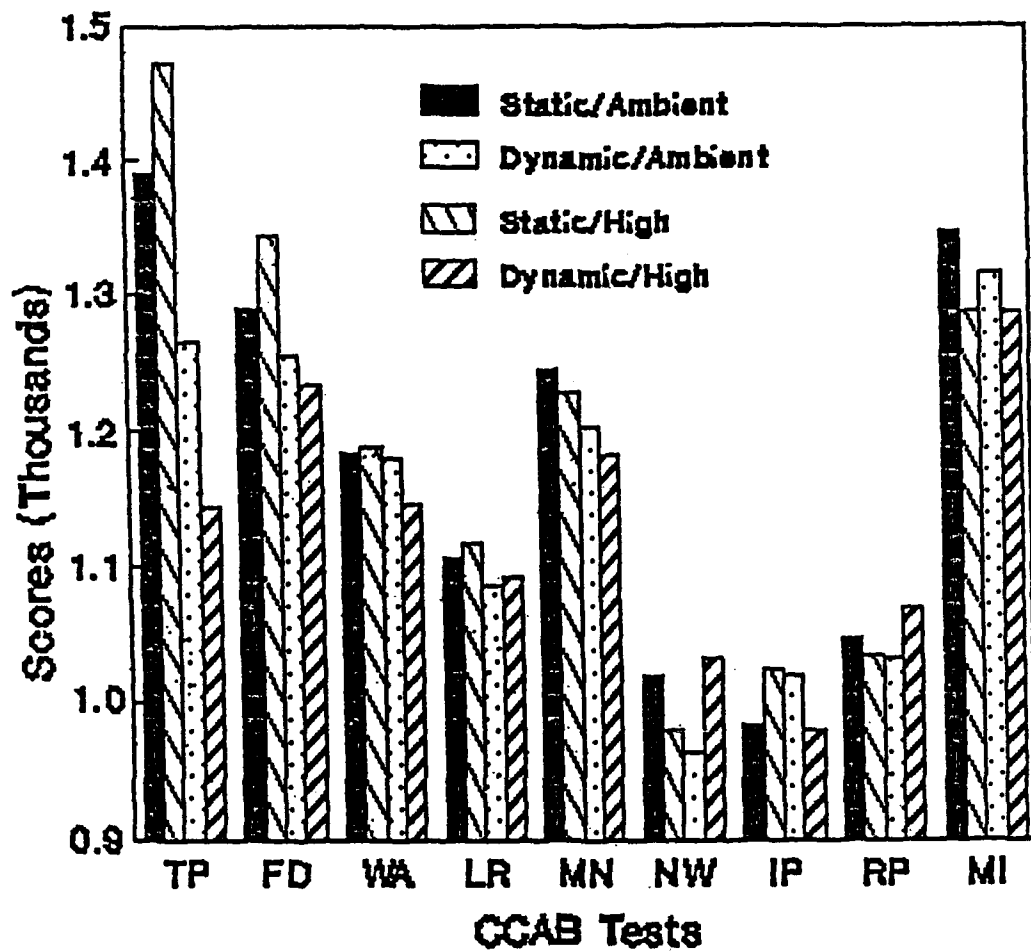


FIGURE 4. PERFORMANCE MEANS FOR EACH COGNITIVE TEST, AS INFLUENCED BY COMBINATIONS OF COCKPIT CONDITIONS.

TABLE 3. ANALYSIS OF VARIANCE OF DATA FROM
AIR SPEED INDICATOR READINGS

Source	df	SS	F
sex	1	0.0092	10.28 *
SUB	28	0.0252	2.64 *
instrument	1	0.0016	4.72 *
noise	1	0.0000	0.02
ERROR	84	0.0287	
total	115	0.0647	

(*) denotes significant difference at 0.05 level

A similar analysis was performed on the percentage correct responses in reading the altimeter. The results of the ANOVA for the mean percentage correct altitude readings are presented in Table 4. Instrument conditions (static versus dynamic) were significant. There was also a significant gender (male versus female) by instrument interaction. Duncan's Multiple Range Test was performed on instrument conditions for males and females. Females performed significantly better during static instrument presentations than during dynamic instrument presentations. For males, there were no significant difference in altitude readings between static and dynamic instrument presentations. For dynamic instruments, there was no significant difference between the performance of males and females. Table 5 presents the mean percentage readings of altitude and the mean percentage readings of air speed.

TABLE 4. ANALYSIS OF VARIANCE OF DATA
FROM ALTIMETER READINGS

Source	df	SS	F
sex	1	0.001	0.37
SUB	28	0.104	1.82 (*)
instrument	1	0.031	15.41 (*)
noise	1	0.001	0.42 (*)
sex*instrument	1	0.012	5.98 (*)
ERROR	83		
total	115		

(*) denotes significant difference at 0.05 level

TABLE 5. MEANS AND STANDARD DEVIATIONS
FOR INSTRUMENT READINGS

Effect	Altitude	Air Speed
Sex		
Male	0.958 (0.051)	0.977 * (0.030)
Female	0.967 (0.054)	0.994 (0.009)
Instrument		
Static	0.978 * (0.036)	0.983 * (0.026)
Dynamic	0.946 (0.061)	0.989 (0.020)
Noise		
Ambient	0.965 (0.047)	0.985 (0.027)
90 dBA	0.960 (0.057)	0.987 (0.020)

(*) denotes significant difference at 0.05 level

In this experiment, gender, instrument, and noise effects were included in the model in order to analyze the subjective workload ratings in

the flight simulator. The NASA Task Load Index (TLX) was the workload measurement procedure used in this experiment. The results of an analysis of variance (ANOVA) of these workload data are shown in Table 6. This ANOVA revealed that instrument conditions had a significant effect on the subjective Task Load Index workload ratings.

TABLE 6. ANALYSIS OF VARIANCE OF NASA TLX OPERATOR WORKLOAD RATINGS

Source	df	SS	F
sex	1	1,416.04	2.82
SUB	27	13,572.90	5.69 *
instrument	1	344.39	3.90 *
noise	1	470.73	5.32 *
ERROR	84	7,426.45	
total	114	23,230.51	

(*) denotes significant difference at 0.05 level

TABLE 7. MEANS AND STANDARD DEVIATIONS OF NASA TLX OPERATOR WORKLOAD RATINGS IN COCKPIT OF FLIGHT SIMULATOR

Effect		NASA-TLX Subjective Rating	
Sex			
	Male	54.4	(14.6)
	Female	61.2	(13.1)
Instrument	(*)		
	Static	55.8	(13.2)
	Dynamic	59.5	(15.2)
Noise	(*)		
	Ambient	55.5	(14.1)
	90 dBA	59.8	(14.3)

(*) denotes significant difference at 0.05 level

Table 7 presents the means and standard deviations for these NASA TLX operator workload ratings. The subjects rated operator workload as being higher (more demanding) during dynamic instrument conditions than during static instrument conditions. Workload ratings for noise were significantly higher during the 90 dBA aircraft noise level exposures than during the ambient noise level (50-60 dBA) condition.

CONCLUSIONS

The results of this experiment lead to the following conclusions.

1. Cognitive performance in the cockpit varied among the different cognitive skill capabilities as measured by the nine cognitive performance tests, suggesting a cognitive performance profile which was above average when compared with the population norm upon which these standardized measures were based.
2. Five clusters of cognitive performance capabilities emerged:
(1) Tower Planning, Missing Items, and Following Directions; consisting of planning, situation assessment, decision making, problem solving, attention to detail, perception of form, comprehension, quantitative reasoning, communication, memory retrieval, time sharing, and verbal reasoning; (2) Mark Numbers, and Word Anagrams; consisting of time sharing, quantitative reasoning, perception of form, memory retrieval, planning, decision making, and creativity; (3) Logical Relations, consisting of comprehension, verbal reasoning, and quantitative reasoning; (4) Route Planning and Information Purchase, consisting of perception of form, planning, situation assessment, communication, problem solving, attention to detail, quantitative reasoning, and decision making; and (5) Information Purchase and Numbers and Words, consisting of attention to detail, planning, situation assessment, decision making, time sharing and quantitative reasoning.
3. There were no significant gender differences among male and female performance means. However, there were significant interactions with instrument conditions.
4. Cognitive performance of the volunteer subjects was more affected by the process of attending to and reading active instruments than it was by attending to and reading static instruments in the cockpit.
5. The presentation of KC 135 noise recordings at 90 dBA did not affect the cognitive performance of the 30 volunteer subjects in the cockpit, as compared with performance of these subjects under ambient (50-60 dBA) noise levels.

6. Using the NASA-TLX workload measures, it was concluded that workload in the cockpit was increased significantly by the KC 135 noise recordings and by the monitoring of active instruments.

REFERENCES

1. Billings, C. E., and Kemmler, R. (1984). Human factors in aircraft incidents: Results of a 7-year study. Aviation, Space, and Environmental Medicine. 55 (10), 960-965.
2. Chambers, R. M. (1988). Current human factors issues in aviation medicine. Proceedings of TECHFEST XV. Annual Meeting of the Wichita Section, American Institute of Aeronautics and Astronautics, and the Institute for Aviation Research. Wichita State University, Wichita, KS.
3. Chambers, R. M. and Kilmer, K. J. (1989). Choosing a Pilot Subjective Workload Scale to Fit Flight Operational Requirements. IAR Report No. 89-21, Institute for Aviation Research, Wichita State University, Wichita, KS.
4. Dille, J. R. (1988). Pilot judgment. Aviation, Space, and Environmental Medicine. October, 997-998.
5. Gerbert, K. and Kemmler, R. (1986). The causes of causes: Determinants and background variables of human factor incidents and accidents. Ergonomics, 29 (11), 1439-1453.
6. Kayton, P. (1988). Human Performance Problems in the 20th Century ATC: What We Must Not Do in the 21st. Paper presented at the Symposium on Aviation Systems Concepts for the 21st Century. Department of Transportation, Transportation Systems Center. Cambridge, MA.
7. Lysaght, R. J., Hill, S. G., Dick, A. O., Plamondon, B. D., Linton, P. M., Wierwille, W. W., Zakland, A. L., Alvah, C. B. and Wherry, R. J. (1989). Operator Workload: Comprehensive Review and Evaluation of Operator Workload Methodologies. Technical Report 851. United States Army Research Institute for the Behavioral and Social Sciences. Alexandria, VA.
8. Samet, M. G., Geiselman, R. E., and Marshall-Mies, R. (1986). Research Report. Analytical Assessments Corporation, Los Angeles, CA.
9. The Federal Aviation Administration Plan for Research, Engineering, and Development. Vols I and II. (1989). U.S. Department of Transportation, Federal Aviation Administration. Washington, D. C.

THE ENHANCEMENT OF AIR TRAFFIC CONTROL SAFETY THROUGH PRE-HIRE
UNIVERSITY BASED TRAINING PROGRAMS

by

Brent D. Bowen
Institute for Aviation Research
The Wichita State University
Wichita, KS 67208-1595

For presentation to the AIAA/FAA Joint Symposium on General
Aviation Systems at the Port O-Call Inn, Ocean City, NJ
on April 11, 1990

THE ENHANCEMENT OF AIR TRAFFIC CONTROL SAFETY THROUGH PRE-HIRE UNIVERSITY BASED TRAINING PROGRAMS

Brent D. Bowen
Institute for Aviation Research
The Wichita State University
Wichita, Kansas 67208-1595

ABSTRACT

This paper proposes a potential means to enhance air traffic control safety through increased human performance capabilities of the nation's Air Traffic Controller Work Force. Research data was gathered from colleges and universities participating in the Federal Aviation Administration's (FAA) Airway Science Program. The Federal Aviation Administration initiated the Airway Science Program in 1983 to facilitate the development of collegiate education programs as a means of meeting future FAA manpower needs, primarily in the area of air traffic control.

The FAA realized that it must update the skill level of its work force to adapt to an increasingly technical and automated environment. This is a major undertaking in that the upgrading of this work force will require the attrition of over 45,000 individuals. Currently, 32 institutions of higher education participate in the Airway Science Program. These institutions represent many established colleges and universities which offer aviation educational programs developed by the FAA.

Research data gathered through this study should allow the Federal Aviation Administration to better understand the potential of the Airway Science Program to enhance air traffic safety. This program allows the availability of a means of pre-hire training through a baccalaureate degree program which stresses technical and managerial capabilities. This will provide an air traffic control work force with the increased human performance capabilities which are required to staff the increasingly difficult systems of our rapidly developing National Airspace System.

INTRODUCTION

Air transportation has become a necessity to this nation. Safe, reliable, and efficient air transportation is a part of everyday life. Aviation has long been at the forefront of technological development. To maintain this vital position of leadership, an increasing level of technological

competence is required of the practitioners in this field. Skilled aviation professionals will be the key to success in the future of aviation. They will be required to have increased technical competence to operate the increasingly difficult systems of our rapidly developing National Air Transportation System. They must also have a significant level of adaptability as our technology progresses.

The mature aviators of today would not have comprehended the ideas of jet engines, of supersonic travel, or of flights into space during their childhoods. Consequently, the young pilots of today may live to see innovations such as hypersonic transportation, e.g., a flight from New York to Tokyo in two hours or less. They may see aircraft utilizing space travel from existing types of airfields. A generation from now, airports and aircraft may be very different from those of today.

The Federal Aviation Administration (FAA) has recognized the need for highly qualified, college-educated aviation professionals for the future. With this need in mind, the FAA developed the Airway Science Program. This baccalaureate college program combines science, management, humanities, and specialty education to meet many of the needs for personnel in the future of aviation ("Careers," 1986, p. 6). As former President Ronald Reagan stated,

Today we stand on the edge of a world in which opportunities are limited only by our own imagination. Our leadership in air and space technology, a leadership we are determined to maintain, has already provided the American people with a rich bounty that has strengthened our economy and bettered our lives.

("Careers," 1986, p. i) The Airway Science Program was designed to provide a sound base of trained professionals which will allow aviation to continue to lead in technological developments in the future. There has never been a more substantial and ambitious training program developed to meet the long-term needs of the aviation industry ("Proposed").

The Federal Aviation Administration has developed the Airway Science Program to meet the needs of the national airspace system of the future. The FAA will spend 15 billion dollars by the end of this century to modernize the air traffic control system and to develop airborne aircraft avoidance systems ("Careers," 1986, p. 4). Through the Airway Science Program, the FAA plans to update its managerial work force to meet the technological demands of the future. The Airway Science Program has as a purpose the training of aviation

professionals for industry as well as for the Federal Aviation Administration ("Careers," 1986).

The Federal Aviation Administration has delegated many aspects of the Airway Science Program to the University Aviation Association (Schukert, 1983, p. IV). The University Aviation Association (UAA) is a membership organization composed of colleges and universities which have aviation educational programs. At the present time, UAA member institutions number 81 ("UAA Membership List," 1988). Of these 81 institutions of higher learning, 32 are recognized as participants in the Airway Science Program (University Aviation Association [UAA], 1989, "AWS"). These recognized institutions must adopt a rigid curriculum which has been developed by the Federal Aviation Administration and approved by the UAA.

The Federal Aviation Administration has pledged to support airway science education through the hiring of up to 500 graduates a year ("Careers," 1986, p. 4). The program was developed in 1983 and offered by 13 participating institutions at that time. The airway science core curriculum consists of 85 credit hours of general studies, math sciences, computer science, management, and aviation.

In the areas of concentration, a student must select one of the five specialized options: (1) Airway Science Management (to train students for air traffic control, air carrier management, airport management, and general aviation operations management); (2) Airway Computer Science (to train students for careers in flight navigation, communications, information processing, and as an FAA computer specialist); (3) Aircraft Systems Management (to train aviation safety inspectors for the FAA and also professional pilots and flight operations managers); (4) Airway Electronic Systems (for troubleshooting, maintenance, testing, development, and FAA electronics technicians); and (5) Aviation Maintenance Management (to train maintenance, troubleshooting, and FAA Aviation Safety Inspectors). ("Airway Science Curriculum")

The FAA has provided grants to the UAA for the purpose of assisting the development of the airway science curriculum in aviation institutions which choose to participate. Grants were given to the University Aviation Association by the Federal Aviation Administration to assist in the cost of designing the implementation procedures for these programs.

Presently, there are 32 recognized Airway Science institutions. The primary attraction for an institution to participate in the Airway Science Program is the pledge by the FAA to hire graduates from these recognized programs and to provide financial assistance in the form of grants to qualifying institutions ("Airway Science Grant"). The Airway Science Program is rigid and insensitive to the academic

requirements of the participating institutions. This has created much difficulty in implementing the program and has forbade the implementation at some institutions.

The Federal Aviation Administration hires non-college educated persons for the same entry-level jobs which are sought by Airway Science graduates. In addition, the FAA hires graduates from "look alike" programs. These programs are similar to the Airway Science Program, yet they do not participate with the University Aviation Association and the Federal Aviation Administration in their guidelines to be a recognized Airway Science Program (Clough, 1988). Therefore, this appearance of a lack of support for the Airway Science Program may present a negative connotation to the participating institutions.

The failure to reach hiring goals has been questioned in that the Federal Aviation Administration has annually increased its hiring for air traffic control positions ("FAA Intensifies," 1988, p. 42). An air traffic controller does not have to go through the Airway Science Program, nor has hiring preference been given to Airway Science graduates. Any person may apply to become an air traffic controller. The applicants go through an evaluation and testing process before being invited to air traffic control school. Upon the successful completion of this program, they become certified air traffic controllers.

Evaluations of the Airway Science Program developed by the FAA seldom have considered the needs, ideas, or opinions of the program coordinators at member institutions. There appears to be a possibility that the delegation of program implementation through the University Aviation Association has put a barrier between the Federal Aviation Administration and the participating institutions. The UAA acts as an intermediary conveying data from participating recognized institutions through themselves to the FAA. These data which are reported by the UAA are basically quantitative and do not contribute subjective information (Gannon, 1989).

STATEMENT OF THE PROBLEM

The Airway Science Program was initiated to meet a perceived need to provide college educated and technically prepared personnel for employment by the Federal Aviation Administration. The expectation was that a significant number of program graduates would be employed each year by the Federal Aviation Administration. The Airway Science Program has not functioned, so far, as it was expected to in making an important contribution to meeting the personnel needs of the Federal Aviation Administration (Clough, 1988).

The problem to be examined in this study may be stated specifically as follows: Why has the Airway Science Program

failed to meet the work force goals for which it was established? Furthermore, it is important to determine if the program will be able to meet these work force goals in the future. Do changes need to be made in the program to allow it to function as was expected? The information which will be collected and analyzed in this study will be used to attempt to answer these questions.

PURPOSE OF THE STUDY

The purpose of this study is to collect and analyze information which can be used in examining the reasons for the failure, thus far, of the Airway Science Program to function as was anticipated. Subjective information about the Airway Science Program as viewed by participating institutions is not available. This is the major type of information which is to be gathered through this study. Each recognized institution has a designated program coordinator who is responsible for the implementation of the Airway Science Program at his or her respective institution (Gannon, 1989). These program coordinators can offer insight into whether or not the Airway Science Program is achieving its objectives. They will also be able to evaluate the current status of program implementation and future needs.

Data should be gathered to gain insight into the needed support by the FAA and UAA for the member institutions. Data concerning students and graduates of the program and other useful information needs to be assembled and summarized to relate the accomplishments of the program.

This study attempts to gain insight from the program coordinators in participating institutions about the progress made in the five years since the program was initiated. Recommendations for improvements which will allow the program to prosper in the next five years and thereafter will be sought.

The information gathered through this study will allow the FAA and the University Aviation Association to better understand the needs of program providers and users. Such information will also be provided to the aviation industry at large on its future prospects for trained aviation professionals. Students will have information available to aid in selecting a program which best suits their needs and aspirations. The identification of any problems encountered during the implementation of the Airway Science Program will certainly be useful to all participants.

The current status of the Airway Science Program needs to be determined before any insight toward its effectiveness or future prospects can be gained. The collection of these data will allow recommendations to be made on how this program may prove to be more useful in the future. The data collected

through this study will allow the reaching of tentative conclusions about ways in which to improve the implementation of the Airway Science Program to meet the Federal Aviation Administration's work force needs.

BACKGROUND LITERATURE

The FAA Airway Science Program was first made public on March 18, 1983, through volume 48, number 54, of the Federal Register. The program was officially titled "Airway Science Curriculum Demonstration Project." The original notice stated that the purpose of the project

... is to compare the performance, job attitudes, and perceived potential for supervisory positions of individuals recruited for several of FAA's technical occupations who have an aviation-related college-level education, or its equivalent, with individuals recruited for the same occupations through traditional methods.

This program was in response to the Federal Aviation Administration's perception of what it called the "... great socio-technological challenge for the 1980's and beyond." ("Proposed," p. 11672)

The program's development came soon after the firing of 12,000 striking air traffic controllers by President Ronald Reagan ("Airway Science Curriculum: Approval"). The work force of the Federal Aviation Administration is composed primarily of persons with technical occupations and high school educational backgrounds. The FAA's purpose for the Airway Science Program is to broaden the base of knowledge of its supervisory and managerial work force ("Airway Science Curriculum: Approval"). This work force must be readily adaptable to the increasing technical and automated environments being developed within the FAA at this time. This is a major undertaking in that the upgrading of this work force will require the attrition of over 45,000 individuals ("Proposed").

The objectives of this program were to provide for: (1) the recruitment/hiring of individuals who have completed or have the equivalent of a model college-level curriculum of general studies, mathematics, science and technology, management, and aviation courses; (2) the evaluation of the concept that individuals with this background recruited for FAA occupations are better able to perform the functions of the job than individuals recruited through existing methods. If this were the case, then that background could be substituted

for general and specialized experience in hiring at the GS-7 level for specific FAA occupations; (3) the assessment of the performance, job attitudes, and potential of airway science individuals versus those of individuals employed by current procedures; and (4) the determination of the impact of this program on the employment in career professions of women and minority candidates ("Airway Science Curriculum: Approval"). The timing of this study allows the comparison of data which were gathered by the FAA to report on the original five-year demonstration project. These data can then be compared to the perspectives of the program coordinators which will be gathered through this study. The hiring estimates throughout the five-year demonstration project were as follows:

TABLE 1. ESTIMATE OF FAA AIRWAY SCIENCE HIRES

	<u>1984</u>	<u>1985</u>	<u>1986</u>	<u>1987</u>	<u>1988</u>
Air traffic controller	70	215	355	355	355
Electronics technician	25	72	122	122	122
Aviation safety inspector	4	10	18	18	18
Computer science	1	3	5	5	5
Total	<u>100</u>	<u>300</u>	<u>500</u>	<u>500</u>	<u>500</u>

("Airway Science Curriculum," p. 32495)

The Federal Aviation Administration contracted with the UAA to conduct the implementation of the Airway Science Program with the colleges and universities which chose to participate ("Airway Science Curriculum Proposal"). The FAA chose to use the University Aviation Association as an intermediary with participating institutions. The UAA then became responsible for assuring that the FAA guidelines for the Airway Science Program would be carried out. Application to participate in the Airway Science Program is made to the UAA after evaluation of application documents from interested colleges and universities. The UAA then transfers required documentation to the FAA, requesting that a particular institution be recognized as a participant in the Airway Science Program ("Airway Science Curriculum Proposal"). Prior to final recommendation by the UAA, a visit is made to the prospective institution to assure that all requirements have been met and that facilities and faculty are satisfactory ("Site"). Airway science member institutions

coordinate all communication on the Airway Science Program through the UAA ("Airway Science Curriculum Proposal").

The University Aviation Association Airway Science Curriculum Committee consists of 15 representatives elected from recognized airway science institutions. Member institutions vary in size from university wide enrollments of 550 to 36,163. With the UAA acting as an intermediary, it is unlikely that the views of all member institutions are addressed by the Airway Science Curriculum Committee, the UAA at large, and then made known to the Airway Science Director at the FAA ("Airway Science Curriculum Proposal").

Presently, there are 32 recognized institutions participating in this program (UAA, 1989, "AWS"). Some institutions have all five airway science options available, while others may have just one airway science option (UAA, 1989, "AWS"). Options available depend on the size of the institution, the technological ability of the institution to provide the appropriate educational training, and the financial resources of the institution.

Current participation in the Airway Science Program may be lessened by the FAA's hiring practices. The FAA continues to hire persons who have only high school educations or other demonstrated professional experience for job categories and levels for which airway science graduates are recruited ("FAA Intensifies"). Little incentive is given to the potential employee to endure a highly structured, quantitative, scientific curriculum of study which would take five years to complete when one without five years of education could apply for and have equal opportunity to obtain the same position. This lack of incentive for a student to participate in the Airway Science Program shall be one of the measurements in the data collection of this study.

The Federal Aviation Administration is receiving considerable pressure from the public to increase the level of safety in air travel ("McArtor"). This has required the FAA to increase the hiring of air traffic controllers and to engage in substantial hiring of aviation operations and safety inspectors ("FAA Intensifies"). These are both options within the Airway Science Program. These work force needs by the FAA are much greater than those projected in 1983 ("Proposed"). Therefore, more opportunity for the employment of airway science graduates exists now than was perceived when the program was originated. This increased employment by the FAA has been mandated by the public; funds were budgeted by the administration, and disbursed by Congress. This increased employment has been directly related to three job categories of the Airway Science Program. The other two job categories of the Airway Science Program will receive considerable shirt-tail effect.

The measurement of support of the Airway Science Program by the FAA can be viewed by its hiring of airway science graduates during the five-year demonstration project. If the Federal Aviation Administration has not hired the graduates it pledged, then an assumption of its lack of support for the program will generally be made by the participating institutions. The Airway Science Program which was developed by the Federal Aviation Administration is not solely intended to provide graduates with FAA careers, but it is also intended to provide a pool of qualified managers for the entire aviation industry ("Careers," 1986).

RESEARCH

The goal of this research was to collect valuable new opinions and perceptions about the Airway Science Program from program coordinators which would aid in the understanding of whether or not the Airway Science Program will have a role in meeting Federal Aviation Administration work force requirements. Discovery of the needs, ideas, and opinions of member program coordinators can add insight into how the program can achieve maximum potential. Through this, an evaluation of the current status of the program will allow a measure of effectiveness to date. In addition to the primary opinion data, demographic data were collected to provide a basis of supportive, descriptive information which would increase the ability of the reader to understand the environment from which data were collected. Both subjective and descriptive data were collected through a structured telephone interview. The interview questionnaire utilized series of open-ended questions which allowed the participants opportunity to discuss their evaluations of the Airway Science Program.

The target group of respondents was the Airway Science program coordinators at each of the 32 institutions recognized by the Federal Aviation Administration as authorized Airway Science colleges and universities. Multiple attempts were made to reach the program coordinator at each authorized institution. The following Table presents a listing of the 32 authorized and participating institutions at the time this study was initiated. A listing of the Airway Science Program options offered at each institution is also given in the Table. The total number of offerings in each Airway Science option is also given.

TABLE 2. AIRWAY SCIENCE RECOGNIZED INSTITUTIONS

Institution	Airway Science Options				
	<u>MGT</u> ^a	<u>CSC</u> ^b	<u>SYS</u> ^c	<u>ELE</u> ^d	<u>MNT</u> ^e
ARIZONA STATE UNIVERSITY Tempe, AZ 32,253*	X		X		
AUBURN UNIVERSITY Auburn, AL 18,280	X		X		
BRIDGEWATER STATE COLLEGE Bridgewater, MA 7,189	X		X		
CENTRAL MISSOURI STATE UNIV. Warrensburg, MO 10,109				X	
CENTRAL WASHINGTON UNIVERSITY Ellensburg, WA 6,775	X		X	X	X
DANIEL WEBSTER COLLEGE Nashua, NH 550	X	X			
DELAWARE STATE COLLEGE Dover, DE 2,153	X		X		
DELTA STATE UNIVERSITY Cleveland, MS 2,289	X		X		
DOWLING COLLEGE Oakdale, NY 4,036	X	X	X		
EMBRY-RIDDLE AERONAUTICAL UNIV. Daytona Beach, FL 6,816		X	X		X
FLORIDA INSTITUTE OF TECHNOLOGY Melbourne, FL 6,497	X		X		
FLORIDA MEMORIAL COLLEGE Miami, FL 1,951	X	X			
HAMPTON UNIVERSITY Hampton, VA 3,230	X	X		X	
INTERAMERICAN UNIV. OF PUERTO RICO Hato Rey, PR 36,163	X	X		X	
JACKSON STATE UNIVERSITY Jackson, MS 6,777				X	
KEARNEY STATE COLLEGE Kearney, NE 9,094	X	X			
KENT STATE UNIVERSITY Stow, OH 22,753	X	X	X	X	X
METROPOLITAN STATE UNIVERSITY Denver, CO 10,457			X		X
MIDDLE TENNESSEE STATE UNIV. Murfreesboro, TN 13,173	X	X	X	X	X
NATIONAL UNIVERSITY San Diego, CA 10,157	X	X	X	X	X
UNIVERSITY OF NORTH DAKOTA Grand Forks, ND 11,658	X	X	X	X	X
NORTHEAST LOUISIANA UNIVERSITY Monroe, LA 9,875	X	X	X		
OHIO STATE UNIVERSITY Columbus, OH 33,637	X	X	X	X	
OHIO UNIVERSITY Athens, OH 1,277			X		

TABLE 2. Continued

<u>Institution</u>		<u>Airway Science Options</u>				
		<u>MGT</u> ^a	<u>CSC</u> ^b	<u>SYS</u> ^c	<u>ELE</u> ^d	<u>MNT</u> ^e
PARKS COLLEGE		X		X	X	X
Cahokia, IL	1,117					
PURDUE UNIVERSITY		X				
West Lafayette, IN	7,300					
ST. FRANCIS COLLEGE		X				
Brooklyn, NY	610					
SAN JOSE STATE UNIVERSITY		X				
San Jose, CA	20,047					
SOUTHERN ILLINOIS UNIVERSITY		X	X	X	X	X
Carbondale, IL	24,227					
SUFFOLK UNIVERSITY			X		X	
Boston, MA	5,444					
TEXAS SOUTHERN UNIVERSITY		X	X			
Houston, TX	6,634					
UTAH STATE UNIVERSITY					X	X
Logan, UT	12,132					
TOTAL.....		25	16	19	14	10

^aMGT - Airway Science Management.

^bCSC - Airway Computer Science.

^cSYS - Aircraft Systems Management.

^dELE - Airway Electronic Systems.

^eMNT - Aviation Maintenance Management.

* Enrollment according to Patterson's American Education, 1989.

Airway Science Program institutions vary in size of enrollment from 550 to 36,163. They are located throughout the United States. There is no geographical apportionment involved in the recognition process. The response group consisted of 20 of the 32 Airway Science Program institutions for a 63% rate of participation. The 63% response rate exceeded the proposed goal of 55% and represented a wide diversity of colleges and universities.

DEMOGRAPHIC DATA

The interview instrument contained five demographic questions which were utilized to provide a basis for understanding the variety of institutions in the response group. Responding institutions represented all five Airway Science Program options. As can be seen from information in Table 3, some program options are more common than others in the respondent group.

TABLE 3. RESPONDENT GROUP AIRWAY SCIENCE OFFERINGS

<u>Airway Science Program Option</u>	<u>Respondent Group</u>
Airway Science Management	16
Airway Computer Science	9
Aircraft Systems Management	12
Airway Electronic Systems	8
Aviation Maintenance Management	6

The Airway Science Management option was predominant in the response group. This option is also more frequent in the total group of Airway Science options (see Table 2). Second in frequency is the Aircraft Systems Management Option. This is the flight curriculum. Several institutions reported utilizing outside vendors (Fixed Base Operators) to alleviate the overhead costs of aircraft.

All Airway Science Program institutions award a Bachelor's degree upon completion of the program. Of the twenty respondents, four reported having Master's level offerings in Aviation and one had a Master's program pending approval. No institutions offered doctoral degrees in aviation aside from aeronautical engineering. However, several mentioned participatory doctoral programs with other departments such as higher education and business.

The Airway Science Program was initiated in 1983. The respondent group included institutions which were approved in 1983 through 1988. The average length of participation of the twenty respondents was 4.1 years with a range of 1 to 6 years. This figure is useful in representing the maturity of the response group. Representation from institutions recognized in the original year of the program and those recognized in the past year, added a diversity of response.

The range of student enrollments in Airway Science Programs was from 5 to 600 for a mean of 104.7. The range of overall enrollment in Aviation at responding institutions was 5 to 1200 for an mean of 369.5. Of the approximately 7,390 aviation students, 2,094 were participating in Airway Science Programs. Twenty-eight percent of all aviation students are enrolled in Airway Science Programs. Some Airway Science institutions do not have other aviation offerings; in those cases, all students are enrolled in the Airway Science Program.

All respondents project growth potential throughout the next two years. Growth projections ranged from little to a 100% increase over the next two years. Five responding institutions reported that administrative caps had been

placed on enrollment. One of these institutions reported that it had 600 freshman applicants for 35 openings. Another institution is only allowing new students into the non-flying aviation management curriculum. Information in Table 4 shows the projected growth over the next two years.

TABLE 4. PROJECTED INCREASE IN ENROLLMENTS NEXT TWO YEARS

<u>Expected Growth Reported</u>	<u>Frequency</u>
100%	4
50	3
30	1
25	1
20	3
10	2
Little	1
*Capacity	5

*Capacity = Program is at maximum allowed capacity and therefore cannot experience growth.

Perhaps the most significant demographic finding is that of known graduates who have been hired by the Federal Aviation Administration. The cumulative response by the program coordinators to the question "How many Airway Science Program graduates from your program (that you know of) have been hired by the Federal Aviation Administration?" was 31. An estimated 1000 Airway Science students have graduated. Much concern was expressed by the respondents to the low number of graduates who have been hired by the Federal Aviation Administration. These concerns are expressed in the subjective response section of this Chapter.

The highlights of the demographic data show that Airway Science Management is the most frequently occurring curriculum option. The response group varies in length of participation from 1 to 6 years (4.1 years average), and 28% of students enrolled in aviation programs are participating in the Airway Science Program. Also of interest is the fact that all institutions were reporting substantial growth opportunities. However, the most significant finding of the demographic section was the fact that the program coordinators know of only 31 graduates hired by the Federal Aviation Administration. This information will provide a point of reference for the presentation of the remaining findings.

RESEARCH RESULTS

The instrument utilized to gather data was comprehensive and required a generous time investment of up to thirty minutes on the part of the respondents. Therefore, a series of yes/no and scaled rating items was utilized in order to examine the subjective opinions of the program coordinators. Several of the yes/no questions allowed for a "why" or "why not" follow-up. The follow-ups which received a reply will be reported in narrative form following a table of the yes/no and scaled responses. Table 5 provides a listing of the yes/no questions and a cumulate of respondent replies.

TABLE 5. YES/NO QUESTION RESPONSES

<u>Question</u>	<u>Yes</u>	<u>No</u>	<u>No Reply</u>
Do you find that students prefer other aviation academic programs which you may offer over the Airway Science Programs?	15	5	0
Do you offer clearly parallel programs?	16	4	0
Do you feel that the Airway Science curriculum is appropriate to overall existing job markets?	16	4	0
To fulfill work force requirements should the FAA be allowed to hire graduates from look-a-like programs for Airway Science Program jobs?	14	5	1
Do you have any scholarship programs exclusively for aviation students?	14	6	0
Are you having difficulty in attracting new students for the Airway Science Program?	8	11	1
Is this true of your other academic programs?	0	19	1
Do you receive grants from the FAA?	9	11	0
Do you anticipate grants in the forthcoming year?	13	7	0

TABLE 5. Continued

<u>Question</u>	<u>Yes</u>	<u>No</u>	<u>No Reply</u>
Are FAA grants important to the existence of your aviation program?	12	8	0
Do you plan to continue participation in the Airway Science Program?	19	1	0
Is the FAA fulfilling its obligations in support of the member institutions?	11	9	0
Is the UAA fulfilling its obligations in support of member institutions?	16	3	1
Would you support having summer internships for Airway Science Program students at the FAA?	19	0	1
Do you see the need for a changing role in the Airway Science Program for the FAA?	9	10	1
Do you see the need for a changing role in the Airway Science Program for the UAA?	6	13	1

Table 6 lists the responses to the questions which asked the respondent to rate his or her opinion of a particular item.

TABLE 6. RATING RESPONSES

<u>Question</u>	<u>Average Response 5Pt.Scale</u>
On a scale of 1-5 with 5 being the most effective, how do you perceive the overall effectiveness of the Airway Science Program in meeting FAA work force requirements?	3.1

TABLE 6. Continued

<u>Question</u>	<u>Average Response 5Pt.Scale</u>
On a scale of 1 to 5, with 5 being the most adequate, do you feel that the Airway Science curriculum of courses is appropriate to the mission of the program?	3.8
On a scale of 1 to 5, is the FAA fulfilling its obligations in support of the member institutions?	3.4
On a scale of 1 to 5, is the UAA fulfilling its obligations in support of member institutions?	4.3
On a scale of 1 to 5, rate your feelings in regard to the UAA establishing and requiring follow-up accreditation visits?	3.8
On a scale of 1 to 5, rate the overall attitudes of your colleagues in higher education toward the Airway Science Program?	3.1
On a scale of 1 to 5, how do you feel about the FAA's plan to modify the Airway Science curriculum?	4.6

Significant findings also resulted from the use of open-ended and follow-up explanation questions. These items provided the opportunity for the program coordinators to qualify many of their yes/no and scaled rating responses. There was also an opportunity to communicate criticism and praise toward the program. Consequently, a complete summary of the program coordinators' perceptions of the role of the Airway Science Program to meet Federal Aviation Administration work force needs could be identified.

Responses to the question concerning why students would prefer other aviation academic programs to the Airway Science Program were consistently in agreement that the Airway Science Program's curriculum was too rigid. The common problem reported was that there was no flexibility to adapt the curriculum to each institution's standards for general education. This resulted in the Airway Science Program being

a 4 1/2 to 5 year program. Also cited were the rigid technical requirements of the program in physics, chemistry, and math. Other curricula criticisms included the inability to have a minor option, failure to allow the institutions input in curricula design, and the perception by students that the Airway Science Program is only to prepare one for employment by the Federal Aviation Administration.

These criticisms were repeated as responses to why institutions are having difficulty in attracting new students for the Airway Science Program while not experiencing difficulty in attracting students to other aviation academic programs. Curriculum inflexibility was also the predominant response when program coordinators were asked about their first concern in regard to the Airway Science Program. The program coordinators also cite this as the primary reason for changing the roles played by the Federal Aviation Administration and University Aviation Association. They commonly expressed a need for the institutions to have a greater role in determining the curriculum. A concern for upholding institutional academic integrity was expressed.

This perceived rigid curriculum also inhibited the motivation of students to participate in the Airway Science Program. Furthermore, a primary motivation for the students to participate in the program was the potential of immediate placement with the Federal Aviation Administration upon completion of the program. According to a majority of the respondents, the Federal Aviation Administration has failed to support the program through the hiring of graduates. This and a feeling of disproportionate grant funding was cited as the primary areas where the Federal Aviation Administration was perceived as not supporting its obligations to the member institutions and the Airway Science Program as a whole. However, 19 of the 20 respondents reported that they plan to continue participation in the Airway Science Program. When asked why, all responded that they had hopes the support would be increased through hiring and funding.

A majority of the program coordinators replied that even though hiring of Airway Science Program graduates has been weak, they felt that the Federal Aviation Administration should be allowed to hire graduates from look-a-like programs for Airway Science Program jobs. Overwhelming work force requirements by the Federal Aviation Administration were cited as the justification. However, some resentment was apparent in response to the Federal Aviation Administration's hiring of non-college graduates for Airway Science Program job categories.

The respondents expressed a consensus of opinion that the Airway Science Program curriculum is appropriate to overall existing job markets. However, they were experiencing difficulty in communicating this to potential students for

the program. They reported that it was difficult to market the Airway Science Program because added rewards for additional effort and expense are not readily apparent. The respondents reported that students are not able to see benefits of the Airway Science Program over parallel programs offered in their own institutions. Placement in business and industry was not reported to be enhanced through completion of the Airway Science Program.

The role of the University Aviation Association in administering the Airway Science Program was ranked significantly more favorable than that of the Federal Aviation Administration. Respondents perceived a concerned effort by the University Aviation Association in support of the participating institutions. All program coordinators were somewhat favorable towards the University Aviation Association response to curriculum concerns. Efforts are being undertaken to provide relief for this significant issue. However, some feel that it is "too little, too late" and will not benefit existing programs without a nearly complete program restructuring process on the part of each institution. Another criticism of the University Aviation Association was the opinion that the Curriculum Committee of that organization is not representative of the diversity of institutions which are participating in the Airway Science Program. Also criticized were the long terms which committee members serve. Some feel that members' interests would be better served through shorter terms and more representation.

DISCUSSION OF RESULTS

Significant subjective findings include common recurring perspectives of the program as expressed by the program coordinators. They include recommendations that both the Federal Aviation Administration and University Aviation Association become more open-minded toward the needs of the participating institutions. Also, more responsibility for curriculum design should be given to the institutions. Efforts which are being made in curricula restructuring are viewed with skepticism. The curriculum is felt to be a secondary issue which has been given a primary focus.

The primary issue which should be addressed, according to many of the respondents, is the failure to provide the promised number of jobs to Airway Science Program graduates during a time when the Federal Aviation Administration is making thousands of new hires. Secondly, it is perceived that the Federal Aviation Administration is not funding the program adequately with grants to participating institutions. While significant grants were reported from the respondent group, a total of \$14.558 million, they were not considered to have been equitably distributed.

This study has resulted in many diverse findings. Program coordinators perceive the Airway Science Program to be a very good concept to help meet Federal Aviation Administration work force needs. This was the predominant feedback throughout most interviews. Information in Table 6 shows that the respondents rate the overall effectiveness of the Airway Science Program 3.1 on a 5.0 scale. This rating resulted in an above average measure on the scale. In applying this finding to the subjective opinions expressed by the respondents it was apparent that they perceived the program to be of significant value to the field of aviation. However, difficulties in agreeing how the program should be implemented, problems with the current status of implementation, and unfulfilled expectations have resulted in preventing this rating from being higher.

A noteworthy amount of criticism was made about the curriculum of the Airway Science Program. However, the appropriateness of the curriculum was measured at 3.8 on a 5.0 scale. Through comments recorded throughout this study, this high rating could be attributed to the fact that the program coordinators, as scholars, liked the demanding technical curriculum. Yet, as administrators facing rigorous program reviews in an era of academic accountability, they need a less demanding curriculum to attract and retain more students within this degree program. It is interesting to note from the data presented in Table 6, that respondents rated their colleagues' perceptions of the Airway Science Program to be equal to their own 3.1. Additionally, from the information measured in Table 6, it was found that the program coordinators overwhelmingly support the Federal Aviation Administration's plan to modify the Airway Science Program curriculum to allow more flexibility, by rating it 4.6 on the 5.0 scale.

Comparison was made between the Federal Aviation Administration and the University Aviation Association in how the program coordinators perceived each organization's role in fulfilling obligations to member institutions. The Federal Aviation Administration was rated at an average of 3.4 while the University Aviation Association was rated at 4.3 on the 5.0 scale. There are several explanations why this disparity may exist. The respondents are members of the University Aviation Association. Hence, there is a more collegial atmosphere between them and the University Aviation Association. They are able to participate in many of the decisions which are made by the University Aviation Association, whereas, the Federal Aviation Administration is a bureaucratic government agency. Respondents were not without praise or criticism for each. Generally, they commented that both had done well given the circumstances. The consensus was that more flexibility should be given to the institutions.

Highlights of the findings reported in Table 5 include the fact that 16 Airway Science Program institutions offer clearly parallel degree programs to the Airway Science Program. This indicates that the responding institutions feel that they can design programs better suited to institutional needs. Also of significance is the fact that 19 respondents report no difficulty in attracting students for parallel programs. Eight respondents reported difficulty in attracting students to the Airway Science Program. It should also be noted that in some Airway Science Program institutions, all aviation students are in Airway Science Programs. There is no parallel program.

Popularity of aviation programs in higher education is easily identified from information presented in Table 4. All institutions reported growth if the programs were not limited by capacity. Growth projections for the forthcoming two years range from 100% to a minimum of 10% with one reporting "little growth." This popularity was further confirmed by the fact that few institutions reported any type of marketing or promotional activities to recruit students.

Initially, the most attractive feature of a college or university's participation in the Airway Science Program was the potential of receiving grants from the Federal Aviation Administration to fund the program. Nine respondents reported receiving grants totalling \$14.558 million. Revealing the specific range of the grant awards would compromise the confidentiality of this study. Criticisms of the grant program included comments that awards were not being assigned proportionately among participants and that political maneuvering had been used to obtain grants. Thirteen respondents reported anticipation of grants in the forthcoming year. Twelve consider future grants vital to continuing their aviation programs.

The final research objective was to report the opinions of the program coordinators on how to make the program more effective. Information in Table 7 summarizes the responses to this question.

TABLE 7. RESPONDENTS' RECOMMENDATIONS TO INCREASE PROGRAM EFFECTIVENESS

<u>Theme</u>	<u>Number of Responses</u>
Federal Aviation Administration should hire more Airway Science Program graduates.	10

TABLE 7. CONTINUED

<u>Theme</u>	<u>Number of Responses</u>
Curriculum should be more responsive to institutional needs.	8
Industry involvement should be promoted.	5
Federal Aviation Administration should support the program with increased and proportionate grant funding.	4

These recommendations coincide with criticisms which the program coordinators expressed throughout the interview process. The consensus is that the Federal Aviation Administration should act in the areas of supporting the program through hiring, funding, and addressing institutions' concerns about the curriculum. The respondents are extremely favorable about the Federal Aviation Administration's proposed plan to allow more flexibility in the curriculum. It is apparent that the response group does not feel that the Federal Aviation Administration has fulfilled all of its obligations to the Airway Science Program. Until these expectations are met, the Airway Science Program cannot achieve its maximum potential.

CONCLUSIONS

(1) The program coordinators feel that the Airway Science Program is extremely vital to the future of aviation in higher education. They also feel that it is valuable to the overall aviation industry. The program coordinators reported throughout the survey that the Federal Aviation Administration and the University Aviation Association need to work towards the final refinement of the Airway Science Program. They stated that this should include the pursuit of the original plan to utilize the Airway Science Program to meet stated work force needs of the Federal Aviation Administration.

(2) The most commonly recurring criticism of the Airway Science Program was the negligible hiring of Airway Science Program graduates by the Federal Aviation Administration. The mission of the Airway Science Program was to serve as a means of meeting a rapidly increasing Federal Aviation

Administration work force need which has continued to accelerate throughout the duration of the program. Much concern was apparent from the failure of the Federal Aviation Administration to comply with this most important mission of the program. This criticism resulted from visible Federal Aviation Administration practices of hiring graduates from look-a-like parallel programs and especially from the hiring of individuals who have no college degree. Therefore, the Federal Aviation Administration must act on this issue before the perceptions of the program coordinators toward the Airway Science Program will improve.

(3) Curriculum restructuring was viewed with extreme favor by the respondent group. The program coordinators view the Airway Science Program curriculum with favor as scholars and visionaries of industry needs. However, they expressed concern about the inadequacies of the current curriculum to meet institutionally mandated requirements for general education. To meet the requirements, up to an additional two semesters of study are required of the students above the four-year mandated Airway Science Program.

(4) Parallel programs to the Airway Science Program are offered at 16 of the 20 respondent institutions. These look-a-like programs are being utilized to meet the needs of all parties. The FAA hires graduates from these programs to meet their work force needs. The Airway Science Institutions use them to attract students to their aviation departments. Students use them to fulfill their needs for a more responsive academic program. Hence, competition exists between these programs. A parallel program is clearly more popular than the Airway Science Program.

(5) The Airway Science Program is not responsive to the needs of students. Because of this it is difficult for the institutions to market the program and recruit students. The inflexibility of the curriculum, its costly added year of studies, and no significant chance of hiring by the Federal Aviation Administration gives students no above normal motivation to participate in the demanding Airway Science Program. In some regards, participating in the Airway Science Program is even potentially detrimental to students by putting them behind in entering industry for an additional year and for allowing no studies in the areas of business, professional education, or other complementary areas.

(6) It appears that institutions have established Airway Science Programs for the sake of competing for Airway Science Program grant funds. They have an Airway Science Program as an add-on curriculum to serve this purpose. Institutions receiving grants were obviously not critical about the grant program. Those not receiving grants were critical of the grant program and voiced concerns of inequity and political ploy.

SUMMARY

This study has attempted to gain insight from the program coordinators in participating Airway Science institutions about the role of the Airway Science Program in meeting the air traffic control work force needs of the Federal Aviation Administration. Information gathered through this study should allow the Federal Aviation Administration, University Aviation Association, and other participants in the Airway Science Program to better understand the needs of the program providers and users. Such information should also be useful to the aviation industry at large for analysis of the impact of the Airway Science Program.

REFERENCES

- Airway science curriculum proposal (No Date). Washington, DC: Federal Aviation Administration.
- Airway science curriculum: Approval of demonstration project final report (Federal Register Vol. 48, No. 137, No Date). Washington, DC: Office of Personnel Management.
- Airway science grant program (No Date). Washington, DC: Federal Aviation Administration. Airway science recruiting. Washington, DC: Federal Aviation Administration.
- Careers in airway science (1986). (3rd ed.). Washington, DC: Federal Aviation Administration.
- Clough, D. L. (1988). Airway science curriculum demonstration project: Summary of initial evaluation findings (Report No. DOT/FAA/AM-88/5). Washington, DC: Federal Aviation Administration.
- FAA intensifies, streamlines controller recruiting effort. (1988, August 15). Aviation Week & Space Technology, p. 42.
- Gannon, J. N. (1989). University Aviation Association. Telephone interview. January 19, 1989.
- Guidelines for an airway science curriculum. Washington, DC: Federal Aviation Administration.
- McArtor orders industry-wide assessment of pilot training (1987, August 24). Aviation Week & Space Technology, pp. 20-21.

Myers, J. (1989). Federal Aviation Administration.
Telephone interview. January 18, 1989.

Proposed demonstration project: Airway science curriculum
(Federal Register Vol.48, No. 54). Washington, DC:
Office of Personnel Management.

Schukert, M. A. (Ed.). (1982). Collegiate aviation
directory: A guide to college level aviation/aerospace
study. Dubuque: Kendall/Hunt.

Shifrin, C. A. (1986, March 31). FAA implements changes in
controller training program. Aviation Week & Space
Technology, pp. 47-53.

Strickler, N. K. (1983). Guidelines for federal aviation
administration regional aviation education coordinators
and aviation education facilitators (Report No. DTFAOI-
83-Q-82331). Washington, DC: Federal Aviation
Administration. (ERIC Document Reproduction Service No.
ED 247118)

University Aviation Association. (1989). AWS recognized
institutions (Status Rep. 06-09-88). Opelika, AL:
Author.

University Aviation Association. (1988). UAA membership
list - July 1988. Opelika, AL: Author.

**DYNAMIC BEHAVIOR OF THE HUMAN BODY SUBJECTED TO IMPACT
CONDITIONS WITH AND WITHOUT RESTRAINT**

by

Hamid Lankarani
Deren Ma
and
Gayle Ermer
Mechanical Engineering Department
Institute for Aviation Research
The Wichita State University
Wichita, KS 67208

For presentation to the AIAA/FAA Joint Symposium on General
Aviation Systems at the Port O-Call Inn, Ocean City, NJ
on April 11, 1990

DYNAMIC BEHAVIOR OF THE HUMAN BODY SUBJECTED TO IMPACT CONDITIONS WITH AND WITHOUT RESTRAINT

Deren Ma, Graduate Research Assistant
Gayle Ermer, Graduate Research Assistant
Hamid Lankarani, Assistant Professor

Mechanical Engineering Department
Institute for Aviation Research
The Wichita State University
Wichita, KS 67208

ABSTRACT

A simple multiple-segment model of the human body is developed in order to examine its dynamic response under the action of external forcing conditions. The system is modeled as a collection of rigid elements interconnected by an array of kinematic joints constraining the relative motion of the elements. These elements include upper body combined with head and neck, lower legs, and thighs. Nonlinear rotational springs are incorporated at the joints accounting for the anatomical characteristics and limits. The constructed model is used to simulate the post-crash behavior of an aircraft pilot or passenger during surges such as frontal side collisions and crashes in the vertical plane. A mathematical representation of the seat and interaction of the passenger with the seat cushion and back is developed. Restraints representing the seatbelts are also introduced in the model in a few different configurations. The complete model is then subjected to various pulse accelerations or decelerations in different directions. To perform a dynamic analysis, a three-dimensional code is developed that generates and numerically solves the governing differential equations of motion in a systematic fashion. This feature of generality allows future additions to the present simple model or construction of more advanced models in a convenient way. This computerized model and the results of the simulations provide a base for predicting the motion behavior of the human body parts during crashes, understanding the effects of various types of seats and seatbelts on passenger safety, and design of mechanisms for crash protection and cockpit cabin interior elements.

INTRODUCTION

Passenger safety is a major concern for those in the airline industry. The progressively greater number of aircrafts and the need to speed up the travel periods have led to an increase in the

potential for human injury. There is no doubt that studies on vehicles safety - both airplane and automobile, have increased vastly in the past decades, but much still needs to be done in the area of post-crash behavior and crash protection for vehicle occupants.

PURPOSE

One main problem of interest for aerospace and automotive designers is how to arrange seats, restraints, and interior elements of a cockpit cabin or a car to reduce the amount of passenger injury in specific types of collision situations. In order to design for safety, the characteristics and the dynamics of motion of the human body under various external accelerations, generated by surges such as collisions, need to be known. If the motion characteristics of the human body parts can be predicted, a safe design of the elements of a car interior or airplane cockpit / cabin becomes feasible.

The design of passenger restraint systems is also a topic of concern. Lap belts and shoulder harnesses allow different types of body motion, as do other types of restraints such as air bags. Mathematical modeling of these restraints is an essential part of crash protection studies. Prediction of human body motion under the effect of a specific restraint system yields important information on the effectiveness of the system.

Much of the research in the area of the human body crash dynamics is obtained by using dummies, which are biomechanically similar to human bodies, and physically simulating the crash situation to study the different kinds of motion involved. This type of testing, although yielding many good results, is very expensive, and is limited by the physical accuracy of the biomechanics of the dummy. Repeated trials for this type of destructive testing are time consuming, and for aerospace applications, actual crash simulations may not even be possible. A way to study crash response of a human body, by mathematically simulating the effects using a computer model, can be much more convenient. It will also yield more data with much less effort and expense. Such model is used in this study, and various dynamic simulations are performed on the model accordingly.

BACKGROUND

Several studies have been performed in the area of computer simulation of body crash dynamics. Varieties of two- and three- dimensional occupant models have been used over the years to simulate a body motion in crash situations. Some that figure prominently in the literature are listed here. Different versions of CAL2D [1,2], HSRI2D [3], MVMA2D [4], SIMULA [5], PROMETHEUS [6] occupant simulation models use lines, circles, or ellipses as the shape of body segments, and have been used for simulations for a variety of collisions with and without restraints. These models however, are all two-dimensional models, and

cannot be used for simulations of side impact, or when elements have rotations about axes not perpendicular to the plane of impact. CAL3D or CVS model, developed by Bartz [7], and its several modifications by Fleck et. al [8,9], model impact in three dimensions. But, the seat cushion and back interaction with the passenger is not modeled. The MADYMO crash victim simulation program [10] has been used for specific automobile (front and side) collisions. The models developed by Goldsmith, Denny, and Merrill [11,12] have been used to study head-neck response subjected to different impulsive loadings.

The prescribed models and simulations performed on them range in complexity from relatively simple to very complex. Some of these simulation results have been verified by comparing them with the actual test results performed on dummies, and most have been found to accurately represent real events. However, the analyses with these models have been performed for only specific configurations of automobile crashes on ground surface. Crash protection studies for aircraft passengers have drawn little attention. The gross-motion simulators are not formulated to be general purpose programs, which can handle all impact situations. In addition, lack of generality causes major difficulties for minor modifications to the models. The existence of numerical instabilities in the solutions, resulted from numerical integration, has also been a problem encountered by all. It is hoped that the analysis programs developed for this study will yield a very general format for developing human body models, starting with one that is very simple and capable of handling much more complex configurations. Once a general model is constructed, many different types of forcing conditions in both horizontal and vertical planes may be applied to the model in order to simulate a variety of aircraft crash types. In order to enhance the numerical stability of the solution, a state-of-the-art multi-step predictor/corrector numerical integration routine with variable stepsize and variable order selection is employed in the analyses.

The specific goals of this study include the following. A computer environment is to be set up which will allow simulation of a human body movement relative to the passenger seat using a system of constrained rigid elements. Forcing conditions are then applied to the seat to approximate the impact conditions of front and side crashes, as well as vertical impacts resulting from crashes in the vertical plane or from a seat ejection. A rigid element model of the human body is described, and mathematical equations are developed to represent the passenger seat interface. These equations, along with the equations of motion for the constrained multi-element system are solved numerically under different forcing conditions. Graphical results in the form of history of response are presented. The results of the analyses or simulations are also run through a developed post-processing program in order to obtain graphical images of the model at different configurations or time junctures.

MODEL OF THE HUMAN BODY AND THE SEAT

In general, there are two major parts in the study of the behavior of an aircraft passenger in various impact situations. A mathematical model must first be developed such that it

represents the human body and mimics its behavior as closely as possible. This model will be referred to as a multi-element or multi-segment model, and it will contain information on elements, their initial configuration, connectivity or topological information, and the present forces. Once the model is constructed, dynamic analysis must be performed in order to simulate the motion of the system under different excitations. This requires formulation and solution of the governing equations describing the motion of the system. This section describes a simple model containing the physical and the geometrical characteristics of both the human body and the seat. The goal of the study has been the development of capabilities for analysis such that future more complex models may be simulated without much effort. More advanced models which may include pelvis, spine, thorax, neck elements, brain, and also the muscle actions will be further extensions of this study.

A simple human body model resting on a seat is shown in Fig. 1. The seat is described as a prismatic element with two planar rectangular surfaces which are perpendicular to each other. The model of the human body consists of three elements: lower legs, thighs, and upper body combined with head. The elements are connected with revolute joints to mimic the behavior of hip- and knee- joints. Torsional spring-dampers are incorporated at each revolute joint to model the biodynamic muscle tension in the joints. An elastic stiffness with viscous damping determines the joint torque up to the joint limits or stops. A sharply-increasing nonlinear and energy dissipating behavior characterizes the joint, when its angle extends beyond the stops. Due to the muscle actions, the joints tend to settle around an equilibrium or natural angle. The joint spring torque is shown in Fig. 2. Note that the addition of viscous damping and friction provides further dissipation of energy, but does not change the equilibrium angle.

The interaction of different elements with each other or with the surrounding was represented by a Hertzian contact force model with local permanent deformations [13]. If there is a penetration of an element onto another or onto the cockpit /cabin interior, contact forces are generated at the surfaces of colliding elements. These forces, shown in Fig. 3, produce local deformations or indentations at the contact surfaces. The forces, and their corresponding moments about the elements mass centers, are applied on pairs of penetrating elements.

SELECTED COORDINATE SYSTEM

A set of Cartesian coordinates was used to describe the three-dimensional configuration of the modeled system of the human body and the seat at any instant. The use of Cartesian coordinates and resulting formulation of the equations of motion in a Newtonian form allow the modeling of both open chain systems (such as the tree structure of a human body), and closed chain systems (such as the spine-ribs-sternum loop). This selection yields a general model to which various components can easily be added. Furthermore, it enhances simplicity of the numerical formulation or generation of the governing equations of motion and numerical development of the solutions. Since rotations in space are non-cumulative in nature, and angular velocity vector cannot be represented as the time derivative of a set of angles, the

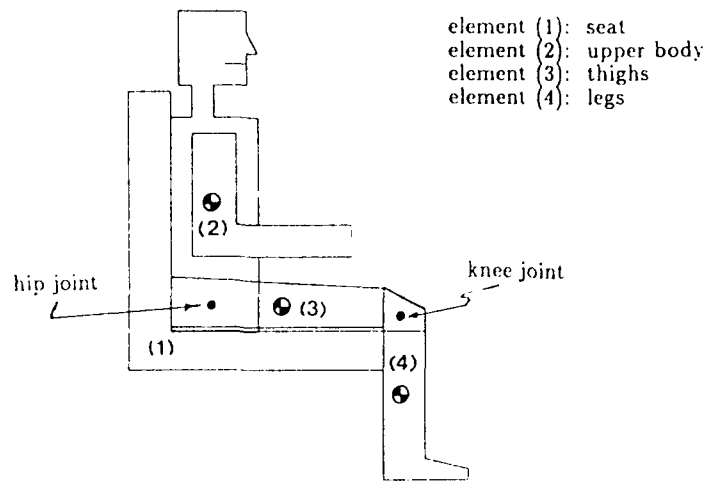


Figure 1. Model of the human body and the seat.

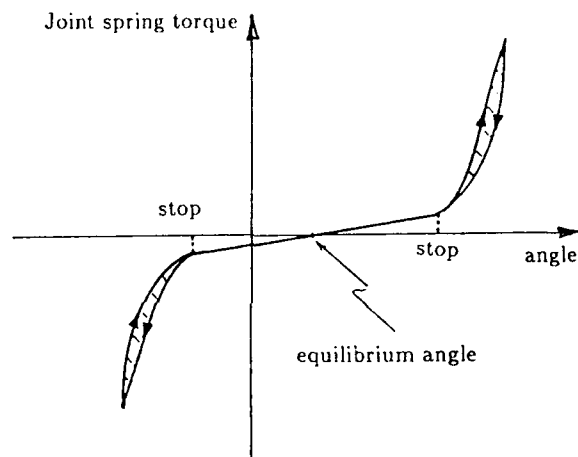


Figure 2. Spring torque at the joints.

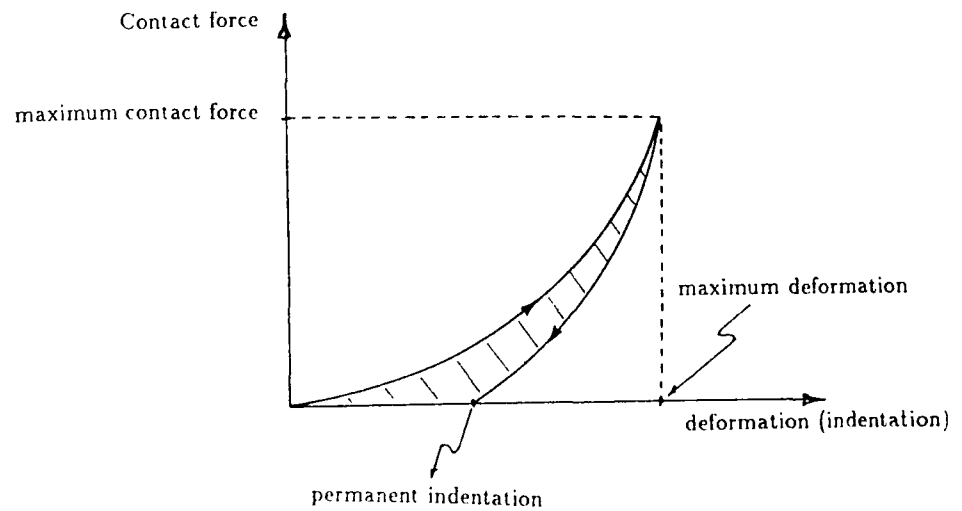


Figure 3. A Hertzian contact force model with local permanent indentation.

selection of rotational coordinates for the three-dimensional modeling and analysis is very important.

A general element "i" of the multi-element system under consideration is shown in Fig. 4. A set of local element-fixed coordinate axes ξ_i, η_i, ζ_i with origin at the element mass center C_i is attached to the element. To obtain the configuration of the element in a non-moving (inertial) reference frame xyz , it is sufficient to specify the spatial location of point C_i and the angular orientation of the local axes. A vector of Cartesian coordinates for the element, \mathbf{q}_i , contains

$$\mathbf{q}_i = [\mathbf{r}_i^T, \mathbf{p}_i^T]^T \quad (1)$$

where $\mathbf{r}_i = [x, y, z]_i^T$; $\mathbf{p}_i = [\mathbf{e}_0, \mathbf{e}^T]_i^T = [e_0, e_1, e_2, e_3]_i^T$; and symbol T performs the transpose operation. The parameters e_0, e_1, e_2 , and e_3 are a set of normalized quaternions known as Euler parameters describing the rotational configurations [14]. These are chosen instead of three independent angles, for the purpose of convenience of transformations, efficiency of manipulations, and their singularity-free nature. These Euler parameters are defined in terms of the components of a unit vector $\bar{\mathbf{u}}$ along the orientational axis of rotation, and an angle of rotation φ as

$$\begin{cases} e_0 = \cos \frac{\varphi}{2} \\ \mathbf{e} = \bar{\mathbf{u}} \sin \frac{\varphi}{2} \end{cases} \quad (2)$$

For the mechanical system of interest, which contains the human body elements and the seat, vector of coordinates \mathbf{q} must contain the Cartesian coordinates of all the elements in the system. It is apparent that the components of vector \mathbf{q} cannot be chosen arbitrarily, since the kinematic joints, namely the hip- and the knee- joints, constrain the relative motion of the elements. Let the dependency of the coordinates be described by some holonomic algebraic constraint equations

$$\Phi(\mathbf{q}) = 0 \quad (3)$$

The velocities $\dot{\mathbf{q}}$ and accelerations $\ddot{\mathbf{q}}$ of the elements must satisfy

$$\text{velocity equations:} \quad \dot{\Phi} = \Phi_{\mathbf{q}} \dot{\mathbf{q}} = 0 \quad (4)$$

$$\text{acceleration equations:} \quad \ddot{\Phi} = \Phi_{\mathbf{q}} \ddot{\mathbf{q}} + \gamma = 0 \quad (5)$$

where

$$\gamma = -(\Phi_{\mathbf{q}} \dot{\mathbf{q}})_{\mathbf{q}} \dot{\mathbf{q}} \quad (6)$$

and dot symbol and subscripts respectively represent the time and the partial differentiation.

The global and the element-fixed local coordinate systems are shown in Fig. 5. The Cartesian coordinates chosen together with the constraint, velocity, and acceleration equations completely describe the geometrical characteristics or the kinematics of the system.

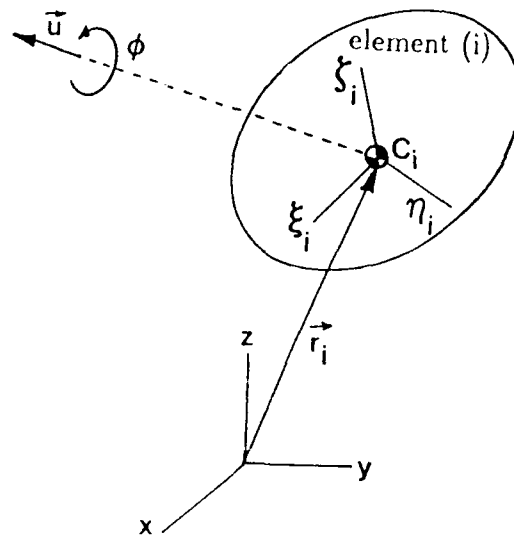


Figure 4. Configuration of an element "i" with respect to the xyz inertial frame of reference.

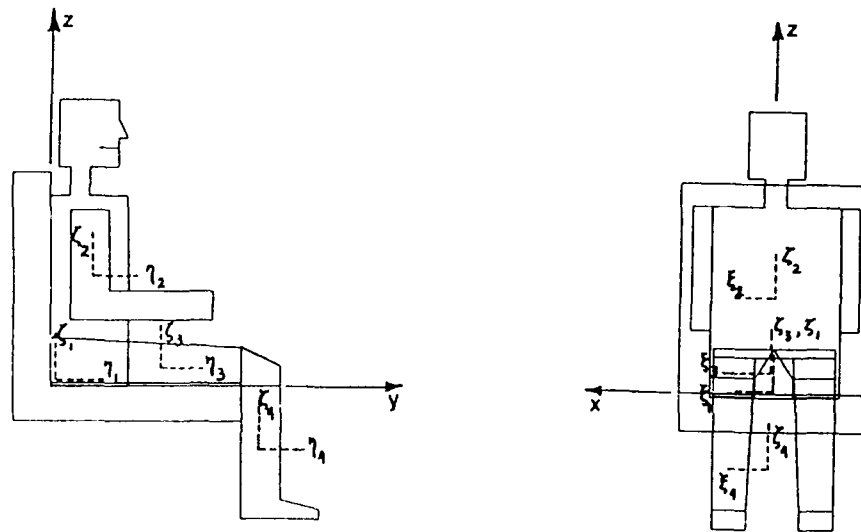


Figure 5. Initial configuration of the body elements and the seat (side and front views).

SEAT/PASSENGER INTERFACE

The interfacial deformation between the seat cushion and back with the passenger is represented by a number of unilateral translational spring-dampers. The corresponding forces are generated only when there is some penetration of back side of the upper body or bottom side of the thighs on the seat surfaces. A general algorithm was developed in order to determine the penetration of any point on the body surface with the seat having any geometry. This general configuration is shown in Fig. 6. Local coordinates are attached to the seat (element "i") and the upper torso (element "j"). The seat has a constant normal vector to its front surface n_0 . The objective is to find the distance d between a point P on the body to the front surface of the seat. Vector ℓ connecting point P to the seat mass center has global coordinates

$$\ell = \mathbf{r}_j + \mathbf{s}_j^P - \mathbf{r}_i \quad (7)$$

where \mathbf{s}_j^P is a vector locating point P on element "j", and \mathbf{r}_i and \mathbf{r}_j are the translational coordinates of the two elements. For the simplicity of the transformations, all vectors may be described with respect to the upper torso (or the $\xi_i\eta_i\zeta_i$ coordinate system). Thus, vector ℓ is evaluated in terms of the rotational transformation matrix of the upper torso \mathbf{A}_i as

$$\ell'_i = \mathbf{A}_i^T \ell \quad (8)$$

where the quantity $(.)'$ describes the component of a vector in local or element-fixed coordinate systems. The distance d to the seat is hence evaluated as

$$d = (\mathbf{n}'_0)_i^T \ell'_i - d_0 \quad (9)$$

and d_0 is the geometric constant distance to the seat front surface as shown in Fig. 6. The time derivative of the distance d is

$$\dot{d} = (\mathbf{n}'_0)_i^T \dot{\ell}'_i \quad (10)$$

where $\dot{\ell}'_i = \dot{\mathbf{A}}_i^T \ell + \mathbf{A}_i^T \dot{\ell}$.

Once there is a penetration d between the surfaces of the body and the seat, the penetration force is evaluated in a Kelvin-Voigt viscoelastic representation as [13]

$$f = kd + c\dot{d} \quad (11)$$

where k is the spring stiffness approximated for a maximum penetration of 2 cm for a 50th percentile male, and c is a damping coefficient taken as the critical value. This unilateral spring-damper force representing the interaction between the seat and the passenger is shown in Fig. 7. An alternative method, which will be the subject of future extensions of this study, is to use a Hertzian type penetration force as

$$f = Kd^{1.5} + \mu d^{1.5}\dot{d} \quad (12)$$

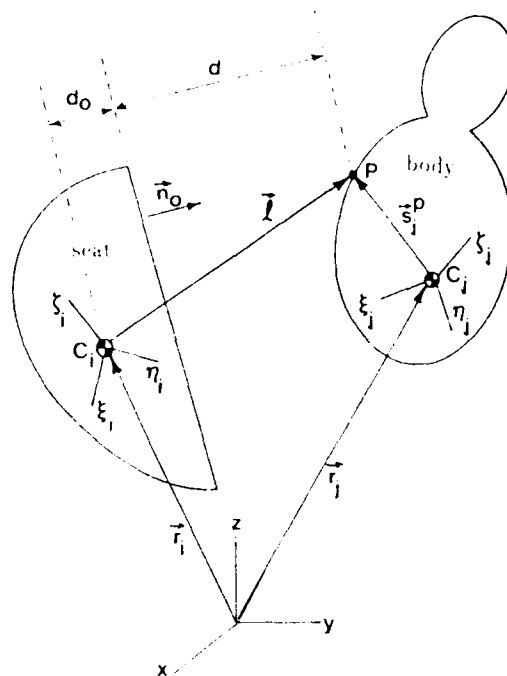


Figure 6. General development of the seat and the occupant interface.

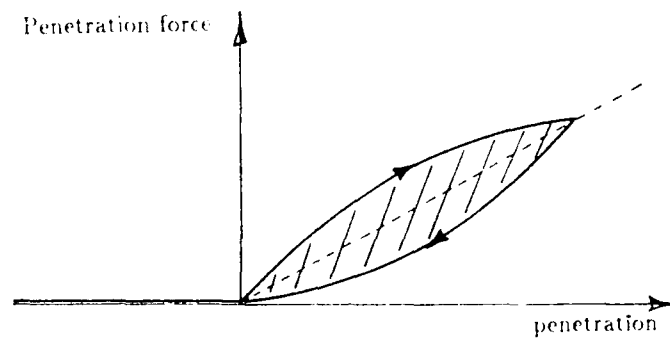


Figure 7. A unilateral viscoelastic model of the penetration force between the seat and the passenger.

where K is a Hertzian generalized parameter, and μ is a hysteresis damping factor related to the amount of energy dissipation [15].

The prescribed procedure has been followed for two checking points P_1 and P_2 on the back side of the upper torso interacting with the seat back, and two checking points P_3 and P_4 on the bottom side of the thighs interacting with the seat cushion. The restraints were represented by spring-dampers in variety of configurations. These configurations were selected in order to model different types of restraint geometry such as lap belts and shoulder harnesses, and to simulate different geometrical configuration of impact such as frontal and side collisions.

DYNAMIC ANALYSIS OF THE MULTI-SEGMENT SYSTEM

The dynamic analysis of a constrained mechanical system requires the solution of a mixed set of differential algebraic equations. The closed-form solutions to these equations cannot usually be obtained even for small systems. Numerical methods and different computational techniques must be used such that stable numerical solutions are obtained. This section describes the steps which were followed in order to perform a dynamic analysis on the constructed model. These include formulation or generation of the governing equations of motion, and development of a numerical solution.

The motion of a free (unconstrained) element "i" is described by a set of differential equations. Let the mass of a rigid element "i" be m_i and its inertia tensor with respect to the element-fixed axes be \mathbf{J}'_i . The three-dimensional Newton-Euler equations of motion for element "i" are written as [16]

$$m_i \ddot{\mathbf{r}}_i = \mathbf{f}_i \quad (13)$$

$$\mathbf{J}'_i \dot{\boldsymbol{\omega}}'_i - \dot{\boldsymbol{\omega}}'_i \mathbf{J}'_i \boldsymbol{\omega}'_i = \mathbf{n}'_i \quad (14)$$

where $\mathbf{f}_i, \mathbf{n}'_i$ are the forces and the moments acting on the element respectively; $\boldsymbol{\omega}'_i, \dot{\boldsymbol{\omega}}'_i$ are the element angular velocity and acceleration vectors; while \wedge performs the cross product operation algebraically. The two equations can be combined as

$$\mathbf{M}_i \ddot{\mathbf{q}}_i = \mathbf{g}_i \quad (15)$$

where \mathbf{M}_i is the element mass matrix containing the mass and the inertia tensor, \mathbf{g}_i contains the applied and gyroscopic forces and moments; and $\ddot{\mathbf{q}}_i$ is the acceleration vector.

For a constrained multi-segment system, such as the model of the human body and the seat, the differential equations of motion will be

$$\mathbf{M} \ddot{\mathbf{q}} = \mathbf{g} - \mathbf{g}^{(c)} \quad (16)$$

where \mathbf{M} is the system mass matrix; $\ddot{\mathbf{q}}$ is the system acceleration vector; \mathbf{g} contains the applied and gyroscopic forces and moments acting on the system; and $\mathbf{g}^{(c)}$ denotes the forces applied at the joints. By means of Lagrange multipliers, these forces are expressible as a linear combination of the rows of the constraints Jacobian matrix $\Phi_{\mathbf{q}}$. That is

$$\mathbf{g}^{(c)} = \Phi_{\mathbf{q}}^T \lambda \quad (17)$$

where λ is a vector of Lagrange multipliers. Corresponding to these second-order differential equations of motion, a set of twice as many initial conditions are needed on the coordinates \mathbf{q} and the velocities $\dot{\mathbf{q}}$ as

$$\begin{cases} \mathbf{q}(0) = \mathbf{q}_0 \\ \dot{\mathbf{q}}(0) = \dot{\mathbf{q}}_0 \end{cases} \quad (18)$$

The differential equations (16) with (17), the constraint (3), velocity (4), and acceleration equations (5), together with initial conditions (18) constitute a "standard" form of the equations of motion. These mixed differential/algebraic differential equations cannot be solved directly, since the multipliers λ are unknown. One simple numerical technique is to append the kinematic acceleration equations (5) to the differential equations (16) as

$$\begin{bmatrix} \mathbf{M} & \Phi_{\mathbf{q}}^T \\ \Phi_{\mathbf{q}} & \mathbf{0} \end{bmatrix} \begin{bmatrix} \ddot{\mathbf{q}} \\ -\lambda \end{bmatrix} = \begin{bmatrix} \mathbf{g} \\ \gamma \end{bmatrix} \quad (19)$$

This linear system can be solved for the accelerations $\ddot{\mathbf{q}}$ and multipliers λ .

To obtain a numerical solution for the response of the system as time progresses, a direct integration algorithm was developed. The linear equations (19) were solved at each juncture of time t^i for the accelerations $\ddot{\mathbf{q}}$ and the multipliers λ , knowing the coordinates \mathbf{q} and the velocities $\dot{\mathbf{q}}$ of all the elements in the system. A vector of integration or state variables \mathbf{y} was used as

$$\mathbf{y} = \begin{bmatrix} \mathbf{q} \\ \dot{\mathbf{q}} \end{bmatrix} \quad (20)$$

In essence, the second-order ordinary differential equations were numerically converted to a system of twice as many first order equations. A numerical integration of the time derivative of the vector \mathbf{y} at the time t^i was performed to obtain vector \mathbf{y} at an updated time t^{i+1} ; i.e.,

$$\dot{\mathbf{y}}^i = \begin{bmatrix} \dot{\mathbf{q}} \\ \ddot{\mathbf{q}} \end{bmatrix}_{t^i} = \underset{\text{Numerical Integration}}{\quad} \cdot \mathbf{y}^{i+1} = \begin{bmatrix} \mathbf{q} \\ \dot{\mathbf{q}} \end{bmatrix}_{t^{i+1}} \quad (21)$$

Knowing the positions \mathbf{q} and the velocities $\dot{\mathbf{q}}$ at time t^{i+1} , the equations of motion were again solved and the numerical integration proceeded as before. As a numerical integrator, a

variable-step/variable-order numerical integration routine, developed by Shampine and Gordon [17], was employed. The use of this routine which included built-in stability checks, and some other developed computational techniques such as the constraint-violation stabilization method [16], resulted in accurate and stable solutions.

The preceding procedure has been installed on a computer program developed at the Wichita State University. The code is written in a general-purpose form, which makes it suitable to a variety of different applications, but it is specifically useful for the dynamic simulations of the developed human body model. Its generality makes modifications of the model extremely convenient, and no need exists to reformulate the governing differential equations of motion. More advanced models of the human body, containing more elements and variety of joints such as spherical or socket joint and universal joint may be added to the model simply by constructing new input data files for the developed analysis program. The code allows the use of the stiffness or hybrid model of crash in a simple form of spring-damper-actuators connecting different elements of the system.

CRASH SIMULATIONS

Once the model of the human body is completed, the interaction between the seat and the passenger accounted for, and the capabilities for automatic generation and stable numerical integration of governing equations of motion are adopted, a variety of input forcing conditions may be applied to the model, and its behavior under each specific condition studied. This section describes a sample, among many, simulations that can be performed on the constructed model. Some results are presented in form of history of response. A simple post-processing graphics program was also developed to draw the configuration of the system at different time junctures. This allows easier understanding of the results. The geometry of each element "i" was described by the local coordinates of all points P on its surface, vector $(s'_i)^P$. From the output of the developed analysis program, the location of the mass center r_i and its rotational transformation matrix A_i were known at any instant. The global coordinates of each geometry-definition point P were then calculated as

$$r_i^P = r_i + A_i(s'_i)^P \quad (22)$$

and these points were connected to each other based on the connectivity or the topological geometry information.

STATIC EQUILIBRIUM ANALYSIS

The static equilibrium analysis is a transitional step which must be followed, before any further simulation is to be performed. It describes the interim process, and determines the equilibrium parameters which are used in further simulations. The starting configuration of

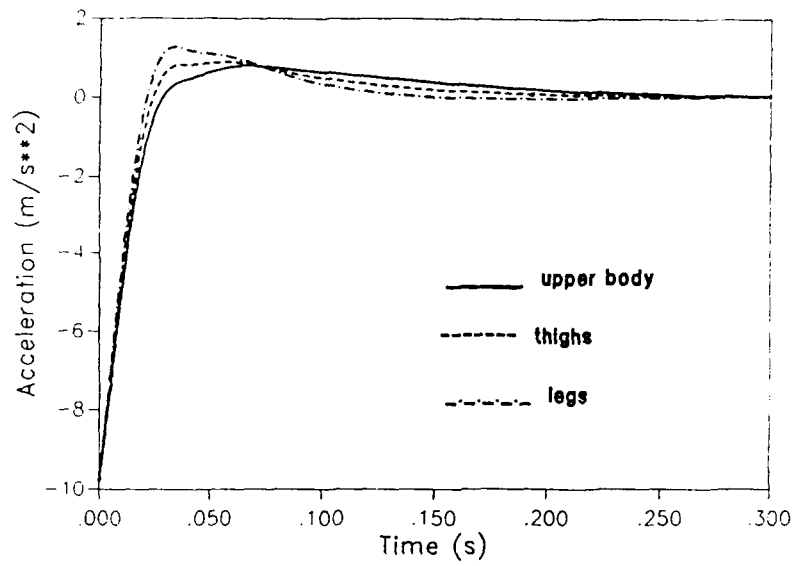
the body was chosen when it was just touching the seat surfaces (cushion and back). Dynamic analysis was performed until the passenger gained his/her balance on the seat. The state of equilibrium was reached for a 50th percentile male at a penetration of about 2 cm on the seat cushion. Some results from the simulation is shown in Fig. 8.

FRONTAL CRASH

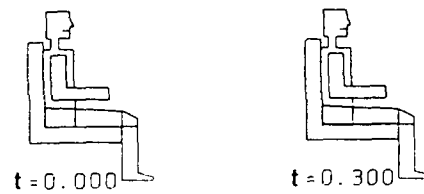
In order to simulate the behavior of a human body during frontal impacts, various pulse decelerations were applied to the seat in the longitudinal direction. The pulses had a half-sinusoidal shape with different peak and duration values. Among a typical set of values used were 10g for the peak and 100 ms for the duration [18]. By adjusting these two parameters, crashes with different degrees of severity may be simulated. The external forces acting on the system contained the impulsive impact loads, the penetration force between passenger and seat, the gravitational forces, the joint torques, and the contact forces between the elements. In addition, the friction force between the seat and the passenger was also accounted for using a dynamic viscous form such that it would be a function of the relative velocities of the contacting surfaces [19].

Different simulations were then performed with and without restraint on the passenger. For an unrestrained passenger with typical crash acceleration parameters, the friction force was not enough to keep the body on the seat. This may result in the passenger divorcing from the seat and colliding with the cockpit/cabin interior causing severe injuries or even casualties. The acceleration of the passenger versus time in the direction of impact is shown in Fig. 9(a). Basically all the elements have the same order of longitudinal acceleration, since the impact loads are all in that direction and little amount of relative rotation occurs among the body elements. A graphical representation of the configurations of the passenger with respect to the seat is provided in Fig. 9(b) for some intermediate time steps.

Restraints representing the seatbelts were then introduced in the model. The belts were represented by unilateral spring-dampers. Two types of simulations were performed with different configurations of the restraint: one with a lap belt and the other with a symmetrical shoulder belt. The existence of the lap belt kept the passenger on the seat; however, it caused excessive rotation of the upper torso about the hip joint. This may not only result in severe frontal head injuries of the passenger on the cockpit/cabin interior, but it may also cause secondary crash of the body's elements onto one another or body's internal organs. Fig. 10(a) shows the acceleration response of the passenger with lap belt subjected to same impact parameters as in Fig. 9. The oscillations are mostly due to the transmission of impact forces from the longitudinal direction to the rotation in the plane of impact about the hip joint. The configurations of the body elements at some intermediate times are also shown in Fig. 10(b).

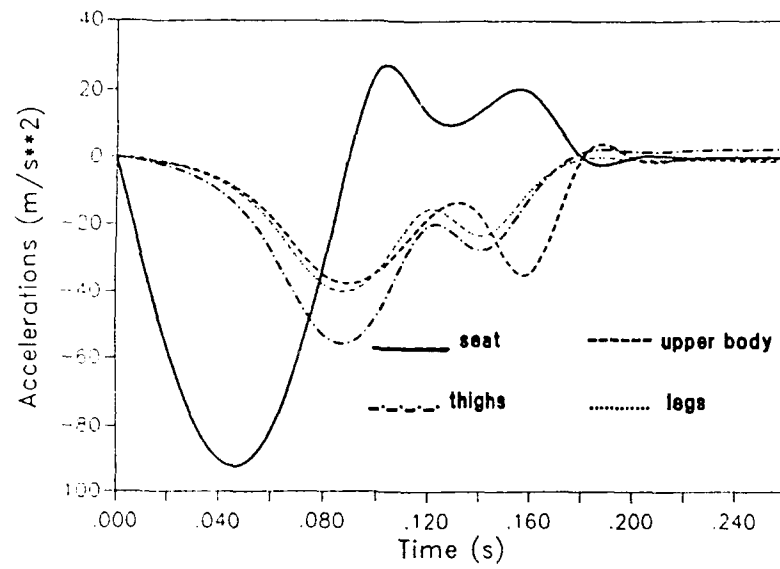


(a)

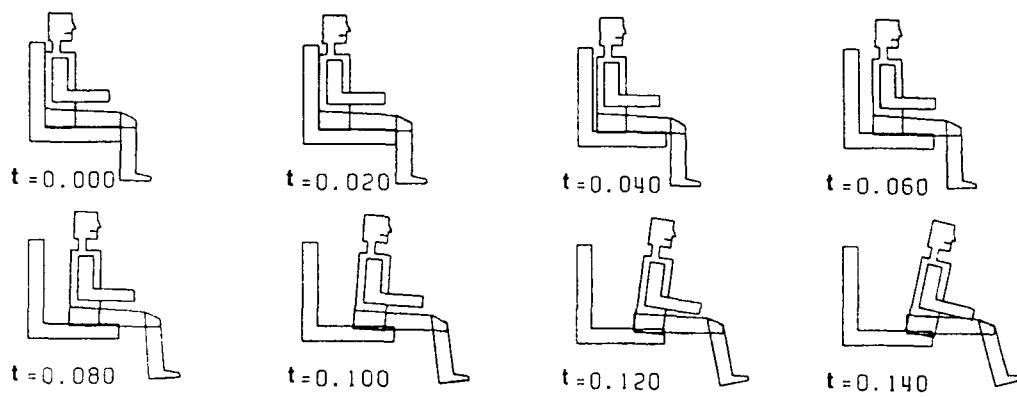


(b)

Figure 8. Static equilibrium analysis: (a) acceleration response of the body elements in vertical direction: (b) initial and final configurations (penetration of the body elements on the seat cushion is small).

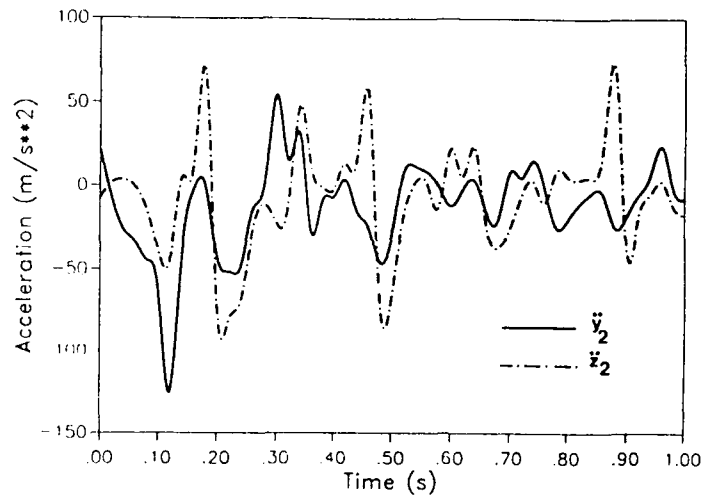


(a)

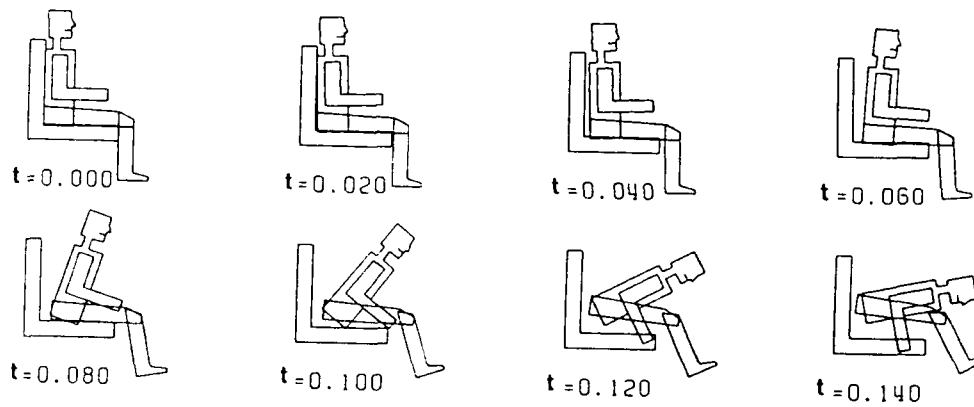


(b)

Figure 9. Frontal collision simulation for an unconstrained passenger: (a) acceleration response in the direction of impact (longitudinal direction); (b) configurations for some intermediate times.



(a)



(b)

Figure 10. Frontal collision simulation for passenger restrained by a lap belt: (a) acceleration response in the longitudinal, the vertical directions; (b) configurations for some intermediate times.

The preceding simulation was then repeated for a passenger restrained by a symmetrical shoulder harness. The corresponding results are shown in Fig. 11, which indicate that the shoulder straps not only keep the passenger on the seat, but absorb most of the energy given to the system by the impact loads. The lower load levels or the corresponding accelerations compare closely in peak values with those of an earlier study on a more advanced model [20].

SIDE CRASH

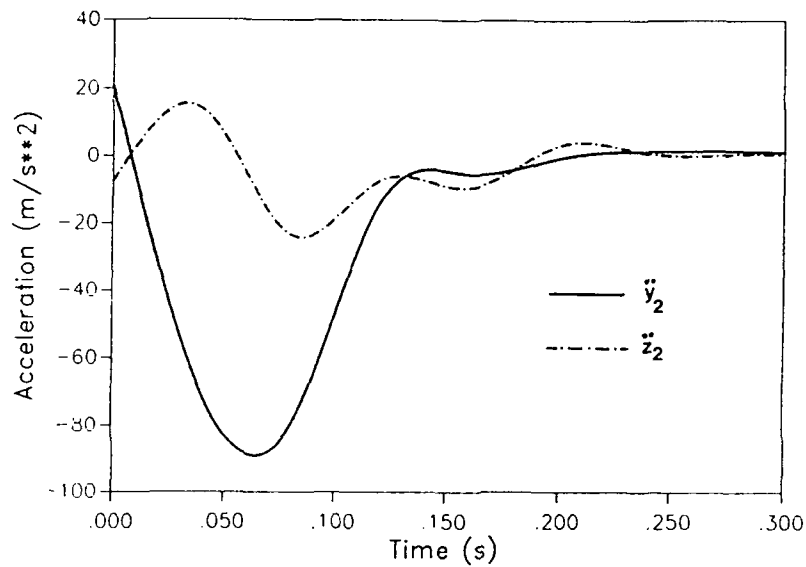
A side impact was simulated by applying a lateral pulse acceleration to the seat. The passenger was restrained to the seat by a symmetric shoulder belt. The same parameters of impact as in frontal collision, (peak and duration), were used in this analysis. The resulting acceleration of the upper torso both in the direction of impact and in the longitudinal directions are shown in Fig. 12(a). The peak values compare closely to an earlier investigation containing results from both simulations and experimental crash tests on dummies [21]. The side view configuration of the passenger is graphically shown in Fig. 12(b). As it is observed, some rotation of the upper torso and the head is encountered in the impact and the longitudinal directions. However, the belt keeps the passenger on the seat, and absorbs much of energy given to the system.

VERTICAL CRASH (SEAT EJECTION)

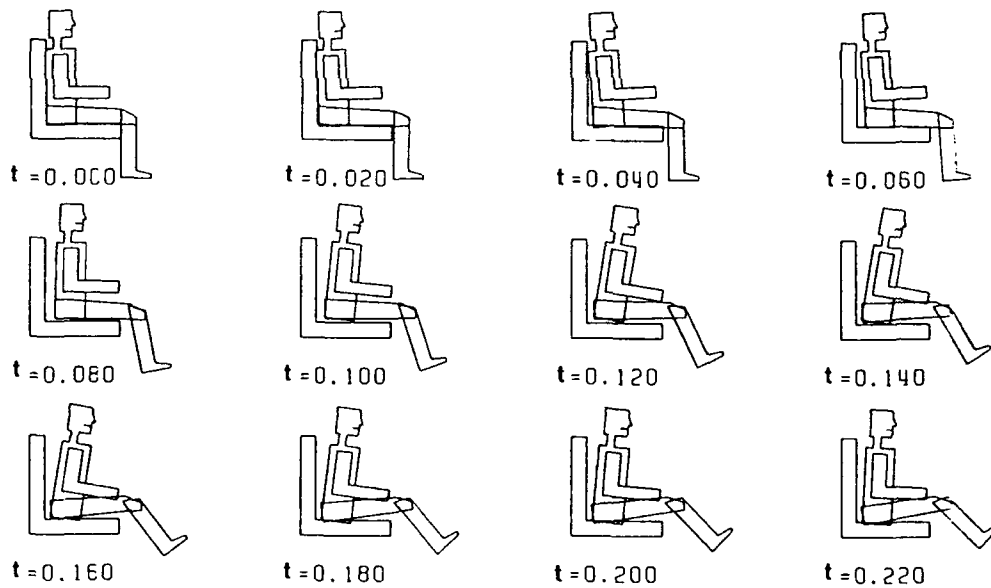
A vertical acceleration was applied to the seat in order to simulate the crashes in the vertical plane or the seat ejections. By selecting different values for the impact parameters and the type of restraints on the passenger, a variety of situations with different degrees of severity and different post-crash behavior of the passenger may be obtained. One interesting result from a seat ejection simulation is the amount of force that is transmitted to the pelvis or to the knee. Fig. 13(a) and 13(b) shows plots of the constraint reaction forces at the hip joint and the knee joints. They are evaluated as components of the joint forces $\Phi_q^T \lambda$. The largest peak corresponds to a secondary vertical impact of the passenger on the seat. Some intermediate configurations of the system are shown in Fig. 13(c). By simulating a variety of impact parameters and development of theories on human survivability criteria, safe designs of seat ejection systems may be proposed, which is one useful aspect of these simulations.

CONCLUSIONS AND RECOMMENDATIONS

A mathematical model of the human body was constructed as a collection of rigid elements interconnected by some kinematic joints. Torsional spring-dampers with energy dissipating characteristics were incorporated at the joints to mimic the behavior of the muscle actions and the joint stops. A Hertzian contact force model with local permanent deformation was employed for the penetration of the body elements onto each other. Crash simulations were

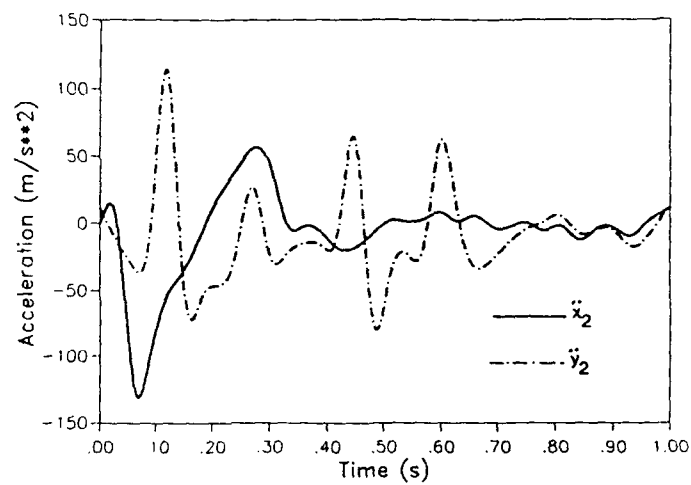


(a)

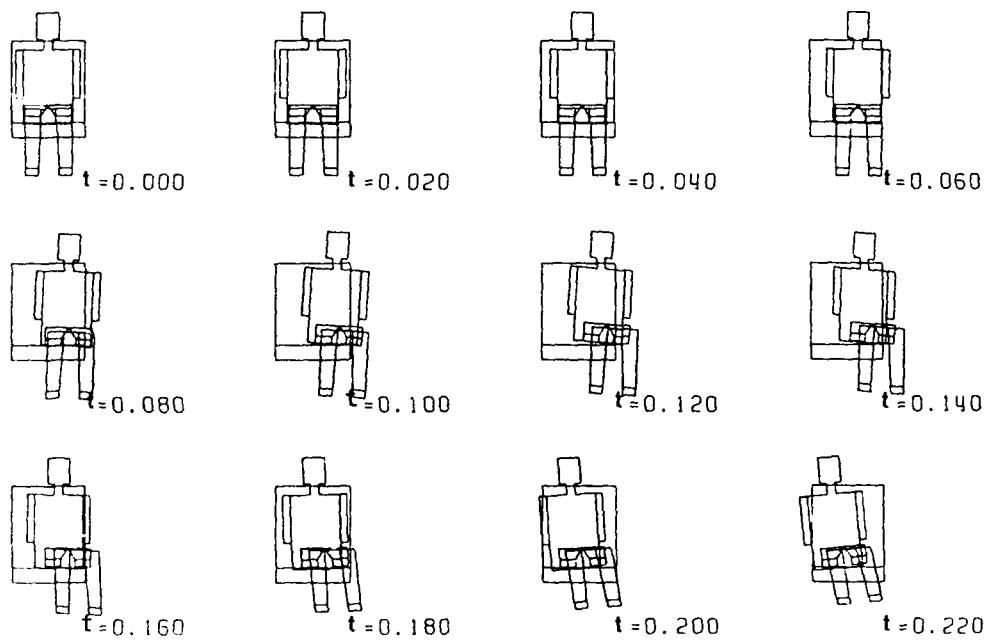


(b)

Figure 11. Frontal collision simulation for passenger restrained by symmetrical shoulder belts: (a) acceleration response in the longitudinal and the lateral directions; (b) configurations for some intermediate times.

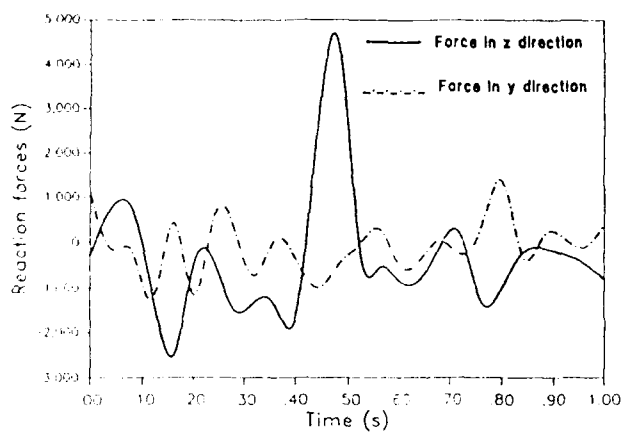


(a)

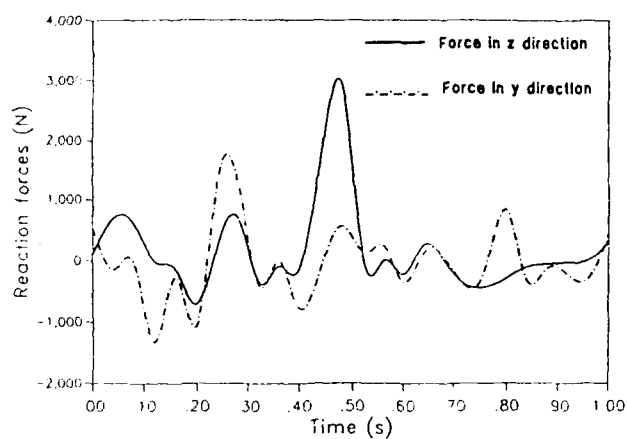


(b)

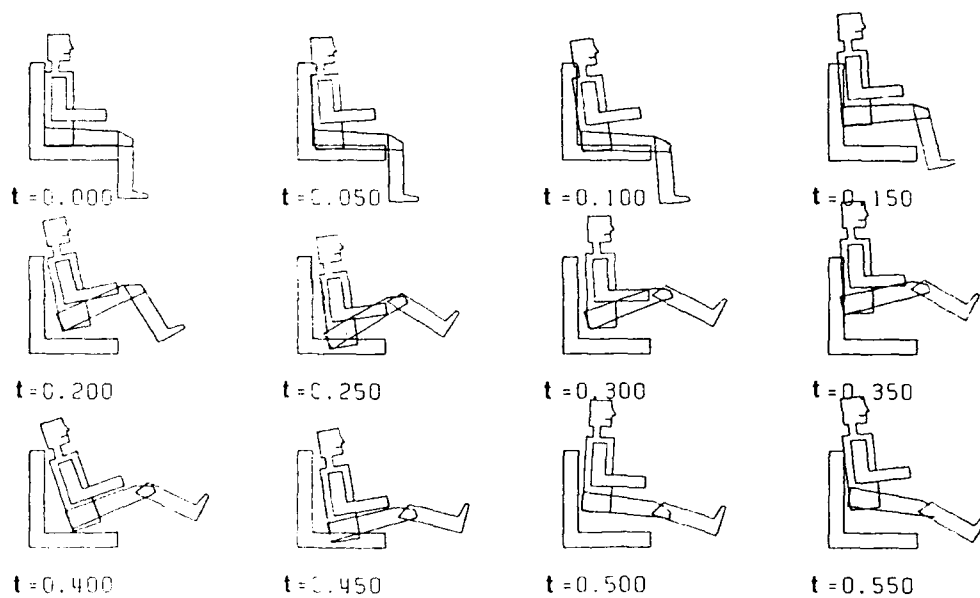
Figure 12. Side collision simulation: (a) acceleration response of the upper torso in the lateral and the longitudinal directions; (b) configurations for some intermediate times.



(a)



(b)



(c)

Figure 13. Seat ejection simulation: (a) hip-joint forces: (b) knee-joint forces: (c) configurations at some intermediate times.

performed by subjecting the human body model, representing an aircraft passenger, to a variety of input forcing conditions. In these analyses, the interaction between the seat and the passenger was modeled by a number of unilateral spring-dampers. Hybrid representation of lap belts and symmetrical shoulder harnesses were also included in the analyses. For each specific simulation, the governing equations of motion for the multi-segment model of the body and the seat were automatically generated and numerically solved. Some typical simulations were performed on the constructed model for various input pulse amplitudes and durations. The simulations of front collision with and without restraint, side collision, and vertical collision (or seat ejection) provided some results that help gain some insight into the behavior of the human body parts during sudden surges.

Much investigation needs to be performed in this area. Some potential areas of research on the continuation of this study include: construction of more advanced model of a human body with more elements representing pelvis, spine, thorax, and arms; Inclusion of head-neck models with muscle actions; Inclusion of variety of joints such as socket and universal joints; biomechanical realistic modeling of the muscles; development of Hertzian contact force models, with either permanent indentation or hysteresis viscous damping, for contact of body parts having any geometrical shapes; creation of some standards for the crash simulators; investigations of seat designs and seat-structure fixture; multiple impacts including primary stage on transmission of impact loads to the seat, secondary stage on impact of body elements onto each other or surrounding, and tertiary stage on impact of internal human organs; modeling of crush behavior and human tolerances; other restraint systems such as airbags and more advanced representation of the seatbelts. These studies will provide a vast amount of information on mechanisms of crash protection, predicting human motion behavior and possible injuries for specific impact conditions, and design of new restraints and interior cockpit cabin elements.

REFERENCES

1. McHenry, R.R., "Analysis of Dynamics of Automobile Passenger-Restraint Systems," Proc. 7th Stapp Car Crash Conf., pp. 207-249, 1963.
2. Segal, D.J., "Revised Computer Simulation of the Automobile Crash Victim," Cornell Aeronautical Lab., Rep. No. VJ-2759-V-2, 1971.
3. Robbins, D.H., Bennett, R.O., and Roberts, V.L., "HSRI Two-dimensional Crash Victim Simulator: Analysis, Verification, and User's Manual - Final Report," University of Michigan, Highway Safety Research Institute, Rep. No. HSRI-Bio-M-70-8, 1970.
4. Robbins, D.H., Bowman, B.W., and Bennett, R.O., "The MVMA Two-dimensional Crash Victim Simulation," Proc. 18th Stapp Car Crash Conf., pp. 657-678, 1972.

5. Glancy, J.J., and Larson, S.E., "Users Guide for Program SIMULA," Dynamic Science. Rep. TDR No. 72-23, 1971.
6. Twigg, D.W., and Karnes, R.N., "PROMETHEUS - A User Oriented Program for Human Crash Dynamics." Boeing Computer Services, Inc., Rep. No. BCS40038, 1974.
7. Bartz, J.A., "A three-dimensional Computer Simulation of a Motor Vehicle Crash Victim." Calspan Rep. No. VJ-2978-V1, 1971.
8. Fleck, J.T., Buttler, F.E., and Vogel, G.L., "An Improved Three-dimensional Computer Simulation of Motor Vehicle Crash Victims," Vol. I-IV, Rep. Nos. DOT-HS-801507, -508, -509, -510, 1974.
9. Fleck, J.T., and Butler, F.E., "Validation of Crash Victim Simulator," Vol. 1-4, Rep. No. ZS-5881-V-1, DOT-HS-6-01300, 1981.
10. Wismans, J., Maltha, J., Van Wijk, J.J., and Janssen, E.G., "MADYMO - A Crash Victim Simulation Computer Program for Biomechanical Research and Optimization of Designs for Impact Injury Prevention," AGARD Meeting, Kooln, Germany, 1982.
11. Merrill, T.H., "Three-dimensional Lumped-parameter Impact Analysis of Head-Neck System," M.S. Thesis, University of California, Berkeley, 1981.
12. Goldsmith, W., Deng, Y.C., and Merrill, T.H., "Numerical Evaluation of the Three-dimensional Response of a Human head-Neck Model by Dynamic Loading." Mathematical Simulation of Occupant and Vehicle Kinematics, Government/Industry Meeting and Exposition, Washington D.C., 1984.
13. Lankarani, H.M., "Canonical Equations of Motion and Estimation of Parameters in the Analysis of Impact Problems," Ph.D. dissertation, The University of Arizona, 1988.
14. Wittenburg, J., "Dynamics of Systems of Rigid Bodies." B.G. Teubner, Stuttgart, 1977.
15. Lankarani, H.M., and Nikravesh, P.E., "A Contact Force Model with Hysteresis Damping for Impact Analysis of Multibody Systems," ASME J. Mechanisms, Transmissions, and Automations in Design, Paper No. 89-DAC-57, 1989.
16. Nikravesh, P.E., "Computer Aided Analysis of Mechanical Systems." Prentice Hall, 1988.

17. Shampine, L.F., and Gordon M.K., "Computer Solution of Ordinary Differential Equations," W.H. Freeman and Co., San Francisco, 1975.
18. . "On-highway Vehicles and Off-highway Machinery," Society of Automotive Engineers handbook, 1989.
19. Gim, G., "Vehicle Dynamic Simulation with a Comprehensive Model for Pneumatic Tires," Ph.D. dissertation, The University of Arizona, 1988.
20. Lestrelin, D., Fayon, A., Tarriere, C., and Mack, P., "Three Applications of a Mathematical Model, PRAKIMOD, in Frontal Collisions," Mathematical Simulation of Occupant and Vehicle Kinematics, Government Industry Meeting and Exposition, Washington D.C., 1984.
21. Segal, D.J., "Side Impact Modelling Using Lumped Mass and CAL3D Simulations," Mathematical Simulation of Occupant and Vehicle Kinematics, Government Industry Meeting and Exposition, Washington D.C., 1984.

**NEURAL NETWORKS: CAN THEY BE USED TO DETECT DEFECTS
IN AIRCRAFT STRUCTURES ?**

by

Behnam Bahr
and
Tarabishy M. Nabeel
Department of Mechanical Engineering
The Institute for Aviation Research
The Wichita State University
Wichita, KS 67208

For presentation to the AIAA/FAA Joint Symposium on General
Aviation Systems at the Port O-Call Inn, Ocean City, NJ
on April 11, 1990

NEURAL NETWORKS: CAN THEY BE USED TO DETECT DEFECTS IN AIRCRAFT STRUCTURES?

Behnam Bahr, Assistant Professor
Tarabishy M. Nabeel, Graduate Student

Department of Mechanical Engineering
The Institute for Aviation Research
The Wichita State University
Wichita, KS 67208

ABSTRACT

There are various nondestructive testing (NDT) inspection methods, such as, vision, eddy current, and ultrasonic, used for crack or corrosion detection of the skin or the structures of aircraft around rivets and fasteners. These methods require a skilled technician to identify the existence of the cracks. Despite the training that a technician goes through, human error is identified to be one of the major contributing factors to problems in the determination of the safety of aircraft. There has been some effort to develop expert systems that can be used by technicians. However, there is currently no expert system developed that can learn and improve its capability as it encounters new situations. In this paper, we review the neural network and its possibility for aiding the technician in detecting defects.

INTRODUCTION

After an aircraft enters service, inspection and maintenance of its structural integrity are essential for its remaining service life. The quality of inspection and the cost of labor are of concern to the airline industry. Millions of dollars are now being spent for maintenance and repair of airplane structures and, generally maintenance labor increases as the aircraft ages [1]. Some of the inspections are costly because of downtime and the number of required man-hours. In general, when an aircraft is removed from service, the loss ranges from \$25,000 to \$50,000 a day [2].

In order to minimize inspection cost and improve the quality of inspection, intelligent systems must be introduced to assist the inspector. For this purpose, we review some of the difficulties encountered in Nondestructive Evaluation (NDE) and how a neural network can be beneficial as a part of a complete integrated system for Nondestructive Inspection (NDI) of the aging aircraft.

The need for automation:

As today's requirements for nondestructive testing are getting tighter, more accurate inspection should be carried out in less time. The shortage of qualified inspectors is more noticeable. It usually takes about five years of training and experience in order to get the level-III NDT certificate. We can realize how important and beneficial it is to integrate NDT equipment with computers; and to develop algorithms that can identify flaws and automatically make decisions about them, releasing the inspector from looking and deciding in each and every case.

Recently it has been recognized that we need to reduce human error in the inspection and maintenance of aircraft, especially aircraft that have been in service a number of years. The failures of aircraft are due to cracks, corrosion, and human errors. Human error in inspection and maintenance of aircraft is especially of concern. There have been numerous incidents that call for immediate action on safety measures. The safety of aging aircraft is of concern to the public and the Federal Aviation Administration (FAA), as well as to the airlines and the aircraft industry.

The studies done by Rummel [3] indicate, with ample evidence, that the decision made by a systematic, automated approach is better than that by the well-trained inspector. The errors caused by the operator are best described by Rummel. Errors in performance by a skilled operator may be classified as: Systematic, Precision, and Sporadic Errors. "Systematic errors may be due to a difference in skill and/or decision criteria input by the operators; or may be due to a difference in equipment or calibration standards. Errors in precision can be caused by slight variations in processing, by inexperience of the operator, or by a shift in decision criteria usually due to a lack of confidence. Sporadic errors are usually associated with lack of motivation, boredom, fatigue, and monotony". It should be pointed out that an improper Nondestructive Evaluation (NDE) is far more dangerous than no test at all, because it leads to false sense of security.

To clarify the preceding remarks, an example is described here on the results of evaluation testing of 24 NDT inspectors from the Structural Assessment Testing Facility located in the Engine Division of the San Antonio Air logistics Center, Kelly AFB, Texas [4]. The samples to be inspected were 150 parts, having 112 flawed parts with defects ranging in size between 0.015 mm (0.006") to 0.44 mm (0.173"), using "A" scan ultrasonic inspection and applying the surface wave technique. No one passed the test with accepted criteria being no less than 80% probability of detection (POD), and no more than 30% false calls. This result indicates how great the impact of the human factor is on the process, and how important it is to consider automation to reduce errors.

There has been some effort to automate the NDT. For example, Smith [5] developed an automatic Eddy current inspection system for turbine engine components. However, there has been no work on the development of automatic interpretation of the data, nor on aid for the inspector in determining the cracks in aging aircraft. There has been some expert system development for pipe inspection in nuclear power plants, but no neural networks or expert systems exist for crack detection in aircraft. Before describing the neural networks and how they might be used for the benefit of of NDE, we need to look at the problem as a whole.

NDT as an integrated system:

The integration of intelligent hardware/software is essential for automation of the inspection of aircraft and can assist the manual inspection of aircraft for better interpretation of the NDE. To reach this goal all the components of the system must be considered [6]:

- 1- Transducers (which transmit and receive signals from the part).
- 2- Software which will receive the data, analyze it, record it, retrieve it, display it and ultimately make decisions about the inspected part.
- 3- The electronic hardware which provides means for data acquisition.
- 4- Transducer positioning and control of motion to place the sensor at the desired location, which is crucial for any successful system.

As nondestructive testing has developed, there has been no real development of the artificial intelligence (expert system) to express results of Nondestructive Inspection (NDI) in quantitative terms. The reason is that different NDI methods result in different probabilities of flaw detection [7]. Furthermore, there is no available data for acceptance/rejection limits for the severity of flaws. Because of the various techniques and interpretations by different operators, one may reach different conclusions. The chance of detecting a given crack depends on many factors such as the location, orientation, and shape of the flaw; materials; inspection environment, and the inspector qualifications.

Therefore, it is a must to have some intelligent system that can handle blurry sets of data which expert systems can not handle effectively. On the other hand, neural nets have inherently the ability to do the "best matching" between a previously learned pattern and a new input pattern. In addition, probably the biggest advantage of using neural nets is that no huge amount of experience is required to train the system. In fact, the

abilities and potentials of neural nets have been demonstrated in a number of applications. The most important ones are in the field of complex pattern recognition, such as continuous speech, handwritten characters, or recognizing a target from different angles [8]. Therefore, the field of nondestructive testing can benefit a great deal from this emerging technology.

NEURAL NETWORK

The idea behind neural nets originated when people were trying to model the human brain and, specifically, to model the basic component of the brain which is called the neuron. When an outside signal stimulates the nerve cell, it triggers a pulse. Once a certain threshold is exceeded, the neuron outputs a signal with strength proportional to the causing stimulator.

The artificial neuron is basically a first order approximation of the biological neurons as shown in Fig. 1. There are a number of inputs each associated with a weight or strength. The net input to the neuron would be the sum of all the inputs after multiplying each with its corresponding strength (weight) as shown in Fig. 2. Usually, a non linear "S shaped" function acts on the net input. For example, the logistic (squashing) function will give:

$$\text{OUTPUT} = 1 / 1 + \text{EXP}(- \text{INPUT})$$

Based on the value of the net input, the neuron will either "fire" an output or not. A group of these simple elements form a layer, and a number of these layers interconnect to form neural network as shown in Fig. 3. This network has capabilities that only humans were once thought to have; e.g., abstraction and generalization [9].

The key point here is the ability to isolate a specific region in space, and to be able to identify the elements belonging to it. To show how neural nets can do this, a two-dimensional input vector space is demonstrated. The input to the first neuron is equal to

$$\text{NET} = X_1 * W_1 + X_2 * W_2$$

If the threshold equals to T, then:

$$T = X_1 * W_1 + X_2 * W_2$$

This is a straight line equation (Fig. 4) that separates the plane into two regions. With proper setting of the threshold, we can choose the region above or below the line. An output can result if for instance the NET is greater than the threshold. Therefore, by using one neuron in the first layer, it is possible to isolate half of the plane. Similarly, by using another neuron,

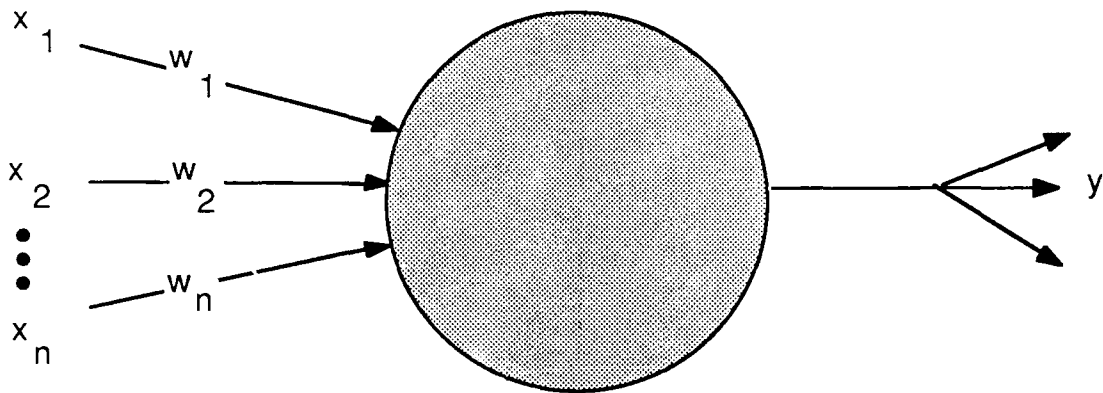


Figure 1 Single neuron.

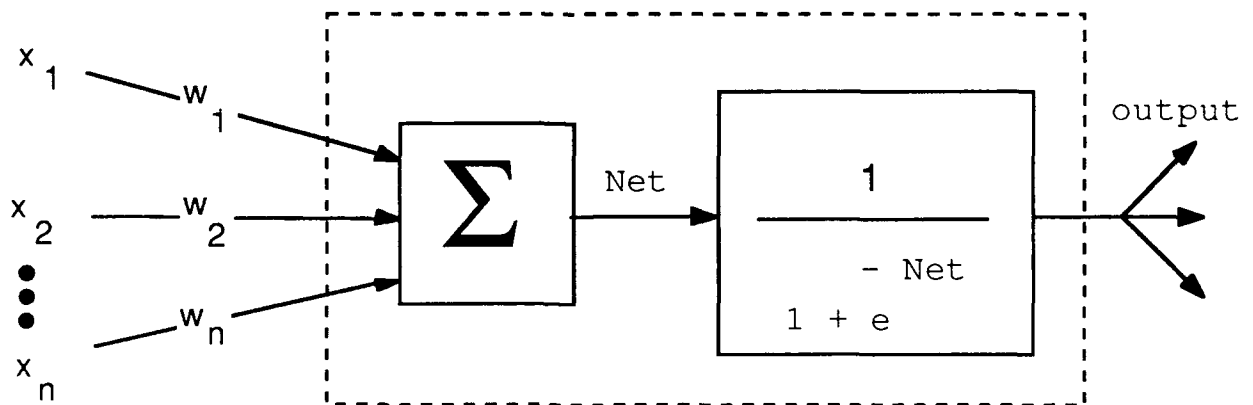


Figure 2 Model of the neuron.

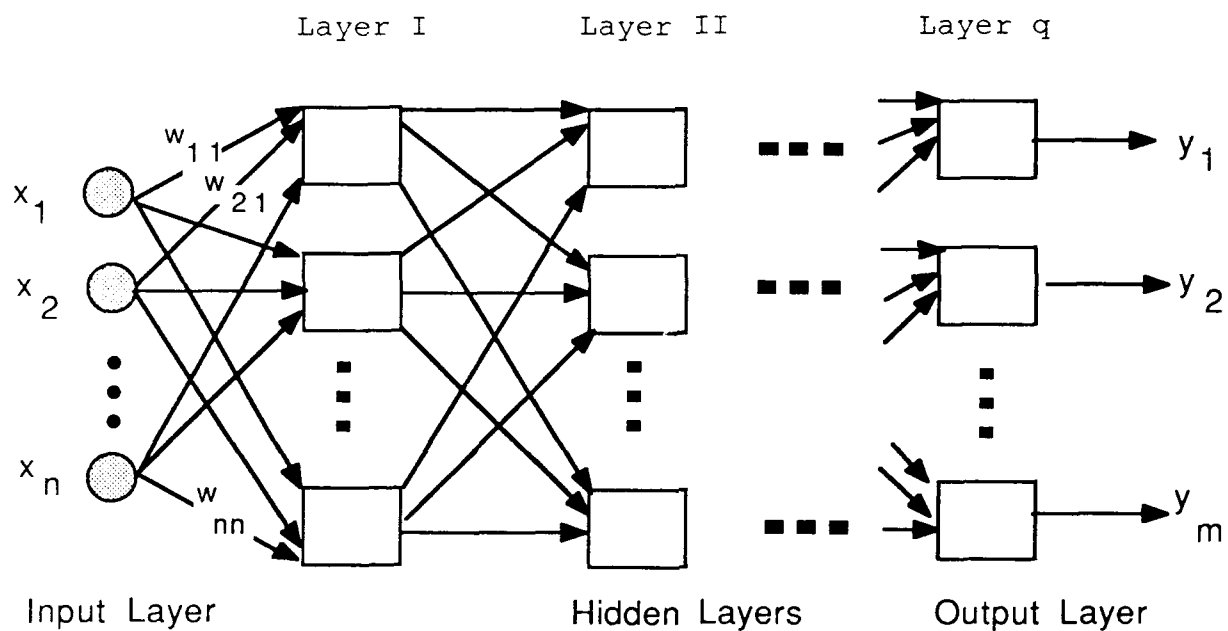


Figure 3 The representation of the general neural network.

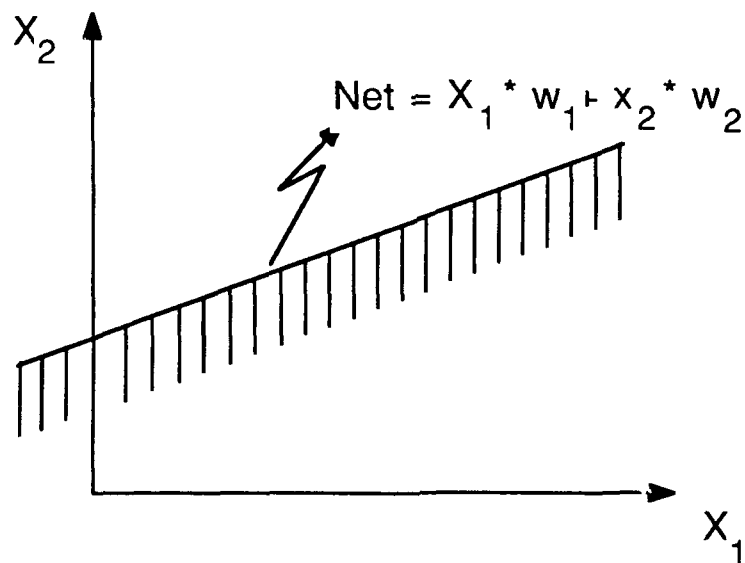


Figure 4 Discrimination by single neuron.

we can have another line and so on. If we now add another layer and assign the neuron located there to do the logical "AND", we can get any convex region in space to the desired degree of accuracy as shown in Fig. 5. However, if the region is more complicated or consists of multiple areas in the space, we can put a third layer with logical "OR" to get that general region as shown in Fig. 6.

Thus the proper selection of the weights can give any general region. It should be noted that these weights are going to be decided by the training process-- starting with random weights. These weights are modified according to one of two ways.

1- Supervised training:

In supervised training, the output of the network is compared with the desired output and the error is used to modify the weights of the last layer. This error is then backpropagated to modify the weights of the network. The modification of the weights of the last layer would be done using the delta rule which is applied as follow:

$$\delta_{out} = f'(OUT) * E \quad (1)$$

where

$f'(OUT)$ = derivative of the squashing function at the output of that neuron,

E = error which is the difference between the desired and actual response of the net.

The change in the weight is then found by substitution of δ for δ_{out} in:

$$\Delta W = r * \delta * OUT_p \quad (2)$$

where

r = The learning rate which is picked to fit the purpose,

OUT_p = Is the output of the neuron in the previous layer associated with that weight.

The modified weights are then evaluated as:

$$W_{new} = W_{old} + \Delta W \quad (3)$$

where

W_{new} = new weight,

W_{old} = old weight.

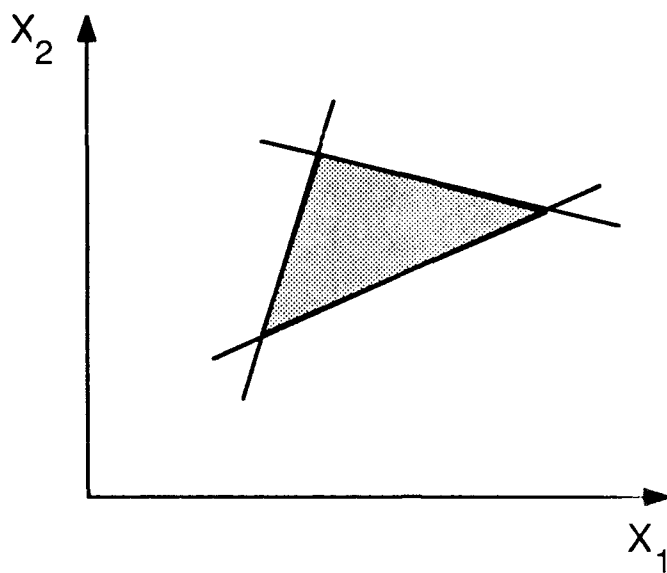


Figure 5 Discrimination by two layers neural network.

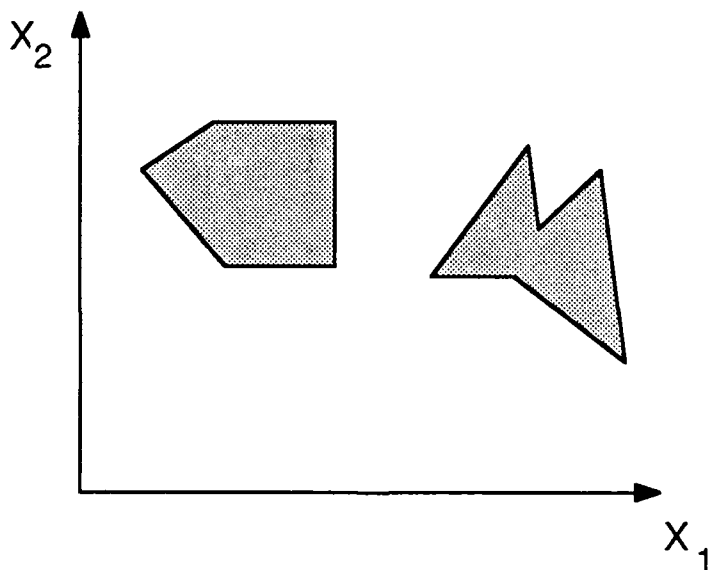


Figure 6 General case of discrimination with multi-layer neural network.

For the hidden layers which have no known output to compare with, a recursive formula is used to calculate δ_h . Starting with the layer directly before the last layer the delta rule relates the " δ " for this layer with the " δ_{out} " 's, and weights of the output layer as follows:

$$\delta_h = f'(OUT_h) * \Sigma (\delta_{out} * W_{out}) \quad (4)$$

where

OUT_h = output of the hidden neuron,

W_{out} = weight of the outer layer,

Σ = summation over all weights and " δ "'s related to this neuron.

By substitution of " δ " in Eq. (2), then using Eq. (3) the new weights of this layer are obtained. This way, the error for each neuron in every layer is calculated, starting with the output layer. This error is then backpropagated throughout the net and the weights are adjusted accordingly. Although the above explained delta rule gives a way to modify the weights, some people improve the performance of the net by adding extra terms like a momentum term, etc., which we will not explain here.

2- Unsupervised training:

In the second method, the net has only an input set and no desired set of corresponding output is available to compare with the output of the network. In this case, the net adjusts itself according to the input.

Great opportunities for neuro-NDE:

One especially suitable application is in interpreting the output results of an advanced ultrasonic inspection station, similar to the one used by Boeing-Wichita in Wichita, Kansas. This system inspects parts for internal voids, delamination, or unbonds. The system is set up such that first, the part is scanned so that the contour of the part is obtained using a contour sensor. It receives a number of points which form a grid-like pattern used to obtain the surface configuration. The information about the part is then used to maintain the ultrasonic search head at a constant distance from the part and perpendicular to its surface during inspection. The resulting data is processed using a computer. The information is then sent to a Versatech V-80 electrostatic plotter that has 200 dots/inch resolution. It is used to form 0.2 mm by 0.2 mm optically-weighted numbers to produce a gray scale plot with 16 different shades of gray. The thresholds are set to represent defects or poor quality as darker

shades of gray. The operator then has to interpret the result according to the indications on the plot and his knowledge of the part geometry. Interpretation of the plots takes about 15 minutes for an experienced operator [10]. On the other hand, automatic interpretation will result in faster, and more consistent and more accurate results; and that will improve the quality of the inspection which might be compromised due to the inspector fatigue.

Another place where neural networks can be used is in the field of Acoustic Emission (AE). Based on the phenomenon that the material emits ultrasonic signals when cracking occurs, detection of these signals can give an early alarm about the material condition. One application that is being investigated is real time monitoring system of the aircraft structural integrity by putting arrays of transducers in "suspected areas." To identify cracking patterns and to locate these cracks are not easy jobs, especially when a great amount of noise is present [11]. This noise can result from different sources such as: Electrical noise, engine vibrations, air stream, hydraulic system, or fretting [12]. The effect of some of this noise can be reduced, to a great extent, by using some methods such as triangulation, or a source localization technique. But some of these noises are hard to separate, especially those associated with fretting. In this case, the solution might lie in a neural network.

CONCLUSION

The problem of the reliability encountered in NDT/NDE was examined in this paper, and the necessity to automate the process was confirmed. This will eventually require the consideration of all the components involved in the process of NDI. Since automatic interpretation of the results is critical for the success of such a system, neural networks with their unique abilities in the field of complex pattern recognition were examined with some very simplified mathematical explanation of how they perform, and how they may be applied to NDE problems. The Neuro-NDE can be an aid to the inspector to locate problem areas with greater confidence, thereby increasing productivity and reliability. It is worthwhile to mention that two cases mentioned as applications to NEURO-NDE are not the only possible cases to use neural networks, but rather they indicate that a lot can, and should be done.

REFERENCES

- [1] Hagemmaier, D.J., "Eddy Current Standard Depth of Penetration," Materials Evaluation, Vol. 43, October 1985, pp 1438-1441.
- [2] Hagamaier, D.J. "Cost Benefits of Nondestructive Testing in

Aircraft Maintenance", Materials Evaluation Vol. 46, September, 1988.

- [3] Rummel, W.D., "Human Factors Considerations in the Assessment of Nondestructive Evaluation (NDE) Reliability," Review of Progress in Quantitative Nondestructive Evaluation, Vol. 3A, Ed. D.O. Thompson and D.E. Chimenti, 1984. Plenum Press, New York and London, UK.
- [4] Thompson, O.D., Dale, E. Chimenti, "Review of Progress in Quantitative Nondestructive Evaluation," Volume 7B, Plenum Press, New York, 1987, pp. 1777-1789.
- [5] Smith, K.D., "Turbine Engine Component Retirement for Cause; Advanced Eddy Current Inspection System", Automated Nondestructive Testing, Volume 4, 1986 pp 185 - 194.
- [6] Dau, J.G., "The Challenge of Automatic Inspection", Automated Nondestructive Testing, Volume 4, 1986 pp 1-7.
- [7] Hagemair, D.J., Abelki, P.R., Harmon M.B., "Supplement Inspection of Aging Aircraft", Materials Evaluation, Vol. 44, pp. 899-997, 1986.
- [8] Hecht-Nielsen, R., "Neurocomputing: Picking the human Brain," IEEE Spectrum, March 1988.
- [9] Wasserman, P.D., "Neural Computing Theory and Practice," Van Nostrand Reinhold, 1989.
- [10] Von Aspe W.B., Stewart K.C., Graebner K.E., "Boeing Military Company's Robotic Ultrasonic Inspection System", 30th National SAMPE Symposium, March, 19-21, 1985.
- [11] Bailey, C. D., Pless W.M. "Lisining Systems to Increase Aircraft Structural Safty and Reduced Costs", Lockheed Horizons, summer 1982.
- [12] Scott, W.R., "Long Term Possibilities for Nondestructive Evaluation for US Navy Aircraft", AGARD Report No. 768, 1988.

ROBOTICS: ANOTHER CHOICE FOR INSPECTION OF AGING AIRCRAFT

by

Behnam Bahr
and
Sami Maari
Mechanical Engineering Department
Institute for Aviation Research
The Wichita State University
Wichita, KS 67208

For presentation to the AIAA/FAA Joint Symposium on General
Aviation Systems at the Port O-Call Inn, Ocean City, NJ
on April 11, 1990

Robotics: Another Choice for Inspection of Aging Aircraft

Behnam Bahr, Assistant Professor
Sami Maari, Graduate Student

Mechanical Engineering Department
Institute for Aviation Research
The Wichita State University
Wichita, KS 67208

ABSTRACT

There have been numerous catastrophic failures of in service aircraft due to cracks, corrosion, and human errors. Unfortunately, experts involved with this problem frequently reach different conclusions about the cause of the failure. But, in general they all agree that we need to reduce human error in inspection and maintenance of the aircraft; particularly aging aircraft which have been in service more than 15-19 years. Therefore, the objective of this work is to illustrate how a robotic system can be used for inspection aircraft. A new mobile robot concept for inspection of aircraft will be presented. This approach will be especially useful for areas that are on the aircraft fuselage and not within easy reach. The robot can be programmed to follow a specified path while inspecting the structure. Vision and other inspection systems will be used to record the surface condition of the aircraft. The results of inspection regardless of technique (vision, eddy current, etc.), can be transmitted to the technician or an expert system for detection of cracks with/without human involvement. By using several robots simultaneously, the inspection time can be reduced with more consistent results.

INTRODUCTION

There have been several reminders of aircraft failures such as the Aloha Airlines accident when the skin of the Boeing 737 peeled off in midair [1], and more recently part of the wing of the United 747 peeled off. These incidents call for increased frequency of inspection and for improvement in the quality of the inspection process.

Despite the training that technicians go through, human error has

been identified to be one of the major factors contributing to aircraft accidents. The inspections are costly because of downtime and the number of required man-hours. In general, when an aircraft is removed from service, the loss ranges from \$25,000 to \$50,000 a day [2]. Therefore, there is an increasing demand for rapid, reliable inspection methods for aircraft. Several reasons that justify the partial-automation of aircraft inspection are listed below:

- 1) Improved repeatability of inspection results.
- 2) Higher sensitivity of the inspection is possible with the use of the modern microprocessors.
- 3) Full scan of the aircraft, with more consistent coverage (The robot will not become fatigued or bored).
- 4) The computerization of the data can generate a data base that can be used for prediction and modification of the interpreted results.

The robotic systems:

As the field of robotics is expanding from structured factory environment to nonstructured environments, robots are expected to work many complex tasks in the open air, underwater and in outer space. Hemami, et al. [3], Isik, et al. [4], Lee, et al. [5], and McGhee et al. [6] have done extensive research in the area of legged locomotion and the computer control of legged robots for various terrains. However, there has not been much research in the area of aircraft inspection. Most of the research that has been in the field of automation of inspection [7,8], has been concerned mostly in the areas of data acquisition, data analysis and presentation. They have designed bulky, expensive pieces of equipment which are specific for only one type of inspection. For example, Smith [7] developed an automatic eddy current inspection system for turbine engine components.

Recently the U.S. Air Force's Sacramento Air Logistics has also developed a robotic inspector for General Dynamics F-111 aircraft. The cost of this robot was more than 25.9 Million dollars [9]. While this technique provides rapid, thorough inspection for small fighter type aircraft, there is a need for application of cost-effective robotics for the inspection of larger commercial aircraft. Another development was a robotic system to direct an x-ray or neutron beam at different parts of the airplane. The cost of a complete system was about \$76 million [10].

Southwest Research Institute has built a robotic Deriveter system for the U.S. Navy, which consist of a T3-776 Cincinnati-Milacron 9robot mounted on a pneumatic tire, electric powered vehicle [11]. This robot is used to derivet and inspect the aircraft wing.

Since the robot is not fixed to a location the operator has to manually move the robot so that the robot touches the wing surface at three locations. These reference points are used to compute the transformation matrix to convert the stored rivet location coordinates to the corresponding points on the wing surface. Thereby, knowing the wing orientation with respect to the wrist of the robot it is possible to move the end effector to the other locations.

There has been no significant work done in the United States on robots which can climb vertical walls. A couple of these robots, using magnetic sticking methods, have been implemented in Japan [12,13]. The foremost of these is a wall-climbing vehicle built at the Tokyo Institute of Technology by Hirose [12]. This robot uses an internally balanced magnetic unit to allow it to move on the iron walls of steam boilers in nuclear power plants. In addition, Akir, et al. [13] designed and demonstrated a robot that could climb a vertical wall of a building using a novel idea of vacuum suction mechanism as the robot was moving upward. The limitations with these robots are that they are heavy (250 lb. or more) and are not able to climb the curved surfaces typical of aircraft. The idea of a robot which could climb over the major areas of a large aircraft with on-board capability of carrying a variety of inspection devices has not been pursued. In this paper we present the initial conceptual design of a new surface-climbing robot to aid in the inspection of aircraft. Advantages of this robotic system are:

- * eliminating need for large maintenance stands,
- * eliminating risk of personnel injuries from falling,
- * greatly reducing inspector fatigue and associated errors,
- * ease of adaptability to a variety of aircraft types and sizes,
- * automatic logging of all inspection data for later analysis,
- * ease of incorporation of vision system, expert systems to recognize cracks and other abnormalities,
- * real-time image and inspector control of robot.

This multi-purpose robot is to be designed such that it will be capable of carrying a variety of nondestructive testing instruments such as eddy current and ultrasonic devices, and a miniature camera for a comprehensive inspection of the aircraft skin and sub-skin structures. It could also be used in deriveting or paint stripping operations.

METHODOLOGY/APPROACH

The development of a robot to assist in the inspection process is divided into three integral sections. First is the mechanical design and development of a robotics system that can maneuver on the airplane surfaces to the desired location. Second is the development of a control system for locomotion of the robot. Third is the development of a vision system for guidance of the robot, and to aid the inspection of the aircraft.

A) The design of an aircraft maintenance robot:

The goal is to design a robot that can carry a variety with nondestructive testing devices. The robot will use vacuum suction cups for sticking to the surface of the airplane. This robot will be integrated to a vision sensor system for guidance and visual inspection. The robot will be capable of carrying alternate aircraft inspection instrumentation payloads. A schematic for the application of this new robot is shown in Figure-1. This robot can attach itself to the surface of the aircraft, and move around while inspecting the aircraft.

A number of mechanisms will be considered for this purpose. One of the designs to be considered is shown in Figure 2. This robot (flapper type) is able to move on a curved surface in two perpendicular directions. The base of the robot is supported by four rollers that provide smooth motion and establish constant distance from the surface of the aircraft. The flappers are connected to the base via motorized revolute joints. Each flapper can move up and down independently. The linear motors on each flapper are used as bases for suction cups. A forward motion of the robot is accomplished as follows. First, the suction cups on the two side flappers are activated and the front and back flappers are moved upward, in turn their linear motors are moved to the extreme forward positions. Then these flappers are moved downward until their suction cups contact the surface and are activated. At the second stage of the motion, the suction cups of the side flappers are deactivated and these flappers are moved upward. Now, the base and side flappers can move forward by linear motors of the front and back flappers. The procedure for moving the robot side to side is similar. An alternative to this design can be obtained by replacing the angular motion plus linear motion mechanism with a different kinematic arrangement which utilizes double linear actuators. The robot will have a shape like a flat spider with suction cups at the end of each leg (Figure-3).

B) The interfacing of the robot controller:

The controlling mechanism of this type of robot consists of one supervisor microprocessor, with the following functions: a)

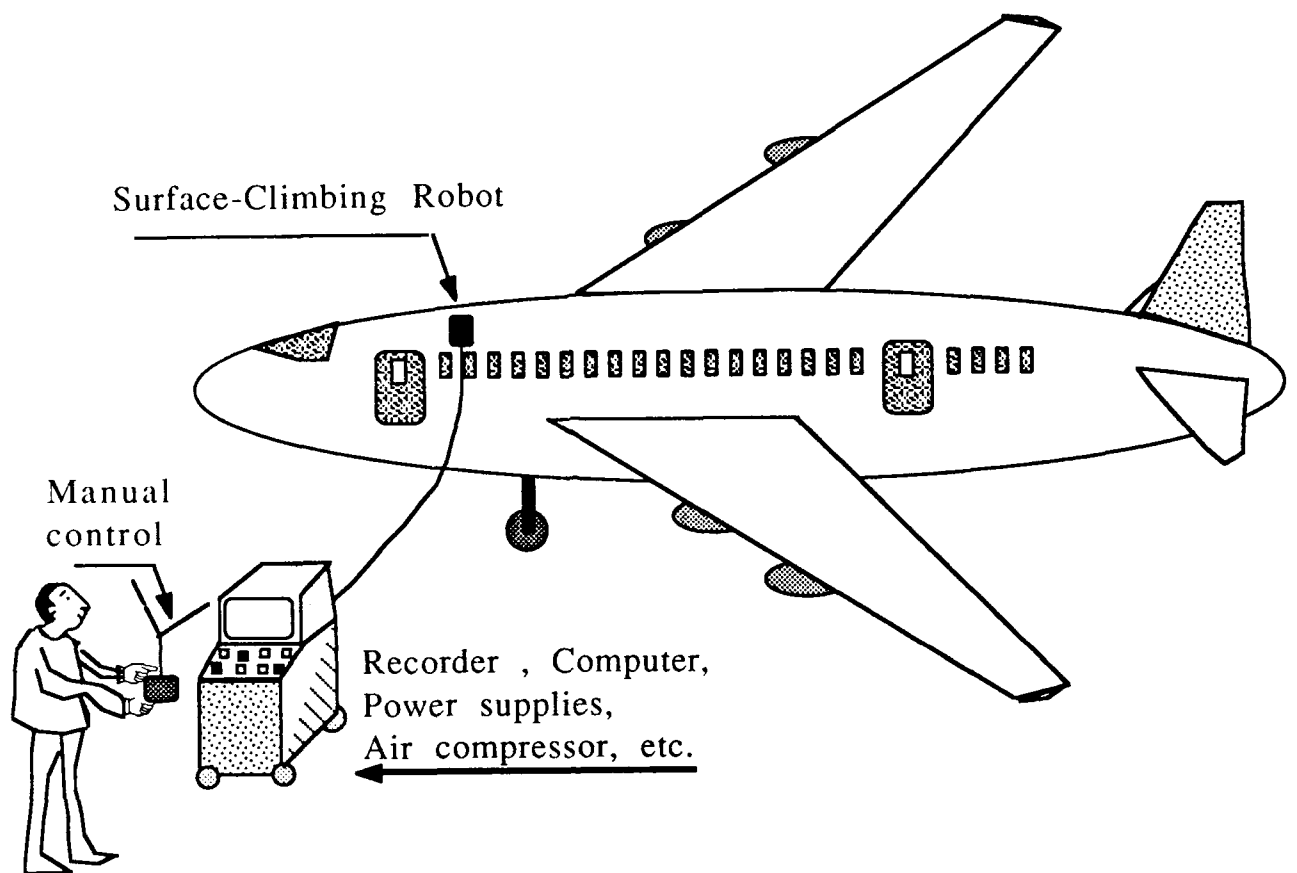


Figure 1 Application of Surface-Climbing Robot.

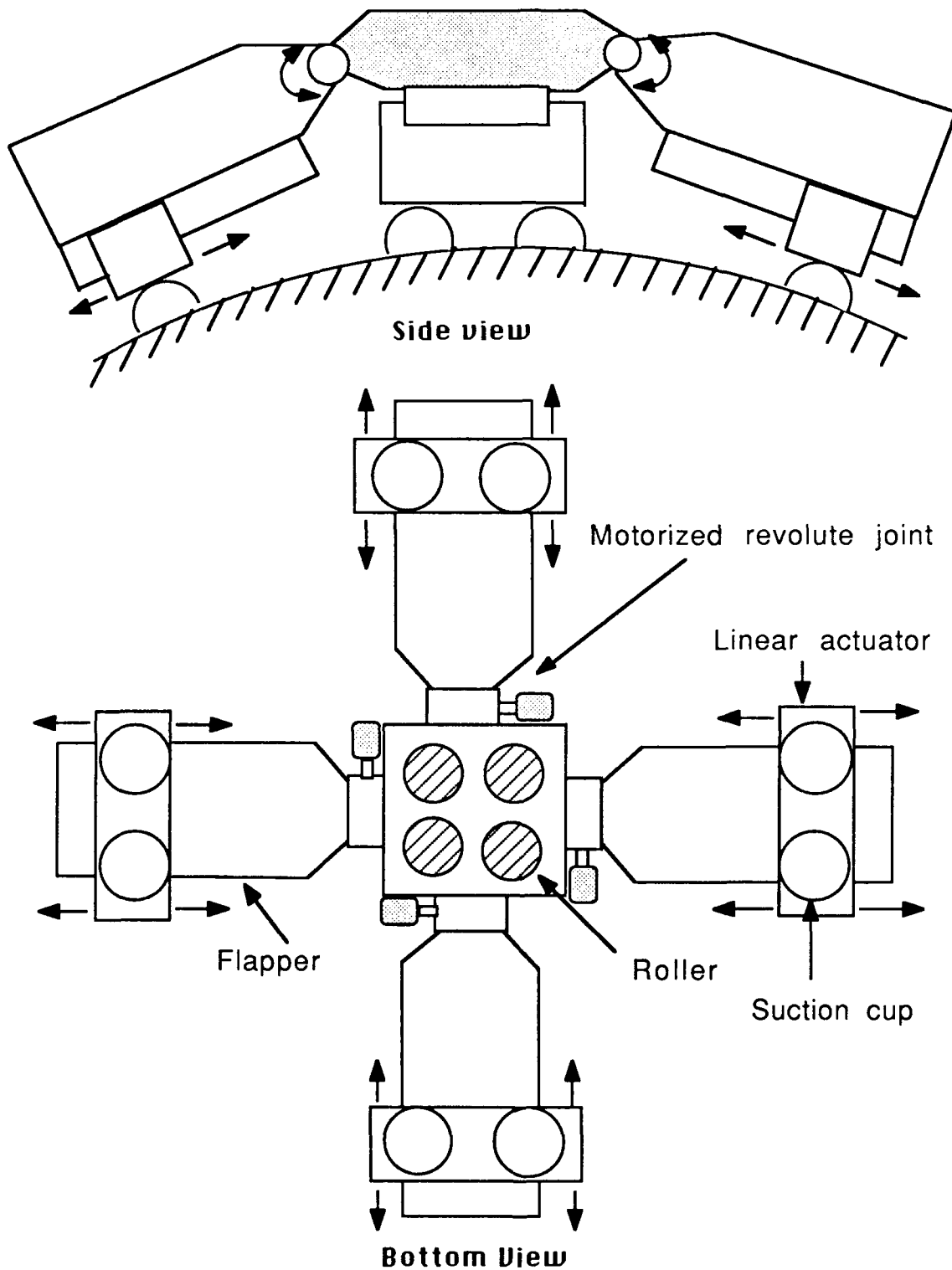


Figure -2 Flapper robot.

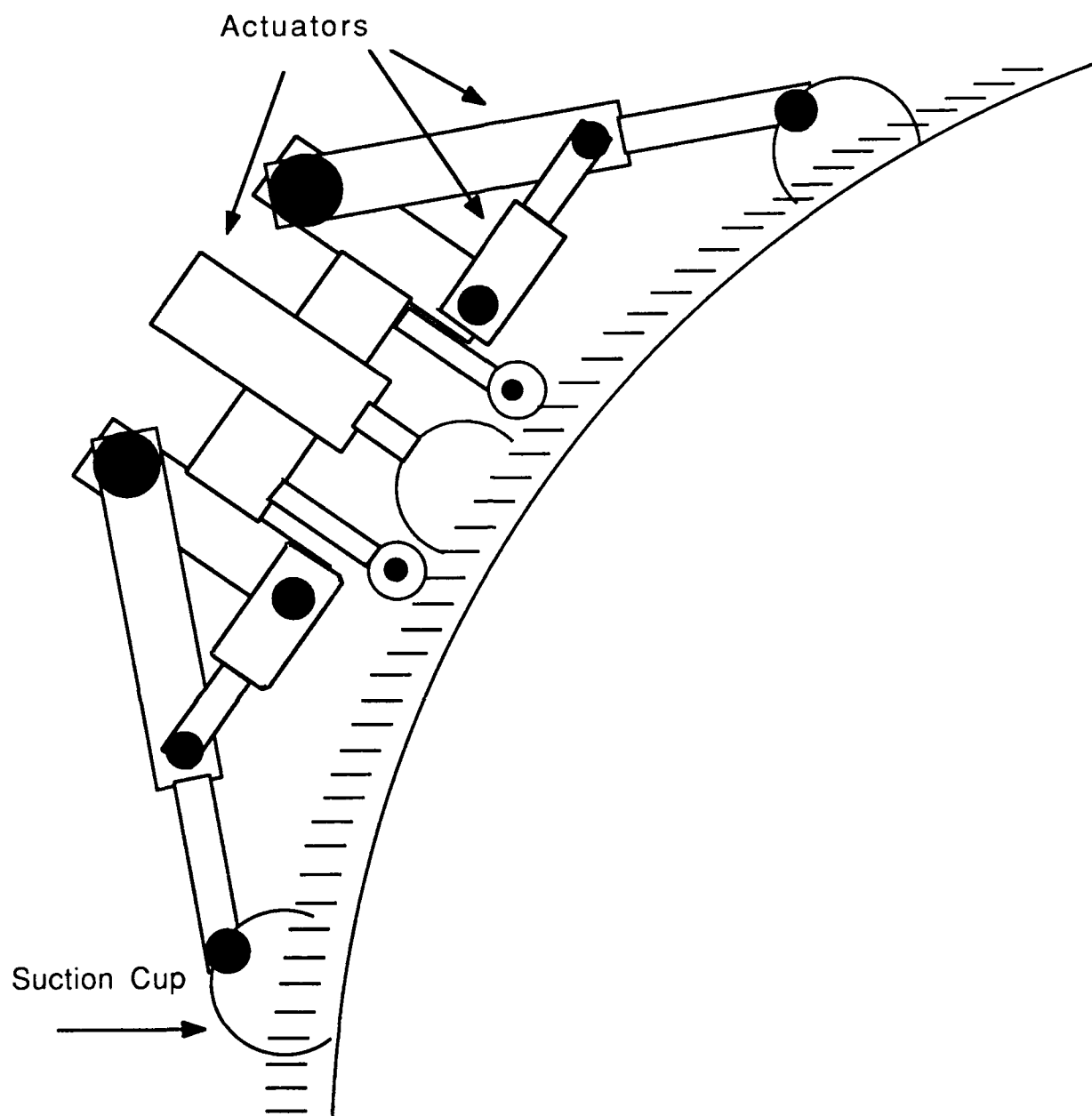


Figure 3 Spider robot.

communicating with user through a joy-stick, or a portable computer, b) supervising all the legs or flappers, and monitoring the status of each leg. At the lower level in the system hierarchy are other microprocessors for sensing and control. Functions include controlling the servomotors, control valves, and air pressure and monitoring movement through sensory feedback, A/D, D/A, encoders and rotation of the whole robot body.

Furthermore, the guidance of the robot can be done by off-line programming for standard rivet lines. A simple joy-stick can be used to over-ride the nominal trajectory of the robot. This feature will be essential for remotely guiding the robot, and is needed for the aircraft that has been repaired where the location of the rivets differ from those of the nominal locations.

C) Robot guidance and inspection of the aircraft:

In this part, a computer vision system will be developed and integrated to the robot so that the operator can remotely guide and control the robot in an arbitrary direction. The vision system also can be used for automatic maneuvering of the robot in order to follow rows of rivets without the operator.

The Miniature camera in conjunction with a frame grabber will be used to digitize the image. Then image processing software will be considered to locate rivets, as well as any inconsistency in the skin of the aircraft due to visible cracks. In addition, the image of the rivets can be recorded with a VCR for further visual inspection.

The gross positioning of the sensor/camera is achieved by the movement of the robot itself. However, the fine positioning of the NDT sensor can be achieved by controlling the sensor relative to the robot. The development of such a positioning system can also be used for other inspection equipment. This sensor system can minimize human error and increase the productivity of the inspector. The collected data and the time history of the inspected parts can be recorded for further detailed inspection or analysis.

CONCLUSION

The preliminary analysis shows that the surface-climbing robot with vision system can:

- 1) Inspect areas that are on the outside surface of the aircraft but not within easy reach (around the fuselage, and the wings).
- 2) Be remotely guided to desired locations.

- 3) Be programmed to follow a specified path
- 4) Remotely micro-position the vision (sensor) system to the specific location with respect to the robot.
- 5) Record the results of inspection by a computer for later analysis.

Therefore, development of such a robotic inspector is the only cost effective way to inspect aircraft and substantially reduce inspection costs by lowering inspection time, and more importantly increase the reliability of inspection.

REFERENCES

- [1] Mecham, M., "Congress Prods FAA to Revise Research in Wake of Crashes" Aviation Week & Space Technology/ Sept. 26, 1988.
- [2] Hagamaier, D.J. "Cost Benefits of Nondestructive Testing in Aircraft Maintenance", Materials Evaluation Vol. 46, September, 1988.
- [3] Hemami, H., Zheng Y.F., and Hines, M.J., "Initiation of Walk and Tiptoe of Planar Nine-Link Biped." Mathematical Biosciences Vol. 61, pp. 163 -189, 1982.
- [4] Isik, C., and Meystel, A.M., "Pilot Level of Hierarchical Controller for an Unmanned Mobile Robot," IEEE Journal of Robotics and Automation, Vol. 4, no. 3, June 1988.
- [5] Lee W.J., and Orin, D.E., "The Kinematics of Motion Planning for Multilegged Vehicles Over Uneven Terrain", IEEE Journal of Robotics and Automation, Vol. 4, No. 2, April, 1988.
- [6] McGhee, R.B., and Pai A.L., "An Approach to Computer Control for Legged Vehicles," Journal of Terramechanics, Vol. 11, No. 1, pp. 9-27, 1974.
- [7] Smith, K.D., "Turbine Engine Component Retirement for Cause; Advanced Eddy Current Inspection System", Automated Nondestructive Testing, Volume 4, 1986 pp 185 - 194.
- [8] Molina, J.I., "Robots Applied to Non-Destructive Inspection", NTIS HC A02/MF A01, 1984.
- [9] Henderson, B.W., "USAF Expects Robotic Inspection Facility to Cut Maintenance Costs", Aviation Week & Space Technology, March 13, 1989.

- [10] Derra, S., "Aging Airplanes: Can Research Make them Safer?," R&D Magazine, January 1990.
- [11] Ernest, F., Luckemeyer, J., "Robotic Removal of Aircraft Wing Rivets," Soc. Manuf. Eng., Paper, No. MS85-563, 1985.
- [12] Hirose S., "Wall Climbing Vehicle Using Internally Balanced Magnetic Unit", Tokyo Institute of Technology, Japan, 1987.
- [13] Akira, N., Yasuo W. and Kazuya W., "Design of a Robot Capable of Moving on a Vertical Wall," Adv. Robotics, Vol. 1, pp. 33 - 45, 1986.

**PERFORMANCE OF A SUPERCHARGED DIRECT-INJECTION STRATIFIED-CHARGE
ROTARY COMBUSTION ENGINE**

by

Timothy A. Bartrand
Sverdrup Tech. Inc., LeRC Group
2001 Aerospace Parkway
Brook Park, OH 44142

and

Edward A. Willis
Propulsion Systems Division
NASA Lewis Research Center
Cleveland, OH 44135

For presentation to the AIAA/FAA Joint Symposium on General
Aviation Systems at the Port O-Call Inn, Ocean City, NJ
on April 11, 1990

PERFORMANCE OF A SUPERCHARGED DIRECT-INJECTION STRATIFIED-CHARGE ROTARY COMBUSTION ENGINE

Timothy A. Bartrand
Sverdrup Tech. Inc., LeRC Group
2001 Aerospace Parkway
Brook Park, Ohio 44142

Edward A. Willis
Propulsion Systems Division
NASA Lewis Research Center
Cleveland, Ohio 44135

ABSTRACT

A zero-dimensional thermodynamic performance computer model for direct-injection stratified-charge rotary combustion engines was modified and run for a single rotor supercharged engine. Operating conditions for the computer runs were a single boost pressure and a matrix of speeds, loads and engine materials. A representative engine map is presented showing the predicted range of efficient operation. After discussion of the engine map, a number of engine features are analyzed individually. These features are: heat transfer and the influence insulating materials have on engine performance and exhaust energy; intake manifold pressure oscillations and interactions with the combustion chamber; and performance losses and seal friction. Finally, code running times and convergence data are presented.

INTRODUCTION

A brief list of the features that make a rotary combustion engine (RCE) a strong candidate as a small aircraft engine would include its large power-to-weight ratio, its ability to be configured into an engine package of small frontal area, its porting simplicity and its inherent balance (1)*. In addition, a direct-injection stratified-charge (DISC) RCE offers the advantages of greater fuel flexibility and improved fuel economy (2). Because of these advantages, research on DISC RCE improvement is ongoing at NASA, in industry and at the university level. As reported in the literature, a DISC RCE has run effectively on gasoline, jet fuel, diesel fuel and methanol (3). Currently, brake specific fuel consumptions (bsfc) of 243–255 g/kW-hr (0.40–0.42 lb/hp-hr) at take-off and 231–249 g/kW-hr (0.38–0.41 lb/hp-hr) at cruise are indicated for an engine with a cruise power of 225 kW (300 hp) (4). These values for bsfc place the DISC RCE well within or under the fuel consumption of horizontally opposed, air cooled conventional piston aircraft engines in a similar power class (5).

In early carbureted RCEs, the positive features mentioned above were offset partially by a number of performance-degrading engine features. Gas seal leakage contributed to reductions in maximum torque, increases in bsfc and increases in hydrocarbon emissions (6). Flame quenching and crevice flows resulted in lost fuel energy and also contributed to bsfc and hydrocarbon emissions increases (7). Finally, slow combustion in the lagging part of the combustion chamber resulted in performance loss and higher emissions (8).

Harder, multi-section apex seals are considered by many to have solved engine sealing problems

* Numbers in parentheses designate references at the end of the paper.

(3). Because the performance of Wankel engines has been improved, it is reasonable to assume the sealing problem has been diminished, although direct measurements of leakage flows in firing engines are difficult to perform. Combustion-related problems have been addressed through the use of dual spark plugs and fuel injection. Suggestions for further improvement of rotary engine performance include insulation of engine components (9), use of improved fuel injection patterns and optimization of rotor pocket and port designs. Fuel injector improvements have been made possible to a large extent through the use of multi-dimensional engine modelling of flow in the combustion chamber (10).

PURPOSE

This report summarizes the results of a computer program written to analyze the performance of a state-of-the-art DISC RCE. A zero-dimensional thermodynamic engine cycle computer model has generated performance data for a single rotor DISC RCE. This satisfied two goals: to map the performance of a hypothetical state-of-the-art RCE and to exercise a modified engine analysis program. In the current study, the intent was not to predict the performance of a specific engine, but to show the general features of DISC RCE performance and to demonstrate the capabilities of an updated computer program.

BACKGROUND

The computer code used in this study (referred to as the MIT code) was initially developed at MIT under the direction of Dr. John Heywood. The first rotary engine code was derived from an existing crank-piston engine thermodynamic model. It predicted the performance of a carbureted RCE (11). The carbureted Wankel model employed a Wiebe function for estimation of burning rate and included crevice/leakage effects. Constant wall temperatures were used and manifold thermodynamic properties were fixed. In its next stage of development at MIT, a DISC combustion heat release model was added. The heat release rate model is described in reference (12). The most complete reference describing the DISC MIT code is the masters thesis presented by Roberts (13). Nguyen et al. applied Roberts' version of the MIT code to a DISC RCE designed by the Outboard Marine Corporation and run at NASA Lewis Research Center (14). Results of a comparable thermodynamic computer model were published by Dimplefeld (15), along with comparisons with engine data. The final development of the MIT code at MIT was performed by Stanten (16), who added the provision for user-defined trochoid housing surface temperatures.

At NASA Lewis Research Center, in addition to funding experimental and industry development of the DISC RCE, computer programs are being written and modified to gain insights into engine performance and in-cylinder processes. Multi-dimensional computer programs under development include those of Raju (17) and Shih et al. (18). In thermodynamic modelling, the MIT DISC engine code has been modified; the modified version was used to produce the results in this paper. A number of major changes have been made to the MIT code at NASA. First, steady state heat transfer models for the rotor face, side housings, trochoid housing and exhaust pipe were added. Also, intake manifold pressure, temperature and mass are now allowed to vary during the intake process. Accounting of crevice mass accumulation was changed, as well as the convergence process and the selection of cycle initial conditions. Finally, kinematic models for seal and bearing friction were added, along with an ad hoc model for estimating losses associated with ancillary components. In the following section of this paper, the basic governing equations of the MIT code will be reviewed briefly and the additions will be described in greater detail.

Due to the MIT code's much shorter computational time, it has many capabilities and can address engine development questions that are not addressed by the multi-dimensional codes mentioned above. On the negative side, the code relies on empirical constants. If experimental data are not

first obtained for an engine, the MIT code can only demonstrate trends. Nonetheless, such a model as the MIT code is useful in preliminary investigations of engine configurations and may be used as part of a larger turbocharged/turbocompounded engine simulation.

MODEL FORMULATION AND CALIBRATION

A brief overview of the original DISC MIT code governing equations is presented in this section, along with a more detailed treatment of the additions made to the code at NASA. For more detailed information, the reader is directed to references (11), (13) and (16).

The MIT code follows the progress of one of the three RCE combustion chambers through a number of engine cycles until steady operation is achieved. The gas in the combustion chamber and in the manifolds is considered well mixed.

Figure 1 is a schematic of a RCE. The indicated chamber is in the minimum volume, top dead center (TDC) position. In the MIT code, this position is designated as crank angle, θ , equal to 0° . The engine cycle begins as the intake port opens (when the lead apex seal begins to uncover the intake port) at crank angle θ_{ipo} and lasts for one rotor revolution. Since the rotor rotates at $1/3$ the rate of the crankshaft, one cycle lasts $3 \times 360^\circ = 1080^\circ$. θ_{ipc} , θ_{sp} , θ_{epo} and θ_{epc} are crank angles for intake port closing, spark firing, exhaust port opening and exhaust port closing, respectively. For the above definition of crank angle, θ_{ipo} , θ_{ipc} and θ_{sp} are negative while θ_{epo} and θ_{epc} are positive. The MIT code is considered converged when the chamber pressure, P_c , the chamber temperature, T_c , the chamber mass, m_c , the intake manifold pressure, P_{im} and the rotor and housing temperatures vary less than a user-input tolerance between engine cycles.

As the code marches in crank angle, the derivatives of chamber temperature, pressure, mass and composition are calculated and integrated. In addition, leakage flow rates, heat transfer rates and rate of change of manifold properties are calculated on a crank angle by crank angle basis. Chamber pressure, temperature, mass and composition are governed by the conservation of mass, species and energy and the ideal gas relation. Thermodynamic properties are calculated using approximate, empirical relations for hydrocarbon-air combustion products (19). Flow rates into and out of the chamber, including intake, exhaust and leakage through gas seals, are quasi-steady, 1-D compressible; the mass flow rate is uniquely determined by upstream temperature, pressure and composition, downstream pressure and user-input discharge coefficient. Port areas and leakage area per chamber are also input. Backflow of chamber contents into the intake manifold is allowed.

Combustion proceeds according to an input empirical heat release rate. As shown in Figure 2, heat release takes place in two phases. First, there is a linear rise to the maximum heat release rate:

$$\frac{dQ}{d\theta} = \left(\frac{dQ}{d\theta} \right)_{max} \left(\frac{\theta - \theta_{sp}}{\theta_{qmax} - \theta_{sp}} \right) \quad (1)$$

where $\frac{dQ}{d\theta}$ is the rate of fuel energy heat release per crank angle degree, $\left(\frac{dQ}{d\theta} \right)_{max}$ is the maximum heat release rate encountered and θ_{qmax} is the crank angle for the maximum heat release rate. After the linear rise, the heat release rate falls exponentially according to

$$\frac{dQ}{d\theta} = \left(\frac{dQ}{d\theta} \right)_{max} \exp \left\{ \frac{-(\theta - \theta_{qmax})}{\tau} \right\} \quad (2)$$

Inputs to the MIT code combustion model are $\left(\frac{dQ}{d\theta} \right)_{max}$ and θ_{qmax} . τ is calculated assuming complete combustion of fuel. Ideally, a set of combustion model inputs would be provided to the code for various engine speeds and loads, depending on the variation of the combustion process

with speed and load. In the absence of engine pressure data to derive these combustion model inputs, the same values were used for all operating conditions in this study. The values used for these constants were chosen based on the authors' experience and the work of Nguyen (14). Using the same combustion model inputs for all engine operating conditions is expected to result in error, especially at high engine speeds when the time for all the fuel to burn becomes a greater fraction of the time to complete one engine cycle for an actual engine.

Heat transfer coefficient between the chamber gas and the trochoid housing inner surface, the rotor face and the side housing surfaces is calculated according to

$$Nu = \beta Re^{\alpha} Pr^{\gamma} \quad (3)$$

where Nu is Nusselt number based on the chamber depth, Re is Reynolds number based on chamber depth, Pr is Prandtl number and β , α and γ are empirical constants. This relation was proposed by Woschni (20). During intake, compression and exhaust, the velocity used in the Reynolds number is the rotor tip speed. During combustion, another term is added to velocity to include combustion turbulence effects. For the results presented, the constants in equation 3 were $\beta = 0.038$, $\alpha = 0.8$ and $\gamma = 1$. An attempt was made to implement an alternative relation proposed by Lee and Schock (21), but this relation did not produce acceptable qualitative results; the peak heat transfer rates did not occur at or near TDC.

Steady state wall temperature calculations are now made in the MIT code. The trochoid housing is divided into 30 segments. The midpoints of these segments are shown in Figure 3. A steady state wall temperature calculation is made at each segment's midpoint. The trochoid housing can be made of up to three materials, each with its own thickness and thermal conductivity. The hot gas side heat transfer coefficient at the segment midpoints is taken as the average of the heat transfer coefficient (equation 3) over the 360° surrounding the segment. The coolant side heat transfer coefficient is calculated internally with user-input coolant properties and flow rate and allowing for nucleate boiling. As can be seen from the thermal resistance schematic in Figure 4, the wall temperature, T_{wall} is

$$T_{wall} = \frac{\overline{h_{hg}} \overline{T_c} + U T_{cool}}{U + \overline{h_{hg}}} \quad (4)$$

where $\overline{h_{hg}}$ is average hot gas heat transfer coefficient, $\overline{T_c}$ is average chamber temperature and U is overall heat transfer coefficient from the inner housing surface to the coolant. For the housing cross section shown in Figure 4,

$$U = \frac{1}{L_1/k_1 + L_2/k_2 + L_3/k_3 + 1/h_{cool}} \quad (5)$$

where L_1 , L_2 and L_3 are thicknesses of materials 1, 2, and 3, k_1 , k_2 and k_3 are thermal conductivities of materials 1, 2 and 3 and h_{cool} is the coolant side convective and boiling heat transfer coefficient. Equation 5 assumes housing curvature effects are small.

A steady state heat transfer model applied at each segment midpoint is the most practical for use with a thermodynamic model. A similar approach was used by Assanis and Badillo (22) and produced adequate results for metal engines, but less satisfactory results for insulated engines. It is likely that errors in using a steady state heat transfer model will be less for the trochoid housing, since each housing position "sees" only a limited part of the cycle and is therefore subject to less severe swings in temperature. Another short-coming of the steady-state heat transfer model is its insensitivity to heat-transfer-driven changes in the combustion process. When wall temperature,

porosity and radiation characteristics are changed, the combustion process may also change. Unless the MIT code combustion model is recalibrated for each set of housing and rotor materials, changes in the combustion process will not be reflected in predicted performance.

Side plate temperatures are calculated similarly to trochoid housing temperatures, with the exception that the coolant side heat transfer coefficient is input and does not include nucleate boiling. The rotor face temperature also is calculated assuming one dimensional steady state heat transfer. The hot gas side heat transfer coefficient and gas temperature are set equal to the cycle averages and the heat transfer coefficient is a user-input value. The value used for rotor coolant heat transfer coefficient was estimated reflecting a "cocktail shaker" type oil flow in the rotor cavity.

Intake manifold thermodynamic properties including intake manifold pressure, P_{im} , temperature, T_{im} , and mass, m_{im} , can either be fixed or allowed to vary during the intake process. Intake manifold volume, V_{im} , does not change. For variable intake manifold properties, the first cycle of the run is made with fixed properties to estimate air mass flow rate to the manifold. For subsequent cycles, the air mass flow rate to the manifold is constant during the cycle and the rate of change of intake manifold mass, \dot{m}_{im} , is given by

$$\dot{m}_{im} = \dot{m}_{ic} - \dot{m}_{int} \quad (6)$$

where \dot{m}_{ic} is mass flow rate into the intake manifold (e.g., from an aftercooler) and \dot{m}_{int} is mass flow rate from the intake manifold to the combustion chamber. The derivative of intake manifold temperature is

$$\frac{dT_{im}}{dt} = \left(\frac{T_{im}}{P_{im}V_{im}} \right) \left(\frac{\dot{m}_{ic}(i_{ic} - i_{im}) + \Re T_{im} \dot{m}_{im} + \dot{Q}_{im}}{c_{p,im}/\Re - 1} \right) \quad (7)$$

where i_{ic} is the enthalpy of the incoming stream, i_{im} is the enthalpy in the intake manifold, \Re is the gas constant for air, \dot{Q}_{im} is heat transfer rate to manifold walls (taken as zero for the current study) and $c_{p,im}$ is specific heat at constant pressure in the intake manifold. Pressure rate of change is

$$\frac{dP_{im}}{dt} = \left(\frac{\Re T_{im}}{V_{im}} \right) \dot{m}_{im} + \left(\frac{P_{im}}{T_{im}} \right) \frac{dT_{im}}{dt} \quad (8)$$

Apex seal friction force is calculated following the approach given by Yamamoto (23), but taking into consideration friction between the seal slot and the seal and also using pressures generated by the MIT code. For any crank angle, θ , calling the pressure ahead of the apex seal P_1 and that behind the seal P_2 , the instantaneous apex seal friction force, F_{sf} , is

$$\begin{aligned} F_{sf} = \frac{\mu_a}{\cos \varphi} \left\{ l_a \left(\frac{b_a}{2} + a_r \sin \varphi \right) (P_1 - P_2) + m_a \left(\frac{d\theta}{dt} \right)^2 \left[\frac{r}{9} + \epsilon \cos \left(\frac{2\theta}{3} \right) \right] - \right. \\ \left. \mu_a m_a \left(\frac{d\theta}{dt} \right)^2 \sin \left(\frac{2\theta}{3} \right) - \mu_a P_1 l_a (h_a - c_a) - \right. \\ \left. \mu_a l_a (P_1 - P_2) (c_a - a_r + a_r \cos \varphi) + F_{sa} \right\} \quad (9a) \end{aligned}$$

when $P_1 > P_2$ or

$$F_{sf} = \frac{\mu_a}{\cos \varphi} \left\{ l_a \left(\frac{b_a}{2} + a_r \sin \varphi \right) (P_2 - P_1) + m_a \left(\frac{d\theta}{dt} \right)^2 \left[\frac{r}{9} + \epsilon \cos \left(\frac{2\theta}{3} \right) \right] - \right.$$

$$\mu_a m_a \left(\frac{d\theta}{dt} \right)^2 \sin\left(\frac{2\theta}{3}\right) - \mu_a P_2 l_a (h_a - c_a) - \mu_a l_a (P_2 - P_1)(c_a - a_r + a_r \cos \varphi) + F_{sa} \} \quad (9b)$$

for $P_2 > P_1$. In equations 9a and 9b, μ_a is the apex seal's sliding coefficient of friction on the trochoid housing, b_a is the apex seal width, a_r is the radius of curvature for the apex seal crown, m_a is the apex seal mass, r is the rotor generating radius, ϵ is the engine eccentricity, c_a is the clearance between the rotor tip and the seal tip, l_a is the seal depth (equal to the chamber depth), F_{sa} is the spring force on the seal and φ is the seal lean angle, given by

$$\varphi = \arccos \left\{ \frac{3\epsilon \cos[\frac{2}{3}(\theta + 180^\circ)] + r}{\sqrt{9\epsilon^2 + r^2 + 6\epsilon r \cos[\frac{2}{3}(\theta + 180^\circ)]}} \right\} \quad (10)$$

Side seal friction force is assumed lumped at the seal center. It arises due to both gas pressure loads and spring force. Side seal friction force, F_{sf} , is given by

$$F_{sf} = \mu_s F_{ss} + (b_s - \mu_s h_s) \mu_s l_s P_c \quad (11)$$

where μ_s is the coefficient of sliding friction for the side seal on the side housing, F_{ss} is the side seal spring force, b_s is the side seal width, h_s is the side seal height, l_s is the side seal length and P_c is the instantaneous chamber pressure. The crank case pressure, P_{cc} , is assumed constant, so the oil seal friction force, F_{of} is given by

$$F_{of} = 2\pi R_o b_o \mu_o P_{cc} + \mu_o F_{so} \quad (12)$$

In equation 12, R_o is the oil seal radius, b_o is the oil seal width, μ_o is the oil seal sliding coefficient of friction and F_{so} is the oil seal spring force. At Michigan State University, modelling work for seal friction is currently underway. This work is expected to result in more sophisticated seal models for use in the MIT code (24).

Ancillary losses were lumped together and estimated in a manner similar to that of other intermittent combustion engine thermodynamic programs. Heywood (25) recommends a relation of the form

$$fmep = C_{F1} + C_{F2} \left(\frac{N}{1000} \right) + C_{F3} \left(\frac{N}{1000} \right)^2 \quad (13)$$

for friction mean effective pressure ($fmep$) in a spark ignition engine. Here, C_{F1} , C_{F2} and C_{F3} are constants and N is engine speed in rpm. The first term is associated with boundary lubrication, the second term with hydrodynamically lubricated surfaces in relative motion and the third with fluid losses (air, water, fuel and oil pumping). Because the MIT code calculates the seal and bearing friction loads separately, equation 13 was modified to

$$fmep_a = C_{A1} + C_{A2} \left(\frac{N}{1000} \right)^2 \quad (14)$$

where $fmep_a$ is the ancillary $fmep$ and C_{A1} and C_{A2} are constants. The only available data for use in calibrating equation 14 were unpublished data (26). Using these data, the constants in equation 14 were set to $C_{A1} = 0.45$ and $C_{A2} = 0.025$.

RESULTS

The MIT code was run for a single rotor engine in the 75 kW class for engine speeds ranging from 3500 to 8500 rpm and for fuel/air equivalence ratios between 0.35 and 0.85. The engine was supercharged to an average boost pressure of 86.1 kPa (12.5 psig) and the exhaust manifold pressure was set at 152 kPa (22 psia). Fuel used was iso-octane. The baseline engine had housings made of aluminum and a rotor made of iron. Engine coolant was a 50/50 mixture of water and ethylene glycol. There were two main bearings, two rotor bearings, three apex seals, six side seals and two oil seals. Leakage area was estimated at 0.1 cm^2 and crevice volumes at 0.57 cc. Discharge coefficients were 0.6 and 0.65 for the intake and exhaust ports, respectively.

PERFORMANCE

A P-V diagram was generated for a baseline engine (Figure 5). Although chamber properties, etc., are calculated at fractional crank angle steps, output was only generated for crank angle increments of 10° . The shape of the plot is expected, but three points should be noted. First, there is a small positive pumping loop (resulting in work added to the system), since the intake pressure is greater than the exhaust and chamber pressures during the scavenging process. Second, the peak chamber pressure location, 28° after TDC, and magnitude, 60.4 atm, are determined by inputs to the combustion model, which was not adjusted to reflect burning rate changes with speed and load. Finally, the peak chamber pressure is well above the critical pressure for *n*-octane, 24.8 atm (27). The thermodynamic cycle description is completed in Figure 6, which shows chamber temperature and the combustion progress for one cycle. Combustion progress is defined as the fraction of the total fuel for one cycle burnt by a given crank angle (0 means combustion has not begun, 1 means combustion is complete). As expected, the temperature drop is more gradual than the pressure drop during the expansion process.

The results of this study are summarized in Figure 7. The performance of a hypothetical DISC RCE is mapped over a domain of engine speeds and loads. Lines of constant equivalence ratio are plotted and contours of iso-bsfc are superimposed. Constant equivalence ratio lines flatten out with engine speed because of volumetric efficiency decreases. The high bsfc's seen at low load arise because the ancillary losses are such a large fraction of indicated power. The engine map shows a fairly large region of operating conditions for which fuel consumption is below 290 g/kW-hr (0.48 lb/hp-hr). Some cautions should be noted, however. First, this engine map was generated for only one boost pressure; to fully map engine performance, a family of these maps should first be generated and then "matched" to the characteristics of the turbocharger in use. Secondly, no attempt was made to optimize engine performance or fuel consumption. Finally, the performance may be worse than predicted at high speeds, because of injector and combustion changes. The engine map of Figure 7 was generated in approximately 1.5 hr CPU time on a VAX 11/780 mainframe computer.

HEAT TRANSFER

To investigate the ability of insulating coatings and materials to enhance engine performance and exhaust gas energy, the MIT code was run for six sets of engine materials: the baseline engine (aluminum housings and iron rotor), an all titanium engine, an engine with a ceramic coated trochoid housing, an engine with a ceramic coated rotor, an engine with all surfaces ceramic coated and a hypothetical, adiabatic engine. Because chamber pressure data were not available for calibration of the combustion model for each of these engines, the same combustion model inputs are used for all six engines. This may lead to inaccurate predictions should the wall temperatures or properties become very different from those of the baseline engine. The exact make-up and material properties of these engine components are detailed in Table 1. The coatings used were chosen to be the same as those of Badgley et al. (9).

Table 1: Engine Materials for the Six Heat Transfer Test Cases

Case	Trochoid Housing	Rotor Face	Side Housing
1	11.25mm Aluminum*	11.25mm Iron**	11.25mm Aluminum
2	10.76mm Titanium***	10.63mm Titanium	10.76mm Titanium
3	10mm Al coated with 0.127mm of coating 1 [†] and 0.635mm of coating 2 [‡]	11.25mm Iron	11.25mm Aluminum
4	11.25mm Aluminum	10mm Iron coated with 0.635mm of coating 2	11.25mm Aluminum
5	10mm Al coated with 0.127mm of coating 1 and 0.635mm of coating 2	10mm Iron coated with 0.635mm of coating 2	10mm Al coated with 0.127mm of coating 1 and 0.635mm of coating 2
6	Hypothetical Struc- ture with near-zero conductivity	Hypothetical Struc- ture with near-zero conductivity	Hypothetical Struc- ture with near-zero conductivity

* For Aluminum, $k=240$ w/m-k

** For Iron, $k=547$ w/m-k

*** For Titanium, $k=19.4$ w/m-k

[†] Coating 1 is Plasma Sprayed Cr_2O_3 , $k=1.21$ w/m-k

[‡] Coating 2 is Plasma Sprayed Zirconia, Post Densified with Cr_2O_3 , $k=2.91$ w/m-k

In Figure 8, predicted trochoid housing inner surface temperatures are plotted for 30 housing positions (see Figure 3 for the 30 positions). Because nucleate boiling was allowed on the coolant side of the housing, coolant heat transfer coefficients became very high when the trochoid housing temperature on the coolant side approached the liquid saturation temperature. The result is very little swing in housing temperature for the aluminum housings. Predicted peak temperature for the coated housing ($T_{wall} = 672$ K, $[750^\circ F]$) was considerably below the prediction of Badgley et al. ($T_{wall} = 991$ K $[1324^\circ F]$) for a liquid cooled engine of the same size category. In predicting their wall temperatures, Badgley et al. used the version of the MIT DISC engine code from MIT without the changes that were made subsequently at NASA. The MIT code was used to generate boundary conditions for a multi-dimensional, finite element steady state heat conduction analysis of the trochoid housing. Badgley's model is steady state, in that averaged chamber temperatures and heat transfer coefficients are used on the hot side of the housing walls. Coolant side heat transfer coefficient and temperature for the finite element analysis were chosen and fixed (apparently the same values for all housing positions). Two possible explanations are offered for the differences between predicted housing temperatures. First, coolant side heat transfer coefficient was determined differently in the two studies. Also, the analysis used in the present study is 1-D, whereas that of Badgley et al. was 3-D (although the boundary conditions were not time dependent). Neither calculation accounted for possible changes in the combustion process.

Also found on Figure 8 are predicted housing temperatures for an all-titanium engine and a hypothetical adiabatic engine. The predicted housing temperatures for all the engines shown in Figure 8 are well below those of a truly adiabatic engine.

Figure 9 illustrates the redistribution of fuel energy from the coolant to work and exhaust when the engine is insulated. In all cases but the adiabatic engine, only modest decreases in coolant load are realized. In general, most of the fuel energy diverted from the coolant appears in the exhaust stream, as demonstrated in the adiabatic engine case. Note that this analysis was performed at only one engine speed, 5500 rpm. At lower engine speeds, since heat transfer is time (and not crank angle) dependent, the fraction of the fuel energy lost to the coolant will be higher and the influence of insulating materials more pronounced. The effect insulating materials have on mean exhaust gas temperature, brake power and bsfc is shown in Table 2. Volumetric efficiency for the coated and titanium engines was nearly the same as that of the baseline engine (93 %). The volumetric efficiency of the hypothetical adiabatic engine was 91 %.

Table 2: Influence of Engine Materials on Performance

Case	% of Fuel Energy to Cooling (%)	\bar{T}_{exh} (K)	Normalized Brake Power (-)	BSFC (g/kW-hr)
1	12.5	964.5	1.0	281
2	11.0	975.5	1.012	278
3	11.7	969.7	1.008	279
4	12.4	965.7	1.002	281
5	11.5	971.3	1.008	279
6	0	1064.6	1.06	260

In Figure 10, the breakdown of coolant heat transfer to the trochoid housing, the rotor face and the sideplates is shown. Since the percentage of heat transfer through the rotor and sideplates is small (in terms of fuel energy), it appears that insulating the trochoid housing would have a greater impact on exhaust gas energy. Because the apex seals scrape the trochoid surface, though, care must be taken in choosing a housing coating and applying it to the surface. Although weight was not analyzed in this study, it is suggested an added benefit of an insulated aircraft engine is its lower cooling system weight.

MANIFOLD PROPERTIES

Since MIT code results were last published, provisions for variable intake manifold pressure, temperature and mass have been added. The formulation is described in this report's Model Formulation and Calibration section. The instantaneous intake manifold pressures for an engine run with an equivalence ratio of 0.75 and engine speeds ranging from 3500 to 8500 rpm are shown in Figure 11. Although a relatively large manifold volume was used (equal to the engine displacement volume), the intake manifold pressure variation during one intake event is large, ~ 30% of the average intake manifold pressure at 3500 rpm. The peak pressure decreases and shifts to later crank angles as engine speed is increased. Since peak pressures are high and early in the intake process (before

the exhaust port closes), there is significant blow-through of fresh air through the exhaust port at low speeds. In addition, since the pressure at the time the intake port closes is higher for low speeds, the volumetric efficiency also is expected to be higher. Volumetric efficiency was calculated based on average manifold pressure and temperature. No comparisons are made with empirical data, since no data were available. In the future, if a need is shown, a more complex, geometry dependent 1-D intake manifold model may be incorporated.

The MIT code was run for the same operating conditions and with both variable and fixed intake manifold thermodynamic properties. Intake manifold volume was not changed for any runs. Figure 12 shows a significant difference between predicted air flow rate and trapping efficiency for the fixed and variable property cases. Trapping efficiency is defined as the percentage of the air flowing through the intake port that is trapped in the chamber when the intake port closes. Both the air mass flow rate and the trapping efficiency are lower for the variable intake manifold thermodynamic property model than for the fixed property model.

In Figure 13, volumetric efficiency and brake power are plotted for the variable and fixed intake manifold property models. Because of the tuning effects described above, the volumetric efficiency of the variable manifold pressure engine is higher at low speeds and lower at high speeds compared to that of the fixed property engine. These volumetric efficiency differences also are reflected in the output power curves.

LOSSES

Figure 14a shows the estimated ancillary f_{mep} , f_{mep_a} , for an engine run at $\phi = 75$. Recalling equation 14, f_{mep_a} rises with the square of engine speed. Note that f_{mep_a} has no load dependency. The f_{mep_a} includes contributions from the water pump, the oil pump, the fuel pump, the alternator and the acceleration of oil in the rotor cavity.

In Figure 14b, seal friction losses for the same engine and a motored engine are plotted against engine speed. The seal f_{mep} is lower than f_{mep_a} . The relatively small influence of equivalence ratio on friction is demonstrated in Figure 14b. Since crank case pressure is not varied, the oil seal friction losses are the same for the motored and the fired engine. Because apex seal losses are dominated by the centrifugal force exerted on the seal, not by gas pressure, apex seal losses are predominantly influenced by engine speed. The side seals show a greater sensitivity to gas pressure, because they have a greater base area (there are six side seals) and are subjected to the chamber pressure.

Friction mean effective pressure is plotted against engine speed for three equivalence ratios in Figure 15. f_{mep} in Figure 15 includes seal friction, bearing friction and ancillary losses. A more revealing comparison of the friction losses at different engine loads is made in Figure 16, where the fraction of the indicated power used to overcome friction losses is plotted against engine speed for 3 equivalence ratios. At low loads, the friction consumes a greater fraction of the engine indicated power. This results in the high bsfc's at low loads shown on the engine map (Figure 7).

CODE STATISTICS

Table 3 shows convergence data and CPU times for a number of runs. Normally the MIT code requires between 3 and 12 engine cycles to converge for one set of engine operating conditions. This equates to between 1 and 3 CPU minutes to run on a VAX 11/780 mainframe computer.

Table 3: Computer Program Statistics

Case	Cycles to Converge	$(\Delta P_c)_{initial}$	$(\Delta T_c)_{initial}$	$(\Delta P_{im})_{initial}$	CPU Time (min)*
$\phi=0.75$, 3500 rpm	6	0.02%	-0.42%	0.05%	1:42
$\phi=0.75$, 5500 rpm	5	0.05%	-0.16%	0.71%	1:24
$\phi=0.75$, 7500 rpm	7	0.10%	-0.08%	0.26%	1:54
Motored, 7500 rpm	6	0.04%	-0.13%	0.86%	1:45
Motored, 7500 rpm, $P_{im} = \text{constant}$	4	0.06%	-0.06%	0.00%	1:03

* On a VAX 11/780 Mainframe Computer

CONCLUSIONS

A hypothetical, one rotor DISC RCE was analyzed with a zero-dimensional thermodynamic engine cycle computer program. The program predicted a broad range of operating conditions over which the engine could run at desired power for fuel consumption below 290 g/kW-hr (0.48 lb/hp-hr). Insulating the engine with a thin coating of ceramic material resulted in small reductions in the coolant load and very small improvements in performance. It is possible the steady state approach used to calculate heat transfer resulted in underprediction of the positive effects of insulation. In addition, it was assumed changes in wall temperature and wall material properties did not have a large influence on the combustion heat-release rate.

A new intake manifold model was demonstrated. There are significant differences in predicted air mass flow rate and volumetric efficiency when the intake manifold properties are allowed to vary, as opposed to using a fixed intake pressure and temperature. There is a significant variation in pressure in the intake manifold during the intake process.

Engine losses were estimated using kinematic models for all seals and bearings, and using an ad hoc model to estimate all other ancillary losses. In general, losses are more influenced by engine speed than load. It would be desirable to incorporate separate models for the ancillary components such as water pump, fuel pump, oil pump and alternator.

When engine pressure data become available for a DISC RCE for a number of loads and speeds, a set of combustion model inputs for the MIT code will be calculated. The domain over which a set of combustion rate model inputs is valid will be determined with these values. Until that time, the MIT code can only be used to make qualitative studies on engine performance. Other model constants that need to be calibrated include friction and heat transfer model inputs.

The MIT code is an inexpensive tool for analyzing DISC Wankel engines. It normally runs in less than 3 min on a VAX 11/780 computer and produces information for a wide range of engine performance indicators. It has been shown to be flexible enough to incorporate submodels for friction and other engine processes and it appears compatible for use in a turbocharged/turbocompounded engine system analysis.

REFERENCES

- (1) Jones, C., "The Curtiss-Wright Rotating Combustion Engines Today," Paper 886D, SAE Transactions, pp.127-147, 1965.
- (2) Willis, E. A. and Wintucky, W. T., "An Overview of NASA Intermittent Combustion Engine Research," Paper AIAA-84-1393, AIAA/SAE/ASME Joint Propulsion Conference, Cincinnati, Ohio, 1984.
- (3) Jones, C., "An Update of Applicable Automotive Engine Rotary Stratified Charge Developments," SAE Paper 820347, International Congress and Exposition, Detroit, Michigan, 1982.
- (4) Mount, R. E. and LaBouff, G. A., "Advanced Stratified Charge Rotary Engine Design," SAE Paper 890324, International Congress and Exposition, Detroit, Michigan, 1989.
- (5) McCormick, B. W., Aerodynamics, Aeronautics and Flight Mechanics, p. 338, John Wiley & Sons, New York, 1979.
- (6) Eberle, M. K. and Klomp, E. D., "An Evaluation of Potential Performance Gain from Leakage Reduction in Rotary Engines," SAE Paper 730117, International Automotive Engineering Congress, Detroit, Michigan, 1973.
- (7) Danieli, G. A., Ferguson, C. R., Heywood, J. B. and Keck, J. C., "Predicting the Emissions and Performance Characteristics of a Wankel Engine," SAE Paper 740186, International Automotive Engineering Congress, Detroit, MI, 1974.
- (8) Ferguson, C. R., Danieli, G. A., Heywood, J. B. and Keck, J. C., "Time Resolved Measurements of Exhaust Composition and Flow Rate in a Wankel Engine," SAE Paper 750024, International Automotive Engineering Congress and Exposition, Detroit, MI, 1975.
- (9) Badgley, P. R., Doup, D. and Kamo, R., "Analysis and Test of Insulating Components for Rotary Engine," SAE paper 890326, International Automotive Engineering Congress and Exposition, Detroit, Michigan, 1989.
- (10) Abraham, J., Wey, M.-J. and Bracco, F. V., "Pressure Non-Uniformity and Mixing Characteristics in Stratified-Charge Rotary Engine Combustion," SAE paper 880624, International Automotive Engineering Congress and Exposition, Detroit, Michigan, 1988.
- (11) Norman, T. J., A Performance Model of a Spark Ignition Wankel Engine: Including the Effects of Crevice Volumes, Gas Leakage and Heat Transfer, Masters Thesis, Massachusetts Institute of Technology, June, 1983.
- (12) Gatowski, J. A., Balles, E. N., Chun, K. M., Nelson, F. E., Ekchian, J. A. and Heywood, J. B., "Heat Release Analysis of Engine Pressure Data," SAE paper 841359, Fuels and Lubricants Meeting and Exposition, Baltimore, Maryland, 1984.
- (13) Roberts, J. M., Heat Release Estimation and Prediction of Wankel Stratified-Charge Combustion Engine, Masters thesis, Massachusetts Institute of Technology, September, 1985.
- (14) Nguyen, H. L., Addy, H. E., Bond, T. H., Lee, C. L. and Chun, K. S., "Performance and Efficiency Evaluation and Heat Release Study of a Direct-Injection Stratified-Charge Rotary Engine," SAE paper 870445, International Automotive Engineering Congress and Exposition, Detroit, Michigan, 1987.

- (15) Dimplefeld, P. and Humke, A., "Heat Release Characteristics of Stratified-Charge Rotary Engines," SAE paper 870443, International Automotive Engineering Congress and Exposition, Detroit, Michigan, 1987.
- (16) Stanten, R. A., Heat Transfer and Performance Calculations in a Rotary Engine, Masters thesis, Massachusetts Institute of Technology, August, 1987.
- (17) Raju, M. S., "Analysis of Rotary Engine Combustion Processes Based on Unsteady, Three-Dimensional Computations," paper AIAA-90-0643, AIAA 28th Aerospace Sciences Meeting, Reno, Nevada, 1990.
- (18) Li, Z., Shih, T. I-P. and Nguyen, H. L., "Modelling and Simulation of Wankel Engine Flow Fields," SAE paper 900029, International Automotive Engineering Congress and Exposition, Detroit, Michigan, 1990.
- (19) Martin, M. K. and Heywood, J. B., "Approximate Relationships for the Thermodynamic Properties of Hydrocarbon-Air Combustion Products," Vol. 15, pp. 1-10, Combustion Science and Technology, Gordon and Breach Science Publishers Ltd., Gr. Britain, 1977.
- (20) Woschni, G., "A Universally Applicable Equation for the Instantaneous Heat Transfer Coefficient in the Internal Combustion Engine," SAE paper 670931, 1967.
- (21) Lee, C. M. and Schock, H. J., "Regressed Relations for Forced Convection Heat Transfer in a Direct Injection Stratified Charge Rotary Combustion Engine," NASA Technical Memorandum 100124, 1988.
- (22) Assanis, D. N. and Badillo, E., "Transient Conduction in Low-Heat-Rejection Engine Combustion Chambers," SAE paper 870156, Automotive Engineering International Congress and Exposition, Detroit, Michigan, 1987.
- (23) Yamamoto, K., Rotary Engine, Toyo Kogyo Co., Ltd., Hiroshima, Japan, 1969.
- (24) Rachel, T. and Schock, H. J., Personal communication, Michigan St. Univ., Dept. of Mech. Engr., December, 1989.
- (25) Heywood, J. B., Internal Combustion Engine Fundamentals, p. 722, McGraw-Hill Book Co., New York, 1988.
- (26) Dimplefeld, P., Personal Communication, John Deere and Company, Rotary Engine Division, Woodridge, NJ, December, 1989.
- (27) Bolz, R. E. and Tuve, G. L., CRC Handbook of Tables for Applied Engineering Science, 2nd Edition, CRC Press Inc., Boca Raton, Florida, 1970.

LIST OF SYMBOLS

Symbol	Description
a_r	apex seal crown radius
b	seal base width
C_{A1}, C_{A2}	ancillary loss constants
C_{F1}, C_{F2}, C_{F3}	friction loss constants
c_a	apex seal clearance above the rotor
c_p	specific heat at constant pressure
F_{af}, F_{of}, F_{sf}	apex, oil and side seal friction forces
F_{sa}, F_{so}, F_{ss}	apex, oil and side seal spring forces
f_{mep}	friction mean effective pressure
h_a, h_s	apex seal and side seal height
\bar{h}_{hg}	average hot gas side heat transfer coefficient

i	enthalpy
k_j	thermal conductivity for material j
L_j	depth of material j
l	seal length
m	mass
\dot{m}	mass flow rate
N	engine speed (rpm)
Nu	Nusselt number
P	Pressure
Pr	Prandtl number
\dot{Q}_{im}	heat loss rate through intake manifold walls
$\frac{dQ}{d\theta}$	rate of release of fuel energy
R	gas constant for air
R_o	oil seal radius
Re	Reynolds number
r	trochoid generating radius
T	temperature
t	time
U	overall heat transfer coefficient
V	volume
α	exponent in heat transfer expression
β	coefficient in heat transfer expression
γ	exponent in heat transfer expression
ϵ	eccentricity
θ	crank angle
μ	sliding coefficient of friction
φ	apex seal lean angle
τ	fuel heat release rate decay constant

Subscript	Description
a	apex seal
c	combustion chamber
cc	crank case
$cool$	coolant
epc	exhaust port closing
epo	exhaust port opening
ic	to the intake manifold (from the intercooler)
im	intake manifold
ipc	intake port closing
ipo	intake port opening
max	maximum
o	oil seal
$qmax$	at the time of maximum heat release rate
s	side seal
sp	at the time the spark fires
$wall$	at the trochoid housing wall
1	upstream
2	downstream

LIST OF ABBREVIATIONS

bsfc	brake specific fuel consumption
DISC	direct-injection stratified-charge
f _{mep}	friction mean effective pressure
MIT	Massachusetts Institute of Technology
NASA	National Aeronautics and Space Administration
RCE	rotary combustion engine

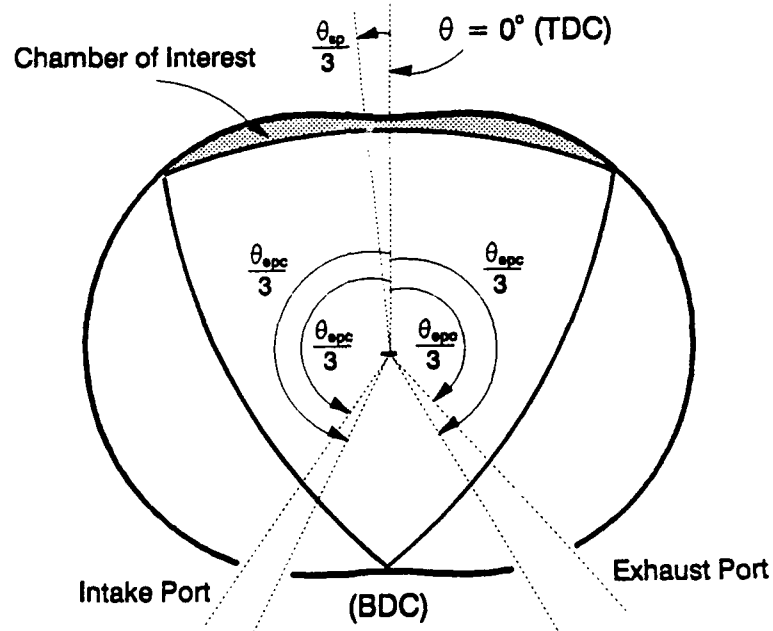


Figure 1: Rotary Engine Schematic

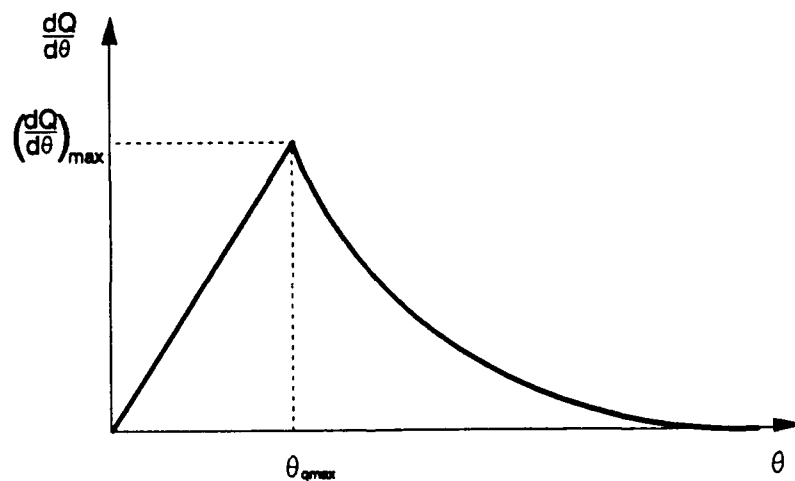


Figure 2: DISC Engine Heat Release Rate

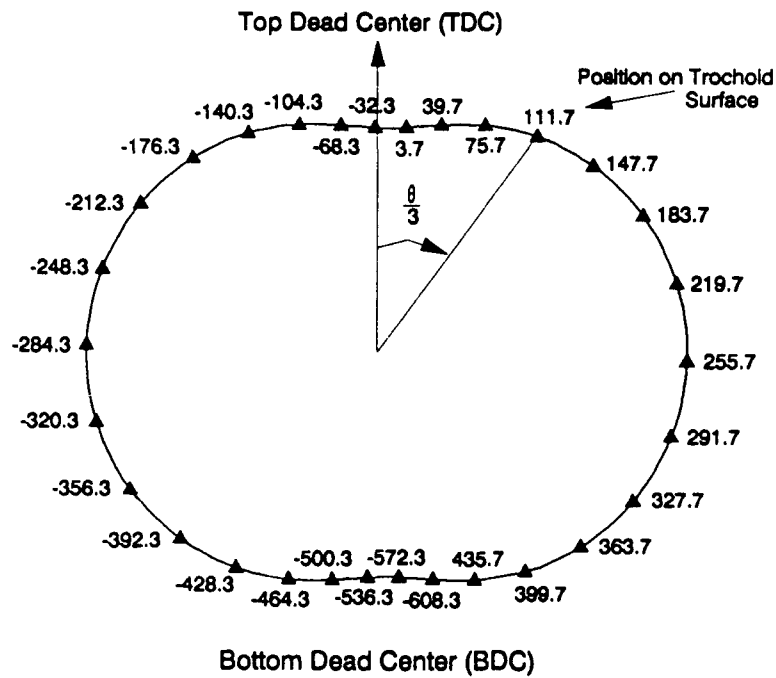


Figure 3: Trochoid Housing Geometry and Crank Angle Definition

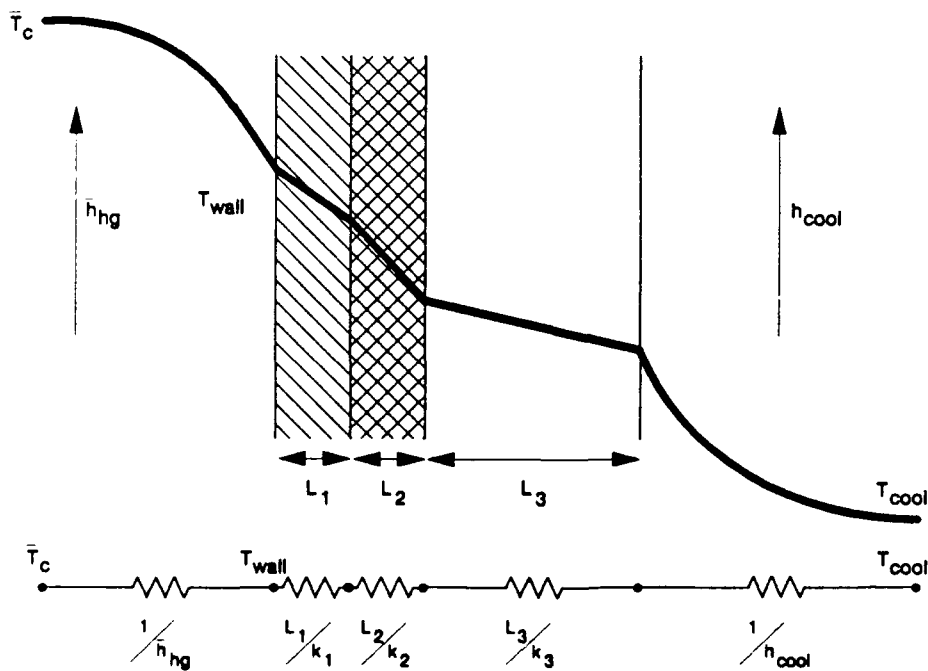


Figure 4: Trochoid Housing Cross Fiction

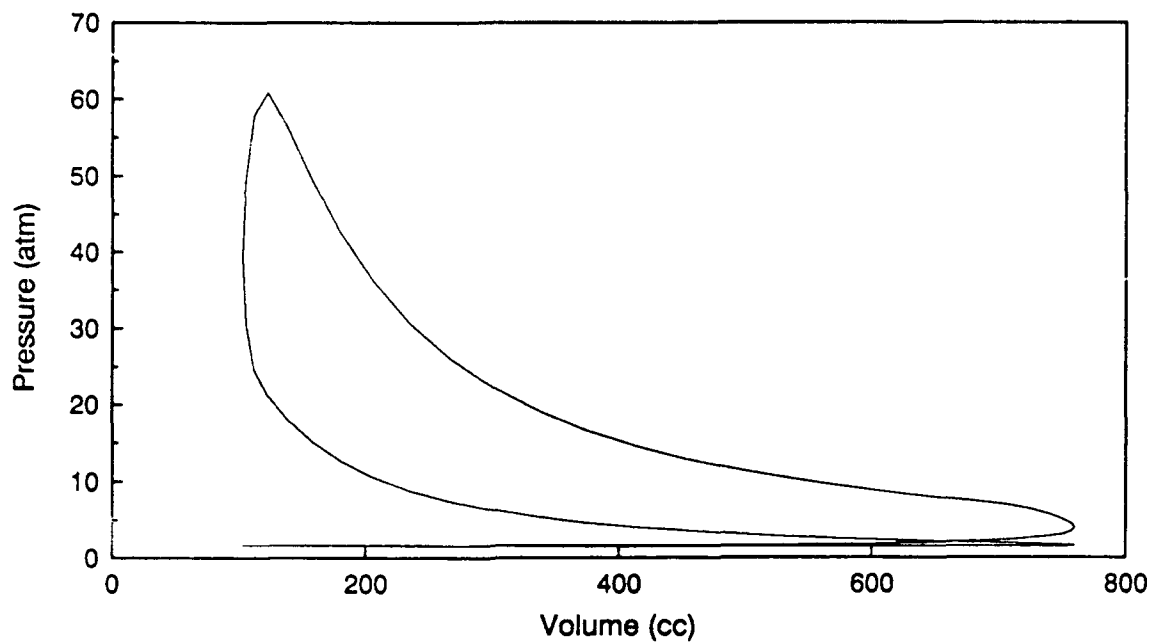


Figure 5: P-V Diagram for DISC RCE, $\phi = 0.75$, 5500 rpm

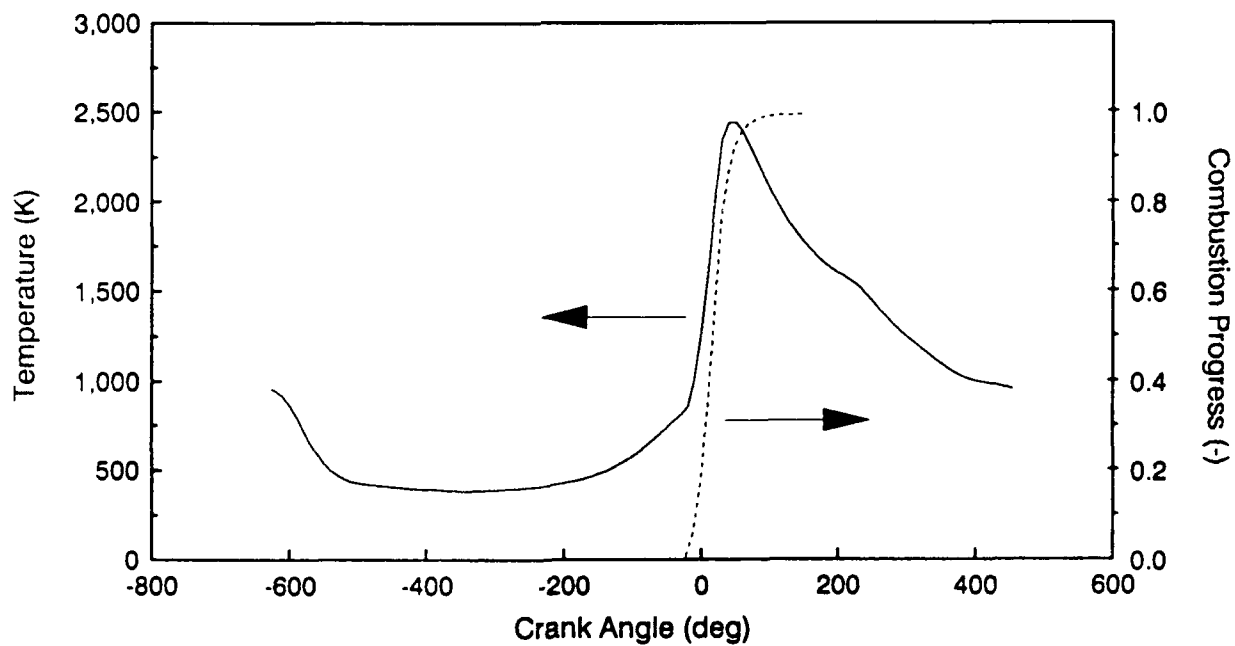


Figure 6: Chamber Temperature and Combustion Progress Histories for
a DISC RCE, $\phi = 0.75$, 5500 rpm

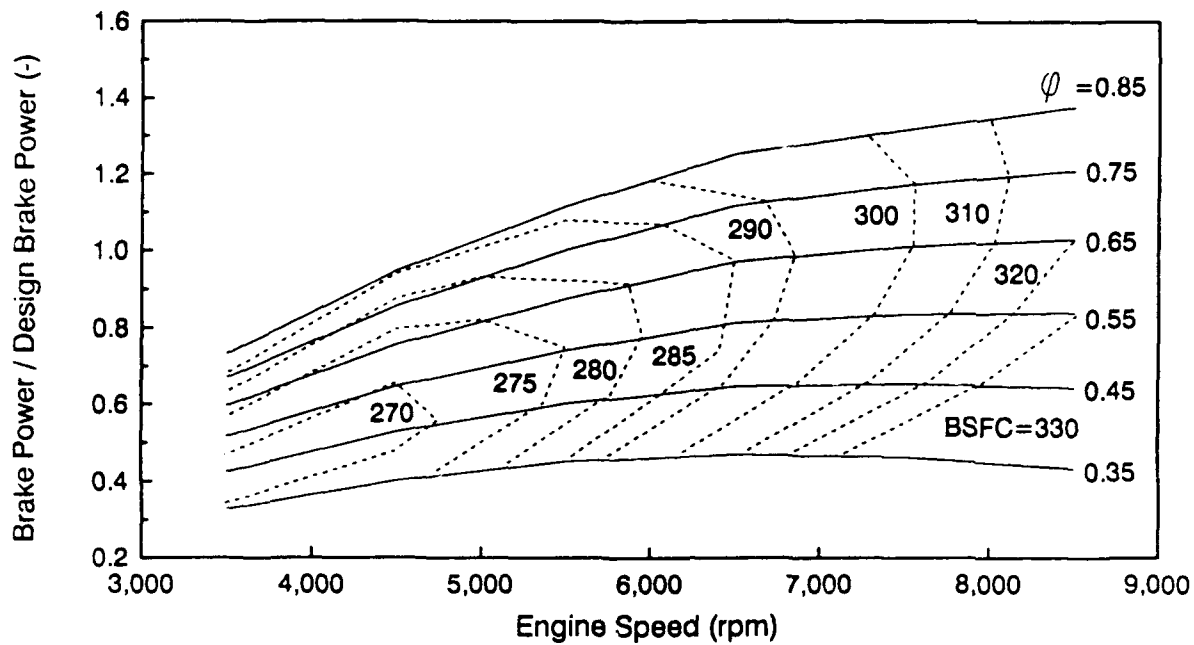


Figure 7: Engine Map for a Single Rotor DISC RCE

— Line of Constant ϕ - - - - - Line of Constant BSFC
(BSFC in g/kW-hr)

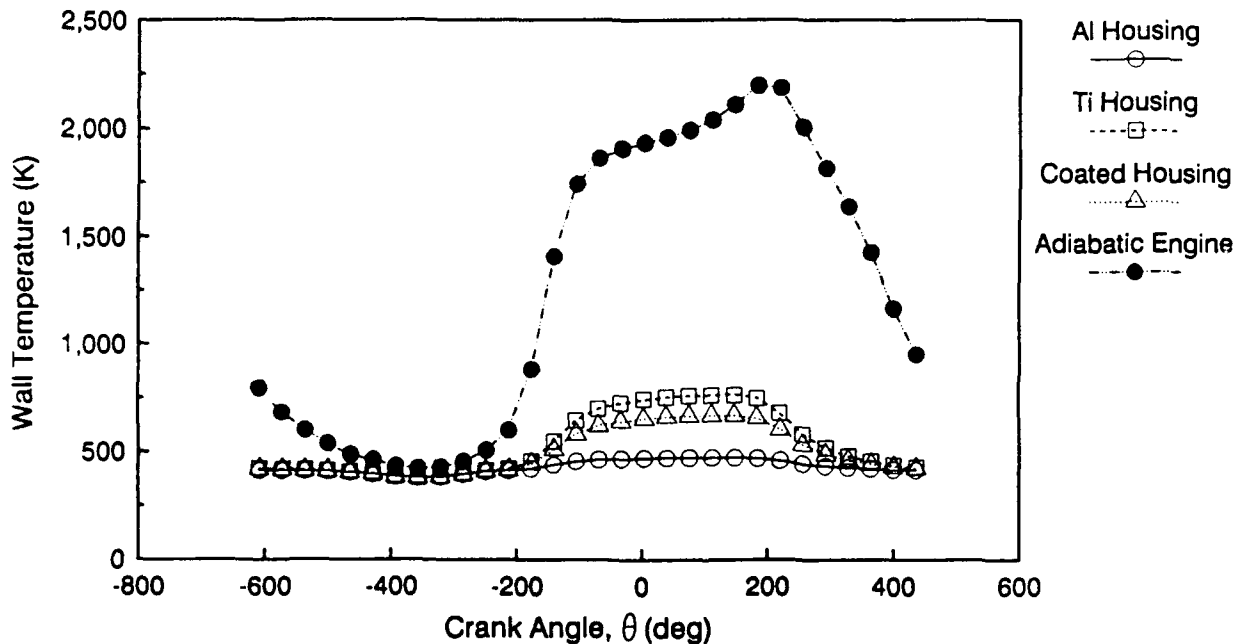


Figure 8: Trochoid Housing Hot Side Wall Temperature for $\phi=0.75$, 5500 rpm and Various Housing Materials

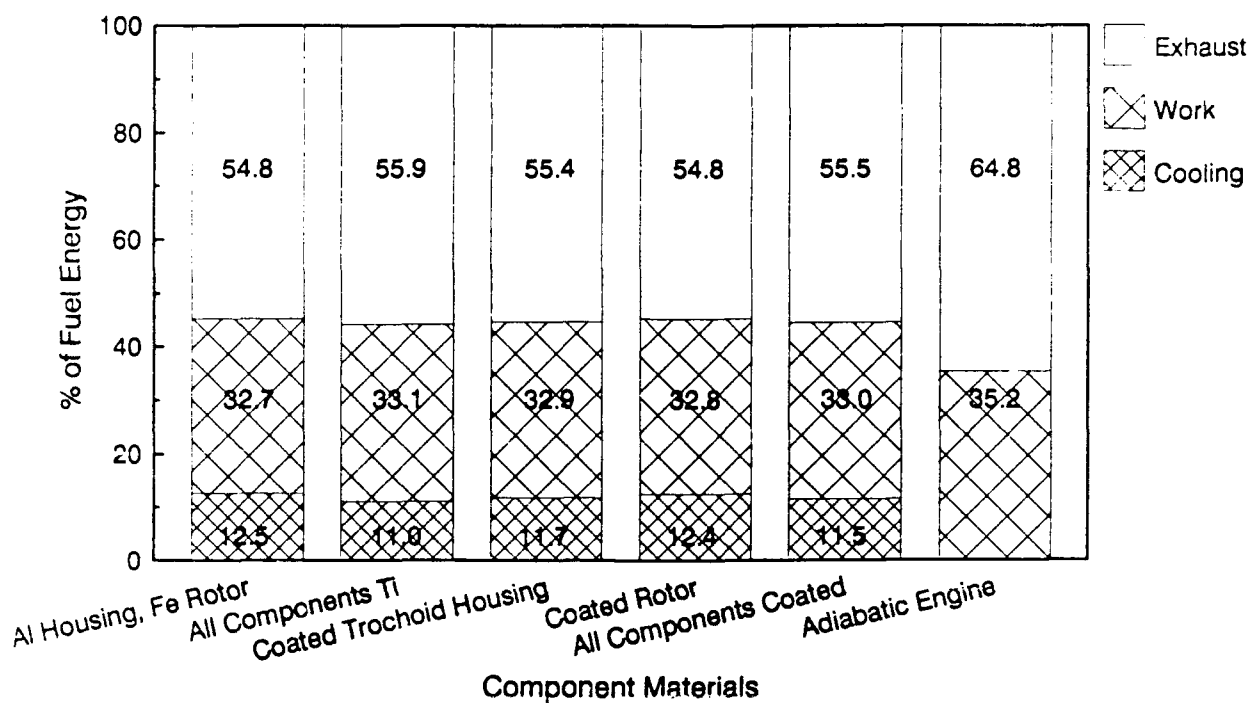


Figure 9: Fuel Energy Diagram for Engines With Various Component Materials, Equivalence Ratio = 0.75, 5500 rpm

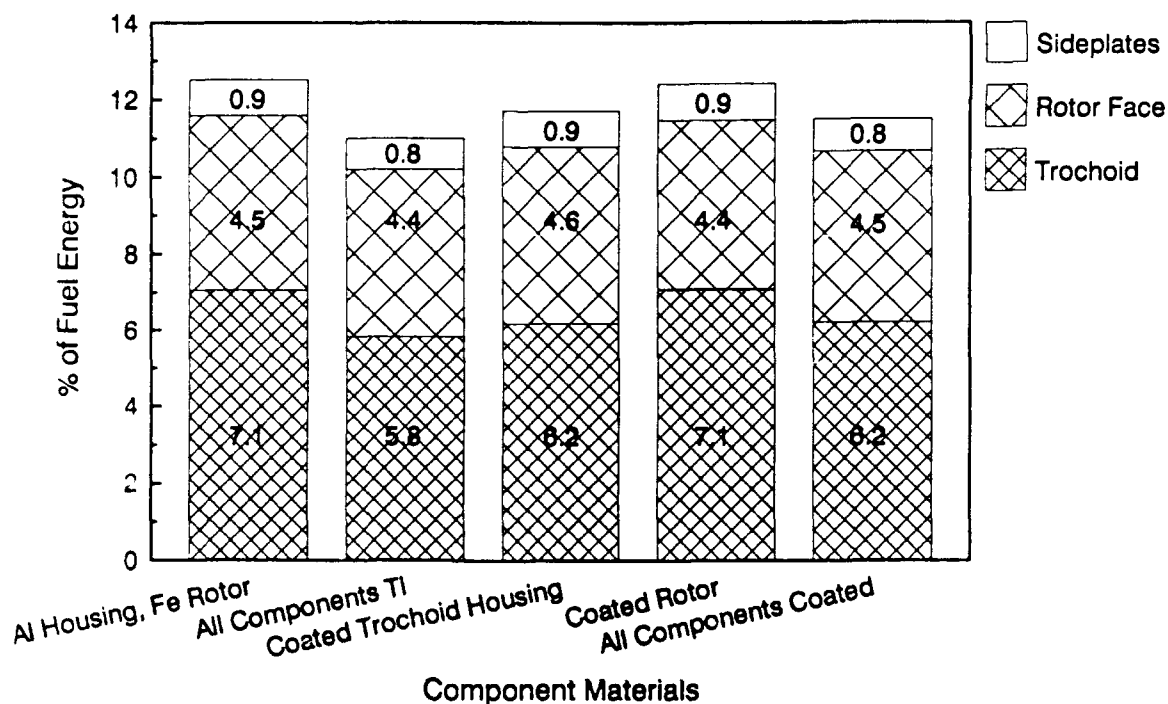


Figure 10: Fuel Energy to Engine Components for Various Component Materials, Equivalence Ratio = 0.75, 5500 rpm

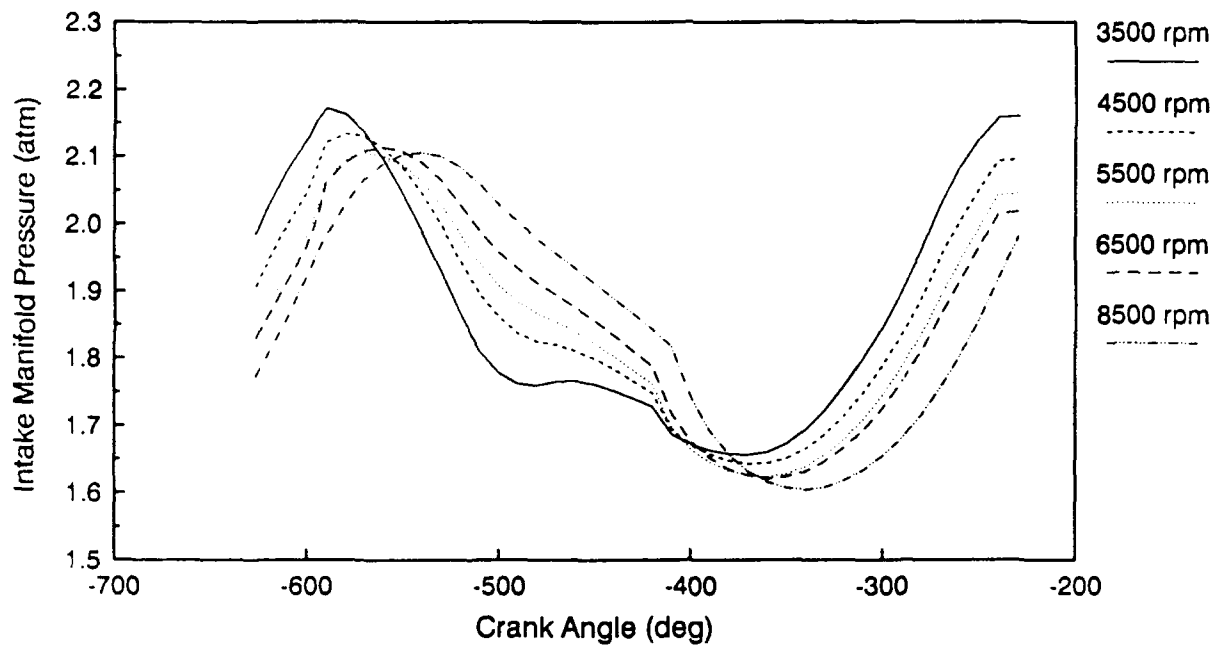


Figure 11: Intake Manifold Pressure Variation During One Intake Event

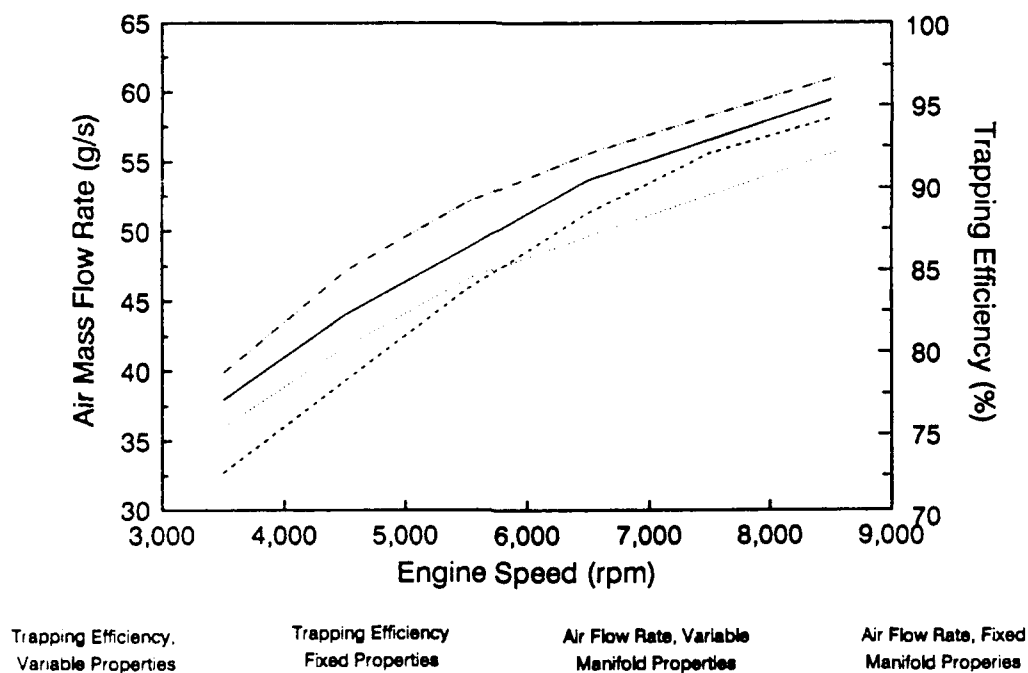


Figure 12: Average Air Mass Flow Rate and Trapping Efficiency for Constant and Variable Intake Manifold Thermodynamic Properties

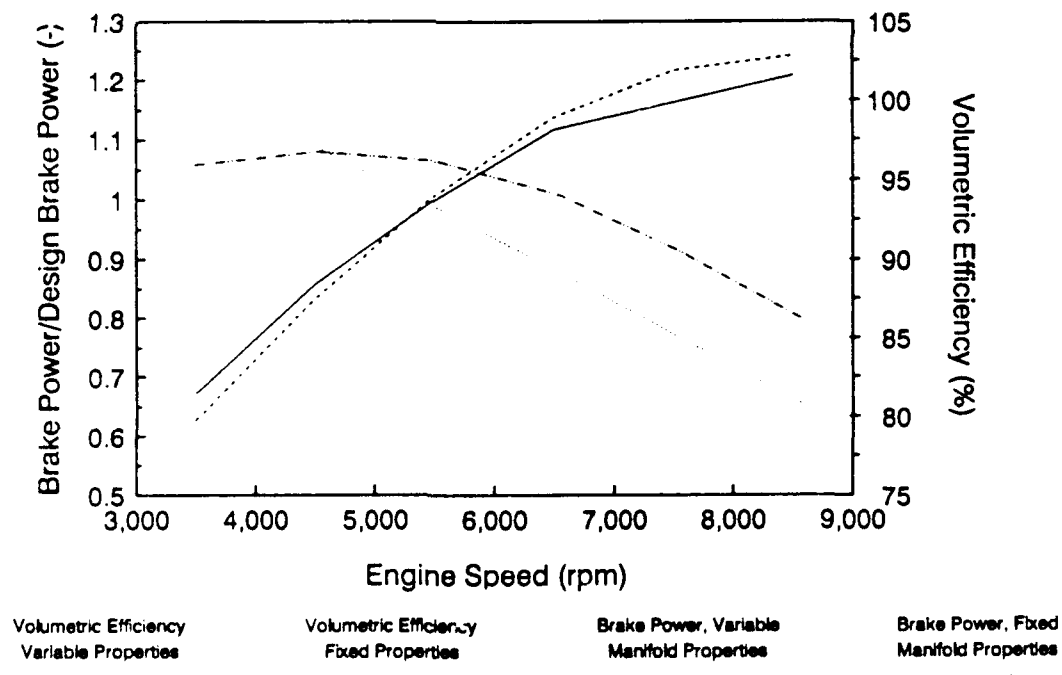
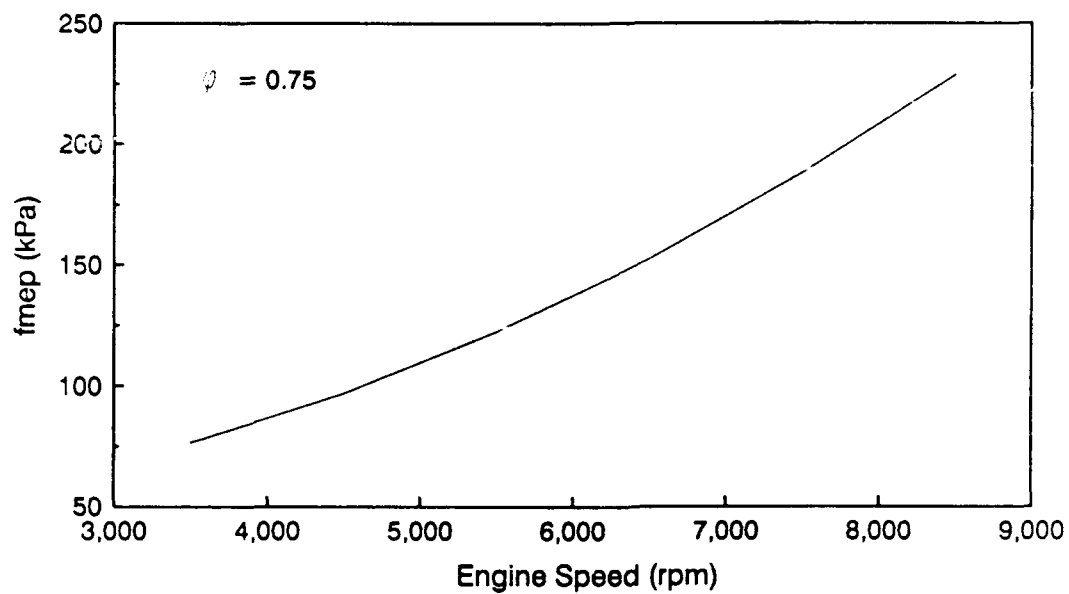
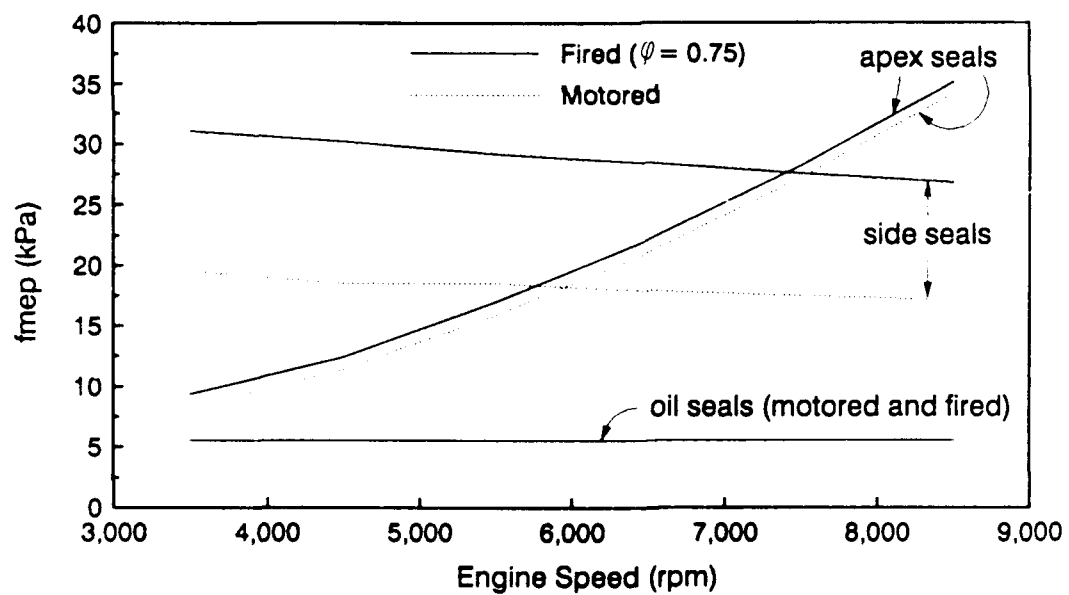


Figure 13: Normalized Brake Power and Volumetric Efficiency for Variable and Constant Intake Manifold Properties



(a) Ancillary Losses



(b) Motored and Fired Seal Losses

Figure 14: Components of Friction Losses

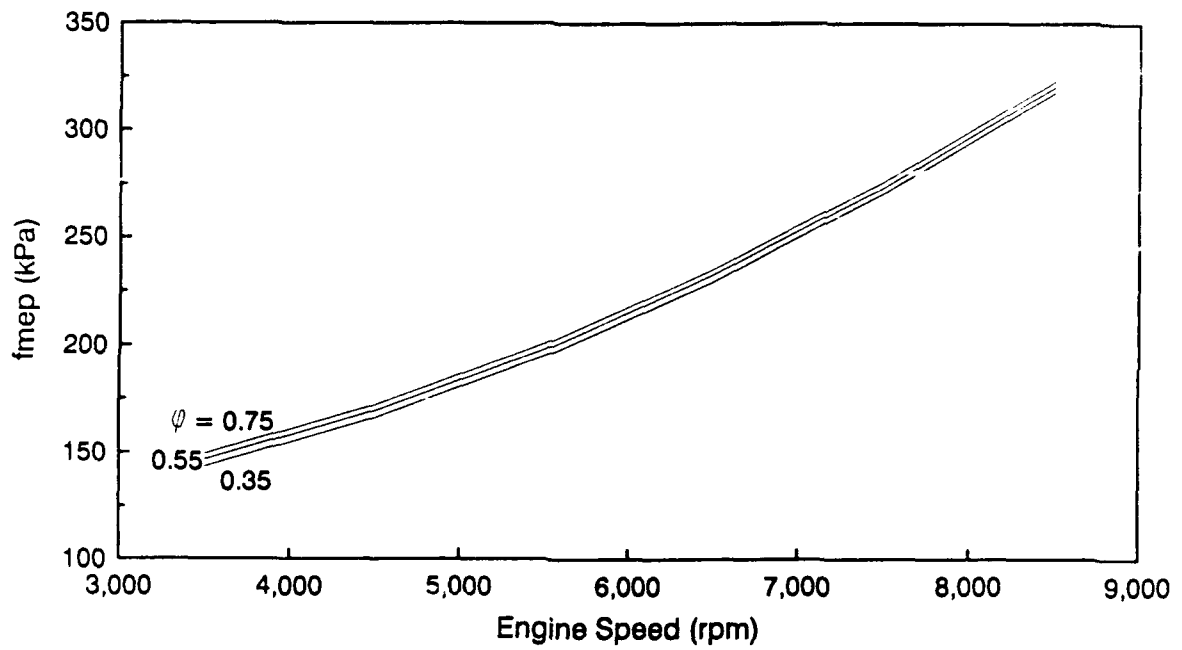


Figure 15: Friction Map

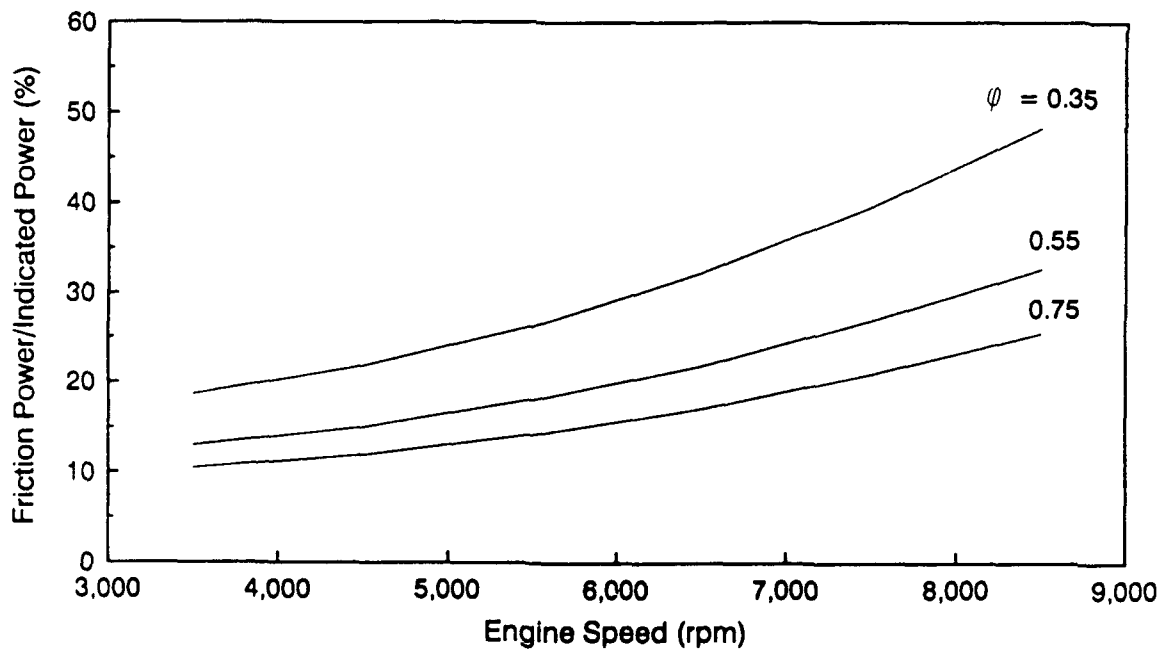


Figure 16: Relative Friction Losses

**COMPUTATIONAL EXPERIENCE WITH 3-D ROTARY ENGINE
COMBUSTION MODEL**

by

M. S. Raju
Sverdrup Tech. Inc.
NASA Lewis Research Center
Cleveland, OH
and
E. A. Willis
NASA Lewis Research Center
Cleveland, OH

For presentation to the AIAA/FAA Joint Symposium on General
Aviation Systems at the Port O-Call Inn, Ocean City, NJ
on April 11, 1990

COMPUTATIONAL EXPERIENCE WITH A 3-D ROTARY ENGINE COMBUSTION MODEL

M. S. Raju[†]

Sverdrup Tech., Inc., NASA Lewis Research Center, Cleveland, Ohio

E.A. Willis[‡]

NASA Lewis Research Center, Cleveland, Ohio

ABSTRACT

A new computer code has been developed to analyze the chemically reactive flow and spray combustion processes occurring inside of a stratified-charge rotary engine. Mathematical and numerical details of the new code were recently described by the present authors. This paper presents the results of limited, initial computational trials as a first step in a long-term assessment/validation process. The engine configuration studied was chosen to approximate existing rotary engine flow-visualization and hot-firing test rigs. Some typical results, in terms of pressure and temperature histories, torque generated due to the non-uniform pressure distribution within the chamber, energy release rates and various flow-related phenomena are discussed and compared with other predictions reported in the literature. The adequacy or need for improvement in the spray/combustion models and the need for incorporating an appropriate turbulence model are discussed.

INTRODUCTION

The rotary combustion engine (RCE) would be a desirable powerplant for light aircraft, drones (including high-altitude applications), auxiliary and ground power units, and marine and industrial applications, if its efficiency could be made closer to that of diesel engines. It has inherent advantages over reciprocating engines such as higher airflow capacity, higher power-to-weight ratio, low frontal area, and less vibration. An initial attempt to introduce a gasoline-fueled rotary engine into the general aviation market in the mid-1970s was unsuccessful, however, because of poor fuel economy, uncertain availability of avgas, and marginal weight advantage over contemporary reciprocating engines. Subsequent research sponsored by industry, NASA, and the Navy has led to the development of the stratified-charge rotary engine (SCRE) concept. This work has already demonstrated a substantial improvement in specific power, multifuel capability and a reduction of cruise brake specific fuel consumption (BSFC) from 0.5 lb/bhp-hr to a value of approximately 0.42 lb/bhp-hr. A major factor in this improvement was the use of CFD methods to analyze the airflow, spray and combustion events of the RCE. Continuing R&D sponsored by NASA is aimed at further reducing the cruise BSFC from the current value to 0.35, or less by the end of 1992. Much of expected improvement will be enabled by further CFD - driven fuel injection, spray, and nozzle optimization, rotor pocket and nozzle relocations, and related modifications. Thus, the availability of accurate, reliable and fast operating CFD

[†]Senior Research Engineer, Member AIAA

[‡]Chief Engineer, Propulsion Systems Division, Member AIAA

simulations of the RCE internal processes is clearly a key element in the future development of this promising engine concept.

Early modelling efforts on the Wankel engine were based on thermodynamic models^{1,2} and also on one-dimensional modelling of premixed-charge combustion.³ Multi-dimensional models of the Wankel engine are of more recent origin; Grasso et al.⁴ presented the first three-dimensional computations of a SCRE during the early stages of flame propagation. Subsequent computations performed by Abraham and Bracco^{5,6} have led to some important design changes in the rotary engine development at Deere & Co., especially in the fuel injector configuration. Their code, REC-3D-FSC-86, is a modified version of the KIVA code developed at Los Alamos National Laboratory⁷ for the modelling of reciprocating engines. KIVA makes use of a conditionally stable algorithm, and the stability of the KIVA scheme is improved by making use of an acoustic subcycling step in order to alleviate the stiffness problems arising from compressibility effects. There appears to be considerable room for improvement in the code, since it neglects the spatial gradients whenever the grid spacing becomes smaller than some predefined value and also requires excessive CPU time when the engine speed becomes small. Shih et al.⁸ presented the first two-dimensional computations of a motored Wankel engine in the absence of combustion. Their code, LEWIS-2D, is based on the Beam-Warming type of ADI method. Their computations have subsequently been extended to three dimensions in Steinthorsson et al.⁹ Linear stability analysis has shown that the ADI method is unconditionally stable in two dimensions but is unconditionally unstable in three dimensions. Although artificial dissipation has some stabilizing effect, an excessive amount can impair stability and reduce accuracy and convergence. Recently, Li et al.¹⁰ have modified their LEWIS-3D code based on upwind schemes together with the incorporation of a $k-\epsilon$ turbulence model.

The present solution procedure differs from the above in terms of the numerics and the submodels used for turbulence, combustion, and sprays. Mathematical and numerical details of the new code were recently described by the present authors.¹¹ This paper presents the results of limited, initial computational trials as a first step in a long-term assessment/validation process. The engine configuration studied was chosen to approximate an existing rotary engine test rigs. Representative results, in terms of pressure and temperature histories, torque generated due to the non-uniform pressure distribution within the chamber, energy release rates and various flow-related phenomena are discussed in comparison with other predictions reported to date in the literature. The objective is to evaluate the adequacy or need for improvement in the spray/combustion models and to assess the need for incorporating an appropriate turbulence model.

PHYSICAL DESCRIPTION

A schematic of the Wankel engine is shown in Fig. 1. The Wankel engine is composed of a trochoid housing (1) with peripheral intake and exhaust ports, fuel injector and spark igniter, a three-flank rotor, and a crank shaft. The contour of the inner surface of the outer casing of the Wankel engine is a two-lobe peritrochoid. The contour of a rotor revolving along an outer housing is a peritrochoid inner envelope. The rotor surface is modified to include rotor pockets (2,3,4). The presence of the rotor pockets not only alters the expansion and compression ratio of the engine, but also plays an important role in modifying the flowfield, mixing and combustion characteristics of the combustor.

The present rotor configuration is adopted from Steinthorsson et al.⁹ In its other dimensions, the engine

has a generating radius (R) of 0.1064 m, eccentricity(E) of 0.01542 m, clearance(C) of 0.004 m, chamber width(W) of 0.07 m, and port width(W_p) of 0.05 m. These dimensions give rise to maximum and minimum volumes of 750 c.c. and 115 c.c., respectively, yielding a compression ratio of about 6.5.

The rotor turns eccentrically at one third of the crank shaft speed. The three combustion chambers of the Wankel engine are the three regions enclosed between the three rotor faces and the peritrochoid housing, two side housings, two side seals, and lead and lag apex seals. In the present calculations, only one of the three combustion chambers is considered, since leakage through the seals is assumed to be negligible. As the rotor revolves around the crank shaft, each of the combustion chambers is continually deformed. This produces the necessary compression and expansion of the fluid for the required engine performance during each one of the cyclic operations.

It should be noted that each combustion chamber has two minimum-volume and two maximum-volume positions. Hence, the top-dead-center (TDC) and bottom-dead-center (BDC) positions are defined differently than would be the case in a reciprocating engine and it will be important to keep the following conventions in mind. In this study, a crank angle of zero radians corresponds with the minimum volume that occurs near the ports. This position is referred to as the BDC. The other position, corresponding with the minimum volume near the fuel injector location, is referred to as the TDC. Thus, combustion occurs near TDC as in a reciprocating engine; but the BDC position has a different meaning. The exhaust port opens at a crank angle of 5.96 rad before BDC and closes at 1.07 rad after BDC and the exhaust back-pressure is maintained at 0.85 atm. The intake port opens at 1.26 rad before BDC and closes at 5.96 rad after BDC. Fresh air enters through the intake while the intake stagnation temperature, $T_{s, int}$, and static pressure, P_{int} are maintained at 400K and 1.25 atm, respectively. The fuel injector has eight holes and is located near the middle of the trochoid housing as shown in Fig. 1. The fuel emerges in a fan-shaped pattern consisting of eight sprays. The initial spray distribution is given by a Rosen-Ramler distribution with the initial droplet sizes ranging from $10 \mu m \leq r_{k,i} \leq 30 \mu m$. The initial droplet velocity and temperature are taken to be 100 m/s and 300 K, respectively. The fuel injection begins at 8.6 rad after BDC and ends at 9.25 rad after BDC. The liquid fuel injection is simulated by injecting a specified number of discretized parcels of fixed mass associated with a given droplet-size group at uniform intervals corresponding with the fuel-injection time-step. The ignition process begins at 8.65 rad after BDC and ends at 8.75 rad after BDC. The spark ignition is simulated by raising the temperature of the few nodes of the computational domain on the wall at the spark ignitor location from 400K to 1500K. A complete physical description of the engine was provided in our earlier paper.¹¹

RESULTS AND DISCUSSION

Numerical solutions are obtained for the engine flowfield under motoring conditions for a single case with all the ports closed; and also under firing conditions for two cases with the equivalence ratios 0.45 and 0.75. For all the cases studied, the computations are initiated before the opening of the exhaust port for only one of the three combustors (formed with the second rotor flank as shown in Fig. 1). Here we present the results obtained for the three different cases for an engine speed of 4000 rpm. The temperatures of the rotor and housing surfaces are maintained at 300K for the case considered under motoring conditions and at 400K for the firing conditions. The initial conditions correspond to the conditions of quiescent air at pressure, $P_{in} = 1$ atm, and temperature, $T_{in} = 300K$ for the motoring engine and at 1 atm, and 400 K for the firing engine.

All the computations are performed with a uniform time-step size such that 15,000 time-steps span the 6π radians of one entire rotor cyclic-rotation. The calculations are performed on a grid with a mesh size of $i=31$, $j=16$, and $k=20$, where i , j , and k represent the coordinate surfaces in the direction extending from the trailing-edge surface to the leading-edge surface of the combustor, from the rotor to housing surface, and from the side wall to the symmetry plane of the domain between the end-to-end side walls, respectively.

MOTORIZING RESULTS

The usefulness of any numerical scheme lies in its ability to generate meaningful predictions for a wide variety of engine operating conditions. Both the numerics and the models used for turbulence, combustion and sprays determine the accuracy of the predictions. The selection of a finite-difference formulation is mainly dictated by a careful balance between the numerical stability, efficiency, and accuracy considerations for the problem under consideration. Stability is often achieved at the expense of accuracy and efficiency. It is also instructive to note that a numerical scheme is often made stable either by explicitly adding some amount of artificial dissipation or by the numerical dissipation that inherently arises from a given finite-difference formulation. For the predictions to be meaningful, the numerical dissipation required for stability considerations should be small compared with the dissipation arising from the actual physical processes governing the flowfield.

The best way to assess the accuracy of a numerical scheme is to compare the predictions with experimental data. In our previous paper¹¹ a good measure of the qualitative agreement was reported between the predictions and experimentally obtained flow-visualization pattern during the intake process. In the absence of any experimental data in terms of the average pressure and temperature variation versus crank angle, a numerical experiment was performed for a motoring engine with all the ports closed, so that comparisons can be made between the predictions with results obtained from isentropic conditions.

Fig. 2 shows the mass-averaged temperature and volume-averaged pressure versus crank angle. Also shown in the figure are the corresponding results obtained from the isentropic conditions. The computations predicted a temperature of 490 K and a pressure of 8.4 atm at BDC. The corresponding differences from the isentropic conditions are found to be 15.8% and 23%, respectively. Although it is hard to ascertain the validity of the predictions in the absence of any experimental data, the observed differences between the isentropic conditions and the predictions can be explained for the following reasons. (a) Both the stagnation pressure and temperature would be slightly higher than the corresponding static conditions near BDC, since the flow velocities at this position approach around 50 m/s. (b) Viscous effects become increasingly significant near BDC as the surface area to volume ratio becomes very large near the clearance regions of the apex seals and also due to a strong squish flow resulting from the non-uniform pressure distribution. The squish flow is a unique feature of the rotary engines that has no counterpart in the reciprocating engines. (c) The heat losses to the walls also contribute to the observed differences since the walls temperatures are maintained at 300 K. (d) Because of the nature of the combustor, all the gas within the combustor may not undergo the same degree of expansion or compression simultaneously and, in fact, while some gas undergoes compression the other is likely to undergo expansion as the rotor moves around BDC. This process allows more time for heat transfer to the walls. Finally (e), numerical dissipation is also likely to contribute to the observed differences. Li et al.¹⁰ made similar comparisons between the various numerical schemes studied for a two-dimensional motoring engine. We have not attempted to make any direct comparisons with their predictions because

of the different engine configurations used in the respective studies. At the end of the computations the predictions indicate there is an accumulation of mass by about 3%. Even though our governing equations are formulated in a strong-conservation law form,¹¹ the way in which the boundary conditions are implemented makes the finite-difference formulation weakly-conservative. However, the observed discrepancy in mass could be reduced further by increasing the number of grid points of the computational domain.

Fig. 3 shows the computed torque about the center of the rotor (as opposed to output torque about the center of the crankshaft). This is generated due to the non-uniform pressure distribution on the rotor surface and also due to a difference of the pressure forces acting on the trailing and leading apex seals. If a uniform pressure prevailed throughout the combustor, the resulting torque would be zero. However, the effect of pressure non-uniformity clearly results in a negative torque contribution opposing the rotor motion. Hence, work needs to be performed to overcome this torque induced by the non-uniform pressure distribution. From the predictions, it is evident that the pressure becomes more non-uniform near BDC and, in fact, the torque has a maximum negative value at this location. The corresponding values of the torque averaged over one cyclic period is found to be -0.9357 Nm (rotor) and -0.1259 Nm (seals).

To provide a better understanding of the observed nonuniformities in the flowfield, the pressure and temperature contours together with the flow velocity at the symmetric plane, $k=19$ and crank angle of 19.3 are shown in Fig. 4. In these figures showing the iso-contour plots, the iso-contour lines near the maximum are shown as dotted lines and near the minimum are shown as solid lines. In the velocity vector plot, only three different sizes of arrow symbols are used to distinguish the variation between the maximum and minimum values in magnitude. Both the pressure and temperature have a maximum value in the region near the trailing apex seal and the flow velocity is essentially determined by the rotor movement.

FIRING RESULTS

In this section we present the results for two other cases that were conducted under firing conditions for which the operating conditions are described earlier in the paper. The equivalence ratio of fuel/air (Φ) is taken to be 0.45 for one case and 0.75 for the other.

Here the results of the three-dimensional computations describing the overall behaviour of the combustor in terms of the volume-averaged pressure versus combustor volume (p-v diagrams), and the variation of mass-averaged temperature, of torque due to pressure non-uniformity, and of vaporization and combustion rates versus the crank angle are first presented before we proceed on to examine the flowfield in detail during the fuel vaporization and combustion. The details of the flowfield during the opening of the exhaust and/or intake were presented in detail in our earlier paper.¹¹

The computations are initiated just before the exhaust port opens. The initial pressure and temperature of the gas are taken to be 1 atm and 400 K, respectively. After the exhaust port opens the residual gas moves out of the combustion chamber, since the imposed pressure of 0.85 atm in the exhaust remains lower than the interior engine pressure during most of the compression cycle. Both the engine pressure and temperature remain fairly uniform during the exhaust process as shown in Fig. 5. As the rotor moves further, the intake port opens and fresh air moves into the combustion chamber. Most of the intake process occurs during the expansion stroke of the engine. The slight rise in the pressure during the intake process is caused by the intake pressure, which is maintained at 1.25 atm.

After the intake port closes, the gas undergoes nearly isentropic compression until the fuel vaporization and combustion take place. During the combustion process, both the pressure and temperature rise sharply to about 33 atm and 1450 K, reaching their maximum values near TDC. During the expansion stroke, the gas undergoes nearly isentropic expansion until the exhaust port opens again. Both the pressure and temperature fall off sharply until the interior pressure near the exhaust port reduces to a value below the imposed exhaust back-pressure of 0.85 atm. When this condition is reached near the crank angle of 16 rad, the temperature remains fairly uniform at 650 K for a brief period before the intake charge at 400 K enters the combustor. The temperature falls to 400 K during the remainder of the opening of the intake port.

The torque variation versus crank angle in Fig. 6a shows that the pressure distribution on the rotor surface undergoes a kind of beating phenomena associated with acoustic resonance during the intake and/or exhaust port opening period. The beating phenomena is characteristic of the unsteadiness associated with the jet movement. It is also noteworthy that positive torque is generated during the overlapping period in which both the exhaust and intake ports are open simultaneously. Once again the maximum negative torque is generated near the minimum volume as in the previous case considered under motoring conditions. The corresponding values of the torque averaged over one cycle is found to be -0.817 Nm (rotor) and +0.508 Nm (seals). Comparison with the previous case shows that the average rotor torque due to the pressure non-uniformity under both motoring and firing cases has a similar value. This indicates that the resulting pressure gradient on the rotor surface is a result of the fluid motion associated with the rotor movement. However, the average torque due to pressure acting on the seals for a firing engine is found to be positive while it had a negative value for the motoring case.

Fig. 6b shows the crank angle variation of the evaporated fuel and also the amount of reacted fuel. The total amount of liquid fuel injected is equal to 0.23 gm which corresponds to an equivalence ratio of about 0.45. The slope of these curves indicates that most of the fuel, after it evaporates, reacts quickly with oxidizer to form products. This in turn implies that most of the fuel burns in a premixed-flame environment. While the validity of the results can be verified only after proper experimental data become available, the extremely fast combustion rates observed in the present study are in contradiction to the numerical predictions presented by Abraham et al.⁵; in which they reported lower rates for both fuel vaporization and combustion. Our present computations are based on the assumption of laminar fluid motion and chemical kinetics. In a turbulent reacting flow, the combustion rates are normally rate-controlled by the mixing rate rather than the Arrhenius reaction rate.¹² Also one expects to predict lower temperatures for the gas near the walls, when the effect of turbulence is properly accounted for in the heat transfer calculations. This, in turn, might reduce both the vaporization and combustion rates.

The effect of increasing the equivalence ratio from 0.45 to 0.75 is shown in Figs. 7-8. While the qualitative behaviour for both cases remains the same, the increase in heat input, as a result of increasing the fuel content, is shown to result in an increase in the maximum temperature and pressure observed from 1450 to 1750 K and 33 to 44 atm, respectively.

FLOWFIELD PHENOMENA

We now turn our attention to the details of the flowfield at the beginning of, during, and after the combustion and vaporization for the case with an equivalence ratio of 0.75. Fig. 9 shows the iso-contours of pressure and temperature, and the velocity vector plot at a crank angle of 8.6 rad. This is before the fuel injection begins. Both the pressure and temperature distributions remain fairly uniform in the region extending all the way from the trailing apex seal to the end of the rotor pocket near the leading apex seal. The maximum values for the pressure and temperature are observed to occur within this region. Fairly large gradients in the distribution of both temperature and pressure are also observed in the clearance region near the leading apex seal. The fluid motion is shown to be strongly influenced by the rotor movement.

Figs. 10 to 12 show the droplet trajectories, iso-contour lines of fuel, oxydizer, cabron dioxide, and temperature, and the velocity vector plot at a crank angle of 9.3. The figures showing the rotor pocket cross-section are drawn in an elongated scale compared with the others in order to provide a better graphic illustration of the results. The polydisperse character of the spray is represented by different sized circles which are indicative of the size of the initial droplets. While the particles retain the fan-shape configuration during this later part of the fuel vaporization process, the deflection of the particles in the direction of the gaseous flow is evident from the path originally dictated by the particle initial conditions.

A very small region near the fuel injector location is found to be fuel rich. While stratified charge gives rise to a gaseous diffusion flame, a careful examination of Fig. 10 also reveals an absence of fuel concentration in the region near the rotor pocket surface where fuel concentration is expected otherwise from the presence of liquid fuel in that region. It is more likely that the combustion characteristics in that region might be influenced by an isolated-combusting droplet behaviour. The oxygen concentration is found to be lower near the high temperature region than the regions near the seals. An opposite trend is observed for the carbon dioxide distribution. The temperature in the flame region is around 3106 K and on the walls is 400 K. Again the fluid motion is found to be essentially dictated by the rotor motion.

During the expansion stroke, after the combustion is completed, the distributions of temperature and of oxidizer and carbon dioxide concentrations are found to become fairly uniform throughout the chamber as shown in Fig. 13.

CONCLUDING REMARKS

We have presented preliminary results for a Wankel engine under both motoring and firing conditions, obtained from the solution of unsteady, three-dimensional Navier-Stokes equations. These results are based on the assumption of laminar fluid motion and chemical kinetics, with the use of appropriate submodels for combustion and sprays.

The results show the average rotor torque generated by the non-uniform pressure distribution is nearly the same for the different cases considered under both motoring and firing conditions. This indicates that the pressure non-uniformity is determined mostly by the rotor-induced fluid motion. The pressure is higher near the trailing apex region than near the leading apex region.

One indication of our study is that, under the present assumptions, vaporization appears to be more rate-controlling than mixing during the combustion process. This finding is contrary to the numerical predictions reported by Abraham et al.⁵ While considering the fact that the present engine configuration is somewhat different from the one used in their studies, it should be noted again that the present computations are performed without attempting to describe the turbulent aspect of the fluid motion. Both the heat transfer, fluid mechanics, and combustion characteristics in a engine flowfield will be influenced strongly by the turbulent fluid motion. Our solution procedure must be modified to include an appropriate turbulence model.

The code takes about 10 CPU-hours on a CRAY Y-MP, when the calculations are performed on a $31 \times 16 \times 20$ grid. This covers for one entire cyclic period of 6π rads for a firing case. It appears that we are the first to have reported numerical predictions obtained from 3-D computations for an entire cyclic period. The code appears to be potentially very efficient compared with the other schemes used in the modelling of a Wankel engine.

ACKNOWLEDGEMENTS

The work of the first author (MSR) was supported under contract NAS3-26266 from the NASA Lewis Research Center.

REFERENCES

1. Danielli, G.A., Keck, J.C., and Heywood, J.B., "Experimental and Theoretical Analysis of Wankel Engine Performance," SAE Paper 780416, 1978.
2. Roberts, J.A., Norman, T.J., Ekchian, J.A., and Heywood, J.B., "Computer Models for Evaluating Premixed and DISC Wankel Engine Performance," SAE Paper 860613, 1986.
3. Bracco, F.V. and Sirignano, W.A., "Theoretical Analysis of Wankel Engine Combustion," Combustion Science and Technology, Vol. 7, No. 3, 1973, pp. 109-123.
4. Grasso, F., Wey, M.-J., Bracco, F.V., and Abraham, J., "Three-Dimensional Computations of Flows in a Stratified-Charge Rotary Engine," SAE Paper 870409, 1987.
5. Abraham, J., Wey, M.-J., and Bracco, F.V., "Pressure Non-Uniformity and Mixing Characteristics in a Stratified Charge Rotary Engine," SAE Paper 880604, 1988.
6. Abraham, J. and Bracco, F.V., "Comparisons of Computed and Measured Pressure in a Premixed-Charge Natural-Gas-Fueled Rotary Engine," Rotary Engine Design: Analysis and Developments, SAE SP-768, SAE, Warrendale, PA, 1989, pp. 117-131.
7. Amsden, A.A., Ramshaw, J.D., O'Rourke, P.J., and Dukowicz, J.K., "KIVA: A Computer Program for Two- and Three- Dimensional Fluid Flows with Chemical Reactions and Fuel Sprays," LA-10245-MS, Los Alamos National Laboratory, Feb. 1985.

8. Shih, T. I.-P., Yang, S.-L., and Schock, H.J., "A Two-Dimensional Numerical Study of the Flow Inside the Combustion Chamber of a Motored Rotary Engine," SAE Paper 860615, 1986.
9. Steinthorsson, E., Shih, T.I-P, Schock, H.J., and Stegman, J., "Calculations of the Unsteady, Three-Dimensional Flow Field Inside a Motored Wankel Engine," SAE Paper 880625, 1988.
10. Li, T., Steinthorsson, E., Shih, T. I.-P., and Nguyen, H.L., "Modeling & Simulation of Wankel Engine Flow Fields," SAE Paper 900029, 1990.
11. Raju, M.S., and Willis, E.A., "Analysis of Rotary Engine Combustion Processes Based on Unsteady, Three-Dimensional Computations," AIAA Paper 90-0643, 1990.
12. Raju, M.S. and Sirignano, W.A., "Multicomponent Spray Computations in a Modified Centerbody Combustor," AIAA Paper 88-0638, 1988.

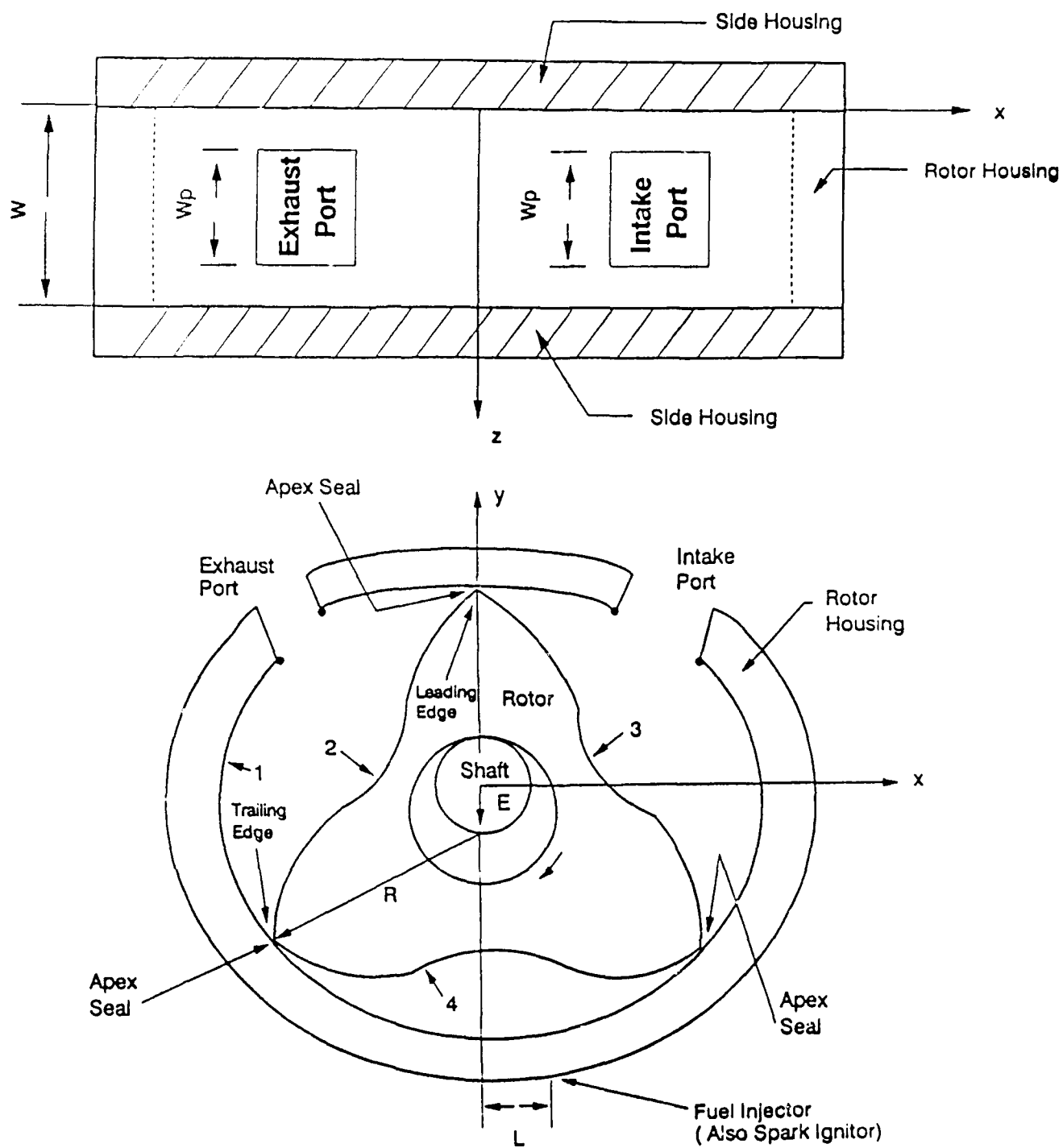
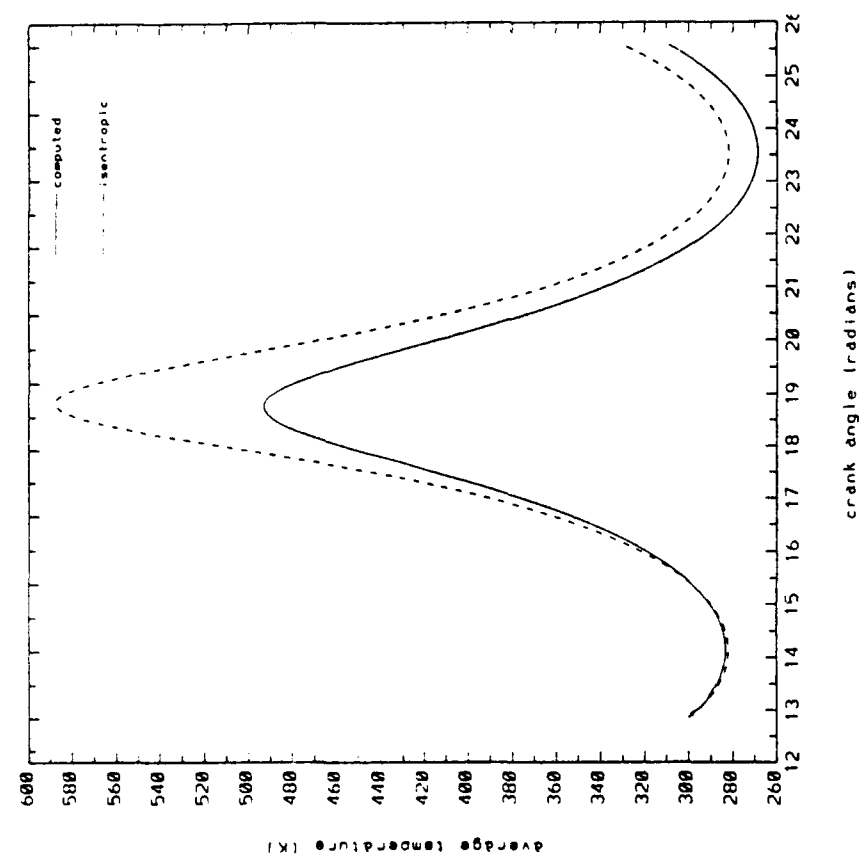
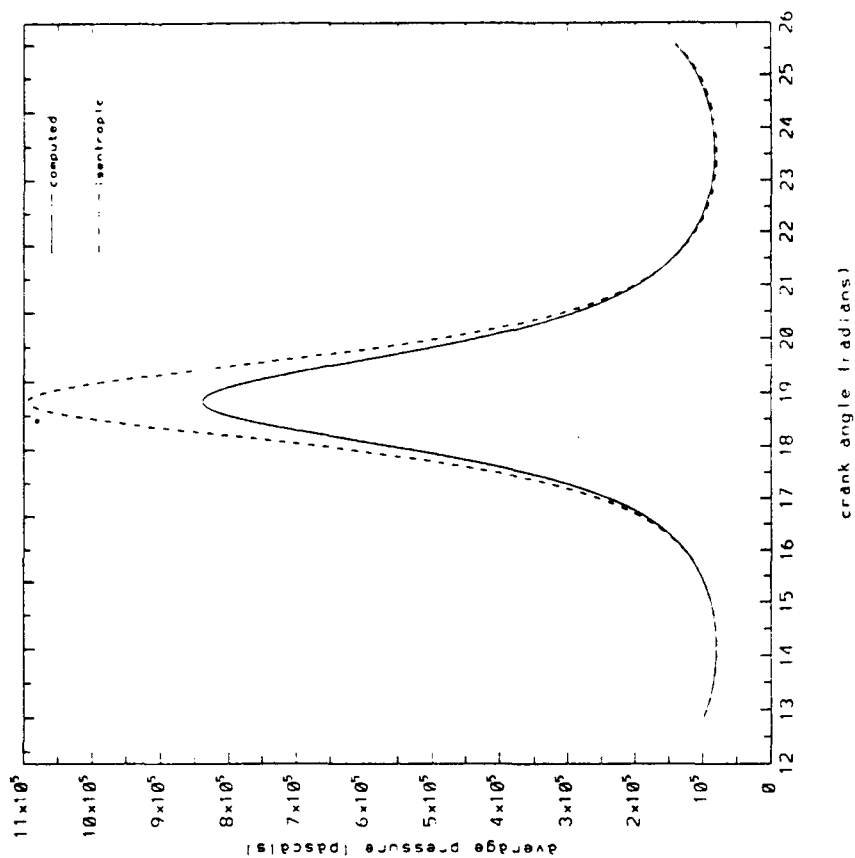


Fig. 1 Schematic of the Wankel engine that was studied.



(a)



(b)

Fig. 2 (a) Mass-averaged temperature versus crank angle with all ports closed.
(b) Volume-averaged pressure versus crank angle with all ports closed.

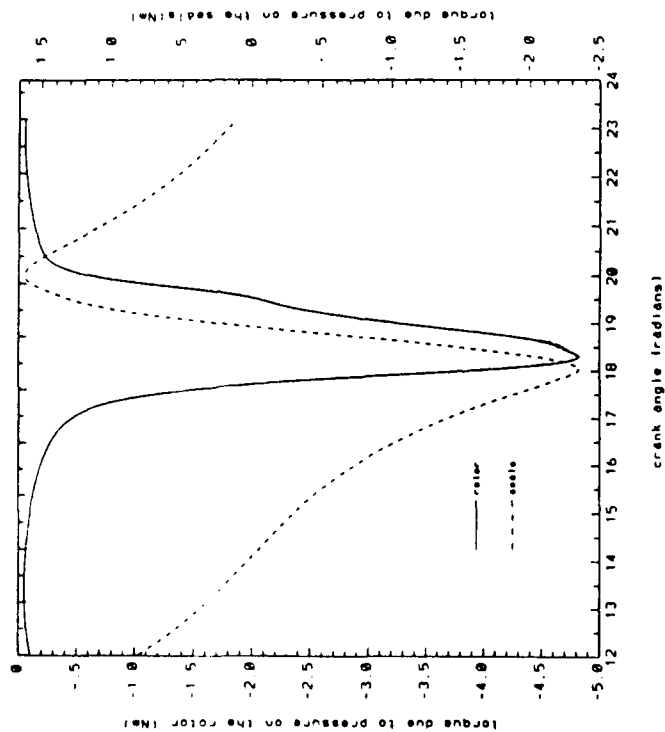


Fig. 3 Torque versus crank angle with all ports closed.

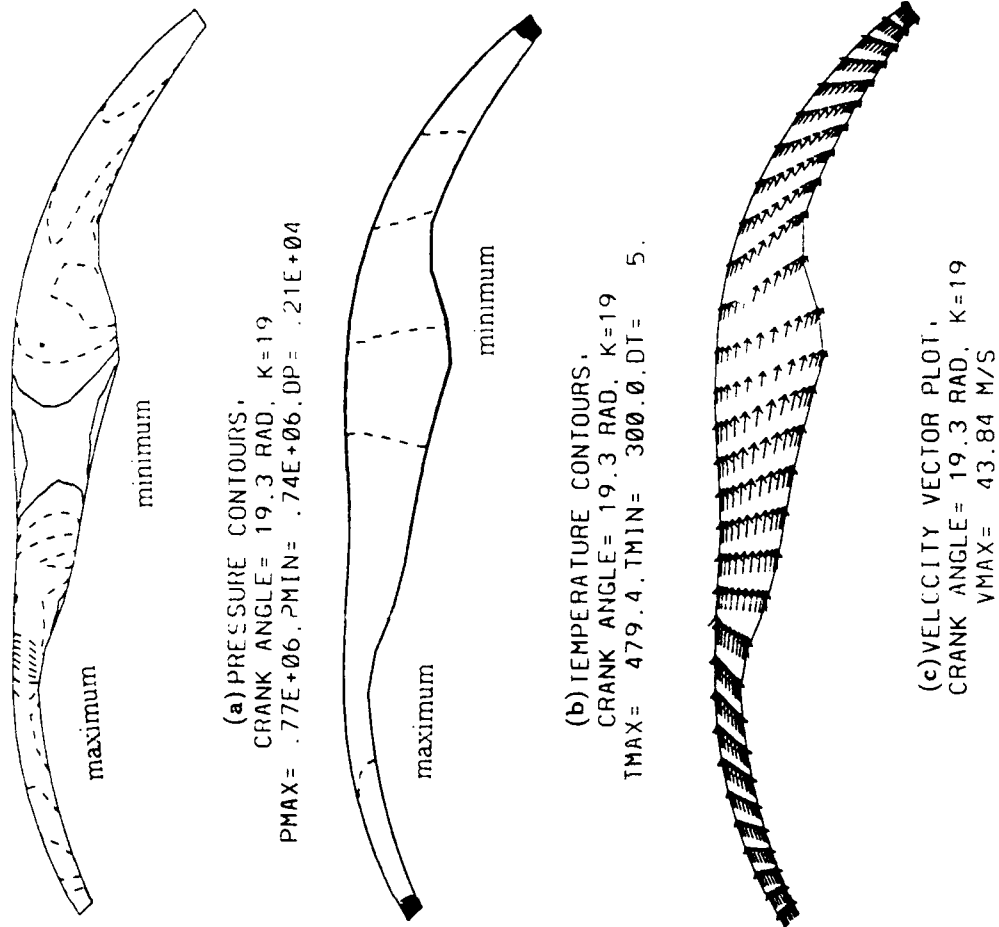


Fig. 4 Gas pressure, temperature, and velocity at $\theta = 19.3$ rad with all ports closed.

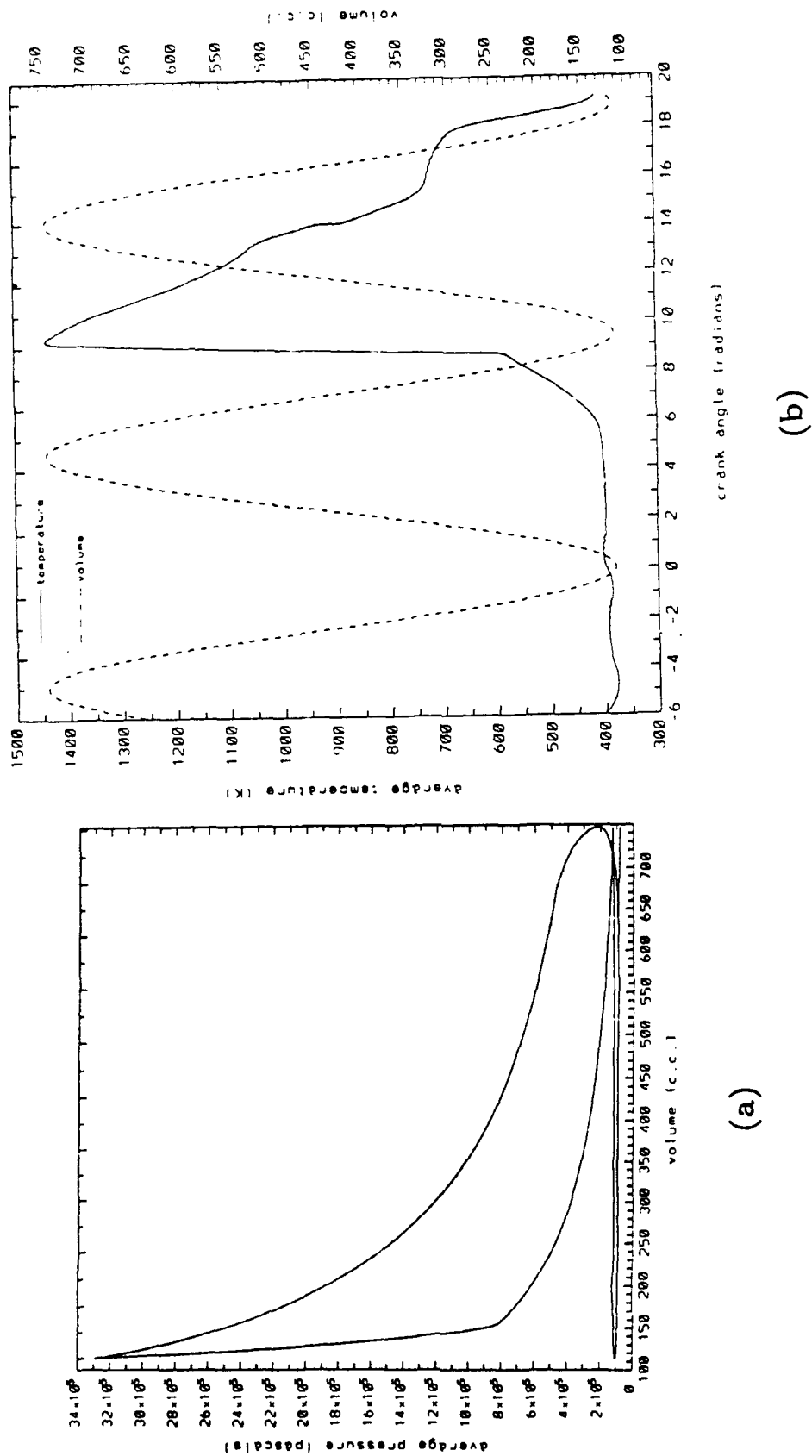
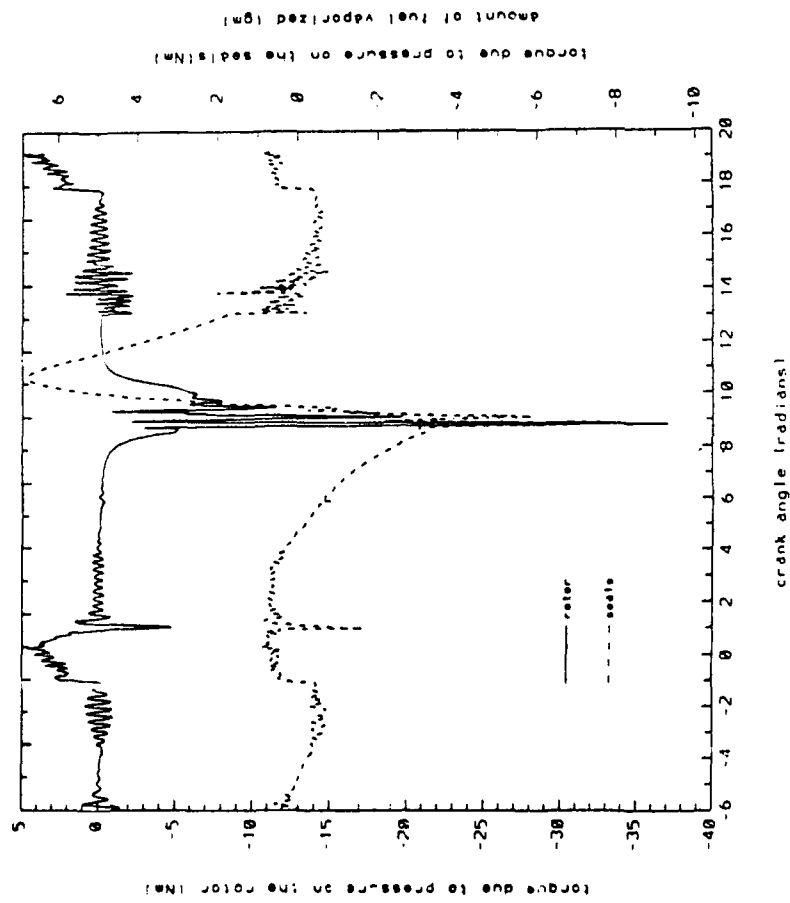
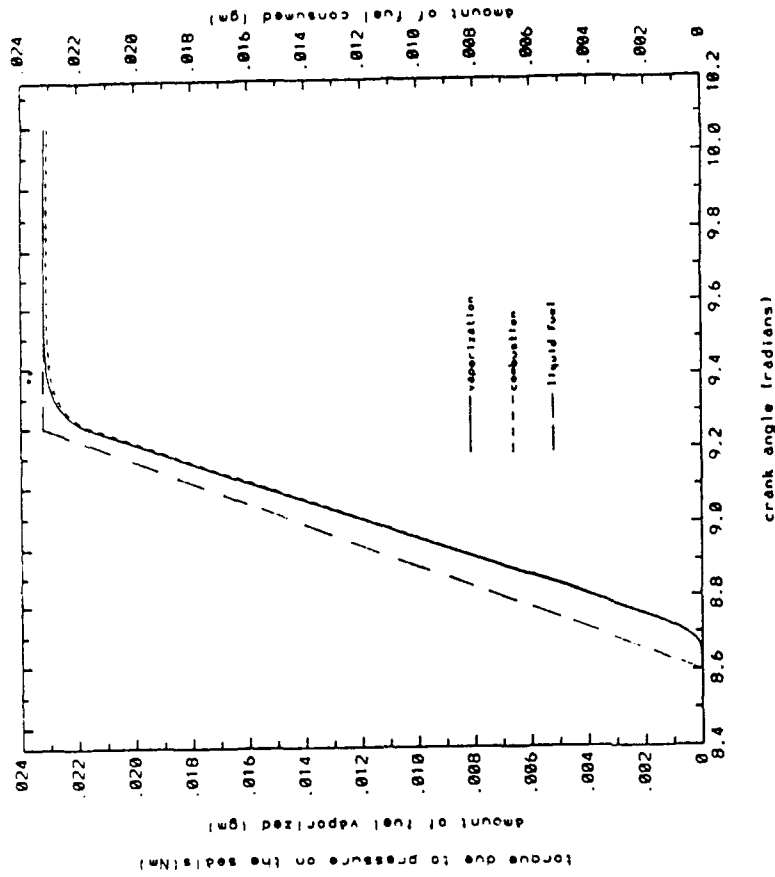


Fig. 5 (a) Pressure versus volume for the case with $\Phi = 0.45$.
 (b) Temperature and volume versus crank angle for the case with $\Phi = 0.45$.



(a)



(b)

Fig. 6 (a) Torque versus crank angle for the case with $\Phi = 0.45$.
(b) Variation of amounts of fuel evaporated and reacted
versus crank angle for the case with $\Phi = 0.45$.

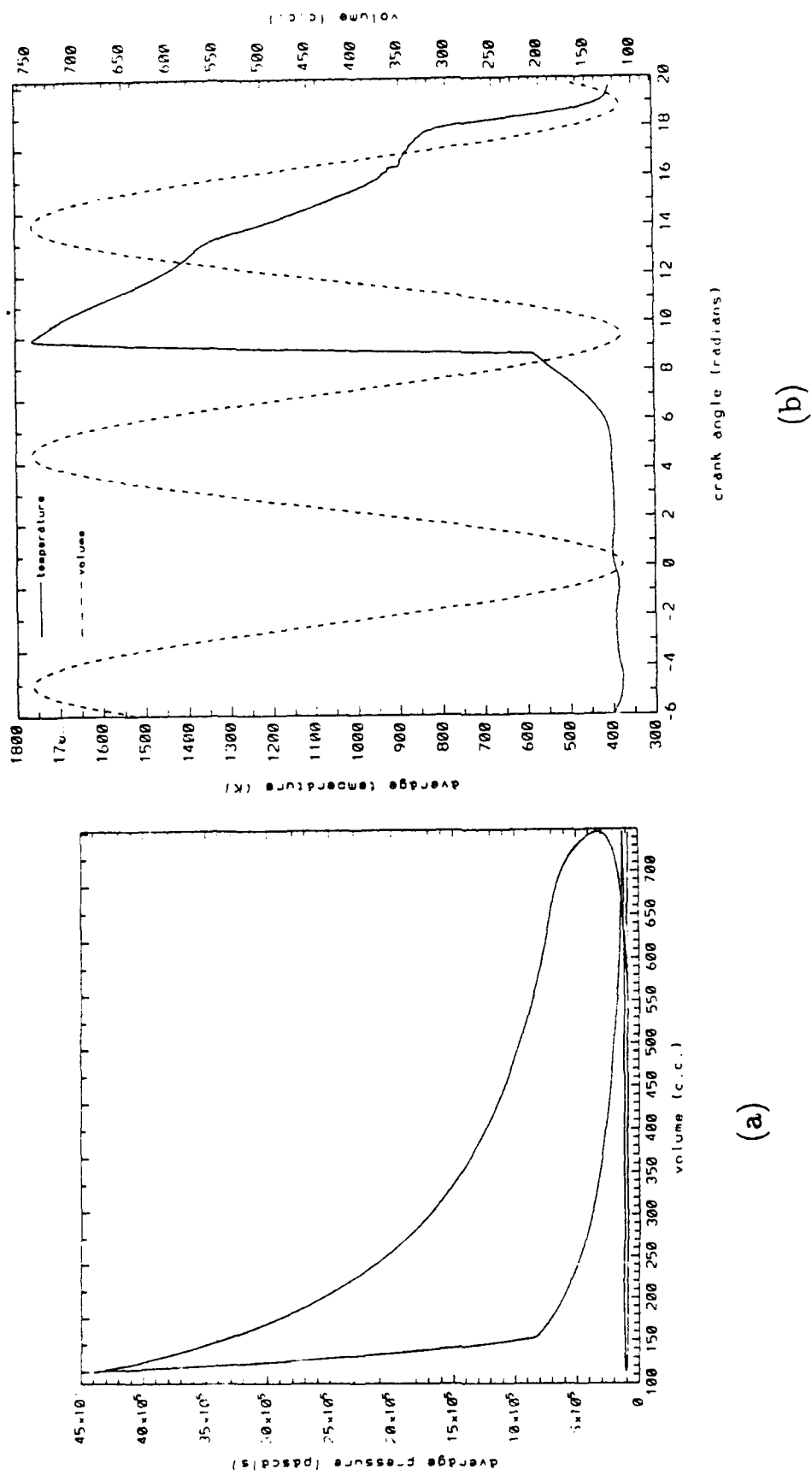
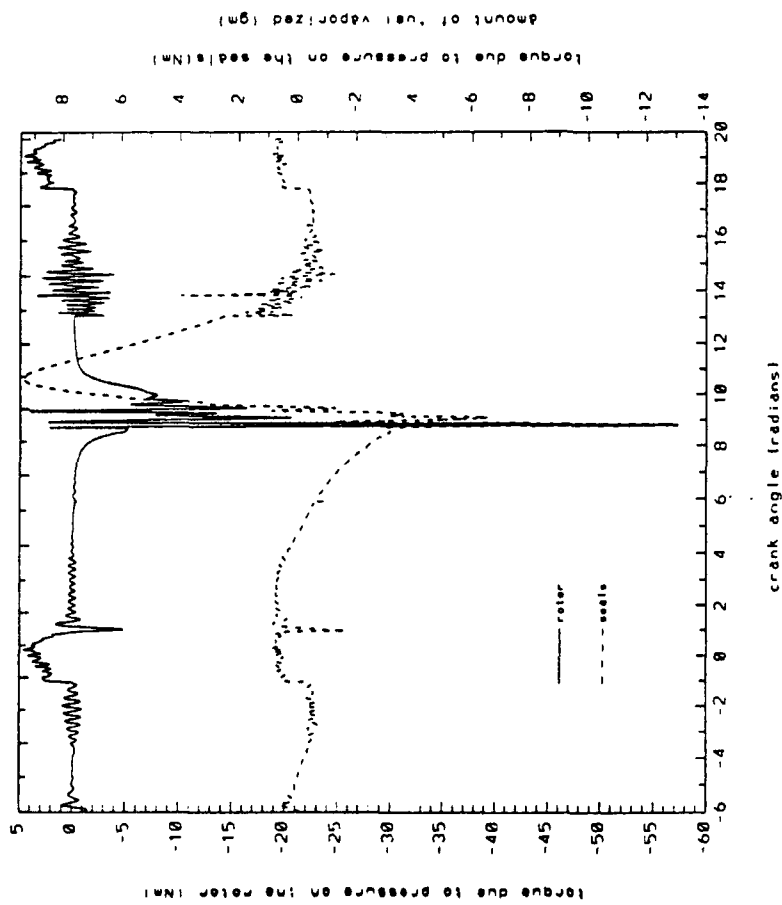
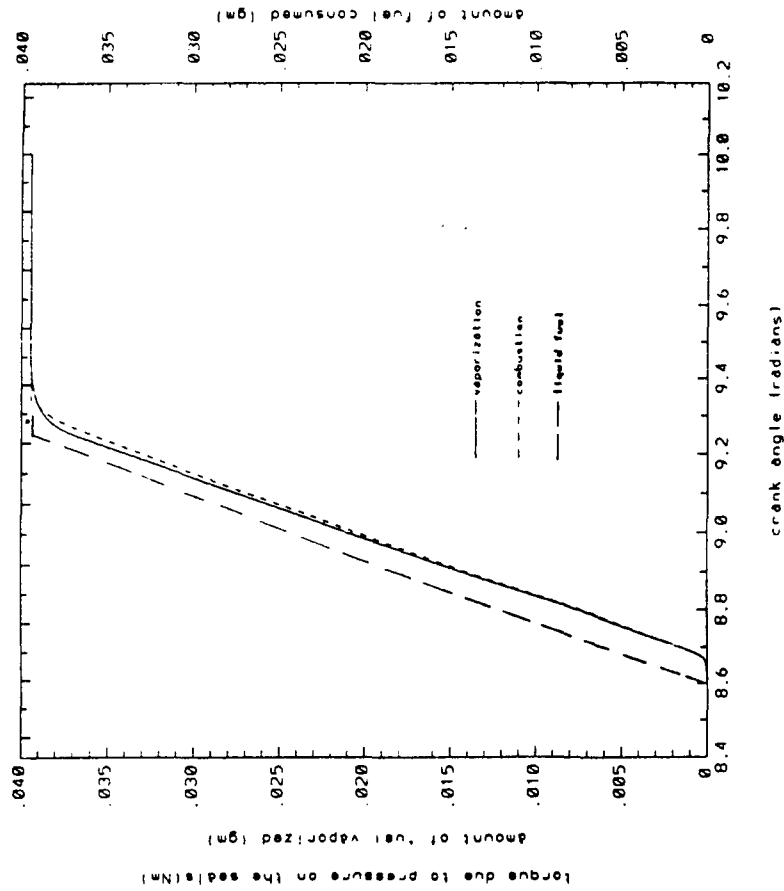


Fig. 7 (a) Pressure versus volume for the case with $\Phi = 0.75$.
 (b) Temperature and volume versus crank angle for the case with $\Phi = 0.75$.



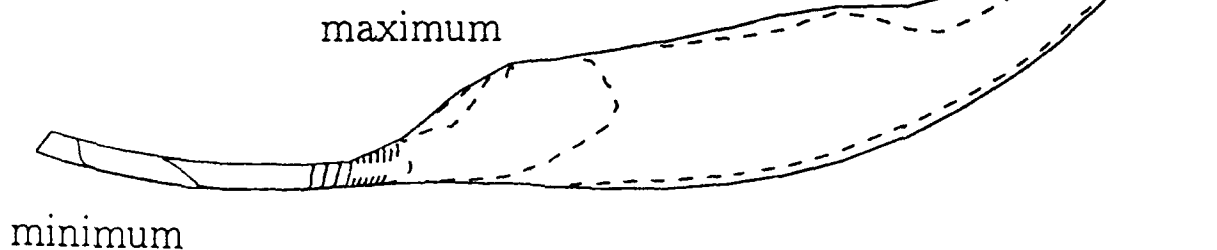
(a)



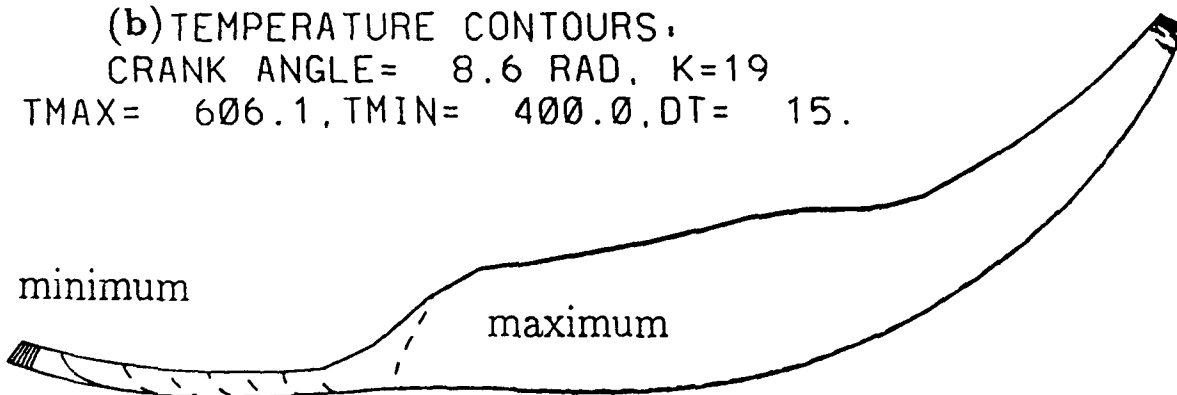
(b)

Fig. 8 (a) Torque versus crank angle for the case with $\Phi = 0.75$.
(b) Variation of amounts of fuel evaporated and reacted versus crank angle for the case with $\Phi = 0.75$.

(a) PRESSURE CONTOURS.
 CRANK ANGLE= 8.6 RAD, K=19
 $P_{MAX} = .80E+06$, $P_{MIN} = .76E+06$, $DP = .26E+04$



(b) TEMPERATURE CONTOURS.
 CRANK ANGLE= 8.6 RAD, K=19
 $T_{MAX} = 606.1$, $T_{MIN} = 400.0$, $DT = 15$.



(c) VELOCITY VECTOR PLOT.
 CRANK ANGLE= 8.6 RAD, K=19
 $V_{MAX} = 35.34$ M/S

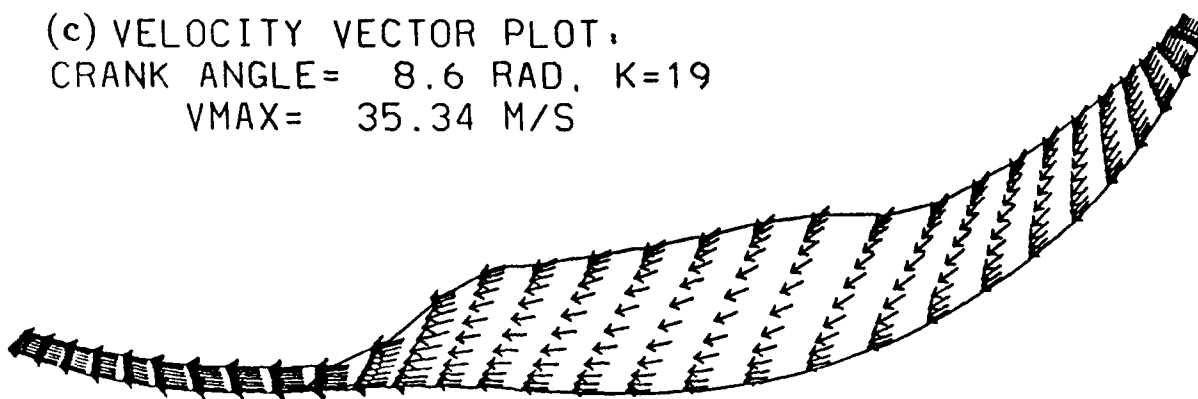
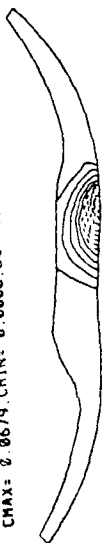
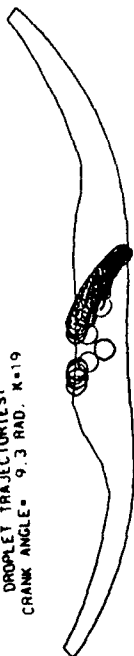


Fig. 9 Gas pressure, temperature, and velocity at $\theta = 8.6$ rad for the case with $\Phi = 0.75$.

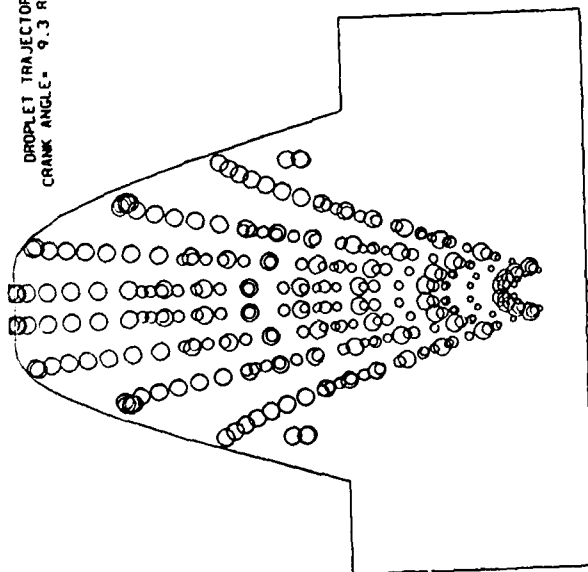
FUEL CONCENTRATION CONTOURS.
 CRANK ANGLE= 9.3 RAD. $K=19$
 CHAX= 0.0679. CHIN= 0.0000. DC= .005



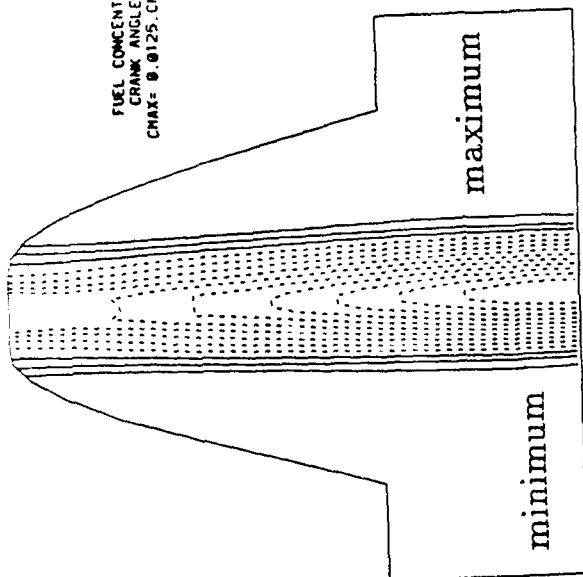
DROPLET TRAJECTORIES.
 CRANK ANGLE= 9.3 RAD. $K=19$



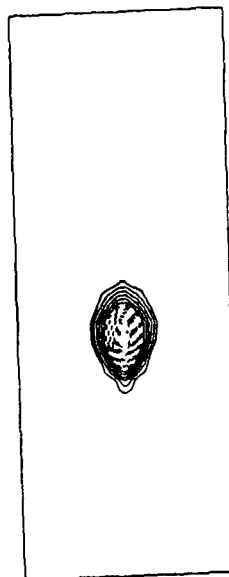
DROPLET TRAJECTORIES.
 CRANK ANGLE= 9.3 RAD. $I=13$



FUEL CONCENTRATION CONTOURS.
 CRANK ANGLE= 9.3 RAD. $I=15$
 CHAX= 0.0125. CHIN= 0.0000. DC= .001



FUEL CONCENTRATION CONTOURS.
 CRANK ANGLE= 9.3 RAD. $J=7$
 CHAX= 0.0198. CHIN= 0.0000. DC= .001



DROPLET TRAJECTORIES.
 CRANK ANGLE= 9.3 RAD. $J=1$

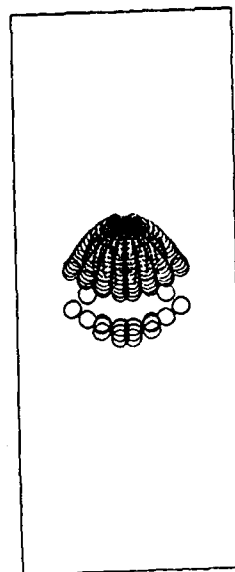
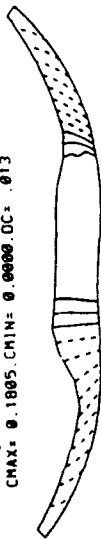


Fig. 10 Droplet trajectories and fuel mass fraction contours
 at $\theta = 9.3$ rad for the case with $\Phi = 0.75$.

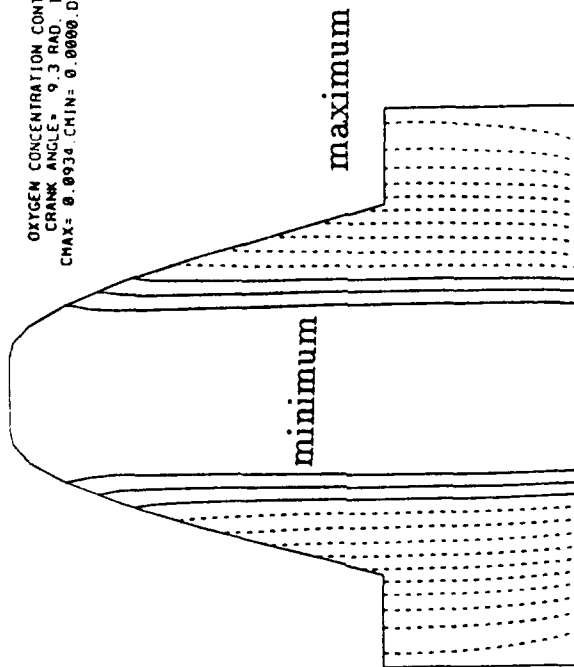
OXYGEN CONCENTRATION CONTOURS
 CRANK ANGLE= 9.3 RAD. $K=19$
 CHAX= 0.1895, CHIN= 0.0000, DC= .013



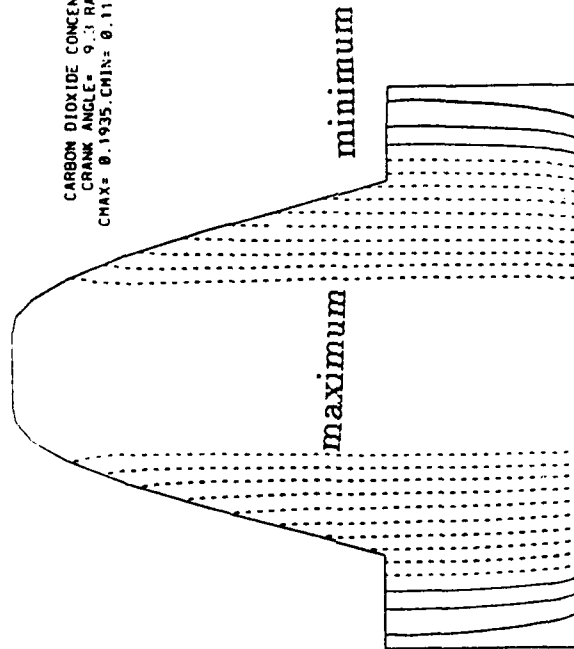
CARBON DIOXIDE CONCENTRATION
 CRANK ANGLE= 9.3 RAD. $K=19$
 CHAX= 0.1935, CHIN= 0.0437, DC= .011



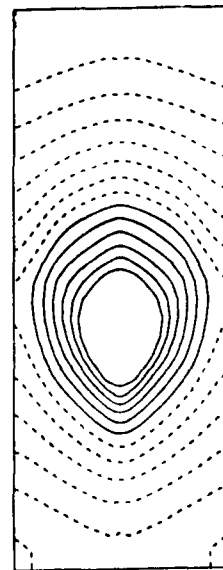
OXYGEN CONCENTRATION CONTOURS
 CRANK ANGLE= 9.3 RAD. $I=15$
 CHAX= 0.0934, CHIN= 0.0000, DC= .007



CARBON DIOXIDE CONCENTRATION
 CRANK ANGLE= 9.3 RAD. $I=15$
 CHAX= 0.1935, CHIN= 0.1162, DC= .006



OXYGEN CONCENTRATION CONTOURS
 CRANK ANGLE= 9.3 RAD. $J=7$
 CHAX= 0.1814, CHIN= 0.0000, DC= .013



CARBON DIOXIDE CONCENTRATION
 CRANK ANGLE= 9.3 RAD. $J=7$
 CHAX= 0.1935, CHIN= 0.0430, DC= .011

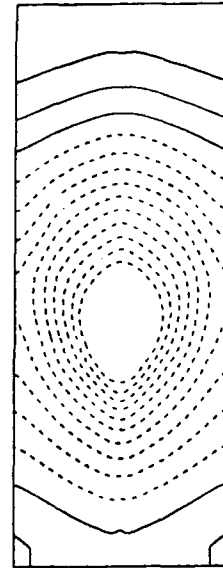


Fig. 11 Oxygen and carbon dioxide mass fraction contours
 at $\theta = 9.3$ rad for the case with $\Phi = 0.75$.

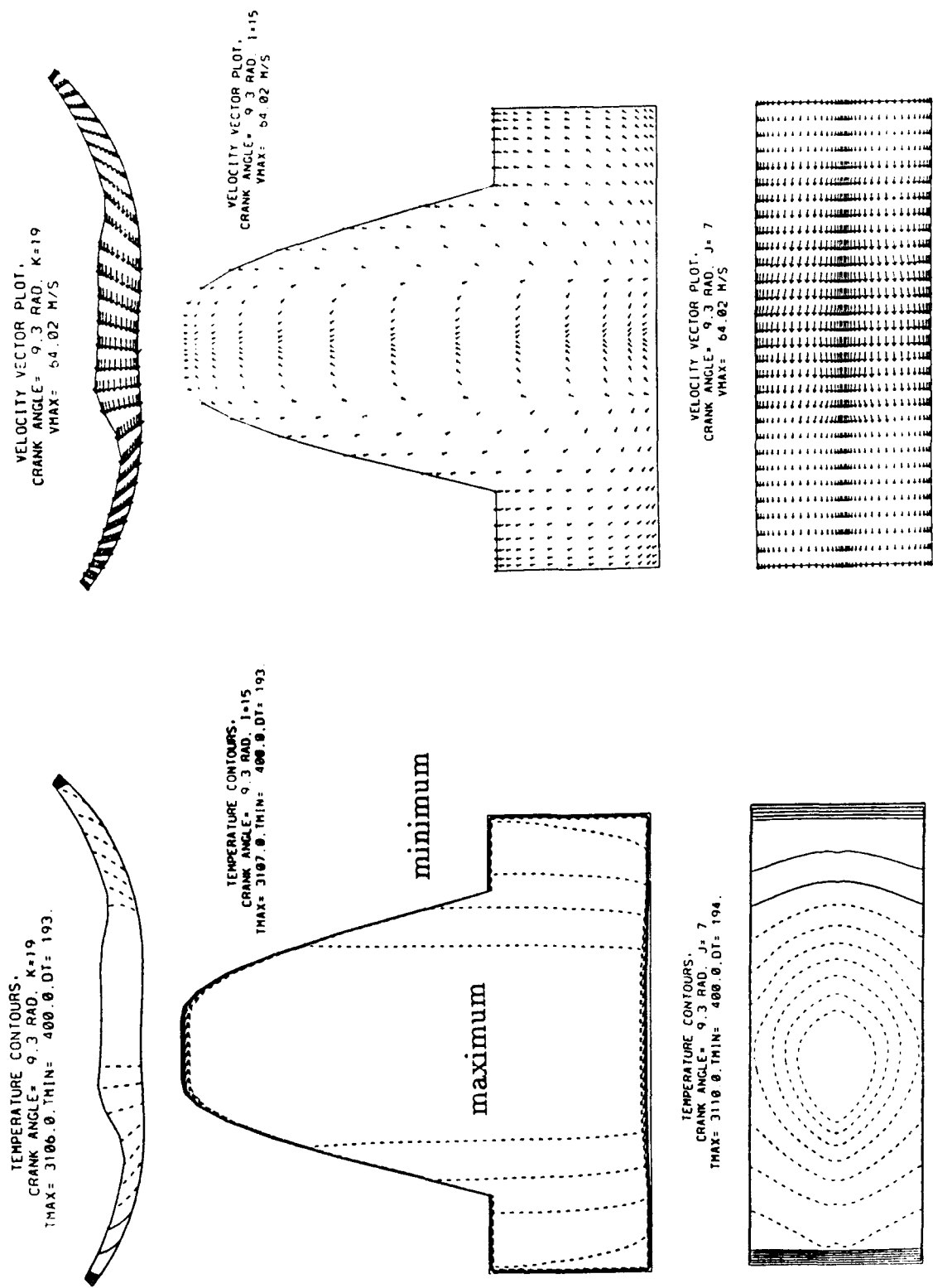


Fig. 12 Isotherms and gas velocity at $\theta = 9.3$ rad for the case with $\Phi = 0.75$.

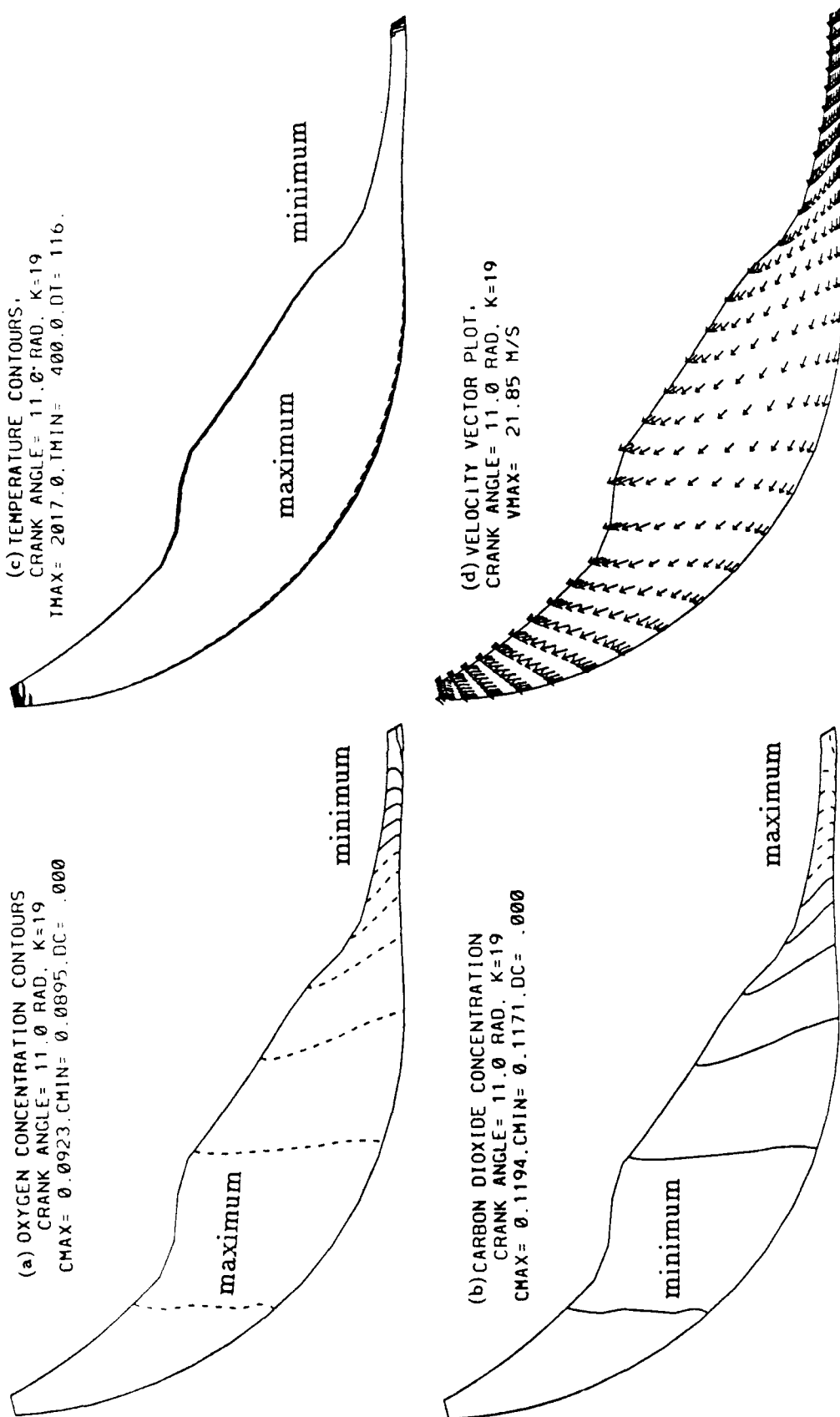


Fig. 13 Oxygen, carbon dioxide, and temperature contours and gas velocity at $\theta = 11$ rad for the case with $\phi = 0.75$.

**ADVANCED STRATIFIED CHARGE ROTARY ENGINE TECHNOLOGY FOR
GENERAL AVIATION SYSTEMS**

by

Robert S. Mount
and
Edward S. Wright
John Deere Technologies International Inc.
P.O. Box 128
Wood-Ridge, NJ

For presentation to the AIAA/FAA Joint Symposium on General
Aviation Systems at the Port O-Call Inn, Ocean City, NJ
on April 11, 1990

ADVANCED STRATIFIED CHARGE ROTARY ENGINE TECHNOLOGY FOR GENERAL AVIATION SYSTEMS

ROBERT E. MOUNT,
Executive Program Manager

AND

EDWARD S. WRIGHT,
President

John Deere Technologies International, Inc.
P.O. Box 128
Wood-Ridge, New Jersey

ABSTRACT

This paper discusses technology enablement activities in progress at John Deere Technologies International, Inc., Rotary Engine Division, toward advanced stratified charge rotary engines. Specific references are made to critical component technology needs and the supportive research and technology in progress. Included are multi-fuel aspects, fuel economy, combustion modeling, advanced turbomachinery, fuel injection systems, performance objectives and progress to date. Long range goals and potential for meeting advanced aviation system needs, in propulsion and auxiliary power unit areas for commercial and military systems, are discussed, including projected market potential and strategies.

INTRODUCTION

Deere & Co. established the Rotary Engine Division of John Deere Technologies International, Inc. at Wood-Ridge, New Jersey in February, 1984. The Rotary Engine Division's mission is to "design, develop and place into production a quality, cost effective and reliable product line of several stratified charge rotary engine families and rotary engine products." A fundamental requirement toward achieving the stated mission is to advance critical component technologies through appropriate research and development activities. These activities are in progress at the Rotary Engine Division in Wood-Ridge, New Jersey and receive substantial support from Deere Management and other Deere & Co. units, i.e. the Deere Technical Center, Moline, Illinois and the Product Engineering Center, Waterloo, Iowa.

Development of three families of SCORE™ stratified charge rotary engines is in progress (Figure 1). The acronym SCORE™ stands for Stratified Charge Omnivorous Rotary Engine with the word "Omnivorous" reflecting multifuel or wide fuel tolerance capabilities. This new propulsion technology for the 1990's has progressed to prototype production status for the SCORE™ 70 Series (0.66 liter, 40.4 cu.in./rotor), the smallest of the three families. Initial emphasis is on the two rotor version and for limited application at near term, conservative ratings. The intermediate size, SCORE™ 170 Series, and largest size SCORE™ 580 Series will enter prototype production at a later date. The

SCORE SERIES	DISPLACEMENT/ROTOR LITERS (CU. IN.)		BHP/ROTOR	
			NEAR TERM	GROWTH
70	0.67	(40)	100	200
170	1.72	(105)	200	300
580	5.80	(350)	375	650

PRODUCT DIRECTION
(COMMERCIAL & MILITARY)

- ENGINES, CAPTIVE AND OEM
- INTEGRATED PROPULSION SYSTEMS
- GEN SETS/AUXILIARY POWER UNITS/ENVIRONMENTAL CONTROL UNITS
- LICENSING TECHNOLOGY

FIGURE 1 JOHN DEERE SCORE™ FAMILIES (ONE TO EIGHT ROTORS)

three families, with variations in the number of rotors from one to six, and horsepower growth cover a wide power range from 80-3000 HP (60-2237 Kw) and are applicable to a wide variety of commercial and military applications.

One potential application is general aviation systems. The jet fuel capability and other features available in the SCORE™ engines make the technology particularly well suited to aviation systems, in main propulsion or auxiliary applications. Research work toward the advancement of critical technologies necessary to achieve the advanced aircraft propulsion system capabilities is in progress under contractual and in-house supported activities. Business arrangements, influenced by market potential, industry experience, sales and service capability and product liability considerations are being explored.

PURPOSE

The purpose of this paper is to discuss the rotary engine technology in general and as related to general aviation systems, the activities in progress toward that end, critical component technologies being investigated and advanced, methodologies and ultimate application including problem areas. Also, supportive technology developments in progress toward other applications (vehicular, marine, ground support) are discussed. Potential aerospace applications of this technology are advanced general aviation aircraft, unmanned aircraft and auxiliary power units (both airborne and ground). Contractual work under the direction of NASA Lewis Research Center and Naval Air Development Center involve higher specific output and improved efficiencies combined with high altitude capabilities. The inherent alternate fuel capability (permitting the usage of Jet-A fuel), high specific output and low fuel consumption offer significant advantages over current reciprocating aircraft engines. Lower initial cost, improved fuel consumption and lower maintenance costs are projected for the rotary in comparison to turbines.

STRATIFIED CHARGE ROTARY ENGINE TECHNOLOGY. An inherent compatibility exists between the rotary engine and unthrottled, direct chamber injection stratified charge combustion. With rotation of the triangular shaped rotor, all of the air for a given lobe on the rotor passes by the top dead center zone when traversing from compression to the expansion portions of the cycle (Figure 2).

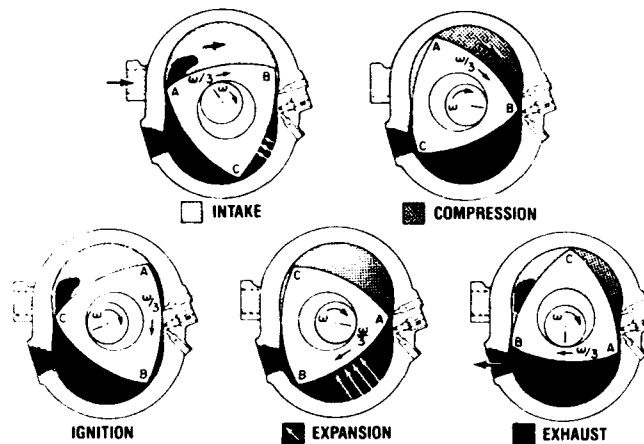


FIGURE 2 BASIC GEOMETRY AND OPERATING CYCLE
STRATIFIED CHARGE ROTARY ENGINE

By placement of a high pressure pilot injection nozzle in this zone, in close proximity to an ignition source, a locally rich fuel-air mixture region can be generated and ignited. Overall fuel-air mixtures that would be too lean for normal spark ignition can be ignited by the initiation of combustion in the locally rich zone. Octane and cetane sensitivities are not present and therefore, operation on a variety of fuels (i.e. Jet-A, diesel, JP-4, JP-5, JP-8, gasoline) can be accommodated and has been demonstrated.

Early versions of the stratified charge rotary engine utilized a single fuel injector. This resulted in limitations over the full speed and load range with the large variations in fuel flow through the light-off zone in responding to variations in load demand. Operation at selected conditions could be optimized, however, at the compromise of other conditions. A significant breakthrough in achieving full load and speed range operation, including starting, idling, efficient part load and full load operation and cold starting occurred during the late 1970's period with introduction of a dual injector configuration, (Figure 3). This configuration permitted consistent light-off over the full operational range by maintaining the volume of fuel per stroke through the pilot nozzle at a constant level, optimized for consistent ignition. Since the $\text{mm}^3/\text{stroke}$ were held constant, conditions in the light-off zone were essentially constant regardless of speed and power changes. Large variations

of fuel flow through the main injector, separated from the pilot injector/light-off zone, could vary widely as a function of load demand with no effect upon the light-off action.

Further development work examined variations in the nozzle positions and culminated in the current configuration as depicted in Figure 4. This basic configuration is used in all current engine designs.

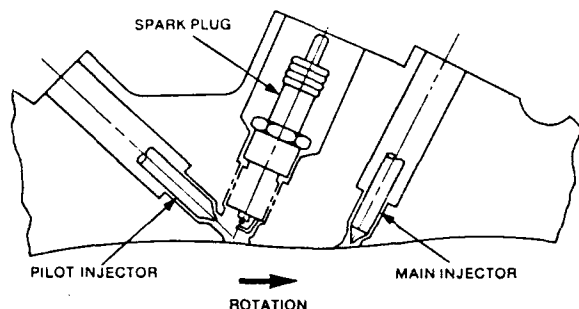


FIGURE 3 ORIGINAL DUAL INJECTOR STRATIFIED CHARGE ROTARY ENGINE CONFIGURATION BTC (Before Top Center) PILOT

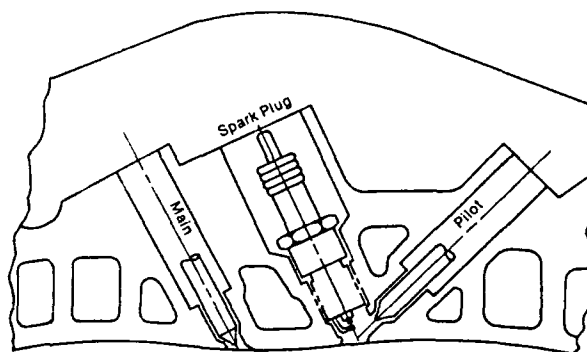


FIGURE 4 ATC (AFTER TOP CENTER) PILOT DUAL INJECTOR CONFIGURATION

INJECTION AND IGNITION SEQUENCE. The sequence of ignition, pilot injection and main injection is presented in Figure 5. As can be noted the ignition source is available prior to start of pilot injection and overlapped by a portion of the pilot injection which in turn is overlapped by the main injection. Timing and variation in durations can easily be accommodated in conventional control systems.

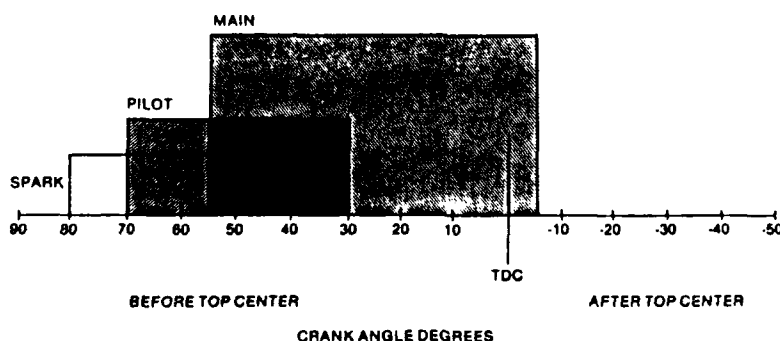


FIGURE 5 TYPICAL IGNITION AND INJECTION TIMINGS

SCORE™ 70 AIRCRAFT ENGINES

Early Studies. Initial work defining the characteristics of an advanced stratified charge rotary aircraft engine design was conducted under contract to NASA Lewis Research Center, Cleveland, Ohio, during 1982 (Reference 1). Detailed studies by

general aviation airframe manufacturers compared overall effects on airplane design, performance, operational and life cycle costs for four engine candidates in advanced and high advanced categories.

- o Stratified Charge Rotary
- o Small Turbine
- o Spark Ignited Reciprocating Engine
- o High Speed Lightweight Air-Cooled Diesel.

These studies (Reference 2 and 3) ranked the stratified charge rotary as the number one candidate.

The Research Rig Engine. A research rig (Figure 6) was designed and built for explorations of power, BMEP and speed levels above and beyond those required for the highly advanced aircraft engine projections. The intent was to provide a working unit capable of exploring performance trends up to and above actual engine maximum design point conditions. This permits the evaluation of component technologies throughout the advanced and highly advanced regimes without mechanical or thermal restrictions in the base rig engine. The research rig is currently operational under NASA contract.

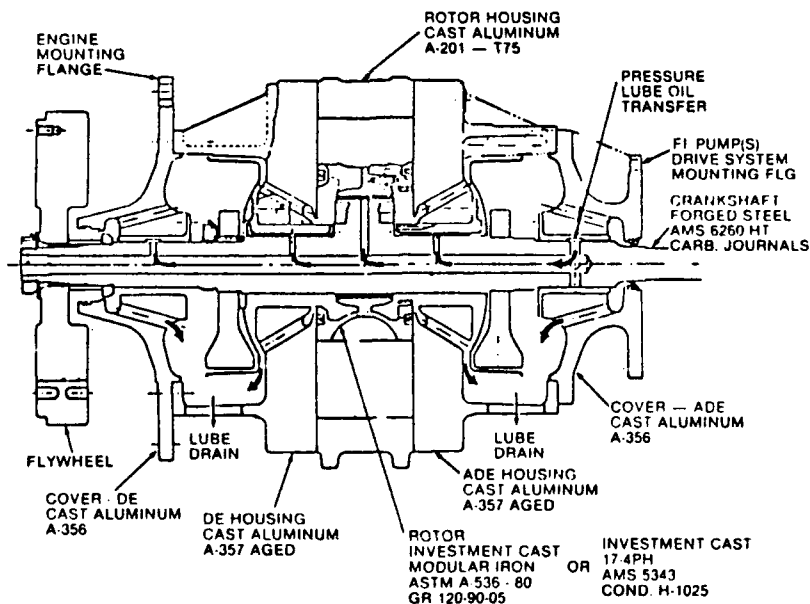


FIGURE 6 0.66 LITERS, (40 CU.IN.) LIQUID COOLED POWER SECTION

Figures 7 and 8 show the basic research rig engine. In Figure 8, a Deere technician is installing a tool for crankshaft positioning purposes during the assembly/measurement process. General construction, cooling passages and basic size can be

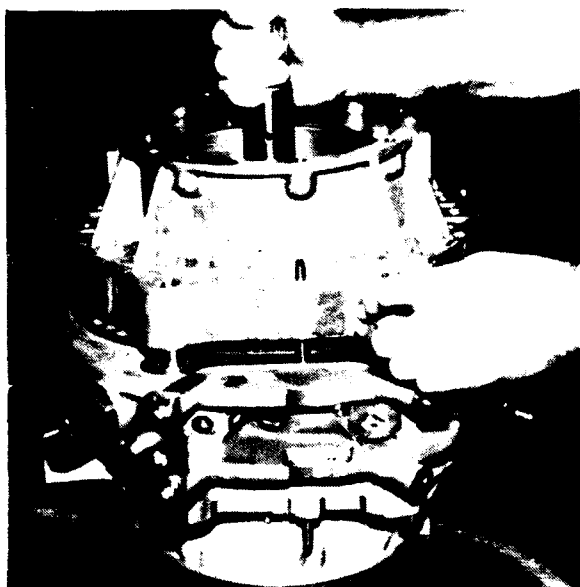


FIGURE 7 1007R SINGLE ROTOR RESEARCH
RIG ENGINE



FIGURE 8 1007R RESEARCH RIG ENGINE COMPONENTS

noted in this photograph. Conventional stratified charge rotary engine materials are used including cast aluminum housings, investment cast steel (or nodular iron) rotor and a carburized steel crankshaft. Detailed design features for the 1007R research rig have been published in Reference 4.

Figure 9 presents the power output demonstrated between late 1989 and March 1990. These tests culminated in the 200 HP (149 Kw) level in late March.

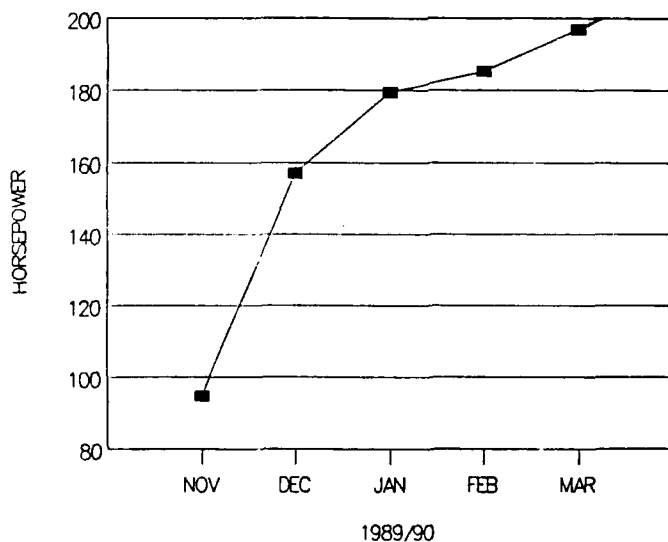


FIGURE 9 MAXIMUM POWER
1007R SCORE 70 ENGINE

The work under NASA contract involves advancing the technology to high power density 5 HP(3.72 Kw)/in³ and improving thermal efficiency. The target brake specific fuel consumption is 0.37 lbs/BHP-Hr at take-off and 0.355 lbs/BHP hr at mid-range.

The critical technologies being addressed are those involving combustion improvement (supported by extensive three dimensional computational fluid dynamics investigations), fuel injection configurations (high speed, high flow), ceramics and adiabatic features (rotors, side and rotor housing coatings), extensive tribological/sealing investigations, control systems, lightweight/low conductivity parts, catalytic surfaces, airplane mission modeling and turbomachinery effective at altitudes of 33,000 feet (10,058 meters) general aviation and 66,000 feet (20117 meters) military.

These detailed research investigations require teams of specialists in the wide ranging areas of technology. Figure 10 reflects the teaming arrangement for the NASA program currently in progress at the Rotary Engine Division and identifies the areas of investigation.

As noted previously, the combustion improvement and power output pursuits are supported extensively by computational fluid dynamics studies. These studies are conducted at the Rotary Engine Division on a TITAN graphics mini-computer. The model has been developed in close collaboration between the Rotary Engine

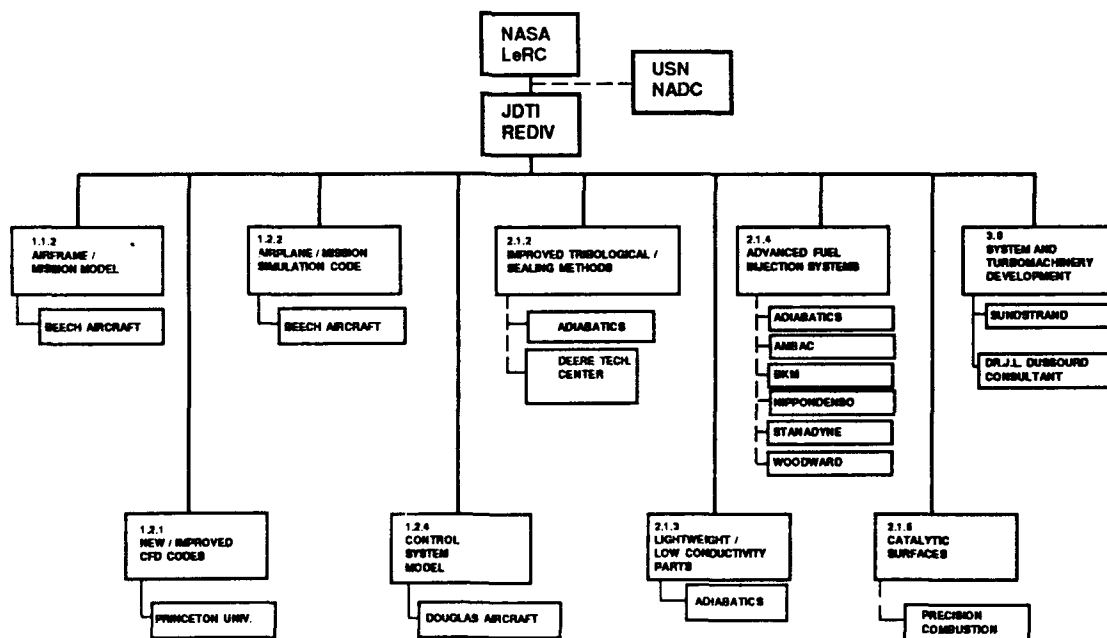


FIGURE 10 STRATIFIED CHARGE ROTARY ENGINE
CRITICAL TECHNOLOGY ENABLEMENT PROGRAM TEAM

Division of John Deere Technologies International, Inc. and the Engine Laboratory of Princeton University which is headed by Prof. F. V. Bracco. Since the early 70's the Engine Laboratory at Princeton has pioneered the development of multidimensional models for engines including detailed measurements in engines which have been used to assess the accuracy of the models. During 1989, substantial correlation was established between the computer model and actual engines test data. This has permitted the prediction of performance anticipated for changes in housing and ignition/injector geometry and other variables. This capability facilitates the technology enablement process and reduces the cost and schedule time required to evaluate proposed modifications.

Two Rotor Aircraft Engine. Figure 11 illustrates a conceptual overall aircraft engine package based on a Model 2013R configuration. This depicts an advanced general aviation engine

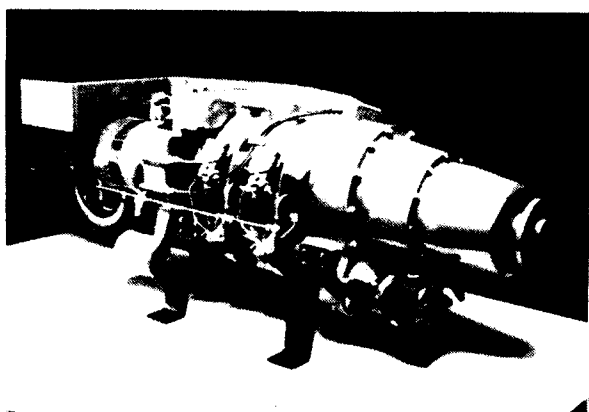


FIGURE 11 CONCEPTUAL AVIATION ENGINE
BASED ON 2013R CONFIGURATION

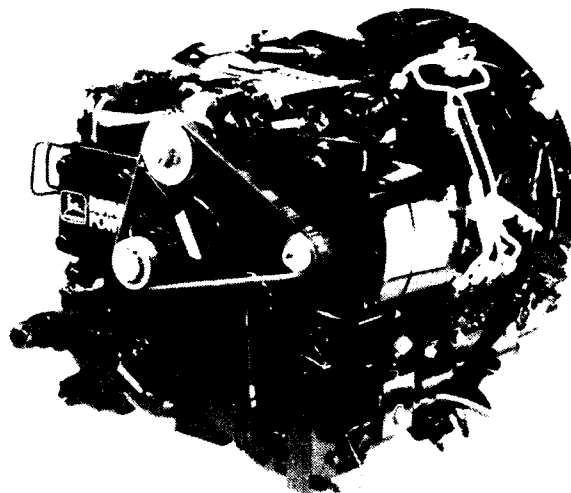


FIGURE 12 70 SERIES, MODEL 2013R

with a full complement of accessories. The two rotor power section is integrated into the complete aircraft engine configuration by the addition of a reduction gear and prop shaft at one end (or direct drive for helicopter application). The accessory gear box and turbocharger-intercooler equipment are located at the opposite end with accessories placed at selected positions at either end. The resultant package is one of small frontal area 272 sq.in (0.176 sq. meters). The arrangement shown is a dry sump and would require airframe mounting of the oil tank. Cooling equipment for coolant and oil are not shown. These components, including the weight of the liquids, were included in the configurations examined by NASA, Cessna and Beech in the studies previously referred to in this paper wherein rotary, turbine, reciprocating spark ignition and compression ignition engines were compared. The 2013R engine is currently of interest for several high altitude, long endurance military

aircraft applications using unmanned aircraft vehicles (UAV's). For the high altitudes, multiple stages of turbocharging and intercooling are necessary with that equipment approaching or exceeding the size of the core engine. Advanced, high pressure ratio turbomachinery is being pursued to minimize the weight and size additions at altitudes up to at least 65,000 feet (19,812 meters). Three and four rotor versions are also of interest.

Supportive Technology-Non Aircraft Configurations. The 2013R engine at its near term power ratings of 120 HP (89.5 Kw) and a non-aircraft version (Figure 12) is currently being utilized for ground power units. Figure 13 shows an industrial version of the 2013R engine. These are the prototype engines produced in 1989. Increased ratings at both 160 HP (119Kw) and 200 HP (149 Kw) are anticipated during 1990. Marine versions of up to 200 HP (149 Kw) are presently being prepared for boat testing during 1990. Also, an installation in a John Deere Model 2955 tractor is in progress (Figure 14).

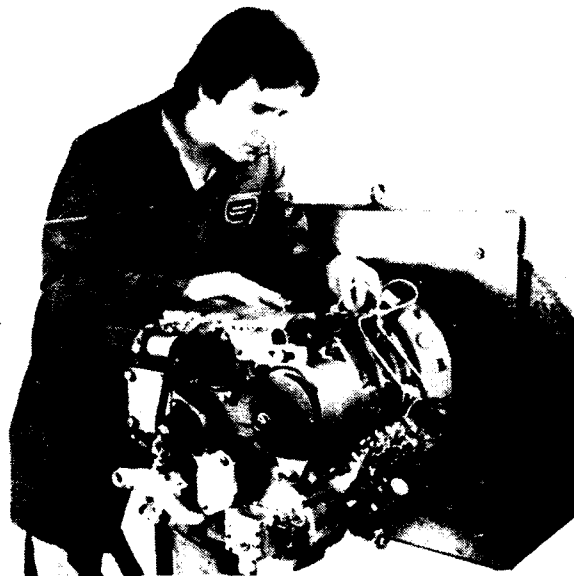


FIGURE 13 SCORE™ 2013R INDUSTRIAL ENGINE

Near Term Aircraft Engine. A 400 HP (298 Kw) stratified charge rotary engine was designed and tested at JDTI, Inc. during the 1985-1989 time period (Figure 15). This engine (References 5, 6, 7 and 8) operates at a take-off BMEP of 130 psi (896 kPa) and at 5800 RPM. It is a two-rotor 1.72 liter (105 cu.in.) per rotor engine and represents a nearer term technology level than that being pursued in the longer range, more aggressive NASA/NADC efforts.



FIGURE 14 SCORE™ 2013R
TRACTOR INSTALLATION



FIGURE 15 2034R AIRCRAFT ENGINE
400 HP/5800 RPM FUEL INJECTION
SIDEVIEW

The preliminary specification of this engine is presented in Figure 16. The designation 2034R SCORE™ 170 engine refers to two rotors, 3.4 liters total displacement and R for rotary.

2034R SCORE 170 ENGINE
FUEL INJECTED, TURBOCHARGED, LIQUID COOLED, GEARED,
INTERCOOLED, WITH CABIN BLEED AIR PROVISIONS

Take-off Power	300kW (400hp)
Take-off Crankshaft Speed	5800 RPM
Take-off Altitude Capability	Sea level to 6000m (20,000 Ft.)
Cruise Power (75% Cruise)	225kW (300HP)
Cruise Crankshaft Speed	4350 RPM
Cruise Altitude Capability	To 7500m (25,000 Ft.)
Engine Weight Goal	228kg (506 Lbs.)
BSFC at Take-off	243-255 g/kW-Hr. (.40-.42 Lbs./BHP-Hr.)
BSFC at 75% Cruise	231-249 g/kW-Hr. (.38-.41 Lbs./BHP-Hr.)
TBO	2,000 Hours
Fuel, Aviation Grade	Jet-A
Oil Consumption (Based on 75% Cruise)27kg/Hr. (0.6 Lbs./Hr.)

FIGURE 16 PRELIMINARY ENGINE SPECIFICATION

The engine is rated at 400 HP (298 Kw) at 5800 RPM in take-off conditions (Figures 17 & 18) and will maintain this to 20,000 ft. (6096 meters) altitude. Cruise conditions for the engine are 300 HP (224Kw) at 4350 RPM and this power can be maintained to 25,000 ft. (7620 meters) altitude. The engine is liquid cooled with a 50/50 mixture of ethylene glycol and water. Liquid cooling in an aircraft engine offers advantages over air cooled engines since the warm coolant can be used for de-icing and safe cabin heat. The liquid cooling provides the advantage of being able to better control the engine operating temperature while maintaining an

even temperature distribution. An air-cooled oil cooler is incorporated with the radiator.

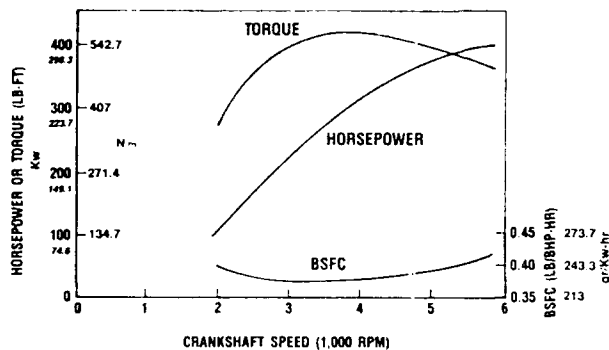


FIGURE 17 ESTIMATED FULL LOAD PERFORMANCE OF ENGINE MODEL 2034R

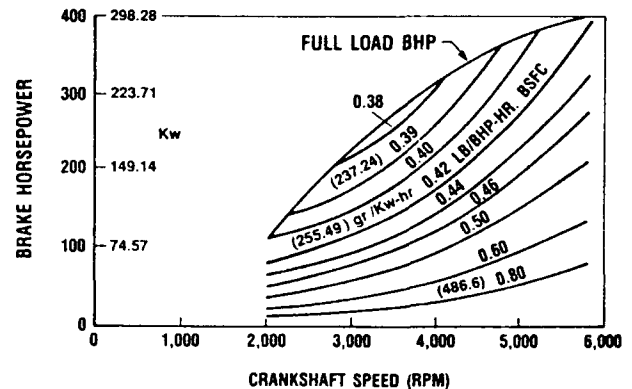


FIGURE 18 ESTIMATED PART LOAD PERFORMANCE OF ENGINE MODEL 2034R

Testing. Testing of the 2034R engine was initiated in late 1987 with the initial test consisting of operation of a highly instrumented engine for the acquisition of housing strain gage data over a wide range of internal pressures. The objective was to validate the finite element models used to design the core engine. Once validated, the finite element models can then be used to facilitate weight control.

Initial testing was accomplished to 200 HP (149 Kw) using Jet-A fuel. This included investigations necessary to obtain uniform ignition, combustion and stable operation and a degree of trial and error in accommodating the dual spark plug configuration at the pilot nozzle, necessary for FAA Certification.

The second phase of testing was initiated in 1988 with operation through full take-off power. This testing was accomplished in conjunction with a Douglas Aircraft Company/USAF contract to investigate the stratified charge rotary engine as a potential candidate prime-mover for an energy efficient APU. The testing involved operation to the take-off condition of 400 HP (298 Kw)/5800 RPM and operation on three different fuels, Jet-A, 100 Octane low lead AVGAS and No. 2 diesel. Also, cold starting was demonstrated on the three fuels in unaided cold starts at -25°F (-32°C).

Take-off Power and Fuel Consumption. Full load performance through the 5800 RPM take-off speed with Jet-A fuel is shown in Figure 19. A maximum power of 430 BHP (320 Kw) was demonstrated at 5800 RPM. The specific fuel consumption of approximately 0.44 lbs/BHP-hr (268 gr/Kw-hr) at the maximum power in this initial testing was slightly above the 0.42 lbs/BHP-hr (255.5 gr/Kw-hr) projected for the engine take-off condition at the end of the overall development program.

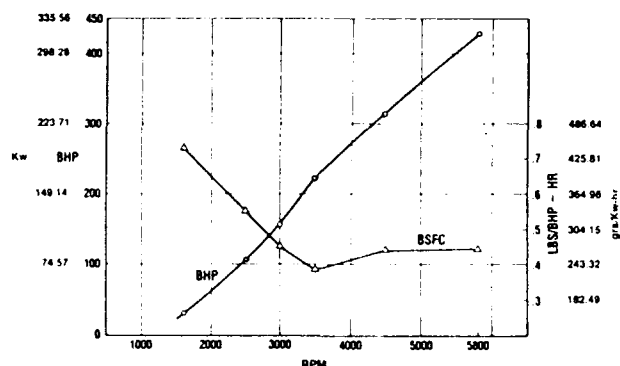


FIGURE 19 STRATIFIED CHARGE ROTARY
AIRCRAFT ENGINE-MODEL 2034R
BASIC PERFORMANCE

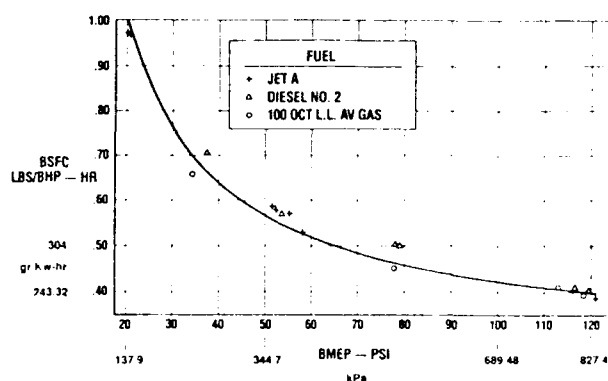


FIGURE 20 STRATIFIED CHARGE ROTARY
AIRCRAFT ENGINE-MODEL 2034R
FUEL CONSUMPTION AT 3500 RPM

Multifuel Testing and Cruise Power Fuel Consumption. In the multifuel testing, Jet-A, 100 Octane low lead AVGAS and No. 2 diesel fuels were used. Starting and general operation through take-off power was essentially equal for the three fuels. Figure 20 shows the resulting specific fuel consumption for the mid-cruise range speed of 3500 RPM over the 20 to 120 psi (138 to 827 kPa) BMEP range. The best BSFC noted was 0.387 lbs/BHP-hr (235.4 gr/Kw-hr) on JET-A, 0.390 lbs/BHP-hr (237.3 gr/Kw-hr) on AVGAS and 0.405 lbs/BHP-hr (246.4 gr/Kw-hr) on No. 2 diesel, all at the 225 HP (168 Kw)/3500 RPM condition.

Cold Starting. Cold Start demonstrations were conducted consisting of unaided starts after a 24 hour cold soak period at -25°F (-32°C). Batteries were not at the low temperature for these tests. Successful starts were achieved on the three fuels (Jet-A, 100 Octane low lead AVGAS and No. 2 diesel) at -25°F (-32°C).

These tests have confirmed operation of the SCORETM engine in a complete aircraft configuration which demonstrated power and fuel consumption on Jet-A and other fuels. Discussions with a wide range of current aircraft industry airframe and engine manufacturers are in progress toward directing that technology to the specialized field of aviation prime propulsion and auxiliary power. More details are provided on the attempts to bring this technology to the General Aviation field in a subsequent portion of this paper.

SCORETM 580 SERIES

John Deere Technologies International, Inc. has been under contract with the United States Marine Corps since 1985 to design and develop its 580 series engines for the Marine Corps toward the usage in Advanced Amphibious Assault Vehicles. A demonstration and validation engine (Figure 21) with total swept-volume displacement of 11.6 liters (5.8 liters or 350 cubic-inches displacement per rotor), rated at 750 BHP successfully

completed the 400-hour NATO test cycle. This cycle is the most vigorous of the 3000 hours of durability and reliability testing conducted under this contract.

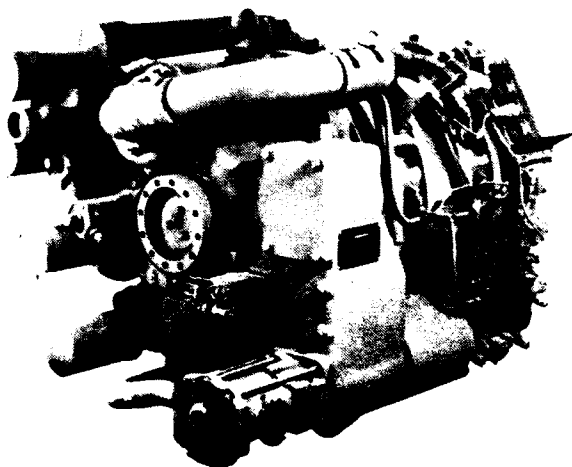


FIGURE 21 580 SERIES, MODEL 2116R



FIGURE 22 SCORE™ 580 POWERED FMC MTTB

Apex seal wear has been reduced to a level significantly below the original goal. Measured wear rates of one to two thousandths of an inch per hundred hours of operation correspond to seal life exceeding three times the required service life. The engine operated successfully on various fuels including DF-1, DF-2, DF-A, JP-8 and combat gasoline. In addition, the engine completed shock tests and demonstrated unassisted cold-start capabilities within five seconds at -25 degrees F.

To date, approximately 6000 hours of contract testing has been completed including performance, environmental, 600 and 1000 hour mission profile reliability testing, and the aforementioned 400 hour NATO test. Power output up to 825HP (615 Kw), equivalent to a ten percent overload condition, has been demonstrated repeatedly.

An installation of this engine has been made in conjunction with FMC Corporation, San Jose, California in their MTTB (high mobility test bed) Vehicle (Figure 22). The overall power pack for this installation, including the Model 2116R SCORE™ 580 rotary engine, transmission and associated equipment is shown in Figure 23.

With successful completion of the two rotor USMC contract, a follow-on demonstration and validation contract has been awarded for development and delivery of two and three rotor models of a 580 Series family. The family of engines will consist of one through six rotor engines covering a range of 375 to 2250 horsepower (280 to 1678 Kw) at current ratings. The design of this family will incorporate the maximum degree of commonality

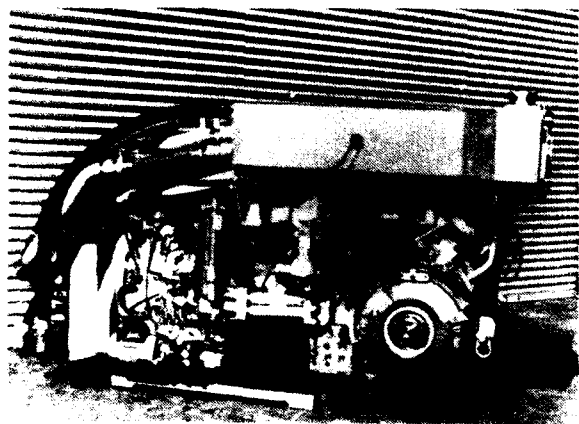


FIGURE 23 SCORE™ 580 IN FMC MTTB POWER PACK

- KEARNEY & TRECKER ORION 2300
- WELDON VERTICAL CNC GRINDER
- GRIND EQUIPMENT MACHINERY TROCHOID LAPPER
- CONE BLANCHARD SURFACE GRINDER

FIGURE 24 MACHINE SELECTION FOR ROTARY ENGINE HOUSINGS

between the six models providing the potential of significant savings in operational and support costs. Both two rotor and three rotor models, producing 750 and 1125 horsepower respectively will be delivered late in 1991 following 400 hour NATO and 1000 hour mission profile durability and reliability testing.

Initial, Low Volume, Production Machines. During 1989 selected machining systems for production of the rotary engine housings were installed and started-up at the Rotary Engine Division, Wood-Ridge, New Jersey. A pilot production run is in progress with the SCORE 70 model 2013R engines during early 1990. Also, SCORE 580 housings have been machined on this equipment. Initial capacity is for 6 engines/day. The machinery is capable of producing parts for Series 70, 170 and 580 engines. Capacity can be expanded to 30 engines/day by 1993 for the 70 Series engines. The machines selected are noted in Figure 24.

Figure 25 presents the Kearney & Trecker Orion 2300 4-axis machining center.

Figure 26 presents the custom built Weldon CNC grinder.

Figure 27 presents the Grind Equipment Machinery trochoid lapper.

Figure 28 presents the Cone Blanchard Surface Grinder (Model 22 AD 42).

Also, a production test cell with fully automated data acquisition equipment and quick disconnect features has been installed and is fully operational (Figure 29).

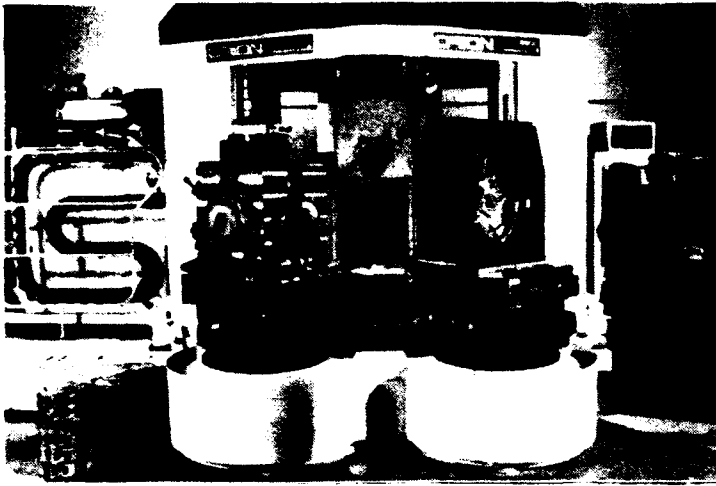


FIGURE 25 KEARNEY AND TRECKER ORION 2300

- 4-AXIS MACHINING CENTER
- TWO FIXTURES WITH THREE STATIONS, EACH MANUFACTURE ALL FOUR 70 SERIES POWER SECTION HOUSINGS
- TWENTY 70 SERIES HOUSINGS PER DAY CAPACITY
- EQUIPPED WITH 10,000 RPM SPINDLE



FIGURE 26 WELDON VERTICAL CNC GRINDER (CUSTOM BUILD)

- FINISH GRINDS ROTOR HOUSING TROCHOID SURFACE
- CAPABLE OF GRINDING 70 AND 580 SERIES ROTOR HOUSINGS
- PRODUCES SURFACE FINISH OF 10 Ra



FIGURE 27 GRIND EQUIPMENT MACHINERY TROCHOID LAPPER

- ONLY MACHINE OF ITS KIND (SERIAL #JDTI #1)
- CAPABLE OF LAPPING 70, 170 AND 580 SERIES TROCHOID
- PRODUCES SURFACE FINISH OF 2 Ra
- UTILIZES MOLY-FILM ABRASIVE



- FOR GRINDING FLAT SURFACES ON POWER SECTION HOUSINGS
- TWO HUNDRED 70 SERIES HOUSINGS PER DAY CAPACITY
- 42" DIAMETER GRINDING TABLE

FIGURE 28 CONE BLANCHARD SURFACE GRINDER (MODEL 22 AD42)

General Aviation Systems. The foregoing discussion has described the extensive research and development in progress at the Rotary Engine Division and early production considerations including low volume production tooling. While initial applications sought are in ground or marine vehicles, the General Aviation market is one wherein the SCORE™ technology can contribute significantly. The provision of jet fuel capability (at lower costs for the engine and lower operational costs than turbines) combined with the size, weight and altitude capabilities competitive with reciprocating engines would permit aircraft designers new freedom in low cost, high performance, reliable aircraft design.

General aviation system prospects wherein SCORE™ technology can be of interest in the 200-1600 HP range are noted in Figure 30.

Estimates by JD TI, Inc. for a family of SCORE™ engines of 1 through 6 rotors, at 200-250 HP (149-186 Kw)/rotor and potential engine sales are summarized in Figure 31.

Figure 32 presents a possible military rotocraft retrofit analysis for SCORE™ vs. turboshaft engines resulting in a substantial ten year life cycle O & S (operational and support) cost saving for a 500 unit fleet.

Figure 33 examines a military UAV application for rotary vs. turboprop engines. Here it is recognized that the specialized multi-stage turbomachinery for the basic SCORE™ engines results in an additional approximately 1200 lbs. of system weight. However, the SFC difference for the long range mission results in a significant overall mission weight saving.

Figure 34 examines a general aviation twin engine installation for SCORE™ engines vs. turbine engines. A substantial annual saving is projected for the SCORE™ installation.

Figure 35 considers a commercial retrofit possibility for engines in the 400-500 HP (298-373 Kw) class showing a savings for SCORE™ in the installation costs, operating cost and projected licensee's potential market.



FIGURE 29 PRODUCTION TEST CELL

- XXX Series Engines
 - 1, 2, 3, and 4 rotor versions
 - @ 200-250 hp/rotor (200-1000 hp)
 - 6 rotor version possible (1500 hp)
 - Parts, service, development commonality
- 5,000-10,000 engines per year
- @ 500 hp average and \$100 hp → \$50,000 average price → \$250 to \$500 million/year
- 20 year total → \$5-\$15 billion
- Development and facilitization cost under \$100 million

FIGURE 31 JETI ESTIMATES

EXAMPLE: Two SCORE™ 2013R Engines
@ 200 HP FLAT RATED TO 66,000 FT.

MISSION WEIGHT	ROTARY	TURBOPROP
Engine weight (lbs.)	600	600
Multi-Stage Turbomachinery System Weight (lbs)	1200	0.0
SFC @ 50% POWER (Lbs/hp-hr)	0.35	0.70
Fuel per hour @ 50% power (lbs)	70	140
Fuel Weight (120 hrs @ 75% power) (lbs)	8,400	16,800
Tankage @ 10% mission fuel weight (lbs)	840	1,680
Mission weight (lbs)	11,040	19,080

SAVINGS: 8,040 lbs

POSSIBLE TRADE-OFFS: power, range, speed, loiter time, system weight, etc

FIGURE 33 MILITARY UAV - USN

- | | |
|---------------------------------------------------------------------------------------------------------------------------------------------------------------------------------------------------------------------------------------------------------------------------------------------------------------------------------------------------------------------------------------------------------------------|-----------------------------------------------------------------------------------------------------------------------------------------------------------------------------------------------------------------------------------------------------------------------------------------------------------------------------------------------|
| MILITARY <ul style="list-style-type: none"> - Helicopters - Retrofit (O&S advantage) - UAV - Coast Guard - Energy-efficient APUs GENERAL AVIATION <ul style="list-style-type: none"> - Sport Aircraft - Piston Twins - Turboprop Twins - Turboprop Singles - Retrofit - Helicopter | OVERSEAS <ul style="list-style-type: none"> - Indigenous Aircraft and Rotorcraft - Export GA & Military Aircraft AIR CARRIER <ul style="list-style-type: none"> - Commuter - APU OTHER <ul style="list-style-type: none"> - A rotary driven prop-fan? |
|---------------------------------------------------------------------------------------------------------------------------------------------------------------------------------------------------------------------------------------------------------------------------------------------------------------------------------------------------------------------------------------------------------------------|-----------------------------------------------------------------------------------------------------------------------------------------------------------------------------------------------------------------------------------------------------------------------------------------------------------------------------------------------|

FIGURE 30 AVIATION PROSPECTS 200-1600 HP

EXAMPLE: One SCORE™ 6060 Engine @ 1500 hp or
Two SCORE™ 3030 Engine @ 750 hp each or
Three SCORE™ 2020 Engine @ 500 hp each

MISSION WEIGHT	ROTARY	TURBOSHAFT
Engine weight (lbs)	1100	550
Average SFC (lbs/hp-hr)	0.35	0.60
Avg. fuel per hour @ 80% power	420	720
2-1/2 hours fuel (lbs)	1030	1800
Mission weight (lbs)	2130	2320
Payload increase (lbs)	190	
OPERATING COST	ROTARY	TURBOSHAFT
Original engine cost	\$150K	\$400K
Annual cost of capital @ 15%	23K	60K
Annual spares, maintenance & overhaul @ 30%	45K	120K
Annual fuel @ 500 hrs usage and 20¢/lb	42K	72K
Total annual cost	110K	250K
Annual savings for rotary	140K	
Users payback period for Retrofit	1.1 yrs	-
Ten year life cycle O&S cost savings for 500 unit fleet	700 mil	-

FIGURE 32 MILITARY ROTORCRAFT HUEY RETROFIT
1500 HP TOTAL POWER REQUIRED

EXAMPLE: Two 400 hp SCORE™ 2013R
engines flat rated to 20,000 ft.

MISSION WEIGHT	ROTARY	TURBINE
Engine - each (lbs)	300	200
Average SFC @ 75% power (lbs/hp-hr)	0.35	0.60
Fuel for 4 hour mission (lbs)	400	720
Reserve fuel for 1 hour (lbs)	100	180
Total mission weight (two engines) (lbs)	1600	2200
Payload reduction for equal range (lbs)	-	600
OPERATING COST	ROTARY	TURBINE
Engine original cost (ea.)	\$ 40K	\$ 80K
Annual capital cost @ 20%	8K	16K
Annual spares, maintenance & overhaul @ 25%	10K	20K
Annual fuel cost @ 25¢/lb & 500 hrs	12-1/2K	22-1/2K
Total annual cost (two engines)	61K	117K
Annual savings with SCORE	56K	-
Engine-related cost per passenger mile (assumes 125,000 miles per year and 6 passengers for rotary, 4 for turbine)	8¢	23¢

FIGURE 34 GENERAL AVIATION TWIN

EXAMPLE: Cessna CE 425 with PT-6A-112
turbines replaced by 450 hp rotaries

INSTALLATION		
Overhaul cost for 2 turbines		\$ 180K
New engine cost for 2 rotaries		120K
Cost to convert CE 425		75K
Resale of used turbines		50K
Money saved by converting		35K
LICENSEE'S POTENTIAL MARKET		
Fleet size		5,000
Annual overhauls (number of engines)		1,000
Penetration @ 50%		500
Annual licensee sales (1,000 engines @ 50K)		\$ 50 mil
Annual installer sales		\$100 mil
USER OPERATING ADVANTAGE		
Cruise power (hp)	+32	(8%)
Cruise speed (knots)	+6	(3%)
Lbs/hour fuel	-124	(-25%)
Range (miles)	+360	(36%)
Hourly cost		(-27%)
Payload increase (1000 miles) (lbs)	525	50%

FIGURE 35 COMMERCIAL RETROFIT
400 - 500 HP CLASS

Marketing Approaches. Deere & Co. is advancing the technology of the stratified charge rotary engine to new levels through both contractual and internally funded research and development efforts. The potential applications vary widely including ground, marine, and airborne systems both commercial and military. Deere & Co.'s experience and primary thrust is in the ground and marine areas. We believe the application of this technology to aircraft systems may be best accomplished by organizations presently active in that field, with established product lines, product liability protection and existing marketing and service networks.

The SCORE™ Series, Model 2034R engine resulted from a joint program established with Avco-Lycoming, Williamsport Division. Avco's involvement in that program was halted in late 1987 after they experienced a large increase in their overall product liability insurance costs. Subsequently, we have reviewed rotary engine technology with a variety of organizations in the aircraft engine/airframer field, with their interests including both propulsion engines and APU's. These discussions are proprietary and confidential in nature however, a variety of licensing approaches are being examined and are actively being pursued. Discussions have also been held with NASA on this subject to define our position and to explore solutions. We cannot predict the final outcome, but we are confident that a means to bring this exciting technology to the General Aviation community will be defined in the near future.

CONCLUSIONS

1. SCORE™ rotary engine basic technology is proven.
2. SCORE™ technology is advancing rapidly as a result of Deere, U. S. Government, customer and licensee investments.
3. The SCORE™ licensee will have an unprecedented opportunity in the small aviation engine market for APU's, propulsion for new airplane designs, retrofit of existing airplanes, helicopters and unmanned aviation vehicles.

Acknowledgments

The authors would like to express their appreciation to Dr. Edward Willis and Mr. Jack McFadden at NASA Lewis Research Center, Cleveland, Ohio; to Dr. Ken Green and Mr. Joe Franz at Naval Air Development Center and to Dr. Buryl Mc Fadden, USAF Wright Paterson Propulsion Lab (for their continued support in the advanced technology enablement activities toward aviation systems) and to Mr. Kent Taylor and USN/USNC personnel (for their continued support toward SCORE™ for amphibious marine propulsion systems).

REFERENCES

1. P. Badgley, M. Berkowitz, et all "Advanced Stratified Charge Rotary Aircraft Engine Design Study", Curtiss Wright Corp., Wood-Ridge, N.J, CW-WR-81.021, Jan. 1982. (NASA CR-15-65398).
2. G. L. Huggins and D. R. Ellis, "Advanced General Aviation Comparative Engine/Airframe Integration Study", Cessna Aircraft Co., Wichita, KA, Cessna Aircraft Co., Wichita, KA, Cessna-AD 217, 1981. (NASA CR-165564).
3. Beech Aircraft Corporation Report No. 165565, "Advanced General Aviation Comparative Engine/Airframe Integration Study", prepared under Contract NASA-22220, March 1982.
4. C. Jones and R. E. Mount: "Design of a High Performance Rotary Stratified Charge Aircraft Engine", AIAA Paper 84-1395. June 1984
5. R. E. Mount and W. L. Greiner, "High Performance, Stratified Charge Rotary Engines for General Aviation" AIAA-86-1553, AIAA/ASME/SAE/ASEE 22nd Joint Propulsion Conference, June 16 - 18, 1986.
6. R. E. Mount, A. M. Parente and W. F. Hady, "Stratified Charge Rotary Engine for General Aviation", 86-GT-181, The American Society of Mechanical Engineers, New York, June 8-12, 1986.
7. Robert E. Mount and Gaston Guarda, "Stratified Charge Rotary Engines for Aircraft", 88-GT-311, The American Society of Mechanical Engineers, Amsterdam, The Netherlands, June 6-9, 1988.
8. R. E. Mount, G. A. LaBouff, "Advanced Stratified Charge Rotary Engine Design," 890324, Society of Automotive Engineers, International Congress and Exposition, Detroit, Michigan, February 27 - March 23, 1989.

EVALUATION OF ADD-ON DRAG REDUCTION DEVICES FOR
LIGHT AIRCRAFT

by

Hubert C. Smith
Assistant Professor, Aerospace Engineering
The Pennsylvania State University
University Park, PA

For presentation to the AIAA/FAA Joint Symposium on General
Aviation Systems at the Port O-Call Inn, Ocean City, NJ
on April 12, 1990

EVALUATION OF ADD-ON DRAG REDUCTION DEVICES FOR LIGHT AIRCRAFT

Hubert C. Smith
Assistant Professor, Aerospace Engineering
The Pennsylvania State University
University Park, PA

ABSTRACT

Commercially produced drag reduction devices were applied to a Piper Cherokee Arrow II and flight tested to determine their effect on performance. This was done to verify the producer's claims for improved performance, which were largely based on customer reports and some crude, uncontrolled tests. Specifically, the devices consisted of aileron gap seals, flap gap seals, flap hinge fairings, inboard wheel well fairings, and fuel tank attach screw fairings.

Speed-power tests and stall speed tests were conducted with the aircraft after installation of the drag reduction modifications and compared with previously obtained data for the original configuration. Analytical prediction of change in drag coefficient from installation of the various devices was also made.

Results showed that, with all devices installed, the parasite drag coefficient of the aircraft was reduced about 7%. This reduction resulted in a 2.5% increase in maximum speed, a 4.3% increase in maximum rate of climb, and a 3.7% increase in ceiling. However, the gap seals seemed to slightly increase stall speed, which increased landing distance by about 4%.

The following pages are reproductions of the slides used in this presentation. This was originally published as AIAA Paper No. 89-2050.

MODIFICATIONS

1. FUEL TANK ATTACH SCREW FAIRINGS
2. WHEEL WELL FAIRINGS
3. FLAP GAP SEALS
4. AILERON GAP SEALS
5. FLAP HINGE FAIRINGS

HOERNER'S METHOD FOR THEORETICAL ΔC_D

$$\text{COMPONENT: } C_{D+} S_+ = \frac{D}{g} (=f)$$

$$\text{AIRPLANE: } \Delta C_{Dp} = \left(\frac{D}{g}\right) \frac{1}{S}$$

THEORETICAL RESULTS

<u>DEVICE</u>	<u>ΔC_D</u>
FUEL TANK SCREW FAIRINGS	0.0000472
WHEEL WELL FAIRINGS	0.0008235
FLAP GAP SEALS	0.0000871
AILERON GAP SEALS	0.0001565
FLAP HINGE FAIRINGS	<u>0.0000551</u>
TOTAL	0.0011694

FLIGHT TEST DRAG DETERMINATION

$$V_{ew} = V \sqrt{\sigma} \left(\frac{w_s}{w} \right)^{1/2}$$

$$THP_{ew} = THP \sqrt{\sigma} \left(\frac{w_s}{w} \right)^{3/2}$$

$$THP_{ew} V_{ow} = K_1 f V_{ew}^4 + K_2 \frac{1}{e} \left(\frac{w_s}{b} \right)^2$$

SLOPE $\rightarrow f$

INTERCEPT $\rightarrow e$

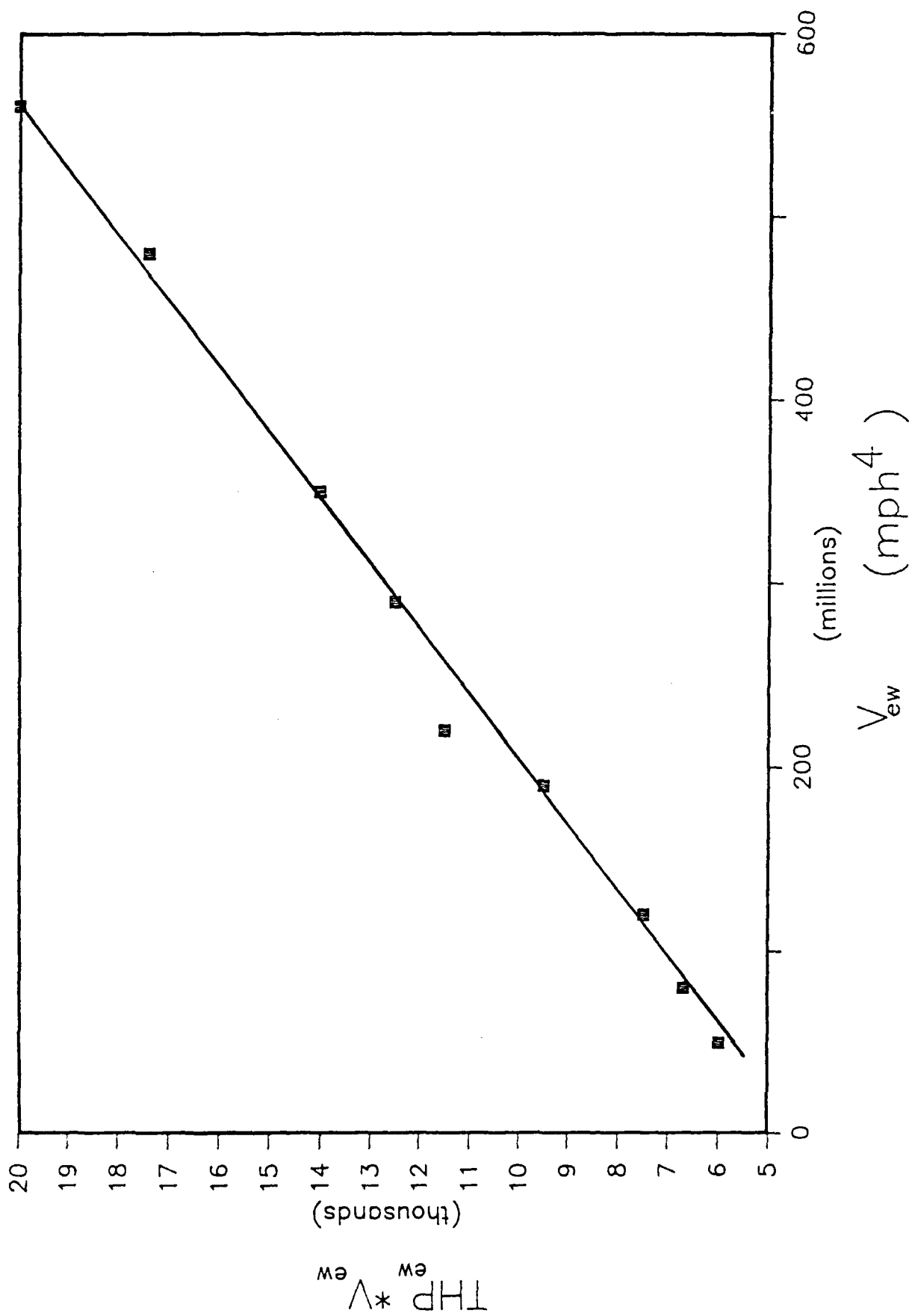


Figure 5 Linearized, standard weight, speed—power relationship for modified aircraft

RESULTS

		<u>C_D</u>	<u>E</u>
ORIGINAL	EXP.	0.02600	0.53
MODIFIED	EXP.	0.02420	0.53
	THEO.	0.02483	

PERFORMANCE PREDICTION EQUATIONS

$$RANGE = 375 \frac{hp}{SFC} \frac{C_L}{C_D} \ln\left(\frac{W_1}{W_2}\right)$$

$$LDG. DIST. = \underbrace{\frac{1}{2} \frac{(1.15 V_S)^2}{a}}_{GROUND} + \underbrace{\frac{L}{D} \left[\frac{0.3675 V_S^2}{2g} + 50 \right]}_{AIR}$$

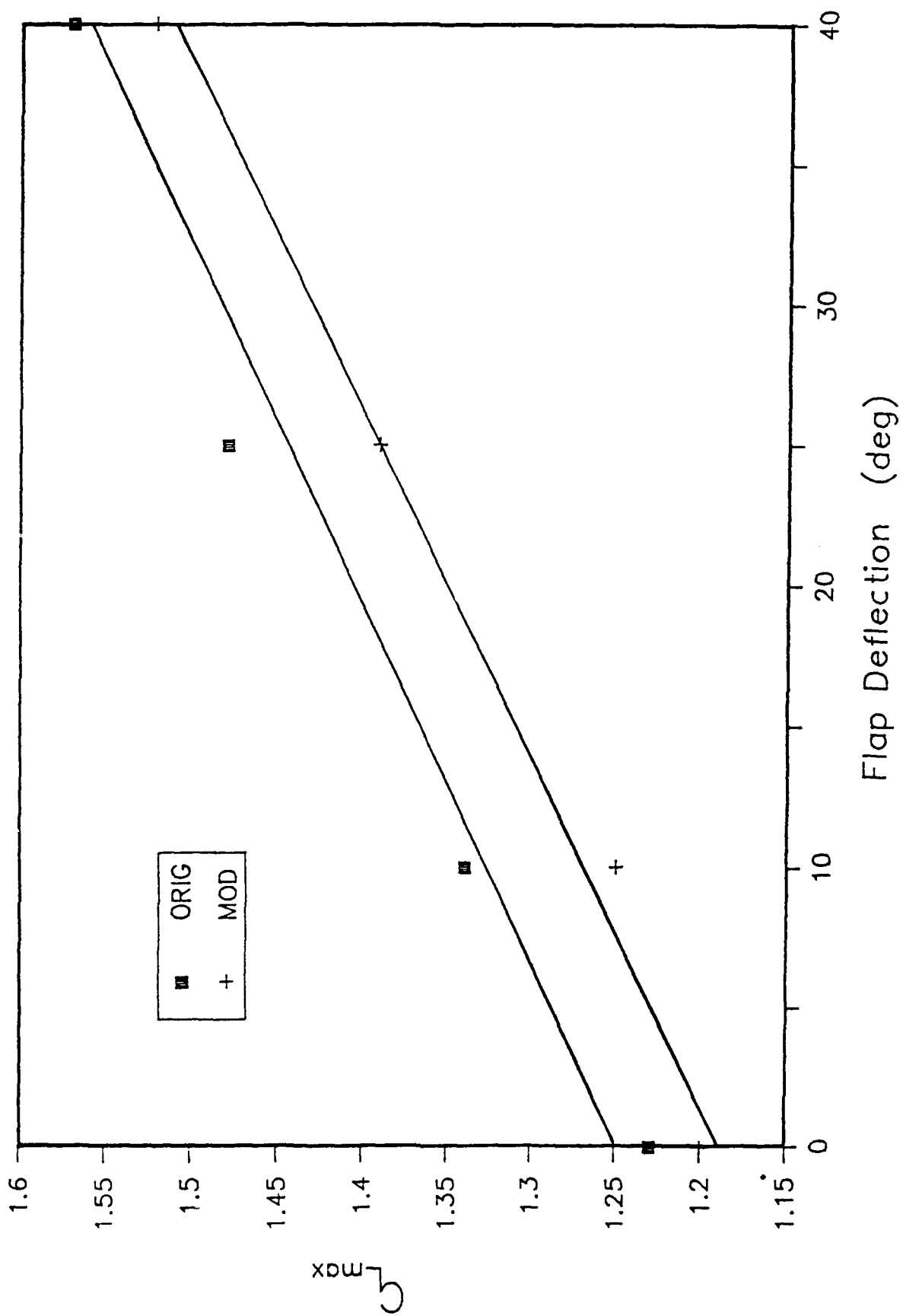


Figure 6 Maximum lift coefficient vs. flap deflection for original and modified aircraft

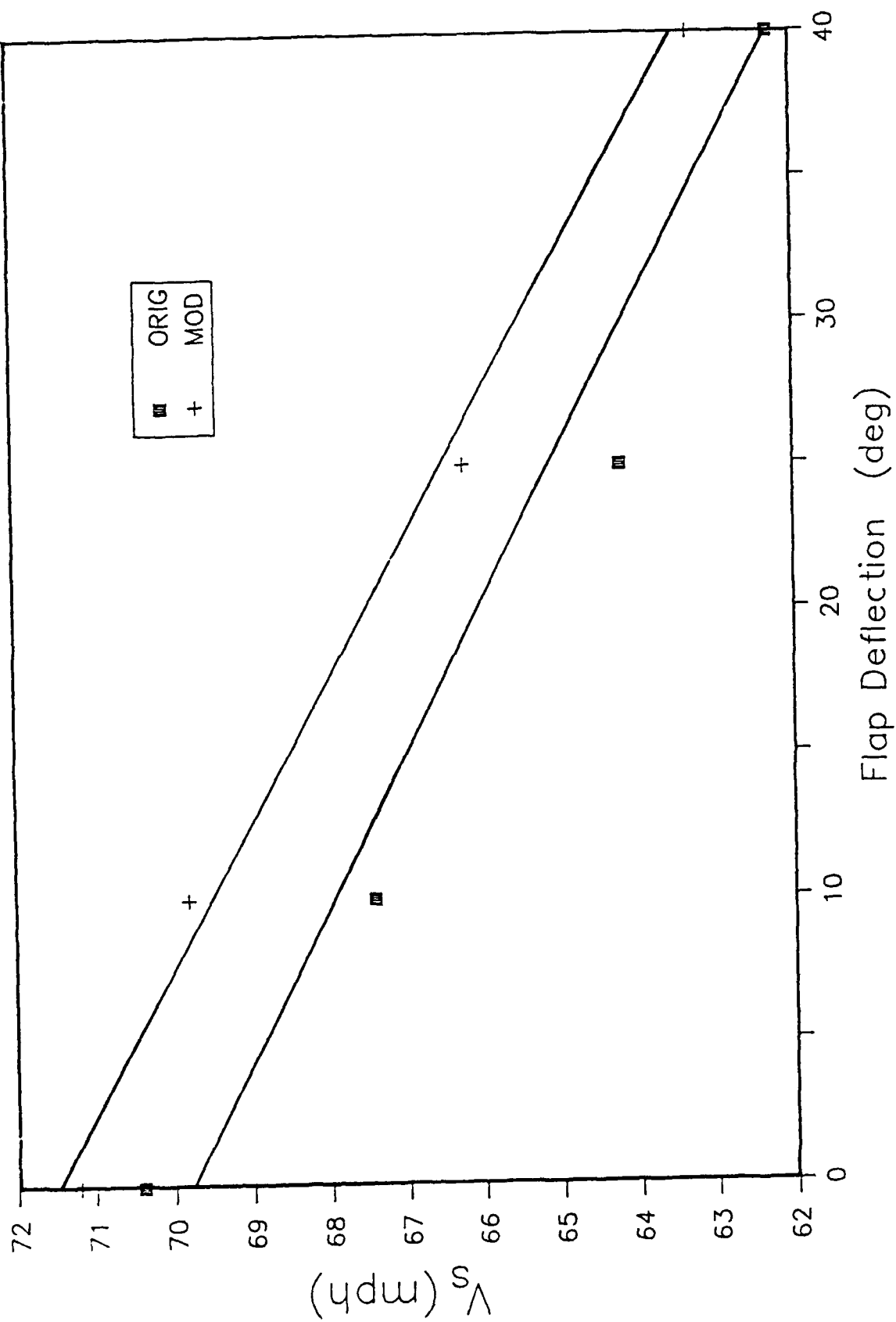


Figure 7 Stall velocity vs. flap deflection for original and modified aircraft

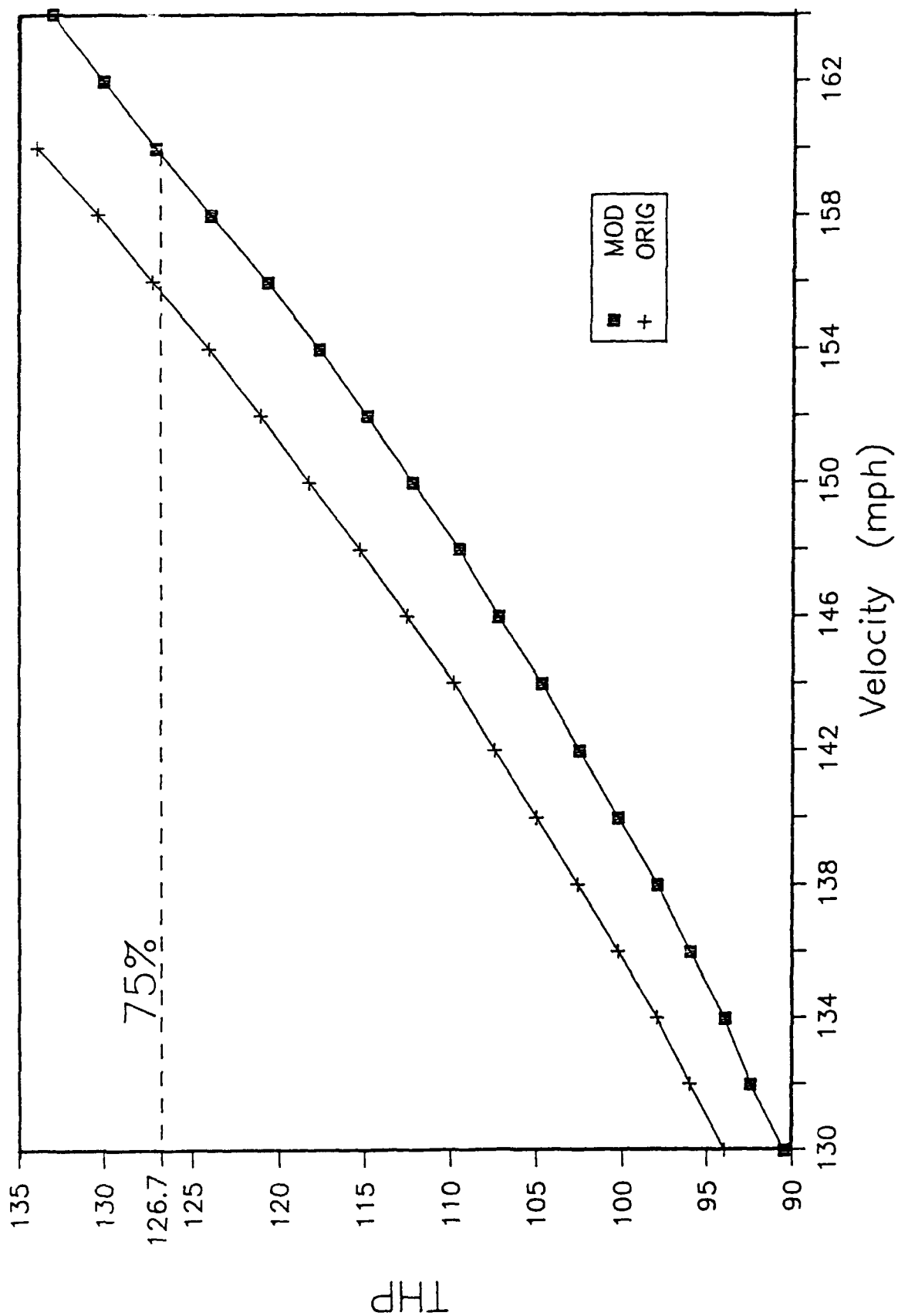


Figure 8 Power curves at 6500 feet for original and modified aircraft

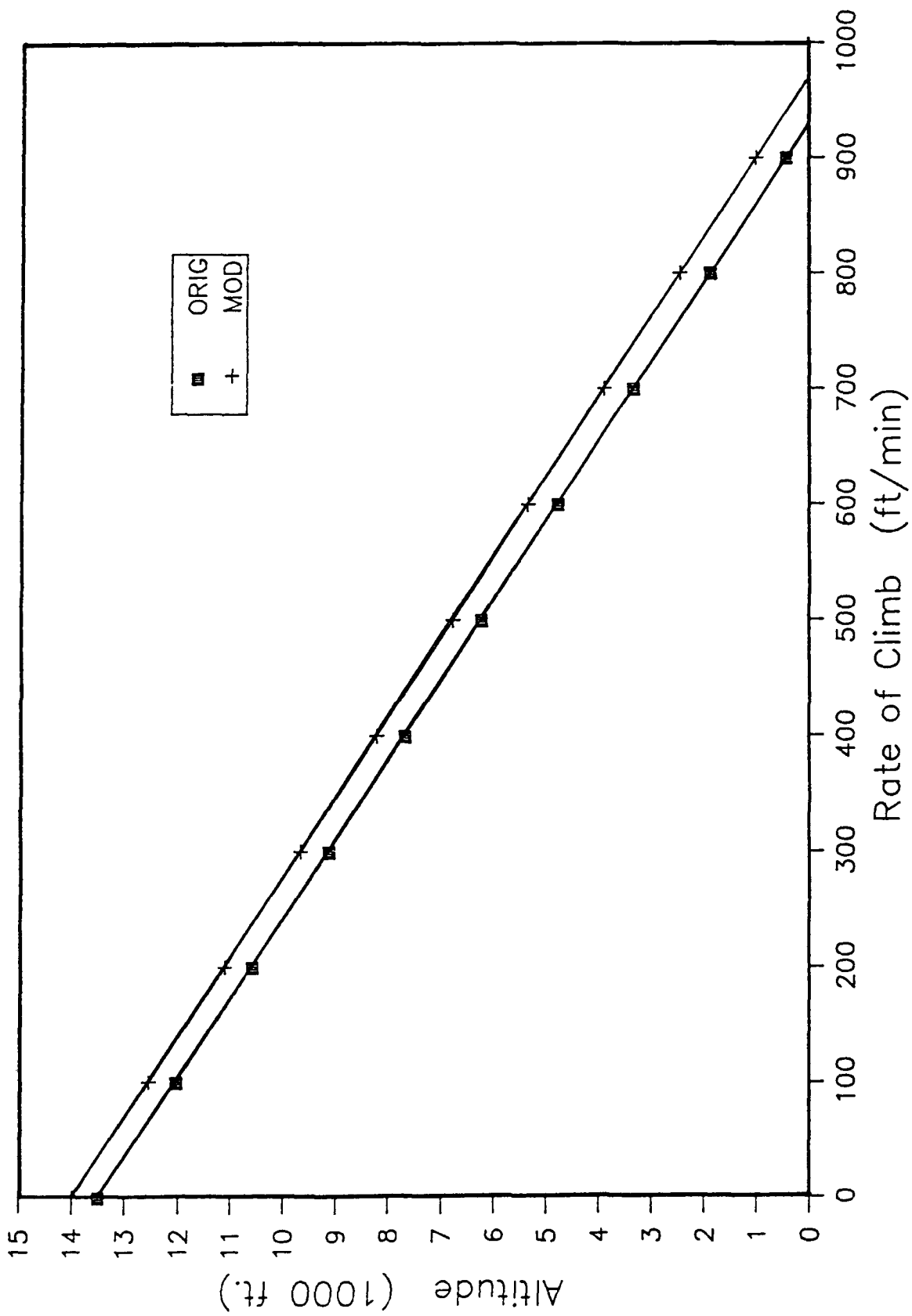


Figure 9 Altitude vs. rate of climb for original and modified aircraft

Table 1 Performance Changes of Modifications

<u>Item</u>	<u>Orig.</u>	<u>Mod.</u>	<u>% Change</u>
Cruising speed	156 mph	160 mph	2.5
Rate of climb (max)	930 ft/min	970 ft/min	4.3
Absolute ceiling	13,500 ft	14,000 ft	3.7
Range at max cruise	685 mi	723 mi	5.5
Landing ground roll	332 ft	346 ft	4.2
Landing over 50-ft obstacle	1032 ft	1032 ft	3.8

CONCLUSIONS

- * MODS MAKE SLIGHT BUT SIGNIFICANT REDUCTION IN C_D
- * CORRESPONDING PERFORMANCE IMPROVEMENT INDICATED
- * SLIGHT BUT INSIGNIFICANT STALL SPEED INCREASE
- * FURTHER STUDY OF LAMINAR FLOW IMPROVEMENT PHASE DESIREABLE

**AN EVALUATION OF AUTOMATIC CONTROL SYSTEM CONCEPTS
FOR GENERAL AVIATION AIRPLANES**

by

**E. C. Stewart
NASA Langley Research Center**

**For presentation to the AIAA/FAA Joint Symposium on General
Aviation Systems at the Port O-Call Inn, Ocean City, NJ
on April 12, 1990**

**AN EVALUATION OF AUTOMATIC CONTROL SYSTEM CONCEPTS
FOR GENERAL AVIATION AIRPLANES**

**E. C. Stewart
NASA Langley Research Center**

ABSTRACT

A piloted simulation study of automatic longitudinal control systems for general aviation airplanes has been conducted. These automatic control systems were designed to make the simulated airplane easy to fly for a beginning or infrequent pilot. Different control systems are presented and their characteristics are documented. In a conventional airplane control system each cockpit controller commands combinations of both the airspeed and the vertical speed. The best system in the present study decoupled the airspeed and vertical speed responses to cockpit controller inputs. That is, the cockpit throttle lever commanded only airspeed responses, and the longitudinal wheel position commanded only significantly reduced the pilot workload throughout an entire mission of the airplane from takeoff to landing. An important feature of the automatic system was that neither changing flap position nor maneuvering in steeply banked turns affected either the airspeed or the vertical speed. All the pilots who flew the control system simulation were favorably impressed with the very low workload and the excellent handling qualities of the simulated airplane.

The following pages are reproductions of the slides used in this presentation.

SIMULATION STUDY OF EASY-TO-FLY GENERAL AVIATION AIRPLANES

by

Eric C. Stewart

Flight Applications Division

Langley Research Center

1990 AIAA/FAA

Joint Symposium on General Aviation Systems

April 11-12, 1990

Ocean City, N. J.



OUTLINE

- Background
- Control description
- Display description
- Evaluation procedure
- Results (Video)
- Conclusions
- Follow-on activities

PURPOSE

Increase utility and productivity of general aviation airplanes by

- **Making them easier to fly**
- **-Reduce initial training requirements**
- **-Reducing proficiency requirements**
- **Making them safer to fly**
- **-Reducing pilot blunders**
- **-Eliminating stalls**



RESEARCH OBJECTIVES

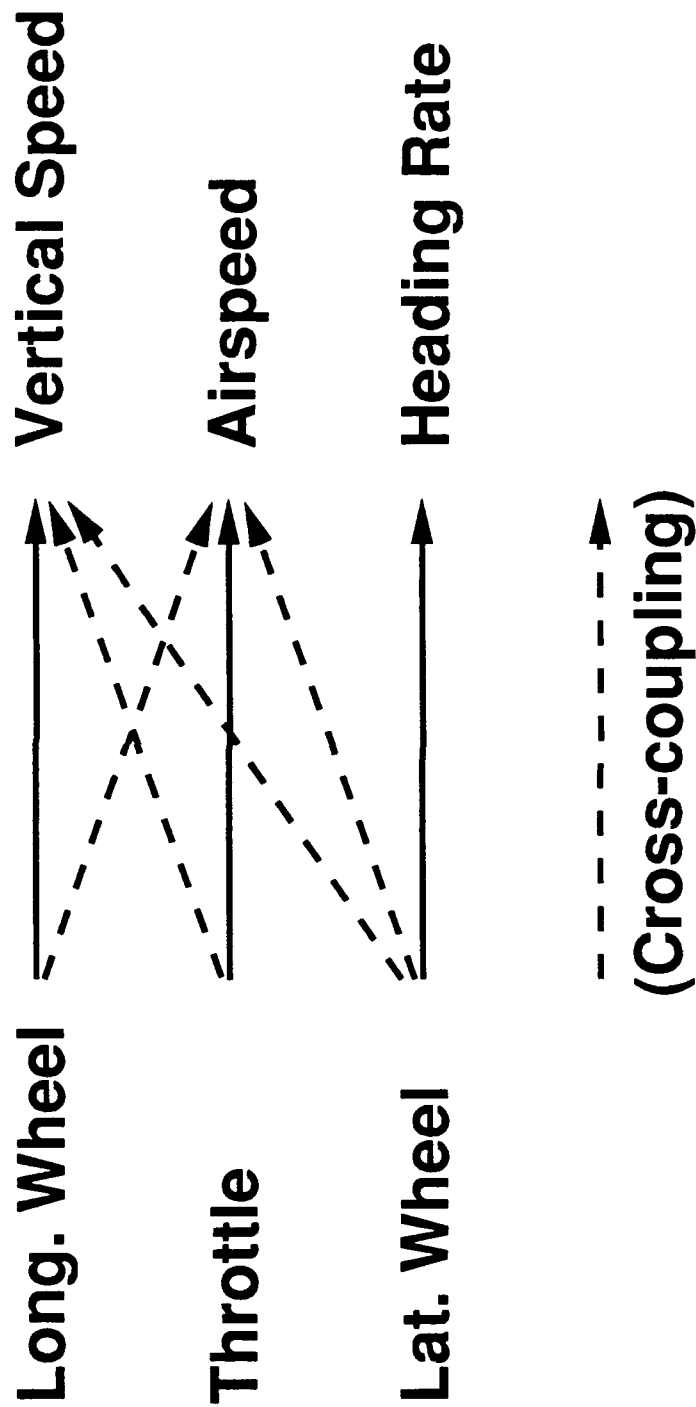
- Simplify control--more "car-like"
- Improve display--more intuitive

STUDY METHOD

- Develop control system
- Develop display
- Evaluate combined system

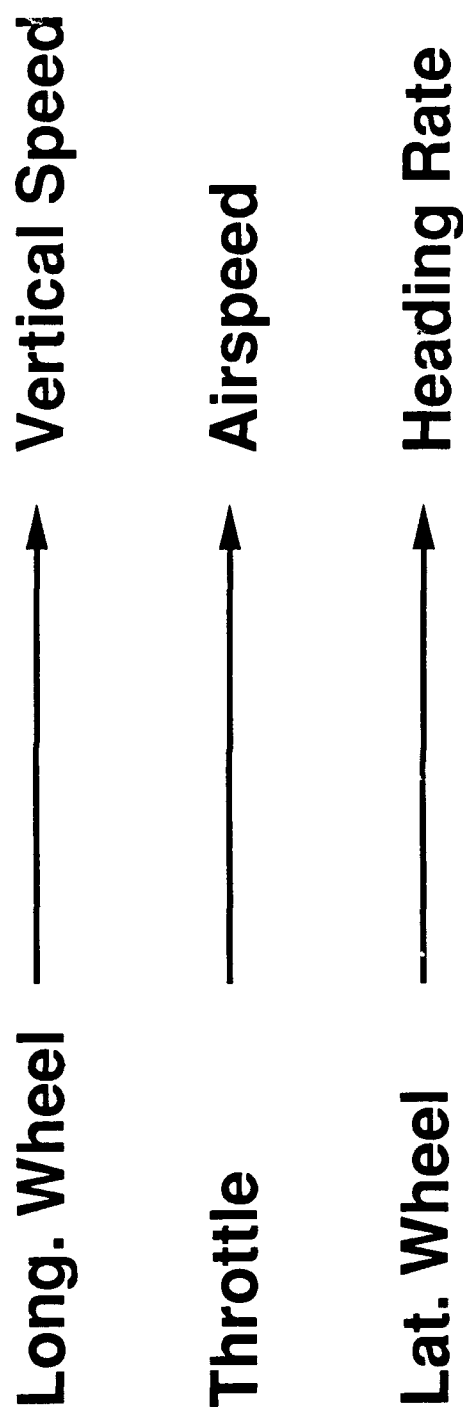
CONVENTIONAL CONTROL

(Coupled)



ADVANCED CONTROL

(Decoupled)



NASA

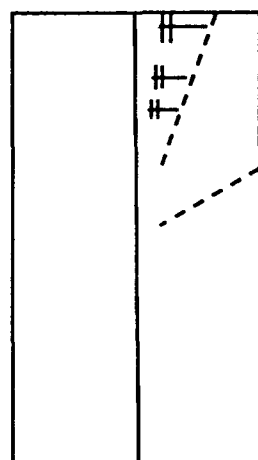
PICTURE FROM A CAR



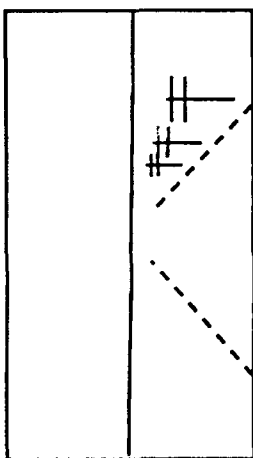
PICTURE FROM AN AIRPLANE



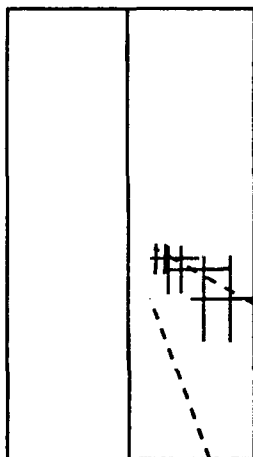
HIGHWAY IN THE SKY(HITS) POSITION GUIDANCE



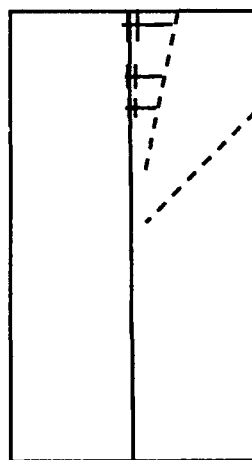
High, Left



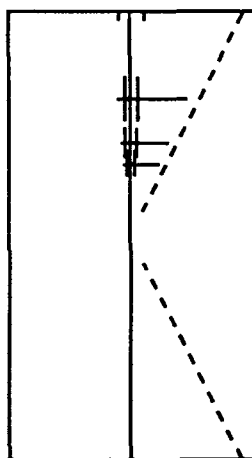
High



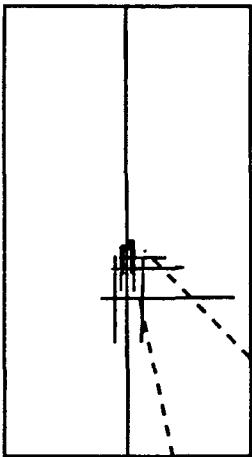
High, Right



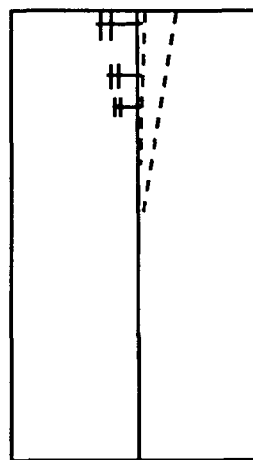
Left



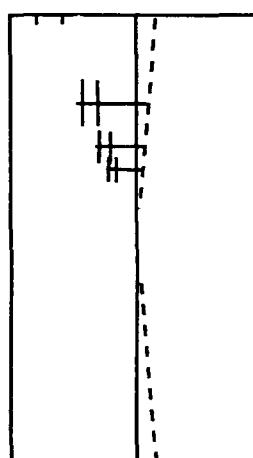
On Path



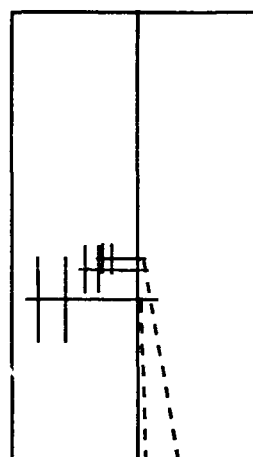
Right



Low, Left

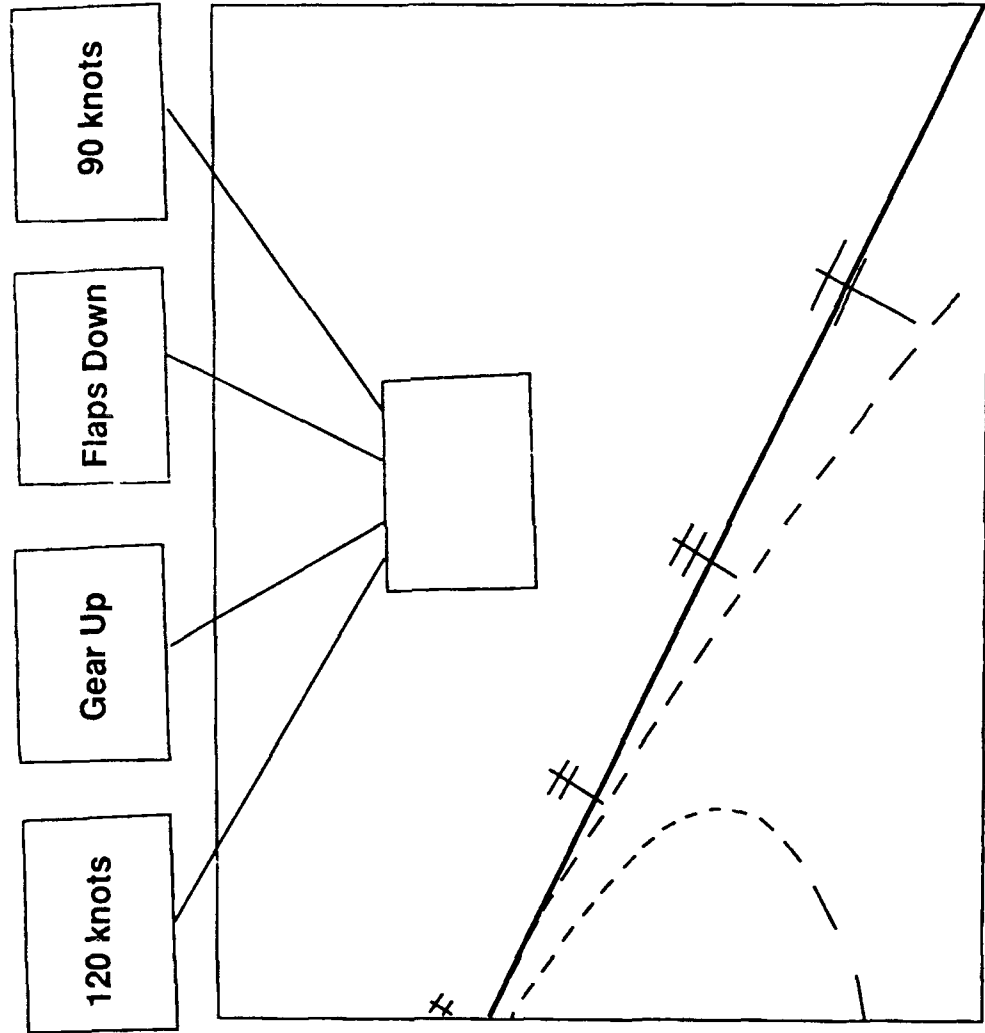


Low



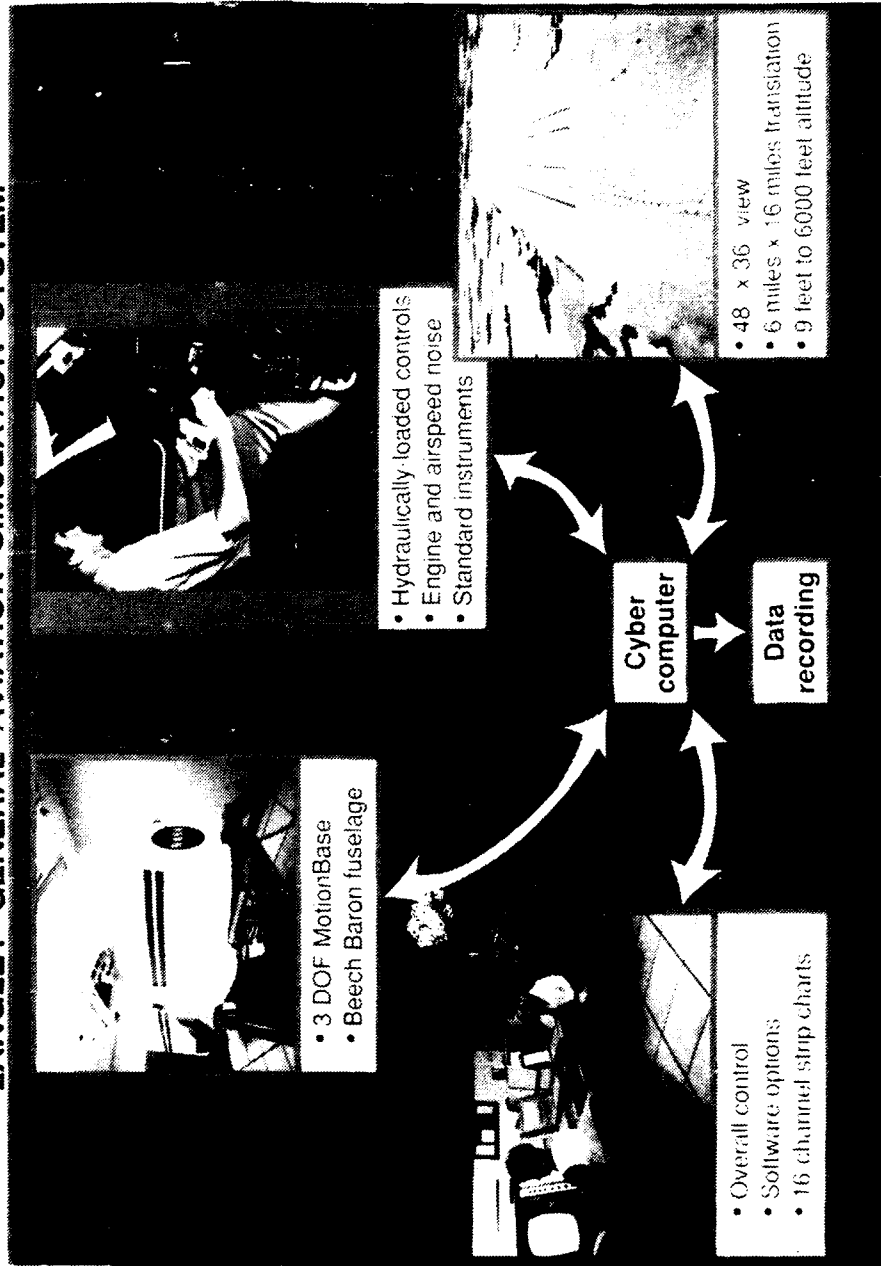
Low, Right

HIGHWAY IN THE SKY (HITS) FORMAT

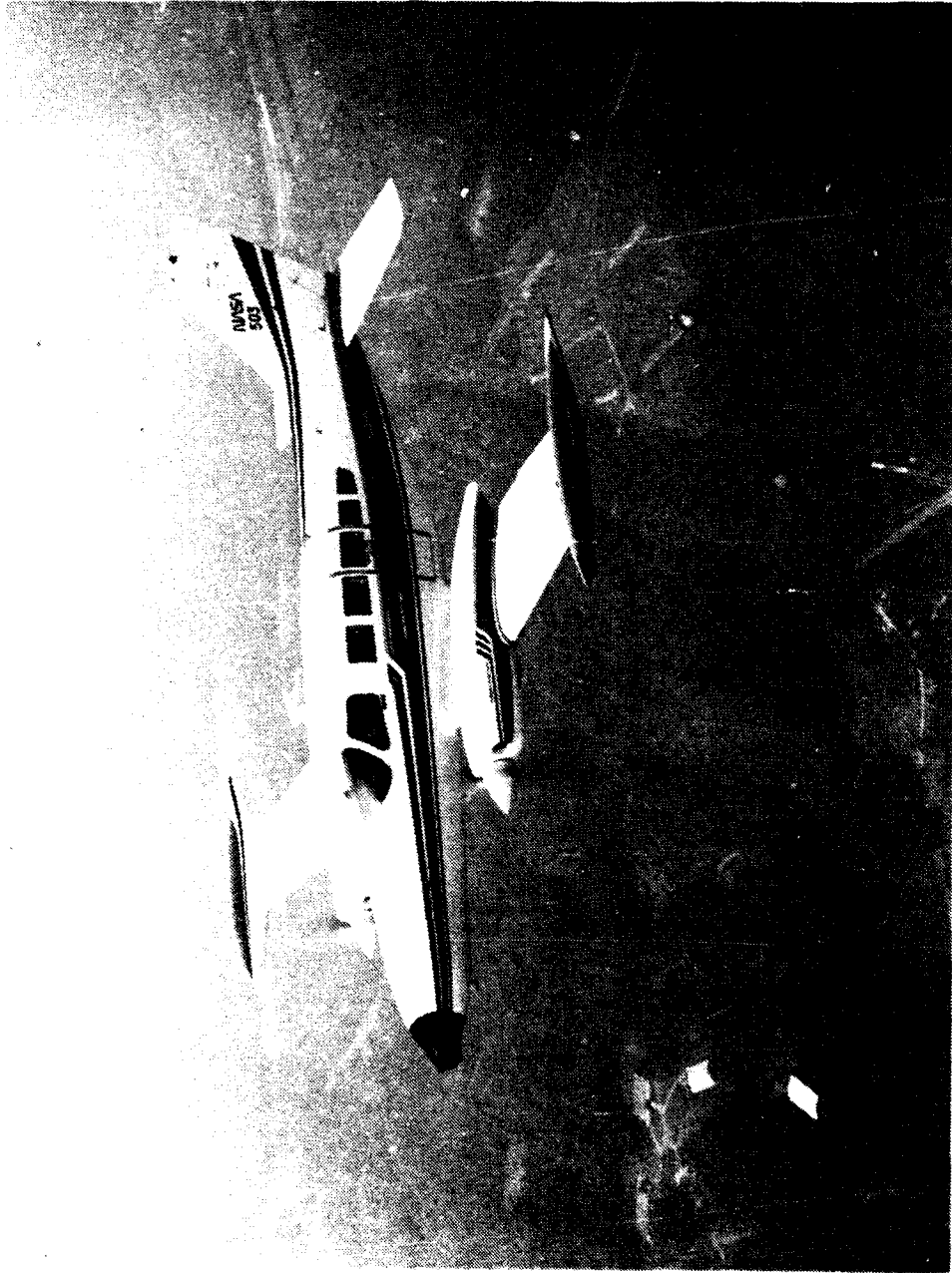


SIMULATOR SYSTEM

LANGLEY GENERAL AVIATION SIMULATION SYSTEM



PICTURE OF C-402B

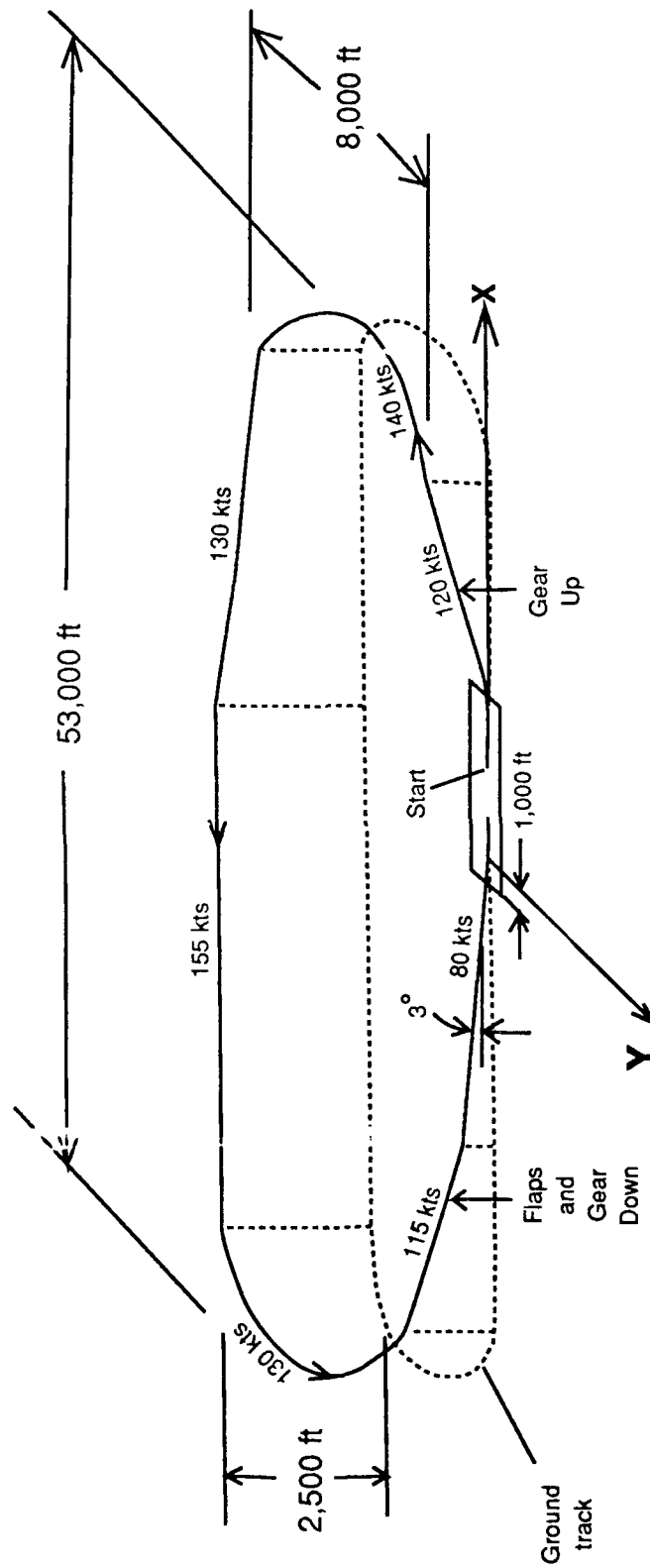


EVALUATION PROCEDURE

- **Non-pilots/pilots as test subjects**
- **30 minute briefing**
- **No practice runs**
- **1 st run: Display & Decoupled Control**
- **2 nd run: Display & Conventional Control**



MANEUVER



Note: Not to Scale

(Cloud ceiling = 200 feet)



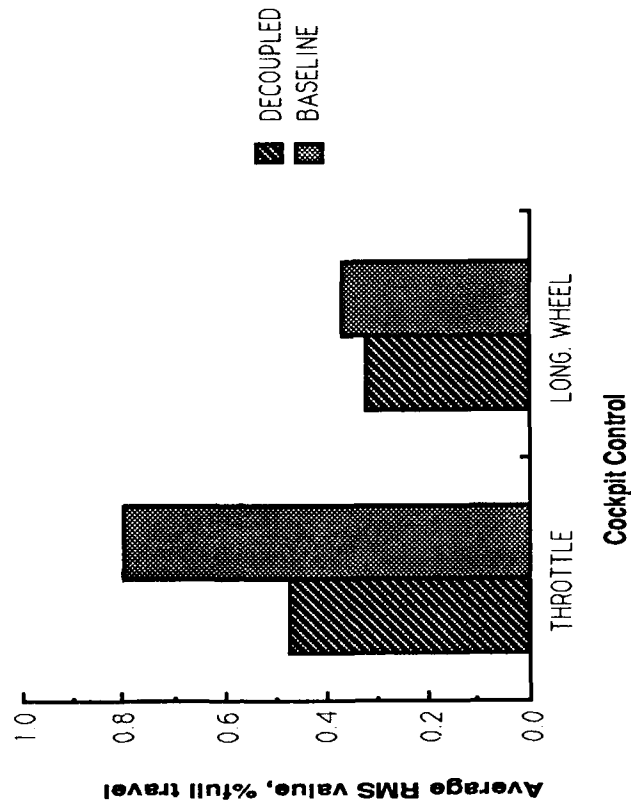
VIDEO

- Research recording
- Recorder over the pilot's shoulder
 - Pilot actions
 - Instruments
- Superimposed visual scene in upper right corner

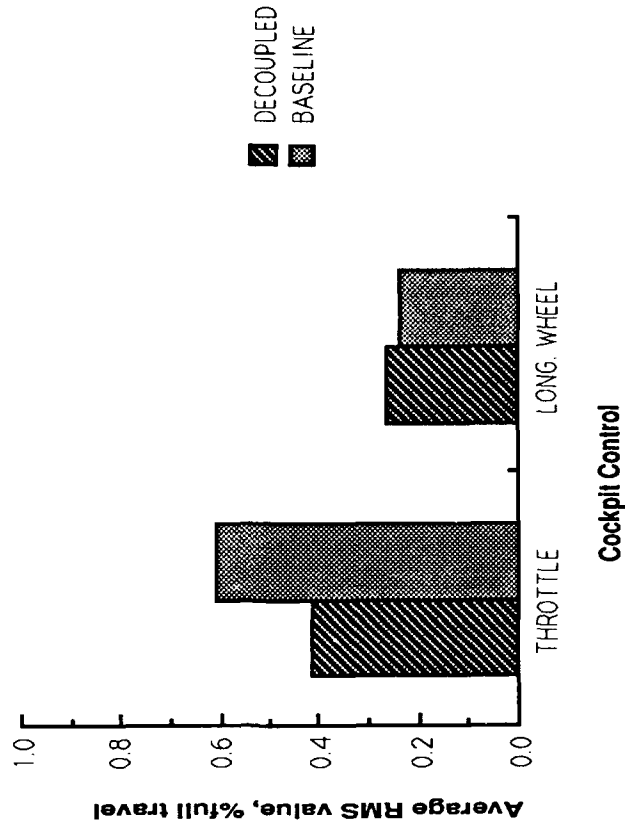
CONTROL ACTIVITY

(With Pictorial HITS Display)

Non-Pilots



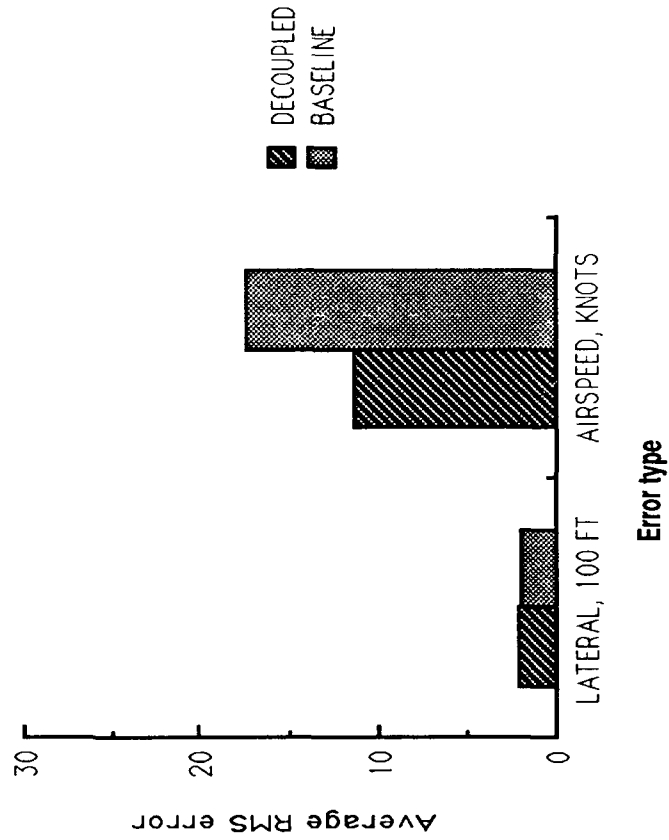
Pilots



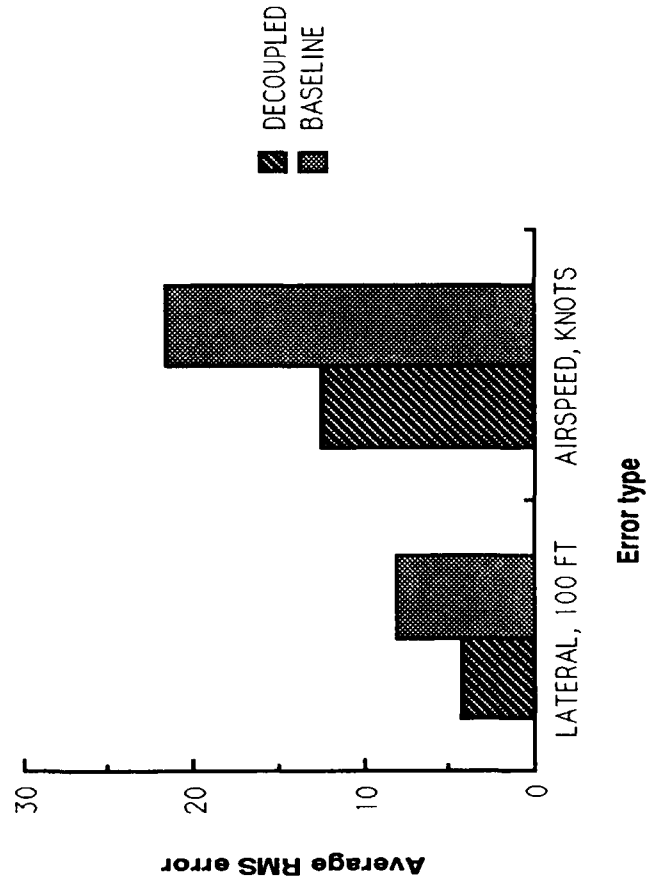
IN-FLIGHT PERFORMANCE

(With Pictorial HITS Display)

Pilots



Non-Pilots



RESEARCH RESULTS

- One-half of novices completed maneuver on first attempt
- Vertical degree-of-freedom is most troublesome
- Pictorial visual cues are unfamiliar

Horizon line

Telephone poles

-Longitudinal wheel force trim

-Landing maneuver

Narrow field of view on simulator



CONCLUSION

- Decoupled controls and pictorial display necessary for novice

FOLLOW-ON ACTIVITIES

- **Command arrows
 - **Rotation**
 - **Tracking**
 - **Flare****
- **Automatic pitch control force trim**
- **Additional pictorial altitude cues**
- **Flight Evaluation**

PERFORMANCE INSTRUMENTATION FOR MULTIENGINE SAFETY

by

Arthur W. Hoadley, P. E.
Aircraft and Automotive Engineering
Western Michigan University
Kalamazoo, MI 49008

For presentation to the AIAA/FAA Joint Symposium on General
Aviation Systems at the Port O-Call Inn, Ocean City, NJ
on April 12, 1990

PERFORMANCE INSTRUMENTATION FOR MULTIENGINE SAFETY

Arthur W. Hoadley, P.E.
Associate Professor
Aircraft and Automotive Engineering
Western Michigan University
Kalamazoo, MI 49008

ABSTRACT

Many accidents in multiengine aircraft are caused by the pilot's inability to retain control and/or obtain maximum performance when an engine fails. In order to maintain control of the aircraft, the pilot must not allow the aircraft to stall with the asymmetric thrust caused by a failed engine. The strong yawing moment that results, coupled with the stall, will most likely result in a spin. Several training accidents have been caused by demonstrating V_{mc} (minimum controllable airspeed) at a sufficiently high altitude, where the lower engine thrust causes the V_{mc} to be below the stall speed of the aircraft. When the aircraft stalls before V_{mc} is reached, an unrecoverable spin can occur. Instrumentation designed to give the pilot a continuous display of the aircraft's stall margin (the percent of lift coefficient available but not being used) allows the pilot to know where the aircraft is relative to stall, regardless of its load factor, weight, or configuration. The same technology can be used to detect the sideslip of an aircraft with asymmetric thrust. An aircraft's best single engine performance is obtained when the sideslip is zero and the stall margin for best climb is flown. During an engine out emergency, the pilot would control the stall margin with pitch changes and the sideslip by adjusting the bank angle, while using the rudder to maintain directional control. This paper covers the theory and hardware necessary to provide both stall margin and sideslip indications.

NOMENCLATURE

AR	= Aircraft Aspect Ratio.
AR _F	= Fuselage Side Aspect Ratio.
β	= Aircraft sideslip angle (assumed not to be affected significantly by the aircraft).
C _{Do}	= Aircraft zero lift drag coefficient.
ΔC_D	= Change in aircraft drag coefficient due to sideslip.
CL	= Aircraft Lift Coefficient.
CL _{MAX}	= Aircraft Maximum Lift Coefficient.
CL _{vβ}	= Slope of the CL _v vs β curve.
CL _{vδ}	= Slope of the CL _v vs δ curve.
CL _v	= Lift Coefficient of the vertical stabilizer.
C _{SF}	= Fuselage Side Force coefficient.
C _{SFβ}	= Slope of C _{SF} vs β curve.
D ₁	= Aircraft drag with one engine inoperative.
D ₂	= Aircraft drag with two engines running.
ΔD	= Change in aircraft drag due to sideslip.
δ	= Rudder deflection angle.
δ_M	= Maximum rudder deflection angle.
ϵ	= Aircraft Oswald's efficiency factor.
ϵ_F	= Fuselage Oswald's efficiency factor.
F	= Aerodynamic lift force of the vertical stabilizer.
F _H	= Horizontal aerodynamic force component from the vertical stabilizer.
L	= Aircraft Lift
P _A	= Power Available.
P _R	= Power Required.
ϕ	= Aircraft bank angle.
ρ_{sl}	= Standard Sea-level air density
ρ	= Air free stream density.
ROC ₁	= Aircraft rate of climb with one engine.
ROC ₂	= Aircraft rate of climb with two engines.
ΔROC	= Change of rate of climb due to sideslip.
S	= Aircraft Reference Area.
S _F	= Fuselage Reference Area
SF	= Fuselage side force due to sideslip.
S _v	= Vertical stabilizer reference area.
SM	= Stall Margin.
T, T ₁	= Thrust of one engine.
T ₂	= Thrust with both engine operating.
V	= Free stream airspeed.
V _{mc}	= Aircraft minimum controllable airspeed, with one engine inoperative.
Vs	= Calibrated Stall Speed (straight and level flight).
W	= Aircraft Weight.
X	= Distance between the aircraft center of gravity and aerodynamic center of the vertical stabilizer.
Y	= Distance from center of thrust to Fuselage Reference Line (FRL).

INTRODUCTION

Flight safety requires that both aircraft and pilot be properly tested and certified per the Federal Aviation Regulations (FARs). These regulations require an aircraft's design be sufficient so as to avoid in flight failures and on those rare occasions when one does occur that the flight can be brought to a safe termination by the pilot. In order for this scenario to work, the pilot must be properly trained to deal with the emergency.

In the case of an in flight engine failure on a single engine aircraft, the pilot needs to maintain proper airspeeds and be able to execute the safest emergency landing possible given the circumstances. A similar failure on a multiengine aircraft presents the pilot with a few more choices. If the aircraft has insufficient power available to maintain altitude, then the pilot must perform the same landing as the single engine pilot. If, however, the aircraft has sufficient power, the pilot must properly manage the aircraft, in order to minimize the power required for flight, and thus maximize the aircraft's potential climb performance. In either case, the multiengine pilot must maintain directional control of an aircraft that has asymmetric thrust.

For the multiengine pilots to perform successfully when an engine fails, their training must emphasize the aerodynamic relationships governing the aircraft's performance and controllability. In addition, the pilot must be given sufficient real time data upon which to make critical decisions.

RESULTS

The failure of an engine, during the landing and takeoff phases of a multiengine flight, taxes a pilot's abilities to the limit. The pilot must maintain directional control of the aircraft, while managing the remaining performance. Failure to maintain directional control occurs when the asymmetric thrust, caused by the single engine situation, cannot be checked by the lift generated by the rudder and vertical stabilizer. This failure often leads to a fatal flat spin.

Maximum performance is obtained by maximizing the available power and minimizing the power required for flight. Obviously, maximum available power is obtained by setting the operating engine controls to their maximum position. As will be shown later, if the airspeed is too low, directional control may not be possible at full power and the maximum power setting will be limited. Failure to do so will cause the aircraft directional control to be lost and a flat spin will ensue.

To minimize the power required, the pilot must minimize the aircraft drag. Standard engine out procedures call for the pilot

to feather the non operating engine and retract the landing gear and flaps, as appropriate. What is not as well understood is the need to keep the fuselage at zero sideslip and how to determine when this condition has been obtained.

SPIN AVOIDANCE

When the aircraft has asymmetric thrust, the rudder must be deflected in order to maintain a zero yawing moment. Equation (1) gives the value of the required rudder deflection at a given airspeed, altitude, thrust, and bank angle.

$$\delta = \left[\frac{T Y}{CL_{v\delta} \frac{1}{2} \rho V^2 S_v \cos(\phi) X} \right] - \frac{CL_{v\beta}}{CL_{v\delta}} \beta \quad (1)$$

During the aircraft certification process, the aircraft manufacturer determines the minimum speed at which the aircraft can be flown with an engine inoperative. This speed, termed the minimum controllable airspeed (V_{mc}), occurs when the rudder deflection reaches its maximum and is given by equation (2).

$$V_{mc} = \sqrt{\frac{T Y}{(CL_{v\beta} \beta + CL_{v\delta} \delta_H) \frac{1}{2} \rho S_v \cos(\phi) X}} \quad (2)$$

The derivation of these equations is presented in the Appendix and is depicted in figures 1 and 2.

The V_{mc} is determined under the worst case conditions, such as, aft center of gravity (CG) location and maximum thrust from the operating engine. Under most flight conditions, the actual V_{mc} is less. If the thrust (T) is reduced by either reducing the throttle setting or flying a non turbocharged aircraft at higher altitudes, the V_{mc} will be decreased. Likewise, if the aircraft's CG is moved forward, the distance from the CG to the vertical stabilizer's aerodynamic center (X) will be increased and thus the value of V_{mc} will decrease. The actual value of V_{mc} at any given time cannot be determined by the pilot. In fact the pilot always has the option of making $V_{mc} = 0$ by shutting the operating engine down.

An engine failure below the actual V_{mc} causes the aircraft to undergo a strong yawing that cannot be counteracted by the use of the rudder. The pilot may be unable to reduce power on the operating engine fast enough to avoid an uncontrollable aircraft

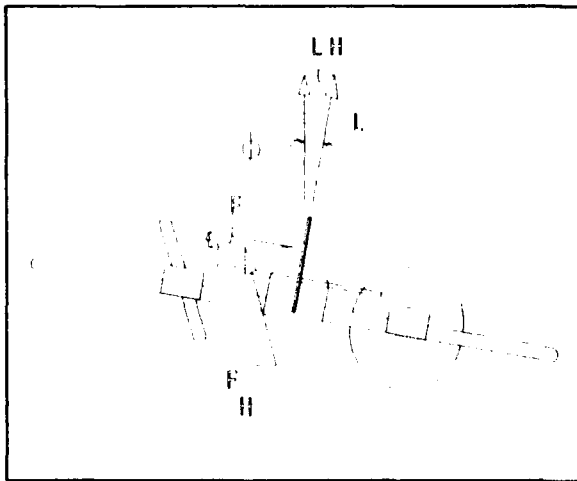


Figure 1 TAIL VIEW

attitude. Pilots are trained to fly at speed greater than the published V_{mc} , because this will most likely keep them at airspeeds greater than the actual V_{mc} .

During pilot training, the characteristics of the aircraft at the actual V_{mc} are demonstrated by flying at a safe altitude, while slowing the aircraft to the point where full rudder is just able to maintain directional control. The aircraft's speed is reduced slowly and the encounter with V_{mc} is usually quite docile, that is,

unless the aircraft stalls before slowing to the actual V_{mc} . This situation occurs when the engine thrust (T) become low, due to the altitude chosen for the V_{mc} demonstration. As can be seen in equation (2), the V_{mc} decreases proportionately with the square root of the thrust.

When the aircraft stalls, the wing with the inoperative engine stalls at the root, while the prop wash from the operating engine delays the other wing's stall. This causes the aircraft to roll toward the inoperative engine. The rolling action increases the angle of attack on the falling wing and decreases it on the rising wing. The descending wing goes into a deeper stall, thus further decreasing its lift and increasing its drag. The roll rate increases and the added drag on the descending wing causes a yawing toward the inoperative engine. The aircraft finally ends up spinning about an earth vertical axis. The mass and placement of the engines cause this spin to become flat with the aircraft's nose just below the horizon. Because of this flat spinning attitude, normal spin recovery techniques are not effective and an uncontrolled crash will be imminent.

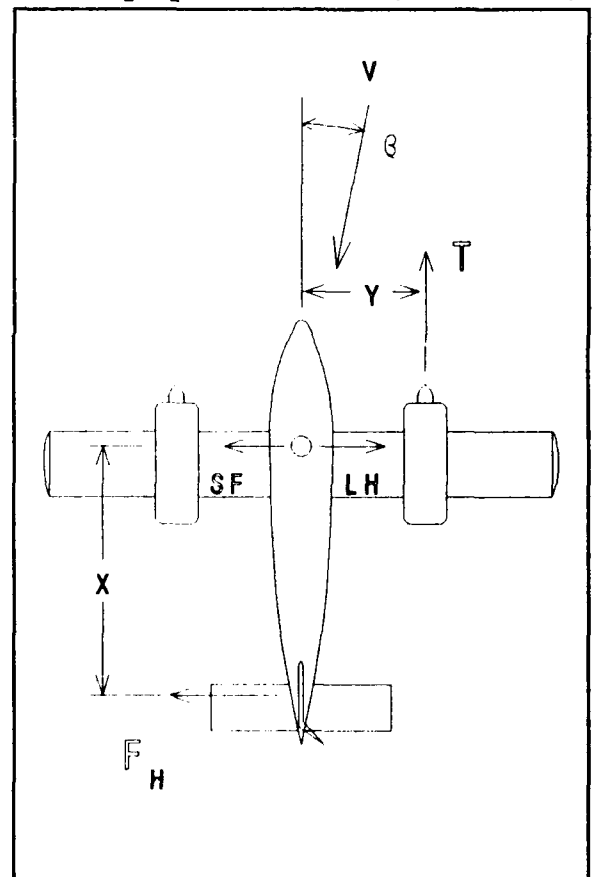


Figure 2 TOP VIEW

The key to avoiding this type of accident is the prevention of the stall, by maintaining an airspeed greater than the stall speed of the aircraft. The problem is to determine the stall speed for the aircraft under the conditions of the flight. Assuming straight and level flight, the power off calibrated stall speed for an aircraft is given by equation (3).

$$V_s = \sqrt{\frac{2 W}{C_{L_{MAX}} \rho_{sl} S}} \quad (3)$$

Generally the pilot will not know the aircraft's in-flight weight and thus will not know the stall speed of the aircraft. In addition, the airspeed indicator system has a high level inaccuracy at speeds near stall. For these reasons, a pilot can not, with any confidence, avoid a stall condition during a V_{mc} demonstration. This is also true during an actual engine out emergency. The pilot needs real time data on the aircraft's proximity to stall.

STALL MARGIN INSTRUMENTATION. Instruments such as the Stall Margin Indicator (SMI) have been designed to provide a pilot with an instantaneous readout of the percentage of aircraft lift coefficient that is not being used. The Stall Margin (SM) of an aircraft is given by equation (4).

$$SM = \left(1 - \frac{C_L}{C_{L_{MAX}}} \right) 100\% \quad (4)$$

Where:

$$C_L = \frac{L}{\frac{1}{2} \rho_{sl} V^2 S}$$

and

$$C_{L_{MAX}} = \frac{L}{\frac{1}{2} \rho_{sl} V_s^2 S} \quad (5)$$

By substituting equations (5) into (4), the Stall Margin can be written as a function of velocities.

$$SM = \left(1 - \left(\frac{V_s}{V} \right)^2 \right) 100\% \quad (6)$$

The Stall Margin can be derived from the aircraft's angle of attack and flap position. Equipment is currently available that provides the pilot with a normalized lift coefficient (CL/CL_{MAX}), which can be directly converted to Stall Margin. The SMI uses wing surface pressures to sense the Stall Margin and its theory and prototype hardware are described in references 1-6.

SPIN AVOIDANCE USING SMI. When an engine fails during a simulated or actual emergency, the aircraft will be at an airspeed greater than stall. The pilot's task is to maintain directional control, while maintaining an airspeed greater than stall. The SMI gives a direct display of the aircraft's lift state, thus, if the aircraft is decelerating toward a stall, the SMI will indicate a reduction in the SM. Where as, the stall speed changes with both flaps and aircraft weight, the SM has been corrected automatically and gives the pilot the needed information on one simple display. As will be described later, the SM can also provide critical data for maximizing the aircraft's climb performance.

During a V_{mc} demonstration, the SM can be monitored as the aircraft slows toward V_{mc} . If, due to low thrust, the airspeed approaches too close to stall before reaching V_{mc} , the instructor can increase the effective V_{mc} by limiting the rudder travel from within the cockpit by blocking it with his foot. The student obtains the same benefit from the demonstration. The function of the SMI in this case was to remove doubt as to how close the aircraft was coming to stall.

MAXIMUM CLIMB PERFORMANCE

Whether the aircraft can climb on one engine or not, the pilot must maximize the performance of the aircraft. If the aircraft cannot climb, the pilot will be minimizing the glide angle and thus be increasing the number of possible emergency landing sights. If, on the other hand, sufficient power is available, the climb angle will be maximized, giving the aircraft the best chance to climb to a safe maneuvering altitude.

DRAG DUE TO SIDESLIP. One of the least understood engine out phenomenon is the sideslip that occurs if the bank angle is not correct. This sideslip increases the drag of the fuselage, which

in turn, increases the total drag of the aircraft. Equation (7) gives an approximation of this drag. See the appendix for the its derivation.

$$\Delta C_D = \left[\frac{C_{SF\beta}^2}{\pi AR_f \epsilon_f} \right] \beta^2 \quad (7)$$

As can be seen from this equation, the drag increases as a function of the square of the sideslip angle (β). In order for the pilot to maximize the aircraft's performance, this angle must be maintained at zero. As shown later, this can be accomplished by banking the aircraft toward the operating engine.

SIDESLIP ANGLE WITH ZERO BANK ANGLE. If the pilot is unaware of the phenomenon, a wings level attitude may be chosen instead of the proper wing down attitude. By doing so, the aircraft will develop a sideslip governed by equation (8).

$$\beta = \frac{-CL_{V\delta} \delta S_V}{C_{SF\beta} S_F + CL_{V\beta} S_V} \quad (8)$$

By substituting equation (1) into (8) and setting the bank angle to zero, the sideslip angle for zero bank angle can be determined.

$$\beta = - \frac{T Y}{\frac{1}{2} \rho V^2 S_F X C_{SF\beta}} \quad (9)$$

Without special instrumentation the pilot has no way of determining either the direction or magnitude of the sideslip. This makes the task of maximizing the performance, by keeping the sideslip angle zero, a matter of educated guess work.

RATE OF CLIMB LOSS DUE TO SIDESLIP. The additional drag resulting from the sideslip, as given in equation (7), results in a loss in the aircraft's rate of climb (ROC). This change in the ROC is derived in the appendix, by taking the difference between the ROC with both engines running and with one engine inoperative. The component of this ROC that can be directly attributed to the sideslip angle is given in equation (10).

$$\Delta ROC = \frac{-\left(\frac{C_{sf}\beta^2}{\pi AR_f \epsilon_f}\right) \frac{1}{2} \rho V^3 S \beta^2}{W} \quad (10)$$

With all other things held constant, the change of the ROC varies as the square of the sideslip angle. Figure (3) illustrates the effect of the sideslip angle on both the rate of climb, derived from equation (10), and the minimum controllable airspeed, given by equation (2).

To maximize the aircraft's performance, the pilot must minimize the ΔROC by holding the sideslip angle zero. The proper method for accomplishing this is to hold a small bank into the running engine.

BANK REQUIRED FOR ZERO SIDESLIP. The general sideslip equation is derived in the appendix and expressed in equation (A13). If the sideslip angle (β) is set to zero and this equation solved for the bank angle (ϕ), the following equation results.

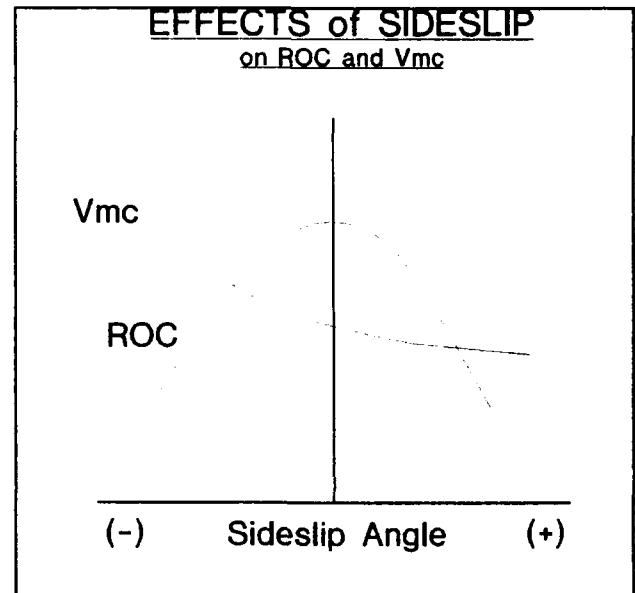


Figure 3

$$\phi = \text{ARCTAN} \left[\frac{CL_{V_\delta} \delta \frac{S_v}{S}}{CL} \right] \quad (11)$$

This equation may be of academic interest, but will be of little use to the pilot, who is trying to maintain a $\beta=0$ condition. None of the independent variables in this equation will be available to the pilot in real time. The pilot requires real time knowledge of β if it is to be maintained at zero.

SIDESLIP INSTRUMENTATION. A simple string taped to the wind screen will provide a pilot with an indication of the sideslip. Such a device is cheap and effectively used by many flight instructors to demonstrate the effect bank angle has on the sideslip. It is rare to find a string taped to a multiengine aircraft for use in the event an actual engine fails. There are several reasons that can be sighted for this:

- * Pilot's lack of knowledge pertaining to sideslip.
- * The string does not measure up to the normal sophistication associated with flight instrumentation.
- * A string quickly wears out and can wear the aircraft's surface upon which it moves.
- * A string also does not work well when wet.

One solution to all but the first of these is to employ the same technology used in the SMI. As shown in figure (4), a small, fixed, symmetrical fin could be mounted on the top or bottom of the fuselage. The fin would be parallel to the aircraft's FRL slightly back from the nose. This fin would have a hole on each side, each connected to one side of a sensitive differential pressure transducer. The fin would be at zero angle of attack when the aircraft's sideslip angle is zero. Any sideslip would cause the pressures to be different and thus the pressure transducer would output a proportional signal. This output would drive a simple sideslip indicator next to the SMI. Such an instrument would remove the guess work, as to the correct bank angle to be held for best performance.

MAXIMIZING RATE OF CLIMB USING SMI. As described earlier, the SMI and similar technology, can be used to both avoid a stall and to minimize the rate of climb lost due to a sideslip. In addition, the SMI gives useful data upon which the pilot can maximize the performance components other than those associated with sideslip. The Stall Margin to be flown for a maximum rate of climb is given by equation (12).

$$SM = \left(1 - \frac{\sqrt{3 C_{D0} \pi AR \epsilon}}{C_{L_{MAX}}} \right) \quad (12)$$

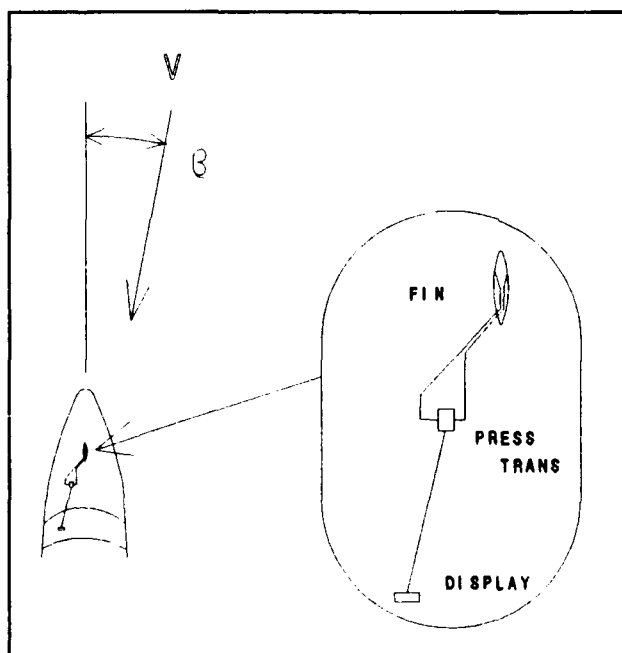


Figure 4 SIDESLIP INSTRUMENTATION

For a given configuration, this number is a constant for the engine out situation. After an engine failure, the pilot needs only adjust the aircraft's pitch to maintain this SM, along with holding the sideslip zero, and the aircraft will perform the best that it can under the circumstances.

CONCLUSIONS

The fatality rate associated with engine failure on a multiengine aircraft is unacceptably high. Due to the high reliability of modern aircraft engines, pilot's are seldom faced with this type of emergency situation. Without regular recurrent training at a well equipped simulator facility, the pilot is generally unprepared to deal with the situation. For numerous reasons, many pilots do not obtain the necessary training to stay current in the engine out emergency procedures.

Although not a substitution for adequate training, good real time data pertaining to aircraft performance can significantly reduce the pilot workload. By having precise information on the aircraft's Stall Margin and its sideslip angle, the pilot can maximize the aircraft's single engine performance. The pilot will not have to rely so heavily on recent single engine emergency training.

Regardless of whether the aircraft climbs or not, it is critical that the pilot retain control. If this control is lost the result will most likely be fatal. The technology presented in this paper would clearly improve the pilot's situation.

REFERENCES

- Hoadley, Conversion of Wing Surface Pressures Into Normalized Lift Coefficient, SAE 790567, 1979 SAE Transactions.
- Hoadley, Normalized Coefficient of Lift Indicator, US Patent No. 4,235,104
- Hoadley, Wing Mounted Stall Condition Detector, US Patent No. 4,350,314
- Hoadley, Stall Margin Indicator Development, AIAA 86-2694.
- Hoadley, Stall Margin Indication, AIAA 86-2595
- Hoadley, Stall Margin Indication, Engineering, Technical Note, Vol. 25, No. 4, Journal of Aircraft, April 1988.

APPENDICES

DETERMINATION OF MINIMUM CONTROLLABLE AIRSPEED. When one of the engines on a twin engine aircraft fails in flight, the yawing moment created by the asymmetric thrust must be balanced by the moment created by the vertical stabilizer in conjunction with the rudder. The total or sum of all yawing moments exerted on the aircraft, during single engine operation, can be expressed by the following equation: (see Figure 2)

$$Y_m = -T Y + F_H X \quad A(1)$$

Applying the definition of the lift coefficient, the vertical's lift force can be written as:

$$F = CL_V \frac{1}{2} \rho V^2 S_V \quad A(2)$$

The horizontal component of the vertical stabilizer's lift vector can be derived as follows: (see Figure 1)

$$F_H = F \cos(\phi) \quad A(3)$$

If the vertical stabilizer's lift force is assumed to vary linearly with both the sideslip angle and the rudder deflection, then its lift coefficient can be expressed in terms of the corresponding slopes. (see Figure A1)

$$CL_V = CL_{V\beta} \beta + CL_{V\delta} \delta \quad A(4)$$

By substituting equations A2 and A4 into A3, the horizontal force generated by the vertical stabilizer can be determined.

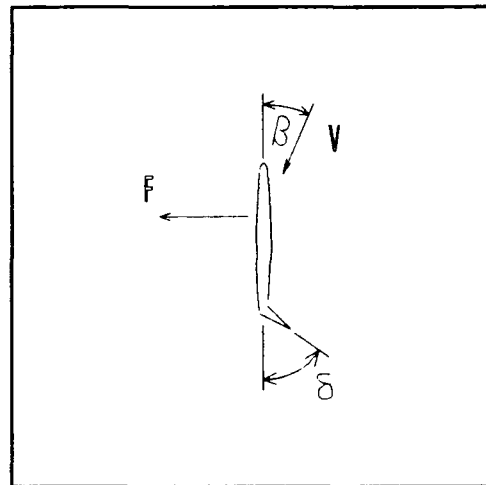


Figure A1
VERTICAL STABILIZER

$$F_H = (CL_{V\beta} \beta + CL_{V\delta} \delta) \frac{1}{2} \rho V^2 S_V \cos(\phi) \quad A(5)$$

Substituting equation A5 into equation A1, yields the following form of the yawing moment equation.

$$Y_m = -T Y + (CL_{V\beta} \beta + CL_{V\delta} \delta) \frac{1}{2} \rho V^2 S_V \cos(\phi) x \quad A(6)$$

This equation shows the relationships between the key variables affecting the aircraft's yawing moment. By setting the yawing moment to zero and solving for the rudder deflection (δ), the following equation is obtained.

$$\delta = \left[\frac{T Y}{CL_{V\delta} \frac{1}{2} \rho V^2 S_V \cos(\phi) x} \right] - \frac{CL_{V\beta}}{CL_{V\delta}} \beta \quad A(7)$$

By setting the rudder deflection to its maximum value, the slowest speed, for which the aircraft will not yaw, can be determined.

$$V_{mc} = \sqrt{\frac{T Y}{(CL_{V\beta} \beta + CL_{V\delta} \delta_H) \frac{1}{2} \rho S_V \cos(\phi) x}} \quad A(8)$$

DETERMINATION OF MAXIMUM CLIMB PERFORMANCE. In order to maximize the performance of the aircraft, a zero sideslip angle must be maintained. With one engine inoperative, a side load must be created by the vertical stabilizer sufficient to off set the yawing moment caused by the operating engine. If the wings are held level, this force will cause the aircraft to accelerate sideways until an opposing force is created by the fuselage side force as a result of the sideslip.

By assuming the fuselage to be symmetrical and to respond in a linear fashion to a sideslip, the side force can be written as follows:

$$C_{SF} = C_{SF\beta} \beta$$

$$SF = C_{SF\beta} \beta \frac{1}{2} \rho V^2 S_F \quad A(9)$$

Referring to figures 1 and 2, the sum of all side forces can be expressed by:

$$\sum F_{Horizontal} = L \sin(\phi) - F_H - SF \quad A(10)$$

By assuming unaccelerated flight and substituting for (SF), the horizontal force generated by the vertical stabilizer can be written as:

$$F_H = L \sin(\phi) - C_{SF\beta} \beta \frac{1}{2} \rho V^2 S_F \quad A(11)$$

If the pilot maintains a wings level attitude after an engine failure, a sideslip will develop. By setting equation A5 equal to A11, the equation for sideslip angle can be obtained for the wings level attitude.

$$(CL_{V\beta} \beta + CL_{V\delta} \delta) \frac{1}{2} \rho V^2 S_V \cos(\phi)$$

$$= L \sin(\phi) - C_{SF\beta} \beta \frac{1}{2} \rho V^2 S_F \quad A(12)$$

Which gives,

$$\beta = \frac{\left[-CL_{V\delta} \delta S_V \cos(\phi) + \frac{L \sin(\phi)}{\frac{1}{2} \rho V^2} \right]}{C_{SF\beta} S_F + CL_{V\beta} S_V \cos(\phi)} \quad A(13)$$

As will be shown later, the performance is reduced for any sideslip angle other than zero. In order to keep $\beta = 0$, the pilot can bank the aircraft into the operating engine. The magnitude of the bank can be determined by solving the above equation for ϕ with β set to zero.

$$\phi = \text{ARCTAN} \left[\frac{CL_{v\delta} \delta \frac{S_v}{S}}{CL} \right] \quad \text{A(14)}$$

The increase in the total aircraft drag coefficient due to the sideslip can be written as an induced drag coefficient. This coefficient takes the form of the induced drag component produced by the wings but is based on the efficiency (ϵ_f) and vertical aspect ratio (AR_f) of the fuselage.

$$\Delta C_D = \frac{(C_{sf\beta} \beta)^2}{\pi AR_f \epsilon_f}$$

or

$$\Delta C_D = \left[\frac{C_{sf\beta}^2}{\pi AR_f \epsilon_f} \right] \beta^2 \quad \text{A(15)}$$

Whenever the sideslip angle is not zero, an additional drag component is created, which will degrade the aircraft's performance. By placing this component into the rate of climb equation, its effect can be written:

$$ROC_2 = \frac{(T_2 - D_2) V}{W}$$

$$ROC_1 = \frac{(T_1 - D_1 + \Delta D) V}{W} \quad \text{A(16)}$$

and

$$\Delta ROC = ROC_1 - ROC_2$$

Substituting gives:

$$\Delta ROC = \frac{(T_1 V - D_1 V - \Delta D V)}{W} - \frac{(T_2 V - D_2 V)}{W}$$

or

$$\Delta ROC = \left[\frac{(T_1 - T_2) - (D_1 - D_2)}{W} \right] V - \frac{(\Delta D V)}{W} \quad A(17)$$

The first term of this equation represents the performance reduction due to the loss of one engine's thrust and the drag associated with that engine. The second term represents the loss of performance due to any sideslip. By considering only the last term and substituting, the equation representing the change in performance can be determined.

$$\Delta D = \Delta C_D \frac{1}{2} \rho V^2 S$$

$$\Delta ROC = \frac{- \left(\frac{C_{sf}^2}{\pi A R_f \epsilon_f} \right) \frac{1}{2} \rho V^3 S \beta^2}{W} \quad A(18)$$

DETERMINATION OF SMI FOR MAXIMUM CLIMB PERFORMANCE. The maximum rate of climb can be found by setting the first derivative of the rate of climb to zero.

$$ROC = \frac{P_A - P_R}{W} \quad A(19)$$

If P_A and W are assumed to be constant with respect to V , then,

$$\frac{\partial (ROC)}{\partial (V)} = - \frac{1}{W} \frac{\partial (P_R)}{\partial (V)} \quad A(20)$$

Setting this to zero gives,

$$\frac{\partial (P_R)}{\partial (V)} = 0 \quad \text{A(21)}$$

If the Lift is assumed equal to the weight, then the power available can be expressed as:

$$P_R = C_{D0} \frac{1}{2} \rho V^3 S + \frac{2 W^2}{\pi AR \epsilon \rho V S} \quad \text{A(22)}$$

Differentiating and substituting gives,

$$C_{D0} \frac{3}{2} \rho S V^2 - \frac{2 W^2}{\pi AR \epsilon \rho S V^2} = 0 \quad \text{A(23)}$$

Further manipulation of this equation yields the optimum lift coefficient necessary for the maximum rate of climb.

$$V^2 = \frac{2 W}{\rho S} \sqrt{\frac{1}{3 C_{D0} \pi AR \epsilon}} \quad \text{A(24)}$$

Given That,

$$CL = \frac{W}{\frac{1}{2} \rho V^2 S} \quad \text{A(25)}$$

Then,

$$CL = \sqrt{3 C_{D0} \pi AR \epsilon} \quad \text{A(26)}$$

Substituting this into the Stall Margin equation (4), the SM for max climb rate can be determined.

$$SM = \left(1 - \frac{\sqrt{3} C_{D0} \pi AR \epsilon}{CL_{MAX}} \right) \quad A(27)$$

AN AIRFOIL FOR GENERAL AVIATION APPLICATIONS

by

Michael S. Selig
Mark D. Maughmer
Pennsylvania State University
Department of Aerospace Engineering
233 Hammond Bldg.
University Park, PA 16802
and
Dan M. Somers
NASA Langley Research Center
Hampton, VA 23665-5225

For presentation to the AIAA/FAA Joint Symposium on General
Aviation Systems at the Port O-Call Inn, Ocean City, NJ
on April 12, 1990

AN AIRFOIL FOR GENERAL AVIATION APPLICATIONS

Michael S. Selig † and Mark D. Maughmer ‡

The Pennsylvania State University
Department of Aerospace Engineering
233 Hammond Bldg.
University Park, PA, 16802

Dan M. Somers §
NASA Langley Research Center
Hampton, VA, 23665-5225

ABSTRACT

A new airfoil, the NLF(1)-0115, has been recently designed at the NASA Langley Research Center for use in general-aviation applications. During the development of this airfoil, special emphasis was placed on experiences and observations gleaned from other successful general-aviation airfoils. For example, the flight lift-coefficient range is the same as that of the turbulent-flow NACA 23015 airfoil. Also, although beneficial for reducing drag and having large amounts of lift, the NLF(1)-0115 avoids the use of aft loading which can lead to large stick forces if utilized on portions of the wing having ailerons. Furthermore, not using aft loading eliminates the concern that the high pitching-moment coefficient generated by such airfoils can result in large trim drags if cruise flaps are not employed.

The NASA NLF(1)-0115 has a thickness of 15%. It is designed primarily for general-aviation aircraft with wing loadings of 718 to 958 N/m² (15 to 20 lb/ft²). Low profile drag as a result of laminar flow is obtained over the range from $c_l = 0.1$ and $R = 9 \times 10^6$ (the cruise condition) to $c_l = 0.6$ and $R = 4 \times 10^6$ (the climb condition). While this airfoil can be used with flaps, it is designed to achieve $c_{l,max} = 1.5$ at $R = 2.6 \times 10^6$ without flaps. The zero-lift pitching moment is held at $c_{m_0} = -0.055$. The hinge moment for a .20c aileron is fixed at a value equal to that of the NACA 63₂-215 airfoil, $c_H = -0.00216$. The loss in $c_{l,max}$ due to leading edge roughness, rain, or insects at $R = 2.6 \times 10^6$ is 11% as compared with 14% for the NACA 23015.

INTRODUCTION

With increasing use of modern/composite structures in general-aviation aircraft, it is possible to obtain tolerances and levels of surface smoothness such that the use of laminar flow airfoils can result in significant gains in aircraft performance¹. In the past, some of the attempts to use such airfoils were not fully successful. For example, the loss of the laminar flow due to surface contamination, etc. sometimes resulted in a significant reduction in the maximum lift coefficient which could produce very dangerous situations with regard to take-off and landing. Also causing concern was the fact that some earlier laminar-flow airfoils were aft pressure

† Graduate Assistant, Student Member AIAA

‡ Assistant Professor, Senior Member AIAA

§ Currently with Airfoils, Inc., 601 Cricklewood Dr., State College, PA, 16801

loaded in order to have long regions of favorable pressure gradients resulting in significant runs of laminar flow. For some applications, the use of such airfoils can result in trim-drag penalties due to large nose-down pitching moments. Likewise, if such airfoils are used over the regions of the wings in which control surfaces are located, large control forces can exist and the control surfaces can have a tendency to "float."

Using the experience obtained with laminar-flow airfoils over the years, a new airfoil has been developed which provides the performance gains possible with laminar flow but without the concerns associated with some of the earlier efforts. The result of this design effort is an airfoil having performance better than those traditionally used for such applications while not giving up any of the desirable characteristics of those older airfoils.

AIRFOIL DESIGN

OBJECTIVES AND CONSTRAINTS

Many of the design requirements for a modern general-aviation airfoil can be derived from other successful general-aviation airfoils. Most notably the turbulent-flow NACA 23015 airfoil² has been a popular choice for general-aviation applications for many years. This fact stems not only from the broad lift range and low pitching moment, but also from small loss in $c_{l,max}$ due to surface contamination. The laminar-flow NACA 63₂-215 airfoil² has also had wide appeal owing to its low-drag, yet it suffers from a narrow usable lift range as compared with the NACA 23015.

The principle goal of this airfoil-design effort is to maintain the lift range of the NACA 23015 while realizing low-drag characteristics like those of the NACA 63₂-215. In particular, low profile drag is desired over the range from $c_l = 0.1$ at $R = 9 \times 10^6$ (the cruise condition) to $c_l = 0.6$ at $R = 4 \times 10^6$ (the climb condition). While the new airfoil can be used with flaps, it is required that without flaps $c_{l,max} \geq 1.5$ at $R = 2.6 \times 10^6$ (the takeoff/landing condition). In case of surface contamination, the loss in $c_{l,max}$ should be no larger than 14%, the same as that suffered by the NACA 23015. To minimize trim drag penalties, it is desired that $c_{m,o} > -0.055$. Furthermore, for a control surface of $0.2c$, the hinge moment coefficient should be no less than that of the NACA 63₂-215, $c_H > -0.0022$. In this case stick forces and control surface "float" will not be excessive. Lastly, the airfoil thickness is set at 15%.

DESIGN PROCEDURE

The airfoil-design process was carried out using the Eppler Airfoil Design and Analysis Program³. Briefly, the design method employs inverse conformal mapping to obtain the airfoil through specification of the velocity distribution. It is particularly valuable as a design tool in that it allows different parts of the airfoil to be designed for different operating conditions. In this way, the desired performance envelope is a consequence of the actual design effort rather than that which is obtained when a point-designed airfoil is operated off-design. The analysis method implemented in the program uses the integral boundary-layer momentum and energy equations to predict airfoil performance. Transition is predicted by a method which will be discussed later. The iterative process of designing and analyzing candidate airfoils is

concluded when the airfoil-design objectives and constraints are satisfied and the performance maximized.

NASA NLF(1)-0115 AIRFOIL AND COMPARISONS

The result of the present design effort is the NASA NLF(1)-0115 †, shown in figure 1 along with three inviscid velocity distributions corresponding to the key flight conditions: cruise, climb, and takeoff/landing. The accompanying theoretical airfoil characteristics are shown in figure 2 for $R = 9 \times 10^6$ and 4×10^6 , the cruise and climb conditions, respectively. The zero-lift pitching- and hinge-moment coefficients fall within the design specifications, $c_{m,o} = -0.055$ and $c_H = -0.0022$ for a $0.2c$ control surface. The airfoil thickness is 15% as desired.

A comparison between the airfoil characteristics of the NASA NLF(1)-0115 and those of the NACA 23015 at the cruise flight Reynolds number is presented in figure 3. As seen, the design goal of maintaining a broad lift range like that of the NACA 23015 has been obtained. The low-drag benefit due to laminar flow is achieved in the cruise-flight lift-coefficient range of the new airfoil. It should be noted that one of the prices paid for the lower drag coefficient is an increase in the nose-down pitching-moment coefficient.

The effects of surface contamination are shown in figure 4 for the takeoff/landing Reynolds number of 2.6×10^6 . It is observed that the predicted value of $c_{l,max}$ for the NLF(1)-0115 airfoil is not overly sensitive to surface roughness. In fact the lift loss due to contamination is only 11% as compared with 14% for the NACA 23015.

In order to have limited sensitivity to surface roughness, the NLF(1)-0115 airfoil embodies upper-surface velocity distributions which behave as generally depicted in figure 5. The velocity distribution for $c_l = 0.6$ (the upper limit of the low-drag range at $R = 4 \times 10^6$) is prescribed such that with increasing angles of attack the transition point moves rapidly forward to the leading edge from a point just upstream of the main pressure recovery at the midchord. Thus for $c_l < 0.6$, the pressure gradients confine transition to the short instability region just upstream of the main pressure recovery. For $c_l > 0.6$, however, the adverse pressure gradient over the forward portion of the airfoil moves transition to very near the leading edge. Consequently, because turbulent flow is predominate on the upper surface at the maximum lift coefficient, $c_{l,max}$ is not dramatically influenced by surface roughness.

In figure 6, a comparison is made between the airfoil characteristics of the NASA NLF(1)-0115 and those of the NACA 632-215 at $R = 9 \times 10^6$. At the cruise condition ($c_l = 0.1$), the NLF(1)-0115 airfoil has 25% less drag than the NACA 632-215, and this advantage is maintained over most of the operational envelope. Although both airfoils are designed to have significant runs of laminar flow, significant differences exist in the way in which this is achieved. These differences are best interpreted using the theoretical boundary-layer development plot, such as that shown in figure 7, which requires some preliminary discussion.

In figure 7, the local Reynolds number based on the momentum thickness and local boundary layer edge velocity (R_{δ_2}) is plotted against the shape factor based on the energy and momentum

† Coordinates for the NASA NLF(1)-0115 airfoil may be obtained directly from the authors.

thickness (H_{32}). Note that the logarithmic scale for R_{δ_2} has the tendency to expand the boundary layer near the leading edge and compress it downstream. Starting from the airfoil stagnation point, R_{δ_2} increases monotonically along the upper and lower surfaces of the airfoil. The value of H_{32} can vary significantly, although certain values correspond to specific, laminar boundary-layer phenomena. An H_{32} of 1.620 corresponds to stagnation, 1.573 to the flat-plate Blasius boundary layer, and 1.515 to laminar separation. It is noted that H_{32} has the opposite tendency of the perhaps more familiar H_{12} , which contains the displacement thickness rather than the energy thickness. That is H_{32} , unlike H_{12} , decreases from stagnation toward laminar separation.

The Eppler method of predicting transition is based on the local values of H_{32} and R_{δ_2} . Within the dotted-line boundaries given in figure 7, the flow is assumed to be laminar. The vertical boundary to the left corresponds to laminar separation ($H_{32} = 1.515$), while the upper transition-criterion curve corresponds to natural boundary-layer transition. This transition criterion was empirically derived from wind tunnel and flight test data, and should therefore be considered as a band since it is merely a fairing through the experimental data points. Once transition is predicted, the method switches to the turbulent boundary-layer equations.

The two boundary-layer developments shown in figure 7 are for the upper surface of the NACA 63₂-215 at $c_l = 0.4$ and 0.8 for $R = 4 \times 10^6$. In the figure both boundary-layer developments begin in the lower right at the stagnation point (point A). For $c_l = 0.4$, the curve meets the transition-criterion curve (point B) at which location transition is assumed to take place. As the angle of attack increases, the boundary-layer development curves skew toward the left as the pressure gradients become steeper. For $c_l = 0.8$, the steep adverse pressure gradient immediately downstream of the velocity peak near the leading edge (point C) results in a more rapid decrease in H_{32} and causes transition via a laminar separation bubble.

When the boundary-layer data is provided in this fashion, it reveals valuable information relating to transition and thereby offers clues as to how to sustain laminar flow in the design of a new airfoil. For example, referring back to figure 7 at $c_l = 0.8$, transition is predicted to occur immediately downstream of the stagnation point. If the adverse pressure gradient in the region were reduced through modification of the velocity distribution, transition would be postponed. By adjusting the velocity distribution based on the boundary-layer development plot, laminar flow can be extended further back on the airfoil and is limited only by boundary-layer separation or one of the design constraints. As discussed by Somers⁴ and first suggested by Eppler, the widest possible low-drag range is achieved when the laminar boundary layer is held on the verge of laminar separation and then on the verge of boundary-layer transition. Such a scenario would be characterized by a boundary-layer development that follows the dotted lines in figure 7. This concept has been exploited in the design of other airfoils, such as those presented in Refs. 5-7, and is now employed in the NLF(1)-0115.

Figure 8 shows the boundary-layer development for the lower surface of the NLF(1)-0115 at $c_l = 0.0$ and $R = 9 \times 10^6$ and corresponds to the lower limit of the low-drag range (see figure 2). First the laminar-separation limit is approached quickly and is followed for a short distance up to point A. The boundary-layer development then essentially follows the transition-criterion curve. The beginning of the pressure recovery at point B causes the transition criterion to be satisfied which, in turn, invokes the turbulent boundary-layer calculations.

For the upper surface, the critical design condition occurs at the upper limit of the low-drag range. The corresponding boundary-layer development is shown in figure 9 for $c_l = 0.6$ and $R = 4 \times 10^6$. Unlike the design of the lower surface, the upper surface is not designed to rapidly approach laminar separation. Rather from the stagnation point to 0.1c, the design of the upper surface is dictated by $c_{l,max}$ and surface roughness considerations as previously discussed. From 0.1c to 0.5c, however, the boundary layer is again forced to be everywhere on the verge of transition.

Based on this discussion, it should be clear that if the design specifications were altered somewhat, this would warrant a different airfoil. For example, if the upper limit of the low-drag range was desired to occur at $c_l = 0.7$ and $R = 3 \times 10^6$, then this would mainly require modification of the upper-surface velocity distribution while simultaneously keeping within the other constraints. Put simply, for maximum performance, the airfoil should be tailored specifically to its mission requirements.

CONCLUSIONS

The latest in a series of natural laminar-flow airfoils designed at NASA Langley Research Center, the NASA NLF(1)-0115, is intended for use in general-aviation applications where high speed and long range are paramount. Incorporated into this design are favorable features derived from several previously existing successful airfoils. These features, coupled with significant drag reductions made possible through the use of extended lengths of laminar flow, should prove to make the NLF(1)-0115 airfoil successful in application to general-aviation aircraft.

ACKNOWLEDGEMENTS

The support of the NASA Langley Research Center under Grant NGT-50341 is gratefully acknowledged.

REFERENCES

1. Holmes, B.J., Obara, C.J., and Yip, L.P., "Natural Laminar Flow Experiments on Modern Airplane Surfaces," NASA TP-2256, 1984.
2. Abbott, I.H., von Doenhoff, A.E., Theory of Wing Sections, Dover Publications, New York, 1959.
3. Eppler, R. and Somers, D.M., "A Computer Program for the Design and Analysis of Low-Speed Airfoils," NASA TM-80210, 1980.
4. Somers, D.M., "Subsonic Natural-Laminar-Flow Airfoils," in Natural Laminar Flow and Laminar Flow Control, edited by R.W. Barnwell and M.Y. Hussaini, Springer-Verlag, to be published.
5. Somers, D.M., "Design and Experimental Results for a Flapped Natural-Laminar-Flow Airfoil for General Aviation Applications," NASA TP-1865, 1981.

6. Somers, D.M. and Horstmann, K.H., "Design of a Medium-Speed, Natural-Laminar-Flow Airfoil for Commuter Aircraft Applications," Institut fur Entwurfsaerodynamik, Braunschweig, IB 129-85/26, April 1985.
7. Maughmer, M.D. and Somers, D.M. "Design and Experimental Results for a High-Altitude, Long-Endurance Airfoil," J. of Aircraft, Vol. 26, No. 2, Feb. 1989, pp. 148-153.

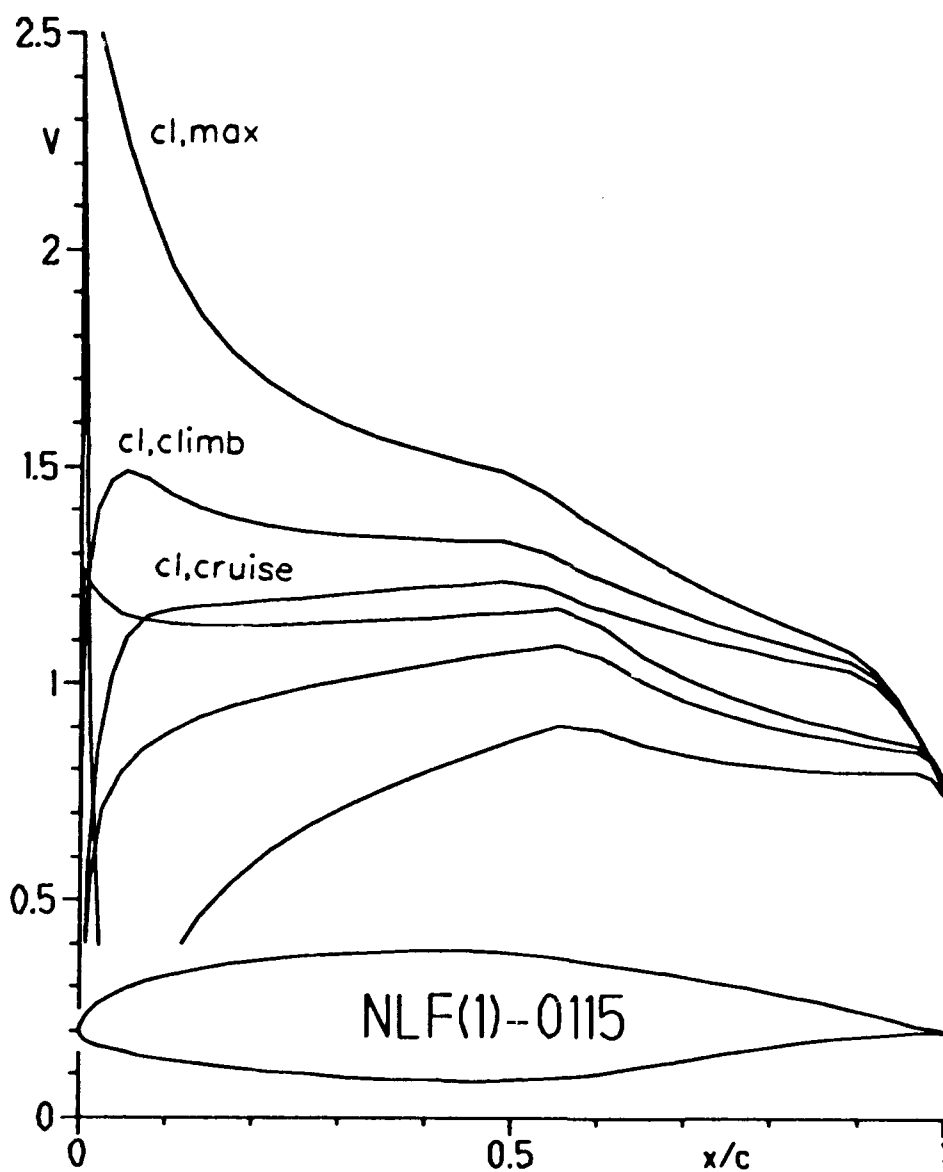


Figure 1. NASA NLF(1)-0115 airfoil and three inviscid velocity distributions.

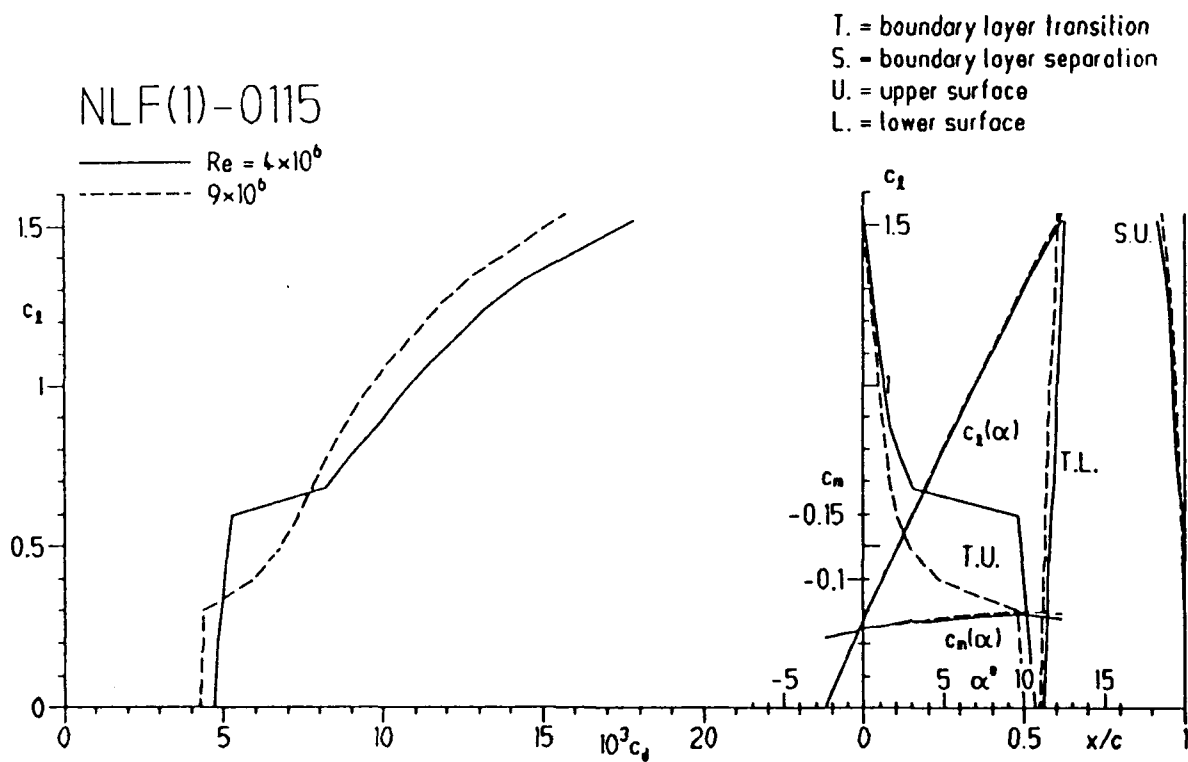


Figure 2. Theoretical airfoil characteristics for the NASA NLF(1)-0115 airfoil.

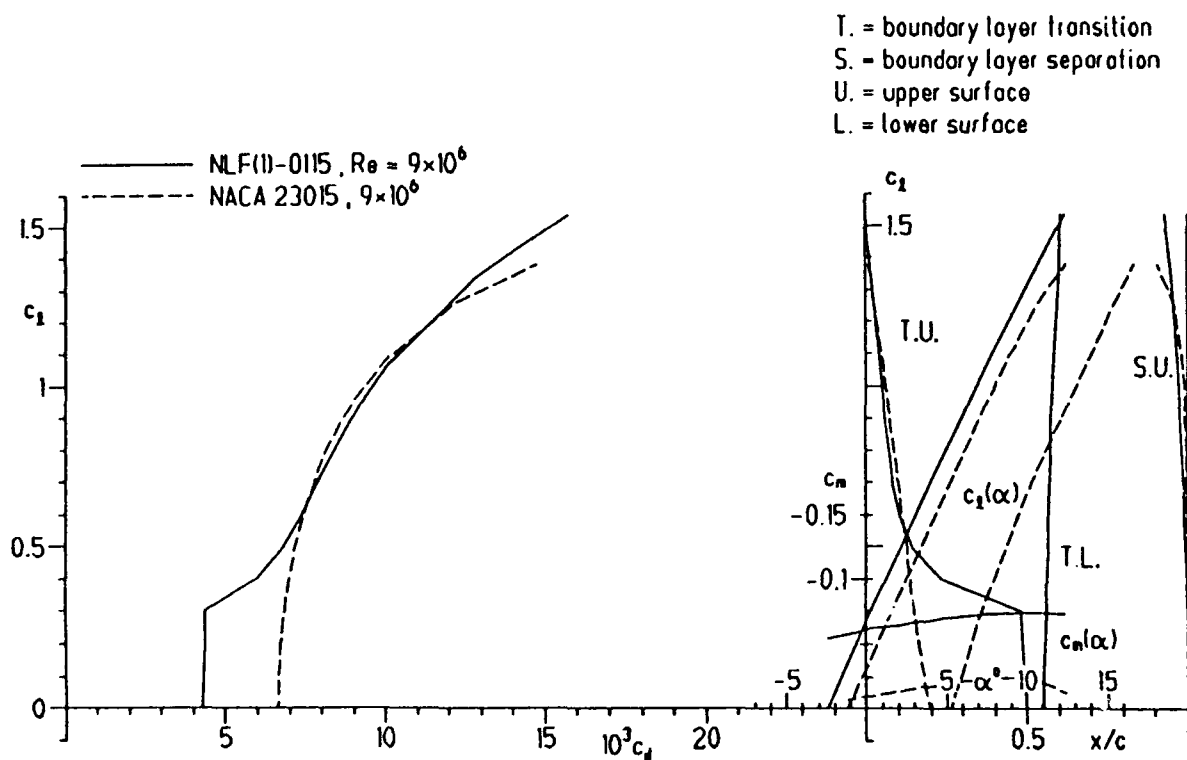


Figure 3. Comparison of the NASA NLF(1)-0115 and NACA 23015 theoretical airfoil characteristics for $R = 9 \times 10^6$.

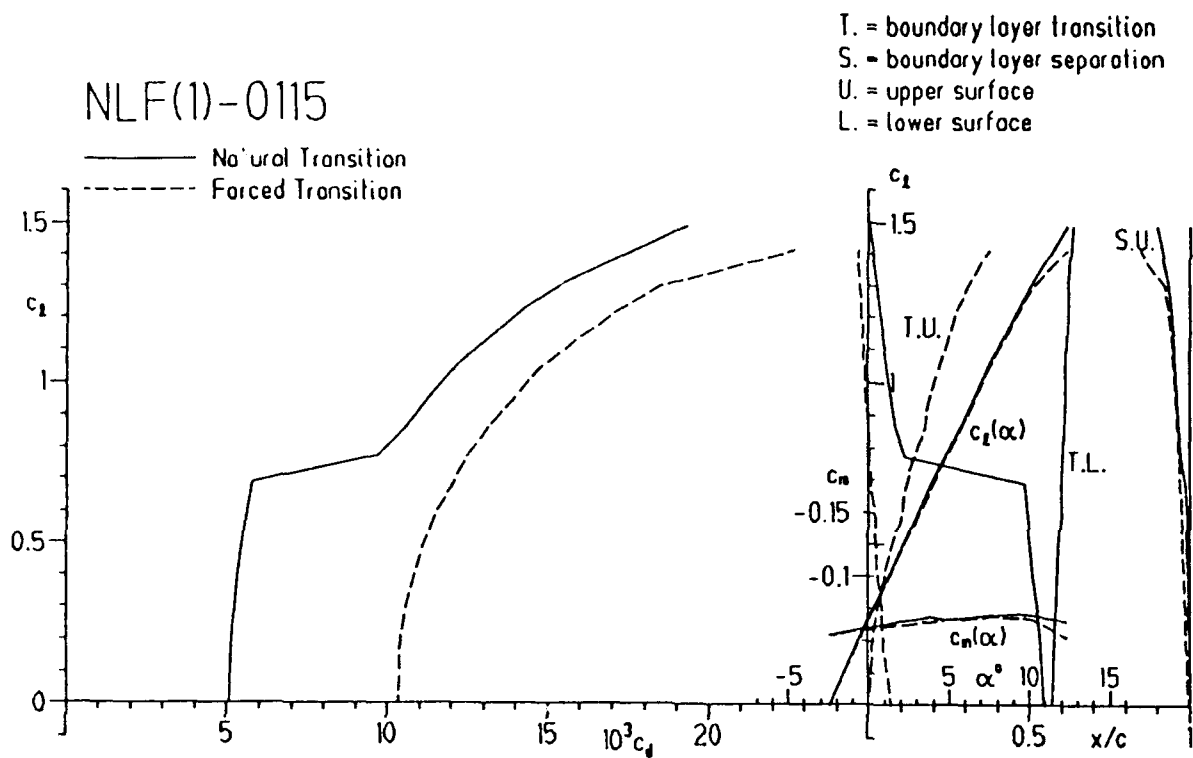


Figure 4. The effects of surface roughness on the theoretical airfoil characteristics of the NASA NLF(1)-0115 airfoil for $R = 2.6 \times 10^6$.

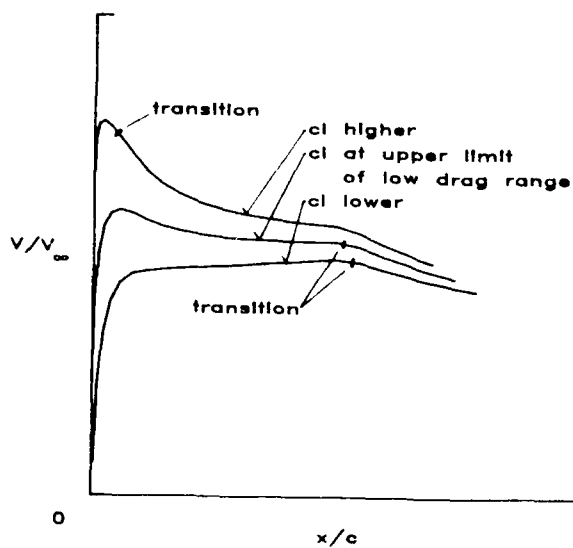


Figure 5. Behavior of the upper-surface velocity distribution that limits $c_{l,max}$ sensitivity to surface roughness.

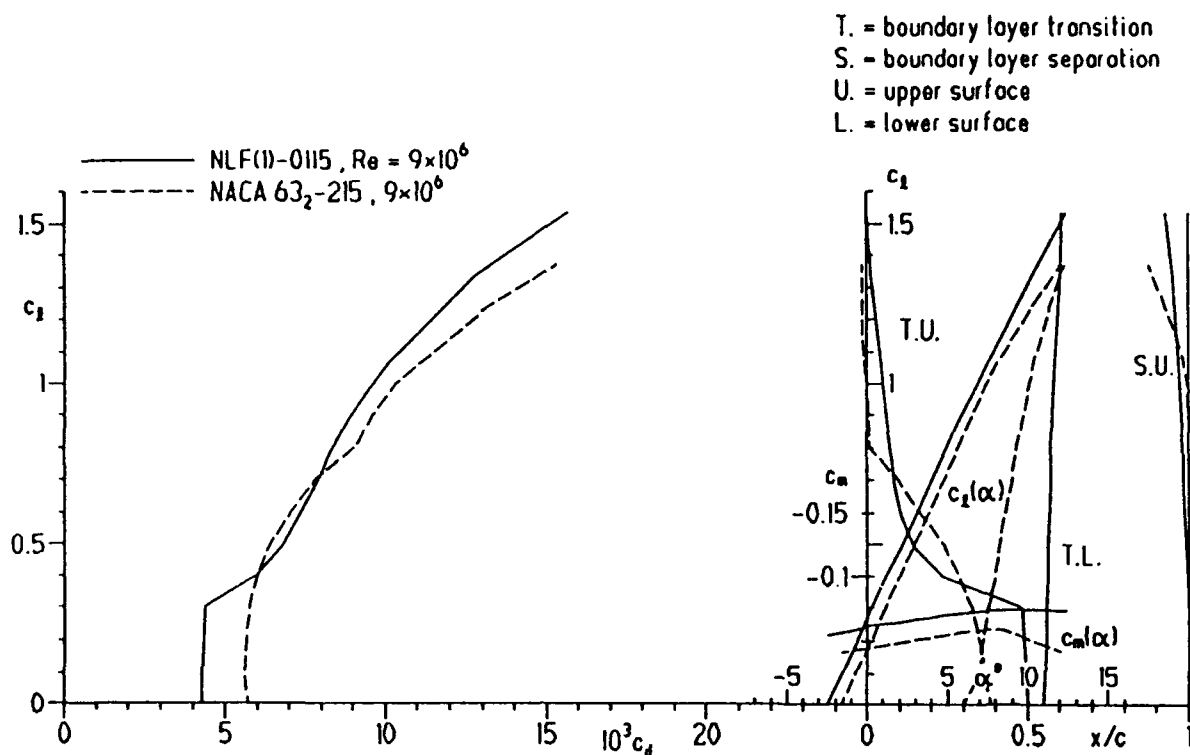


Figure 6. Comparison of the NASA NLF(1)-0115 and NACA 632-215 theoretical airfoil characteristics for $R = 9 \times 10^6$.

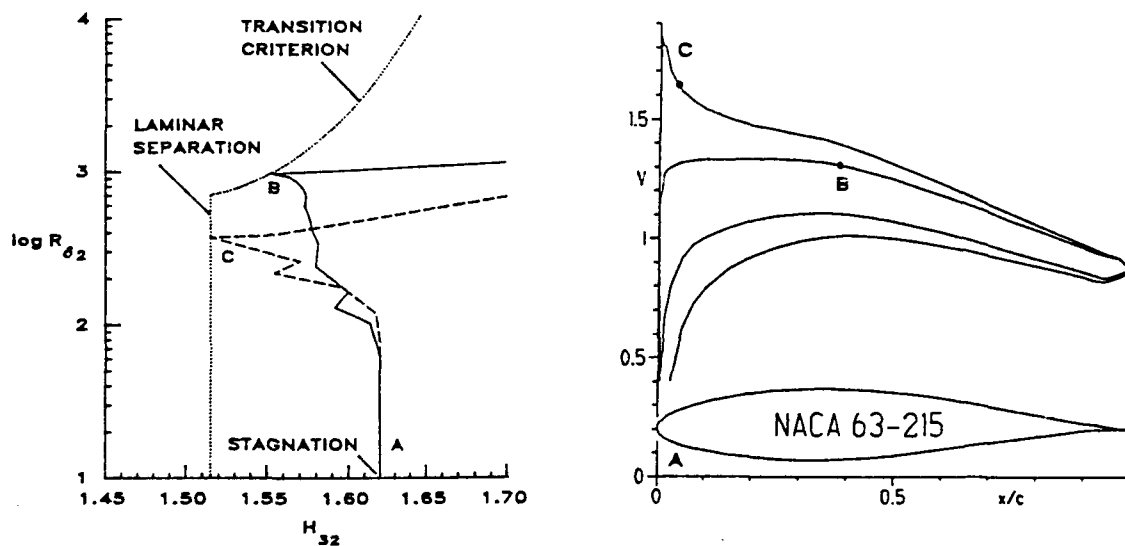


Figure 7. Theoretical boundary-layer development for the NACA 632-215 airfoil lower surface at $c_l = 0.4$ (solid-line) and 0.8 (dotted-line) for $R = 4 \times 10^6$.

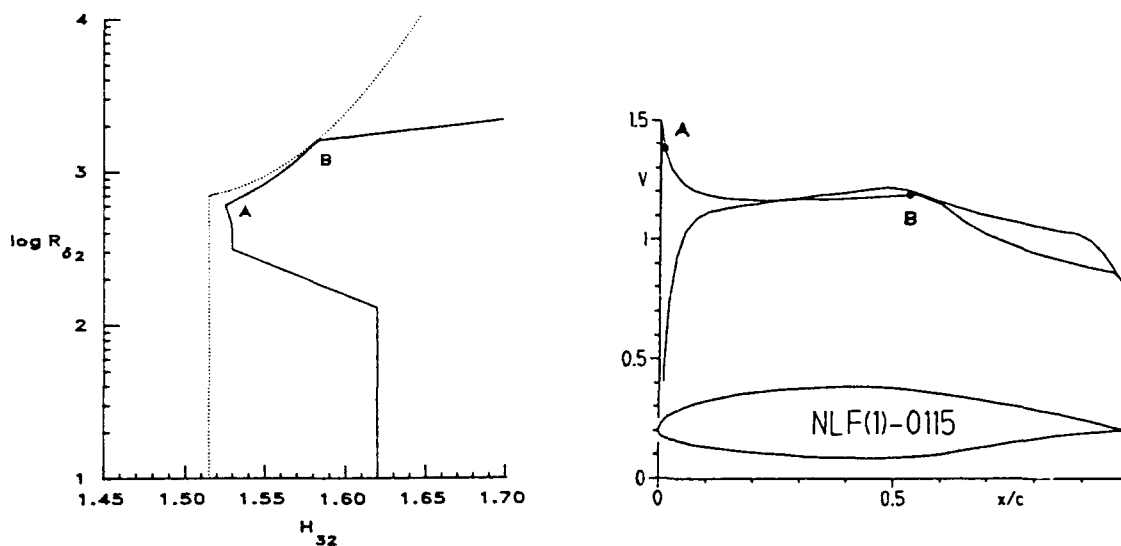


Figure 8. Theoretical boundary-layer development for the NASA NLF(1)-0115 airfoil lower surface at $c_l = 0$ and $R = 9 \times 10^6$.

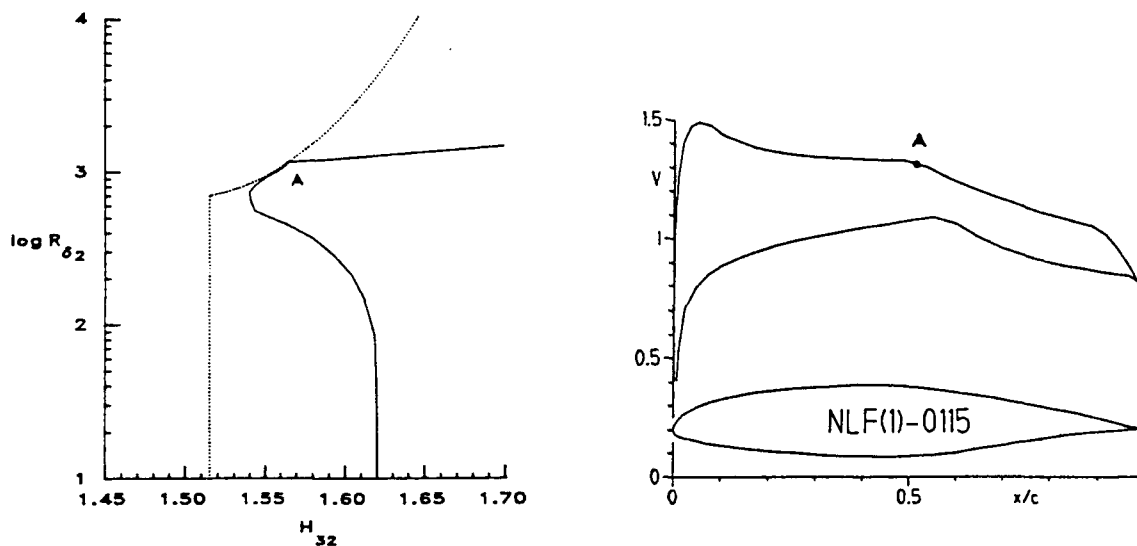


Figure 9. Theoretical boundary-layer development for the NASA NLF(1)-0115 airfoil upper surface at $c_l = 0.4$ and $R = 4 \times 10^6$.

**AERODYNAMIC TRANSPORT EFFICIENCY OF GENERAL AVIATION:
AN OVERVIEW**

by

Fabio R. Goldschmied
Consulting Engineer
1782 McClure Road
Monroeville, PA 15146-2027

For presentation to the AIAA/FAA Joint Symposium on General
Aviation Systems at the Port O-Call Inn, Ocean City, NJ
on April 12, 1990

AERODYNAMIC TRANSPORT EFFICIENCY OF GENERAL AVIATION: AN OVERVIEW

Fabio R. Goldschmied*
Consulting Engineer
1782 McClure Road
Monroeville, PA 15146-2027

ABSTRACT

An extensive overview has been carried out on the Aerodynamic Transport Efficiency, as defined by Gabrielli and von Karman, of General Aviation aircraft, using data from many published sources, including the 1988 and 1989 Tri-aviathon races and the 1970 Oshkosh Aircraft Efficiency Contest races. The best result from the races was an efficiency of 6.19 at 91 m/s (204 MPH) for a four-seat aircraft. It was also shown that an efficiency of 14.8 can be achieved with a NASA fuselage/wake-propeller configuration and 12.9 with a Navy fuselage/pressure-thrust configuration of comparable gross weight and speed. On the basis of the Kraus cruise Figure-of-merit, this would mean that new advanced aircraft would have the same merit value as used conventional aircraft, for the same purchase price; thus the buyer would be strongly motivated to buy the new aircraft, revitalizing the General Aviation industry.

INTRODUCTION

PURPOSE

The purpose of this brief preliminary study is to review the current state-of-the-art of General Aviation aerodynamics, focusing on the Aerodynamic Transport Efficiency (ATE), first introduced by Gabrielli and von Karman (1) in 1950, and then to show how it can be doubled by the rational application of extensive NASA (2), (3) and Navy (4), (5), (6) subsonic wind-tunnel test programs on self-propelled fuselages. This means that a given GROSS WEIGHT could be flown at a given SPEED with half the best current POWER or that the GROSS WEIGHT could be doubled for given SPEED and POWER. In terms of General Aviation market rejuvenation, if the Kraus (7) Figure-of-merit formula is used, it can be seen that new advanced aircraft would be as attractive to the buyer as used conventional aircraft, for the same price.

BACKGROUND

In the current phase of sharp deep decline of the General Aviation industry, it is high time for aeronautical engineers to take a serious look at aircraft aerodynamics, to forego tradition and to go back to basics, i.e. the primitive concept of essentially independent DRAG and THRUST. Already in 1865

*Associate Fellow, AIAA. Member, EAA.

Froude (8) believed that the Rankin drag/thrust concept was an anachronism from the days when canal barges were towed by horses; when a force in one medium must be overcome by power input in another medium or more generally, when there is an impedance-matching problem, the drag/thrust concept may have great merit. In steady motion through a single fluid, however, as with aircraft flight, the drag/thrust concept is highly misleading in its apparent simplicity and it invariably results in the adoption of much reduced performance targets. For instance, when a fuselage is said to have a certain drag at a given speed, it is tacitly implied and accepted that its wake's momentum is condemned to useless dissipation, without possible recourse of any kind. It is implied and accepted that the drag can only be balanced by an equal independent thrust, in accordance to the totally inadequate Rankin perception; already in 1957 Cerreta (4) demonstrated in a Navy wind-tunnel that the measured wake-drag of an axisymmetric subsonic body could be reduced by a factor of 25 from a volume drag coeff. $C_{DW} = 0.048$ to $C_{DW} = 0.0018$ by the application of power for boundary-layer control suction (not thrust generation!).

The Aerodynamic Transport Efficiency (ATE) is defined as follows:

$$ATE = \frac{\text{Gross Weight (N)} \times \text{Max. Speed (m/s)}}{\text{Rated Engine Power (w)}}$$

which is equivalent to the definition below:

$$ATE = \frac{\text{Lift}}{\text{Drag}} \times \text{Propulsive Propeller Efficiency}$$

The computed value of ATE will be the same if lbf, ft/sec and ft lb/sec units are used.

GABRIELLI - VON KARMAN (1) LIMIT TABULATION

SPEED		ATE
m/s	(MPH)	
40	(89.4)	62.5
60	(134.2)	43.5
80	(178.9)	33.5
100	(223.0)	26.5
120	(268.0)	22.3
140	(313.0)	18.7
160	(358.0)	16.7
180	(402.0)	14.7

The ATE computation for a given aircraft allows its assessment against the Gabrielli-von Karman (1) limit at the same speed, as a measure of its overall aerodynamic efficiency (aerodynamic design quality).

OVERVIEW OF AERODYNAMIC TRANSPORT EFFICIENCY

In order to assess the extent of any proposed improvement, it is necessary first to present an adequate documented overview of the current situation.

Tabulations are given below, presenting the following six parameters:

Aircraft Designation
Number of Seats
Gross Weight kN (lbf)
Rated Engine Power KW (HP)
Maximum Speed m/s (MPH)
Aerodynamic Transport Efficiency ATE

It can be noted here that the Gross Weight is used, rather than the Payload, because this study is focused on AERODYNAMICS: it is the Gross Weight that is carried by the aerodynamic lift.

COMMERCIAL AIRCRAFT

Table 1 presents the data for 60 aircraft which are, or have been supplied by the following seven aircraft manufacturing companies:

- 1) Beech Aircraft Corp.
- 2) Cessna Aircraft Company
- 3) Piper Aircraft Corp.
- 4) DeHaviland Aircraft Company
- 5) Mooney Aircraft Corp.
- 6) Maule Aircraft Corp.
- 7) Taylorcraft Aviation Corp.

The number of seats range from 2 to 22, the gross weight from 7.45 kN (1675 lbf) to 55.62 kN (12,500 lbf), the rated engine power from 80 KW (108 HP) to 970 KW (1300 HP) and the speed from 54 m/s (121 MPH) to 135 m/s (302 MPH). The ATE values range from 4.24 to 7.94 with an average of 6.19; all the data are plotted against speed in Fig. 1. In the figure there is plotted the curve corresponding to 33% of the Gabrielli-von Karman limit because it appears to be the upper boundary of the data points; thus Table 1 may be classified as 33% G-K. The top values occur in the top speed range 100 m/s (220 MPH) to 130 m/s (300 MPH) while the bottom values are at the low speed; on the other hand the G-K plot descends with speed. This means that the aerodynamic design quality of the low-speed aircraft is extremely primitive and needs major updating.

SPORT AIRCRAFT

Data for 21 sport kit aircraft are presented in Table 2; the kits are or have been available to enthusiastic private builders. The number of seats range from 1 to 4, the gross weight from 2.22 kN (500 lbf) to 10.68 kN (2400 lbf), the rated power from 16.4 KW (22 HP) to 223.5 KW (300 HP) and the speed from 49.1 m/s (110 MPH) to 123.3 m/s (276 MPH). The ATE values range from 4.00 to 7.80, with an average of 6.13; Table 1 had 4.24 to 7.94 with an average of 6.19. The agreement between Table 1 data and Table 2 data appear to be good. Table 2 data are plotted in Fig. 2 against speed: it can be seen that all points are on or below the 25% G-K plot. Thus Table 2 may be classified as 25% G-K.

Next is Table 3, where the measured results for 28 aircraft at the annual Triaviathon races are listed for 1988 and 1989, as given by Seeley (9), (10)

TABLE 1. AERODYNAMIC TRANSPORT EFFICIENCY OF COMMERCIAL AIRCRAFT

Aircraft Designation	Seats	Gross Weight		Rated Power		Max. Speed		ATE
		kN	(lbf)	KW	(HP)	m/s	(MPH)	
<u>Beech Aircraft Corp.</u>								
77 Skipper	2	7.45	(1675)	85	(115)	54	(121)	4.68
C-23 Sundowner	4	10.79	(2425)	134	(180)	64	(145)	5.26
C-24R Sierra	4	12.23	(2750)	149	(200)	70	(158)	5.77
76 Duchess C/R	4	17.35	(3900)	268	(360)	85	(191)	5.50
F-33A Bonanza	4-5	15.13	(3400)	212	(285)	88	(198)	6.28
V-35B Bonanza	4-5	15.13	(3400)	212	(285)	88	(198)	6.28
A-36 Bonanza	4-6	16.24	(3650)	223	(300)	94	(212)	6.86
B-55 Baron	4-6	22.69	(5100)	387	(520)	96	(216)	5.63
B-36TC Bonanza	6	17.13	(3850)	223	(300)	102	(230)	7.85
E-55 Baron	4-6	23.58	(5300)	424	(570)	102	(230)	5.62
58 Baron	4-6	24.47	(5500)	447	(600)	106	(239)	5.82
58 P Baron	4-6	27.59	(6200)	484	(650)	114	(256)	6.49
B-60 Duke	4-6	30.14	(6775)	566	(760)	123	(275)	6.52
58 TC Baron	4-6	27.59	(6200)	484	(650)	124	(277)	7.02
<u>Cessna Aircraft Company</u>								
152	2	7.45	(1675)	80	(108)	54	(122)	5.03
172 Skyhawk	4	10.71	(2407)	119	(160)	61	(138)	5.52
172 Cutlass	4	11.38	(2558)	134	(180)	62	(140)	5.29
172 Cutlass RG	4	11.82	(2658)	134	(180)	72	(161)	6.32
182 Skylane	4	13.83	(3110)	171	(230)	72	(163)	5.86
185 Skywagon	6	14.96	(3362)	223	(300)	75	(169)	5.03
206 Stationair 6	6	16.07	(3612)	223	(300)	75	(169)	5.41
207 Stationair 8	8	16.96	(3812)	223	(300)	75	(169)	5.74
182 Skylane RG	4	13.83	(3110)	175	(235)	80	(180)	6.34
Turbo 182 Skylane	4	13.79	(3100)	175	(235)	81	(182)	6.38
T-207 Turbo Stationair	8	16.98	(3816)	230	(310)	82	(185)	6.05
Turbo 182 Skylane RG	4	13.84	(3112)	175	(235)	84	(189)	7.00
T-206 Turbo Stationair	6	16.09	(3616)	230	(310)	86	(192)	5.97
210 Centurion	6	16.96	(3812)	223	(300)	88	(197)	6.65
P-210 Centurion	6	17.87	(4016)	230	(310)	93	(208)	7.16
T-210 Turbo Centurion	6	17.87	(4016)	230	(310)	101	(226)	7.75
T-303 Crusader	6	23.03	(5176)	372	(500)	101	(226)	6.22
402-C Business Liner	6-10	30.63	(6885)	484	(650)	108	(242)	6.81
414 Chancellor	6-8	30.19	(6785)	461	(620)	115	(258)	7.51
340-A	6	26.81	(6025)	461	(620)	118	(264)	6.82
421 Golden Eagle	6-8	33.37	(7500)	558	(750)	124	(277)	7.36
<u>Piper Aircraft Corp.</u>								
PA-38-112 Tomahawk 2	2	7.43	(1670)	83	(112)	56	(127)	5.03
PA-28-161 Warrior 2	4	10.85	(2440)	119	(160)	65	(146)	5.92
PA-28-181 Archer 2	4	11.34	(2550)	134	(180)	66	(149)	5.61
PA-28-236 Dakota	4	13.35	(3000)	175	(235)	73	(165)	5.60
PA-32-301 Saratoga	6	16.02	(3600)	223	(300)	77	(173)	5.52
PA-28 RT-201T Arrow 4	4	13.30	(2990)	149	(200)	88	(198)	7.63
PA-32 R-301T Saratoga	6	16.02	(3600)	223	(300)	91	(204)	6.51
PA-46-310P Malibu	6	18.24	(4100)	231	(310)	93	(209)	7.35
PA-34-220T Seneca 3	6	21.13	(4750)	327	(440)	99	(222)	6.37

TABLE 1 (continued)

PA-31-325 Navajo CR	6	28.92 (6500)	484 (650)	113 (253)	6.72
PA-31-350 Chieftain	10	31.15 (7000)	521 (700)	114 (255)	6.78
PA-31P-350 Mojave	7	32.04 (7200)	521 (700)	120 (269)	7.35
PA-60-602P Aerostar	6	26.70 (6000)	432 (580)	127 (284)	7.81
PA-60-700P Aerostar	6	28.10 (6315)	521 (700)	135 (302)	7.24
<u>DeHaviland Aircraft Company</u>					
DHC-1 Chipmunk	2	8.45 (1900)	104 (140)	62 (140)	5.08
DHC-3 Otter	12	35.60 (8000)	447 (600)	71 (160)	5.70
DHC-2 Beaver	7	20.02 (4500)	335 (450)	80 (179)	4.78
DHC-6 Twin Otter	22	55.62 (12500)	971 (1304)	93 (208)	5.33
<u>Mooney Aircraft Corp.</u>					
M20J 201	4	12.19 (2740)	149 (200)	90 (201)	7.32
M20K 231	4	12.90 (2900)	167 (225)	103 (231)	7.94
<u>Maule Aircraft Corp.</u>					
M6-235	4	11.12 (2500)	175 (235)	67 (150)	4.24
M5-180C	4	10.68 (2400)	134 (180)	70 (156)	5.53
M5-235C	4	11.12 (2500)	175 (235)	77 (172)	4.86
M5-210TC	4	11.12 (2500)	156 (210)	87 (196)	6.20
<u>Taylorcraft Aviation Corp.</u>					
F21B Taylorcraft	2	7.78 (1750)	83 (112)	55.8 (125)	5.22

NOTE: Weights, powers and speeds quoted from Aviation Week & Space Technology, March 12, 1984 and from AIAA Studies Series, "A Case Study on the DeHaviland Family of STOL Aircraft," by R. D. Hiscocks. Taylorcraft data quoted from manufacturer's specifications.

in the September 1988 and 1989 issues of Sport Aviation, the monthly publication of the Experimental Aircraft Association. The gross aircraft weight is measured before takeoff and the maximum speed is measured at 1830 m (6000 ft), while the power is the rated engine power. The seats ranged from 2 to 4, the gross weight from 5.03 kN (1132 lbf) to 12.50 kN (2811 lbf), the power from 67 KW (90 HP) to 223 KW (300 HP) and the speed from 52.7 m/s (118 MPH) to 132.2 m/s (295 MPH). The ATE values ranged from 3.50 to 6.19, with an average of 4.61; it can be noted that these measured values are considerably below those of Tables 1 and 2. The data are plotted in Fig. 2, with the data of Table 2 for comparison. The best aircraft is the Turbo Arrow Piper, with 4 seats, a gross weight of 10.11 kN (2272 lbf), a power rating of 149 KW (200 HP), a speed of 91.2 m/s (204 MPH) and ATE = 6.19.

At this point, it is extremely cogent to assess the aerodynamic progress in General Aviation over the past 20 years: Table 4 lists the measured results of 29 aircraft at the 1970 Oshkosh Aircraft Efficiency Contest races, as given by Borst (11) in the July 1971 issue of Sport Aviation. It can be recalled that the 1970's were boom years for the aviation industry, with sales peaking at 17,500 aircraft in 1978. As in the Triaviathon, the aircraft takeoff weight was measured and the max. speed was recorded. The number of seats ranged from 1 to 2, the gross weight from 2.46 kN (553 lbf) to 7.97 kN (1792 lbf), the power from 31 KW (42 HP) to 167 KW (225 HP) and the speed from 40.4 m/s (90.5 MPH) to 83.5 m/s (187 MPH); the ATE values ranged from 2.99 to 5.80 with an average of 4.08. Table 3 ATE values ranged from 3.50 to 6.19

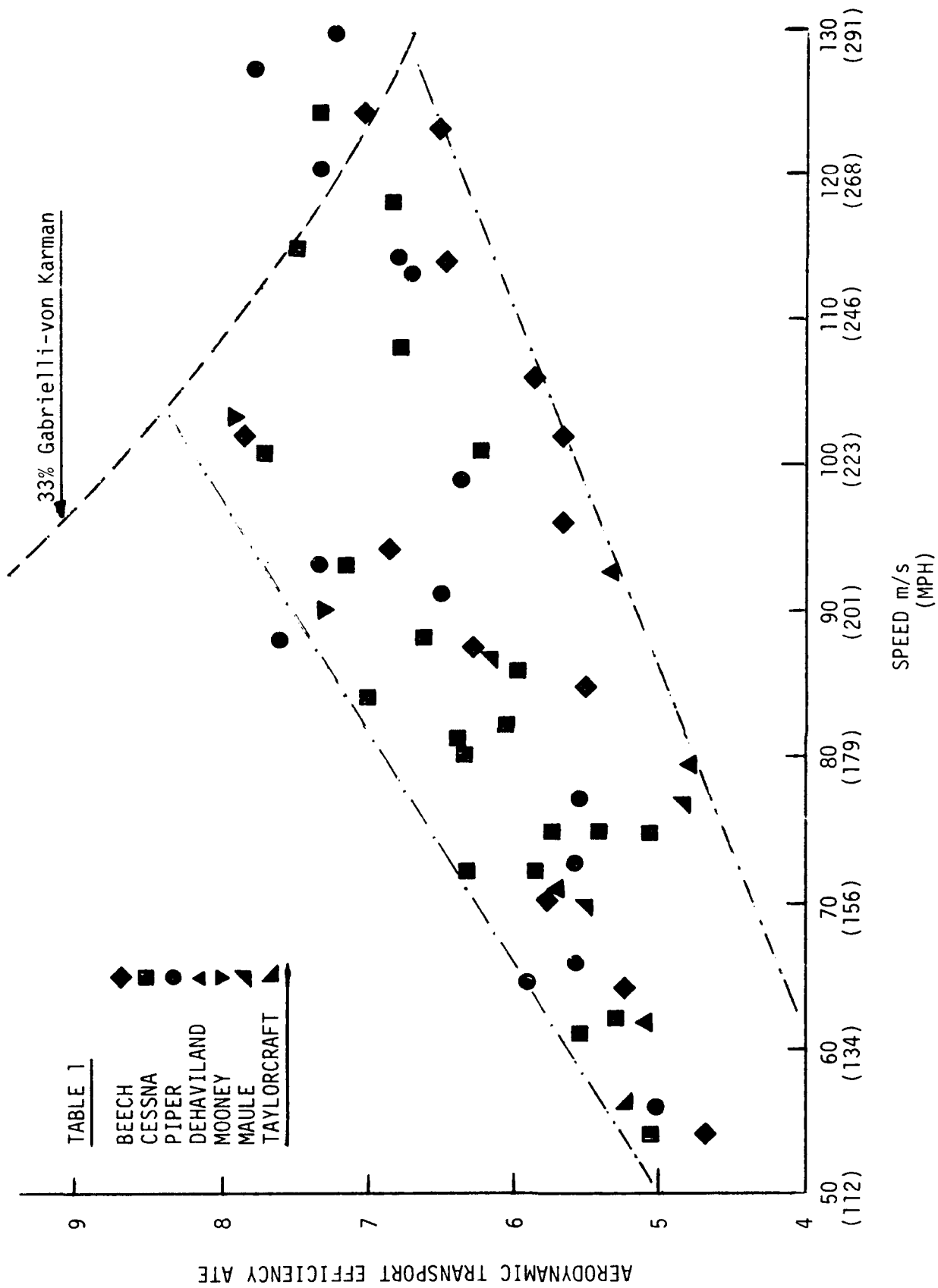


FIGURE 1. AERODYNAMIC TRANSPORT EFFICIENCY OF COMMERCIAL AIRCRAFT (TABLE 1).

TABLE 2. AERODYNAMIC TRANSPORT EFFICIENCY OF SPORT AIRCRAFT

Aircraft Designation	Ref.	Seats	Gross Weight		Rated Power		Max. Speed		A/E
			kN	(lbf)	KW	(HP)	m/s	(MPH)	
Sparrow Hawk Mk. II	14	2	4.45	(1000)	37.2	(50)	49.1	(110)	5.86
Moni Tri-gear	7	1	2.49	(560)	16.4	(22)	51.4	(115)	7.80
Moni	6	1	2.22	(500)	16.4	(22)	53.6	(120)	7.27
Star-Lite	10	1	2.22	(500)	29.8	(40)	53.6	(120)	4.00
Silhouette	11	1	3.11	(700)	32.7	(44)	53.6	(120)	5.09
Windex 1100	5	1	2.25	(506)	16.4	(22)	55.8	(125)	7.66
Laminar Magic	20	1	2.51	(575)	22.3	(30)	56.6	(126.7)	6.38
Pulsar	19	2	3.87	(870)	47.6	(64)	58.1	(130)	4.72
Taylor Mini-1 mp	1	1	3.56	(800)	44.7	(60)	67.0	(150)	5.33
Taylor Bullet	2	2	7.34	(1650)	74.5	(100)	67.0	(150)	6.60
Whitehawk-65	16	2	4.22	(950)	134.1	(180)	70.1	(157)	6.12
Whitehawk-100	17	2	5.56	(1250)	59.6	(80)	81.3	(182)	6.06
Prescott Pusher	8	4	10.68	(2400)	87.9	(118)	82.2	(184)	6.50
KR-2	21	1	3.55	(798)	119.2	(160)	83.1	(186)	4.95
Cozy	15	2	6.67	(1500)	119.2	(160)	83.5	(187)	6.80
RV-6A	18	2	7.12	(1600)	74.5	(100)	88.9	(199)	5.32
Falco	4	2	8.04	(1808)	119.2	(160)	94.7	(212)	6.38
Lancair 200	12	2	5.67	(1275)	74.5	(100)	95.2	(213)	7.24
Whisper	9	2	8.01	(1800)	119.2	(160)	100.5	(225)	6.75
Glasair FT-180	13	2	7.56	(1700)	134.1	(180)	107.2	(240)	6.04
Swearingen SX-300	3	2	10.68	(2400)	223.5	(300)	123.3	(276)	5.88

NOTE: Sport Aviation: (1) August 1984; (9) March 1986; (10) April 1986; (11) March 1985; (12) April 1985; (13) August 1985; (14) June 1985; (18) November 1988; (19) July 1988; (20) January 1990; (21) January 1988. Homebuilt Aircraft: (2) May 1986; (3) October 1985; (4) August 1985; (8) May 1986; (15) April 1986. Builder's Specifications: (5), (6), (7), (16), (17).

with an average of 4.61: the best 1989 ATE value is 6.7% higher than the corresponding 1970 value. It seems clear that we had 20 years of aerodynamic stagnation which caused the present decline of General Aviation. The data of Table 4 are plotted in Fig. 2, with those of Tables 2 and 3, against speed.

MILITARY AIRCRAFT AND ADVANCED DESIGNS

As a conclusion of this overview of Aerodynamic Transport Efficiency, the data of three military aircraft are given in Table 5 as a possibly useful reference. The Northrop XB-35 Flying Wing achieved 96% of the Gabrielli-von Karman limiting value, i.e. 14.65 as against 15.2 in 1946; it was scrapped and destroyed in 1949.

It may be interesting to add that a new thick-wing span-loader cargo aircraft design has been proposed by Goldschmied (12) with the 31.5% thick GLAS II suction boundary-layer control airfoil. The gross weight is 356.00 kN (80,000 lbf), the power is 1788 KW (2400 HP) and the speed is 112 m/s (250 MPH). The ATE value is 22.3 or 95% of the Gabrielli-von Karman limit, in excellent

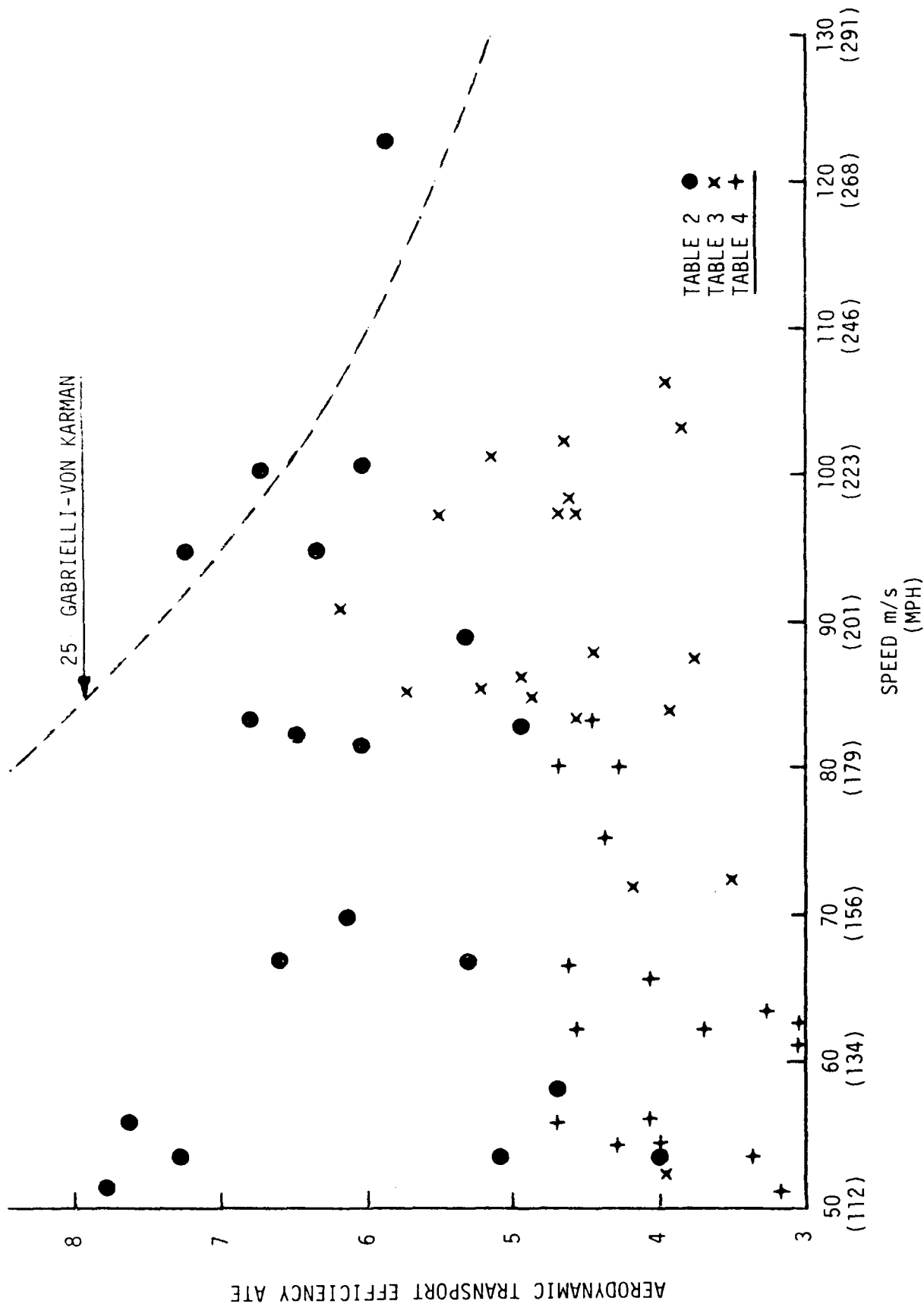


FIGURE 2. AERODYNAMIC TRANSPORT EFFICIENCY OF SPORT AIRCRAFT (TABLES 2, 3, 4).

TABLE 3. AERODYNAMIC TRANSPORT EFFICIENCY: TEST RESULTS
OF 1988 AND 1989 TRIAVIATHON RACES

Aircraft Designation	Seats	Gross Weight		Rated Power		Max. Speed		ATE
		kN	(lbf)	KW	(HP)	m/s	(MPH)	
Encoupe 415D	2	5.03	(1132)	67	(90)	52.7	(118)	3.97
Cessna C177	4	7.79	(1752)	134	(180)	71.8	(160.6)	4.18
Cherokee 235	4	8.42	(1893)	175	(235)	72.6	(162.5)	3.50
Grumman AA5B	4	7.56	(1700)	134	(180)	77.5	(173.4)	4.38
Trinidad TB-20	4	9.81	(2206)	186	(250)	81.9	(183.2)	4.32
Comanche 250	4	10.21	(2296)	186	(250)	83.3	(186.5)	4.58
RV-6	2	5.55	(1249)	119	(160)	84.1	(188.2)	3.93
Mooney M20E	4	8.59	(1931)	149	(200)	84.9	(190.1)	4.90
V-35 Bonanza	6	10.82	(2433)	212	(285)	85.1	(190.5)	4.35
Turbo Arrow Piper	4	9.99	(2245)	149	(200)	85.6	(191.5)	5.74
RV-4	2	5.54	(1247)	119	(160)	85.5	(191.3)	3.98
Mooney M20E	4	9.12	(2051)	149	(200)	85.6	(191.6)	5.25
Mooney M20C	4	8.55	(1922)	149	(200)	86.6	(193.8)	4.97
RV-4	2	5.76	(1296)	134	(180)	87.5	(195.9)	3.77
V-35 Bonanza	6	10.72	(2410)	212	(285)	87.8	(196.5)	4.45
Cessna 210	6	11.10	(2496)	212	(285)	89.7	(200.7)	4.70
Turbo Arrow Piper	4	10.11	(2272)	149	(200)	91.2	(204.0)	6.19
Cessna T210N	6	12.50	(2811)	223	(300)	95.2	(213.1)	5.34
Siai Marchetti SF260	4	9.10	(2045)	193	(260)	97.3	(217.8)	4.58
Glasair Ft	2	6.50	(1461)	134	(180)	97.1	(217.4)	4.72
Glasair RG	2	6.74	(1516)	119	(160)	97.3	(217.8)	5.52
Siai Marchetti SF260	4	9.08	(2041)	193	(260)	98.5	(220.4)	4.62
Glasair RG	2	6.78	(1524)	134	(180)	101.7	(227.6)	5.15
Glasair RG	2	6.75	(1519)	149	(200)	102.5	(229.3)	4.65
Super BD-4	2	8.27	(1860)	223	(300)	103.4	(231.4)	3.83
Super BD-4	2	8.30	(1867)	223	(300)	106.2	(237.7)	3.95
Glasair III	2	9.83	(2209)	223	(300)	118.3	(264.7)	5.21
Venture Questair	2	7.07	(1590)	208	(280)	132.2	(295.8)	4.49

NOTE: Weights, powers and speeds are quoted from Refs. 9 and 10 (Sport Aviation, September 1988 and September 1989).

agreement with the XB-35 rating. A comprehensive review of the GLAS II airfoil flight test data in Australia has been provided by Goldschmied, (13) focusing on the static-pressure thrust on the airfoil. Finally, the very extensive advanced work carried out at the NASA Langley Research Center must be considered for this overview: Holmes and Croom (14) performed an aerodynamic optimization program for a 6-seat single-engine 154 m/s (300 kN) aircraft. A current-technology design (designated 810625-A) was computed with 22.41 kN (5036 lbf) gross weight and 339 KW (456 HP) power, yielding ATE = 10.1; an advanced-technology design (designated 810625-B), maximizing laminar flow over wing and fuselage, was computed with 17.40 kN (3910 lbf) gross weight and 211 KW (284 HP), yielding ATE = 12.6, for a 24% improvement. It is also interesting to note that the 810625-A configuration reaches 59% of the Gabrielli-von Karman limit, while the 810625-B configuration reaches 73%, well below the XB-35.

TABLE 4. AERODYNAMIC TRANSPORT EFFICIENCY: TEST RESULTS
OF 1970 OSHKOSH AIRCRAFT EFFICIENCY CONTEST

Aircraft Designation	Seats	Gross Weight		Rated Power		Max. Speed		ATE
		kN	(lbf)	KW	(HP)	m/s	(MPH)	
Mod-Cub	1	4.29	(966)	48	(65)	40.4	(90.5)	3.60
Taylorcraft	2	4.73	(1064)	48	(65)	41.0	(91.7)	4.01
Flybaby	1	4.05	(912)	48	(65)	42.5	(95.2)	3.57
Jeanie Teeny	1	2.46	(553)	31	(42)	48.6	(108.8)	3.83
Sky Hopper	1	4.33	(973)	48	(65)	51.7	(115.8)	4.63
Taylor	1	3.52	(792)	31	(42)	51.5	(115.2)	5.80
Sky Coupe	2	5.63	(1266)	93	(125)	51.8	(116.0)	3.14
Playmate	2	5.78	(1299)	93	(125)	53.7	(120.2)	3.34
Pipit	1	4.33	(975)	59	(80)	54.4	(121.8)	3.97
Mooney Mite	1	3.79	(852)	48	(65)	54.5	(122.0)	4.27
Cliff	1	4.03	(907)	48	(65)	56.2	(125.7)	4.69
VS-1	2	5.35	(1203)	63	(85)	57.2	(128.0)	4.84
Lark	1	3.92	(883)	56	(75)	57.6	(129.0)	4.06
Davis	2	4.48	(1008)	63	(85)	58.8	(131.7)	4.17
Tailwind	2	5.67	(1275)	80	(108)	59.0	(132.0)	4.16
PL-2	2	6.45	(1450)	93	(125)	60.7	(135.8)	4.21
Star Duster	1	4.49	(1011)	93	(125)	61.7	(138.2)	2.99
Elchiporosa	1	2.84	(640)	48	(65)	62.2	(139.2)	3.66
Daphne	2	4.64	(1043)	63	(85)	62.5	(139.8)	4.58
PJ 260	2	7.97	(1792)	167	(225)	63.3	(141.7)	3.01
Tailwind	2	4.76	(1070)	93	(125)	63.8	(142.7)	3.26
Tailwind	2	4.53	(1018)	74	(100)	65.9	(147.6)	4.02
Tailwind	1	4.34	(976)	63	(85)	67.0	(150.0)	4.60
Swift	2	7.12	(1602)	108	(145)	69.0	(154.5)	4.56
T-18	2	5.58	(1254)	111	(150)	71.9	(161.0)	3.60
Skeeter	2	5.38	(1211)	93	(125)	75.4	(168.8)	4.37
Mustang II	2	6.31	(1420)	119	(160)	80.4	(179.9)	4.27
Sidewinder	2	5.42	(1219)	93	(125)	80.5	(180.1)	4.69
T-18	2	5.38	(1211)	100	(135)	83.5	(187.0)	4.48

NOTE: Weights, powers and speeds are quoted from Ref. 11 (Sport Aviation, July 1971).

NASA FUSELAGE/WAKE-PROPELLER CONFIGURATION

In 1962 an extensive wind-tunnel test program was carried out by McLemore (2) at the NASA Langley Research Center with an axisymmetric self-propelled body of 1.290 m (50.8") diameter and 6.248 m (246") length, corresponding to a full-scale 4-seat fuselage, at the speed of 44.7 m/s (100 MPH). The main research objective was to demonstrate the propulsive efficiency of true stern wake-propellers with streamlined bodies; the body's wake was first carefully measured and then a stern pusher propeller was designed to the measured wake velocity profile. The propeller diameter was 0.609 m (24") with four blades; the propeller speed ranged from 5200 to 8300 RPM and it produced up to 225N (50 lbs) net thrust beyond fuselage self-propulsion. Since this research program was labeled "Airships," it was ignored by the General Aviation industry. To the

TABLE 5. AERODYNAMIC TRANSPORT EFFICIENCY OF MILITARY AIRCRAFT

Aircraft Designation	Ref.	Gross Weight		Rated Power		Max. Power		ATE
		kN	(lbf)	KW	(HP)	m/s	(MPH)	
Grumman F7F-3 Navy Fighter/Bomber	1	114.36	(25,700)	3129	(4,200)	194	(435)	7.11
B-24J Liberator Air Force Bomber	2	289.25	(65,000)	3576	(4,800)	129	(290)	10.50
Northrop XB-35 Air Force Bomber	3,4	784.04	(168,100)	8940	(12,000)	175	(391)	14.65

NOTE: (1) Sport Aviation, October 1986; (2) Sport Aviation, January 1990;
(3) Maloney (15); (4) Woolridge (16).

author's knowledge, there has been no other wind-tunnel test of self-propelled fuselages with wake propellers; it must be made clear that stern pusher propellers are not necessarily wake-adapted, just because of their location. Finally in 1986 Goldschmied (3) carried out a preliminary design study on the application of the NASA full-scale experimental results to General Aviation aircraft. It can be noted that no mention was made in the 1986 AIAA General Aviation Technical Committee Annual Report, although the paper of Ref. 3 was presented at the AIAA Aircraft Systems, Design and Technology Meeting.

Table 6 presents a partial summary of the computed design results, to be compared to those of Tables 3 and 4. It can be seen that the 1.397 m (55") diameter fuselage offers ample seating volume for four and the 10.68 kN (2400 lbf) gross weight is quite realistic. At the speed of 80 m/s (180 MPH) the ATE value of 14.8 outstrips the best measured 6.19 value from Table 3 by a factor of 2.39. The propeller would have a 0.660 m (26") diameter, 8 blades and 7000 RPM (direct drive from a rotary engine). The data of Table 6 are plotted in Fig. 3 against speed, together with the measured data of Tables 3 and 4; the 50% Gabrielli-von Karman line and the 25% line are also shown for convenient reference.

NAVY FUSELAGE/PRESSURE-THRUST CONFIGURATION

The U.S. Navy has carried out extensive wind-tunnel test programs at the David Taylor Research Center in 1957, as reported by Cerreta (4) and then in 1982, as reported by Goldschmied (5), (17) on subsonic axisymmetric self-propelled bodies. The test model, used in 1957 and modified in 1982, had 0.508 m (20") diameter and 1.475 m (58.8") length, with a fineness ratio of 2.9, and was tested at speeds up to 111 m/s (250 MPH); thus it was one-third scale and full speed for General Aviation fuselage application. The propulsion force to this body, to overcome the skin-friction drag, was not supplied by air momentum enhancement, i.e., propellers, but the novel concept of static-pressure thrust on the body itself. It can only be achieved by effecting a stepwise pressure-recovery well aft on the body, i.e., 80% to 90% length by the rational combination of body shape and suction-slot boundary-layer control. Considerable pumping power is required to bring the suction flow back to free-stream's total-pressure; the wake-drag, however,

TABLE 6. AERODYNAMIC TRANSPORT EFFICIENCY OF NASA
FUSELAGE/WAKE-PROPELLER AIRCRAFT

Aircraft Designation	Fuselage Diameter		Gross Weight		Power		Speed		ATE
	m	(in.)	kN	(lbf)	KW	(HP)	m/s	(MPH)	
86-2693-I	1.066	(42)	5.34	(1200)	19.0	(25.2)	62.5	140	17.7
-II	1.219	(48)	6.23	(1400)	22.5	(30.3)	62.5	140	17.2
-III	1.397	(55)	10.68	(2400)	36.8	(49.5)	62.5	140	17.9
-IV	1.651	(65)	14.24	(3200)	50.0	(67.2)	62.5	140	17.7
-I	1.066	(42)	5.34	(1200)	31.3	(42.0)	80.4	180	13.6
-II	1.219	(48)	6.23	(1400)	37.9	(50.9)	80.4	180	13.1
-III	1.397	(55)	10.68	(2400)	60.1	(80.7)	80.4	180	14.2
-IV	1.651	(65)	14.24	(3200)	80.8	(108.5)	80.4	180	14.1
86-2693-V	1.066	(42)	5.34	(1200)	20.9	(28.1)	62.5	140	15.8
-VI	1.219	(48)	6.23	(1400)	25.2	(33.8)	62.5	140	15.4
-VII	1.397	(55)	10.68	(2400)	41.3	(55.5)	62.5	140	16.1
-VIII	1.651	(65)	14.24	(3200)	55.5	(74.6)	62.5	140	16.0
-V	1.066	(42)	5.34	(1200)	30.3	(40.8)	80.4	180	14.0
-VI	1.219	(48)	6.23	(1400)	37.1	(49.8)	80.4	180	13.4
-VII	1.397	(55)	10.68	(2400)	57.8	(77.7)	80.4	180	14.8
-VIII	1.651	(65)	14.24	(3200)	78.4	(105.3)	80.4	180	14.5

TABLE 7. AERODYNAMIC TRANSPORT EFFICIENCY OF NAVY
FUSELAGE/PRESSURE-THRUST AIRCRAFT

Aircraft Designation	Fuselage Diameter		Gross Weight		Power		Speed		ATE
	m	(in.)	kN	(lbf)	KW	(HP)	m/s	(MPH)	
84-2163-I	1.143	(45)	6.23	(1400)	44.7	(60)	89.4	(200)	12.1
-II	1.143	(45)	7.45	(1675)	50.6	(68)	89.4	(200)	13.0
-III	1.143	(45)	8.01	(1800)	52.8	(71)	89.4	(200)	13.3
-IV	1.524	(60)	11.12	(2500)	81.9	(110)	89.4	(200)	12.8
-V	1.524	(60)	12.90	(2900)	89.4	(120)	89.4	(200)	12.9
-VI	1.524	(60)	15.13	(3400)	98.3	(132)	89.4	(200)	13.7

is practically zero. The suction flow is discharged axially through a nozzle: the experimental total-pressure was carefully measured at the nozzle's outlet and was shown by Goldschmied (18) to be equal to free-stream's, with zero "momentum thrust." Also the same author (19) carried out the radial integration of the experimental body pressures to show directly that the pressure thrust does indeed occur.

In 1984 a preliminary design study was carried out by Goldschmied (6) for the application of the Navy self-propelled fuselage to General Aviation aircraft. It can be noted that no mention was made in the 1984 AIAA General Aviation

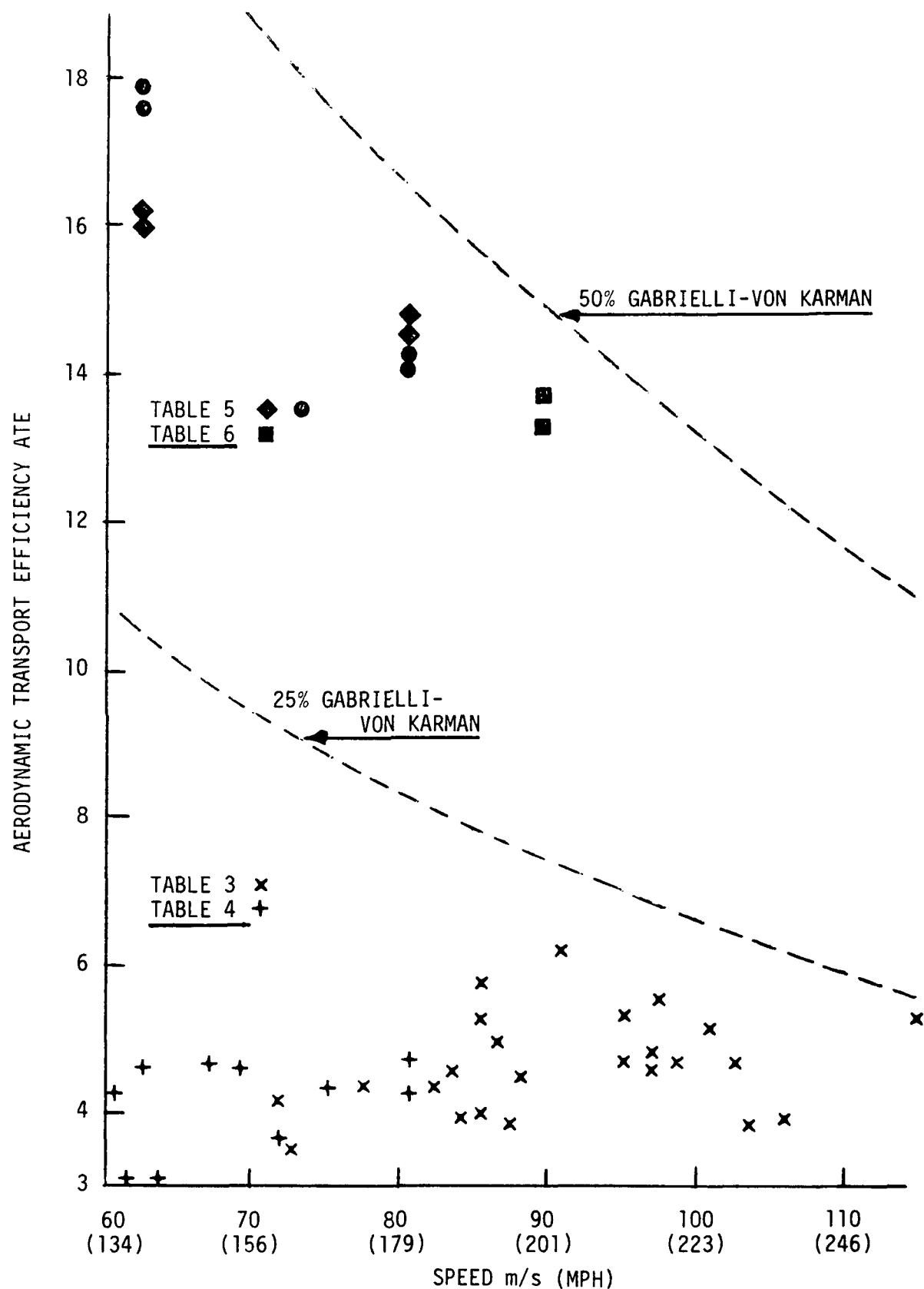


FIGURE 3. AERODYNAMIC TRANSPORT EFFICIENCY OF SELF-PROPELLED FUSELAGE CONFIGURATIONS (TABLES 5 AND 6).

Technical Committee Annual Report, although the paper of Ref. 6 was presented at the AIAA Applied Aerodynamics Conference. Table 8 gives a summary of the computed results for 2-seat, 1.143 m (45") diameter and 4-seat, 1.524 m (60") diameter fuselages at the speed of 89.4 m/s (200 MPH), to be compared to the data of Tables 3 and 4. A value of 13.7 is reached for ATE, to be compared to the best 6.19 of Table 3, for a factor of 2.21. The computed data are shown in Fig. 3.

OVERALL REVIEW

An overall review of the Aerodynamic Transport Efficiency against aircraft speed can be achieved by consideration of Fig. 4 for the complete speed range from 70 m/s (156 MPH) to 180 m/s (400 MPH). On the one hand, the Gabrielli-von Karman limit plot can be observed, with the two points for the XB-35 and the 90-3198 thick-wing span loader design (12) above the 90% line, and on the other hand the 50% plot can be seen, with the concomitant points for the 86-2693, the 84-2163, the B-24J and the 810625-A. The advanced optimized design of Holmes and Croom (14) lies on the 75% plot. None of the points from Tables 1, 2, 3 and 4 can be shown in Fig. 4 because they are all well below the ATE = 10 level. A conclusion can be reached that it would be very helpful to classify the aerodynamic design quality of General Aviation aircraft by their ATE percentages as against the corresponding Gabrielli-von Karman value. From the evidence of Fig. 4 it would seem that the 50% level represents the acceptable minimum goal of aerodynamic design, while 90% can be reached only with flying wing configurations.

REVITALIZING GENERAL AVIATION

There is no disagreement that the General Aviation industry is moribund; the question is how it can be revitalized to a viable level of activity through technological improvements. The 1987 AIAA General Aviation Technical Committee Annual Report (Aerospace America, Dec. 1987) reaches high in the sky to the birds to disclose their secret of flight and deep in the sea to the fish to reveal their secret of propulsion. Steugel (20) states that it is time to reinvent the General Aviation aircraft and that it is the opportunity, if not the imperative, of the aeronautical engineering profession to do so. DeMeis (21) also writes about innovation in a generalized manner. Carson (22) gives a thorough and comprehensive review study of the fuel efficiency of small aircraft, with a very good discussion of the Gabrielli-von Karman criterion for limiting performance. However, it is only the excellent work of Kraus (7) that provides the quantitative means to recognize the technical improvement levels needed to make a difference. The difference can be defined as follows: it is the decision of an aircraft buyer, with a given amount of money to spend, to purchase a used aircraft or a new aircraft. The decision is assumed to be based on the relative Figure-of-merit of the two aircraft available at the same price. Kraus (7) has introduced a formula for the computation of a cruise Figure-of-merit F , which is based on his trade studies and marketing analysis at the Cessna Aircraft Company, to reflect the value a customer places on the several parameters for high-performance single-engine 4-6 seat aircraft. The formula does not apply to 2-seat aircraft.

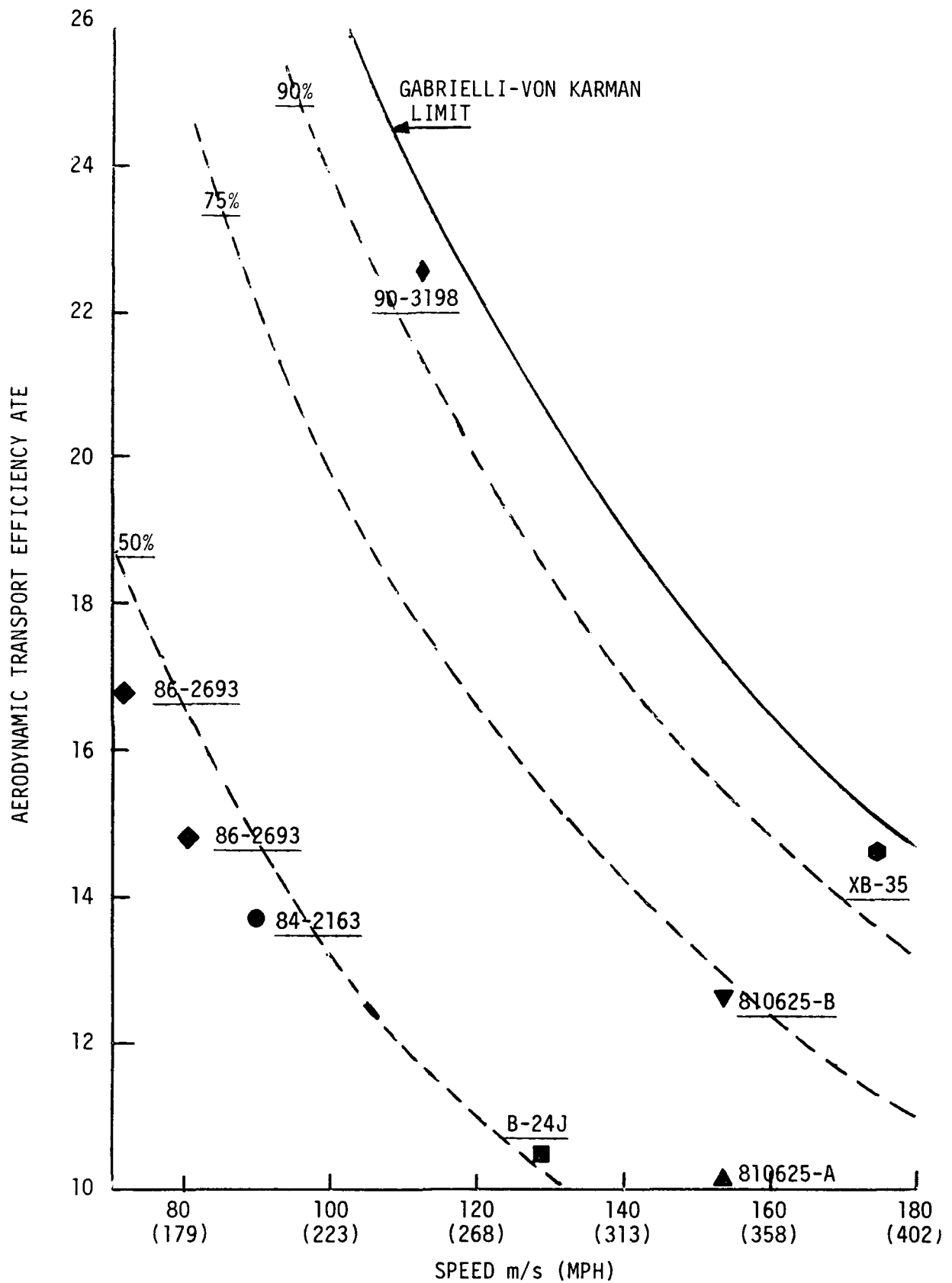


FIGURE 4. OVERVIEW OF AERODYNAMIC TRANSPORT EFFICIENCY VS. SPEED.

$$F = (P)(R)^{0.5} (V)(Q)^{0.5} (S)^{0.3} \times 10^{-7}$$

where P = Payload, lbf
 R = Range at full payload at cruise speed, NM
 V = Cruise speed, kn
 Q = Cabin volume, ft³
 S = Specific Range at cruise speed, NM/lbf.

Kraus (7) presents the 1987 situation in his Fig. 19, which is reproduced below as Fig. 5.

Considering the \$200,000 price, it can be seen that the new aircraft has F = 5 while the used aircraft has F = 11, i.e. the same \$200,000 delivers in the used market a purchase twice as attractive. This is why the General Aviation industry is in its moribund condition. Kraus (7) presents Level 1 technology improvements to F = 6 and Level 2 improvements to F = 7; both the levels are clearly inadequate to make the difference as defined above. Quoting Kraus (7): "Level 1 involves optimum resizing for efficiency, resulting in higher aspect-ratio wings and a better match of engines with air frames ...

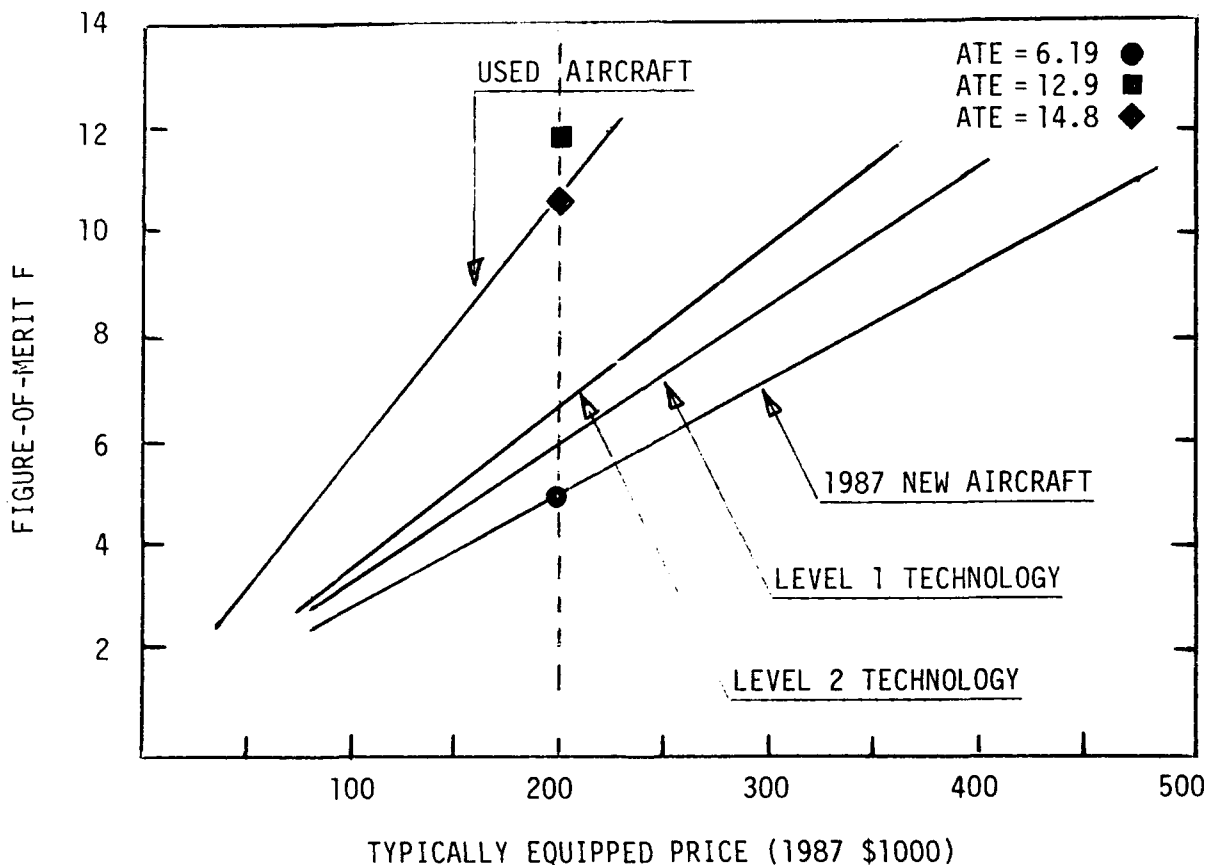


FIGURE 5. VALUE IMPROVEMENTS EXPECTED FROM ADVANCED TECHNOLOGIES

The wings are assumed to achieve 30% chord laminar flow. Wing tips are sheared for lower drag. Propulsive efficiencies are improved by partial liquid cooling and installation refinements. Level 2 technologies include Level 1 items plus composite wings with 50% laminar flow and full liquid cooling. Canard surfaces and pusher propellers are not considered."

Now let us use the best from Table 3 as the baseline ($F = 5$) and consider comparable configurations from Tables 6 and 7:

Table 3:	10.11 kN (2272 lbf) 149 KW (200 HP) 91.2 m/s (204 MPH)	<u>ATE = 6.19</u>	<u>F = 5</u>
Table 6:	86-2693-VII AR=8 10.68 kN (2400 lbf) 57.8 KW (77.7 HP) 80.4 m/s (180 MPH)	<u>ATE = 14.8</u>	<u>F = 11.9</u>
Table 7:	84-2163-IV AR=10 11.12 kN (2500 lbf) 81.9 KW (110 HP) 89.4 m/s (200 MPH)	<u>ATE = 12.9</u>	<u>F = 10.4</u>

Assuming that the payload P is linearly proportional to the gross weight, then the 86-2693-VII would achieve $F = 11.9$ and the 84-2163-IV would achieve $F = 10.4$ by the ratio of the ATE values (2.39 and 2.08). Parity is achieved between the Figure-of-merit ratings of the used conventional aircraft and of the new advanced aircraft. The customer would now buy the new aircraft, thus revitalizing the industry.

CONCLUSIONS

An overview has been carried out of the Aerodynamic Transport Efficiency of General Aviation aircraft. It has been shown that the NASA and the Navy self-propelled fuselage configurations would revitalize the General Aviation industry by making new advanced aircraft reach Figure-of-merit parity with used conventional aircraft for the same price and thus motivating buyers to purchase new units.

REFERENCES

1. Gabrielli, G. and von Karman, T., "What Price Speed," Mechanical Engineering, Vol. 72, October 1950.
2. McLemore, H.C., "Wind-Tunnel Tests of a 1/20-Scale Airship Model with Stern Propellers," NASA TND-1026, January 1962.
3. Goldschmied, F.R., "Aerodynamic Design of Low-Speed Aircraft with a NASA Fuselage/Wake-Propeller Configuration," AIAA Paper 86-2603, October 1986.

4. Cerreta, P.A., "Wind-Tunnel Investigation of the Drag of a Proposed Boundary-Layer Controlled Airship," David Taylor Research Center Aero Report 914, 1957.
5. Goldschmied, F.R., "Wind-Tunnel Test of the Modified Goldschmied Model with Propulsion and Empennage: Analysis of Test Results," David Taylor Research Center ASED-CR-02-86, February 1986.
6. Goldschmied, F.R., "On the Aerodynamic Optimization of Mini-RPV and Small General Aviation Aircraft," AIAA Paper 84-2163, August 1984.
7. Kraus, E.F., "Technical Thresholds for Revitalizing General Aviation," AIAA Paper 87-2933, Sept. 1987.
8. Froude, W., "Discussion of Paper by W.J.M. Rankin," Transactions of Institute of Naval Architects, Vol. 6, 1865, pp. 35-37.
9. Seeley, B.A., "1989 CAFE 400 and Triaviathon Technical Discussion," Sport Aviation, September 1989.
10. Seeley, B.A., "1988 CAFE 400 Discussion of Results," Sport Aviation, September 1988.
11. Borst, R., "1970 Oshkosh Aircraft Efficiency Contest," Sport Aviation, July 1971.
12. Goldschmied, F.R., "Thick-Wing Span Loader All-Freighter: Design Concept for Tomorrow's Air Cargo," AIAA Paper 90-3198, Aircraft Design and Operations Meeting, September 1990.
13. Goldschmied, F.R., "Airfoil Static-Pressure Thrust: Flight-Test Verification," AIAA Paper 90-3286, Aircraft Design and Operations Meeting, September 1990.
14. Holmes, B.J. and Croom, C.C., "Aerodynamic Design Data for a Cruise-Matched High Performance Single Engine Airplane," SAE Paper 810625, April 1981.
15. Maloney, E T., "Northrop Flying Wings," World War II Publications, Corona Del Mar, CA, 1988.
16. Wooldridge, E.T., "Winged Wonders: The Story of the Flying Wings," Smithsonian Institution Press, Washington, DC, 1988.
17. Goldschmied, F.R., "Integrated Hull Design, Boundary-Layer Control and Propulsion of Submerged Bodies: Wind-Tunnel Verification," AIAA Paper 82-1204, June 1982.
18. Goldschmied, F.R., "Jet-Propulsion of Subsonic Bodies with Jet Total-Head Equal to Free-Stream's," AIAA Paper 83-1790, July 1983.
19. Goldschmied, F.R., "Fuselage Self-Propulsion by Static-Pressure Thrust: Wind Tunnel Verification," AIAA Paper 87-2935, September 1987.

20. Stengel, R.F., "Time to Reinvent the General Aviation Aircraft," Aerospace America, August 1987, pp. 24-26.
21. DeMeis, R., "Innovation in General Aviation," Aerospace America, August 1989, pp. 30-35.
22. Carson, B.H., "Fuel Efficiency of Small Aircraft," AIAA Paper 80-1847, August 1980, AIAA J. Aircraft, Vol. 19, No. 6, June 1982, pp. 473-479.

GULFSTREAM IV FLIGHT MANAGEMENT SYSTEM

by

Steven C. Runo
Honeywell Inc.
Commercial Flight Systems Group
Business and Commuter Aviation Systems Division
Glendale, Arizona

For presentation to the AIAA/FAA Joint Symposium on General
Aviation Systems at the Port O-Call Inn, Ocean City, NJ
on April 12, 1990

GULFSTREAM IV FLIGHT MANAGEMENT SYSTEM

Steven C. Runo
Honeywell Inc.
Commercial Flight Systems Group
Business and Commuter Aviation Systems Division
Glendale, Arizona

ABSTRACT

In February 1990, the Gulfstream IV (G-IV) received Federal Aviation Administration (FAA) certification of the most advanced flight management system (FMS) available on business aircraft. This certification completed the Honeywell SPZ-8000 Digital Automatic Flight Control System (DAFCS) that is standard on all G-IVs. Vertical guidance, aircraft performance management, and an autothrottle are the primary additions to the previous capabilities of the SPZ-8000.

INTRODUCTION

At an operating weight of over 60,000 pounds, the G-IV is among the largest of the business jets in the General Aviation market (see Figure 1). In many respects, the G-IV more closely resembles commercial airliners. The two Rolls-Royce Tay engines that power the G-IV also power the Fokker 100, a 100-passenger airliner. At 88 feet long and with a wing span of 78 feet, the G-IV is about 85 percent the size of McDonnell-Douglas DC-9 and Boeing 737 airliners. And the G-IV paces the latest airliners with one of the most advanced cockpits flying.

SPZ-8000 DAFCS

The advanced SPZ-8000 DAFCS of the G-IV were developed by the Business and Commuter Aviation Systems Division of Honeywell Inc. The SPZ-8000 is a second-generation glass cockpit that features six large (eight by eight inches) color displays to depict all flight information (see Figure 2). The Primary Flight Displays (PFD) provide altitude, speed, attitude, and heading information in the "standard T." The companion Navigation Displays (ND) present the flight plan and navigation information. Engine Indicating and Crew Advisory System (EICAS) information is presented on two central displays.

The standard G-IV Honeywell SPZ-8000 DAFCS also includes weather radar, fault warning, air data, dual fail-operational Flight Guidance Computers (FGC), dual fail-passive autothrottles, and dual FMS. All of the separate units are integrated with the Avionics Standard Communication Bus (ASCB). The ASCB permits high-speed exchange of data between units connected to the bus (see Figure 3). Integration of the avionics suite is facilitated by each unit having access to all data transmitted by the other units on the bus.

The highly-integrated nature of the SPZ-8000 means operation is consistent, coordinated, and straight-forward. This is demonstrated best in the dual FMS that virtually automate flight from takeoff to touchdown.

HISTORICAL OVERVIEW

The term "Flight Management System" was first popularly applied to the Boeing 757 and 767 airliners. Boeing used FMS to describe the integrated avionics in these first-generation "glass cockpits." Thus, the 757/767 FMS includes flight guidance, fault warning, inertial navigation, and flight management computers (FMC). The Honeywell (formerly Sperry) FMC for the 757 and 767 integrates navigation and performance management functions, and serves as the focal point for the complete FMS.

Sperry pioneered navigation management with the TERN 100. First certified in 1976, the TERN 100 introduced a navaid database and multi-sensor area navigation (RNAV). This commercial system was capable of automatic tuning, and lateral and vertical guidance. Navigation management of this type was also naturally suited to the increasingly sophisticated business jets in the General Aviation market.

Performance management was developed for Boeing 727, 737, and 747 aircraft to conserve fuel as a result of the 1973 Oil Crisis. These systems utilize air data, engine, and aircraft configuration inputs to optimize speed, altitude, and throttle-setting. Optimization is based on sophisticated aircraft and engine models developed by the airframe and engine manufacturers. As a result, performance management has found less General Aviation application than navigation management.

Today's General Aviation navigation management systems interface with a variety of sensors, including IRS, LORAN C, and Global Positioning System (GPS). Navigation databases have grown to include worldwide airways, Standard Instrument Departures (SIDs), Standard Terminal Arrival Routes (STARs), and runways. And the latest systems have ability to optimize the flight laterally and vertically. These capabilities have caused the title "Flight Management System" to be applied to the latest General Aviation navigation management systems.

PHASE II

The G-IV was initially certified in 1987 with the Honeywell NZ-800 Navigation computer as the Flight Management System. The NZ-800 includes full-featured navigation management with limited performance management functions. However, the G-IV specification called for performance management capabilities equal to those on the latest airliners. A full-flight-regime autothrottle was also specified. Neither was available in General Aviation.

A Phase II program was planned to follow the initial G-IV certification. Gulfstream would develop the detailed aircraft performance data required. Simultaneously, Honeywell would design and build the hardware and software for performance management and autothrottle. These powerful new features would integrate directly into the existing and successful SPZ-8000 DAFCS.

Each G-IV was provisioned for dual Honeywell PZ-800 Performance/Autothrottle computers. Servo-clutches for the autothrottle were also installed in each delivered G-IV. Addition of the PZ-800 and software updates to other SPZ-8000 components would complete the G-IV development.

In February 1990, Phase II received FAA certification. The certification effort focused on the Honeywell FMS and its unique navigation, performance and autothrottle capabilities. The G-IV Phase II FMS is composed of dual NZ-920 Navigation and PZ-800 Performance/Autothrottle computers with dual CD-810 color Control Display Units (CDU) and a DL-800 Data Loader. All units are built by Honeywell Inc., Business and Commuter Aviation Systems Division. The ASCB provides communication between FMS functions and the other functions of the SPZ-8000.

NAVIGATION MANAGEMENT

The Navigation Computer provides high-accuracy, long range navigation and guidance data to the pilot and the other components of the SPZ-8000 system. Various sensors, including multiple inertial reference systems and radio navigation devices (e.g., Omega/VLF and VOR/DME), provide position information. By blending the sensor inputs, the Navigation Computer develops a position which is more accurate than any single sensor. The optimum mode of navigation is selected based upon the available sensors. Once the navigation mode is selected, the optimum flight profile is computed, utilizing detailed performance management predictions.

Guidance outputs include advisory information and steering signals for the pilot or Flight Guidance Computers to steer the aircraft along the desired route. Routes are defined from the aircraft present position to a destination via a direct great-circle route or via a series of great-circle legs connected by intermediate waypoints. Published high and low-altitude routes, RNAV approaches, SIDs, and STARs may be entered and automatically navigated. At any time, the pilot may deviate from the entered route and fly direct to a waypoint. In addition to flying direct, the FMS can intercept a specific course to a waypoint.

FEATURES

The Navigation Computer includes the following features:

- Navigation Radio Tuning
- DME/DME and VOR/DME Navigation
- Long Range Navigation
- Automatic Leg Transitions
- Support Display of Guidance/Map Information
- Lateral Steering Commands
- Vertical Steering Commands
- Holding Patterns and Parallel Offset Entry
- Radio/Sensor Management
- Cross-loading of Flight Plans, Pilot-Entered Data, and Navigation Databases

The Navigation Computer provides the following navigation data to the pilot via the Control Display Unit:

- Present Position
- Wind Direction
- Wind Velocity
- Magnetic or True Track
- Cross Track Deviation
- Bearing to Active Waypoint
- Groundspeed
- Estimated Time of Arrival at waypoints
- Desired Track
- Time to any Waypoint
- Distance to any Waypoint
- Distance to Active Waypoint
- Bearing to any Waypoint

NAVIGATION DATABASE

The NZ-920 worldwide navigation database is four times larger than the NZ-800 database initially certified on the G-IV. The navigation database can include nearly 1.3 million bytes of data, and is divided into custom and Jeppesen areas. The Jeppesen portion of the database is updated on a 28-day cycle with the Data Loader (DL-800). The DL-800 may also be used to enter a flight plan from a flight planning service. The Jeppesen area of the navigation database contains:

- Nav aids
- Airport/Runways
- SID/STAR Procedures
- Airways
- Waypoints (Intersections, VORs only, etc.)

The custom area is used to tailor the database to the requirements of individual pilots or customers. Custom data, programmed by the pilot, can include pilot-defined waypoints and routes.

The functions above are also generally available on other Honeywell Navigation Computer installations, such as Beechcraft Beechjets, British Aerospace HS125s, Canadair Challengers, Cessna Citations, and Dassault Falcons.

The Navigation Computer installed on the G-IV is distinguished by enhancements to Vertical Navigation (VNAV) and the interface with Performance Management. VNAV guidance is generated by the Navigation Computer based on extensive performance management inputs. On the G-IV, VNAV is therefore a true Flight Management function.

VERTICAL NAVIGATION

The FMS automatically computes the top-of-climb (TOC) and top-of-descent (TOD) points, as well as the relevant speed predictions. VNAV can be coupled to Flight Guidance (autopilot) and the Autothrottle for automatic climbs, cruise, descents, and transitions. Holding patterns and step climbs can be similarly automated. Performance management ensures the predicted speeds, altitudes, fuel burn, and distances are accurate.

During climbs, and without speed or altitude constraints in descent, the airmass mode is utilized. In this mode, VNAV is simple to use. The pilot need only dial the preselector altitude to the FMS target altitude. When engaged in VNAV, the climb or descent is automatically initiated and terminated as shown on the Control Display Unit. Speed control is maintained by elevator inputs from the FMS through the flight guidance system. Descents including waypoints with speed or altitude constraints are accomplished in the path mode.

VERTICAL PROFILE

The real power of VNAV is revealed in profile descents with multiple crossing restrictions. The waypoint crossing restrictions may be speeds and/or altitudes ("at," "at or above," or "at or below"). Visualizing such complicated descents is often difficult. Honeywell solved this problem with a unique vertical profile on the Navigation Display of the G-IV.

The vertical profile presents the TOC, TOD, vertical path, and any intermediate level-offs. The preselector altitude is shown as a dashed line. Horizontal scaling is controlled with the weather radar range adjustment. The vertical profile is presented immediately below the lateral navigation map for easy reference (see Figure 4).

The vertical profile allows the pilot to preview the flight profile before it is flown. Even complicated SIDs and STARs are easily visualized. And since the SIDs and STARs are contained in the Honeywell FMS navigation database, the whole process requires only a few keystrokes.

PERFORMANCE MANAGEMENT

The primary addition to the SPZ-8000 DAFCS for Phase II is the PZ-800 Performance/Autothrottle computer. Previously, detailed performance information was only available by laboriously consulting the aircraft performance manuals. With PZ-800 performance management, the pilot has an easy-to-use, computerized performance manual.

The pilot is supplied with flight-planning information before takeoff such as fuel and time required. In flight, the system provides the pilot with real-time information based on current aircraft and atmospheric conditions. In case of changes to the flight plan, the pilot can be updated immediately on the consequences of the changes. Pilots have especially appreciated the automatic speed and engine rating selection. And Performance Management can be coupled to the autopilot and autothrottle for increased ease, safety, comfort, and fuel economy.

Tailored to the corporate pilot, the PZ-800 is easy to operate. While performance management typically requires many pilot inputs, the PZ-800 minimizes entries by using sensed values, the navigation database, and by "remembering" selections from flight to flight. In addition, the CD-810 Control Display Unit used with Navigation Management is also used for Performance Management. Integration of navigation and aircraft performance data, and consistent formats cause the pilot to only see one unified Flight Management System.

The complete capabilities of Performance Management are described below and summarized in Figure 5.

APPROVED FLIGHT MANUAL DATA

FAA certification of the Phase II marked the first civil onboard Approved Flight Manual (AFM) takeoff and landing prediction computer. Pilots that frequently use AFM "chase-around" charts will especially appreciate the PZ-800. Complex reduced-thrust (FLEX), or performance-limited takeoff predictions are now literally at the "push of a button."

TAKEOFF. PZ-800 performance management computes all FAA-approved G-IV AFM predictions for takeoff, including:

"V-speeds":

- Decision (refusal) speed, V_1
- Rotation speed, V_R
- Safety (second-segment) speed, V_2
- Final segment speed, V_{FS}
- Single-engine speed, V_{SE}
- Reference speed, V_{REF}

Engine setting/Takeoff rating

Distances:

- Accelerate-stop
- Accelerate-go
- Required field length

Annunciations are provided for the following conditions:

- Maximum takeoff weight
- Configuration mismatch
- Field-length-limited
- Tire-speed-limited
- Obstacle-limited
- Climb-limited
- Brake-energy-limited
- V_{1mcg} -limited

Performance Management takeoff computations are based on pilot selections of:

Full-thrust (MIN EPR) or reduced-thrust (FLEX EPR)

Runway parameters:

- Heading (can be obtained from Navigation database)
- Length (can be obtained from Navigation database)
- Clearway
- Stopway
- Slope

Atmospheric parameters:

- Pressure altitude/elevation (can be obtained from Navigation database) and barometric setting
- Wind: Magnitude and magnetic direction
- Outside air temperature (can be sensed value)

Obstacle:

- Distance
- Elevation

V_1 between computed minimum and maximum V_1 values

Aircraft configuration (approved configurations only):

- Takeoff weight (can be computed from basic initialization)
- Flap selection
- Anti-ice bleeds
- Anti-skid
- Ground spoilers

Takeoff Checks. A unique series of tests is incorporated into the selections, computations, and display of takeoff data. The selection check ensures only valid, approved aircraft takeoff configurations are initialized. This is accomplished by removing certain takeoff initialization selections from the CDU based on other selections. For example, selecting anti-skid "off" removes selections for ground spoilers inoperative, 10-degree flaps, and reduced-thrust. This is because the G-IV AFM requires ground spoilers operative, flaps at 20-degrees, and full-thrust for takeoffs with the anti-skid system off.

The computation checks include both internal and external comparisons of the predicted takeoff speeds. Internally, the PZ-800 continuously evaluates sensed weight, altitude, and temperature for differences that could change the predicted V-speeds. A half-knot change triggers re-computation of the complete takeoff predictions. Takeoff computations are "frozen" when the throttles are advanced to takeoff. This prevents changes and annunciations during the takeoff run.

External computation comparisons are performed by the Honeywell FC-880 Fault Warning Computer. The V-speed predictions of the dual PZ-800s are compared for consistency. A difference in the independent computations triggers a message on the EICAS and inhibits display of the V-speed target bugs on the PFD. The PZ-800 also removes the V-speed bugs from the PFD speed-tape when the aircraft configuration does not match the initialized configuration. The out-of-configuration item is highlighted on the CDU. In either case, a prominent PFD annunciation on the speed-tape alerts the pilot to the loss of V-speed target bugs.

LANDING. Performance Management computes all FAA-approved G-IV Airplane Flight Manual predictions for landing, including:

Speeds:

- Landing speed (1.3 V_{stall} landing configuration)
- Approach climb speed
- Landing climb speed
- Reference speed (1.3 V_{stall} current configuration)

Distances:

- Landing distance
- Required field length dry
- Required field length wet

Engine setting: Go-around and climb

Annunciations are provided for the following conditions:

- Maximum landing weight
- Approach-climb-limited
- Field-length-limited
- Landing-climb-limited

Performance Management landing computations are based on pilot selections of:

Runway parameters:

- Heading (can be obtained from Navigation database)
- Length (can be obtained from Navigation database)

Atmospheric parameters:

- Pressure altitude/elevation (can be obtained from Navigation database) and barometric setting
- Surface winds: Magnitude and magnetic direction
- Airport temperature

Aircraft configuration (approved configurations only):

- Flap selection
- Anti-ice bleeds
- Anti-skid
- Automatic spoilers

PERFORMANCE ADVISORY DATA

Like commercial airliner Flight Management Systems (FMS), the PZ-800 utilizes aerodynamic and propulsion models provided by the airframe and engine manufacturers. Over 300,000 bytes of aerodynamic, propulsion, and aircraft performance information are contained in the PZ-800.

Performance Management computes and displays on the Control Display Unit advisory information for optimization of flight profiles. Performance Management data is also used by the Navigation Computer for optimum Vertical Navigation predictions. Performance Management advisory information includes:

CLIMB PREDICTIONS.

Speeds:

- Gulfstream-recommended CAS/Mach schedule
- Pilot-selected CAS/Mach schedule "remembered"
- Speed restrictions (e.g., US Rules)

Time, fuel, and distance to top-of-climb

Engine setting and maximum climb thrust rating

CRUISE PREDICTIONS.

Speeds:

- Pilot-selected CAS/Mach "remembered"
- Long range cruise
- Maximum endurance (hold)
- Maximum speed (V_{MO}/M_{MO} -, buffet-, thrust-limited)

Step Climbs:

- Pilot-selected altitude increment
- Time and distance to step point

Altitudes:

- Initial cruise: Optimum or pilot-selected
- Current optimum
- Step altitude

Range: Time, fuel remaining, and distance

Engine setting and maximum cruise thrust rating

DESCENT PREDICTIONS.

Speeds:

- Gulfstream-recommended CAS/Mach schedule
- Pilot-selected CAS/Mach schedule "remembered"
- Flightpath angle

Speed restrictions (e.g., US Rules)

Time, fuel, and distance to bottom-of-descent

Engine setting

ACTIVE FLIGHT PLAN PREDICTIONS. Minimum speed (1.3 times the stall speed for the current configuration) and other operating limits are protected in all Performance Management predictions. Time, fuel, and distance to the top-of-climb, top-of-descent, destination, and alternate are displayed. Reserve requirements can be computed on time, fuel weight, or National Business Aircraft Association (NBAA) rules. Data for each navigation waypoint includes:

- Time, fuel, and distance
- Groundspeed, airspeed, and vertical speed
- Wind speed and direction
- Temperature: Outside air temperature and ISA deviation
- Speed and altitude constraints

ENGINE-OUT PREDICTIONS. The active flight plan is automatically recomputed to account for engine-out performance when an engine failure is detected. At any time the pilot can examine the following for both fixed altitude cruise and cruise-climb at the engine-out optimum altitude:

- Time and range to reserve fuel
- Time and range to zero fuel
- Engine-out cruise altitude
- Drift-down/-up speed to engine-out cruise altitude

"WHAT-IF" PREDICTIONS. A "What-If" function is provided to permit the pilot to examine changes to the active flight plan without actually making the changes active. The following parameters may be altered from their current settings:

- Speeds: Climb, cruise, and descent
- Cruise wind and temperature
- Speed restriction
- Step increment
- Fuel reserve requirements
- Initial cruise altitude
- Weights: Fuel, cargo, passenger, and gross

With the changes from the active flight plan made, the "What-If" function predicts the effect of the changes on active flight plan predictions of:

- Cruise altitude
- Fuel required and change from active
- Time enroute and change from active
- Step climb time, distance, and altitude
- Range and time to reserve fuel

The conditions selected under "What-If" can be transferred to the active flight plan by pilot selection. The "What-If" capability is a means for the pilot to evaluate proposed Air Traffic Control changes, examine time/fuel options, and determine the optimum altitude/wind tradeoffs.

STORED FLIGHT PLAN PREDICTIONS. A Stored Flight Plan function permits the pilot to examine flight plans other than the active flight plan without actually making the plan active. The function presents a list of flight plans stored in the navigation database for selection by the pilot. The following parameters may be entered with the stored flight plan:

- Speeds: Climb, cruise, and descent
- Cruise wind and temperature
- Speed restriction
- Step increment
- Fuel reserve requirements
- Initial cruise altitude
- Weights: Fuel, cargo, passenger, and gross

The Stored Flight Plan function returns mission predictions of:

- Cruise altitude
- Fuel required
- Time enroute

This capability to examine mission predictions for another flight plan may be used to pre-plan the next day's flight or a return flight, examine destination options, and answer fueling planning questions.

AUTOTHROTTLE

The PZ-800 hardware also provides the autothrottle functions of the SPZ-8000. The PZ-800 Autothrottle is the first digital, full-authority, full-flight-regime automatic thrust control offered in the business jet market.

MODES

Four modes are provided in the Autothrottle. Selection of the modes is automatic with selections for Flight Management and Flight Guidance.

TAKEOFF. The pilot may manually select a takeoff target Engine Pressure Ratio (EPR), a reduced thrust FLEX EPR computed by Performance, or use the takeoff EPR rating computed by the Autothrottle. When properly engaged in takeoff mode, the Autothrottle will rapidly advance the throttles to the takeoff setting and maintain that EPR. At 60 knots, the Autothrottle servo-clutches are de-powered, and HOLD is annunciated on the Primary Flight Display. If the Autothrottle fails to go into the hold mode, the Fault Warning Computer will annunciate the failure on the Crew Alerting System. The Autothrottle remains in the hold mode until pilot action is taken to select a new flight guidance mode. If the new mode is selected below 400 feet above runway, the Autothrottle remains in hold until the aircraft is above 400 feet before seeking the new engine setting.

GO-AROUND. Go-around mode provides smooth, rapid application of power to the go-around EPR rating computed by the Autothrottle when any other mode is engaged. The Autothrottle maintains the go-around power level until the pilot deselects the mode.

FLIGHT LEVEL CHANGE. Flight Level Change (FLCH) mode interacts with the autopilot for smooth climbs and descents. A unique feature sets climb thrust proportional to the amount of climb. This results in smooth step climbs with minimal throttle changes. FLCH automatically transitions to Speed Hold when the preselected altitude is "captured" by Flight Guidance.

SPEED HOLD. Speed Hold mode accurately maintains either a FMS-selected speed or a manually-selected speed entered on the Guidance Control Panel. Both Calibrated Airspeed and Mach number targets are maintained throughout the G-IV flight envelope. Speed Hold will also smoothly control thrust during acceleration and deceleration.

OTHER FUNCTIONS

The Autothrottle provides speed protection for the operating speed limits (V_{MO} and M_{MO}) of the G-IV, as well as flap placard and landing gear placard speeds. With Performance Management speed targets, the Autothrottle will maintain the aircraft within the thrust, buffet, and minimum speed envelope of the G-IV. The Autothrottle will protect the engine EPR ratings, anti-ice (bleed air) engine limits, and the minimum idle level.

The Autothrottle also provides engine synchronization during Speed Hold to the low-rotor speed (LP or %N1) or high-rotor speed (HP or %N2) selected by the pilot. In all other modes, and defaulted for Speed Hold, consistent Engine Pressure Ratios (EPRs) are maintained side-to-side.

The Autothrottle will sense uncommanded throttle movements and disengage (such as when the pilot manually moves the throttles). Engine failures are detected and confirmed rapidly at high and low power settings, and the Autothrottle is automatically disengaged.

SUMMARY

Federal Aviation Administration certification of the Honeywell SPZ-8000 Digital Automatic Flight Control System for the Gulfstream Phase II program ushered in a new era for General Aviation. Phase II introduced the first true Flight Management System specifically designed for business jets. It also extended existing airliner Flight Management System capabilities with the display of vertical profile, Approved Flight Manual takeoff and landing predictions, and extensive engine-out and atmospheric modelling capabilities. And consistent with the high level of integration already exhibited by the SPZ-8000, the autothrottle extends the pilots' ability to safely, economically, and easily guide the Gulfstream IV.



FIGURE 1. GULFSTREAM IV BUSINESS JET BUILT BY GULFSTREAM AEROSPACE CORPORATION

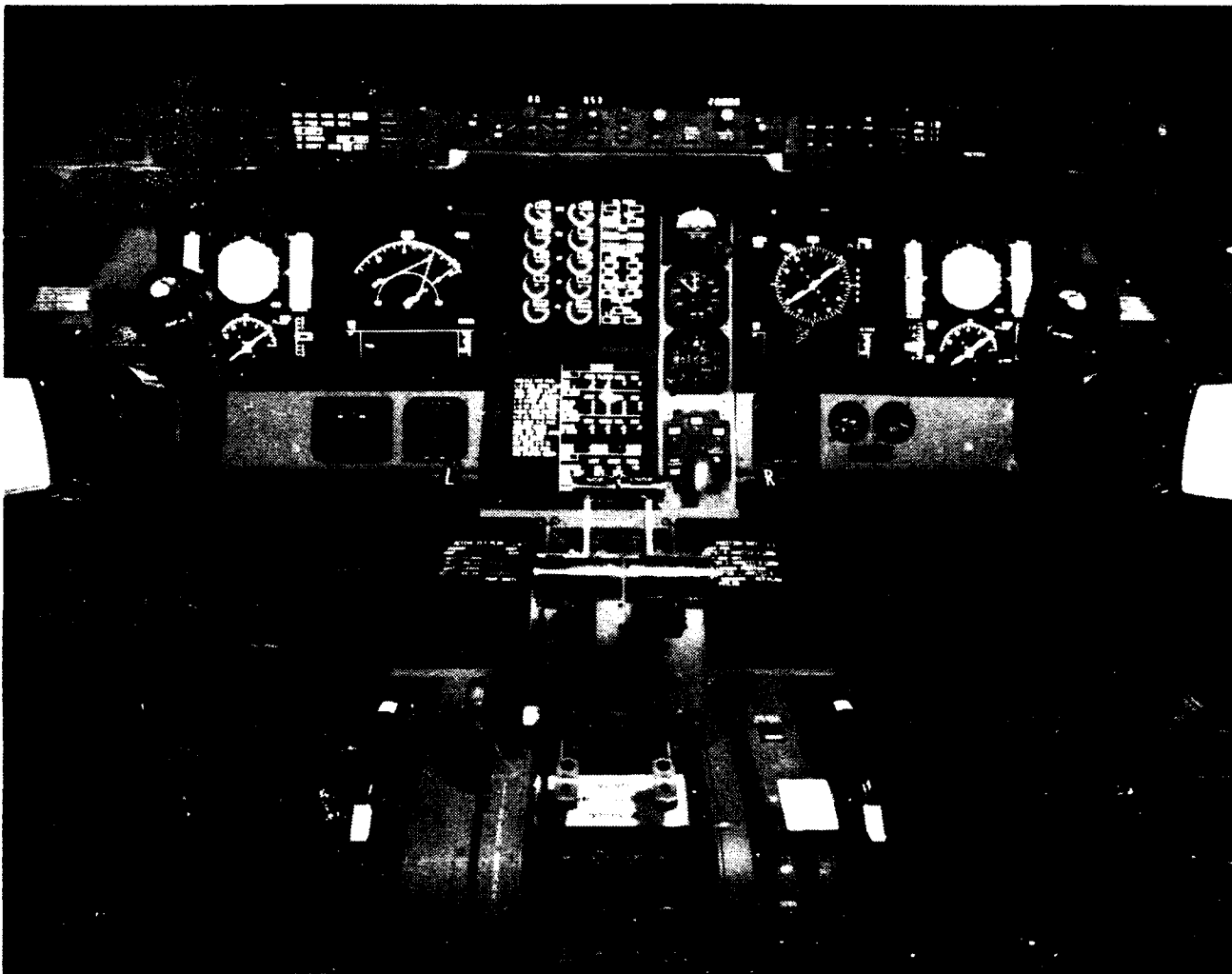


FIGURE 2. GULFSTREAM IV COCKPIT FEATURING HONEYWELL SPZ-8000 DAFCS

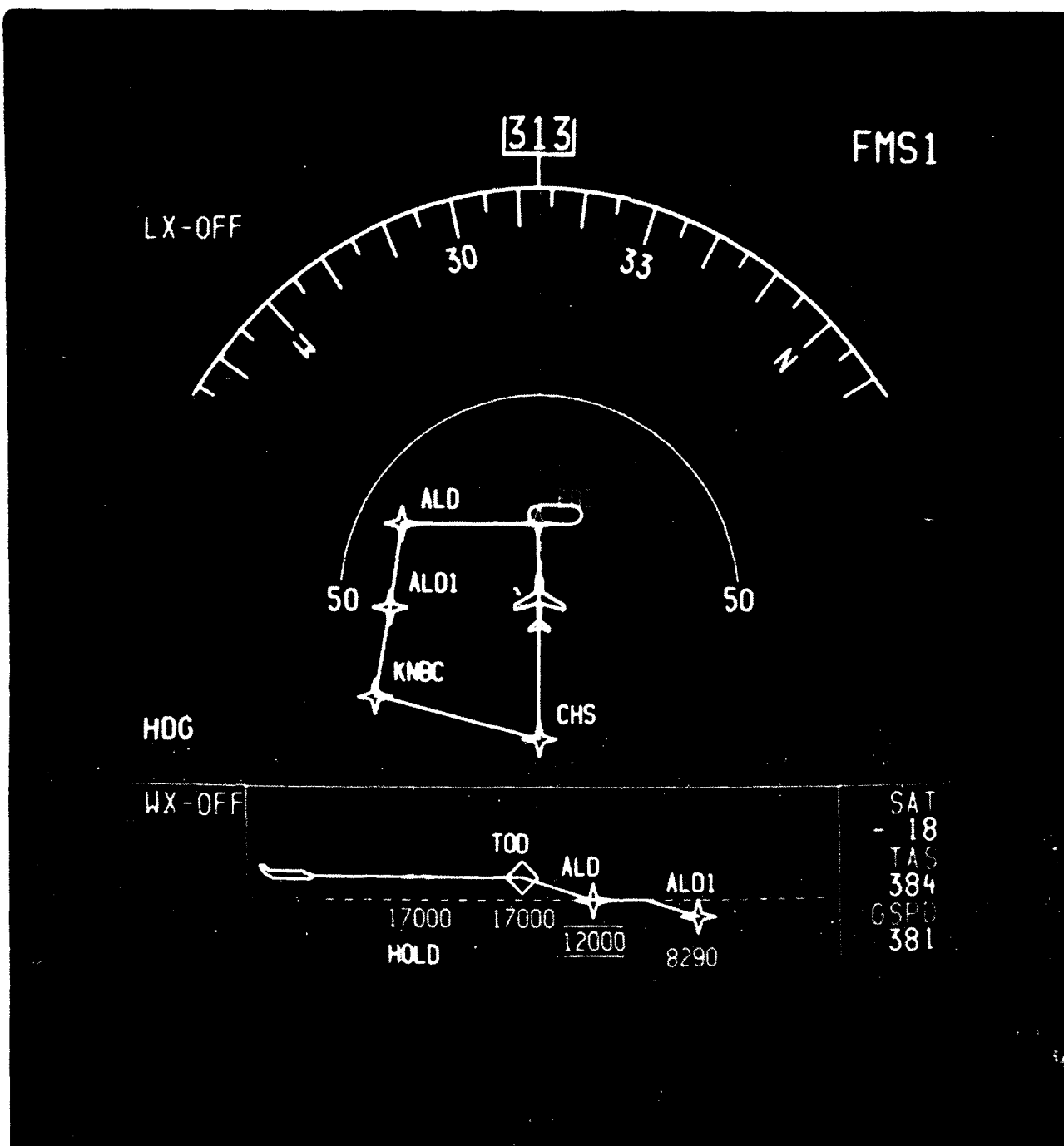
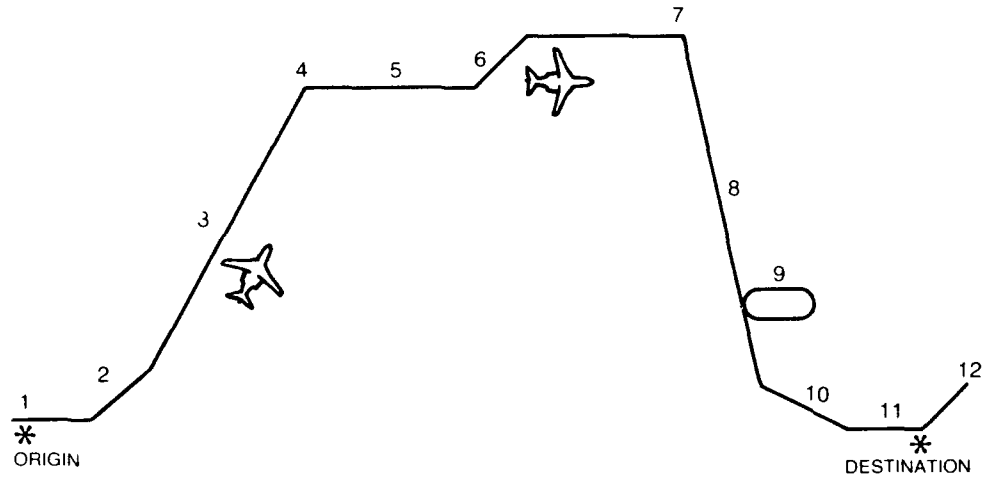


FIGURE 4. FLIGHT PLAN LATERAL AND VERTICAL PROFILES ON THE NAVIGATION DISPLAY



	FLIGHT PHASE	AUTOTHROTTLE FUNCTIONS	PERFORMANCE FUNCTIONS
1	Takeoff	Maximum rated thrust OR "FLEX" reduced-thrust OR Manually-set thrust	Full flight manual: "Vs speeds" distances full- reduced-thrust
2	Climb-Out	Takeoff to climb thrust transition	Flaps-down speeds Minimum speed protection
3	Climb	Climb thrust coordinated with Flight Guidance	Climb speed schedules <i>Engine settings</i>
4	Top-of-Climb	Transition to cruise speed	Time, fuel, and distance Optimum cruise altitude
5	Cruise	Cruise speed maintained	Cruise speed schedules: Long Range Cruise Maximum Speed <i>Engine settings</i>
6	Step Climb	Smooth altitude change	Time and distance to step point Optimum altitude
7	Top-of-Descent	Transition to idle thrust	Time, fuel, and distance
8	Descent	Minimum engine setting <i>anti-ice bleeds protection</i>	Path and speeds <i>Engine settings</i>
9	Holding	Holding speed maintained	Maximum Endurance
10	Approach	Precise speed control Placard speeds protection	Approach speeds
11	Landing	Flare retard (growth)	Speed distances
12	Go-Around	Maximum rated thrust	Speeds <i>Engine settings</i>

AD-16923-R2

FIGURE 5. PZ-800 FUNCTIONS OVER THE FLIGHT PROFILE

**DESIGN AND CERTIFICATION OF AIRCRAFT FOR
THE HERF ENVIRONMENT**

by

Jack Glecier
and
Joseph P. Cross
Beech Aircraft Corporation
Wichita, KS

For presentation to the AIAA/FAA Joint Symposium on General
Aviation Systems at the Port O-Call Inn, Ocean City, NJ
on April 12, 1990

DESIGN AND CERTIFICATION OF AIRCRAFT FOR THE HERF ENVIRONMENT

Joseph P. Cross
Group Engineer - Beechjet Avionics
Beech Aircraft Corporation
Wichita, KS

Jack Glecier
Design Engineer - Electromagnetic Compatibility
Beech Aircraft Corporation
Wichita, KS

ABSTRACT

Certification authorities world-wide are in the process of amending regulations to add new standards which will provide requirements for the protection of aircraft flight critical functions from the effects of high energy radiated electromagnetic fields. Within the industry, these effects have become associated with the acronym "HERF."

In late 1989, the Federal Aviation Administration (FAA) imposed requirements on the Beech Model 2000 Starship airplane requiring qualification of the installed equipment for operation in HERF conditions.

Field levels imposed for aircraft certification to the HERF threat require hardening aircraft electronic systems to a level two orders of magnitude above today's typical equipment qualification levels. Two large design challenges are thereby imposed: 1) hardening equipment requires extraordinary measures to insure performance; and 2) conventional TSO test methods and test equipment used for qualification are not capable of adequately assessing performance at the high field levels.

This paper discusses HERF design considerations and solutions relative to the above subjects and the experience gained by Beech Aircraft during the Starship and subsequent development programs in evaluating flight critical system performance for aircraft certification in the HERF environment.

INTRODUCTION

PURPOSE

Testing was performed to FAA certify the Beech Model 2000 Starship in HERF conditions. Bulk current injection (BCI) and radiated susceptibility (RS) tests designed to reveal the vulnerability of aircraft flight critical systems to high energy radiated fields were specified.

Certification for the HERF Environment

These tests determine whether equipment and interconnecting wiring will operate within performance specifications with a level of RF modulated power coupled into the equipment and wiring either by a radiated field or by injection probe induction into the system through power input and interconnecting circuit configurations.

Testing was performed per methods specified in RTCA DO-160B Section 20 draft dated April 4, 1989. The FAA allowed one of two alternative qualification levels: equipment and component testing at specified field levels, or aircraft testing at the full scale external threat level.

Flight critical systems not adversely affected during BCI and RS testing are determined to be submissive evidence of demonstrated regulatory compliance for the HERF requirement.

BACKGROUND.

Electronic functions are being incorporated into aircraft designs on an increasingly widespread basis. In addition to roles which have traditionally been implemented electronically, such as avionics, other systems which have previously been mechanical in nature are being implemented with electronic or electromechanical control to reduce cost and increase performance. Conversions have progressed to the point that major critical aircraft functions are being accomplished in this manner.

In addition to the above, the electronics design community has been moving away from analog designs in favor of digital techniques. Again, this is being done for cost and/or performance considerations. This trend introduces several new factors into system design. Among these are software integrity, data storage and retention, quality of power, and response to transient effects. The digital electronics field has stressed much improved functionality, increased performance, and flexibility of configuration with a drastic reduction in the size of individual electronic elements.

A natural progression of this phenomenon has been to accomplish major aircraft operational functions using digital control systems. The most visible development within the past few years has been evidenced by the fly-by-wire control concept, in which flight dynamics and control of an aircraft are accomplished electronically. Less obvious examples are the electronic determination and display of aircraft attitude, altitude, airspeed, braking system control, and steering. The trend in this direction will continue to increase due to technical and economic considerations.

When such functions are accomplished in this electronic manner, it is necessary to insure that undesirable effects do not occur from electrical sources outside of the system. Electronic systems have generally not been highly susceptible to external threats, and airframes enclosing these systems have offered a considerable degree of protection.

The increasing trend to accomplish critical and essential functions electronically has

Certification for the HERF Environment

generated the need to evaluate the response of this equipment in current and projected electromagnetic fields which may exist external to the airframe. In addition, the airframe itself is changing with a move away from conventional aluminum structures to non-metallic materials offering improved structural characteristics.

TEST APPARATUS

The Beech Aircraft Electromagnetic Effects (EME) facility includes a 50' L x 40' W x 24' H anechoic room with attached anteroom of 30' L 20' W x 14' H. The production Starship electrical and avionics harnesses designated for aircraft Serial No. NC-12 were provided for this test prior to its installation into the airplane.

This equipment under test (EUT) was a complete ship set with the exception that the right wing harness was omitted. Per the prescribed test method, the harness was installed in the anechoic chamber, separated from an electrical ground plane by a specified distance. Styrofoam pads were placed between the harness and the ground plane to provide this spacing. Testing was performed on the left wing harness only, with sufficient right wing equipment simulated to allow evaluation of simultaneous HERF effects on duplicated critical system equipment components located in that area.

A photo of the EUT is shown in Figure 1, "Test Harness Configuration." The camera is located at a viewpoint which would be just aft of the right hand wing, looking forward.

Signal generators and power amplifiers appropriate to the test matrix were placed in the anechoic chamber and were isolated from the radiating antennas and EUT by portable sections of anechoic material. A survey of fields at the location of the signal generators showed that the hazardous fields were not present in this location, allowing operators to directly control this equipment. There was therefore no need for remote control of signal generation.

A video camera was placed at a location appropriate to monitor the expected effects on the EUT. This camera and associated video cable were isolated as well as possible from the radiated fields. A VHS format video tape recorder and video monitor were located in the anteroom for operation by the personnel witnessing the testing and providing a record of effects experienced.

TEST PROCEDURES

Prior to testing, an analysis of critical systems installed on the aircraft was performed. There was concern that systems not traditionally considered critical may be effected in a critical manner when HERF was imposed. An additional concern was that redundant critical systems may be simultaneously effected, thus negating the advantage of this redundancy.

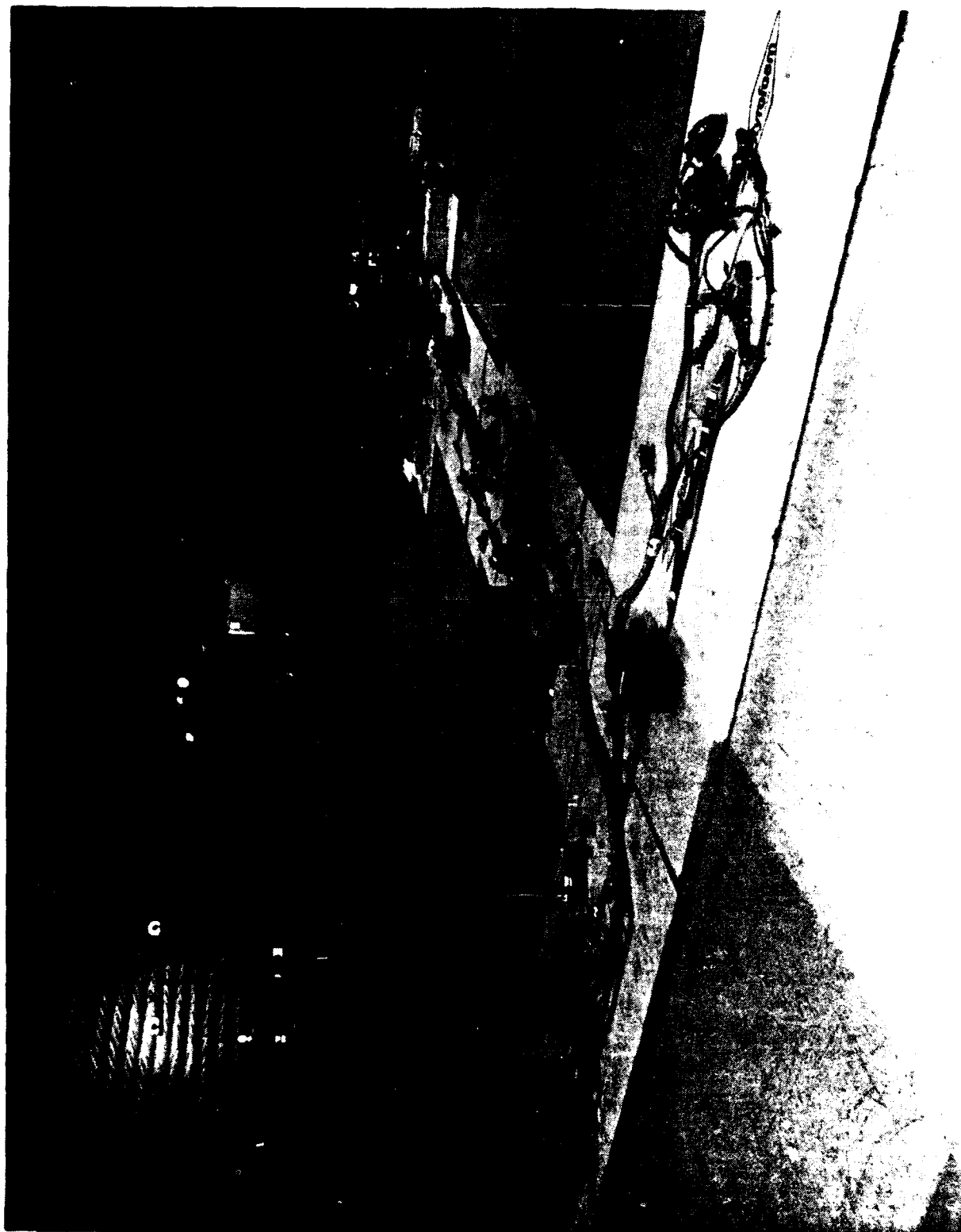


Figure 1 - Test Harness Configuration

Certification for the HERF Environment

Expected effects were anticipated to fall into one of the following categories:

- No effect or slight operational perturbations
- Unflagged, misleading information displayed
- Flagged or obviously misleading information displayed
- Passive equipment failure - failure to operate when expected
- Unscheduled equipment operation - "runaways"
- Burnout

The critical system analysis resulted in categorization of systems as follows:

System cannot be effected	Equipment is not electronic in nature or uses components not susceptible.
Predictable effects	Effects can be predicted and occur in an acceptable manner.
Effects cannot be predicted	Testing is required to determine effects.

Equipment from the systems listed in Table 1, "Systems Requiring Test", were subjected to HERF conditions to show compliance.

Table 1 - Systems Requiring Test

Function	Brief Description
Altitude	Pilot and Copilot displays are electronic (EFIS) and derived from digital air data computers. Standby is pneumatic.
Airspeed	Same condition as Altitude.
Anti-ice/De-ice	System is electronically controlled and sequenced with manual backup. Malfunctions of automatic controller must be recognizable to control ice shedding through propellor disc.
Attitude	Pilot and Copilot displays are electronic (EFIS) and derived from digital attitude/heading (AHRS) system. Standby is electromechanical.
Autopilot	Servo torque limiting may be susceptible. Verify that monitoring detects any runaway conditions induced.
EICAS	Provides electronic display of engine parameters and crew advisory annunciation.
Flap/forward wing	Electronic control system may lose synchronization.
Stall warning/ stick pusher	Electronic system may provide inadvertent push.

Testing was conducted in two parts: conducted susceptibility and radiated susceptibility. For both parts, equipment configuration and test methods were as prescribed in RTCA

Certification for the HERF Environment

Document DO-160B Section 20 Draft dated April 4, 1989. The test conditions are summarized in Table 2, "Specified Test Conditions."

Table 2 - Specified Test Conditions

Type of Test	Frequency Range	Modulation
BCI	10 kHz - 150 kHz	CW
	150 kHz - 30 MHz	1 kHz Square Wave (Rise time < 50 ns)
	30 MHz - 400 MHz	1 kHz Sine Wave at > 80% modulation
RS	30 MHz - 200 MHz	1 kHz Square Wave (Rise time < 50 ns)
	200 MHz - 18 GHz	1% duty cycle Pulse,
		1 kHz PRF, 10 μ s Pulse Width

CONDUCTED SUSCEPTIBILITY

Cable bundles which connect the EUT to other equipment in the aircraft system, including primary power lines, were subjected to BCI testing. Current injection probes capable of handling the required power levels had only recently become available, requiring test facility personnel to become familiar with this new equipment and its operating procedures.

PROBE CALIBRATION. Equipment for probe calibration was set up, and the injection probe installed in the calibration fixture. The calibration fixture is shown in Figure 2, "Calibration Fixture". Equipment arrangement is shown in Figure 3, "Calibration Setup." Beginning at 10 kHz (unmodulated), power was applied to the injection probe and current/power measured in the calibration fixture using a spectrum analyzer until the desired forward current/power was indicated per Figure 4, "CS Test Levels". The drive levels were recorded to determine required input power for BCI testing of the cable harnesses.

TEST SETUP. The EUT, wiring, associated interface circuitry, and test equipment were setup per Figure 5, "CS Test Setup." Prior to performing the conducted susceptibility test, a measurement of the cable was made to identify wiring resonant nodes.

Monitor Probe. The monitor probe was installed 5 cm (2 in) from the EUT. If the EUT connector plus backshell length exceeded this dimension, the probe was placed as close to the backshell as possible and the position noted. The probe was supported as necessary for centering of the harness.

Injection Probe. The injection probe was installed 5 cm (2 in) from the face of the monitor probe. If the interconnecting cable length was less than 0.5 m (20 in), the injection probe was placed at the center of the bundle and the induced current measured 5 cm (2 in) from each connector backshell.

Certification for the HERF Environment

TEST PROCEDURE. At each test frequency, the signal amplitude was gradually increased from zero until either a malfunction occurred or the maximum test level was achieved. Frequency coverage was obtained by slowly sweeping between each test frequency to ensure the lowest susceptibilities had been found and a full malfunction signature measured.

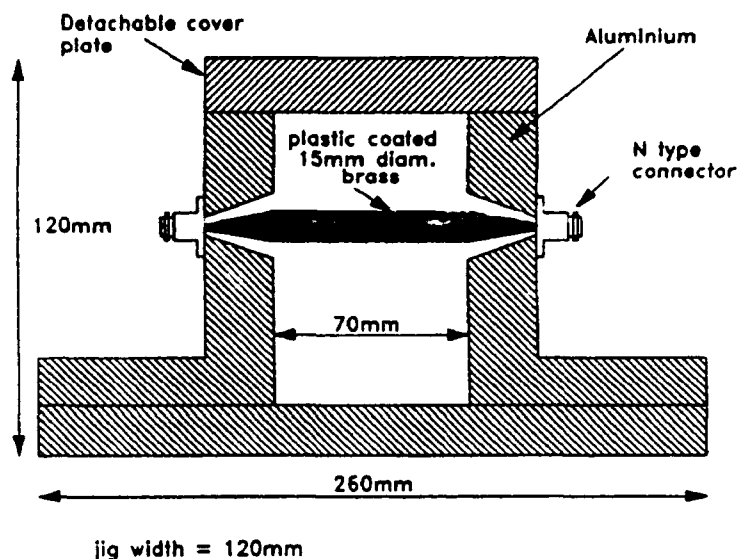


Figure 2 - Calibration Fixture

At frequencies where the EUT displayed susceptibility, the signal amplitude was reduced until a threshold of susceptibility was determined. A check for hysteresis was then performed by alternately increasing and decreasing signal level through the susceptibility threshold. The lesser of the two levels was recorded.

For the frequency range between 10 kHz and 5 MHz, common mode current was monitored and limited to a maximum equivalent field of 100 V/m. For the remainder of the frequency range, this limit was to a maximum equivalent field of 200 V/m. At resonant frequencies, power was carefully monitored and reduced as necessary to remain within these limits. Modulation was per Table 2.

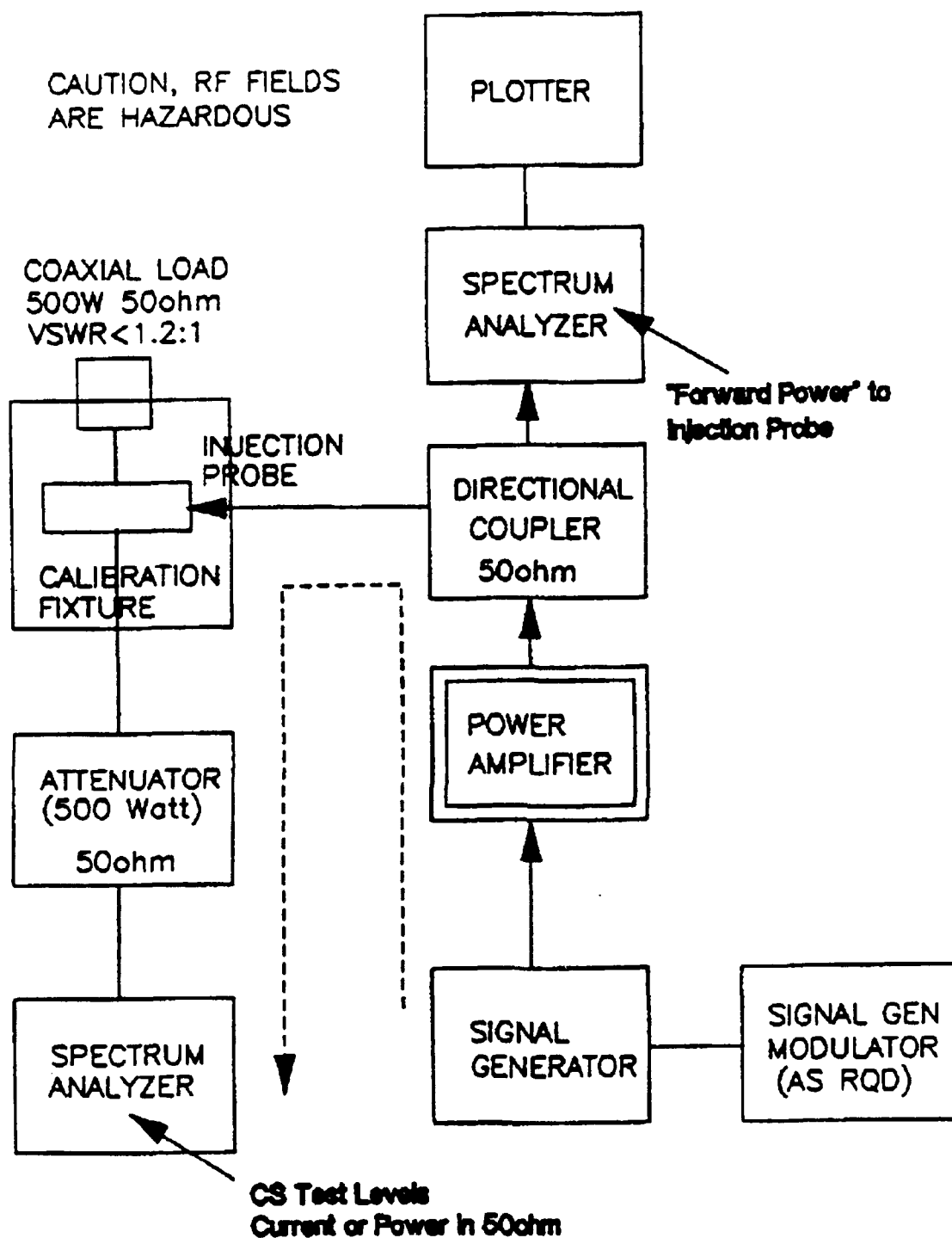


Figure 3 - Calibration Setup

Certification for the HERF Environment

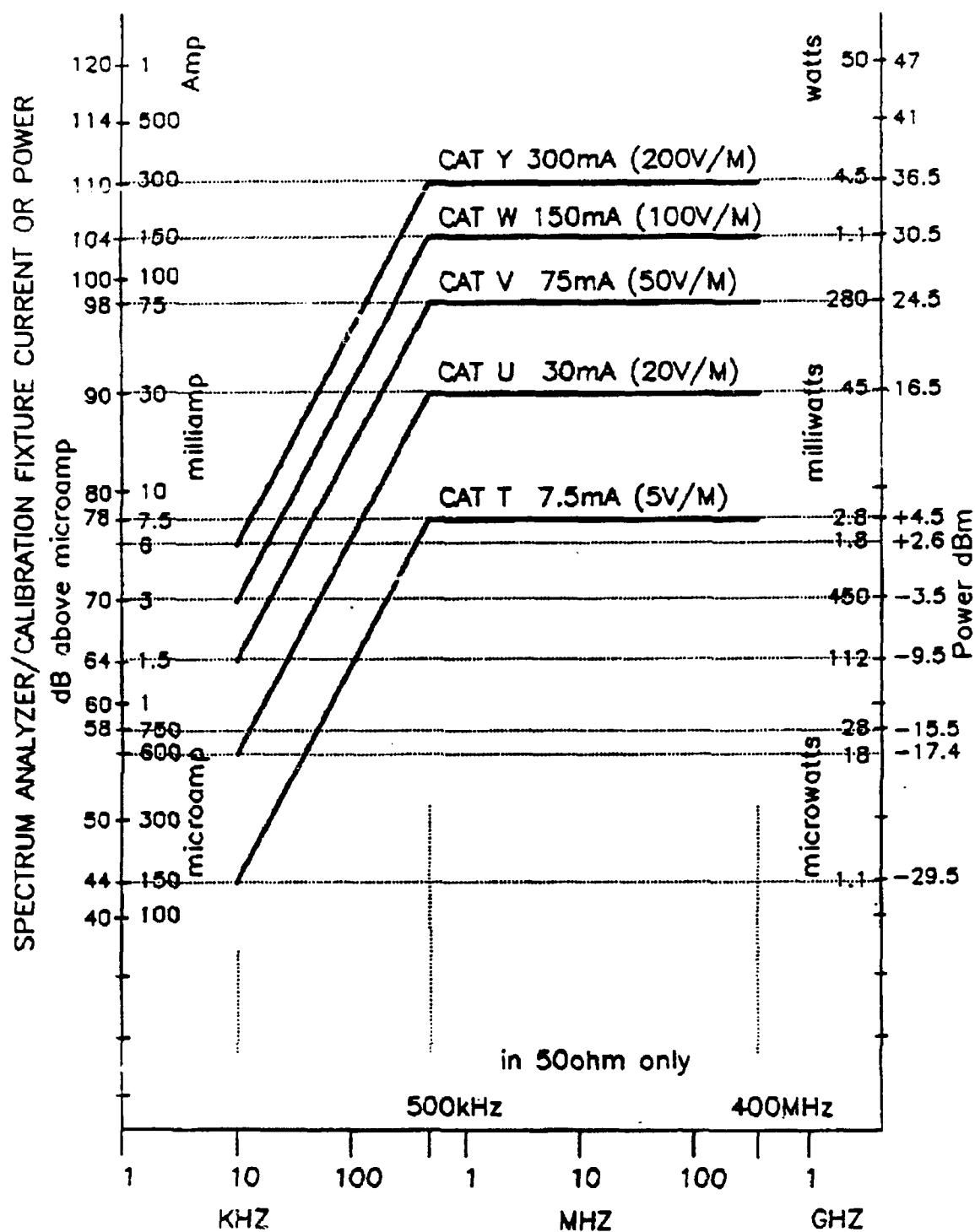


Figure 4 - CS Test Levels

Certification for the HERF Environment

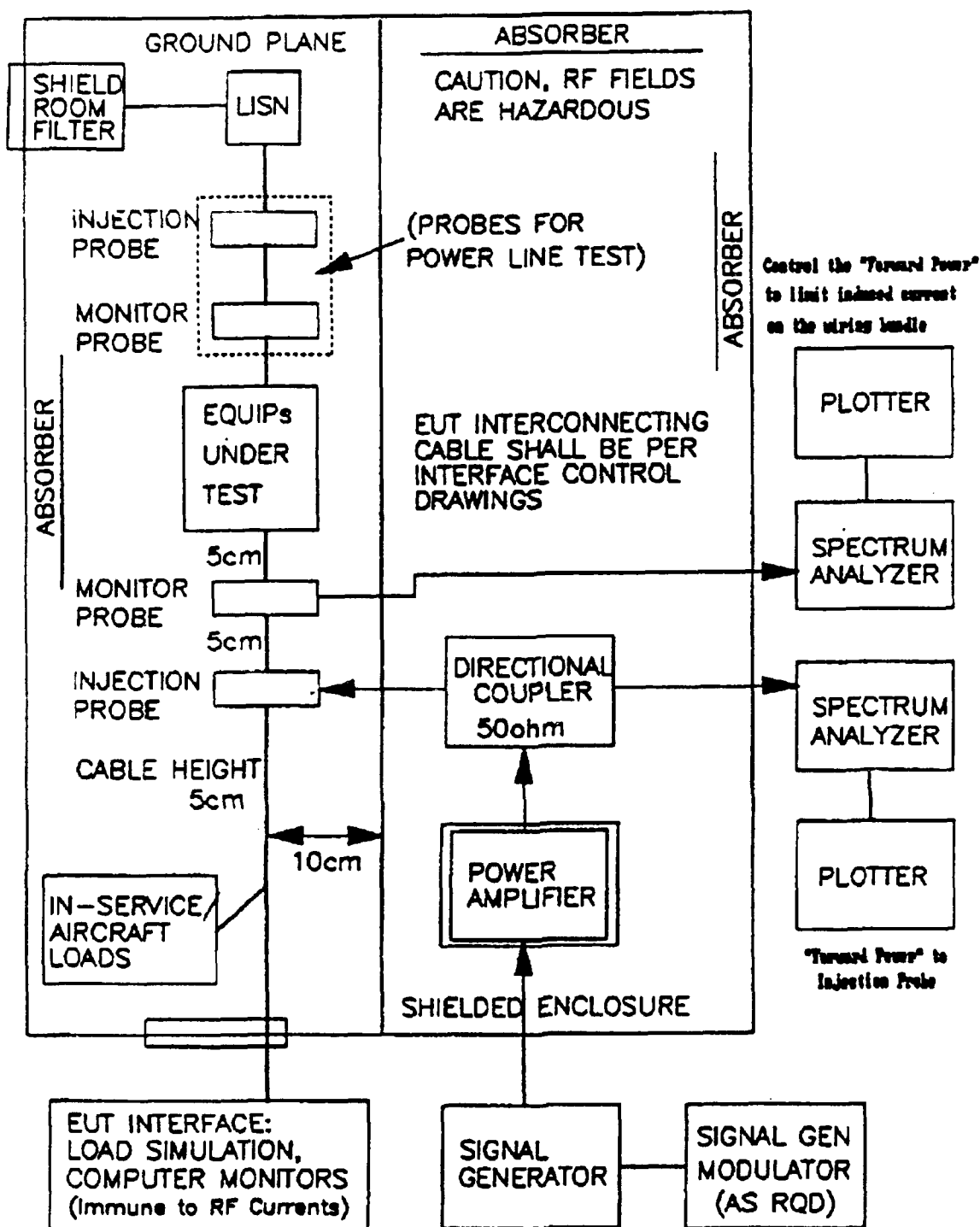


Figure 5 - CS Test Setup

Certification for the HERF Environment

RADIATED SUSCEPTIBILITY

Test Setup. Cable bundles which connect the EUT to other equipment in the aircraft were subjected to RS testing. The test setup consisted of the EUT, wiring, associated interface circuitry, and test equipment per Figure 6, "RS Test Setup."

Proper antenna and sensor locations were established. Equipment modes of operation which were to be evaluated were achieved. Radiating antennas which generated the test field levels were placed at sufficient separation from the EUT to ensure overall uniform illumination.

Test Procedure. The EUT and interconnecting cables were subjected to the CAT Y RF fields of Figure 7, "RS Test Levels" as described below.

The signal generator was set to 30 MHz, unmodulated, and the signal generator/power amplifier adjusted for a field strength level (200 V/m) as indicated by a field sensor located adjacent to the specific equipment component under test.

The RF signal was amplitude modulated with a 1 kHz square wave or 1% duty cycle pulse as appropriate to the frequency range of operation per Table 2.

A frequency range was scanned and EUT operation evaluated to determine compliance with EUT performance standards. Where susceptibility occurred, the threshold was determined in a manner similar to that used during BCI testing.

At frequencies above 1 GHz, apertures in the EUT, such as CRT faces, were exposed directly to the transmitting antenna. Vertical and horizontal orientations were tested where polarized antennas were used.

Certification for the HERF Environment

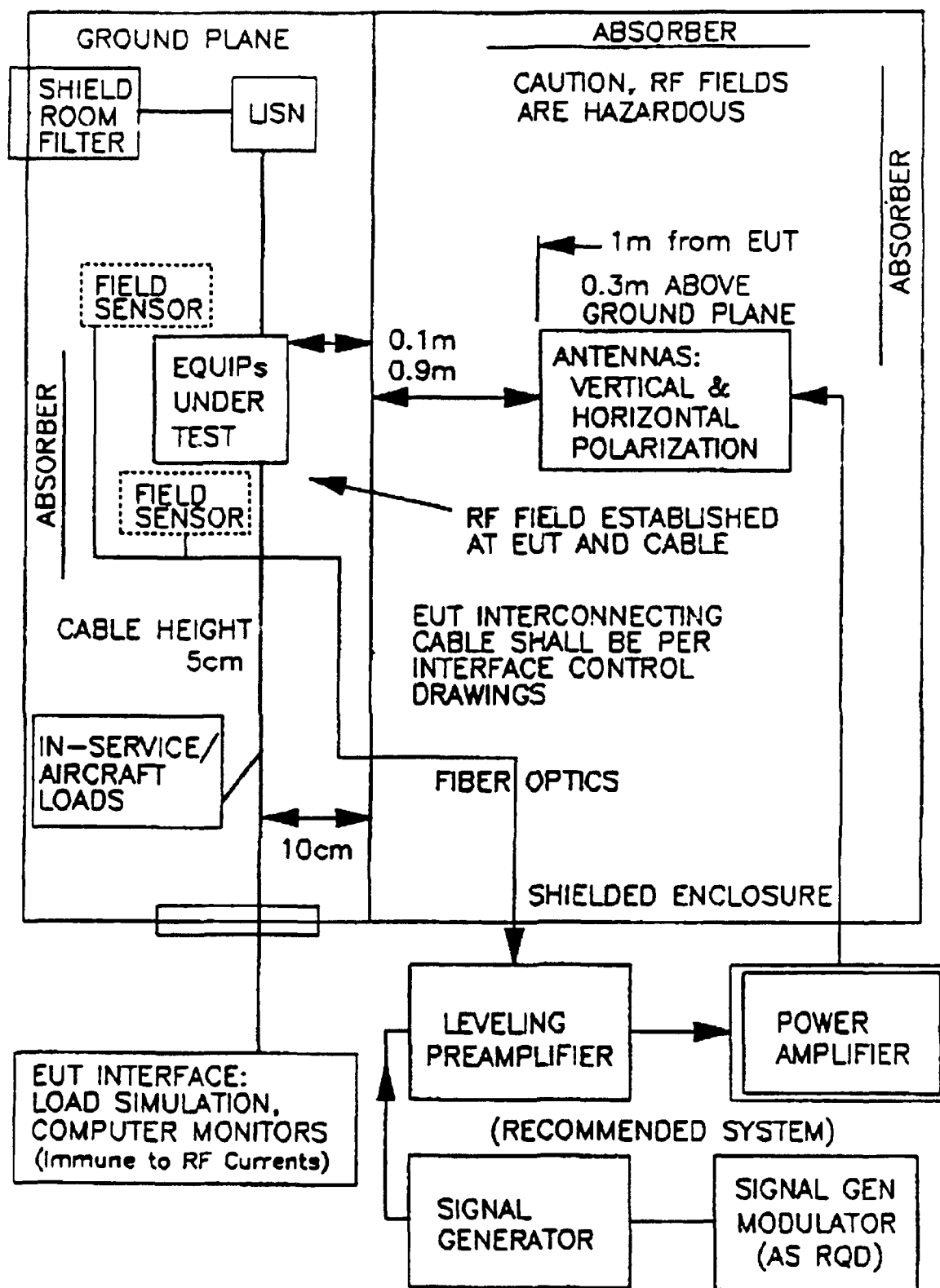


Figure 6 - RS Test Setup

Certification for the HERF Environment

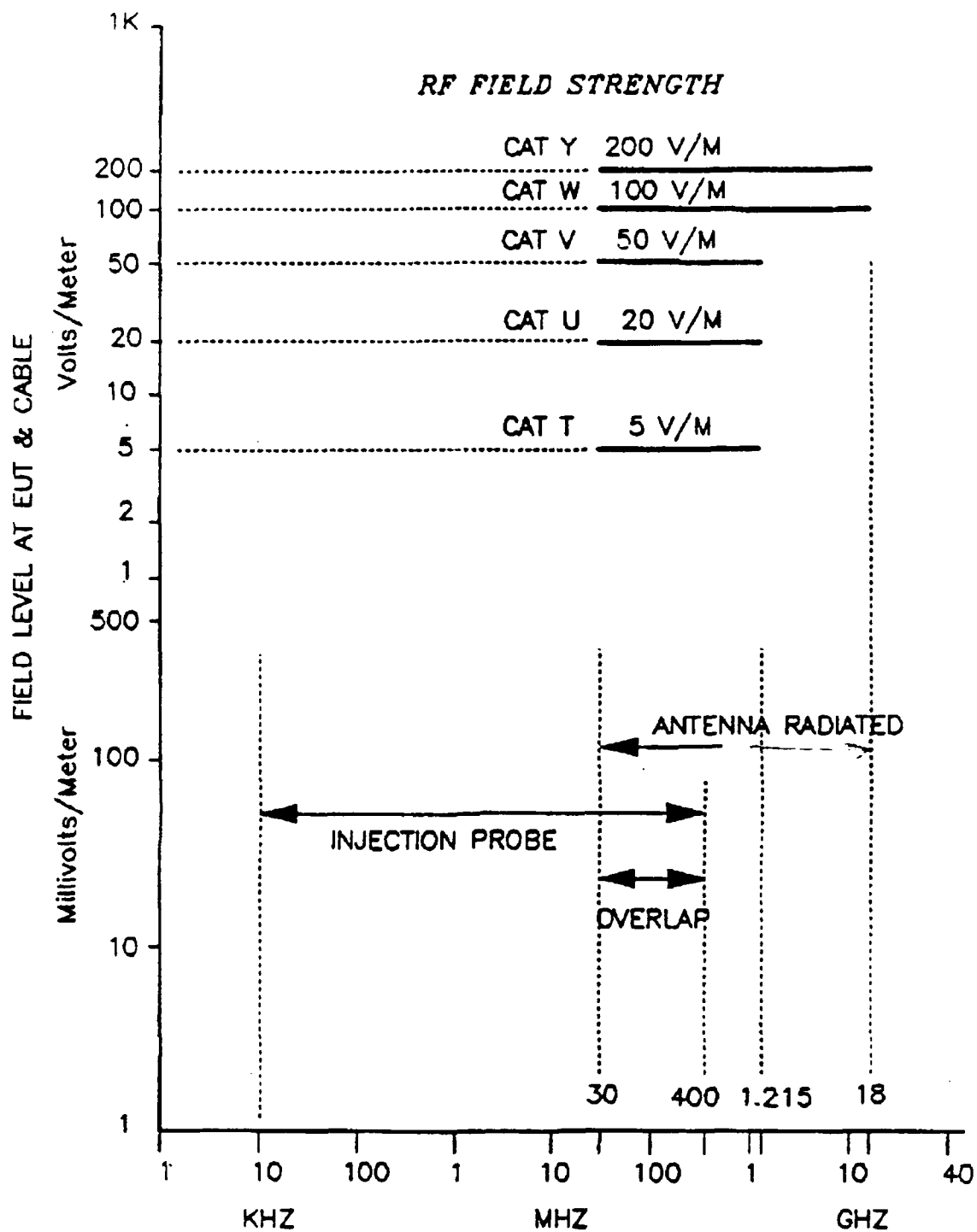


Figure 7 - RS Test Levels

Certification for the HERF Environment

RESULTS

QUANTITATIVE RESULTS.

A considerable volume of data was generated as a result of the testing performed. A complete description of the results cannot be provided due to publishing limitations for this document and for proprietary reasons.

Quantitative results for the electronically displayed attitude system are graphically summarized in Figures 8 and 9 as an example of the type of information typically obtained after reduction of the data collected. A susceptibility was considered to be an unreadable display, misleading display of information, or loss of displayed information. Pitch and/or roll errors in excess of 2 degrees were considered to be misleading.

QUALITATIVE RESULTS.

The type of susceptibilities experienced included all of those expected prior to the test with the exception of passive equipment failure. Only one case of equipment burn out was experienced, which was less than originally expected.

For equipment demonstrating unflagged, misleading information, such effects occurred only within a narrow range of RF levels. Typical experience was a noticeable deviation from normal indications, followed by abrupt blanking of information display when power levels were increased by less than 10%.

For evaluation of the availability of critical functions for HERF effects, individual susceptibilities were considered relative to their effects on operation of the airplane. It was required that no hazardous effects occur and that individual susceptibilities within critical functions be obvious.

Example - Attitude Evaluation. To illustrate this point, the example of attitude display will be discussed. Attitude in the Starship is provided by separate, electronic (EFIS) attitude director indicators (ADI) for pilot and copilot. Each ADI is provided digital data for display by separate, redundant digital systems. Display symbol generators are integral to each display.

In the event that an ADI should fail, the affected crew member may select a composite display of attitude and navigational information on a separate, electronic horizontal situation indicator (HSI) display. This is accomplished by selecting a reversionary mode.

An additional display of attitude is provided by a separate, mechanical standby indicator. The standby display utilizes a separate DC battery power supply which is constantly recharged from aircraft power, when available.

Certification for the HERF Environment

Two types of susceptibilities were evident in the electronic attitude display system.

1. Attitude "slow over" effects occurred, but were annunciated by an attitude comparator system prior to the time that excessive deviations occurred.
2. Blank displays occurred. This effect is an obvious failure, and the affected crew member would transition to backup display.
3. The standby mechanical system displayed no susceptibilities at the maximum test level of 200 V/m, and was available for backup reversion at all times.

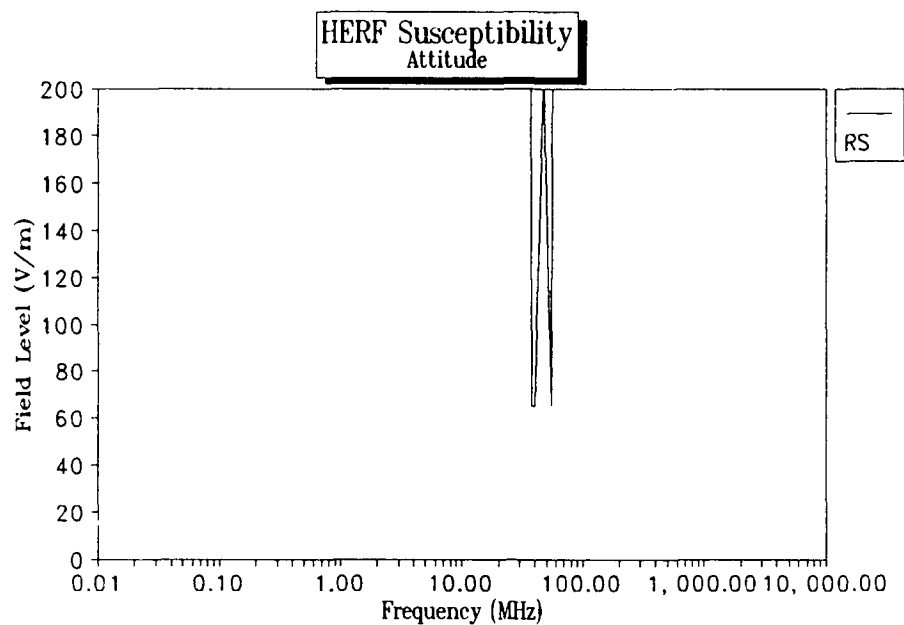


Figure 8 - Attitude, Radiated Susceptibility

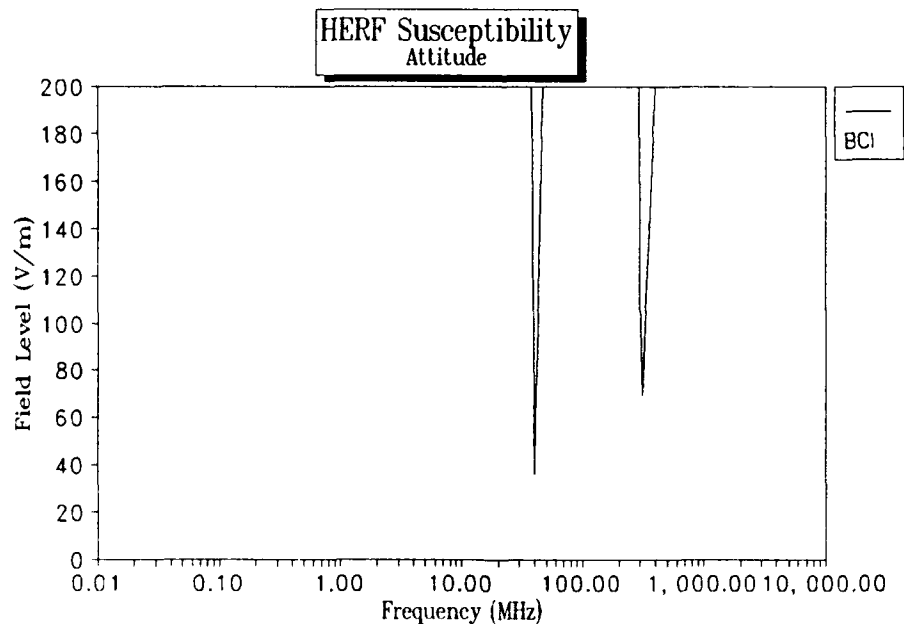


Figure 9 - Attitude, Conducted Susceptibility

Certification for the HERF Environment

CONCLUSIONS

The criteria for FAA certification was that critical functions demonstrate and certify that their operation and capabilities pertaining to safe flight and landing not be adversely affected by HERF.

This testing demonstrated that critical functions were not adversely affected by HERF when tested in accordance with the RTCA/DO-160B (Section 20, draft) procedures at levels of 100 and 200 V/m levels as described in Table 2.

RECOMMENDATIONS:

Results obtained using the BCI methods indicate that conducted susceptibility test requirements are more severe than is necessary by up to one order of magnitude, and do not accurately simulate "real world" radio field encounters. Additional analysis and testing is recommended to establish reasonable fuselage RF transfer characteristics and BCI test levels appropriate to the expected radio fields which are expected to be encountered. In cooperation with other member companies, Beech is currently in pursuit of such test development through the General Aviation Manufacturers' Association (GAMA).

THE FAA TECHNICAL CENTER'S AVIONICS DATA LINK INITIATIVE

by

Albert J. Rehmann
FAA Technical Center
Atlantic City Int'l Airport
Atlantic City, NJ 08405

For presentation to the ...IAA/FAA Joint Symposium on General
Aviation Systems at the Port O-Call Inn, Ocean City, NJ
on April 12, 1990

THE FAA TECHNICAL CENTER'S AVIONICS DATA LINK INITIATIVE

Albert J. Rehmann

FAA Technical Center

Atlantic City International Airport, NJ 08405

ABSTRACT

Weather and ATC services have been developed at the Federal Aviation Administration Administration (FAA) Technical Center to be delivered to aircraft via Data Link. The six weather and three air traffic control (ATC) services have been designed to meet with the needs of pilots and air traffic controllers. To assess the suitability of Data Link services to both user groups, two mini studies and a full fidelity operational evaluation were conducted. In the mini studies, pilots were asked to view Data Link cockpit presentations depicted on a personal computer (PC) display. In the operational evaluation, four general aviation pilots flew a GAT II B cockpit simulator configured as a Cessna 421. Four airline crews flew a B-727 cockpit simulator. Subjective and objective data were collected on pilot performance during the operational evaluation.

Results showed that the pilots' interaction time with Data Link was comparable to the time spent in voice communications. Furthermore, thirteen errors/callbacks/repeats were logged in with voice communications while none were logged with Data Link.

The Technical Center plans to continue the human factors research to broaden the pilot performance data base. Research will also continue to provide low cost solutions to expensive avionics.

INTRODUCTION

The Federal Aviation Administration (FAA) has aggressive programs underway to develop air to ground communications using Data Link as opposed to relying on voice communications.

The term "Data Link" is a rather generic term referring to digital data transmission. It is not meant to imply a specific system or type of transmission medium. For example, the FAA is procuring surveillance radars called Mode S which will replace the present day Mode A and C radars. Mode S, by virtue of its selective addressing feature, also supports a highly reliable Data Link capability. However, Data Link service is not limited to Mode S.

Part of the FAA's data link program is the development of a concept called the Aeronautical Telecommunications Network (ATN). Based on the International Standards Organization's Reference Model (ISORM), the ATN concept calls for the open interconnection of Data Links into a communication network. Thus, the term Data Link applies to an air to ground link whether the medium is satellite, Mode S, or very high frequency radio, (VHF).

In the near term, the FAA plans to offer weather services on the Mode S link only. In the longer term, ATN-compatible ground equipment will mean that these same services will be available over multiple links. At the same time that the ATN equipment is commissioned, air traffic control (ATC) services will also be available to ATN compatible avionics.

A brief description of planned Data Link weather and ATC services follows.

Weather:

Terminal Forecast (FT) - A 24-hour prognosis of weather conditions within the immediate vicinity of a selected location; includes sky and ceiling, visibility, weather, obstructions to vision, cloud heights, and whether visual or instrument conditions are expected.

Winds/Temperatures Aloft (FD) - A report of projected winds and temperatures for a range of altitudes; includes wind speed, wind direction, and temperature.

Surface Obstruction (SA) - A report of current ground weather at a selected station; includes sky conditions, ceiling, visibility, weather, obstructions to vision, wind direction/speed, altimeter setting, and additional remarks.

Pilot Reports (PIREPS) (UA) - Pilot reports of inflight conditions which may include information on sky cover, flight visibility, flight weather, and indications of icing or turbulence, etc.

Hazardous Weather (HZ) - Includes AIRMET, SIGMET, Urgent SIGMET, and Convective SIGMET. Convective SIGMET includes thunderstorm activity, turbulence, windshear icing, and lowering visibilities.

Radar Summaries (SD) - A low resolution graphic presentation of precipitation levels using ASCII characters. Radar Summaries are transmitted in six reports, each representing a region of the country.

Air Traffic Control:

Altitude Assignment (AA) - An ATC command to change to assigned altitude. The command may also contain time or crossing references and, if required, an altimeter setting.

Frequency Change (FC) - Also called sector handoff, this is an ATC command to a pilot to change to a new traffic control center frequency.

Both of these ATC services have been developed for en route airspace. They are part of a larger group of services called menu text. The menu text function allows an air traffic controller to compose a message, say at the beginning of a shift, and repeatedly send the message during the shift using trackball slewing and one function pushbutton. Menu text has the attractive feature of being reconfigurable as system conditions change.

Progress in the development of the ATC and weather services just described is

well along. In June of this year, the FAA Technical Center, near Atlantic City, N.J., will begin acceptance testing of a ground Data Link processor (DLP). The DLP has the necessary interfaces and software to access weather products from the National Weather Service, and route them to aircraft via Mode S.

ATC service development has matured to the point where detailed specifications can be written to incorporate the menu text services into the FAA's en route Host computer system. ATC service development is being performed by a team of Terminal and En route air traffic controllers from various centers across the nation.

While just two menu text (ATC) functions have been fully developed, work is ongoing in service development, and more services are expected to be added.

PURPOSE

What about the users of the system -- specifically general aviation? What services are useful to GA pilots? How much will data link cost? What about rulemaking? Can a single pilot flying Instrument Flight Rules (IFR) even use Data Link?

About 2 years ago, the Technical Center included General Aviation in their research plan for Data Link avionics. The work described in this paper describes the human factors and avionics initiatives which compose the research plan.

Historically, ground-based ATC facilities and equipment and airborne equipment have been developed, essentially, independently. The FAA perceives a serious pitfall in continuing this practice into the design of Data Link. Pilot/controller communications require a mutual understanding of the rules imposed, especially when communication is electronic in nature.

To best serve the needs of both the pilot and controller, the Technical Center conducted a series of mini studies culminating in a full fidelity operational evaluation.

Test Procedures

In the mini studies, controllers were asked to view options for Data Link services on plan view display (PVD) equipment and select preferred options. Pilots from the Air Transport Association (ATA) and from the Aircraft Owners and Pilots Association (AOPA) were asked to view cockpit-type displays of services, implemented on a personal computer. The pilots were asked to select display options, suggest appropriate responses, rule out inappropriate responses, and suggest operational procedures.

When the mini study analysis was complete, a full fidelity operational evaluation was conducted. The Technical Center's Air Route Traffic Control Center simulation facility was configured for the experiment. In addition, two aircraft simulators, a B-727 and a GAT II B, configured as a Cessna 421, were connected by telephone lines and flew as targets in the scenario.

Four airline crews flew the B-727, and four GA pilots flew the Cessna 421. The GA pilots flew single pilot IFR operations, three runs each. Average experience for the pilots was 2600 hours. The flight plan was a simulated route between Dupont (DPQ) VOR and Philadelphia International Airport.

The man-machine interface (display) in these experiments consisted of a fairly low resolution display with a touch sensitive surface (figure 1). It was intended to represent a low cost display suitable for GA applications. During the experiments, subjective, and objective data were gathered on non-Data Link runs and runs with Data Link in two degrees of difficulty (reference 1).

Of prime importance was the determination of just how suitable (or unsuitable) data link services, as designed, were for the GA pilot.

RESULTS

Pilots were asked to rate Data Link as presented from 0 (poor) to 7 (very good) in the following areas:

- a. Appearance
- b. Clutter
- c. Amount of Information
- d. Information Clarity
- e. Ambiguity
- f. Time to interpret

Data Link received the ratings listed in table 1:

<u>Rating</u>	<u>Alt Assignment</u>		<u>Freq Change</u>	
	<u>Avg</u>	<u>Std</u>	<u>Avg</u>	<u>Std</u>
Appearance	6.25	0.96	6.25	0.96
Clutter	6.5	1.0	6.25	0.96
Amount of Information	7.0	0.0	7.0	0.0
Information Clarity	6.25	0.5	6.5	0.58
Ambiguity	6.75	0.5	7.0	0.0
Time to Interpret	6.5	1.0	6.25	0.96

Table 1. GA Pilot Ratings of ATC Services

Negative comments were:

1. "Too many words to read"
2. "Color 'Green' is hard on the eyes."

Positive Comments were:

1. "Much clearer than voice"

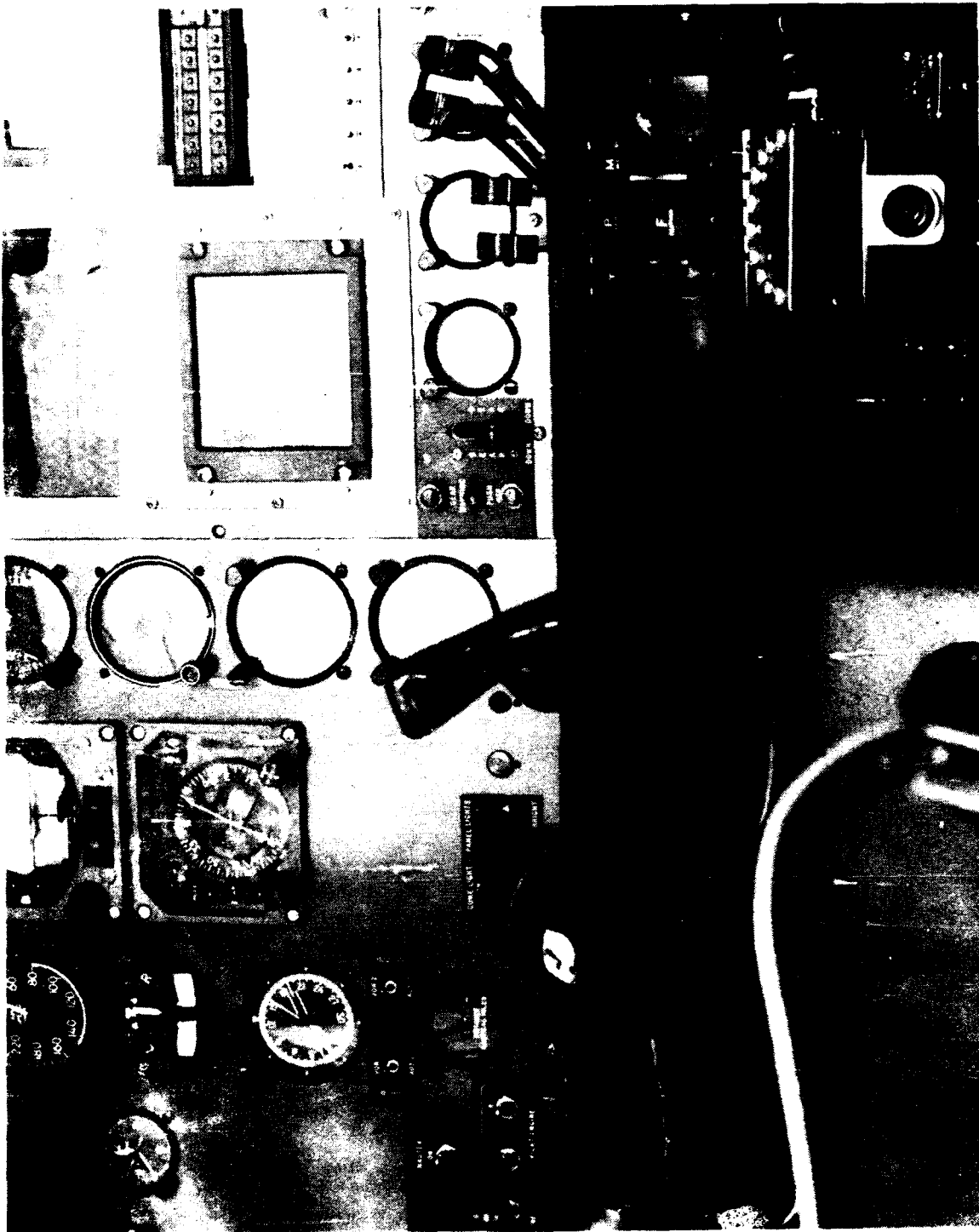


Figure 1. Data Link Avionics
Installed in Cessna 421 Simulator

2. "Having current plus new frequency can eliminate errors by pilot misunderstanding new frequency or forgetting old frequency."

Some interesting objective data were also collected. Measurements of pilot response time and errors were made for voice-only and voice plus Data Link communications.

A total of 13 errors were recorded in voice communications; none were recorded with Data Link. Aggregating the total time required to request and process spoken messages versus Data Link messages, a comparison shows that less pilot involvement time is spent using Data Link. It must be understood that this comparison is strictly pilot involvement time and is irrespective of link delays due to antenna rotation, etc. When one considers the time spent in callbacks and repeated messages, the real significance of Data Link becomes clear. These results are presented graphically in figure 2.

It should be remembered that a non-optimized man-machine interface was used in this experiment. Results were generally expected to be positive, while pointing to areas where improvements could be made. Instead, the results showed that the services as presented were entirely useful, and actually reduced voice communications errors.

Results for the B-727 pilots were generally the same, although the air carrier crews generally responded more slowly than the Cessna-421 pilots.

Specific details regarding the experiment are available in a two-volume final report to be published at the Technical Center in the next month or so.

CONCLUSIONS/FUTURE CONSIDERATIONS

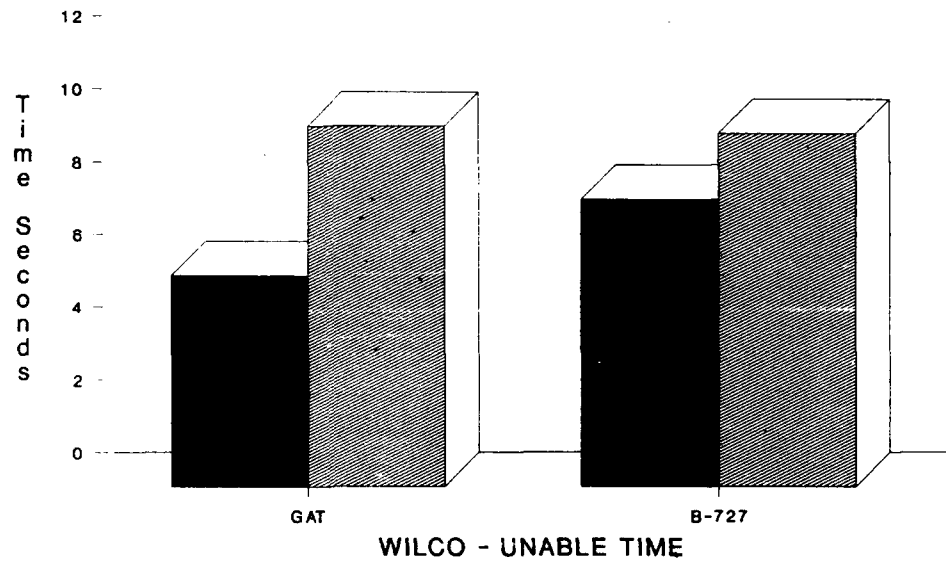
Even though more data will be gathered, the operational evaluation data suggests that Data Link is entirely suitable for single pilot IFR. But what about other questions such as cost and rulemaking?

The FAA has no plans to mandate Data Link. If, however, a pilot wishes to use Data Link, his ship's avionics will have to be ATN compatible. Two comments apply. First, the Technical Center has research underway to develop OSI-compatible layers to implement a communications protocol suitable for general aviation.

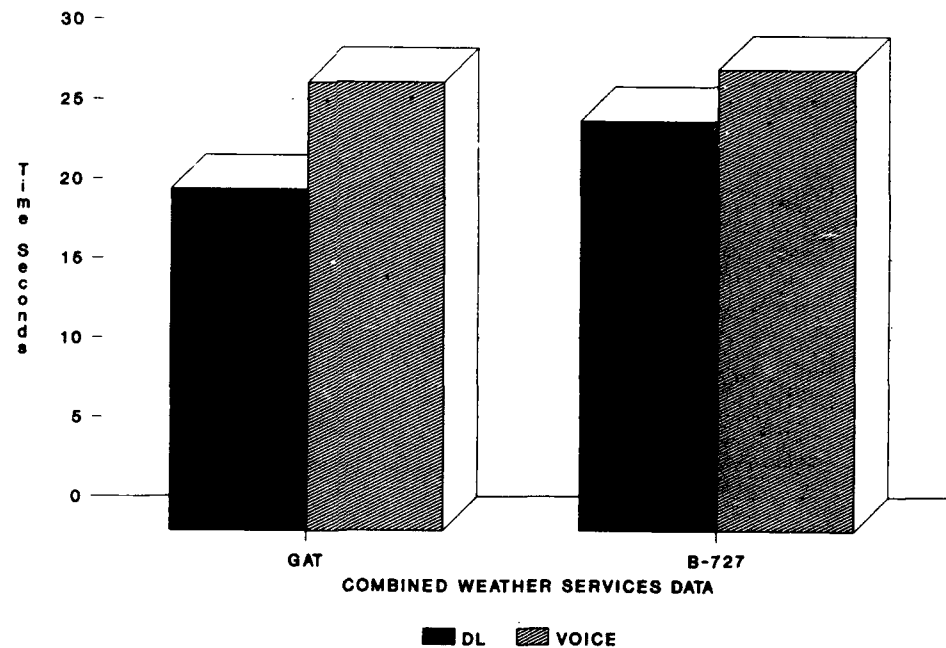
Recognizing that light aircraft will likely carry only one Data Link, or two at the most, the full range of ATN options is not necessary, and can be eliminated to reduce cost.

The second comment pertains to Mode S. Carrying an altitude reporting Mode S transponder with Data Link capability will provide access to Data Link services. It will also enhance access to Terminal Control Areas (TCA) and other controlled airspace, and will provide safety by making your aircraft visible to other aircraft carrying TCAS equipment.

DATA LINK VS. VOICE Overall - ATC



DATA LINK VS. VOICE TOTAL PILOT INTERACTION TIME



TPIT = MCT + RL + MPT

Figure 2. Pilot Performance
Data Voice vs Data Link

The FAA is working closely with avionics manufacturers to bring down the cost of airborne equipment. However, prices for Mode S Data Link equipment are a long way from being affordable to the light aircraft owner.

The high cost of avionics stems from low production quantities and segregated functions. It is believed that by integrating functions, the combined cost of avionics will be substantially lowered. To this end, the Technical Center is sponsoring research to examine new approaches to communication/navigation management, fuel and engine control, and flight following, to find ways to integrate aircraft systems and to allow multiple functions to be performed by single components.

To answer difficult questions regarding ATN cost and overhead, research is being sponsored to develop large-scale-integration (LSI) integrated circuits to implement ATN functions. Additional research involves avionics prototyping to demonstrate low cost flyable systems.

Tying all the research together, the Technical Center plans a second series of mini studies, culminating in a full fidelity operational evaluation. Data Link products and services will be evaluated using minimum cost avionics. The operational evaluation will anticipate ATC and weather service availability on Data Link. Current FAA planning is to offer weather services on Mode S beginning in December 1990, following with ATC services in early 1994.

The General Aviation segment represents a group of users of prime importance to the FAA. Through structured research and development the FAA intends to go well beyond just meeting your needs in Data Link. The goal is to provide the kind of service to General Aviation that allows pilots to attain the highest performance possible.

Researchers at the FAA Technical Center strive to be receptive, and to ensure that the proper questions are asked, and answered, from the GA perspective, in the development of airborne Data Link.

Reference:

1. An Operational Evaluation of a Prototype Airborne Data Link System, MSR-TR-89-1001, Midwest Systems Research Inc., Dayton, Ohio.

GENERAL AVIATION AND TCAS

by

Carl B. Jezierski
FAA Technical Center
Atlantic City Int'l Airport
Atlantic City, NJ 08405

For presentation to the AIAA/FAA Joint Symposium on General
Aviation Systems at the Port O-Call Inn, Ocean City, NJ
on April 12, 1990

General Aviation and TCAS

Carl B. Jezierski
Department of Transportation
Federal Aviation Administration
Technical Center
Atlantic City International Airport, New Jersey 08405

ABSTRACT

The amended Traffic Alert and Collision Avoidance System (TCAS) rule was published in the Federal Register on April 9, 1990. It requires TCAS-II equipment of all civil aircraft with more than 30 passenger seats operating in the United States by December 30, 1993. The same rule also requires turbine powered aircraft with 10 to 30 seats to be equipped with TCAS-I by February 9, 1995.

This paper briefly describes the technical operation of the different types of TCAS and how General Aviation participates in the TCAS environment. Development efforts of a low cost airborne collision avoidance system are also addressed.

INTRODUCTION

Several approaches to airborne collision avoidance were developed and tested by industry and the government over the past 30 years. The collision avoidance system development and implementation program in its present form, TCAS, was initiated by the Federal Aviation Administration (FAA) in 1981.

TCAS was envisioned to have two major elements: the threat evaluation or traffic alert function and the response or collision avoidance function. Systems implementing the traffic alert function only are classified as TCAS-I. They are intended to be low cost systems for use in general aviation (GA) and small commuter aircraft. Systems implementing the collision avoidance function were initially classified as TCAS-II. This class was then further subdivided as it became evident that directional antenna information could be exploited to provide another dimension for escape maneuvers. TCAS-II refers to systems providing resolution advisories (RA) in the vertical dimension. TCAS-III, when fully developed, provides RAs in both the vertical and horizontal planes. A Mode S transponder is intrinsic to the TCAS-II/III configuration and is used by TCAS to coordinate RAs with a second TCAS unit to ensure complementary maneuvers. These systems would typically be found in airliners and large corporate aircraft. Figure 1 shows the parameters of TCAS by type.

Parameter	TCAS-I	TCAS-II	TCAS-III
User	GA, military, turbine powered aircraft with 10 - 30 seats, rotorcraft	Large aircraft, turbine powered aircraft with more than 30 seats	Large aircraft, turbine powered aircraft with more than 30 seats
Traffic Advisories	Yes	Yes	Yes
Resolution Advisories	None	Vertical	Vertical & Horizontal
Coordination	None	Yes	Yes
Bearing Data	Traffic Display only	Traffic Display only	RA solution and display
Display Range	4 nmi Maximum	4 nmi Minimum	4 nmi Minimum

FIGURE 1. CHARACTERISTICS OF TCAS EQUIPMENTS

GA OPERATIONS IN THE TCAS ENVIRONMENT

TCAS operates by detecting and tracking proximate traffic equipped with ATCRBS or Mode S transponders. Traffic advisories (TAs) and RAs are issued based on time to closest point of approach (CPA), range, and relative altitude at CPA. TA and RA issuance times are approximately 40 and 25 seconds, respectively, and vary by altitude.

Range and direction to the nearby aircraft from own aircraft are displayed to the pilot as well as TAs. Relative altitude and RAs will also be displayed if the other aircraft is reporting altitude. A typical TCAS-II/III display is shown in figure 2. A modified instantaneous vertical speed indicator (IVSI) is also part of the TCAS-II configuration. A TCAS-I display has the same characteristics except that the red intruder symbol and data would not be displayed. The display range would also be limited to 4 nmi.

There are two ways for own aircraft to take part in the TCAS environment. First, as a minimum, own aircraft would be equipped only with either a standard ATCRBS or Mode S transponder. Optimum TCAS performance against own aircraft is obtained when altitude encoding is used with the transponder. The TCAS equipped aircraft

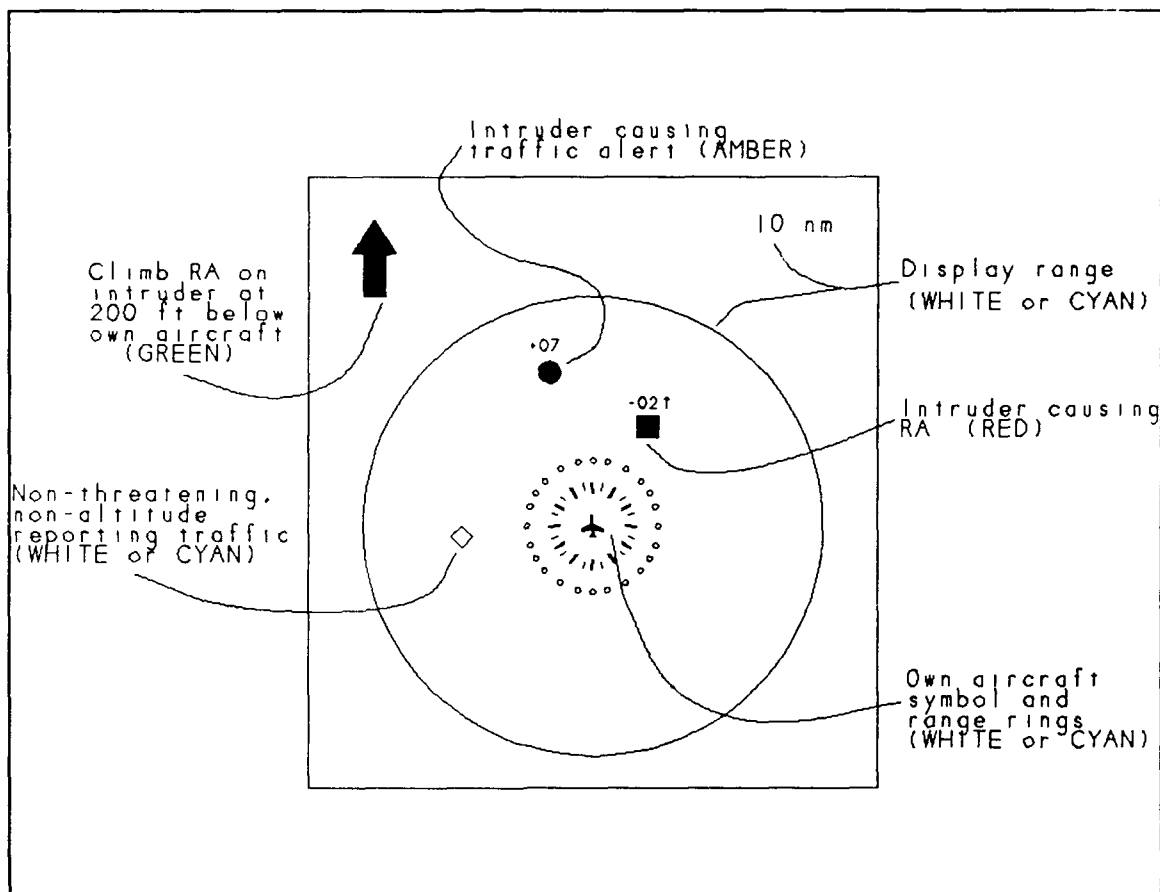


FIGURE 2. SAMPLE TCAS-II/III DISPLAY

performs its maneuver without mode-S coordination with own aircraft. The limitation here is that own aircraft, with this minimum configuration, can not detect any other aircraft independent of air traffic control (ATC).

Second, own aircraft may participate in the TCAS environment by being equipped with TCAS. If the system is a TCAS-I, it performs as a set of electronic eyes to aid the pilot in visually acquiring the intruder. The pilot then chooses his course of action based on the visual (windshield) information available to him. He does not maneuver solely on the basis of his traffic display. If the system is a TCAS-II or TCAS-III, then the maneuvers are coordinated between aircraft via Mode S. The pilot does not maneuver on TAS but waits for an RA. Flight testing during the TCAS-II Limited Installation Programs (LIP) indicate that most TAS are resolved by ATC or clear themselves because of geometry and do not develop into RAs.

DEVELOPMENT OF TCAS-I

TCAS-I is intended to be used with GA, small military aircraft, and turbine powered aircraft with 10 to 30 seats. Early development work includes the design of a TCAS-I by MIT Lincoln Laboratory (MITLL) and its test on a Bell 206-L helicopter at MITLL and a Sikorsky helicopter at the FAA Technical Center. The FAA awarded contracts for the development of "proof of concept" models and low cost systems.

The Minimum Operational Performance Standards (MOPS) document for TCAS-I was completed by the Radio Technical Commission for Aeronautics (RTCA) in March, 1987. The FAA subsequently issued a TSO based on this specification for TCAS-I.

The FAA initiated a TCAS-I LIP to provide technical, operational, and certification data required for commuter/air taxi operators in the shortest possible time to meet the TCAS Rule requirements. The LIP will provide seed money for one manufacturer to produce a more capable commuter TCAS-I system. It is expected that some of the technology developed during the LIP will be applicable to GA TCAS-I systems.

The formal request for proposals was issued by ARINC Research, the FAA support contractor for this project, on December 29, 1989, with responses due from prospective manufacturers by February 20, 1990. The RFP is for the production and delivery of a minimum of six shipsets of TCAS-I avionics, displays, antennas, recorders, and engineering support for all phases of the project. A contract award is expected to be made by April 30.

A 1 year in-flight evaluation of the systems will be conducted aboard regional airline aircraft. Recorded data will be archived and analyzed at the FAA Technical Center for TA rate and geometry computations and MITLL for surveillance considerations.

TCAS observers will accompany the flight crew on many of the scheduled flights to record operational procedures, pilot and ATC issues, and crew opinion of the system's utility. The crews will also be asked to fill out questionnaires. These responses will be analyzed and tabulated by ARINC Research for inclusion in the project report.

The lessons learned from this evaluation will then be used to fine tune system parameters and operational procedures.

CONCLUSIONS

TCAS will result in a safer flight environment. Small, transponder equipped, aircraft are protected in an encounter with a TCAS aircraft. Situational awareness is improved because TCAS alerts

the pilot to the presence of transponder equipped proximate traffic and indicates its location.

While TCAS-II is the closest to implementation (20% equippage of large aircraft with more than 30 seats by the end of 1990), the specifications for TCAS-I are formalized and an implementation program is funded and well underway. Development efforts for TCAS-III continue with flight test, simulation, and research.

Bibliography

AIR SAFETY, FAA's Traffic Alert and Collision Avoidance System, U.S. General Accounting Office, February 1988.

R.M. Handley, TCAS - A Lengthy But Beneficial Development Effort, ICAO bulletin, October 1989.

Federal Register, Monday, April 9, 1990.

Traffic Alert and Collision Avoidance System (TCAS), Status and Future Plans, DOT FAA Advanced Systems Acquisition Service, Ground to Air System Division, October 18, 1988.

Technical Standard Order: TSO-C118, Traffic Alert and Collision Avoidance System (TCAS) Airborne Equipment, TCAS-I, DOT FAA Office of Airworthiness, August 5, 1988.

**SUMMARY OF THE FAA LOW DATA RATE VOICE CODEC EVALUATION
AND DEMONSTRATION PROGRAM**

by

Markus R. Grable
CTA Incorporated
English Creek Center
The Courtyard, Suite 204
McKee City, NJ 08232

For presentation to the AIAA/FAA Joint Symposium on General
Aviation Systems at the Port O-Call Inn, Ocean City, NJ
on April 12, 1990

SUMMARY OF THE FAA LOW DATA RATE VOICE CODEC EVALUATION AND DEMONSTRATION PROGRAM

Markus R. Grable
CTA INCORPORATED
English Creek Center
The Courtyard, Suite 204
McKee City, NJ 08232

ABSTRACT

This paper summarizes the Federal Aviation Administrations (FAAs) low data rate voice coder/decoder (CODEC) evaluation and demonstration program. This program will assess the performance and operational characteristics of low data rate voice digitizing equipment in an aeronautical satellite link environment for Air Traffic Control (ATC) applications. A concern of the FAA is to achieve acceptable voice performance for ATC in the most efficient manner. The FAA will recommend a low data rate voice CODEC standard for inclusion to Aeronautical Mobile Satellite Service (AMSS) voice communications based on the program results. This paper will focus on the Phase II CODEC evaluation and results.

INTRODUCTION

The Federal Aviation Administration (FAA) is conducting a low data rate voice coder/decoder (CODEC) evaluation test program. This program will assess the performance and operational characteristics of low data rate digitized voice digitizing equipment in an aeronautical satellite link environment for Air Traffic Control (ATC) applications. A concern of the FAA in this assessment is to achieve acceptable voice performance for ATC in the most efficient manner.

PURPOSE

The program objectives include:

- 1) Evaluate the performance of low data rate voice CODECs in an aeronautical satellite link environment for Air Traffic Control (ATC) applications.
- 2) Support the development of Standards and Recommended Practices (SARPs), prepared by the International Civil Aviation Organization (ICAO), as well as Minimal Operational Performance Standards (MOPS), prepared by the Radio Technical Commission for Aeronautics (RTCA), for Aeronautical Mobile Satellite Service (AMSS) voice communications.

3) Develop a test bed replicate both aircraft and ATC room environments in which digitized voice can be demonstrated.

4) Recommend a low data rate voice CODEC standard for inclusion to AMSS voice communications.

BACKGROUND

The ICAO has developed requirements for the AMSS for use by the civil aviation community. Satellite and avionic systems are being developed for this purpose. Such systems will eventually provide data and digitized voice communication capabilities with aircraft for safety related services such as air traffic services (ATS) and aeronautical operational control (AOC), as well as non-safety related services such as aeronautical administrative communication (AAC) and aeronautical passenger communication (APC).

The ICAO committee on Future Air Navigation Systems (FANS) established digital transmission of voice as a requirement of AMSS. The FANS report notes the numerous advantages of digital voice techniques for air-ground satellite communications. The details of data rates and speech coding algorithms have not been determined.

The digitized voice transmitted via satellite will enhance current communications in many ATC related environments. In particular, this technology will improve voice communications in oceanic airspace, where high frequency (HF) radio communications currently provides marginal service. This service can also be useful in continental airspace with low traffic density (such as low altitude, offshore and remote areas), where very high frequency (VHF) service is poor or nonexistent. In addition, this technology will preserve the ATC safety margin as well as provide more efficient air traffic services.

The equipment that converts analog voice signals to a digital representation of the speech signal is called a coder/decoder (CODEC). The digital representation is transmitted to the remote location as a sequence of binary bits. Digital transmission provides a considerable measure of signal-to-noise improvement. At the receiving location, the CODEC converts the digital representation back to an analog signal for reception by a human operator.

The selection of a suitable CODEC and data rate for digital transmission involves the consideration of many parameters. For example, higher data rates are desirable for optimum voice quality. However, lower data rates are desirable for accommodating more users on a satellite link channel that have inherent limitations of bandwidth and power.

A 9600 bit per second (bps) data rate CODEC algorithm standard for aeronautical satellite voice services was recently selected by the Airline Electronic Engineering Committee (AEEC) Satellite Systems

Subcommittee's Voice Coding Working Group. The AEEC selected this CODEC based primarily on the results of subjective listening tests conducted by British Telecom Research Laboratory (BTRL). The BTRL tests were based on the presumption that the initial use of the satellite voice channel is for aeronautical passenger communication (APC) telephone service. The UK Civil Aviation Authority (CAA) conducted an independent evaluation of the same CODECs for pilot/ATC communication applications. The CAA evaluations were a secondary selection criteria for the AEEC based on assumptions that APC quality service will be suitable for an ATC service. When the AEEC CODEC standard was selected, it was concluded that CODEC technology at a 9600 bps data rate was a minimum for near toll quality. Recent advances in new coding techniques and implementations have shown dramatic improvements in low data rate technology.

The FAA has initiated the investigation of lower data rate CODECs (4800 bps and lower) for use with AMSS. The FAA recently completed a two phase CODEC test program which evaluated and demonstrated low data rate voice CODEC technology (4800 bps and 2400 bps).

The FAA Phase I test program involved inviting manufacturers of 4800 bps and 2400 bps data rate voice CODECs to participate in a prequalification evaluation based on subjective listening evaluations. The eight respondents were each sent an audio cassette test tape to process through their respective CODEC algorithms. This tape, prepared with the cooperation of Rome Air Development Center (RADC), contained controller-pilot dialog and Diagnostic Acceptability Measure (DAM) sentences. DAM sentences are sets of phonetically balanced sentences used as industry standard material for subjective speech evaluations. The CODEC processed tapes were returned to the FAA for evaluation by ATC personnel from the New York Air Route Traffic Control Center (ARTCC). The controllers were asked to evaluate voice acceptability and intelligibility based on the Mean Opinion Scoring (MOS) system, an industry standard for subjective speech quality evaluations. In the simplest form of this system, an MOS evaluator rates the acceptability of processed speech on a scale of one (poor) to five (excellent). An MOS score of five indicates perfect quality, a score of four or more indicates high quality (toll quality in the telephony field), while MOS scores of three to four are referred to as "communication quality."

The MOS results of the Phase I evaluation were used to qualify a select number of CODECs for further testing in Phase II. The manufacturers of the selected CODECs were asked to submit equipment to the FAA for direct CODEC testing and evaluation in Phase II.

In addition to the FAAs independent Phase I and II CODEC testing, a joint FAA/JPL experiment was performed to evaluate JPL's ground mobile satellite experiment (MSAT-X) terminal equipment in an aeronautical mobile satellite environment. The 4800 bps CODEC used in the experiment was developed for JPL by the University of California at Santa Barbara (UCSB). The experiment involved using

the INMARSAT Marecs B2 satellite which provides coverage of the Atlantic ocean. The experiment was conducted using the FAA's Boeing 727 B100 aircraft during a flight path over the Atlantic ocean. A full duplex satellite communications link was established between the aircraft and the COMSAT ground earth station located in Southbury Connecticut. A prepared script was spoken through the link and exhibited acceptable voice quality and favorable intelligibility.

The following sections describes the FAA Phase II CODEC testing and results in further detail.

TEST APPARATUS

The FAA CODEC test bed (CTB) was established for Phase II of low data rate voice evaluations and demonstrations. Five CODEC manufacturers were asked to submit hardware based on Phase I results. Some of the manufacturers provided CODECs with multiple data rates or different versions of their algorithm for a total of eleven CODECs tested; one at 9600 bps, five at 4800 bps and five at 2400 bps. The test configuration (figure 1) included operating the CODEC pairs back-to-back via a digital bit error rate (BER) simulator. The simulator is designed to insert bit errors into the digital bit stream typical of satellite link performance degradation. A channel simulator was also included in the test configuration to model the effects of an analog telephone link to a pre-CODEC processed message. The processed audio was recorded for evaluation and further comparative studies.

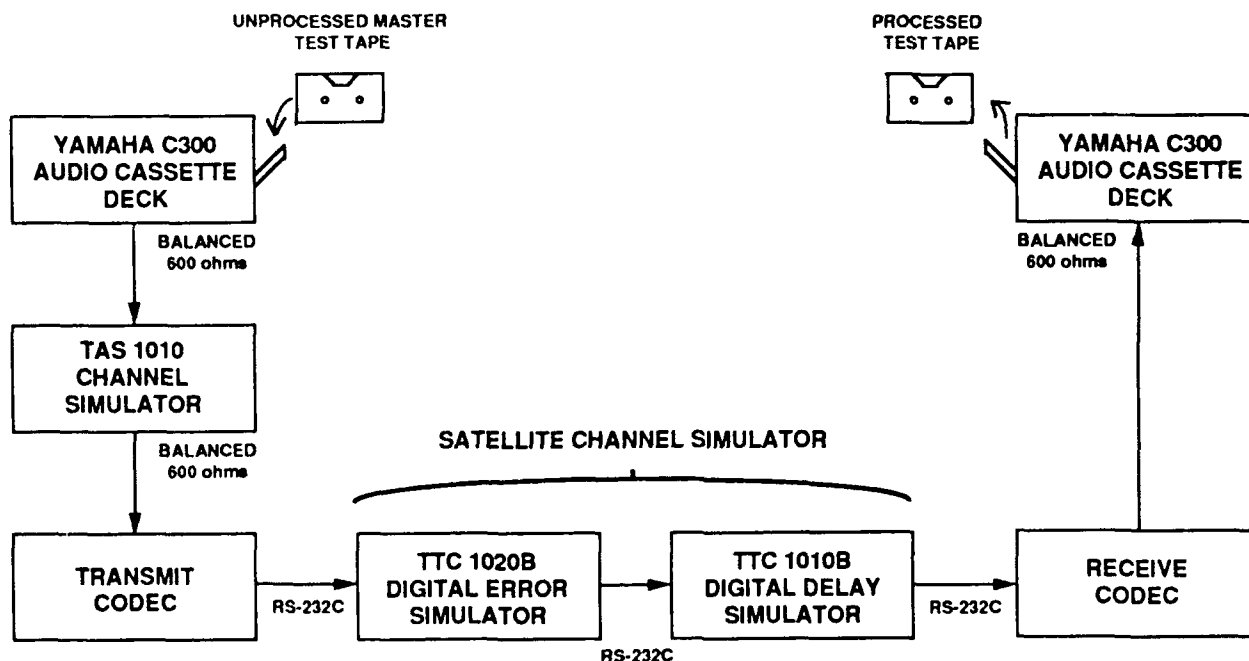


FIGURE 1. PHASE II TEST CONFIGURATION

TEST PROCEDURES

The source recordings were generated with messages spoken by eight volunteer ATC controllers from the New York ARTCC and four pilots from the FAA Technical Center. The volunteers first recited the messages in a quiet environment, then with ATC room and cockpit background noise introduced at the appropriate levels through speakers. The cockpit noise level was 83 dBa recorded in the FAA Boeing 727 cruising at 14,500 ft. The ATC room noise level was 73 dBa recorded during a peak hour at the Washington ARTCC.

Three types of test speech material were used for the three part test evaluation. The material in part 1 was a set of close rhyming/related word pairs. This test type is similar to the Diagnostic Rhyme Test (DRT) or Modified Rhyme Test (MRT), which are common forms of industry standard intelligibility tests. The FAA differs from the industry standard in that a number of ATC related words were included in the text without regard to the phonetic balance of the resulting word pair. The evaluator in this type of test was asked to distinguish between the given word pair.

Part 2 material consisted of typical pilot-ATC related sentences. The evaluator in this test type had to identify certain spoken numerals within each sentence.

Part 3 consisted of a majority of pilot-ATC related single words or phrases. The evaluator was asked to identify these words or phrases.

In addition, each evaluator was asked to fill out a questionnaire regarding the acceptability of the CODEC under test and to compare the CODEC processed audio to current voice communications.

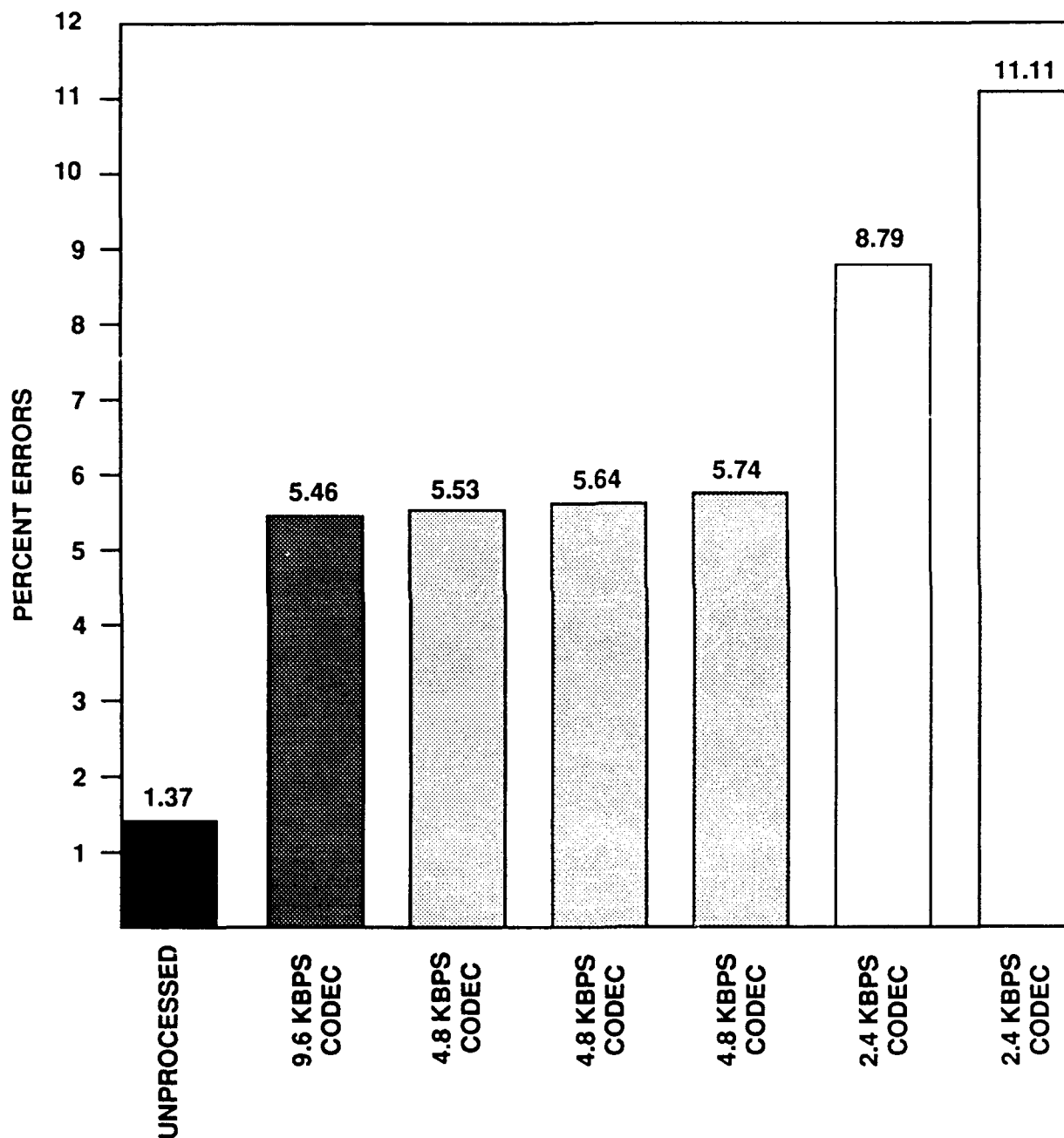
Three listener groups were used for evaluating the CODEC processed tapes; non-ATC personnel, ATC personnel with mostly en route controller experience (Washington ARTCC), and ATC personnel with mostly oceanic controller experience (Oakland ARTCC). The non-ATC personnel evaluated the initial set of eleven CODECs first in order to limit the number of CODECs to six and minimize evaluation time for the ATC personnel. The original unprocessed audio tape was included in the evaluation for control purposes.

RESULTS

Each CODEC received a score based on a percentage of wrong answers averaged over the three part test (table 1). The results established that the intelligibility of the 4800 bps CODECs are essentially equivalent to the intelligibility of the 9600 bps CODEC. The intelligibility scores of the 2400 bps CODECs were a few percentage points lower.

The results of the subjective acceptability questionnaire indicated that the best 4800 bps CODEC was considered as acceptable as the 9600 bps CODEC. In addition, the majority of controllers expressed

TABLE 1. PHASE II INTELLIGIBILITY RESULTS



NOTE: AVERAGE CODEC INTELLIGIBILITY SCORES OVER EACH SECTION (DRT, FILL IN #, AND WORD RECOGNITION), BACKGROUND NOISE (QUIET, ATC ROOM, AND COCKPIT), AND BIT ERROR RATES (10E-5, 10E-3, 10E-2)

that the 9600 CODEC and the best 4800 bps CODEC were nearly equivalent to current communications. The controllers who distinguished between very high frequency (VHF) and high frequency (HF) rated the CODECs higher than HF, but equivalent to or worse than VHF. The 2400 bps CODECs were considered not acceptable by most controllers with VHF background, and by some controllers with HF background.

Individual scores categorized by background noise and BER conditions were calculated. These results indicated that the intelligibility scores were lowest under the combined conditions of operational background noise and high bit error rates. It should be noted that these combined conditions fluctuated rapidly, some of which were worse than normal operating conditions. Even under these conditions, the intelligibility of the 9600 and 4800 bps CODECs remained high.

CONCLUSIONS

The following conclusions were drawn from the results of the Phase II test program:

- 1) The intelligibility of the 4800 bps CODECs were nearly as high as the 9600 bps CODEC in a simulated ATC environment. High intelligibility persisted under conditions combining operational background noise and BER,s.
- 2) That the acceptability of the 4800 bps CODEC range from approximately equivalent to slightly worse than the 9600 bps CODEC. The opinion of the ATC personnel was divided over the acceptability of the 9600 bps and the 4800 bps CODEC's, with roughly half of the controllers stating that the CODEC's were acceptable for ATC use.
- 3) The intelligibility and acceptability measures of the 2400 bps CODECs as compared to the 4800 bps and 9600 bps CODECs were significantly lower.

FUTURE PLANS

A Phase III CODEC test program has been initiated as a result of the previous evaluations. Phase III will include more comprehensive testing of two CODEC pairs chosen based on Phase II results, as well as CODEC pairs previously unavailable to the FAA. A low data rate voice CODEC standard for inclusion to AMSS voice communications will be identified and recommended from the Phase III results.

Future flight tests will continue with the CODEC(s) selected from Phase III testing. The FAA is currently establishing a communications test facility equipped with avionics, satellite, and test equipment for the flight tests.

Technologies for voice CODECs operating at data rates of 2400 bps and lower are maturing rapidly. CODEC manufacturers are contacted periodically concerning developments of low data rate coding techniques that could possibly improve voice intelligibility. As the lower data rate technology improves, tests will be conducted to evaluate the potential benefits to ATC operations.

REFERENCES

1. Child, J., Cleve, R., and Grable, M., Evaluation of Low Data Rate Voice CODECs for Air Traffic Control Applications, Technical Note, CTA INCORPORATED for the FAA Technical Center, DOT/FAA/CT-TN89/13, January 1989.
2. Dehel, T., Grable, M., Child, J., Phase II Testing and Evaluation of Low Data Rate Voice CODEC Equipment, Technical Note, CTA INCORPORATED for the FAA Technical Center, DOT/FAA/CT-TN89/49, August 1989.
3. International Civil Aviation Organization (ICAO), Report of the Fourth Meeting of the Special Committee on Future Air Navigation Systems (FANS/4), Montreal, 1988.
4. Airline Electronic Engineering Committee (AEEC), Report of Satellite Subcommittee's Voice Coding Working Group Meeting held December 13, 1988, in Arlington, Virginia, AEEC Letter 89-006/sat-96, February 13, 1989.
5. Quackenbush, S., Barnwell, T., Clements, M., Objective Measures of Speech Quality, Prentice-Hall, 1988.
6. Jayant, N. S., Coding Speech at Low Bit Rates, IEEE Spectrum, Vol. 23, no. 8, August 1986, pp.58 - 63.

THE PILOT'S AUTOMATED WEATHER SUPPORT SYSTEM CONCEPT

PAWSS

Prepared for
FAA ARD-42 & ARD-300
on
Contract NAS1-18585, Task 62

by
Ernie R. Dash
ViGYAN, Hampton, Virginia
and
Norman L. Crabill
Aero Space Consultants, Newport News, Virginia

For presentation to the AIAA/FAA Joint Symposium on General Aviation Systems
at the Port-of-Call Inn, Ocean City, New Jersey
on April 12, 1990.

~~PROPRIETARY RIGHTS RESERVED~~

THE PILOT'S AUTOMATED WEATHER SUPPORT SYSTEM CONCEPT

Ernie R. Dash
ViGYAN, Hampton, Virginia
and
Norman L. Crabill
Aero Space Consultants, Newport News, Virginia

ABSTRACT

The FAA is initiating an investigation of the Pilot's Automated Weather Support System (PAWSS). The PAWSS concept is to provide the enroute pilot with a continuous assessment of surface and aloft weather conditions automatically acquired and presented in pilot-oriented map depictions. Other system concepts include a data link with a short update cycle, color-coded map depictions with alpha-numeric backup, an automated assessment of weather trends with hazardous conditions alerting, and a non-keyboard control system. PAWSS will also assist the pilot through expert system procedural guidance for preflight as well as inflight decision support.

INTRODUCTION

Pilots need timely and accurate weather data to make informed decisions for both preflight and inflight operations. The present National Airspace System (NAS) weather support system provides pilots access to extensive weather data for preflight planning but only limited data is available to the enroute pilot; primarily through voice broadcast and request/reply procedures. New National Weather Service (NWS) and FAA weather data sources and new planned data link communication systems will provide the enroute pilot access to more weather data. The weather support procedures for both the current and planned weather support systems, however, require extensive effort for the pilot to acquire and assimilate an adequate view of the existing and forecast weather, especially under adverse conditions. The Pilot's Automated Weather Support System (PAWSS) concept is being developed to determine if automation techniques can be used to provide pilots with a better view of flight weather conditions with much less work. In this paper we will review our preliminary systems concepts and illustrate some pilot-oriented PAWSS products. While the initial focus is on the enroute pilot, the PAWSS concepts and techniques will also benefit the preflight pilot.

SYSTEM CONCEPT

The PAWSS concept is to provide pilot-oriented weather products automatically and directly to the pilot in near real-time. These products will be displayed on a map background and the weather information will be coded into discrete operationally significant categories. The basic alpha-numeric data will also be available for backup and for presentation of detailed information for specific locations. In addition, the aviation weather data will be analyzed and displayed in a format that will accentuate trends in the actual

weather conditions and accentuate deviations in the actual weather from the forecast conditions. The PAWSS program will also alert the pilot to the appearance of any significant or hazardous weather conditions.

With PAWSS, the weather data will be communicated directly to the aircraft via a data link mode. An on-board processor will then select and display the appropriate data effecting the route.

SYSTEM DESCRIPTION

A schematic of the PAWSS System is shown in Figure 1. On the left, conventional weather data are continuously received by the Communications Processor. There it is automatically checked and edited for quantitative and format errors. The edited data are then packaged into compressed data blocks and transmitted to the aircraft via a digital data link. On board the aircraft, the data blocks are expanded and decoded into several types of graphic depictions for display on a small screen using shapes and colors to define the various pilot-oriented display classifications. A non-keyboard control system is envisioned, similar to those used on many LORAN systems today. The Ground Station Processor with the Control and Display on the left is not necessary for the automatic operation of the system; it would be used for preflight briefing support.

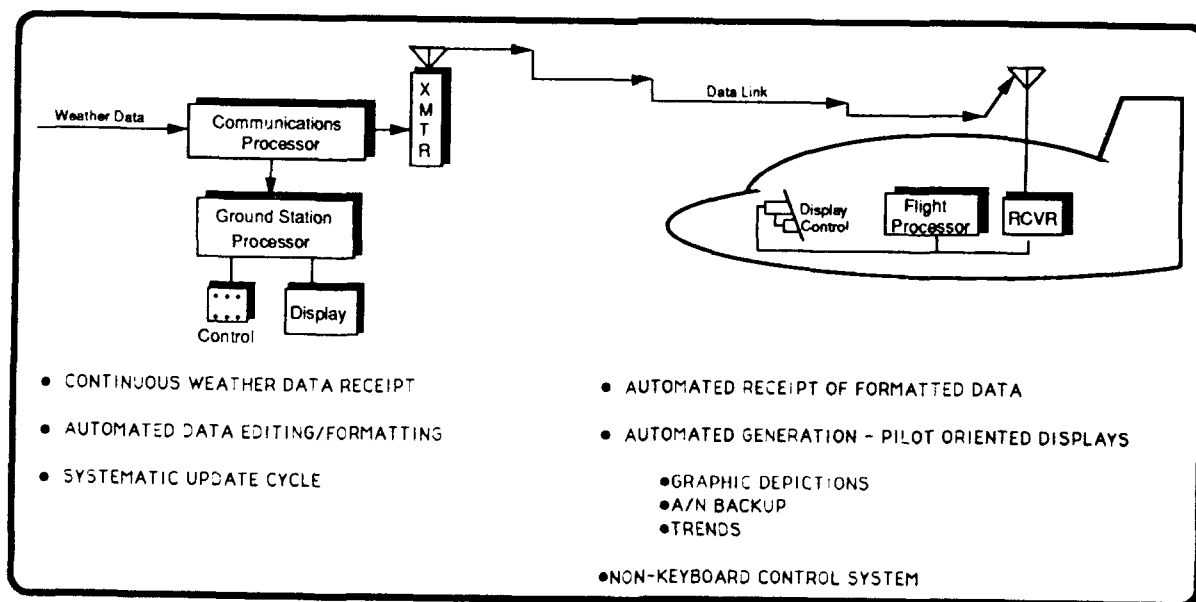


Figure 1. PAWSS System Description

DISPLAYS

In our initial studies, we have used only the following weather data types:

- Airport surface observations
- Airport terminal forecasts
- Near real-time ground weather radar mosaics.

Our approach is to encode the ceiling, visibility, present weather, and precipitation into operationally useful classification levels. The results are then displayed on map-type depictions. Figure 2 lists the classification levels and associated color and non-color keys for the PAWSS depictions described later in this paper. The non-color key has been developed for use in this paper; the PAWSS system will employ color depictions.

OPERATIONAL CATEGORY			WEATHER			GROUND RADAR		
Color		Non-Color	Color		Non-Color	Color		Non-Color
Clear	NO REPORT		Clear	NO REPORT				
Clear	VFR ($> 3000 / 5$)		Clear	NO WEATHER		VIP Levels	<1	
Green	MVFR ($\leq 3000 / 5$)		Green	CEILING ≤ 3000 & NO WEATHER		Green	1-2	
Blue	IFR ($< 1000 / 3$)		Blue / Clr	RAIN / DRIZZLE				
Yellow	LIFR ($< 500 / 1$)		Clr / Yel	VISUAL RESTRICTION		Yellow	3-4	
Red	$< \text{Cat I}$ ($< 200 / 1/2$)		Red	HAZARDOUS WEATHER		Red	5-6	

Figure 2 - Classification Key

In displaying the Operational Categories, we used the five existing ceiling and visibility levels which are representative of VFR, MVFR, IFR, LIFR or less than Category I IFR conditions. The Weather classifications represent significant weather elements which may impact on airport operations varying from hazardous weather (involving thunderstorms and ice forms) to visibility restrictions, to rain forms, to cloud only, to no weather. The Ground Radar classifications are based on the video integrated processor (VIP) assessments of the

precipitation intensities from today's National Weather Service (NWS) weather radars.

Using these classification types we can develop many different levels of PAWSS depictions. Figure 3 is a matrix which shows examples of the type of depictions which could be developed using three weather data types (surface observations; terminal forecasts and ground radar) and applying the data classification keys (Operational Category and Weather). For example, it is possible to create forecast depictions for the same time (synoptic view) or time-phased along the route based on the applicable forecast. By combining some of these depictions, you can also develop displays of weather trends which depict the representativeness (or accuracy) of the forecast conditions, i.e. compare the actual surface observations with the applicable terminal forecasts over the last three hours.

Data Analysis	WEATHER DATA TYPES		
	Surface Observations	Terminal Forecasts	Ground Radar
Operational Category	• Airport Category	<ul style="list-style-type: none"> • Synoptic Forecast Category • Route Forecast Category (Time Phased) 	
Weather	• Airport Weather	<ul style="list-style-type: none"> • Synoptic Forecast Weather • Route Forecast Weather (Time Phased) 	• Precipitation Depictions
Trends	COMBINED ANALYSIS <ul style="list-style-type: none"> • Airport Category Trend = Observed Category vs Forecast Category • Airport Weather Trend = Observed Weather vs Forecast Weather • LIST = Observed Airport Category & Weather vs Forecast Airport Category & Weather 		

Figure 3 - PAWSS Depiction Matrix: Phase I. Boxed Items Are Subsequently Illustrated.

In this paper we will illustrate the four depictions shown in the boxes. Software has been developed that will read the surface observations and terminal forecasts from the conventional FAA data service, and then automatically create these depictions and display them on a personal computer (286 PC with EGA). The depictions included here are illustrations which were created on a Macintosh computer.

THE AIRPORT OPERATIONAL CATEGORY DEPICTION (FIGURE 4). In this display, the airport ceiling and visibility are depicted in pilot-oriented operational categories as shown in the legend. The ceiling and visibility category status for each airport is determined by the on-board processor from the surface observation data included in each data block transmission. A solid course line is drawn between the departure and destination airports; a dotted line from the destination to the alternate. The airplane position is also displayed.

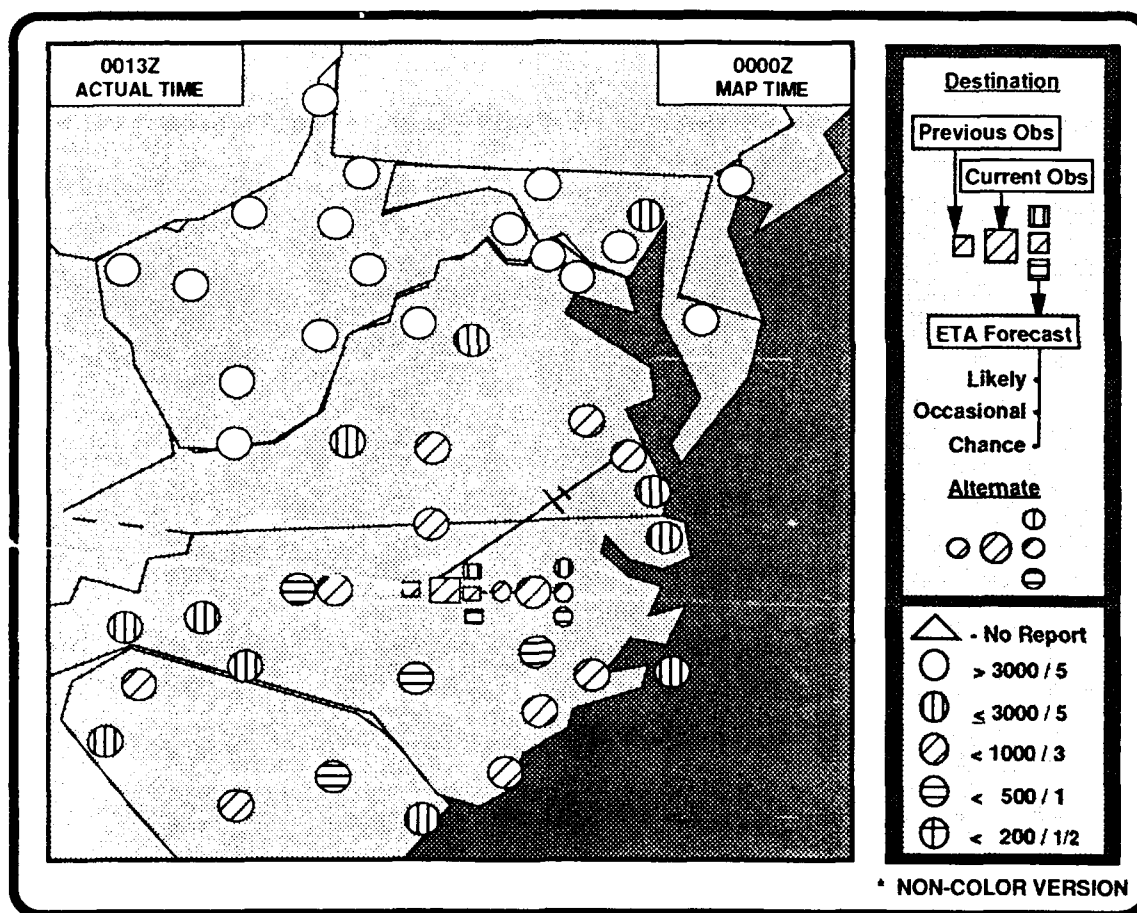


Figure 4 - Airport Operational Category Depiction

Some additional information is shown at the destination and alternate airports. At the 9 o'clock position, the category for the last observation is shown; at the 2, 3, and 4 o'clock positions, the categories depicted represent the Operational Category valid at the flight's ETA based on the currently valid terminal forecast. The current Zulu (actual) and map times are also shown.

The last three hours of this depiction will be stored in on-board memory and displayed in a loop fashion on demand. This type of display will clearly indicate which airports are acceptable for various modes of operation. A variation of this display which will provide a depiction of the Airport Operational Category trends at each airport is being studied.

THE AIRPORT WEATHER ELEMENT DEPICTION (FIGURE 5). For this depiction, the current weather elements are read from the surface observation and displayed for each airport on the map in the seven ways shown in the legend. Hazardous Weather and Visibility Restriction are defined as follows; the other symbols are self explanatory:

Hazardous Weather - Thunderstorms, hail, freezing rain and drizzle, sleet, sleet showers, ice crystals, snow, snow showers, snow grains/pellets

Visual Restriction - Fog, ground fog, ice fog, haze, smoke, dust, blowing dust, blowing sand/snow/spray

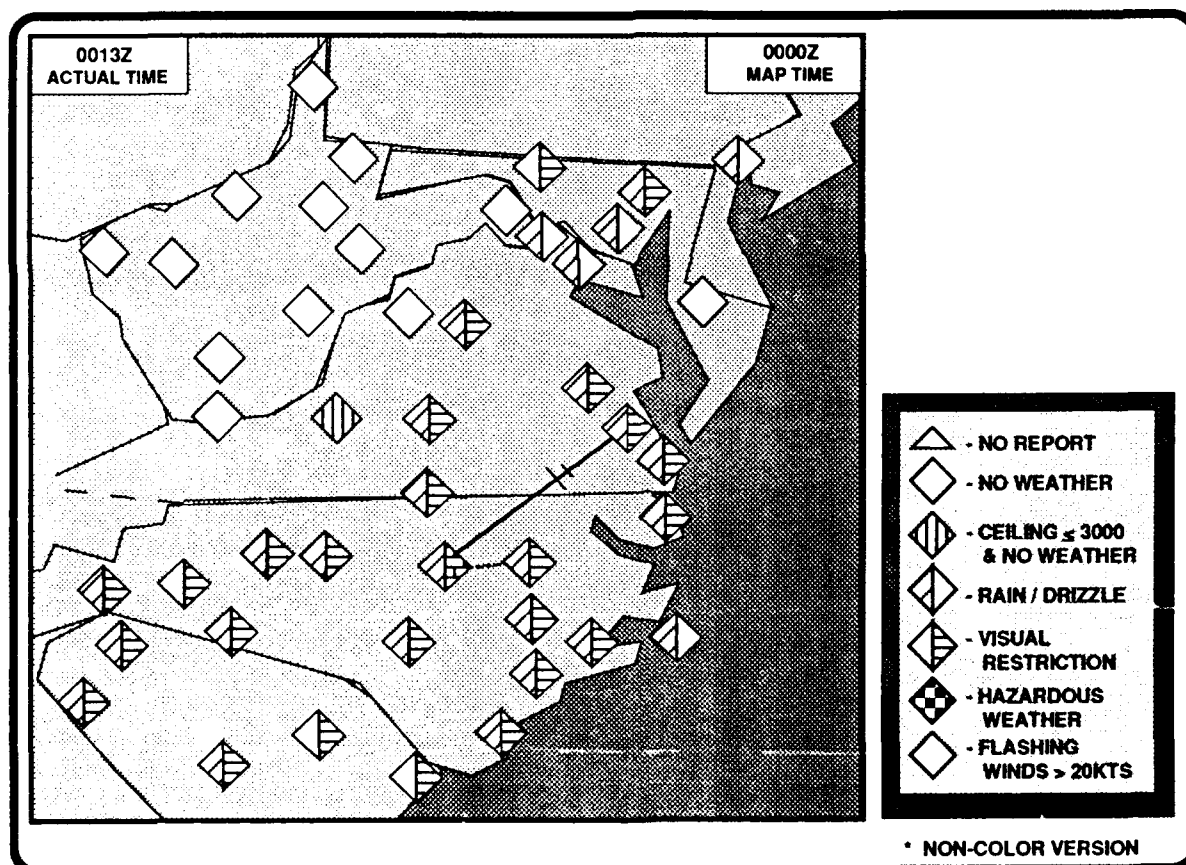


Figure 5 - Airport Weather Element Depiction

As before, the last three hours of this depiction will be stored in on-board memory and displayed in a loop fashion on demand.

THE GROUND WEATHER RADAR DEPICTION (FIGURE 6). This depiction example shows the radar precipitation intensity levels over the area. It was created from the NWS radar summary data. The intensity levels and color codes are shown in the legend. Radar top altitudes are shown in hundreds of feet. A flashing red contour will be shown 20 miles outside each red boundary (the Alert Line). While the data for this example are only available 60-90 minutes after-the-fact in the present weather reporting system, in the PAWSS tests we plan to access near-real-time radar mosaic data at 30 minute intervals initially, and ultimately at 15 minute intervals. The last three hours of these Ground Weather Radar Depictions will be stored on-board and displayed in a loop fashion on demand. They may also be overlaid on the other depictions when desired.

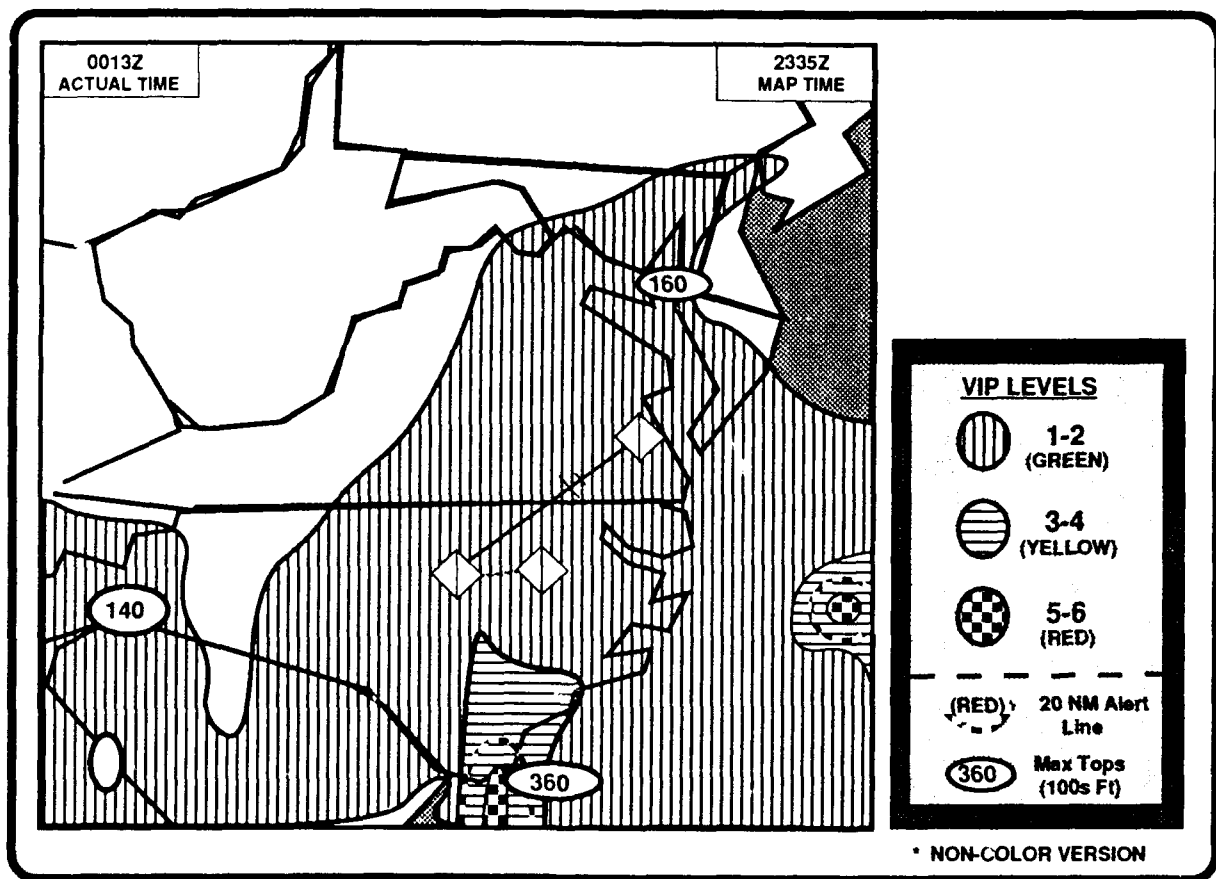


Figure 6 - Ground Weather Radar Depiction

THE SELECTED AIRPORT "LIST" DEPICTION (FIGURE 7). In this display, the current surface observation is displayed completely (at the top) including remarks except that the sea level pressure and special elements such as precip totals, max/min temps are deleted. The observation is wrapped around to a second or third line as necessary. In the following observation summary block, the current and last 3 hours of observations (including specials) are shown in descending chronological order with only the two lowest cloud layers, visibility and present weather displayed. For each observation, the applicable Airport Operational Category based on the terminal forecast (or amended forecast) valid at that time is shown.

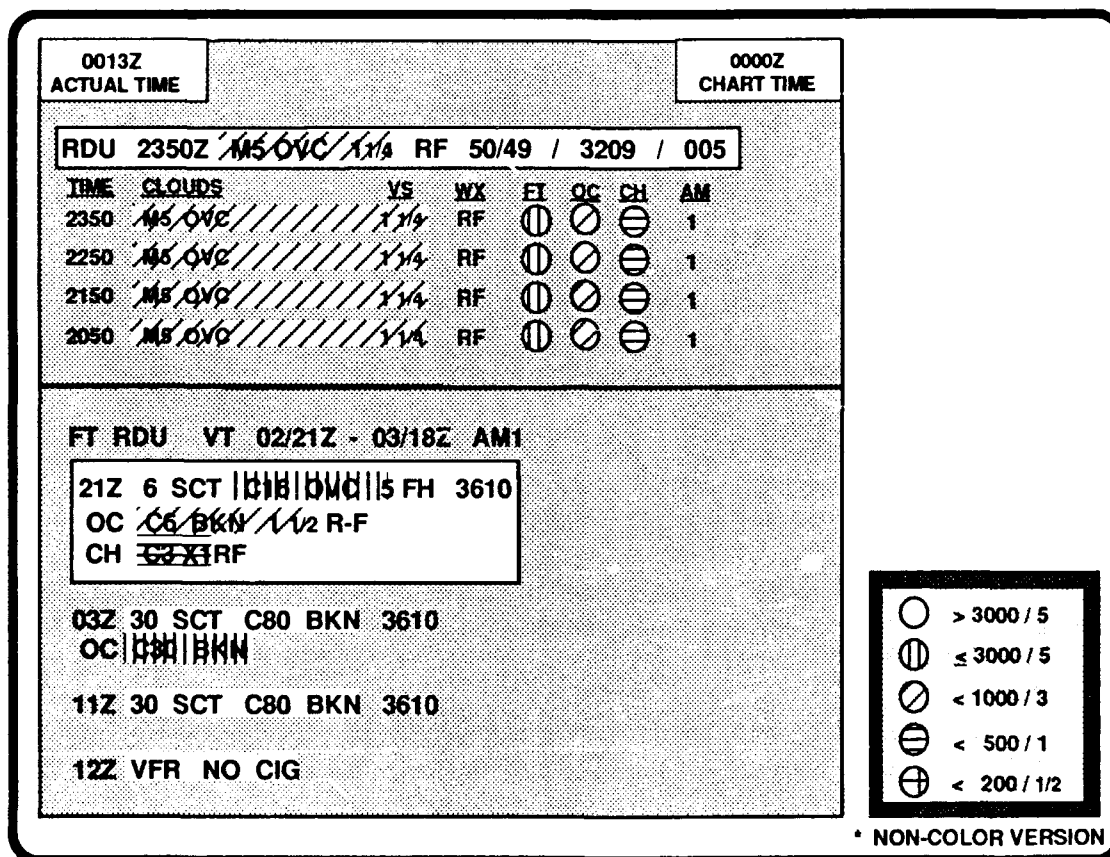


Figure 7 - Selected Airport "LIST" Depiction

The currently valid terminal forecast is also shown in alpha-numeric form below the observation summary block. The forecast has been reformatted into separate time block entries. Color-highlighting is used on each cloud and visibility portion of the surface observations and each line of the terminal forecast. It is easy to see from the "colors" alone that the weather at Raleigh has been worse than the "likely" part of the forecast and has,

in fact been equal to the "occasional" part of the amended forecast for the last three hours.

CONTROLS

The PAWSS will be controlled through the use of rotary knobs and buttons such as those shown in Figure 8.

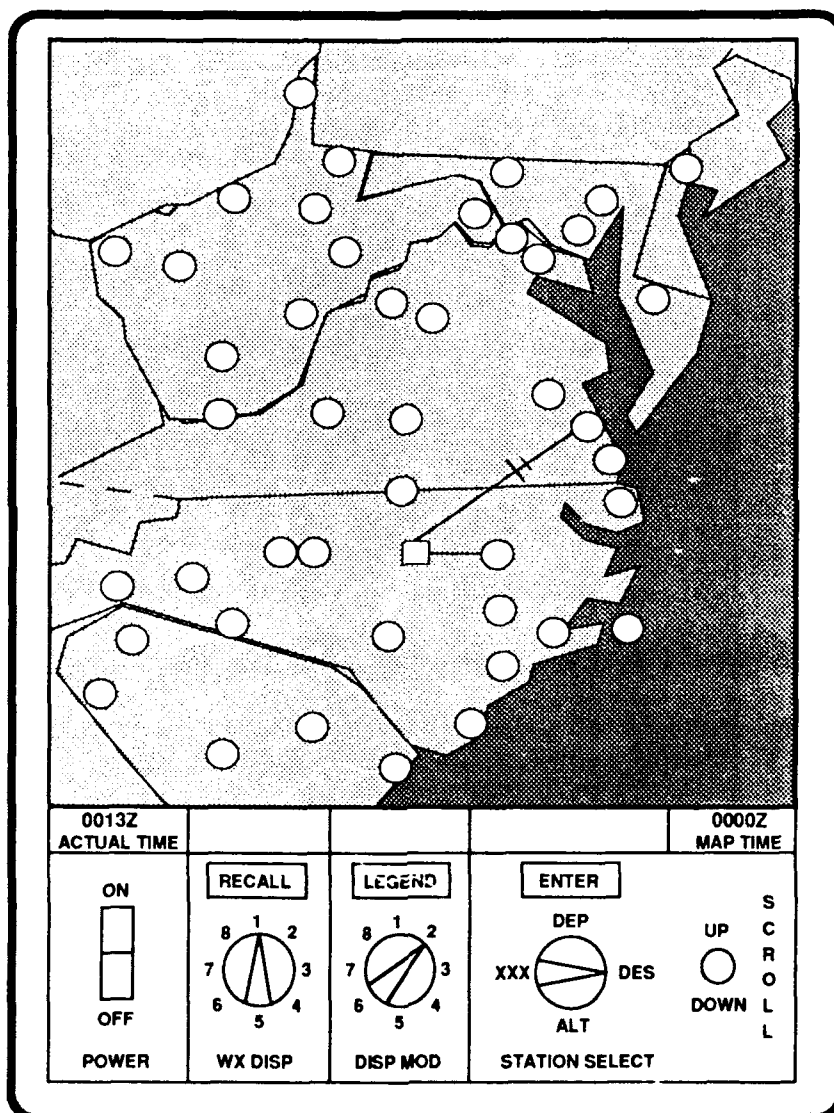


Figure 8 - PAWSS Control System and Display: Phase I

Using these controls the operator will be able to:

1. display any of the four basic displays
2. loop any of the map depictions
3. zoom any map depiction to a higher resolution and bring up any stations eliminated by the clutter algorithm
4. display or remove the appropriate legend on any map depiction
5. overlay the applicable radar mosaic on any map depiction
6. determine the location of any station by its alpha numeric identification
7. designate any airport as Departure, Destination, or Alternate
8. select any airport for the LIST display.

In addition, when a hazardous weather element or below Category I condition is received in any data block, the screen display will be automatically interrupted and the appropriate display will be shown until cancelled.

CONCEPT DEVELOPMENT AND EVALUATION PHASES

The PAWSS concept will be developed in three evolutionary phases. The first phase will be limited to the few data types already discussed and will allow development and testing of the concept in supporting flights within a confined local area. In the second phase, we will automate depictions based on many more data types and expand the coverage to support cross-country flights. The additional data will include products such as area forecast, winds and temperatures aloft, lightning location and intensity, Convective SIGMETs, SIGMETs, AIRMETs, PIREPs and on-board aircraft precipitation, wind and temperature measurements. We will also develop some initial expert system procedural guidance concepts such as automatically determining acceptable airport locations during preflight planning.

In the final phase, the PAWSS concept will be further expanded to cover the continental United States and to provide preflight and inflight expert system procedural guidance. We will also include new data from the planned National Weather Service AWIPS-90 (Advanced Weather Information Processing Systems for the 1990s) and the FAA aviation weather system improvements (i.e. NEXRAD and TDWR Doppler radar data, NWS and FAA automated surface observations, and the near real-time upper level winds measure by the NWS wind profilers). This data will be made available in the future via new data link technology.

The application of new display technologies (higher resolution, 3D . . .) could provide useful benefits to this system. The integration of PAWSS depictions with the new low-cost electronic-moving map displays will be tested and evaluated.

CONCLUDING REMARKS

The FAA is examining the use of automation in providing assistance to the pilot in obtaining and assessing weather data during flight operations. Promising approaches have been identified and testing of the concepts in simulators and in flight will follow.

1990 AIAA/FAA Joint Symposium on General Aviation Systems
Attendees List

Allsup, Jerry
U.S. Department of Energy
1000 Independence Ave., S.W.
Rm. 5G046
Washington, D.C. 20585
(202) 586-8032, FTS 896-8031

Avjian, Robert
Martin Marietta
6 Parsippany Ct.
Gaithersburg, MD 20878
(301) 294-7848

Bahr, Behnam
Institute for Aviation Research
Wichita State University
Wichita, KS 67208
(316) 689-3402

Balena, John
International Aerospace Mfg.
1500 Chiquita Center 250 E. 5th St.
Cincinnati, OH 45202
(513) 762-7860
FAX (513) 721-4628

Barile, Tony
FAA Technical Center
ACD-210
Atlantic City Int'l Airport
Atlantic City, NJ 08405
(609) 484-4457

Bartrand, Tim
Sverdrup Technology Inc.
NASA Lewis Research Center Group
2001 Aerospace Parkway
Mail Stop SVR-2127
Brook Park, OH 44142
(216) 826-6768

Bennett, Dr. A. G.
Mississippi State University
Raspet Flight Research Lab.
Drawer A, MS State, MS 39762
(601) 325-3274

Biehl, Keith
FAA Technical Center, ACN-360
Atlantic City Int'l Airport
Atlantic City, NJ 08405
(609) 484-6480

Bowen, Brent
Institute for Aviation Research
Wichita State University
Wichita, KS 67208
(316) 689-3678

Chambers, Randall
Institute for Aviation Research
Wichita State University
Wichita, KS 67208
(316) 689-3678 or 3425

Crabill, Norman
NASA Langley Research Center
105 Inland View Dr.
Newport News, VA 23603
(804) 865-1400

Dahl, Michael
ACE-111
FAA Central Region
601 East 12th Street
Kansas City, MO 64106
(816) 426-6941

Dash, Ernie
FAA Engineering Field Office
ASD-142, MS-250
NASA Langley Research Center
Hampton, VA 23665-5225
(874) 865-1400

Del Balzo, Joseph
FAA National Headquarters
AXD-1
800 Independence Ave., S.W.
Washington, D.C. 20591
(202) 267-7111 FTS 267-7111

Demko, Paul
FAA Technical Center
ACM-360
Atlantic City Int'l Airport
Atlantic City, NJ 08405
(609) 484-5463

Eiff, Gary
College of Technical Careers
S. Illinois Univ. at Carbondale
Carbondale, IL 62901
(618) 536-3371

Eiff, Mary Ann
S. Illinois Univ. at Carbondale
208 Pineview Dr.
Carbondale, IL 62901
(618) 549-6950

Glecier, Jack
Beech Aircraft Corp.
P.O. Box 85
Wichita, KS 67201-0085
(316) 689-6791

Goldschmied, Fabio
Engineering Consultant
1782 McClure Rd.
Monroeville, PA 15146-2027
(412) 327-8843

Grable, Markus
CTA Inc.
25 N. Jefferson Ave.
Margate, NJ 08402
(609) 646-4510

Gushue, John
Ebasco Services Inc.
210 Clay Ave.
Lyndhurst, NJ 07071-3507
(201) 896-5007

Hoadley, Arthur
Western Michigan University
College of Engineering and Applied
Sci.
Kalamazoo, MI 49008-5062
(616) 387-6491

Holmes, Bruce
NASA Langley Research Center
MS 116
Hampton, VA 23665-5225
(804) 864-6048

Hooper, Steve
Institute for Aviation Research
Wichita State University
Wichita, KS 67208
(316) 689-3678

Hopkins, Grant
Industry Science and
Technology Canada
235 Queen St.
Ottawa, Ontario K1A 0H5
(613) 954-3268

Ingels, Frank
Mississippi State University
819 Pine Circle
Starkville, MS 39759
(601) 325-3912

Johnson, Bill
Galaxy Scientific
2310 Parklake Dr., Suite 300
Atlanta, GA 30345
(404) 270-2855

Jezierski, Carl
FAA Technical Center
ACD-320
Atlantic City Int'l Airport
Atlantic City, NJ 08405
(609) 484-6913

Khatiwala, Bart (co-op student)
FAA Technical Center
911 E. Landis Ave.
Vineland, NJ 08360
(609) 484-5048

Knopp, Ken (co-op student)
FAA Technical Center
ACD-240
Atlantic City Int'l Airport
Atlantic City, NJ 08405
(609) 484-6539

Kosinski, Robert
Ebasco Services Inc.
210 Clay Ave.
Lyndhurst, NJ 07071-3507
(201) 896-5007

Lamprecht, Richard
FAA Technical Center
494 SaraAnn Ct.
Linwood, NJ 08221

Lankarani, Hamid
Institute for Aviation Research
Wichita State University
Wichita, KS 67208
(316) 636-4410

Lee, Siu (co-op student)
FAA Technical Center
ACD-330
Atlantic City Int'l Airport
Atlantic City, NJ 08405
(609) 484-4572

MacDermott, Frazier
756 Shropshire Dr.
West Chester, PA 19382
(215) 692-1386

Marshall, Bill
NIPER
P.O. Box 2128
Bartlesville, OK 74005
(918) 337-4253

Maughmer, Mark
Pennsylvania State University
Dept. of Aerospace Engineering
233 Hammond Building
University Park, PA 16802
(814) 863-4485

McFadden, John
NASA Lewis Research Center
21000 Brookpark Rd.
Cleveland, OH 44107
(216) 433-3386

Mount, Robert
JDTI Inc.
P.O. Box 128
Wood-Ridge, NJ 07075-0128
(201) 470-7005

Murillo, Margaret
(co-op student)
FAA Technical Center
ACD-320
Atlantic City Int'l Airport
Atlantic City, NJ 08405
(609) 484-6386

Nissley, Bill
FAA Technical Center
ACD-210
Atlantic City Int'l Airport
Atlantic City, NJ 08405
(609) 484-4147

Rehmann, Al
FAA Technical Center
ACD-320
Atlantic City Int'l Airport
Atlantic City, NJ 08405
(609) 484-5733

Nixon, Barry
Consultant
30 Merritt Dr.
Lawrenceville, NJ 08648
(609) 883-9456

Rose, Raymond
NASA Headquarters
600 Independence Ave. S.W.
Washington, D.C. 20546
(202) 453-2828

Owens, John
Mississippi State University
Raspet Flight Research Lab.
Drawer A
Mississippi State, MS 39762
(601) 325-3274

Runo, Steve
Honeywell Inc.
P.O. Box 29000, MS AV5710
Phoenix, AZ 85033-9000
(602) 863-8930

Perez, Jose (co-op student)
FAA Technical Center
ACD-310
Atlantic City Int'l Airport
Atlantic City, NJ 08405
(609) 484-5112

Sarino, Joslin (co-op student)
FAA Technical Center
ACD-320
Atlantic City Int'l Airport
Atlantic City, NJ 08405
(609) 484-4577

Perrotta, Pat
FAA NYACO
ANE-174
181 S. Franklin Ave.
Valley Stream, NY 11581
(609) 791-7421

Schroer, Robert
Martin Marietta Air Traffic Systems
475 School St. S.W.
Washington, D.C. 20024
(202) 646-6992

Pierce, Harold
Honeywell Inc.
8840 Evergreen Blvd.
M/S MN51-1390
Minneapolis, MN 55433-6040
(612) 785-4292

Schuler, Gregg
International Aerospace Mfg.
1500 Chiquita Center
250 E. 5th St.
Cincinnati, OH 45202
(513) 762-7860
FAX (513) 721-4628

Raju, M.S.
Sverdrup Technology Inc.
NASA Lewis Research Center Group
2001 Aerospace Parkway
Brook Park, OH 44142
(216) 826-6710

Selig, Michael
Pennsylvania State University
233 Hammond Building
University Park, PA 16802
(814) 865-9611

Shin, Kem (co-op student)
FAA Technical Center
Atlantic City Int'l Airport
Atlantic City, NJ 08405
(609) 484-5630

Singh, Trib
Martin Marietta
FAA Technical Center
SEI-540
Atlantic City Int'l Airport
Atlantic City, NJ 08405
(609) 484-5133

Smith, Hubert
Pennsylvania State University
233 Hammond Building
University Park, PA 16802
(814) 865-2569

Smith, William
Facet Aerospace Products Co.
1048 Industrial Park Rd.
Bristol, VA 24201
(703) 669-5555

Snyder, Mel
Institute for Aviation Research
Wichita State University
Wichita, KS 67208
(316) 689-3678

Stewart, Eric
NASA Langley Research Center
MS 247
Hampton, VA 23665-5225
(804) 864-3939 FTS 928-3939

Stewart, Robert
Gulfstream Aerospace Corp.,
B-08
P.O. Box 2206
Savannah, GA 31402
(918) 897-4192

Sweeney, Dave
FAA Technical Center-MITRE
Building 270
Atlantic City Int'l Airport
Atlantic City, NJ 08405
(609) 484-5538

Talia, Jorge
Institute for Aviation Research
Wichita State University
Wichita, KS 67208
(316) 689-3402

Truont, Y. (co-op student)
FAA Technical Center
ACN-210
Atlantic City Int'l Airport
Atlantic City, NJ 08405
(609) 484-5436

Walsh, Joseph
4942 Herkimer St.
Annandale, VA 22003
(203) 354-3778

Werth, Mark
Illinois Dept. of Agriculture
Div. of Marketing- State Fairgrounds
P.O. Box 19281
Springfield, IL 62794-9281
(217) 782-6675

Willis, Ed
NASA Lewis Research Center
MS 86-6
Cleveland, OH 44135
(216) 433-3398

Wright, Edward
Deere and Company
John Deere Rd.
Moline, IL 61265-8098
(309) 765-5462

York, Paul
Institute for Aviation Research
Wichita State University
Wichita, KS 67208
(316) 689-3678

Yang, S. L.
NASA Lewis Research Center
Mail Stop 86-6
Cleveland, OH 44135

Yulo, Carlo
FAA Technical Center
P.O. Box 771
Ocean City, NJ 08226
(609) 399-3144